SKB

Methodology for discrete fracture network modelling of the Forsmark site

Part 1 – concepts, data and interpretation methods

Jan-Olof Selroos

Diego Mas Ivars

Raymond Munier

Lee Hartley

Simon Libby

Philippe Davy

Caroline Darcel

Paolo Trinchero

SVENSK KÄRNBRÄNSLEHANTERING

Methodology for discrete fracture network modelling of the Forsmark site

Part 1 – concepts, data and interpretation methods

Jan-Olof Selroos, Diego Mas Ivars
Svensk Kärnbränslehantering AB

Raymond Munier, Terra Mobile Consultants AB

Lee Hartley, Simon Libby
Golder Associates UK, Ltd.

Philippe Davy, Géosciences Rennes, Université de Rennes 1, CNRS

Caroline Darcel, Itasca Consultants s.a.s.

Paolo Trinchero, Amphos 21 Consulting S.L.

Preface

A series of methodology reports support the programmes for investigation and modelling during the execution of planned underground constructions at Forsmark. The series includes the following disciplines: geometric modelling of ground elevation and regolith, deterministically modelled geological structures, discrete fracture network (DFN) modelling (stochastic, semi-stochastic and deterministic modelling of structural-hydraulic fracture data), rock mechanics modelling, thermal properties modelling, integrated hydrological and hydrogeological modelling, hydrogeochemical modelling, and transport modelling. Report numbers (ID), acronyms, and titles are shown below. The acronyms are recommended for internal referencing.

ID	Acronym	Title
R-20-10	**DGMM**	Methodology for deterministic geologic modelling of the Forsmark site
R-20-11	**DFNMM1**	Methodology for discrete fracture network modelling of the Forsmark site Part 1 – Concepts, Data and Interpretation Methods
R-20-12	**DFNMM2**	Methodology for discrete fracture network modelling of the Forsmark site Part 2 – Application examples
R-20-13	**RMMM**	Methodology for rock mechanics modelling of the Forsmark site
R-20-14	**HGMM**	Methodology for hydrological and hydrogeological modelling of the Forsmark site
R-20-15	**HCMM**	Methodology for hydrochemical modelling of the Forsmark site
R-20-16	**ERMM**	Methodology for elevation and regolith modelling of the Forsmark site
R-20-17	**TRPMM**	Methodology for site descriptive and safety assessment transport modelling of the Forsmark site
R-20-18	**THPMM1**	Methodology for modelling of thermal properties of the Forsmark site Part 1 – Recommended data and interpretation methods
R-20-19	**THPMM2**	Methodology for modelling of thermal properties of the Forsmark site Part 2 – Background and methodology development

The present report provides the methodology for Discrete Fracture Network (DFN) modelling. The report consists of two parts; Part 1 (R-20-11, the current report) provides theoretical foundations, conceptual frameworks and analysis techniques with which to interpret site data and construct quantitative descriptions of fracture systems, while Part 2 (R-20-12) provides practical guidance and methods for numerical modelling of fracture systems.

Although the present report focuses on the Forsmark site and SKB's needs for DFN modelling during the underground construction of the spent fuel repository, it is noted that the methodology has been devised to also inform DFN applications involving other geological and hydrogeological settings or other types of repositories.

The work forming the basis of the present report has been performed by a project group consisting of the listed authors. However, the project group has greatly benefitted from discussions also with the authors of several of the other modelling methodology reports. The project was led by Jan-Olof Selroos, with substantial support from Raymond Munier, while all project members provided expert knowledge on various aspects of the DFN modelling methodology covered.

Abstract

Prior to the planning of detailed site investigations at Forsmark, Simpevarp and Laxemar (2003–2010), SKB presented methodologies and strategies for the analysis and construction of Site Descriptive Models (SDMs). These strategies were manifested in the form of a series of methodology reports which offered the theoretical underpinning for the methods and best practices that should be applied to the various aspects of site modelling.

Lessons learned during the safety assessment SR-Site and its review by the authorities and the scientific community revealed both the strengths and weaknesses of these methodologies. In particular, though adequate for the SDM and the safety assessment, SKB identified a need to update the methodology for DFN modelling to meet expected challenges anticipated during the construction of the repository and to reflect the state-of-the-art in this increasingly complex field of science.

In contrast to previous DFN methodologies reported by SKB, the governing principle of this work has been to ensure the creation of a common, generalised and multidisciplinary DFN framework that can be used in any application required for modelling in support of site-description, safety assessment or repository engineering. Other main new features of the methodology include hydromechanical coupling, introduction of in-plane heterogeneity of individual fractures, genetic fracture generation, description of deformation zones through a DFN approach and a framework of uncertainty management.

The methodology for DFN modelling presented here also includes recommended methods and best practices. Due attention is paid to other methodologies being developed by SKB, in particular the methodologies for geological modelling, for rock mechanical modelling, for hydrogeological and transport modelling. The methodology is aimed towards a broad audience, thereby enabling both practitioners and theoreticians alike to appreciate the information provided. Due emphasis has been paid also to uncertainty assessment, and how to handle different types of uncertainties given the applications at hand.

Sammanfattning

Inför planeringen av platsundersökningar I Forsmark, Simpevarp och Laxemar (2003–2010), publicerade SKB metodiker och strategier för analys och generering av platsbeskrivande modeller (SDM). Dessa strategier bestod av ett antal metodikrapporter vilka beskrev det teoretiska ramverket och rekommendationer om bästa förfarande vid applicering för olika modelleringsaspekter.

Erfarenheter vunna i samband med genomförandet av säkerhetsanalysen SR-Site, samt dess gransking av myndigheter och det vetenskapliga samfundet, tydliggjorde såväl metodikernas svagheter som styrkor. I synnerhet identifierade SKB ett behov av en uppdatering av metodiken för DFN-modellering för att kunna möta de utmaningar som förväntas i samband med konstruktionen av slutförvaret och för att spegla de senast vunna rönen i detta allt mer komplexa vetenskapliga område.

I kontrast mot de tidigare av SKB rapporterade metodikerna, har den styrande principen för föreliggande arbete varit att säkerställa ett gemensamt, generaliserat och multidisciplinärt ramverk som kan tillämpas för samtliga modelleringsinsatser som krävs som stöd för platsbeskrivningar, säkerhetsanalyser eller förvarsutformningar. Dessutom har tidigare metodik utökats med hydro-mekaniska kopplingar, ytheterogenitet av enskilda sprickplan, genetisk sprickgenerering, modellering av deformationszoner medelst DFN-metodik, samt ett utökat ramverk för osäkerhetshantering.

Föreliggande DFN-metodik omfattar även rekommendationer av metoder och om bästa praxis. Koppling har säkerställts till övriga metodikrapporter, i synnerhet metodikerna för geologisk modellering, bergmekanisk modellering, hydrogeologisk modellering och för modellering av transportprocesser.

Metodiken som presenteras här är riktad mot en bred läsekrets vilket möjligör både för praktiker och teoretiker att tillgodogöra sig det förmedlade innehållet. Osäkerhetsanalyser betonas liksom hanteringen av osäkerheter för olika tillämpningar.

Contents

1 Introduction

1.1 Context and purpose of report

The Swedish and Finnish systems for handling the long-term storage of spent nuclear fuel, KBS-3, has been developed since the late seventies (KBS 1983 a, b, c, d, SKBf/KBS 1983, SKB 2010c). The system is based on multiple interacting barriers (Figure 1-1) of which the geosphere is the main focus of this report. The research and development program "FoU-PROGRAM 89" (SKB 1989a, b) identified key aspects of the geosphere, important for containment and retardation of radionuclides, which were further detailed and expanded as a result of SKB's first formal safety assessment SKB 91 (SKB 1992). Ever since, the methods for characterization and modelling of fractures have been refined and developed as a response to the feedback provided by collaborators, downstream users, peer reviewers, regulators and their experts, partly summarized in SSM (2018) and references therein, to meet the needs required by safety assessments and planning of the construction of the repository.

The description of brittle deformation structures i.e., fractures and fractures zones, their properties, and representation in Discrete Fracture Network (DFN) models provides a cornerstone for several components of a site description, principally concerning structural geology, rock mechanics, hydrogeology, hydrogeochemistry and solute transport. It also underpins assessment of several safety functions (Posiva SKB 2017) including consideration of mechanical, hydraulic and chemical stability of the buffer and backfill, as well as retardation of the migration of harmful substances from the repository. For example, groundwater flow through the void space of the interconnected fractures in the bedrock is the dominant pathway for the migration of any contaminant releases from a repository. At the same time, sorption onto the minerals on fracture surfaces and the adjoining rock matrix via molecular diffusion through porewater are significant retardation mechanisms for migration. The same physical processes are significant factors determining the evolution of groundwater composition, which is an important consideration in assessing long-term integrity of the engineered barrier system and performance of the overall disposal system through processes such as chemical erosion of the buffer and corrosion of canisters. Safety assessment also has to consider the possibility of a major earthquake leading to canister failure due to induced, secondary, movements on fractures intersecting canister positions, especially at a time of ice-sheet retreat, which requires knowledge of fracture mechanical and geometrical properties in an intricate interplay with transient stress states.
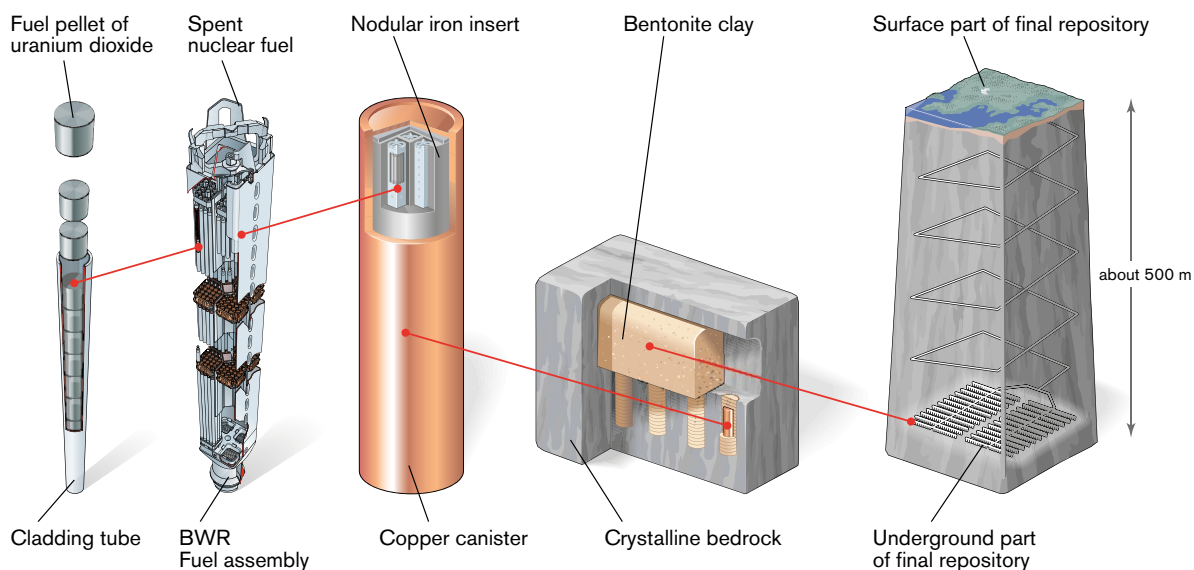
Figure 1-1. *The KBS-3 method. The method involves encapsulating the spent fuel in copper canisters which are then emplaced, surrounded by a buffer of bentonite clay, in vertical deposition holes in a tunnel system at a depth of 400–700 metres in the bedrock.*

Geometrical, hydraulic and mechanical properties of fractures are also relevant to planning construction and operation of a disposal facility through their implications to managing water inflows and bedrock stability. Related fracture characteristics are also important when assessing compliance relative to requirements of the disposal system and design (Posiva SKB 2017), including support to rock engineering.

The term DFN modelling defines how a fractured rock mass (the natural fracture system) can be equivalently and quantitatively represented as a population of individual, *fracture-like*, idealized tabular objects, including their geometrical and physical properties. The generic term fracture used in the report refers to these idealized objects (which cover a broad range of geological fractures). In the modelling process, the geometry of the individual fractures is first determined, as a basis for the definition of their individual hydraulic and mechanical properties and for the determination of the properties of the population of fractures (the DFN), as a whole. The complexity of the modelling process is dependent on the complexity of the natural fracture pattern and on the degree of bedrock exposure, both at the scale of individual fractures and at the scale of the entire fracture population. DFN models typically involve the determination of the following properties for the fractures (Munier 2004, Milnes 2006):

- Each individual fracture of a DFN has a location, size, shape and orientation, as given by the spatial density distribution of the whole population, including the size, shape and orientation distributions. The density-size distribution may reflect a scale dependency (Bonnet et al. 2001), expressing the relation between large and small fractures at different modelling scales.

- The combination of the preceding distributions, over a certain volume and range of parameters, results in a cumulative fracture area per unit volume, the fracture intensity noted (e.g. P_{32}, Dershowitz 1985).

- Variations of the abovementioned properties in terms of spatial correlations to other fractures or lithology.

- Fracture aperture and surface morphology, e.g. the presence of voids/asperities, contact areas, roughness and undulations of surfaces.

- Fracture mineralogy, e.g. mineral infillings, alteration, fault gouge and adjacent host-rock alteration.

- Fracture mechanical properties, e.g. shear stiffness, normal stiffness, shear- and tensile strength, and shear dilation.

- Fracture hydraulic properties, e.g. transmissivity, storativity, diffusivity with relationships to aperture.

- Fracture transport properties, e.g. the volumes (transport aperture) accessible by advection and hydrodynamic dispersion, the diffusion and sorption properties of the adjoining rock matrix and transport aperture that scales flux to advective velocity.

The DFN model is the recipe for creating a numerical system of fracture objects in which the mechanical, flow and transport processes taking place in fractures are represented explicitly in a discrete system, thus mimicking as much as possible the reality. The interplay between fractures and adjacent matrix rock may also be considered.

When simulation conditions and model dimensions are too demanding for a discrete representation of the complete DFN, the DFN model itself can be partially or fully upscaled in an Equivalent Continuous Medium model (see e.g. Chapter 6), where the properties of individual fractures are averaged in some way over a volume typically containing several or many fractures.

The DFN representation of a site model commonly encompasses deterministic, semi-stochastic and stochastic fractures (see Subsection 1.3.5 for definitions). For some large-scale structural features, the above-mentioned fracture properties can be assigned to the modelled objects by integration of geophysical, surface-based boreholes, outcrop, monitoring, and underground characterisation. However, for most fractures in the volume of interest it is not possible to determine more than a small fraction of the properties and their spatial distributions, if at all. Hence, they are described in terms of probability distributions, with statistical models and through correlation structures. This stochastic

aspect of fractures is necessary in order to predict the nature of fracture networks, in a statistical sense, between observations, that are below the resolution of geophysical methods, in boreholes and in underground openings. Similarly, it is necessary to use a statistical approach to describe fractures in the subsurface that are known to exist but for which there are no direct observations.

Approaches to fracture characterisation and the use of DFN modelling are long established in SKB's programme since development of their application at the Stripa mine (Gnirk 1993) and at the Äspö Hard Rock Laboratory (Billaux et al. 1994, Uchida et al. 1994, Gustafson et al. 1995, Follin and Hermanson 1996, Geier 1996, Geier and Thomas 1996, Dershowitz et al. 1999, 2000, 2003a, Doe 1999, Gale 1999, Andersson 2002, Andersson P et al. 2002, Rhén and Smellie 2003, Fox et al. 2005, Sawada et al. 2015). DFN models of Forsmark have been used in SDM-Site (Follin et al. 2007b, Fox et al. 2007b) SR-Site (Joyce et al. 2010, Svensson and Follin 2010, Vidstrand et al. 2010), and SFR-PSU (Odén et al. 2014) but also developed in parallel branches beyond the framework of safety assessments or site descriptions (Darcel et al. 2006, 2009, 2013). It has also been used in Laxemar-Simpevarp (Darcel et al. 2004, La Pointe et al. 2008, Rhén et al. 2008) and by Posiva at Olkiluoto (Hartley et al. 2018b).

A new suite of site descriptive models (SDMs) will be needed to support the preparation of a Safety Analysis Report (SAR) required as part of the Operational Licence Application (OLA) for the spent fuel repository in Forsmark. In preparation for these efforts, a series of methodology reports are being prepared in support of the operational programmes for characterisation and modelling of the access ramps, shafts and technical facilities, and, ultimately, for the deposition areas. The methodologies may also be applied in the creation of intermediate modelling steps toward the planning for SAR and assist characterisation taking place during construction of the accesses.

The application for the construction of a repository for spent nuclear fuel, which was submitted in 2011, regarded the Forsmark site exclusively. On the other hand, the location of the Final Repository for Long-lived Radioactive Waste, SFL, has not yet been decided. Though theories, tools and most methods discussed herein are applicable to an arbitrary site for nuclear waste disposal in crystalline bedrock, nevertheless focus of this report is on the Forsmark site, with the intention to update the report, should it be needed, in light of the future site investigations for the SFL facility.

The current report describes the methodology for performing DFN modelling, which forms a bridging activity between the descriptions of bedrock geology, rock mechanics, hydrogeology, hydrogeo-chemistry and solute transport. It is intended as a handbook for the modelling concepts, data analysis, numerical techniques appropriate to description and numerical modelling of naturally fractured rocks.

The target audience for the report is twofold; first, the report is intended for the SKB experts and modellers, both internal and external, who will do the DFN modelling in the coming stages of SKB's stepwise program. Second, the report is intended as an account for the authorities and their external experts on the DFN methodology to be employed by SKB henceforth. These dual target groups imply that the report must be both specific on details and instructive at the same time. Each chapter and section meets these objectives by presenting a context and the major ideas, followed by the theoretical, and mathematical framework, and concluding with examples of applications based on simplifying assumptions. Where more than one set of assumptions may be valid, multiple applied methodological variants may be presented. The more theoretically inclined readers are encouraged to read also the mathematically inclined sections, whereas practitioners should be able to take home the main messages by reading the introductory and applied sections only.

This report is divided into two volumes: Part 1 (Chapters 1–11) provide conceptual frameworks and analysis techniques with which to interpret site data and construct quantitative descriptions of fracture systems, while Part 2 provides practical guidance and methods for numerical modelling of fracture systems.

1.2 The discrete fracture network (DFN) modelling concept

As stated above, the concept of DFN modelling involves a simulation framework that represents a fractured rock mass (the natural fracture system) as an equivalent population of individual, *fracture-like*, idealised objects. Depending on the modelling conditions, the scale and the fracture pattern, specific groups of "real" fractures may be idealised geometrically as single objects with effective properties that represent the aggregation of multiple fractures, and possibly the intervening rock. A simple example would be to assign the aperture of the single object according to the sum of aperture of apertures within a zone intersected by the same hole or tunnel. A more complex example would be to generate a heterogeneous field of transmissivity over the plane of the single object that represents the inter-connectivity (or lack of it) and lateral conductance of the fractures within a zone.

The first attempts for modelling the structural and hydraulic characteristics of naturally fractured rock with the DFN concepts date back to the mid- or late eighties (Robinson 1984, Dershowitz 1985, Long et al. 1985, Cacas 1989). Since these pioneering works, the conceptualization of natural fracture systems (e.g. Bonnet et al. 2001) as spatial and multiscale patterns, the relationship between structural information, fracture statistics and bedrock hydraulic and mechanical properties, and also the numerical tools adapted to perform DFN based numerical simulations (Figure 1-2), have evolved considerably.
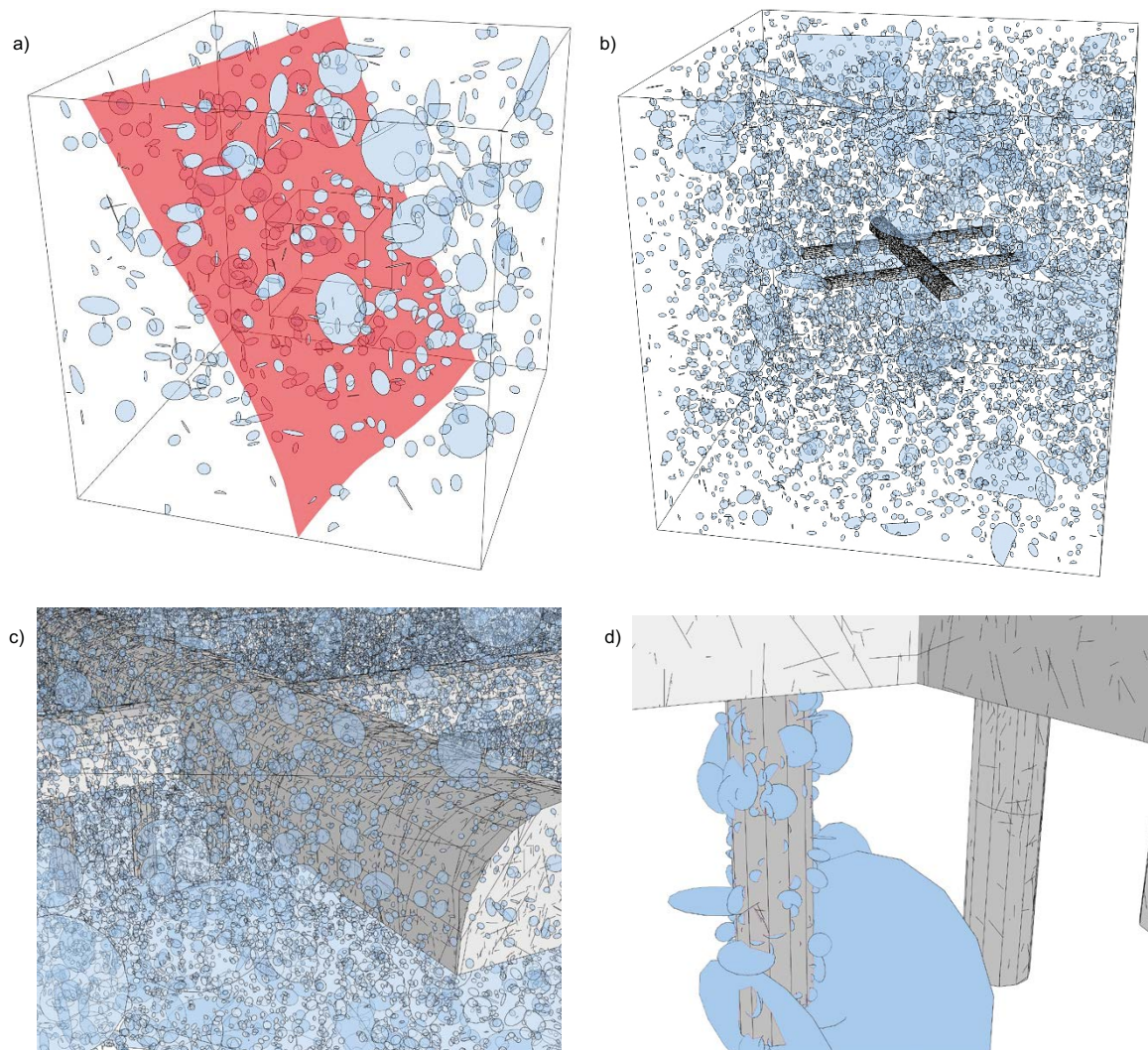
Figure 1-2. *Example of a multiscale, nested, DFN model. Figure a) shows an included deformation zone which is modelled deterministically. Figure b) shows hypothetical tunnels, in the model cube shown in the centre of Figure a). Figure c) displays a detail of Figure b) which shows the traces used to condition the DFN model. Figure d) shows a detail of Figure c) in which only fractures intersecting a deposition hole are shown, for clarity.*

There are two main advantages of using the DFN concept (Davy et al. 2018b) *i*) the model of the medium mimics the real system and consequently the geoscientific information collected in the field is easily integrated into the modelling process, *ii*) no pre-existing homogenization scale is required, in contrast to continuum approaches. This presumes the case, as at Forsmark, that structural mapping along with high resolution geophysical and hydraulic logging of boreholes are the standard for borehole characterisation, as opposed to homogenised methods such as double packer tests. The DFN modelling approach is also particularly suited to crystalline rocks (like in Forsmark), where the fractures are orders of magnitudes more permeable than the rock itself and where the rock matrix is much stiffer than the fractures.

Therefore, the characterisation of individual fracture properties has been one cornerstone of the data acquisition strategy at SKB. The major supporting data for defining the elementary components of the DFN modelling at Forsmark are so far:

- Structural interpretations of the oriented borehole image logs and borehole cores. These have been collated as a database of fracture properties, e.g. orientations, locations, infillings (see e.g. Stephens et al. (2007) for governing principles; Rauséus and Petersson (2020) for complete data set and application).

- Detailed outcrop fracture mapping at nine locations including, but not restricted to, records of fracture orientation, lithology, fracture morphology (planarity, roughness, and geometry), fracture termination relationships, fracture aperture and, where applicable, fracture infill mineralogy (Stephens et al. 2007).

- Hydraulic characterisation focused on interpreting the transmissivity of both short consecutive borehole intervals using Pipe String System, PSS, (Follin et al. 2007b), and of individual fractures using the Posiva Flow Logging tool, PFL (Rouhiainen and Sokolnicki 2005).

SKB has more than 30 years of experience in all stages of DFN modelling. As part of this experience, it is recalled below the main concepts and terminology which are used at the different levels of the DFN methodology, from in situ data acquisition, geological description, DFN model building leading up to risk assessment analyses.

1.3 Key concepts and terminology

The process of producing a **Site Descriptive Model** (SDM) of which DFN models constitute a vital component, is an iterative and integrative process that include collaboration of a large number of professionals with widely different backgrounds, nationalities and expertise (Munier 2008, Ström et al. 2008, Andersson et al. 2013). Naturally, to ease collaboration and avoid costly misunderstandings, it is vital to unite around a common terminology for terms that are commonly used in such context.

We therefore here re-iterate and refine the terminology that was established during the surface-based Site Investigations, subsequent modelling and safety assessments, to maintain backwards compatibility with previously published work and ensure a stringent and coherent nomenclature for coming phases of the construction and deposition processes.

The terminology covers two main aspects. One relates to the real world and classical geological description (Subsections 1.3.1 to 1.3.4) the other relates to the idealized volumes and objects handled in the SDM and DFN models (Subsection 1.3.5 and Chapters 2, 5, 6, 8).

1.3.1 Lithology and Structural geology

The **lithology** of a rock volume is a description of its physical characteristics such as texture, grain size, or composition (e.g., Bates and Jackson 1987). It may, in addition, describe the gross physical character of the rock, which may also include its constituent fractures.

Structural geology is the study of the three-dimensional distribution of rock units with respect to their deformational histories, more precisely the processes that resulted in the formation of geologic structures and how these structures affect the rock. Geological structures include a variety of essentially

planar features such as bedding planes, foliation, fault- and fracture planes, linear features such as shear striae (slickenlines, grooves) on fracture surfaces and irregularly shaped volumes or surfaces which includes folds and rock contacts which may, in addition to their original shape, have been reworked by geological processes such as folding, shearing or faulting. It follows therefore that structural geology, with direct implications on DFN modelling, is essentially the art of unveiling the deformation history by the study of changes in geometry with time and space.

1.3.2 Deformation

Rock deforms in essentially three types of deformation: Ductile deformation, semi-ductile deformation and brittle deformation. Pervasive, or dissipated, deformation is dispersed throughout the rock mass whereas localised deformation concentrates in restricted volumes of the rock. The connection to DFN modelling is strong: Fractures and shear zones are structural features that accommodate deformation.

Ductile deformation is the response to stress of rock which undergoes irreversible deformation without fracturing. This produces permanent strain marked by smooth variations of properties and fabrics within the deformed rock. Ductile behaviour is enhanced where high confining pressures are combined with high temperatures (Figure 1-5) and low rates of strain, conditions characteristic of deeper crustal levels (after Allaby 2013). In Swedish bedrock, such deformation typically represent the outcome of the oldest geological events and act as guides to subsequent deformation by various reactivation processes (Saintot et al. 2011). The structures formed during ductile deformation include folds and shear zones as exemplified in Figure 1-3 and Figure 1-4, respectively.

Semi-ductile deformation, also referred to as "semi-brittle deformation", occurs in the so-called **brittle-ductile transition zone** (Figure 1-5) which is located at a depth of about 15 km (12–18 km) in the continental crust. The brittle strength of rock is increased by confining pressure (depth) whereas its ductile strength decreases with increasing temperature (depth). The transition zone is defined as the depth interval in the crust where the downwards increasing brittle strength equals the upwards increasing ductile strength (Duba et al. 1990). Typically, rocks deformed in the transition zone, now exposed in outcrops or drill cores, consist of cataclasites (Figure 1-6) and microbreccias often with inclusions of older mylonite. At the base of the crust, the rock type changes to peridotite, a rock rich in olivine which is stronger than most minerals that make up the crust, and, therefore, the upper part of the mantle is again strong. However, just as in the crust, the effects of increasing temperature dominate and at a depth of about 40 km the brittle-ductile transition zone in the mantle occurs below which rocks behave in an increasingly ductile manner.

Brittle deformation occurs when competent (stiff) rocks lose their internal cohesion along certain surfaces when the elastic limit is exceeded under applied stress. Brittle deformation results in fractures and is common in the upper crustal regions (Figure 1-5) where temperatures and pressures are relatively low (after Allaby 2013).

Figure 1-3. Ductile deformation in the ductile high-strain belt north–east of the Forsmark tectonic lens. Left: Folding with S-asymmetry of a thin band of fine-grained felsic rock in amphibolite. Right: Highly-strained folds dominated by a S-asymmetry (from Stephens 2010).
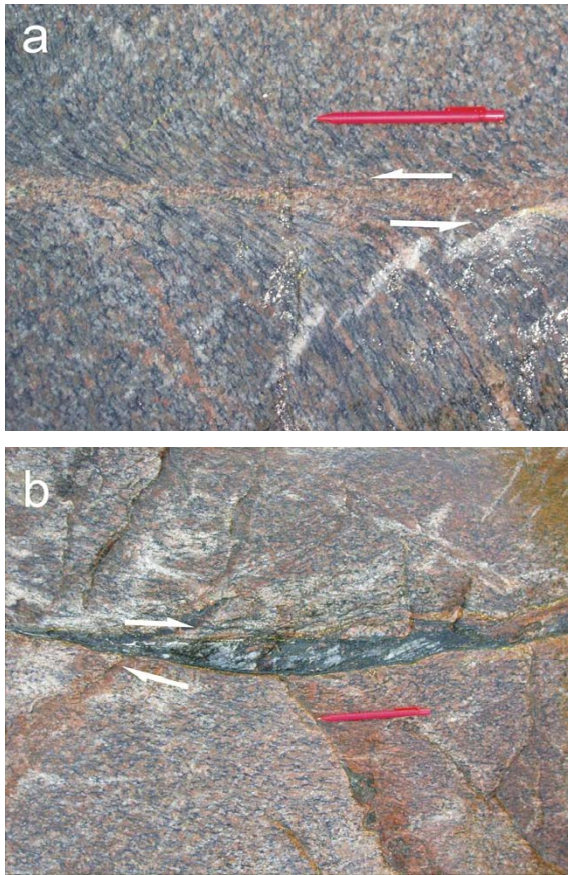
Figure 1-4. *Figure (a) shows a localised, ductile and sinistral shear zone in medium-grained metagranite, and (b) shows a well-defined section of a semi-ductile deformation zone; N.B. the internal foliation planes, indicating a dextral movement. Length of the pencil shown is 14 cm (from Forssberg et al. 2007).*
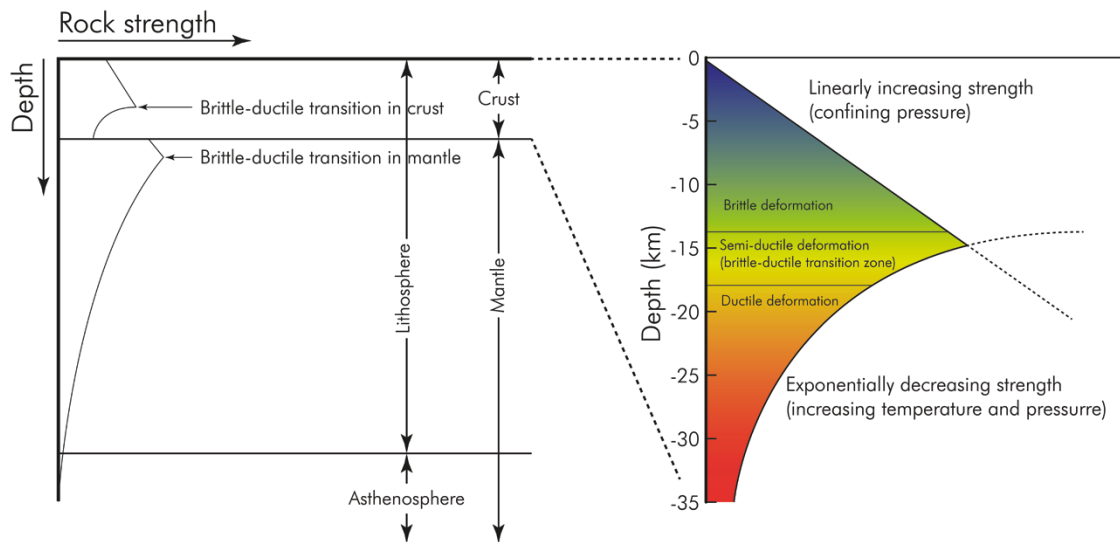
Figure 1-5. *Illustration of various deformation regimes. The rock strengths vary with depth as function of temperature and confining pressure.*
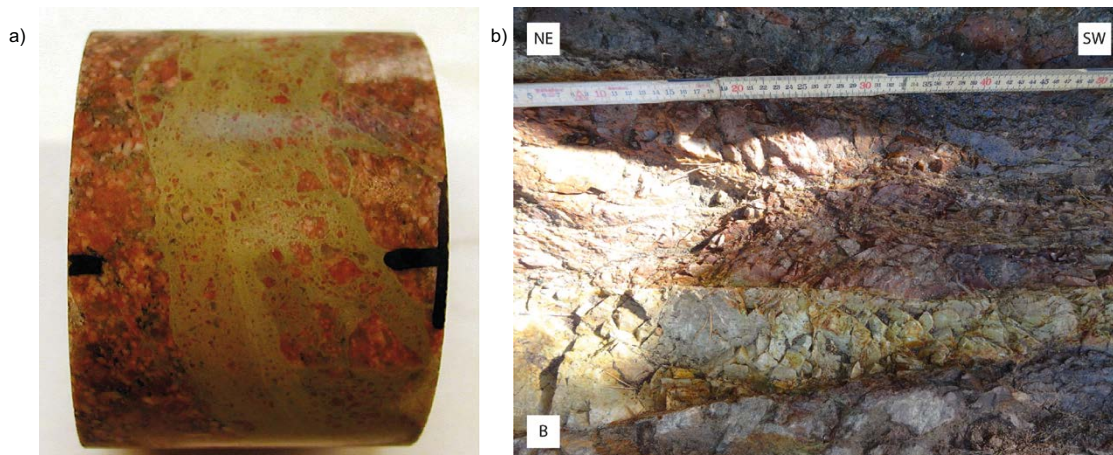
Figure 1-6. *a) Epidote sealed cataclasite from drill core KFM06A (core length 268.77–268.82 m), Forsmark. The diameter of the drill core is c 5 cm (from Sandström and Tullborg 2005). b) Cataclasite in the core of the Äspö shear zone near the Äspö HRL (from Grigull and Luth 2018).*

The **deformation history** for an area is an interpreted reconstruction of the origin and evolutionary history of strain in the rocks, to understand the evolution of the stress field through time, that resulted in the observed strain and geologic structures. Deformation history is usually described as a sequence of deformation phases, relating to time periods during which structures deformed within a region, with a common expression that can be linked to a particular stress or strain field or kinematic pattern. The timing of geological events, by relative or absolute dating of rocks and fracture minerals (Tullborg et al. 2001), combined with study of kinematics (Nordgulen and Saintot 2006, 2008, Stephens and Simeonov 2006, Saintot and Nordgulen 2007), by which we mean the study of the movements along structures or within the surrounding rock mass, constitute key input (Munier 1993, Viola et al. 2009, 2011, Saintot et al. 2011). Figure 1-7 shows how a portion of the deformation history of the rocks in Forsmark can be unveiled by kinematic analysis of outcrop-scale structures.
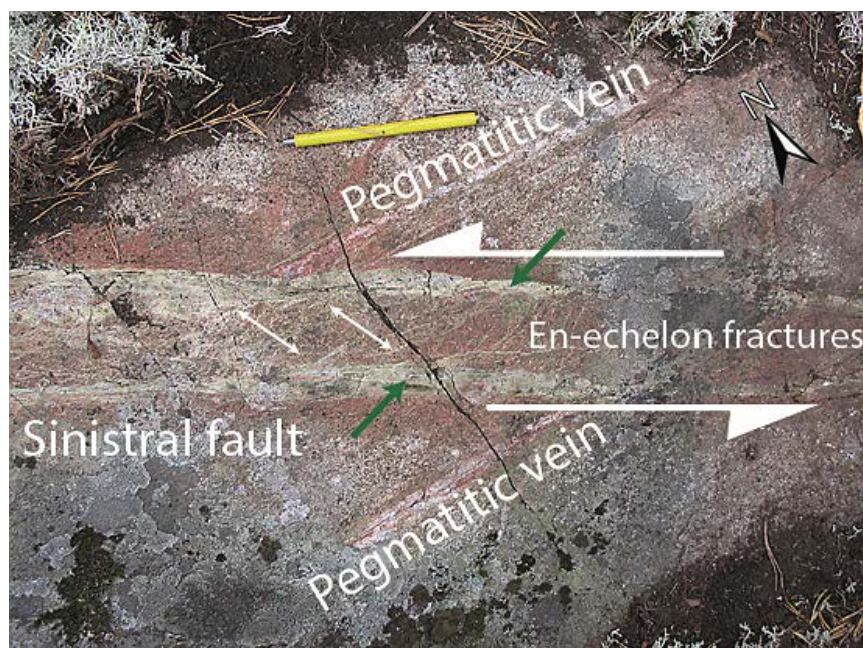
Figure 1-7. *Photograph from outcrop PFM007088 at Forsmark showing epidote-filled faults in reddish metagranite. Kinematic interpretation indicates sinistral movement along the NNW–SSE fault indicated by (1) sinistral offset of a feldspar-rich pegmatitic vein and (2) en-echelon distribution of NW–SE tension fractures within the fault (indicated with green arrows). The extension direction (perpendicular to the tension fractures) is indicated by small white arrows (from Nordgulen and Saintot 2006).*

The relations between types of rock deformation and the terms used in this report to refer to the resulting geological structures are sketched in Figure 1-8. The term **deformation zone** thus designates a structure in which deformation has been **localised** (concentrated) or is being localised, in the case of active faults. Deformation zones can be further qualified as **brittle-**, **ductile-** or **semi-ductile deformation zones**. Commonly in old continental crust, deformation zones show evidence of **brittle reactivation**, i.e., brittle deformation of rocks already deformed in a ductile or semi-ductile regime along the same zone.

The simplest expression of a brittle deformation zone is a **single fracture** (see Subsection 1.3.3), where the zone is reduced to a single discontinuity of the rock. More generally, the commonly used term **fracture zone** (see Subsection 1.3.4), in its geological meaning, can be used to denote an ensemble of fractures forming a brittle deformation zone or the brittle part of a semi-ductile deformation zone.

The commonly used term **ductile shear zone** can be used to denote a **ductile deformation zone** or the ductile part of the semi-ductile or reactivated deformation zone. For the purpose of DFN modelling, **pervasive deformation**, e.g. expressed as bedrock foliation, is of secondary importance and is therefore not expanded upon herein. The different types of deformation zones, and their relationship, considered relevant for the understanding of this report are summarised in Figure 1-8.
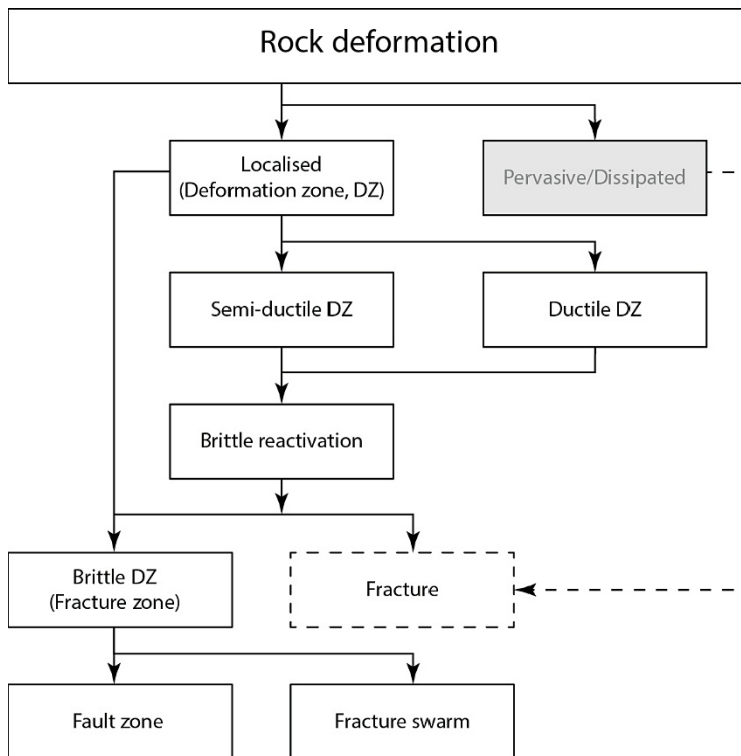
Figure 1-8. *Terminology relations relative to the geological characterization of deformation localisation.*

During the surface-based site investigations in Forsmark and Simpevarp-Laxemar, significant brittle deformation zones were identified throughout the site and ranked into three categories according to their presumed extent (from largest to smallest below):

- **Regional deformation zones** for zones with extents exceeding tens of kilometres, e.g. the Singö deformation zone at Forsmark, typically with widths of tens of meters.

- **Local deformation zones** with extensions typically in the size range 1–10 km, typically with width of several meters.

- **Minor deformation zones** (MDZ), with estimated extents typically in the order 100–1 000 m and with width generally less than one meter.

1.3.3 Fractures

A geological **fracture** is an essentially two-dimensional structure, i.e., a sub-planar structure with a small thickness relative to its lateral extent, that divide the bedrock into blocks and forms as a result of external (e.g. tectonic) or internal (e.g. thermal- or residual) stress.

Fractures can be further subcategorised into **shear fractures** (faults) and opening or **tension fractures** (joints) which reflects the **mode** (Figure 1-9) of deformation, steered by the combination of past and current stress state. Relevant terms, and their relationship, are summarised in Figure 1-10. The term "fracture" thus constitutes the highest level of abstraction and hence is always correct to use whereas terms such as "joint", "fault" requires that additional information about formation, kinematics etc can be positively demonstrated.

Tension fractures (Mode I, Figure 1-9a) have at some stage of their lifecycle experienced a displacement perpendicular to the fracture walls which may have enabled precipitation of minerals on the fracture surface. **Mineralised fractures** are sometimes referred to as **veins** and, if filled with igneous material, **dykes**. **Sheet joints** (also referred to as "sheeting joints" or "exfoliation joints") are a special kind of tension fracture that occur near the ground surface and develop parallel to the upper rock surface (Gilbert 1904, Martel 2006, Hencher et al. 2011). In Forsmark (Figure 1-11), such sheet joints are extensive and, due to locally extremely high transmissivities, they to a very large degree control the near-surface bedrock hydrology. Typically, these sheet joints are filled with unconsolidated, glacial sediments and can attain widths of tens of centimetres.

a)   b)   c)

Mode I   Mode II   Mode III
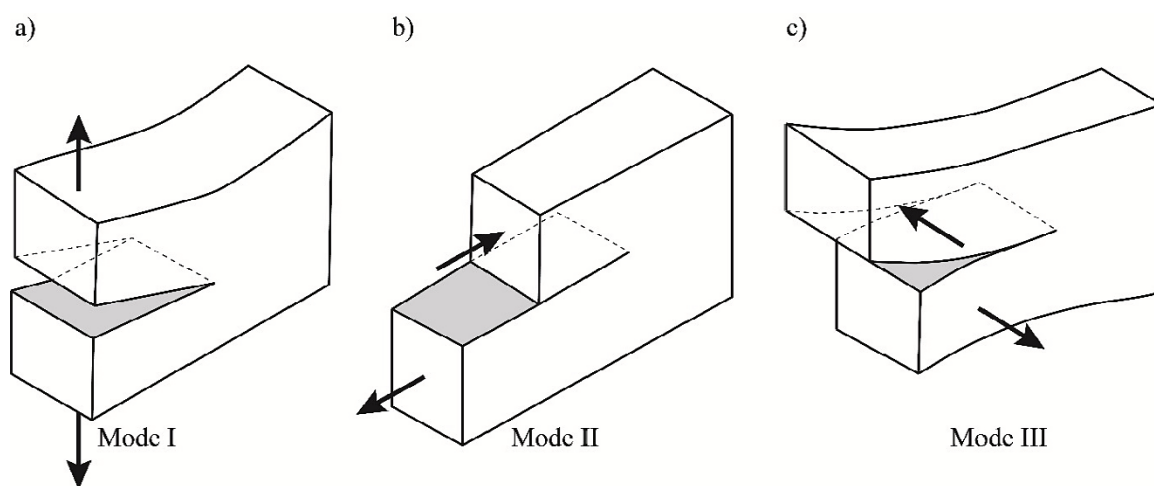
Figure 1-9. *Schematic illustration of the fundamental modes of fractures. Figure a) shows Mode I, tensile or opening mode, b) Mode II, in-plane shear or sliding mode and c) Mode III, anti-plane shear or tearing mode (reworked from Paris and Sih 1965).*
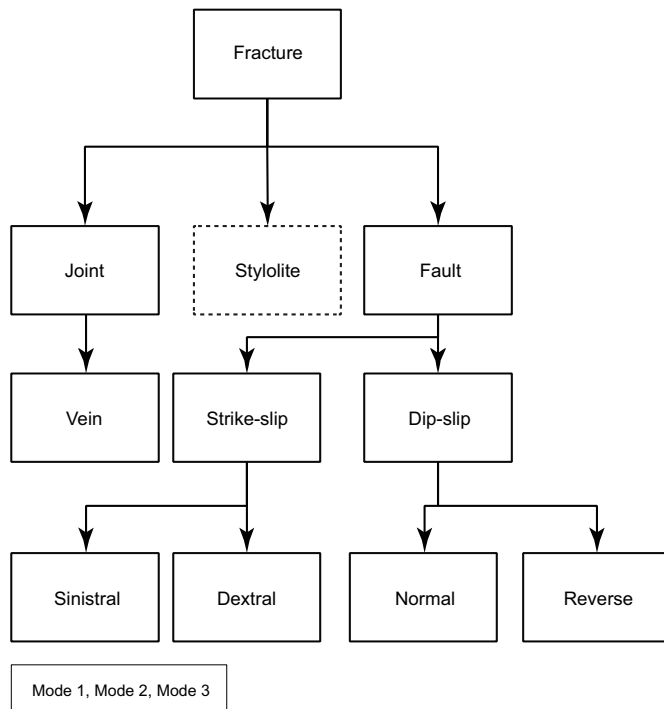
Figure 1-10. *Hierarchical relation between terms related to the geological fractures which are represented in DFN modelling. Terms such as "crack", "fissure" etc, common in the literature, should be avoided to avoid ambiguity.*

Figure 1-11. *Picture from the construction of the 13 m deep and more than 1 km long canal between the Baltic Sea and the nuclear power reactors at Forsmark. Horizontal sheet joints are encountered along the entire excavation. The sheet joints follow the undulations of the bedrock surface (Photo: G. Hansson).*

Based on a property, or a number of properties, geological fractures may be grouped into so called "**fracture sets**". Traditionally, the term "set" has been used almost exclusively for categorising fractures according to their orientation, e.g. "NW set", "sub-horizontal set" by identification of cluster maxima on (contoured) stereonets. For instance, the Q-system for rock mass classification (Barton et al. 1974) utilises a parameter J_n (joint number) which stands for the number of "Joint sets" (Barton's terminology). Though less common, sets can be equally used for grouping fractures according to genesis (e.g. "Precambrian set"), mineralogy (e.g. "epidote-quartz set") or kinematics (e.g. "sinistral set"). Nevertheless, unless otherwise stated, orientation is the presupposed parameter when using the term "set" within this report to ensure compatibility with established nomenclature in geology and rock engineering.

In addition to the geological and geometrical description of the fractures and of the fracture pattern, properties of individual fractures are also required to subsequently determine the flow, mechanical and transport processes in the fractured rock mass. Most of these physical properties are likely to vary throughout the fracture planes, thus raising the DFN modelling aspect of fracture in-plane heterogeneity (see Sections 6.7 and 8.1). For instance, the fracture aperture, which is the perpendicular width between the intact wall rock, can be measured on a certain scale (core) and location (see Section 6.7 and Chapter 7). But this simple "point" measurement may not capture the hydraulic or mechanical behaviour of the fracture when considered over its full surface due to the reality of fracture wall roughness (e.g. Brown and Scholz 1985, Brown 1987, Power and Tullis 1991, Renard et al. 2006, Stigsson and Mas Ivars 2018), degree of mineral or gouge infill, shear, degree of matedness and many other factors controlling the aperture, its variability and how it responds to stress changes. The aperture, therefore, can vary considerably across the fracture and is, consequently, both difficult to measure and quantify. Mechanical aperture is measured as the mean aperture over a rock sample, while measurement of transport aperture also represents an effective average over a scale determined by the experiment of e.g. tracer test or resin/grout injection. From all practical purposes related to flow modelling, the concept of aperture is used qualitatively to infer whether or not a fracture may contain voids and if connected, participate in the hydraulically active fracture network, in which case the notion of hydraulic aperture can be useful in describing flow magnitudes (see Sections 6.7 and 8.1).

For that purpose, the characterisation of fractures in drill cores and borehole imagery during SKB surface based site investigations, classified fracture aperture into three classes: **Open**, **Sealed** and **Partly Open** (see Figure 1-12, Figure 1-13 and Figure 1-14 for examples). This terminology and its application is defined in one of the SKB standard guides ("*SKB MD 143.006 Metodbeskrivning för Boremap-kartering*") which are internal documents accessible upon request. It should be noted, however, that the fracture is intersected in a very small portion in relation to its lateral extent and the mapping of e.g. apertures using core and borehole imagery may not reflect a representative value or situation, due to the in-plane heterogeneity (Figure 1-15). Similarly, different generations of mineralisations may be unevenly distributed on the fracture plane due to aperture variations over time. A borehole sample through such a fracture will record different mineral coatings depending on where the borehole intersects the fracture.

Figure 1-12. *Epidote sealed fracture cut by a sealed fracture filled with hematite stained adularia. KFM05A 692.00–692.15 m. The diameter of the drill core is c 5 cm.*

Figure 1-13. *Open fracture coated with a thin coating of euhedral quartz together with calcite and clay minerals. Hardened asphaltite droplets are found on this coating. KFM06B 90.60–90.85 m. The diameter of the drill core is c 5 cm.*

Figure 1-14. *Partly open fracture with a mixture of euhedral calcite, small euhedral quartz crystals, asphaltite and small pyrite crystals. The diameter of the drill core is c 5 cm.*
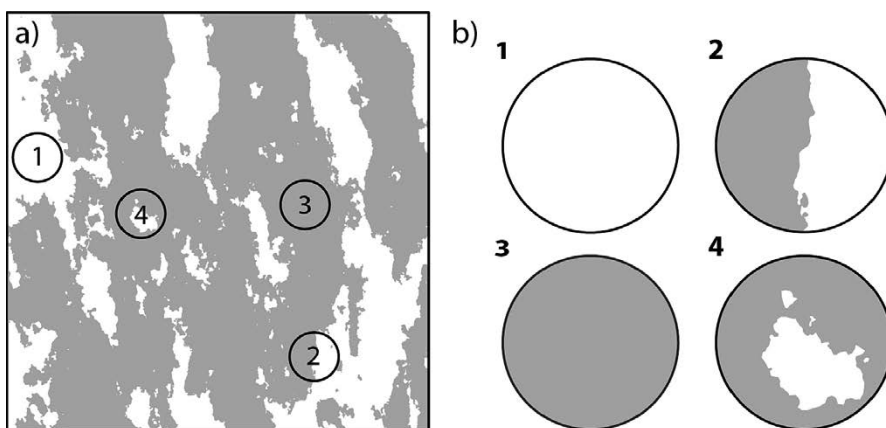
Figure 1-15. *a) conceptual view of an in-plane spatial distribution of open (white zones) and sealed (grey zones) portions on a hypothetical fracture plane. b) Resulting apparent filling as intercepted by a core log (black circles), where the fracture in core log 1 would be open, 3 as sealed and 2 and 4 as partly open.*
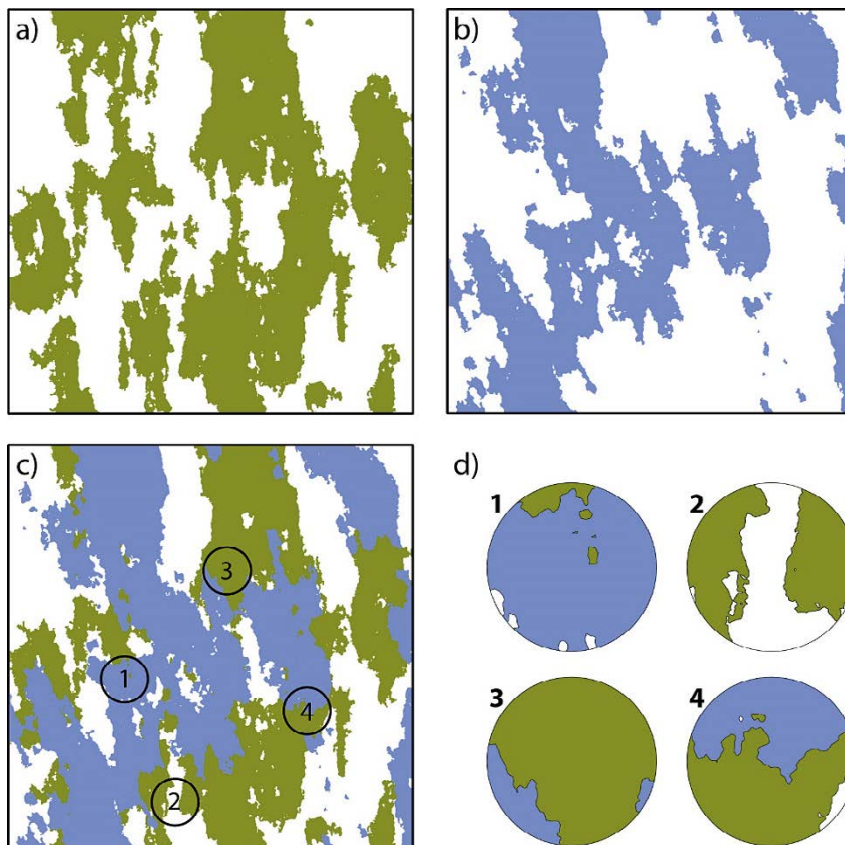
Figure 1-16. a) and b) shows a conceptual view of an in-plane spatial distribution of different mineralisations on a hypothetical fracture plane. The relative frequency of minerals sampled from drill cores (d) will depend on where the borehole intersects the fracture plane, (c). Accordingly, the same fracture can, during core mapping, be classified as either joint or vein and either open or sealed depending on where the borehole happens to intersect the fracture.

1.3.4 Fracture zones

Fracture zones constitute a subclass of brittle deformation zones (Figure 1-8). The simplest form of fracture zone is constituted of subparallel, fractures appearing as a **fracture swarm (**Figure 1-17).

Close inspection of more mature fracture zones (Figure 1-18), however, reveal a complex network of interplaying structures with different impact on e.g. flow and mechanical stability. Typically, the deformation zone contains one or several **cores**, within which accumulated strains have been concentrated over millions or several hundred million years. The core often contains **fault rock** (e.g. breccia, cataclasite, gouge) formed by the comminution of the rock and associated alteration, though we note the absence of mapped fault gouge at Forsmark. Slip surfaces may display **shear striae** that reveal the (latest) direction of shear. The degree of comminution and fragmentation decrease outwards from the core, where cataclasites and breccias may be found (Caine et al. 1996).

Deformation zones grow during each reactivation episode both in area, by propagation of the tip through the rock, and by thickening. This growth (Cowie 1992, Cowie and Scholz 1992b) takes place in the so called **damage zone** (Kim et al. 2004, Kim and Sanderson 2005, Choi et al. 2012, 2016), a volume of rock with increased fracturing and alteration surrounding the core(s) of the deformation zone, which can be regarded as the large-scale equivalent of the **process zone** (Vermilye and Scholz 1998), i.e., the volume of rock that develops microfractures to allow propagation of the macroscopic fracture plane. The damage zone may often be asymmetric around the more deformed parts of the deformation zone (see e.g. Winberg et al. 2013 for example). At SKB, the thickness of deformation zones, as used in the Site Descriptive Models, includes the thickness of the damage zone (see also Chapter 5) which is essentially estimated by the fracture intensity or fairly well established correlations between length of faults and their damage zone (Scholz et al. 1993, Schultz and Fossen 2002, Faulkner et al. 2011, Choi et al. 2016, Callahan et al. 2019).
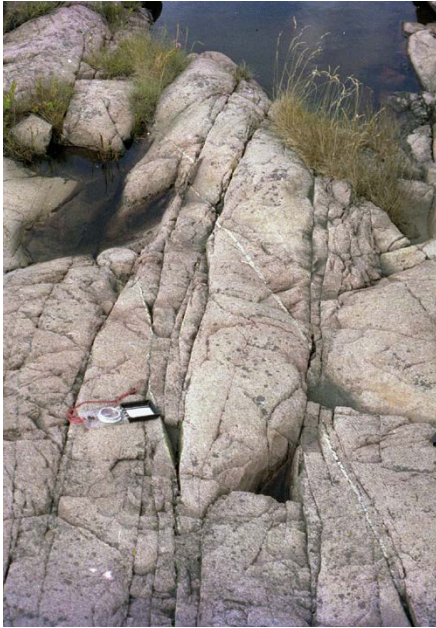
Figure 1-17. *Fracture swarm, or fault swarm as evidenced by offset quartz veins, at Kråkelund, SE Sweden (Photo, R. Munier).*
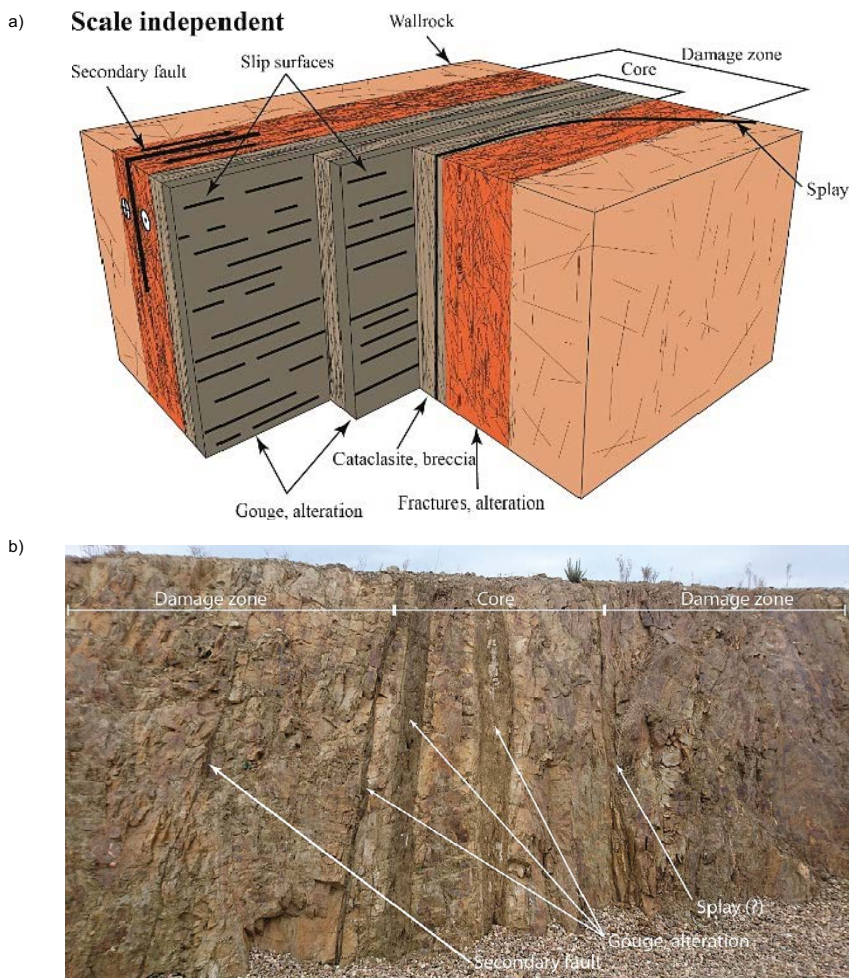
Figure 1-18. *a) Idealised deformation zone with its typical constituent features. b) Cross section (the face is ca 3 m high) through a deformation zone (El Cabril, Spain) displaying multiple cores, splays, and damage zones (photo: R. Munier).*

1.3.5 Current SDM modelling concepts

All the fractures (sealed, open and partly open), fracture zones and brittle deformation zones of the target volume, are potentially represented in the DFN model incorporated into any given SDM. The challenge of the DFN modelling is to determine how the model should be divided into sub-volumes (domains), delimited by deformation zones and/or lithological boundaries, within which fracture idealisations are created according to a specified concept or recipe. It is also a challenge to decide whether or not deformation zones should be included in the DFN conceptualisation and whether to represent them as single features or as zones populated with fractures.

These aspects are developed throughout the next chapters of the Part 1 of the DFN methodology, while considering all the geological, geometrical, mechanical, flow and transport aspects. Here the main concepts and used terms are only briefly introduced. They reflect the best knowledge of the DFN methodology at the time being and are open to improvement in the future.

Former investigations and modelling efforts at the Forsmark site, up to and including SDM v.2.2 (Stephens et al. 2007), defined two types of major conceptual domains: the **Deformation Zone** (DZ) and the **Fracture Domain** (FD) as the primary divisions of the target volume. Assuming that all the regional- and local-scale deformation zones of the site can be identified during the investigations, their dimensions (location, extent, thickness, orientation/geometry) are known and thus are modelled deterministically, as DZs, in the SDM. They are modelled as tabular volumes, where the thickness of the zone is much smaller than its lateral extents.

All the remaining volumes outside the Deformation Zones are set as Fracture Domains. The latter are defined as rock volumes between Deformation Zones where fracture statistics are distinct from adjacent domains (Munier and Hermanson 2001, Munier et al. 2003, Olofsson et al. 2007, Darcel et al. 2012, 2013, Stephens et al. 2015). The definition of fracture domains is predominantly based on fracture network geometry: Adding hydraulic and mechanical properties to Fracture Domain descriptions gives them value for conceptual models of the site hydraulic behaviour and rock mechanical response to construction (see Chapters 7 and 8).

In practice, the envelopes which define the spatial boundaries of the DZ and FD domains are **deterministic**, that is, they are fixed. Then, in each domain, a DFN model is potentially defined, which reflects the fracture pattern and the fracture statistics in the given domain. The components of a DFN model (as briefly listed in the introduction) encompass all the fracture geometrical and physical properties (e.g. transmissivity for flow computation, shear and normal stiffness for analysis of elastic deformation, etc) necessary to perform flow and mechanical numerical simulations based on the generated DFN. These DFN models are defined in a statistical sense: Only the statistical distributions and the spatial correlation rules are defined, but the generation process itself, which takes the model parameters to generate a DFN realization, is **stochastic**: As in any stochastic process, changing the generation seed to create the fracture network results in a different, equiprobable, realization of the fracture network.

In between the stochastic and deterministic representation, a large number of fractures may be **semi-stochastically** modelled, i.e., when only some of their properties are known locally and deterministically while others are not (e.g. the trace of a fracture on a tunnel wall defines the position of a fracture whose extent is not known). In general, if no fractures are conditioned locally to observations, predictions of quantities such as fractures in deposition tunnels, flow around deposition holes, groundwater pathways and shear failure are made purely by stochastic simulation, with potentially different outcomes at each location between realisations. Conditioning of fractures to known intercepts provides a means of honouring observations, in terms of location, orientation and flow, while still maintaining stochasticity in terms of centre, size and shape. This adds a conditioning element to the DFN model, **semi-stochastic** (or semi-deterministic, both terms are interchangeable) fractures in addition to purely stochastic fractures or purely deterministic structures in the model. The amount of semi-stochastic elements will increase progressively when new information will be available during construction and operation.

The spatial boundaries of the domains, together with the concepts and parameters of the statistical DFN models, constitute the basis of the SDM for DFN applications. They may evolve in the future thanks to addition of new data (each version of the SDM is linked to a database identified by a data freeze reference), to new interpretations methods and to new knowledge relative to modelling naturally fractured systems. In that perspective, there is an ongoing incentive to:

- Improve the realism of the stochastically generated DFN in the DZ (fault zones) and in the FD, in particular with the intention to, as far as possible, mimic the growth of fracture networks; and,

- update and refine the definitions and properties of structures especially Minor Deformation Zones, which fractures as may initially be stochastic, but become semi-stochastic or deterministic with the acquisition of more data from boreholes, tunnels, and deposition holes. These refinements may include either upscaling a Deformation Zone to be a single fracture in the DFN model with equivalent hydraulic properties or refining a Deformation Zone to include fracture damage zones and other features internal to the zone. The representations of specific Deformation Zones as single fractures or zones of multiple fractures will depend on their locations relative to deposition locations and their effects on the Safety Assessment.

1.3.6   Critical Structures and Volumes

The terms **critical structure** and **critical volume** refer to geological structures or fracture domains whose behaviours may impact the repository's ability to perform safely after closure. The notion of "critical" refers to a) susceptibility to shear in conjunction with an earthquake, b) mechanical stability of the structure in an underground opening (Munier and Mattila 2015), and c) importance for groundwater flow and/or retention due to the structure's properties and location.

Critical structures and volumes are categorised into three classes with respect to their impact upon the repository layout (Munier and Mattila 2015). Class 1 contain structures (CS1) or volumes (CV1) with properties such that they cannot be accepted within the repository footprint. Such structures (e.g. Forsmark DZ, Singö DZ) have steered the current positioning of the planned repository and define the outer boundaries of the repository volume. Class 2 structures or volumes, CS2 and CV2 respectively, have properties such that they can be accepted between deposition areas but not within a deposition tunnel and, consequently, steer the repository layout. Class 3 structures and volumes (CS3/CV3) have properties such that they are not allowed to intersect deposition holes. Thus, CS3/CV3 structures steer the location of canisters and the degree of utilisation of the repository.

The methodology for the analysis of earthquake impact upon a KBS-3 repository (Fälth 2018) has been evolving ever since it was first implemented in SR-Can and subsequently in SR-Site (Munier 2010, SKB 2010b, 2011a). The recent estimates indicate that the radii of critical structures (CS3/CV3), beyond which they can impose a threat for long term safety of canister, exceed 100 m. With such an extent, these structures are most probably not individual fracture planes but rather small deformation zones. Studies at Olkiluoto (Nordbäck and Mattila 2018) indeed indicate that individual fracture planes reach roughly a maximum radius of 50–100 m before they link to networks and form deformation zones, with the notable exception of some sheet joints.
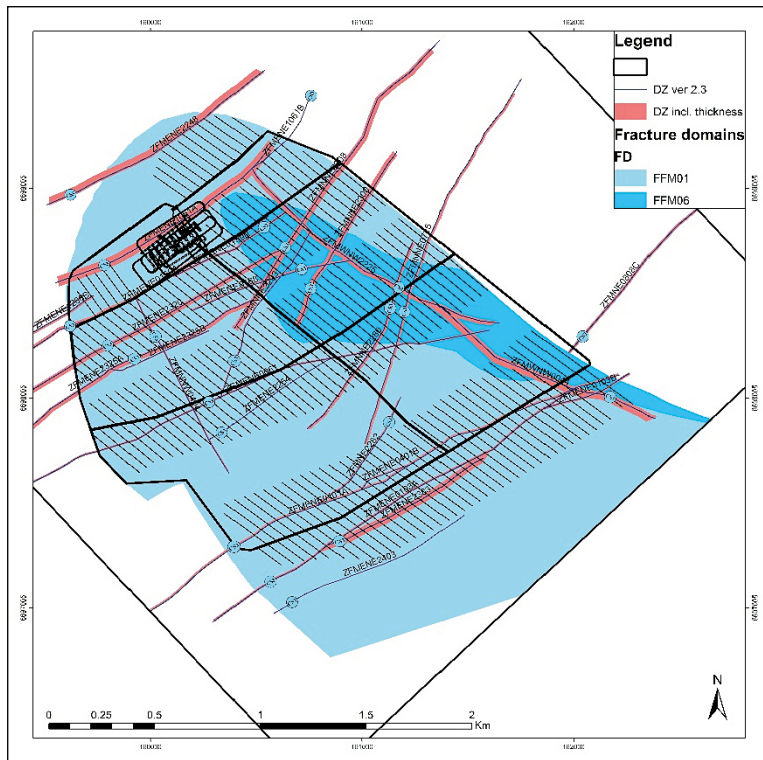
Figure 1-19. CS-classification of deformation zones and large fractures at Forsmark, section at −470 m (see Munier and Mattila 2015 for methodology).

1.4 Relationships between modelling concepts for fractured rock

The DFN concept provides a framework for integrating the various structural, hydrogeological, mechanical and transport characteristics of the bedrock into a unified fracture-network framework. The first step of DFN modelling is developing a conceptual model of the natural fracture system (Figure 1-20) based on both geologic and stochastic information on the site, including deterministic Deformation Zones.

The next step, in the DFN methodology workflow, is to build numerical and synthetic model(s) of the site (cycle "medium model" in Figure 1-20), as a basis for performing the numerical simulations to evaluate the model, to make predictions followed by comparison with measured outcome in situ, and to perform risk assessment evaluations. The computation capacity and the target application steer the type of medium model, fractured medium, equivalent continuous porous medium (ECPM, Figure 1-21) or equivalent channel network. As well as illustrating how a fracture system a) is converted to mesh-based permeability tensors c) and d), the difference between c) and d) shows the strong anisotropy that can occur, with higher horizontal permeability due to dominance of sub-horizontal fracturing and stress effects. The difference between Figure 1-21 b) and c) demonstrates how permeability based on flow simulation c) tends to give lower permeability than when estimated from the geometry and transmissivity b) without accounting for connectivity and low transmissivity bottlenecks in the fracture system. These aspects are further developed in the Part 2 of the DFN methodology and are only briefly introduced here, as they are not critical to how a DFN is constructed, rather they are alternative ways of representing an underlying DFN as a quantitative description of the fracture system.

For most applications related to safety assessments, exhaustive DFN-based numerical simulations require model dimensions and a range of fracture sizes largely beyond available computational resources. For example, radionuclide migration through a fracture network, from a canister position to the biosphere, may require the full range of fracture sizes from millimetre to metre resolution close to canister and up to site scale structures to model transport paths to the surface and the biosphere.
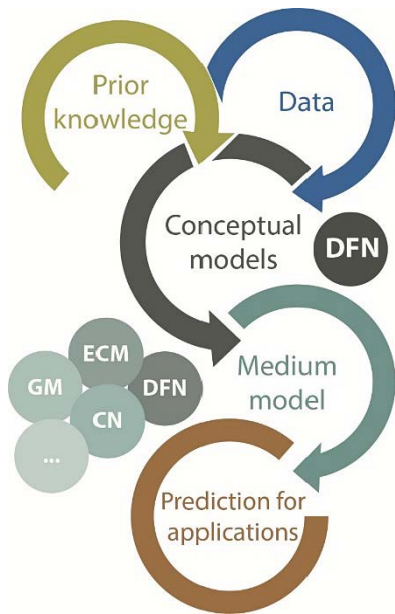
Figure 1-20. *DFN methodology workflow from prior knowledge and data to predictions for applications. Modified from Figure 1 in Davy et al. (2018b).*
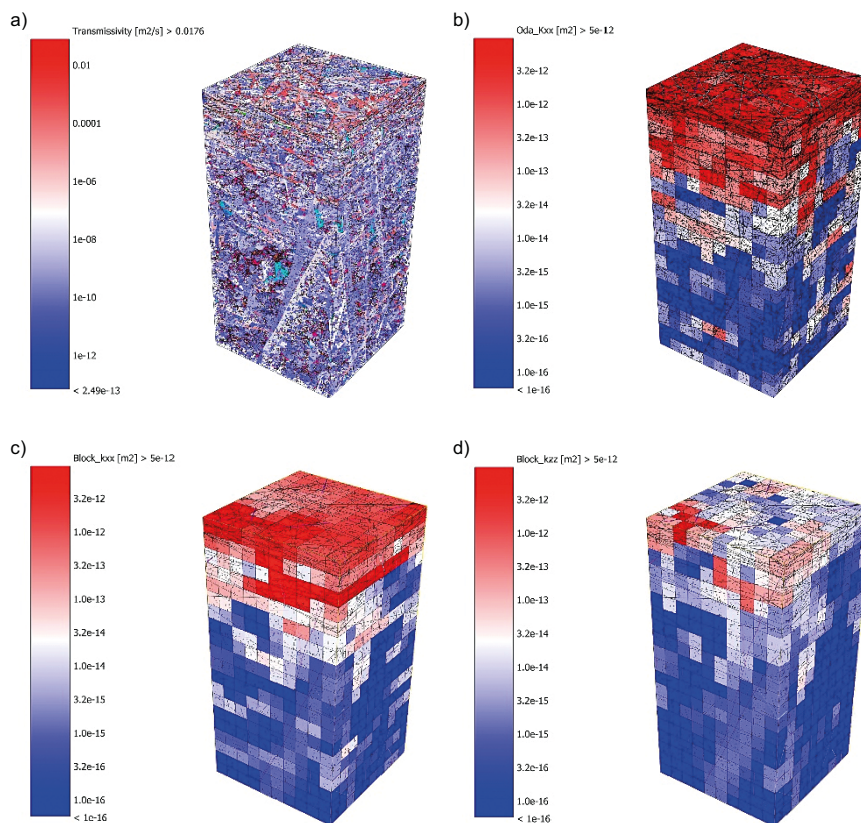
Figure 1-21. *Example of equivalent continuous porous medium representation of a DFN model. a) The DFN model for a 200 m × 200 m × 400 m block with sub-horizontal sheet joints in the near surface and a depth trend of reducing transmissivity with depth. b) shows the result of a basic geometric-based estimate of x-permeability. c) shows the results of a flux-based upscaling method to give more equivalent permeability in the x-direction (E–W) and d) the vertical permeability.*

1.4.1 Parameter reduction and effective properties

The concept of property **upscaling** is commonly used to overcome the computational burden. The purpose of upscaling is simple, it consists of replacing a relatively high-resolution complexity by a coarser, less heterogeneous but assumed equivalent, representation. Upscaling thus defines a meso-scale (e.g. a grid voxel size at which properties are inferred) description of the medium, where heterogeneities smaller than the meso scale are lumped into effective parameters (e.g. DFN density, flow intensity, rock mass mechanical effective properties), which are further used to calculate the macroscale (target scale of the modelling, e.g. volume between repository and surface, or volume around a tunnel, etc) medium behaviour. A key point is that upscaled properties are always defined relative to a particular chosen scale, and their statistics vary with scale because fractures exist in many different scales and fracture properties are often correlated to their scale. The particular approach to upscaling has to be adapted to its purpose considering the underlying processes taking place within the discrete system when attempting to capture them in the continuous system. Upscaling methods may be analytical (Oda 1985, Svensson 2001a, Sævik and Nixon 2017), numerical (Durlofsky 1991, Wen and Gómez-Hernández 1996, Jackson et al. 2000) or a mix of the two. Also, **hybrid ECPM/DFN** models may be considered. These use several model volumes with different resolution and type of medium. Typically, a fine-scale DFN is used in the innermost volume (e.g. repository near field), with a restriction to larger scale fractures or an upscaled ECPM further out. The principle of upscaling is present in most of the medium models (Figure 1-20), as reviewed below.

The most direct conceptual representation of a fractured rock is a *3D* network of meshed *2D* fractures with assigned properties. In that option, the role played by intact rock in between fractures, on the physical process, is neglected and no simplifications are required of the DFN representation. This approach can be selected to perform flow and transport analyses (Selroos et al. 2002, Joyce et al. 2010, Hartley et al. 2013b) or to simulate stress distributions in the medium (Kachanov 1985), as long as the model dimensions are not too computationally demanding. It is in practice limited to specific applications, when the role played by the intact rock is negligible and typically limited to tunnel-scale and facility-scale models.

In addition to direct DFN simulation, three main modelling approaches have been used so far at SKB: *i*) equivalent continuous porous medium methods (noted CPM or ECPM, see below) where both the fractures and rock are modelled as one single equivalent and continuous medium, *ii*) coupled continuous and discrete medium (e.g. Discrete Element Method for rock mechanical modelling, which combine rock blocks and fractures, see below), *iii*) equivalent *1D* channel networks (CN, see below). The properties of these medium models are largely built from the conceptual DFN properties.

The ECPM concept provides a classical representation of groundwater flow (pressure) or stress and strain fields assuming continuity of variables in three dimensions. The properties of the medium represent those of the **rock mass** combining fractures and intervening intact rock. For flow in crystalline rock, the rock mass hydraulics are dominated by the fractures, but mechanics consider both components. The physical properties of the medium (hydraulic conductivity, Young's modulus etc) are expressed as volumetric scalar or tensorial values. A step of upscaling, between the DFN representation and the *3D* equivalent medium is necessary to define the medium properties. There are many ways to do the upscaling.

For rock mechanical applications, the well-known Rock Mass Classification Systems are widely used for standard geotechnical applications. The most widely used are the Rock Quality Designation index (RQD, (Deere et al. 1966)), Rock Mass Quality as measured by the Geological Strength Index (GSI) value, the RMR (Rock Mass Rating) (Bieniawski 1989) or the tunnelling quality index Q (Barton et al. 1974). The limits of these approaches have been recently pointed out (Hoek et al. 2013). They rely on an overly simplified representation of the fracture system, directly deduced from *1D* observations (geotechnical core logging or cell mapping). The conceptualisation of the DFN is there reduced to an indicative number of fracture sets, the fracture frequency and some additional qualitative estimates of the fracture condition (Palmström 2005). These properties neglect the step of true DFN conceptualization and provide a direct empirical upscaling for rock mechanical properties. As of the modelling Stage 2.2 at Forsmark (e.g. Fox et al. 2007b, Stephens et al. 2007, Stephens and Skagius 2007), these empirical methods have been used to estimate rock mass properties alongside the theoretical methods described in the following paragraph (Glamheden et al. 2007) using the structural records from core descriptions and rock mechanical tests in the laboratory.

For computation of stress, strain and failure, Distinct Element Methods (DEM) are adapted to simultaneously model the rock blocks (as assemblies of rigid elements) and the fractures in between. The DEM allows the building of Synthetic Rock Mass specimens (Mas Ivars et al. 2011), with a certain amount of discrete fractures embedded in the synthetic rock. Also, the number of discrete features included in a simulation and the total dimension of a simulation are limited by computational capacities, DEM modelling is potentially a direct implementation of the DFN concept that gives the possibility to represent intact rock deformation and local failure. The DEM approach has been used recently to support analytical developments for rock effective properties determination from the DFN approach (Davy et al. 2018b), modelling of the site stress conditions, dynamic simulations of earthquake consequences on fracture displacements or spalling in the EDZ.

There are not universally accurate analytical or empirical methods for estimating the equivalent permeability of fractured rock masses since the inter-connectivity of a general network in *3D* space can be complex and transmissivities vary between fractures over several orders of magnitude. Several approaches attempt to define the upscaling function between the DFN and the ECPM (grid cell) hydraulic properties (Oda 1985, Svensson 2001a, Sævik and Nixon 2017). Most approaches try to formulate permeability as a function of geometrical proxies. For example, the intensity of fracture networks and size distributions of fractures have long been identified as key determinants on connectivity (Bour and Davy 1997, Renshaw 1999, Berkowitz et al. 2000). However, it has also been shown that mutual arrangement or topology of fractures also has a significant effect (Maillot et al. 2016, Sævik and Nixon 2017).

To apply an ECPPM concept, it is necessary to first develop a DFN model of the bedrock and then represent the hydraulic characteristics of each part of the fracture network on some scale, normally defined by a continuous grid that overlays the DFN model domain. The process thereby "upscales" the fracture network within each grid cell to an equivalent permeability tensor. Numerical methods for upscaling can provide a more consistent level of accuracy in representing the underlying network but is often much slower than analytical based methods. However, once a DFN is converted to an ECPM representation it has the advantage that it is relatively efficient and there is a larger range of tools for modelling a wide range of Thermo-Hydro-Mechanical-Chemical (THMC) coupled processes. Joyce et al. (2010), Svensson and Follin (2010), and Vidstrand et al. (2010) are examples of this concept being applied to Forsmark.

Analytical and numerical methods of upscaling rock mass hydraulic and mechanical properties are discussed and illustrated in Part 2 of the DFN methodology. An important note is that in most cases the equivalent properties are scale-dependent, i.e., it is rare that the rock mass (hydraulic conductivity, say) stabilises as some scale and become representative for all larger volumes. This because as soon as one considers a larger volume, there are usually new and larger structures to consider, and these tend to dominate (as hydraulic and mechanical properties tend to scale with size).

1.4.2 Channel networks

Another hydrogeological concept for modelling fracture flow is the Channel Network (CN) model that considers Darcy flow through a network of intersecting one-dimensional channels (Moreno and Neretnieks 1991, Andersson et al. 1998, Gylling et al. 1998b, Outters and Shuttle 2000, Black et al. 2007, Figueiredo et al. 2016). CN models are often represented on a regular grid using channels of discrete lengths; however, it is possible to distort the network to account for a more realistic geometric understanding of the system or make them unstructured (Dessirier et al. 2018). CN models can also be derived from DFN models, where the channels represent a simplification of the fracture network, usually representing connections through fractures between intersections. The channels in the CN approach are representative of the regions within fractures where flow-rates are highest. Field observations suggest that fracture surfaces are often uneven and mineralised, with the result that groundwater flow is distributed non-uniformly across the fracture in preferential paths, or channels. CN models are essentially a process specific alternative modelling concept appropriate to highly channelised flow systems. Such systems can also be represented within the DFN framework, for example by restricting the portion of a fracture that is open or varying transmissivity over the plane (see e.g. Figure 1-22). Both flow and solute transport processes can be evaluated with the CN approach (see Section 8.2 and Subsection 9.1.4) (e.g. Winberg et al. 2003, SKB 2010d, Poteri et al. 2014).
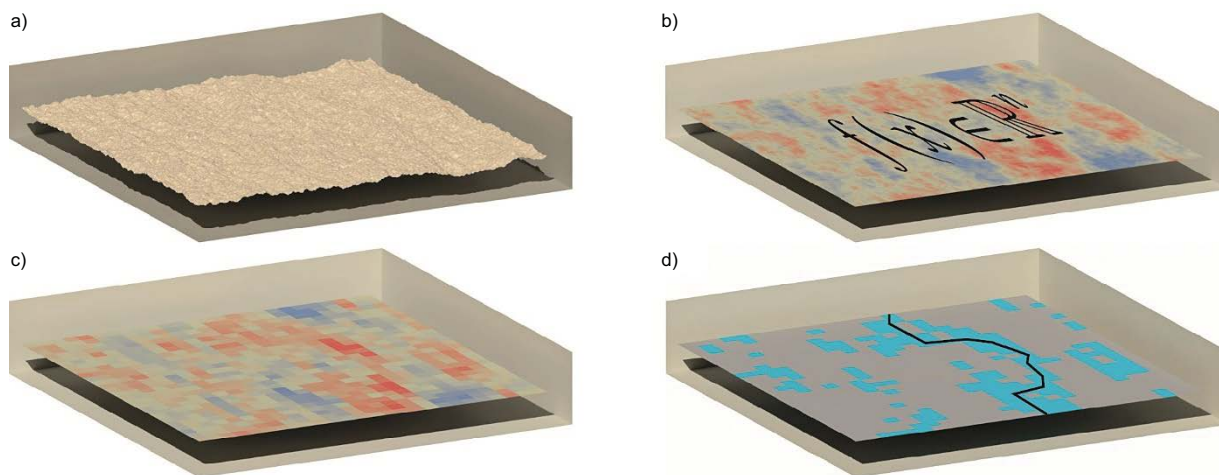
Figure 1-22. *Schematic illustration of fracture in-plane heterogeneity and flow channel concept. a) fracture one-sided roughness, b) representation of a random field, e.g. local aperture or transmissivity distribution projected onto a flat surface, c) discretisation of the random field onto a grid and d) Boolean representation of the grid in c with the main flow path overlain as a 1D channel on the 2D fracture surface.*

1.5   Report structure

Part 1 defines the conceptual frameworks and analysis techniques with which to interpret site data and formulate a site DFN model.

Chapter 1 describes the application of DFN modelling methodologies for end users in safety assessment and repository engineering. Chapters 2 and 3 provide an overview of the methodology for developing an integrated description of fracture systems, how this is formulated to make predictions of properties and processes relevant to both the operational and post-closure periods, and how model reliability is demonstrated and quantified. The geological context for fracturing and *3D* geological site models currently available is presented in Chapter 4. A hierarchical framework for describing spatial variability in fracturing is introduced in Chapter 5. The theoretical frameworks and techniques for describing fracture geometrical properties is given in Chapter 5. How DFN is applied to rock mechanical, hydraulic and transport processes is explained in Chapters 6, 7 and 8, respectively. These chapters include descriptions of the background concepts, available site data, approaches to data analysis, the numerical model and uncertainties for each of these components of the DFN. Chapter 10 outlines approaches for early screening of site models, model prediction-outcome exercises and how to quantify and improve model performance when predicting observable site conditions.

Part 2 provides detailed practical guidance and methods for numerical modelling of fracture systems, including:

*   Generating fracture network realisations,

*   simulating rock mechanics properties and stress,

*   parameter reduction and calculation of effective properties,

*   performing hydraulic calibration on multiple scales,

*   simulating solute transport, and

*   managing uncertainties.

The target group of the second volume is thus primarily modellers who are to generate DFN models of the site.

1.6   A note on modelling scales

Certain aspects of modelling require reference to **modelling scales**. A nomenclature for modelling scales to be used by SKB is available in Winberg (2017) and visualised in Figure 1-23. An approximate horizontal length scales for each scale relevant to DFN modelling is as follows:

- Regional-scale: encompassing a significant part of Northern Upland – c 40 km side;

- Local-scale: encompassing present and future surface water catchments – c 12 km side;

- Facility-scale: encompassing the repository area – c 2.5 km side;

- Facility part-scale: encompassing a repository deposition area – c 0.7 km side;

- Tunnel-scale: encompassing a deposition tunnel – c 300 m long; and

- Deposition hole-scale: encompassing a deposition hole – c 10 m deep.
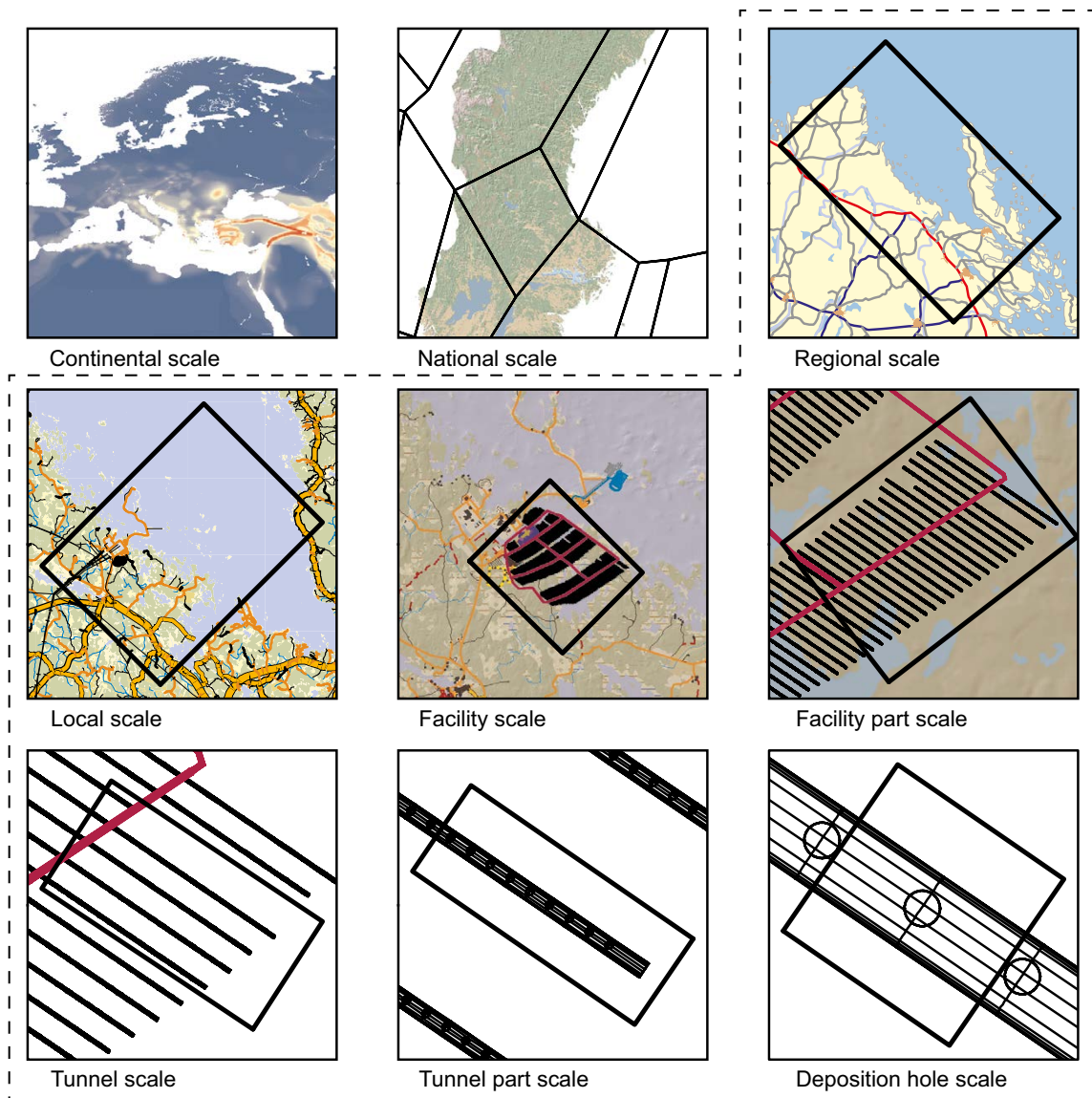
Figure 1-23. *Scales applicable to development of conceptual and descriptive models during development of repository accesses and deposition areas (from Winberg 2017).*

1.7   Acronyms used in this report

CN	Channel Network
CPM	Continuous Porous Medium
DEM	Distinct Element Method
DFN	Discrete Fracture Network
DZ	Deformation Zone
ECPM	Equivalent Continuous Porous Medium
EDZ	Excavation Damage Zone
FPI	Full Perimeter Intersection
FWS	Flow Wetted Surface
GSI	Geological Strength Index [-]
HFM	Percussion borehole at Forsmark (generally surface-based)
HRL	Hard Rock Laboratory
JRC	Joint Roughness Coefficient [-]
KFM	Cored borehole at Forsmark (generally surface-based)
K_n	Fracture normal stiffness [MPa/mm]
MASL	metres above sea level
OLA	Operational Licence Application
PFL	Posiva Flow Log
PSS	Pipe-String System (double packer injection tests)
Q	Rock mass quality designation for design and support recommendations [-]
RMR	Rock Mass Rating [-]
RQD	Rock Quality Designation
SACRe	Sensitivity Analyses, Calibration and Rejection
SAR	Safety Analysis Report
SDM	Site Descriptive Model
SPR	Single Point Resistivity
SRM	Synthetic Rock Mass
THMC	Thermal-Hydro-Mechanical-Chemical (coupled processes)
UFM	(likely) Universal Fracture Model
TRUE	Tracer Retention Understanding Experiments (performed at the Äspö HRL)

2 Applications of DFN in geological disposal

This chapter provides an overview of where DFN modelling fits within the site descriptive process, how it interfaces with other disciplines and with end users in engineering design and safety assessment. Sections 2.2 and 2.3 describe the main applications of DFN modelling for these end users. This is to provide context for the purposes of DFN models, and hence an indication of level of detail required when making predictions. The other piece of context given here is the timeline for versions of the Forsmark DFN relative to the overall programme of site description and the regulatory process, including what types of site specific data support for DFN can be expected along this timeline, see Section 2.4.

2.1 Applications and clients for Forsmark DFN models

A schematic showing the relationships and processes between a site DFN model and other discipline specific models involved in producing a site descriptive model and delivering this to clients is shown in Figure 2-1.

As indicated, site descriptive modelling involves use of the DFN in modelling design and operational decisions during repository development, such as deposition hole acceptance or rejection. The interpretation of fracture data for the DFN model feeds back into the wider Forsmark geological model on issues such as how to model the extent of deformation zones or generating deformation zones semi-stochastically in the area covered by underground openings and stochastically outside of the focused characterisation area (see Subsection 4.3.1). Other examples are DFN models providing a description of hydrogeological properties and groundwater flow to be tested against hydraulic monitoring and hydrogeochemical sampling data and DFN models providing input to modelling of rock deformability and in situ stress that feeds into understanding of rock mechanical properties and hydromechanical effects. Building the overall site descriptive model therefore involves iteration and integration of various conceptual and numerical models. DFN models provides quantitative information to the various disciplines involved in SDM (see Chapters 5 through 8). DFN models also provides numerical models and quantitative inputs to repository engineering and safety assessment. More details are given in the following sections.
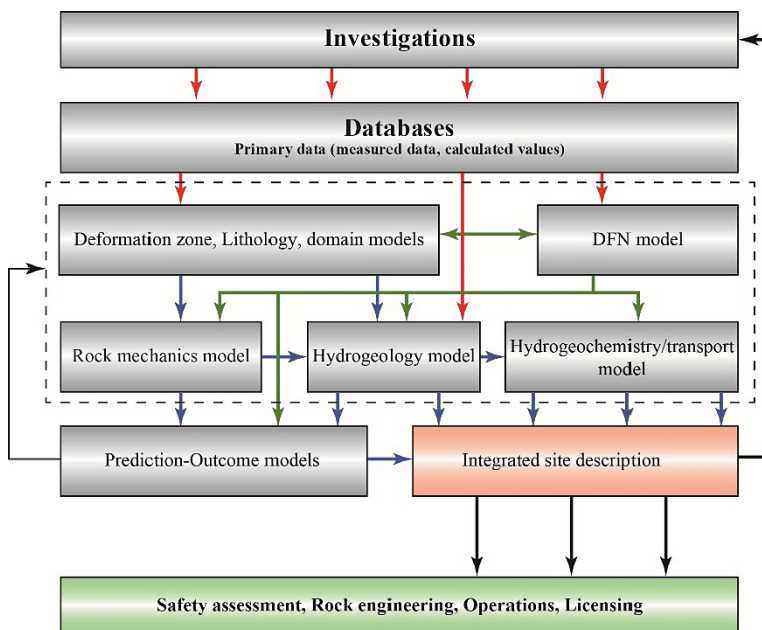
Figure 2-1. *Relationship between DFN modelling and other modelling activities in SKB's spent fuel disposal programme. The dashed line encompasses the vital components of the site descriptive modelling.*

In order to provide a holistic description of bedrock fracturing at Forsmark, the DFN model must describe a system of structures of different types and scales as sketched in Figure 2-2. Repository layout and long-term safety assessment of effects of seismicity are most concerned with deformation zones and the fractures associated with them on scales of hundreds of metres to kilometres. Assessment of rock mass mechanical properties, flow and advective transport is concerned with fractures, particularly those in the deposition areas, on the scale of decimetres to hundreds of metres. Engineering and safety assessment of near surface stability, flow and transport also must evaluate sheet joints which extend tens to hundreds of metres. On the smallest scale, micro-structures of millimetres to decimetres collectively host significant volumes of water and minerals that determine the retardation and retention of contaminants moving through the fracture system.
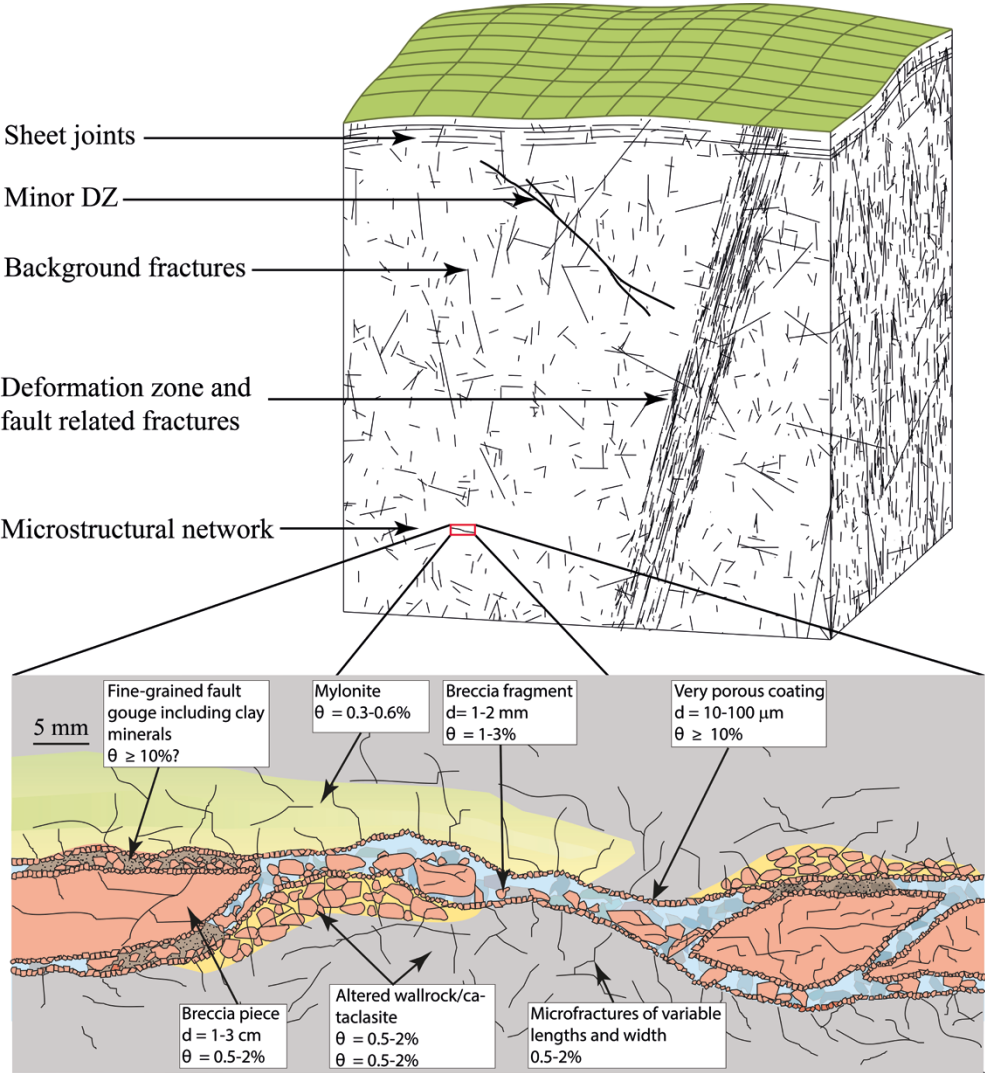
Figure 2-2. *Conceptual framework for fractures of different types and scales. The insert shows a highly magnified schematic of fractures at the microstructural scale after Winberg et al. (2003), which can be down to the scale of the micro-fissures between individual grains.*

2.2   Role of DFN in Safety Assessment

The most recent SKB safety assessment of a spent nuclear fuel repository is the SR-Site assessment (SKB 2011a). The key steps in the assessment of post-closure safety were divided into 11 main components or activities. DFN models play an integral part in four of the 11 main components (the numbering is in accordance to SKB (2011a)):

- 2a. Description of site initial state (i.e., essentially formulation of the site-descriptive model);

- 7. Definition and analyses of the reference site evolution;

- 9. Analyses of selected scenarios with respect to containment and retardation;

- 10. Additional analyses, specifically scenarios related to future human actions, and optimisation and best available technique (BAT).

Bullet 2a: A pre-requisite for assessing post-closure safety of a repository is to have an adequate site-descriptive model, SDM, of the disposal site. Since Swedish sites, and Forsmark in particular, are characterised by sparsely fractured rock, the DFN concept is an amenable representation of the fracture system.

Bullet 7: In the analyses of the reference evolution, the site characteristics are to be described for multiple glacial cycles. The evolution is typically sub-divided into different time periods such as the Construction and operation period, the Temperate period, and subsequent Permafrost and Glacial periods. That is, expected prevailing geological, hydrogeological, hydrogeochemical, and rock mechanical conditions are to be described for the different time periods. For all these scientific disciplines, the underlying DFN models serve as important input, see Figure 2-1.

Bullet 9: SKB and Posiva have jointly formulated the long-term safety principles guiding the design and production of a spent nuclear fuel repository (Posiva SKB 2017). In the safety assessment, compliance during the reference evolution (or any other evolution considered) is assessed using performance targets of given safety functions (Posiva SKB 2017, Figure 1-1).

Bullet 10: Future human actions scenarios that may utilise DFN models include assessing the consequence of drilling of deep boreholes and construction of tunnels, shafts or rock caverns to great depth within the repository area and an incompletely sealed repository. BAT assessments may utilise DFN in comparing the merits/detriments of details of the disposal method (e.g. vertical versus horizontal placement of canisters), closure design (e.g. locations and quality of plugs) and the application of deposition hole acceptance criteria.

Returning to safety functions regarding the Geosphere, these are formulated as follows (Posiva SKB 2017):

The main safety functions of a KBS-3 repository are to, either directly or indirectly by protecting and preserving the safety functions of the barrier system, isolate the repository from the surface environment; contain radionuclides and to retain and retard their dispersion into the environment. The host rock and underground openings shall contribute to these main safety functions of a KBS 3 repository by providing:

- *Isolation from the surface environment,*

and by maintaining:

- *Favourable thermal conditions,*

- *mechanically stable condition,*

- *chemically favourable conditions; and*

- *favourable hydrogeological conditions to limit the transport of solutes.*

The rock has an additional quality contributing to retaining the radionuclides and retarding the dispersion of radionuclides, the capacity to sorb radionuclides if the containment should be breached.

The system of safety functions and performance targets from Posiva SKB (2017) are shown in Figure 2-3. To exemplify, the hydrogeological safety function stated as *favourable hydrogeological conditions to limit the transport of solutes* has the corresponding performance targets:

- Transport resistance (see Subsection 9.1.2 for definition) in fractures intersecting the deposition hole should be larger than 10 000 year/m; and

- flowrate in fractures intersecting the deposition holes (per one metre of fracture width) should be less than 1 L/m per year.

Note that in SR-Site the latter performance measure was posed in terms of an equivalent flow-rate for diffusive exchange at the interface between the buffer and the fracture intersect on the wall of the deposition hole (see e.g. Joyce et al. 2010, SKB 2011a). SR-Site also considered an inflow criterion on deposition holes of 0.1 L/s to avoid buffer erosion during installation (Börgesson et al. 2015).

To quantify these performance targets, explicit DFN models, as opposed to upscaled EPM models, are clearly needed. This follows since the transport resistance is obtained by integrating the ratio of local aperture and velocity along groundwater pathways through the fracture network starting from deposition holes until reaching the accessible environment. Similarly, to assess the flowrate in fractures intersecting deposition holes, an explicit representation of the fractures on the scale of metres (i.e., diameter of a deposition hole) is needed.

The performance targets for chemically favourable conditions include conditions for the canister, buffer and backfill, as well as for limited radionuclide release; however, note that these demands are stated relative to deposition areas as a whole, not for individual deposition hole locations. Still, this again requires assessment of the changes in groundwater chemistry in the fractures adjacent to deposition holes, and the wider evolution of chemical conditions in the deformation zones that provide the primary pathways for changes in surface water chemistry to reach repository depth. Hence, again DFN models representing fractures on the metre to kilometre scale are required to assess compliance with these targets, even if the chemical evolution typically is calculated using upscaled DFN models. However, in principle, explicit DFN models may be available also for these types of calculations in the near future.

The rock mechanical performance targets relate to:

- groundwater pressure at repository depth, including being under an ice sheet during glaciation, such that isostatic load on the canister < 50 MPa; and

- shear movements at deposition holes < 5 cm during seismic events, and with a maximum velocity of 1 m/s.

The first of these requires a DFN description of the vertical groundwater pathways between the ice sheet and the repository. The rock stresses related to glaciation (large rock loads) may induce mechanical processes/deformation of the rock and this may consequently influence the pore water pressure as well as the hydraulic conductivity indirectly through changes in fracture and matrix pore geometry. Of particular relevance here is the change in aperture for fractures of different orientation due to the evolving mechanical load, resulting in changes in hydraulic properties (see e.g. Hartley et al. 2016). Additionally, increased pore pressures and propagation of fractures may change the hydraulic conductivity through changes in the fracture network. Assessing shear movements requires models for stress field, fracture size, strength and stiffness and the connectivity of the fracture system to large structures than can host such movements (Fälth et al. 2014, 2016, 2019).

Compliance of the performance target is ideally achieved for all the time periods analysed. However, the performance targets should be seen as simply targets, not as strict limits (Posiva SKB 2017).

The next step in the assessment is to analyse the selected scenarios with respect to containment and retardation; i.e., the consequences of not honouring one or several performance targets are evaluated and quantified in the analysis of the selected scenarios. Here, radionuclide transport simulations are an important component of the analyses, and the DFN description constitutes a fundamental basis for the conceptualisation of the transport processes. Specifically, advective transport is conceptualised as taking place along the connected fracture network, whereas retention processes may take place on the fracture surfaces and the inner surfaces of the rock matrix where water is assumed immobile.

Provide favourable thermal conditions	Provide chemically favourable conditions
a) $T_{\text{deposition hole}} \geq$ temperature yielding $T_{\text{buffer}} > -2.5\ °C$ b) $T_{\text{deposition hole}} \leq$ temperature yielding $T_{\text{buffer}} \leq 100\ °C$	**Favourable conditions for the canister:** a) Anoxic conditions after the initially entrapped oxygen in the near field is consumed b) pH > 4 and concentration of Cl^- < 2 mol/L c) Concentration of No_2^- < 10^{-3} mol/L, low concentration of $NH4^+$ and acetate d) Concentration of HS^- < 3 mg/L, higher short-term transients can be accepted

Provide favourable thermal conditions

a) $T_{\text{deposition hole}} \geq$ temperature yielding $T_{\text{buffer}} > -2.5\ °C$
b) $T_{\text{deposition hole}} \leq$ temperature yielding $T_{\text{buffer}} \leq 100\ °C$

Provide mechanically stable conditions

a) Isostatic load on canisters < 50 MPa
b) Shear movements at deposition holes < 0.05 m
c) Shear velocity at deposition holes < 1 m/s

Provide favourable hydrologic and transport conditions

a) Transport resistance in fractures intersecting the deposition hole < 10 000 year/m
b) Flow rate in fractures intersecting the deposition holes (per one metre of fracture width) < 1 L/m per year

Provide chemically favourable conditions

Favourable conditions for the canister:

a) Anoxic conditions after the initially entrapped oxygen in the near field is consumed
b) pH > 4 and concentration of Cl^- < 2 mol/L
c) Concentration of No_2^- < 10^{-3} mol/L, low concentration of $NH4^+$ and acetate
d) Concentration of HS^- < 3 mg/L, higher short-term transients can be accepted

Favourable conditions for the buffer and backfill:

a) Salinity; TDS < 35 g/L, short-term transients up to 70 g/L accepted
b) Concentration of K^+ < 0.1 mol/L
c) Total charge equivalent of cations $\sum q\,[M^{q+}] > 8 \times 10^{-3}$ mol/L, where q = charge number of ion and $[M^{q+}]$ = molar concentration of cation
d) pH 5–11

Low release rate of radionuclides and limited radionuclide transport:

a) Anoxic conditions
b) Low organic content of the groundwater
c) High ionic strength

Figure 2-3. *Geosphere Safety functions (bold) and corresponding performance targets (from Posiva SKB 2017). DFN modelling is needed to assess whether or not the safety functions are met by computing safety function indicators and comparing to the performance targets.*

It is emphasised that the DFN-based transport description thus is used both to assess transport of solutes to the repository along recharge pathways (e.g. assessment of favourable chemical conditions), and to assess consequences of radionuclide transport along discharge pathways from potentially leaking canisters to the accessible environment. Also, in the additional analyses, e.g. in the analysis of scenarios related to future human actions, the underlying DFN models are used if any groundwater flow simulations are involved.

It is worth noting that DFN models are likely to be used in a much wider context in the safety case than simply to assess performance targets, and to assess containment and retardation potential. In the safety assessment SR-Site, the hydrogeological modelling performed during different time periods is summarised in Selroos and Follin (2010). Here, we identify additional usages of the DFN-based hydrogeological models in various analyses:

- Rock shear movement and climate evolution;
- Corrosion;
- Buffer and backfill erosion;
- Geochemical analyses;
- Biosphere analyses;
- Surface hydrology;
- Radionuclide transport in nearfield and far-field; and
- Supporting arguments and feedback to reference design.

The instrumental importance of the DFN models for many of the key analyses in the safety assessment is hence acknowledged. This has also been confirmed in various regulatory reviews, e.g. in SSM's review of SR-Site (e.g. Black 2012, Tirén 2012) where the uncertainty in the DFN models is pinpointed as one of the main and most crucial uncertainties of the whole assessment.

2.3 Role of DFN in Repository Engineering

All aspects of rock engineering in hard brittle rock are dominated by fractures and their impact on stress/strain, strength, deformation, failure, and kinematics. Approaches to rock mechanical description include synthetic rock mass (SRM) models, in which fracture geometry and properties are simulated explicitly and combined with a representation of the intact rock in-between to calculate effective rock mass properties, and there are empirical methods where fracture properties (intensity, orientation and strength) are factored into the rock mass classification. The accuracy and realism of rock engineering analyses is increased as the fracture properties are more accurately represented, i.e., as the underlying DFN is more explicitly considered. Therefore, DFN models provide powerful tools for detailed design of reinforcement and grouting. Some examples of practical uses of DFN in rock engineering are given in the following subsections.

2.3.1 Effects of grouting

Tunnel sections characterised by high inflow will be subject to pre-grouting prior to excavation and post-grouting after construction. Grouting may also be employed in pilot /investigation boreholes to safeguard completion of a given borehole. Grouting redistributes pressures in the bedrock, which can cause larger inflows to deposition holes. The use of cement grout can lead to a rise in pH of groundwater leachate, which can have detrimental effects on buffer performance (Luna et al. 2006)). DFN modelling can be used to quantify the number of fractures that may need grouting, grout volumes, and the numbers of deposition holes that may be lost due to avoiding possible effects of cement leachate.

Grouting for groundwater flow control in fractured rock is carried out to specifically plug flow in the most conductive fractures. Grouting design was traditionally based on procedures which combine the use of rock mass quality measures (GSI, RMR, Q) and local hydraulic testing. However, today it is based on the statistical analysis of fracture data – i.e., the DFN model. The rock mass flow and transport properties, after grouting, are governed by the fractures that were not accessed during the grouting process. As a consequence, grout performance evaluation can also be enhanced by interpreting grout results within the context of a DFN approach such as "Aperture Controlled Grouting" (Carter et al. 2015).

During grouting operations, downhole pressures, grout injection rates and grout properties can be used to analyse distribution of hydraulic and transport aperture and also differentiate between *1D* (narrow channels) and *2D* (divergent radial flow) injection behaviour within fractures (Fransson and Gustafson 2006, Hollmén 2008, Funehag 2012). A recent example of the application of these analysis methods and what they imply for fracture aperture description based on grouting operations in the ONKALO shafts is given in Libby et al. (2020).

2.3.2 Excavatability and rock support

The role that fractures play in the excavatability and support requirements of underground facilities can be addressed either through explicit DFN simulation or by utilising DFN models to parameterise and support effective rock mass classification systems. Both approaches can be used to address issues of spatial variability of rock mass quality, the occurrence of specific classes of discontinuities is likely to influence excavatability and may require additional tunnel ceiling and/or wall support. Also, changes in groundwater pressure due to excavation, dewatering and mitigations such as grouting and lining of tunnels can be simulated to make consistent coupled calculations of the effective stresses (i.e., rock stress minus groundwater pressure) around excavations and thereby support assessments of stability (i.e., shear strength) of fractures and rock blocks and inflows into the excavation.

Particularly in the repository environment, it is important for excavation methods and advance rates to be predictable in order to avoid unexpected structural or groundwater problems. DFN models, either directly or through their use as input to effective rock mass classification systems, can improve the local predictability of rock excavatability and support requirements through:

• More accurate identification of rock block size and shape distributions;

- More accurate calculation of effective rock-mass strength and deformability based on mechanical upscaling and the Synthetic Rock Mass (SRM) approach (Mas Ivars et al. 2007, 2011, Pierce et al. 2007, Sainsbury et al. 2008, Elmo et al. 2014, Darcel et al. 2018, Davy et al. 2018a);

- More accurate identification of multiple (> 3) fracture sets and the associated variability in set spacings, and

- identification of unstable wedges and blocks in large excavated underground openings.

Examples of the use of DFN modelling in design alongside excavation is given by Eftekhari et al. (2014), and to rock support and grouting design by Kvartsberg and Fransson (2013).

2.3.3   Rock Mass Deformability

Rock mass deformation in response to repository construction and operation is not expected to be a significant issue for Rock Engineering at Forsmark. It is not anticipated that the horizon of tunnels successively developed at repository depth will cause surface subsidence, or that new tunnels or openings will cause deformation of existing facilities. Nevertheless, it is important to consider rock mass deformability within the context of effective stress evolution – which does affect flow and solute transport in the geosphere.

Rock mass deformability depends on the distribution of rock mass elastic moduli – which are a combination of intact rock properties and local natural fracture geometry, intensity, and properties. Rock mass deformability can be derived (a) from dynamic elastic moduli obtained from *3D* seismic surveys or borehole dipole sonic logs, (b) from rock mass index measures (GSI, RMR and Q/Q'), and (c) from a model covering both fracturing and rock properties, e.g. SRM types of model. The current standard practice for analysis of rock mass deformation is to use effective rock mass deformability approaches at most sites (Davy et al. 2018a).

A DFN model conditioned on local geological properties can be used to derive spatially varying rock mass mechanical properties and thereby improve the accuracy of predictions in specific volumes. Both rock anisotropy and fracture geometry are expected to have a significant effect on the anisotropy of rock mass deformability. Consequently, it can be important to utilise the DFN models to condition the rock mass deformability model to describe the evolution of the three-dimensional stress field. The *in situ* stress field will undergo significant changes with repository construction, resaturation, and also for key process scenarios including the seismic and glacial scenarios (Hökmark et al. 2010). Having a well-conditioned, anisotropic model for rock mass deformability is valuable for improving rock engineering for derivation of the stress field – and fracture response to changes in that stress field.

2.3.4   Excavation Damage Zones

Significant research has been carried out on excavation damage zones (EDZ) by both Posiva and SKB because of its importance for repository resaturation, radionuclide and solute transport, and tunnel/cavern stability. The extent of damage zones induced by excavation needs to be controlled and characterised (Bäckblom 2008, Koittola 2014, Ericsson et al. 2015). Facility-scale DFN models provide the basis for quantifying the degree of fracturing in the pre-excavation rock that can be modified to incorporate effects of the additional EDZ fracturing or rock mass alteration.

The DFN approach can be used to support EDZ analysis at deposition hole, tunnel, and repository scales. Analysis of EDZ effects using the DFN approach includes the following aspects:

- Consideration of the local pattern of natural fracturing before excavation;

- Modelling of the effect of natural fracturing on the pattern of *in situ* stress and rock mass strength before and during excavation;

- Changes to natural fractures, and creation of induced fractures during excavation; and

- Changes to the hydraulic and mechanical properties of natural and induced fractures as stress and groundwater pressure evolves with repository operation, resaturation, and long-term.

2.3.5   Kinematic Wedge Stability

Rock support is generally applied to minimise the kinematic instability of rock blocks that form between the discrete fractures. The stability of blocks depends on the resistance to slip on the bounding faces, the strength and deformability of any rock bridges between blocks and the forces acting on them. Rock support can be applied at two levels:

1. A statistical/empirical approach based upon correlations between required rock support and index measures of rock mass quality. In this approach, the local pattern of fracturing is only used to estimate the rock mass quality index – generally GSI, RMR, or Q. The support design is then based on statistical correlations between required support (using empirical experience) and the index measures.

2. A statistical/kinematic approach, in which DFN based kinematic analysis is carried out at each location, modelling the local tunnel geometry and multiple realisations of the fracture geometries and strength parameters, followed by identification of unstable blocks. In this approach, the reliability of support design depends on the accuracy of the DFN model at that location, and hence the model can be conditioned to local geological conditions and observed fractures. A safety factor on the rock support is still required to account for the degree of confidence in the DFN characterisation.

A DFN model can provide a basis to significantly enhance kinematic rock wedge stability for tunnels, caverns, and deposition holes. By considering the *3D* fracture geometry it provides a more realistic assessment of the risk of block instability and provides input to optimised support design. DFN models can take into account the spatial and statistical variability in fracture orientation, intensity and size, thus being able to provide limits to rock wedge size formed more comprehensively than can be achieved using purely empirical methods.

2.4   Timeline of model development

The DFN Modelling methodology presented in this report will be implemented in site-descriptive models, and then applied by a variety of clients as described in the subsections above. The operational aspects of the applications will be described in dedicated operational programmes for the accesses and ramp, and deposition areas, respectively.

An indication of the likely outputs expected from DFN modelling and the new types of data expected at each phase of modelling along this timeline is given in Table 2-1. The application of the DFN methodology presented in this report has to be adapted to meet the evolving client needs and types of data to be analysed. The methodology is therefore general with some processes only becoming relevant as certain types of data become available, such as tunnel mapping data or monitoring of hydraulic disturbances during construction of the facility. It will first be applied in the stage of Baseline modelling, using existing data from SDM-Site re-analysed according to the revised methodology and augmented by some 20 new shallow, c 50–150 m, cored holes. With the Baseline model in place, the model is iteratively up-dated through the phases leading up to SDM-SAR when new underground and monitoring data are acquired. The methodology is also expected to provide the techniques that will be required during the operational phase.

Table 2-1. An illustrative scheme of how DFN models will likely evolve through the construction process, the new data available and some of the applications.

Modelling phase	Expected types of new information	Expected outputs from DFN modelling
SDM-Site	Structural mapping of fractures on surface outcrops. Structural mapping of fractures and high-resolution flow logging and hydraulic injection tests in deep boreholes. Long-term hydraulic interference tests. Groundwater samples from boreholes.	Facility scale DFN. Stochastic description of fracture geometries. Near-field flow distribution. Hydraulic and transport properties for modelling site evolution and radionuclide transport.
Baseline model for Environmental impact	Structural mapping of fractures and high-resolution Flow logging (PFL) in near-surface (50–150 m) boreholes. Hydraulic interference tests in dense array of near-surface boreholes.	An updated local scale DFN model using this new methodology and data from the accesses area to calculate equivalent hydraulic properties of near-surface and deep bedrock.
Baseline model for Initial state and forecast	As for Baseline model for environmental impact.	On "Facility part scale" (covering repository accesses): Input to grouting and reinforcement design. Initial predictions of fracture properties and state variables (e.g. groundwater pressures and rock stresses) to be compared with measured/modelled outcomes from access ramp and shafts.
DIL Level 50	Structural mapping of fractures and high-resolution flow logging in pilot boreholes in shallow depth. Pressure monitoring in boreholes close to shallow ramp. Information on grout flow-rates, pressures and grout properties from grouting operations in accesses.	On tunnel scale and facility part scale (deposition areas): Prediction-outcome exercises of fracture properties and hydraulic properties relative to pilot boreholes and tunnel data in the upper 200 m of the bedrock. Iteration of DFN concepts and parameters with predicting grouting efficiency.
DIL Level 200	Measurements of in situ stress orientations and magnitudes in excavations. Mapping of cores for establishing indices of mechanical properties of matrix rock, fractures and fractured rock mass. Measurement of inflow in probe/pilot boreholes along the rock excavations (ramp/niche) for early detection heterogeneity and anisotropy of hydraulic properties. Measurements of groundwater inflow to underground openings (water rings and weirs).	On tunnel scale and facility part scale (deposition areas): Mechanical and hydromechanical predictions. Prediction-outcome exercises of fracture properties and hydraulic properties relative to pilot borehole and tunnel data in the lower bedrock.
DIL Level 470	As above but at repository depth. Correlation of structures between several tunnels and their pilot holes. Groundwater samples. Results from application of deposition hole acceptance criteria.	On tunnel scale and facility part scale (deposition areas): Prediction-outcome exercises of fracture properties and hydraulic properties relative to pilot holes and tunnel data at repository depth. Inputs to address needs of grouting and reinforcement. Near-field flow distribution. Hydraulic and transport properties for modelling site evolution and radionuclide transport.

3 Overview and basis for fracture description and modelling

This chapter provides a short overview of the phased workflow (Figure 3-1) for constructing an integrated DFN model suited for the purposes of making structural, mechanical, hydraulic and transport simulations. It also provides a basis for assessing reinforcement and grouting needs and associated designs. The reliability of the model is established and augmented through successive prediction-outcome exercises. This involves all the aspects of the DFN modelling methodology presented in this report. The corresponding phased workflow is structured as four main stages:

1. Building the geometrical sub-model(s), based on the quantitative framework described in Chapter 5, available data, available knowledge (model assumptions) and the division into domains from geological and deformation history models;

2. Building the flow sub-model(s) by assigning individual **fracture process properties** (i.e., mechanic and hydraulic properties) from calibration to in situ experiments and lab tests (Chapter 8);
    a. confirmatory testing (i.e., simulation of data types, events and/or processes different from those used in calibration) and sensitivity testing (i.e., quantifying the significance of assumptions and parameters) are performed alongside the modelling progress;
    b. building the mechanical DFN model(s) is an indirect requirement at this stage, due to its contribution for building a model of the spatial distribution of in situ stresses.

3. Building the transport sub-model(s) by assigning individual fractures and the rock matrix transport properties, from calibration to in situ experiments and lab tests (Chapter 9);
    a. again, confirmatory and sensitivity testing for transport are performed alongside the modelling progress;

4. Prediction-outcome exercises when additional or reserved data are made available, to iterate and establish DFN model reliability when delivered to users (Chapter 10).

The DFN conceptualisation is a holistic integration throughout. For example, the mechanical and transport descriptions are intimately bound with the geometrical models for the spatial descriptions of intact rock and fracture surface minerals. The flow description is closely associated to the stress conditions and hence mechanical description. The transport description only comes last because it requires not only a description of intact rock and fracture minerals, but also the flow field.

The aforementioned "building" phases involve data analyses and model(s) **Sensitivity Analyses, Calibration and Rejection (SACRe)** steps (Figure 3-1):

• **Sensitivity Analyses** – analytical and numerical simulations are essential to identify the key parameters of the model(s) and better target what are the key characteristics of the model(s), where and how different model(s) and/or more data would be required to reduce the overall modelling uncertainties.

• **Calibration** is the process whereby a clearly predefined set of model parameters can be tuned until the model results match the set of selected observations and key characteristics (as identified in the Sensitivity analyses). This is *not* a validation process since many different models can be consistent with observations and characteristics.

• **Rejection** of unviable model(s) is the process of eliminating models for which fundamental inconsistencies between predictions and observations persist at the end of the calibration process.

The process is iterated until satisfactory models are found. If no model is acceptable at the end of the SACRe process, one must go back to an earlier stage of the modelling workflow and reconsider the modelling hypotheses. Complementary to the data analyses and SACRe, **confirmatory tests** evaluate the capacity of the calibrated DFN model(s) to reproduce additional *in situ* hydraulic experiments or monitoring, like for instance i) heads, ii) interference tests, and iii) hydraulic disturbances during underground construction. At any given time, the database available for the modelling may be divided such that part of the data are used as constraints of the model parameters, part as calibration data used

in SACRe, and the remaining part in the confirmatory tests aiming at model validation. New data acquired during the construction of the facility can be used in the confirmatory tests. If the tests fail to match them, the models should be revisited, and new data integrated in the calibration process.
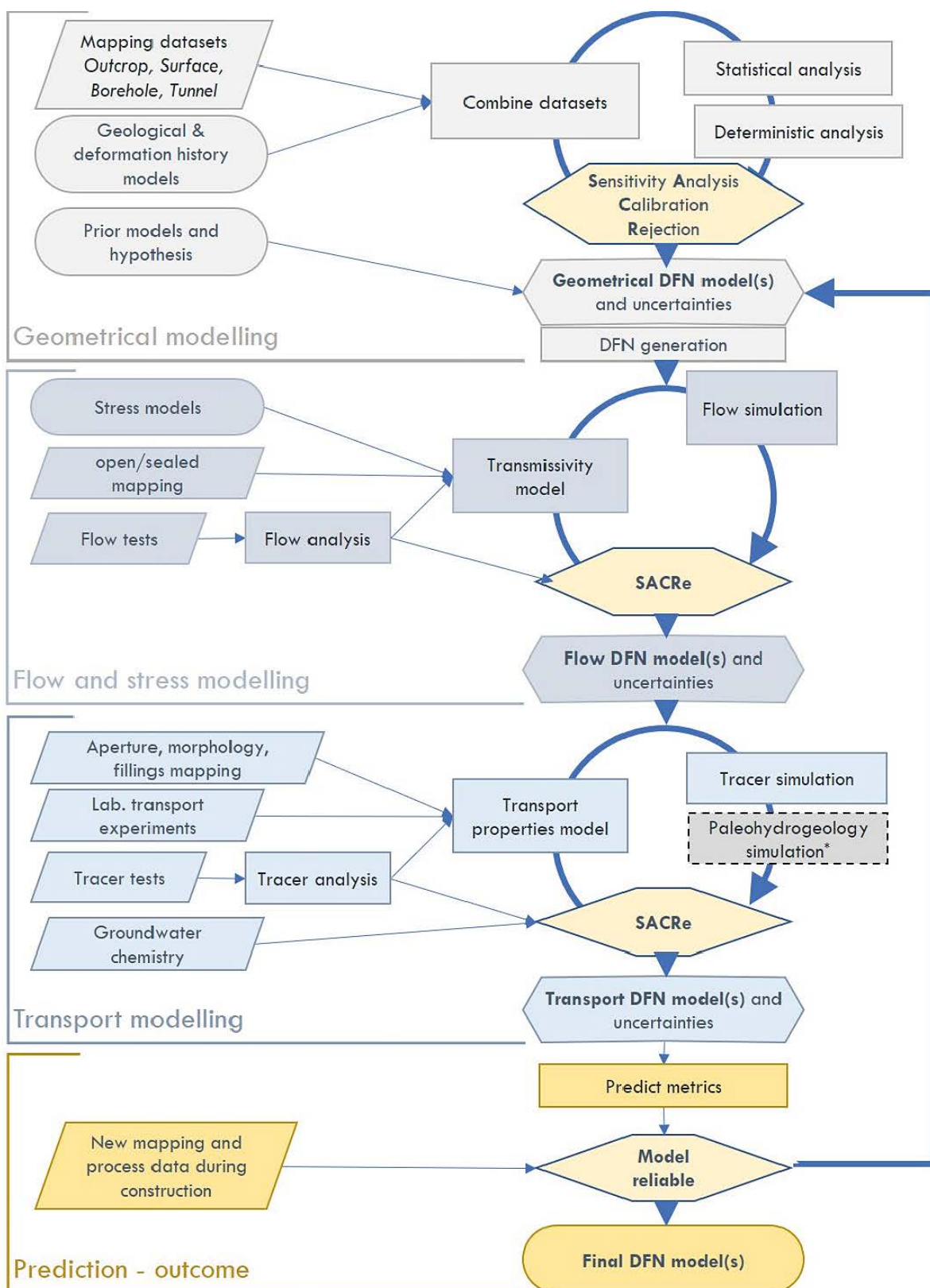
Figure 3-1. *Outline of workflow for DFN modelling divided into main phases. Sensitivity Analysis, Calibration and Rejection (SACRe). *Paleohydrology modelling is not included herein but reported in* **HGMM**.

In summary, sensitivity analyses and confirmatory tests are performed alongside the calibration and rejection tests to quantify the significance of uncertainties for long-term safety.

It is worth emphasising that several models, based on potentially alternative modelling assumptions (e.g. the spatial patterns of fractures and openings or structures not directly characterised), could likely all be consistent with the available data but yield different predictions. Therefore, it is recommended to perform prediction – outcome simulations of metrics and flow indicators that represent measurable proxies for safety related performance measures, such as flows around deposition holes and transport resistance, to assess whether the alternative models have significant implications for the safety case, and therefore identify key alternative models for further assessment.

Figure 3-1 indicates the overall steps performed in building a DFN description of the bedrock system. This is one component of developing an integrated site description. In particular, the hydrogeological site description involves close integration between DFN modelling, interpretation and modelling of hydrogeological and transport measurements, and hydrological models of the surface system. The Hydrogeological Modelling Methodology, **HGMM,** summarises the workflow for this integration, reproduced here in Figure 3-2.
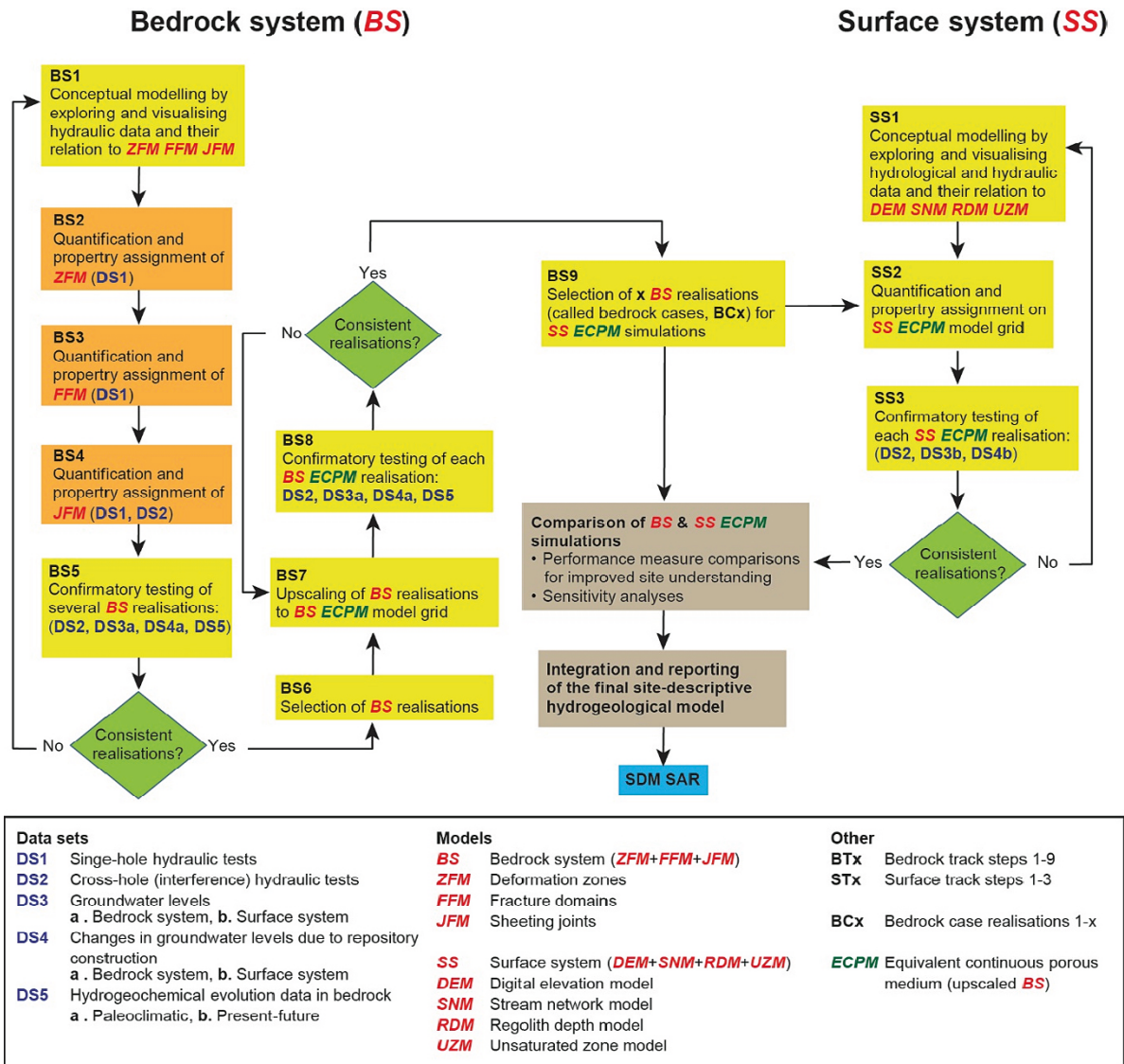
*Figure 3-2. Overall workflow for integration of bedrock structural and hydrogeological models with surface system models (from **HGMM**). Note: The acronyms ZFM and FFM in the figure are Forsmark-specific and are referred to in this report as DZ and FD respectively.*

In this workflow, the DFN focused tasks (BS2 through BS4) are shown in orange in the left-hand column and are structured according to building models for each of the structural components shown in Figure 2-2 and described in Chapter 5. The identification of these structural building blocks (BS1) is an integrated process between Geology, DFN and Hydrogeology, the DFN part corresponding to the first SACRe cycle in Figure 3-1. Steps BS5–BS9 involve integration between DFN, Hydrogeology and Hydrogeochemistry, and correspond to the second and third SACRe cycle in Figure 3-1.

The steps of the flowchart in Figure 3-1 are reviewed in the following sections.

3.1 Geometrical DFN modelling

The geometrical DFN model describes all the geometrical characteristics of individual fractures and the topological structure of the DFN. This includes geometric properties, such as orientation, size, shape/aspect ratio, termination, scaling properties such as spatial and intensity distributions of the fracture-properties, and the fracture in-plane-properties such as planarity/undulation, geologic aperture, morphology and filling minerals. Filling minerals are used to infer relative ages of fractures and associate them to stages of the deformation history, but they also have significance to the description DFN process modelling as described in Section 3.2.

The input data for the geometrical DFN model are firstly *i*) borehole core fracture mapping and image logs, *ii*) detailed tunnel wall and outcrop fracture trace mapping and *iii*) the larger scale mapping of lineaments on the surface.

For brevity, inference of geometrical model includes the following steps (top block in Figure 3-1), which are iterated (loop in the figure) until a satisfactory (range of alternative) model(s) are selected:

- Combination of datasets according to their sampling support (i.e., type and dimensionality of the object from which fractures are sampled such as scanlines, surface outcrops, boreholes, tunnel walls), to their location in the Geological model and to their age in the deformation history (Section 4.2). The latter provides a potential framework for interpreting fracture orientations, size through interactions (e.g. termination, cross-cutting), and infillings;

- Statistical analyses of the combined datasets, primarily:
  - Identification of preferential orientations and fitting of probabilistic models to represent the orientation distributions. In most cases, for each preferential orientation, the resulting distribution is defined by a mean orientation and a variability term to describe the dispersion about the mean (Subsection 6.6.2). Stereographic projections are widely used to visualise qualitatively the fracture orientations. The interpretation into fracture orientation sets can be correlated to deterministic information and expectations from the site deformation history, tectonic domains etc.
  - Analysis of fracture trace size distributions, i.e., how intensity scales with the size of fractures, and any hierarchies in the organisation of fractures of different size. This step is critical to understanding the spatial model and the multiscale nature of the fractured system.
  - Characterisation of the spatial variations of the fracturing properties (e.g. scale analysis of fracture intensity fluctuations along core logs, fracture spatial correlations and terminations types from *2D* maps, etc) to define a spatial model of variability from the core log resolution and up to scales comparable to the site main tectonic and lithological units for each of which different parameter settings are considered. The spatial model in its entirety describes all the spatial variability scales, from well identified geological units and down to the smallest observations.
  - Characterisation of fracture shape and fracture terminations.
  - Characterisation of fracture geologic aperture, i.e., the gap measured between wall rock surfaces. This step involves conceptualisation of the spatial aperture distribution within a fracture over the visible scale, with consideration of open/sealed status, fracture morphology, matedness, alteration and filling mineralogy. These indicators are used to associate fractures to significant geological events of the deformation history or to further define the fracture process properties (see below).

- The preceding statistical analyses and modelling are combined with deterministic information, which covers a wide spectrum, starting from the large-scale geological volume boundaries between major geological units, deterministic deformation zones, down to the local conditioning of the DFN model to honour fracture observations in tunnels or boreholes; and

- Analyses and combination of datasets coming from different sampling supports (e.g. *1D* and *2D*), locations and scales by means of stereological analyses enables the determination of a complete *3D* DFN model. Complementary sensitivity analyses to modelling assumptions reinforce the final *3D* DFN model(s) relevancy.

Where there exist significant uncertainties in interpretations or in extrapolating observations made in boreholes/tunnels to volumes much larger than the one of the support, alternative models are defined to explore different hypotheses and/or assumptions. Alternatives are tested whether they can be screened or calibrated against observed mechanical, hydraulic or transport characteristics and the significance for long-term safety quantified.

3.2 DFN Process modelling for flow

The phase of "DFN process modelling" refers to populating the geometrical fracture network with all the properties required to perform flow modelling and evaluating and calibrating the resulting systems on different types and scales of measurements. This involves assigning fracture mechanical and hydraulic properties (as process properties). The data used are mainly *i*) direct observations of the fracture open fraction as available from the core logging data, *ii*) stress model to infer the local stress conditions acting on the fractures (recognising the effect of stress on fracture mechanical opening and thus indirectly on transmissivity) and *iii*) all available hydraulic tests, as listed in Chapter 7.

The workflow associates the geometric DFN model(s) previously developed with additional data and SACRe analyses to determine the individual fracture hydraulic parameters, i.e., transmissivity and storativity. The calibration targets are a range of flow indicators derived from flow data analyses as listed below:

- Statistics of discrete flows (specific capacities) associated to individual fractures based on continuous flow logging, with distinction between Fracture Domains and Deformation Zones (inside/outside), providing the intensity of flows of different magnitudes at a point (borehole inetrsect);

- The locations of discrete flows from continuous flow logging or short interval double packer tests analyses (scale analysis) for the spatial structure of flows along a line (borehole), e.g., clustering;

- Interference tests due to long-term pumping to detect hydraulic connections (hydraulic tomography) between points (borehole intersects) under controlled induced flow conditions and measure hydraulic diffusivity; and

- Hydraulic disturbances caused by underground drilling and excavation of the accesses and facilities, to detect hydraulic connections (hydraulic tomography) between points (tunnel-borehole intersects) under unintentional induced flow conditions.

The calibration tuning parameters are:

- Geometric DFN model(s) selection;

- Spatial distribution of fracture openness. The fractures of the geometrical DFN are first assigned an **open fraction**. Whilst the total open fraction can be assessed from data, the spatial distribution and arrangement of openness (below and above the fracture scale) is less well constrained, although it is likely a key parameter of the modelling. At this stage, sensitivity analyses of the resulting DFN model(s) connectivity structures are highly recommended to facilitate early rejection of inconsistent connectivity structures, prior to starting flow simulations;

- Relationship between fracture transmissivity and fracture geometry (roughness, size, shape);

- Relationship between fracture transmissivity, orientation and local stress conditions by using the stress field model and a hydromechanical relationship that relies on the normal and shear stiffness and strength models. This relationship may be empirically defined from in situ observations and/or from analyses and lab tests.

- The stress field results from a combination of remote stress conditions and spatial distribution of intact rock and DFN mechanical properties. At a first order the stress model is calibrated against the in situ stress measurements. However, any fracture induces a local stress perturbation whose intensity and spatial reach is controlled by its mechanical properties, size and orientation and with respect to surrounding stress and rock conditions. So, the refined definition of the Stress Field model (**RMMM**) results from the Mechanical model, with a spatial distribution of rock mass elastic and strength properties, which itself results from the Mechanical DFN model (Geometric DFN model with fracture mechanical properties). A special emphasis should be put on the critically stressed regime, for which the fracture transmissivity is likely increasing due to dilation; and

- Estimate of the fracture in-plane heterogeneity in aperture (transmissivity), which is likely controlling the spatial distribution of flow in the fracture plane.

In practice, the calibration shall rely on numerical flow simulations whose constraints and limits (inherent to any numerical modelling tool) should be clearly stated by the DFN flow modeller. Due to the complexity of the calibration process, it is recommended to carry out pre- and post-simulation analysis of the flow models – e.g. a scale analysis of the hydraulic connectivity from analytical indicators, the calculation of the flow channelling – in order to better understand how and if a flow model can match measurements from different types and scales.

Alternative hypotheses for in-plane heterogeneity in fracture properties including transmissivity, that in turn give rise to flow channelling, also need to be considered in this step. A combination of direct measurements, e.g. fracture surface roughness and matedness, and indirect evidence such as spatial and temporal variability in hydraulic tests can be used to quantify heterogeneity.

At the end of the SACRe process for flow modelling, additional confirmatory tests can be defined to test the model(s) predictive capacities.

3.3 DFN Process modelling (transport)

The next phase of process modelling focuses on the additional properties and processes involved in solute transport through the following steps:

- Simulation of single-hole or multi-hole tracer tests to calibrate the equivalent transport aperture and related parameters such as hydrodynamic dispersion.

- Description of the **spatial distribution of transport properties** of the mineral fillings and wall-rock according to statistical models or spatial correlations with different sorts of structures or lithologies inferred from laboratory transport experiments.

- The combined hydraulic and transport description of the network together with a description of the past climate evolution are used to simulate the **palaeohydrogeological evolution** of the site to confirm the overall description against measured hydrogeochemical data in the fracture and porewater systems. Notice that the simulation of porewater and porewater evolution, which is important to assess for possible anion exclusion processes, requires the explicit consideration of mass transfer between the flowing fractures and the immobile water in the rock matrix. This also has the potential to screen alternative models. They may over-predict the flushing of different water types through the fracture system, for example.

3.4 Confidence building

It should be emphasised that a significant part of the DFN model acceptance and confidence building takes place during the testing of the bedrock hydraulic and transport properties predicted by the DFN model(s) during the mechanical, flow and transport process modelling. As indicated by steps BS5–BS9 in Figure 3-2 this is performed as a series of confirmatory tests integrating DFN, hydrogeological, hydrological, hydrogeochemical and solute transport information.

Once the site descriptive models have been defined and developed, there is a need to validate them (at some level). Validation is an inherently difficult matter when groundwater flow models designed for large spatial and temporal scales are considered (see e.g., Nordstrom 2012), but nevertheless an attempt is needed. The definition of validation adopted here is the one by IAEA (2018):

Model validation: The process of testing whether a model is an adequate representation of the real system being modelled by comparing the predictions of the model with observations of the real system.

With this definition of validation, it is presupposed that the numerical code representing the governing equations has been thoroughly verified (against e.g. analytical solutions) before the actual model is developed.

The confidence building in the DFN model is approached through a series of Prediction-Outcome (P/O) exercises comparing model predictions with measurements of fracture and network properties through various metrics. These performance metrics are primarily related to geometrical and hydraulic characteristics. However, in principle also transport-related and rock mechanics-related metrics can be devised. The metrics proposed as part of the present DFN methodology are listed in Section 10.2. The difference between confirmatory testing and P/O is somewhat subtle, but the primary difference is that confirmatory testing is used during model construction, while P/O is a test performed after a model version has been finalized.

The developed model will be stochastic in nature since it will be based on statistical input information; specifically, relevant fracture parameters will be known only in a statistical sense since the fractured rock is heterogeneous, and measured data only exist in a few locations with limited spatial coverage. Thus, the developed model will be stochastic (and locally unconditioned), and comparison of predictions with independent data, also measured in a few specific locations, can only be made in a statistical sense; e.g. checking that measured data are spanned by the distributions of predictions.

If predictions are to be made in a more deterministic fashion, models need to be locally conditioned to location-specific data. Once a model is locally conditioned, additional independent location-specific data should be used for further P/O exercises. Even if such predictions cannot be fully deterministic, the distributions of predicted metrics should be narrower than in the unconditional step.

The type of data that typically can be obtained for P/O exercises will come from pilot holes of (deposition) tunnels and pilot holes of deposition holes, and from tunnels themselves. That is, the data will be very local, and metrics may be fracture-related parameters such as total fracture intensity, or intensity of water conducting fractures. However, the model ultimately needs to be validated on the Facility-scale; i.e., the scale at which the model is used in performance and safety assessment applications. This may be impossible in a strict sense, specifically if the safety assessment time scale also is considered. Thus, the strict validation, which can be applied on deposition hole scale, will have to be replaced by looser validation criteria at the Facility-scale. Here, the notion of fit-for-purpose is useful, i.e., will the developed model be a good tool for the assessments to be made? Multiple lines of evidence will need to be invoked to argue for the fitness. The DFN methodology itself, single-hole calibration, early rejection of un-viable models, confirmatory testing, P/O exercises, and expert-solicitation of obtained results will play important roles in such argumentations.

4 Geological context of the Forsmark site

This chapter summarises the geological setting at Forsmark, lists the currently available geological data, describes the current understanding and geological models, and tabulates the associated uncertainties relevant for creating a DFN model of the Forsmark site. This includes descriptions of current models for lithologies, deformation history, brittle deformation zones and fracture domains.

4.1 Regional geological setting

Forsmark is situated approximately 120 km north of Stockholm in the south–eastern part of Sweden (Figure 4-1a). A gentle relief and a landscape situated below the highest shoreline, i.e., the highest level in Sweden reached by the sea during or after the latest Quaternary glaciation, characterise the region around Forsmark (Lidmar-Bergström 1994, Lundqvist 1994). The bedrock surface beneath the unconsolidated, Quaternary glacial and post-glacial deposits, which is exposed only locally on the ground surface at Forsmark, corresponds to the morphological structure referred to as the sub-Cambrian peneplain (Lidmar-Bergström 1994). This ancient denudation surface formed more than 540 million years ago. It corresponds geologically to a sub-Cambrian unconformity and marks a long period of uplift and erosion with loss of the geological record between the formation of the crystalline bedrock and the deposition of the unconsolidated Quaternary cover.

The bedrock at Forsmark is situated inside the Svecokarelian orogen in the south–western part of the Fennoscandian Shield (Figure 4-1a) which forms one of the ancient continental crustal fragments on Earth. This is bordered by an Archaean continental nucleus to the north–east, by the Sveconorwegian orogen to the south–west and by Neoproterozoic and Phanerozoic sedimentary cover rocks of the East European Platform to the south–east. In the west and north–west, it is overthrust by rocks that belong to the Caledonian orogen. The thickness of the continental crust in the region that includes Forsmark is around 50 km.

Intrusive rocks, felsic volcanic rocks and subordinate sedimentary rocks, the majority of which were affected by pervasive or more localized ductile strain and metamorphism at mid crustal levels, dominate the Svecokarelian orogen in south–eastern Sweden (Koistinen et al. 2001). Both the crystallisation of the igneous rocks and the ductile deformation along with metamorphism occurred between 1.9 and 1.8 Ga. Forsmark lies shortly beyond the north–eastern periphery of one of Sweden's important provinces for the exploitation of mineral deposits inside this orogen (Figure 4-1b), the so-called Bergslagen province (Stephens 2009). The abundant Fe oxide and Zn-Pb-Ag ± (Cu-Au) sulphide deposits along the arc-like structure to the west of Stockholm (Figure 4-1b) are hosted by felsic volcanic rocks dated at 1.91 to 1.89 Ga.

The Svecokarelian orogen in south–eastern Sweden has been divided into six regional tectonic domains (tectonic domains 1 to 6 in Figure 4-1b). These domains have been separated on the basis of differences in either the timing of tectonic activity, i.e., the timing of ductile deformation, metamorphism and igneous activity, or in the character and intensity of the ductile strain (Hermansson et al. 2007, 2008a, Söderbäck 2008). Forsmark is situated in tectonic domain 2.

Tectonic domain 2 contains broad belts of rocks that have been affected by strong ductile deformation under amphibolite-facies metamorphic conditions. These ductile high-strain belts, which strike approximately WNW−ESE to NW−SE and are subvertical, anastomose around tectonic lenses in which the bedrock is commonly folded and, in general, affected by lower ductile strain (Figure 4-1c). They also contain retrograde deformation zones along which deformation occurred in both the ductile and brittle regimes. The overall structural character of the bedrock in tectonic domain 2, in general, and in the Forsmark area, in particular, is strongly anisotropic. The volume at Forsmark targeted as a site for the disposal of highly radioactive spent nuclear fuel is situated in one of these tectonic lenses, the so-called Forsmark tectonic lens.
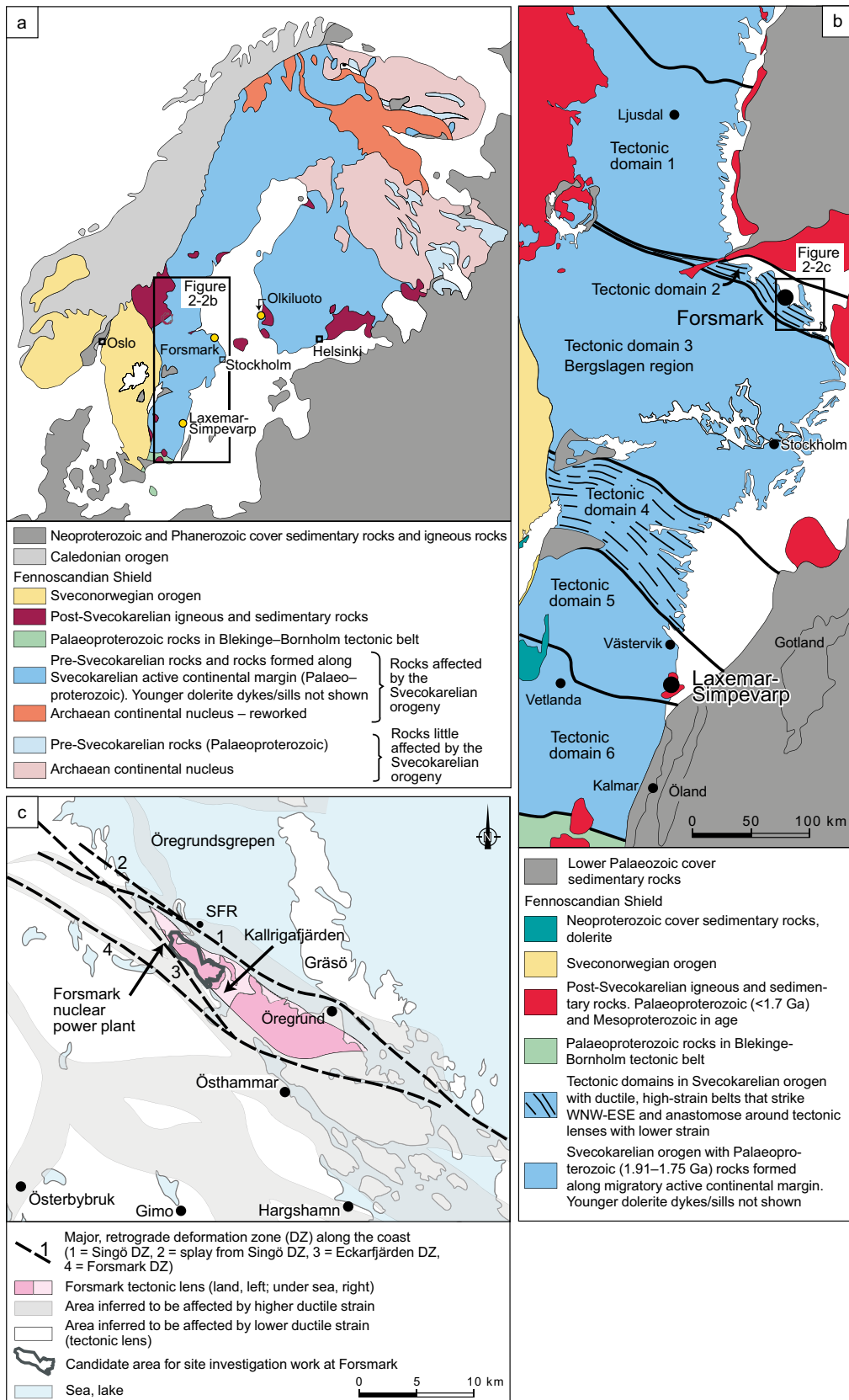
Figure 4-1. *National and regional geological setting of the Forsmark site. (a) Major tectonic units in Fennoscandia at the current level of erosion. The locations of Forsmark and Laxemar-Simpevarp as well as the proposed repository site at Olkiluoto in Finland are also shown on the map. (b) Svecokarelian tectonic domains and post-Svecokarelian rock units in the south–western part of the Fennoscandian Shield, south–eastern Sweden. (c) Inferred high-strain belts and tectonic lenses, including the Forsmark tectonic lens, in the area close to Forsmark, all situated along a coastal deformation belt in the northern part of Uppland, Sweden. Image and caption from Stephens (2010).*

A conceptual tectonic model for the Svecokarelian orogen in south–eastern Sweden has been proposed (Hermansson et al. 2008b, Söderbäck 2008). This model envisages approximately northward-directed oblique subduction beneath an active continental margin to the north–east and a progressive migration of the subduction hinge away from or towards the overriding plate, related to long periods of trans-tensional tectonics and short periods of transpressional tectonics, respectively.

4.1.1 Available geological data

Multiple sources of information have contributed to the current understanding of the geology at Forsmark.

- Geological mapping of the Forsmark area was carried out in two field campaigns during 2002 and 2003 (Stephens et al. 2003, Bergman et al. 2004);

- Detailed mapping of surface fractures was undertaken between 2002 and 2005 (Hermanson et al. 2003a, b, 2004, Stephens et al. 2003, Cronquist et al. 2005, Leijon 2005, Forssberg et al. 2007, Petersson et al. 2007a, b).

- Borehole drilling, which has been undertaken in three phases, 2003–2009, 2011 and 2016. The maximum depth of some of these boreholes is c 1 000 m. Data collected include (Stephens et al. 2007):
  - Oriented drill cores, enabling assignment of absolute fracture orientations.
  - Wireline geophysical logs including image logs of structures.
  - Borehole seismic data (VSP) for boreholes KFM01A and KFM02A collected in 2004 (Cosma et al. 2005).

The more recent drilling phase provides information on structures in the top c 100 m of bedrock, which was typically cased in the earlier boreholes.

- Magnetic surveys were undertaken to aid extrapolation and interpolation of interpretations.
  - 110 km^2 of helicopter based measurements were made in 2002 (Rønning et al. 2003).
  - 11.1 km^2 of ground based measurements were made in 2006–2007 (Isaksson et al. 2007).

- *2D* seismic reflection data were collected in 2002 (Juhlin et al. 2002, Juhlin and Bergman 2004) and 2004 (Juhlin and Palm 2005). Reflection seismic profiles 5b and 8 in the northern Forsmark area were reprocessed to improve the images in the uppermost 500 metres in the SFR area (Juhlin and Zhang 2010). A *3D* seismic dataset (reflection, refraction and tomography) 320×406 m was acquired in 2016 (Lundberg et al. 2018).

- Observations made during shallow bedrock excavation (Bergman et al. 2004, Petersson et al. 2007b).

- Various radiometric methods (see Table 3-3 in Stephens 2010) have been used to date the rocks (Page et al. 2004, 2007, Hermansson et al. 2008a, b, Söderlund et al. 2008, 2009).

Other data sources include *2D* seismic refraction surveys, various additional airborne geophysical methods, radar and historical data (Stephens et al. 2007).

4.1.2 Lithological summary

Four major groups of rocks (Groups A to D), distinguished by their relative age, are present in the Forsmark model area (Stephens et al. 2008, Stephens 2010). Their spatial distribution, composition and grain size are summarised in Figure 4-2.

The rocks are dominated by meta-intrusive rocks that formed between 1.89 and 1.86 Ga (Group B) and between 1.86 and 1.85 Ga (Groups C and D). The Group B meta-intrusive rocks consist of granitoids as well as subordinate ultrabasic, basic and intermediate rocks, metamorphosed under amphibolite-facies conditions. The rocks in the subordinate Groups C and D consist solely of granitoids that show a lower degree of metamorphism. The two suites have been distinguished primarily by their relationships to the penetrative ductile deformation in the area. Both suites intruded into supracrustal rocks dominated by the acid metavolcanic rocks of Group A. The bedrock volume that hosts the proposed repository is dominated by metamorphosed, biotite-bearing granite (to granodiorite) that belongs to the older Group

B suite. Partly due to the lithological homogeneity of the Forsmark tectonic lens (Figure 4-2), there is limited lithological control on fracture distribution within the host rock of the repository. Outside the lens, the lithology is more heterogeneous (Figure 4-2).
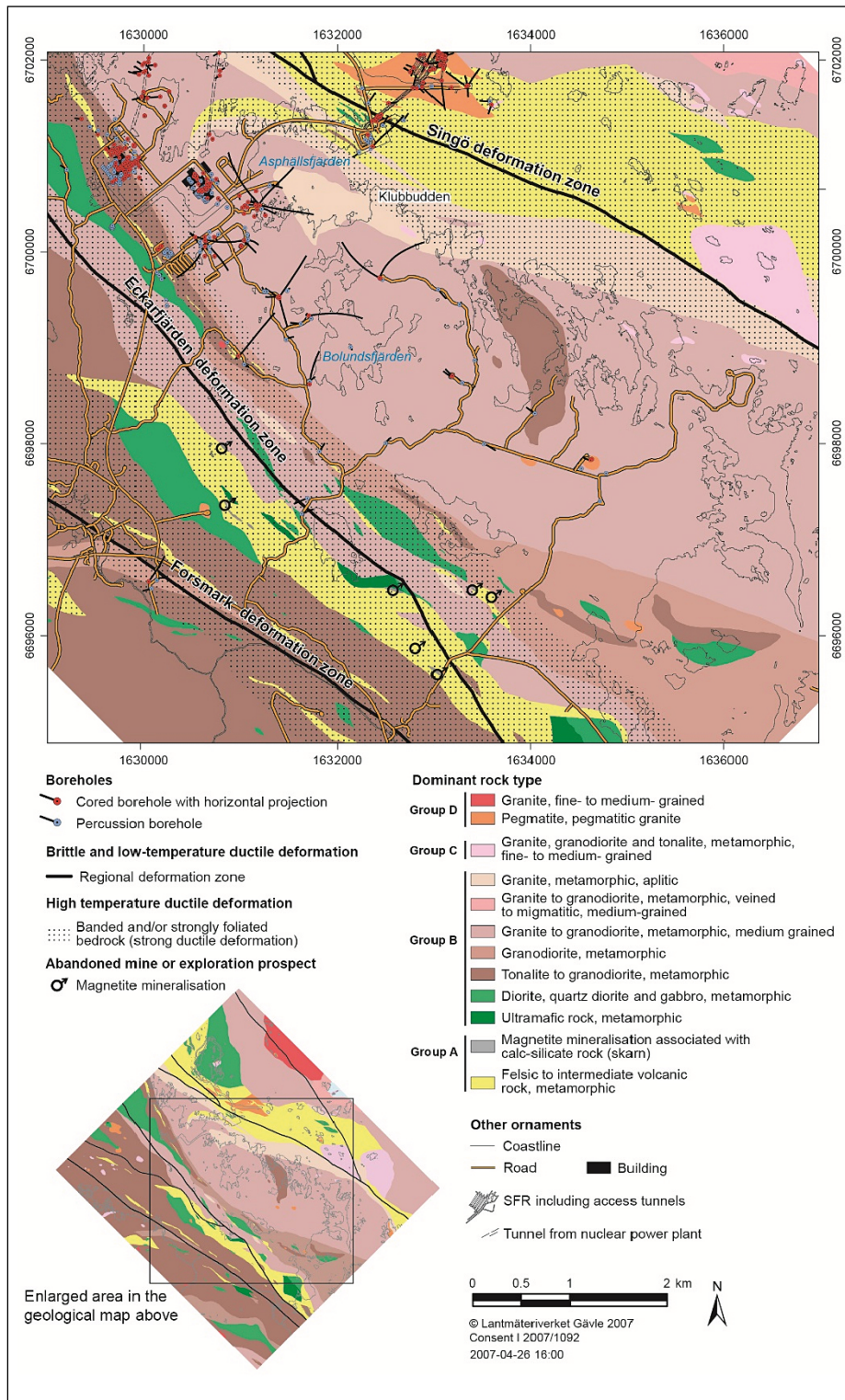
Figure 4-2. *Bedrock geological map of the investigation area at Forsmark modified from Sidborn et al. (2010) by including all cored- and percussion holes up to and including HFM46 registered in Sicada in February, 2018.*

4.2　Deformation history

Various radiometric dating methods have been used to constrain the cooling ages of the Forsmark rocks (Page et al. 2004, 2007, Hermansson et al. 2007, 2008a, b, Söderlund et al. 2008, 2009). In combination with the fracture minerology, this dating has permitted the deformation to be divided into six episodes, the first being purely ductile.

The rocks in the Forsmark area display evidence of a protracted ductile deformational history, with the development of a penetrative fabric under amphibolite-facies conditions followed by folding on different scales between 1.87 and 1.86 Ga (Figure 4-3) (Stephens 2010). The rocks inside the Forsmark tectonic lens display a predominantly linear grain-shape fabric and folds that plunge moderately to the south–east. In contrast, the rocks in the ductile high-strain belts that surround the Forsmark tectonic lens (Figure 4-2) show a generally more intense planar and linear grain-shape fabric.

Between 1.85 and 1.8 Ga uplift to the 500 °C geotherm occurred, which is inferred to contribute to focusing of strain along more spatially constrained zones. Regionally significant structures with a trace length greater than 10 km at the current ground surface, including the Forsmark (WNW), Eckarfjärden (NW) and Singö (WNW) deformation zones, formed during this time (Figure 4-2 and Figure 4-4A).

Cooling to the 300 °C geotherm occurred between 1.8 and 1.7 Ga, possibly initiating brittle deformation during the latest part of the Svecokarelian orogeny (Söderlund et al. 2009, Stephens 2010). Two more significant local structure sets inside the Forsmark tectonic lens formed during this time (Figure 4-4B). They strike ENE−WSW or NNE−SSE and are steeply or gently dipping fracture zones. Between 1.7 and 1.6 Ga the structures continued to develop (Figure 4-4C), possibly in response to the Gothian orogeny (Stephens et al. 2007). Cooling beneath the c 225−200 °C geotherm occurred between 1.6 and 1.5 Ga (Stephens 2010).

Brittle deformation continued as a far-field response to Sveconorwegian tectonic activity between 1 100 and 900 Ma (Figure 4-4D). There is evidence for several relatively minor brittle deformation events after the establishment of the sub-Cambrian peneplain, probably during the Phanerozoic (Stephens et al. 2007). Some reactivation of fractures is occurring under the current stress regime (Figure 4-4E) (Stephens et al. 2007).

A summary of palaeostress field reconstruction using site-by-site and merged data sets from outcrops and oriented drill cores is provided by Saintot et al. (2011) as follows:

Transpressive deformation with a regional NNW–SSE maximum stress axis, associated with clockwise stress deviation inside a tectonic lens, resulted in dextral slip along regionally significant, steep WNW–ESE and NW–SE deformation zones. The semi-brittle and most of the brittle structures, including specifically the epidote-bearing fractures, were established during this oldest regime around 1.8 Ga (latest Svecokarelian). A younger palaeostress field with a NE–SW maximum stress axis, which was also transpressive in character, is inferred to have been active at 1.7–1.6 Ga. The best defined palaeostress field is transpressive in character with a WNW–ESE maximum stress axis that resulted in sinistral reactivation along the WNW–ESE and NW–SE zones. The main set of laumontite-stepped faults developed at this stage at 1.1–0.9 Ga (Sveconorwegian). It is impossible to exclude fully the influence of reactivation during even younger Phanerozoic tectonic events. A similar deformation history has been interpreted at Olkiluoto (Mattila and Viola 2014) across the Gulf of Bothnia.

This conceptualisation of the deformation history at the site provides context for interpretation of fracture orientations, size distribution and terminations, and can potentially be used in genetic fracture generation methods.
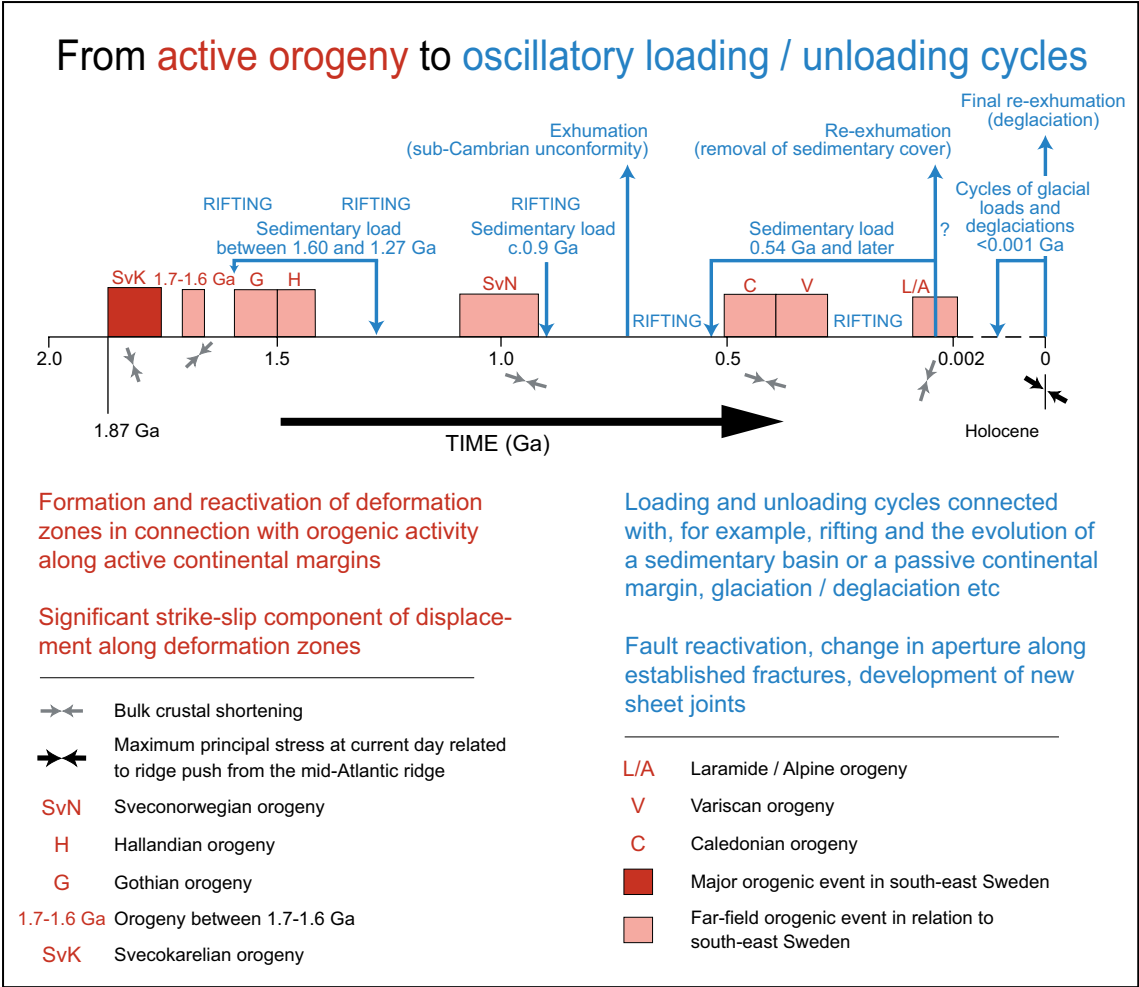
Figure 4-3. *Tectonic activity (red) and oscillatory loading and unloading cycles (blue) from 1.9 Ga to the Holocene in the Fennoscandian Shield in the south–eastern part of Sweden (Stephens 2010).*

A) Activation of zones
Late Svecokarelian (after 1.85 Ga)
Low-T ductile and brittle deformation
Zones follow anisotropy in bedrock related to high-T ductile deformation
Generation 1 minerals
Epidote-quartzchlorite-hematite dissemination

B) Activation and reactivation of zones - stage 1
Late Svecokarelian (after 1.80 Ga)?
Brittle deformation
Generation 1 minerals
Epidote-quartz-chlorite-hematite dissemination
Gently dipping zones follow orientation of contacts to rock units in more gently dipping parts

C) Activation and reactivation of zones - stage 2
Gothian (1.70 –1.60 Ga)?
Brittle deformation
Generation 1 minerals
Epidote-quartz-chlorite-hematite dissemination
Gently dipping zones follow orientation of contacts to rock units in more gently dipping parts

D) Activation and reactivation of zones - stage 3
Sveconorwegian (1,100–900 Ma)
Brittle deformation
Generation 2 minerals
Adularia-prehnite-laumontitecalcite-hematite dissemination (Sveconorwegian and/or pre-Sveconorwegian)

E) Quaternary (after c. 2 Ma)
Minimum principal stress=vertical
Maximum principal stress=140°, horizontal
Generation 4 minerals
Clay minerals-calcite
Also formation of open, sheet joints without minerals or filled by glacial sediment close to surface

Deformation Zone:
— Considerable change
— Moderate change
— Restricted change
⌇ Steeply dipping, transform motion
◄ Gently dipping

➤ Bulk crustal shortening
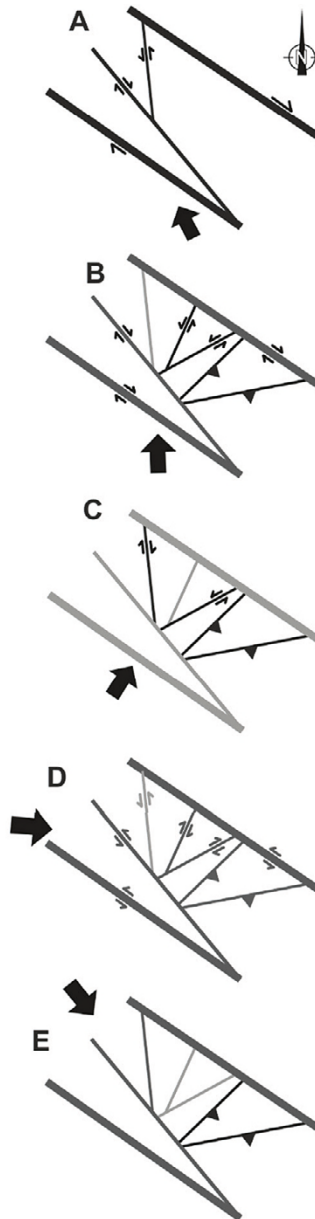
Figure 4-4. *A series of cartoons showing the conceptual model for the activation and reactivation of regional scale deformation zones around Forsmark in response to far-field tectonic activity, and associated fracture fill minerology. The WNW and NW striking deformation zones correspond to the Forsmark, Singö, and Eckarfjärden deformation zones (Figure 4-2). The different generations of minerals are referred to in Section 6.7. Adapted from Stephens et al. (2007).*

4.2.1 Mineralisation chronology

The walls of natural fractures are rarely clean unaltered surfaces defining open apertures, more often mineralisation occurs on the surfaces due to fluid-rock interactions. On the long timescales of shield rocks, filling materials within fractures may undergo several phases of mineralisation, deformation and re-equilibration, or paragenesis. Identification of fracture minerals and textural characterisation both visually (mm scale) and instrumentally (mm scale e.g. microscopy, X-ray diffraction) can be used to infer the order of formation of associated minerals in geological history and the hydrothermal conditions under which they have formed or re-equilibrated.

Fracture mineralogy, i.e., description of fracture filling materials and coatings are available from core description as input to interpretations of deformation history (Section 4.2), descriptions of fracture openings (Section 6.7), fracture mechanical stiffness (Chapter 6) and water-rock interactions (Chapter 8). Four generations of fracture minerals have been identified, as described below after Stephens (2010), as detailed in Table 4-1.

Table 4-1. Summary of the paragenesis of mineralogy at Forsmark, summarised from Sandström et al. (2008b).

Generation	Dominant Minerals	Formation Temp. (°C)	Comments
1	Epidote, chlorite, quartz	> 200	Dominated by fractures sealed with hydrothermally precipitated epidote, quartz and Fe-rich chlorite. This generation formed between 1.8 and 1.1 Ga and is possibly related to late Svecokarelian and/or Gothian tectonothermal events.
2	Adularia, prehnite, laumontite, chlorite, calcite, hematite	~150–280	Consists of a sequence of hydrothermal fracture minerals particularly common along steep, ENE–WSW to NNE–SSW and NNW–SSE fractures. Consists of both reactivation of older fractures and formation of new fractures
3	Quartz, calcite, pyrite, corrensite, adularia, analcime, asphaltite	~50 – 190	Consists of minerals precipitated under low-T conditions during the Palaeozoic. Stable isotopes in calcite and the presence of asphaltite indicate that the formation fluid was influenced by organic material. The orientation of fractures with generation 3 minerals suggests reactivation of fractures filled with older minerals but new fractures were also formed.
4	Clay minerals, chlorite, calcite, ± pyrite, ± FeOOH	< 50	Dominated by chlorite/clay minerals and thin precipitates of calcite in predominantly hydraulically conductive fractures. These minerals are prominent along sub-horizontal and gently dipping fractures but are also present in different sets of steeply dipping fractures. Most of the hydraulically conductive fractures are ancient structures.

The first generation of fracture minerals (generation 1) consists of epidote, quartz and chlorite. The key mineral epidote occurs along cataclastic faults that formed during ductile to brittle conditions (Figure 4-4) and along fractures with solely brittle deformation, all of which are either steeply dipping with an approximately NW−SE strike or are gently dipping. Epidote is also present along fractures in the other steeply dipping sets that strike approximately NE−SW (with ENE−WSW and NNE−SSW sub-sets) and NNW−SSE. Radiometric dating in the Forsmark region infers precipitation of generation 1 minerals between 1.8 and 1.1 Ga, in particular during the late Svecokarelian orogenic stage at 1.8−1.7 Ga. South of Forsmark, alternative radiometric data has yielded ages in the time interval 1.6 to 1.5 Ga (Wickman et al. 1983).

The second generation of fracture minerals (generation 2) is a sequence of hydrothermal minerals that consists of an early phase of hematite-stained adularia, albite and calcite, followed by prehnite and calcite, and a late phase of hematite-stained laumontite, calcite and chlorite/corrensite. The generation 2 minerals are associated solely with brittle deformation in the bedrock, commonly along sealed fractures. Radiometric dating indicates that the generation 2 minerals formed either prior to or during the early part of the Sveconorwegian orogeny (Sandström et al. 2008a, 2009, Söderbäck 2008).

The third generation of fracture minerals (generation 3) is dominated by euhedral quartz, calcite and pyrite with several secondary minerals. The generation 3 minerals are associated solely with brittle deformation in the bedrock and occur along both sealed and open fractures. Generation 3 pyrite and asphaltite are conspicuous along NE−SW steep fractures, along gently dipping or sub-horizontal fractures, particularly at an elevation above approximately −150 m (masl), and along fractures in the other steeply dipping sets (Sandström et al. 2008a). A Palaeozoic age (0.5−0.3 Ga) has been supported by radiometric dating, possibly corresponding to a far-field response to the Caledonian orogeny or due to burial/denudation in response to the development of a Caledonian foreland basin.

The fourth and youngest generation of fracture minerals consists of clay minerals and calcite with subordinate pyrite and goethite. The generation 4 minerals coat open fractures, either as the outermost mineral layer or as a single layer and occur along brittle structures that are hydraulically conductive at the current time. The generation 4 minerals also formed during the Phanerozoic. However distinguishing generation 4 clay minerals from clay minerals formed during earlier generations has proven challenging (Sandström et al. 2008a, 2009).

Hematite dissemination (oxidation) and albitisation are by far the most abundant types of rock-wall alteration at the Forsmark site. Volumetrically subordinate, but nevertheless conspicuous alteration that involves quartz dissolution and the development of episyenite is also present. Hematite alteration, evident as red staining can be extensive in areas of increased fracture intensity.

High spatial resolution *in situ* Rb-Sr dating has been applied to secondary mineral slickenfibres in faults at Forsmark following the methodology presented in Drake et al. (2017)) and Tillberg et al. (2020), see Figure 4-5. Fine-grained secondary assemblages of illite and/or K-feldspar together with co-genetic calcite in the outermost part of the slickenfibres (growth steps) in sub-horizontal and sub-vertical faults were targeted with 50 μm laser ablation triple quadrupole inductively coupled plasma mass spectrometry analyses (LA-QQQ-ICP-MS). The ages obtained from five samples disclose slickenfibre growth at several occasions spanning over 1 billion years: Proterozoic; $1\,527 \pm 28$ Ma (KFM08A, DZ4), $1\,438 \pm 33$ Ma, $1\,074 \pm 74$ Ma (both from a sample in zone ZMF1203, KFM07A) and Paleozoic; 399 ± 5 Ma, 392 ± 19 Ma (both from ZFMA2 in KFM01B and KFM04A intercepts) and 349 ± 9 Ma (KFM06C, DZ1). Tensile conditions are indicated by mineral growth at $355+/-14$ Ma (U-Pb dating of Calcite-Potassium feldspar at Forsmark borehole KFM04A: 306 m depth), and $173+/-8$ Ma (calcite in KFM06C:103 m depth).

The association between fracture minerals and adjoining rock mass alteration for the purposes of transport modelling has been evaluated by Byegård et al. (2008), see Subsection 9.1.5. How minerals may be spatially distributed with respect to deformation zones, fractures, rock domains and depth are also discussed in Subsection 9.1.5.
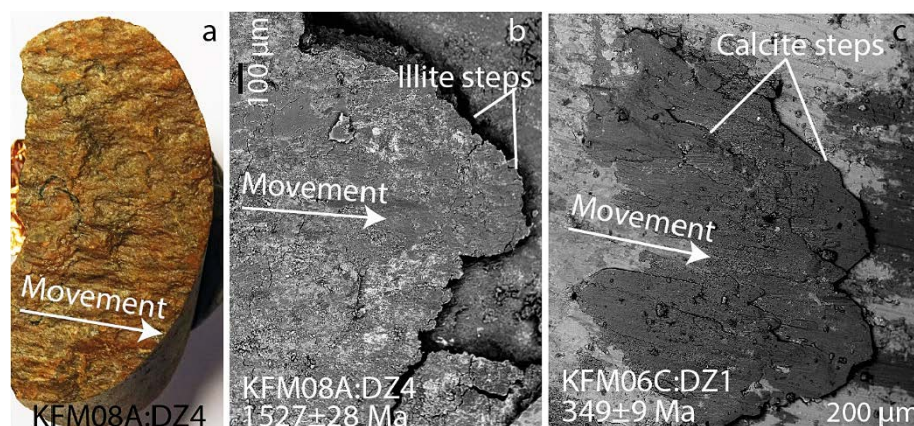
Figure 4-5. *Examples of shear striae (slickenfibres) that were dated using the Rb-Sr method (Photo: Henrik Drake, pers. comm).*

4.3 Current state of geological models

As part of the geological site description, the bedrock has been categorised according to properties of the intact rock and structures. The intact rock being divided according to rock domains (RD), while structures have been used to define volumes associated with deformation zones (DZ). As of SDM-site fracture domains (FD) were defined mainly on the basis of fracture orientations and intensities, but also considering stress magnitudes, rock geochemistry and hydrogeochemistry as additional supports. These divisions of the rock have been applied in boreholes and at the surface, and then represented by deterministic *3D* models as input to the SDM-Site stage of DFN modelling.

4.3.1 Deformation zone model

Surface mapping and borehole data in the Forsmark region have been used to identify deformation zones. These are tabular structures in which there is a concentration of brittle, ductile or combined ductile and brittle deformation. A local-scale *3D* model of these deformation zones has been constructed (Figure 4-6) with the aid of geophysical methods to extrapolate the deformation zones between other data points and beyond when possible. The latest published deformation zone model is version 2.3 (Stephens and Simeonov 2015). An update of this model is ongoing (September 2019) and accessible in SKB's model database SKBMod with access number "1705366-DZ Forsmark DMS 2018:2". The deterministic structures within the model include the kilometre scale composite ductile and brittle, WNW−ESE or NW−SE deformation zones (Singö and Eckarfjärden) that surround the Forsmark tectonic lens (outlined in Figure 4-4), and three other sets of zones interpreted inside the lens resulting from the focused deep drilling in that area.

The two most common sets of facility-scale deformation zones inside the Forsmark tectonic lens strike ENE−WSW to NNE−SSE and are steeply or gently dipping, respectively (Stephens and Simeonov 2015). Subvertical, NNW−SSE oriented zones represent the third, less frequently occurring, set in the Forsmark tectonic lens.
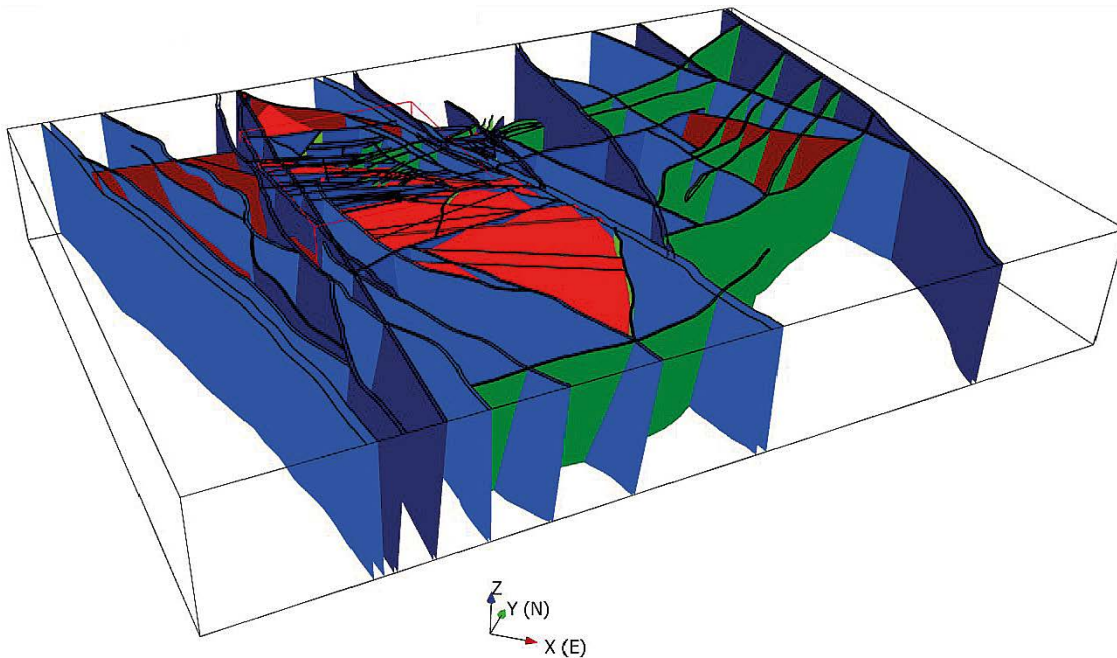
Figure 4-6. *Local-scale 3D model that shows the deterministically modelled deformation zones in the most recent model version. Note that the concentration of vertical and steeply dipping zones in facility scale region is primarily an artefact of the focused investigation in that area.*

4.3.2 Lithological model

For *3D* modelling purposes, the Forsmark bedrock has been divided into different rock domains, differentiated by a combination of the rock composition, grain size, degree of bedrock homogeneity, and degree and style of ductile deformation (Stephens et al. 2007, Stephens 2010), see Figure 4-7.

Legend:
- ■ Regional deformation zone
- ■ Granite, fine- to medium-grained
- ■ Granite, granodiorite and tonalite, metamorphic, fine- to medium-grained
- ■ Aplitic granite, medium-grained granite and felsic volcanic rock, metamorphic and, in part, albitised
- ■ Granite to granodiorite, metamorphic, medium-grained
- ■ Tonalite and granodiorite, metamorphic
- ■ Diorite, quartz diorite, gabbro and ultramafic rock, metamorphic
- ■ Felsic to intermediate volcanic rock, metamorphic and, in part, albitised
- ■ Sedimentary rock, metamorphic, veined to migmatitic

Figure 4-7. *Local scale 3D model for rock domains (numbered) and regional deformation zones (red colour) inside the regional model volume. View to the north. Rock domain RFM029R is unshaded to show the major folding within the tectonic lens at the Forsmark site. Other domains are unshaded to show the south–eastern elongation of several domains. The dominant rock type in each domain is illustrated with the help of different colours (see legend). Image and caption from Stephens et al. (2007).*

4.3.3   Fracture domain model

A vital part aspect of DFN modelling is the decomposition of the model volume into Fracture Domains, FD, (see Chapter 5 for details). Fracture domains provide a framework for describing overall spatial heterogeneity in rock fracturing. The goal behind identifying fracture domains is to find rock volumes with fracture characteristics such that the statistical variability between volumes is larger than the intrinsic fracture variability within volumes (Munier et al. 2003, Darcel et al. 2012, 2013), in line with geologic best practice. As such, fracture domains should form the basic divisions over which spatial heterogeneity in rock fracturing is characterised but may not, necessarily, correspond to the limits of other geologically-significant volumes such as those defined in the Rock Domain (RD) model although this is generally the case. The resulting output of such domain analysis is a number of rock volumes within each a particular set of statistical laws apply to the fracture network (see Chapter 5 for details).

Based on mainly borehole data, six fracture domains (FFM) have been identified inside and immediately outside the proposed repository volume at Forsmark (Olofsson et al. 2007) using a combination of qualitative and quantitative assessment. Most of the site data are focused in FFM01, FFM02, FFM03 and FFM06. Differences in fracture intensity and orientation were important factors in defining the spatial extent of FFM01, FFM02 and FFM03, while FFM06 was differentiated from FFM01 mainly by lithology. These definitions were further supported by distinct hydrogeological and hydrogeochemical characteristics in the different domains. FFM04 and FFM05 had limited data from drilling, being discerned by geophysics to be outside the Forsmark tectonic lens, and with some indications of having different hydrogeological properties. A *3D* model of four of these domains (FFM01, FFM02, FFM03 and FFM06) was constructed where sufficient data permitted (Figure 4-8).
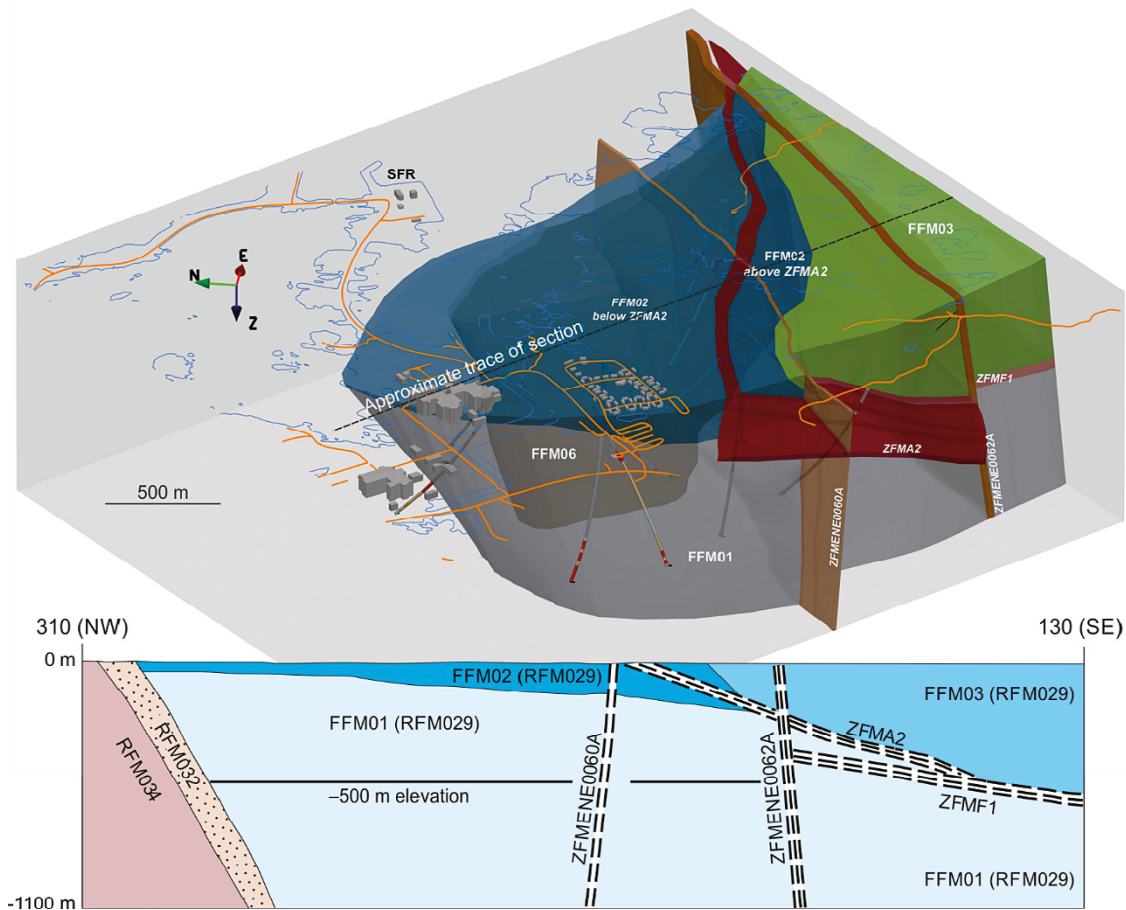
Figure 4-8. *A) Local scale 3D geometric model for fracture domains FFM01, FFM02, FFM03 and FFM06 in the north–western part of the Forsmark tectonic lens, viewed towards the east–north–east; B) Simplified NW–SE trending profile showing the same fracture domains. Only high confidence deformation zones ZFMA2 (gently dipping), ZFMF1 (sub-horizontal), FMENE0060A (steeply dipping, longer than 3 000 m) and ZFMENE0062A (steeply dipping, longer than 3 000 m) are included in the images. Images and caption adapted from Olofsson et al. (2007).*

In the uppermost c 100–150 m of bedrock in the region there is a set of sub-horizontal sheet joints that can, locally, be highly transmissive (Stephens et al. 2007, Follin 2008). The favoured explanation for the origin of these structures is the release of rock stresses during glacial unloading in the Quaternary (Stephens 2010). Martel (2011) points out that compression parallel to a convex surface can cause shallow subsurface fractures to open, and therefore sheet joints may form in areas of topographic curvature. This was also confirmed by Moon et al. (2017) in an application to Forsmark. Some of the shallow fractures including these sheet joints have been filled with glacial sediments (Carlsson 1979, Leijon 2005, Lönnqvist and Hökmark 2010, 2013, Hökmark and Lönnqvist 2014, Talbot 2014).

4.3.4 Geobody and geocellular modelling

Geological structures (e.g. deformation zones) and volumes (such as lithologies and fracture domains) can be bounded by triangulated surfaces enclosing "geobodies" as a representation of discrete objects. When doing spatial or numerical analysis of such objects it is often convenient to represent them on a common continuum grid where each geological property is defined for each cell storing, e.g. the predominant lithology in that cell, within which fracture domain it lies, or if it lies within a deformation zone. This is referred to as a "geocellular model". Rock mechanics properties, such as elastic moduli or stress tensors, can be stored as geocellular properties. Likewise, upscaled ECPM flow and transport properties can be represented on a geocellular properties.

For example, in SDM Site a local scale domain of 15 km × 11 km × 2.1 km was used and the fracture domains as input to DFN modelling were represented on geocells of side 20 m in the facility area, increasing to 100 m outside the focused characterisation area. ECPM models of flow and transport properties were then output for use in palaeohydrogeology calculations.

If the rock is relatively homogeneous, then it may be hypothesised that fracture patterns and spatial variability arises primarily from random processes of fracture nucleation and interaction, see Subsection 6.6.3, and that variability in intact rock properties has only secondary effects on fracture distributions, and hence can be neglected. In that case, there is no need to provide spatially varying inputs to the fracture generation process.

If, however significant correlations between fracturing and other geological properties and structures are apparent, then the spatial variability in the latter can be represented as either geobodies or geocellular properties and provided as inputs to fracture generation. For example, input parameters for mean fracture orientations, intensities, fracture propagation and stress can all be represented on geocells to condition local properties of the network.

4.4 Geological input to DFN

Here the DFN v2.2, from SDM stage 2.2 (Follin et al. 2007b, Fox et al. 2007b), is used to illustrate how geological models are used as input in constructing a site-descriptive DFN model.

- The deformation zone model was used to delimit volumes where fractures are influenced by the larger scale structures, separating them from background fractures in the intervening rock suitable for disposal. Different statistics were then inferred for fractures associated with the deformation zones, ZFMs, and those in the surrounding fracture domains, FFM. Noting the fracture domains are defined in an iterative process starting with geology but refined through DFN analyses and supported by information from other disciplines.

- The lithological model was mainly used as input to delimit appropriate fracture domains in combination with major deformation zones. Again, DFN analyses found relative homogeneity in fracture properties between lithologies, and hence several lithologies could be grouped within a fracture domain.

- Fracture properties were analysed separately for each fracture domain to derive distinct statistical models (Munier 2004, Olofsson et al. 2007, Darcel et al. 2012, 2013).

The deterministic deformation zone model has been updated in 2018 and is now (September 2019) referred to as "DMS 2018:2" (with SKBMod 1705366). The recent shallow drilling in the access area has also provided data to make some limited deterministic interpretation of sheeting joints in the upper part of the bedrock possible.

Once construction of the repository accesses begins, additional minor deformation zones are likely to be encountered, albeit whose extent will only be partly determined. This raises a new challenge in generating semi-stochastic deformation zones. This and other challenges integrating DFN and geological modelling are discussed further in Chapter 5.

4.5 Confidence and uncertainties

The significance of various uncertainties, propagated from the geological description, for the reliability of any DFN model is summarised in Table 4-2, along with potential mitigation options. The status of uncertainties in the geological model components is discussed below.

Uncertainties in the spatial distribution of rock domains inside and immediately around the target volume as of SDM v2.2 are considered to be low, see Section 4.6 of Stephens et al. (2007). Significant uncertainties concerning the rock domains beneath the sea remains.

The most significant uncertainties in the deterministic deformation zone model, are considered inherent or stable, see Section 5.6 of Stephens et al. (2007) for version 2.2 and Section 5.3 of Stephens and Simeonov (2015) for version 2.3:

- The presence of undetected deformation zones;
- The character of the deformation zones inferred from lineaments;
- The length and down-dip extension, the dip and the thickness of deformation zones interpreted with the help of linked lineaments; and
- The length and down-dip extension, and the thickness of the gently dipping zones that are based, to a large extent, on the seismic reflection data.

Additional zones have been interpreted and geometries of existing modelled zones have been refined with new data, but the above uncertainties will essentially remain. The 2018 deformation zone model has been updated based on the *3D* seismic survey and the new drilling 2011–2016.

Table 4-2. List of uncertainties pertinent to the production of a DFN based on the Forsmark geology, a description of their significance and possible options for mitigation of these uncertainties.

Uncertainty	Cause	Effect	Potential Mitigation Options
The borehole data have uneven coverage.	Drilling has been focused on the repository volume and limited to maintain the integrity of the rock barrier.	Modelling involves extrapolation/ interpolation over large distances, to the cost of not capturing local variability.	*3D* seismic data provide a more uniform coverage to identify deformation zones within the acquisition volume. New boreholes will be drilled in the access areas at closer spacing to give more information on scales of variability.
Fracture mapping on cores and borehole imagery suffers from orientation bias.	The intersection probability between a borehole and a fracture is dependent on their dihedral angle. Borehole orientation and location uncertainties affect interpreted fracture orientations.	Fractures intersecting the borehole with small intersection angles are under-represented. Geometric borehole uncertainties result in larger spread of orientation sets.	Employ procedures for correction of orientation bias, using different algorithms and assumptions. Propagate borehole orientation uncertainties to fracture orientations. Employ multiple borehole deviation measurements.
Only a subset of deformation zones will be detected, most of which will be located in the repository volume.	Data from geophysics have a certain resolution and is biased toward vertical zones. Drilling is limited to a few locations.	Smaller scale deformation zones have to be generated stochastically in the repository volume, and a broader size range of deformation zones have to be generated on the local-scale.	DFN models need to generate stochastic deformation zones between the known deterministic deformation zones using consistent rules for their interactions.
The thickness of deformation zones.	Defining the extent of damage zones can be subjective and depend on application, e.g. difference between geologic and hydraulic definitions.	The thickness effects the division of the modelled rock into FD and DZ and, hence, the statistical representation of fractures within each. The assigned thickness also affects the connectivity of structure-related networks.	Determine rules for deciding thicknesses using combination of geologic-, geophysical- and hydraulic data from boreholes. Investigate variability in thickness between boreholes, and correlations with size.
The extent of deformation zones.	The down-dip extent of zones is very uncertain when based on lineaments or seismic reflection.	It is difficult to model the connectivity of the deterministic structures, and the analysis of their size distribution is biased.	Reprocess and analyse *3D* seismic data. Rules based on stochastic modelling of the extent of zones. Testing of assumptions against hydraulic interferences and disturbances during construction.
The extent of fracture domain FFM02.	Casing of boreholes in top 100 m. The lateral extent of sheet joints is uncertain.	The spatial extent of the more intense and connected upper bedrock is uncertain.	Analyse the 2011–2016 boreholes from the access areas to evaluate different DFN variants for FFM02.
Rock heterogeneity in the repository volume.	No horizontal drilling at depth yet.	Unknown how much heterogeneity there is in fracture intensity and if this correlates with geology.	Analyse borehole data from pilot holes during construction of ramp and technical facilities.

5 Describing spatial variability

This chapter presents the hierarchical approach to describe different parts of the fracture system as sketched in Figure 2-2 and how spatial variability within each part can be represented. The bedrock volume is subdivided according to the following hierarchy:

1. Deterministically modelled deformation zones (**DGMM**), each defined as either tabular volumes or surfaces with fixed extent. Where they are tabular their thickness is fixed and typically contain fracturing of relatively high intensity.

2. The rock mass between deformation zones that is divided into fracture domains that displaying consistent structural, hydrogeological and hydrogeochemical characteristics within each domain. The boundaries of fracture domains are coincident with deterministically modelled surfaces: deterministically modelled zones, lithological boundaries or bedrock topography. The fracture domains are modelled to contain stochastic and semi-stochastic structures ranging in size from individual fractures to minor deformation zones.

Modelling a geological structure deterministically, e.g. a deformation zone, requires a high density of information, which involves a need for high spatial density of sources of information such as boreholes, geophysics, surface or tunnel mapping. Even then, the areal coverage of the data must be large in relation to the size of the modelled object to accurately define its extent in *3D*, a requirement typically fulfilled for the largest structures in the model. However, if a structure unequivocally identified as a deformation zone, is only recorded at a single or at a few locations without further information to confirm its lateral extent, it needs to be modelled semi-stochastically to reflect the uncertainty in its size, and termination rules to other objects must be assumed or inferred from information gathered elsewhere. That is, its geometry is constrained at one or more locations but its extent and thickness at distance from the intersections is inferred from some combination of probabilistic descriptions. This is particularly relevant to **minor deformation zones** with their (interpreted) limited lateral extent. Thus, a minor deformation zone is positively demonstrated to have hosted deformation (e.g. using kinematic markers, alteration or other proxies (e.g. Cosgrove et al. 2006)) but its lateral extent is uncertain. It follows then that minor deformation zones need to be modelled stochastically in model volumes that contain no boreholes, tunnels or outcrops.

Other observations may not be sufficiently pronounced to uniquely denote them as intercepts with a deformation zone. Examples of such are e.g. observations of increased fracture intensity in a borehole but being devoid of kinematic or other markers of deformation. For reasons of conservativeness, such observations are used for the modelling of so-called **possible deformation zones**. As larger deformation zones are rarely, if ever, geologically indiscernible, especially not in old cratonic rocks such as those dominant in Fennoscandia, intercepts denoted possible deformation zones could be minor, immature zones. The number of intercepts with minor- and possible deformation zones should match the size-intensity relation of the DFN model or provide input to such, with due respect to the uncertain nature of possible deformation zones. In practice this means that possible deformation zones can be regarded as a subgroup of minor deformation zones and, hence, modelled semi-stochastically as such.

Minor deformation zones will also exist undetected beyond the investigated rock volumes and these need to be modelled there stochastically in order to obtain a geologically plausible structural model over the scale of interest. Therefore, minor deformation zones will likely be modelled semi-stochastically within the focused characterisation area, covered by boreholes and underground openings, and stochastically beyond.

The hierarchy above not only reflects different approaches to how different structures are modelled, e.g. deterministic, stochastic and semi-stochastic, but also how the data are partitioned to characterise volumes with potentially different statistical properties. The data from borehole intervals or mapped rock surfaces corresponding to each of these volumes are subdivided accordingly to facilitate data analysis specific to each volume so that each volume can potentially be conceptualised and parameterised as separate populations.

Another hierarchy to be considered is the distinction between large single fractures and minor deformation zones. A partly determined large single fracture may be modelled semi-stochastically, sampling from property distributions (e.g. size) for the fracture domain in which the fracture is observed. Whereas a minor deformation zone may be modelled using the description of fracturing within deformation zones, treating it as an individual (new) fracture domain and parameterising it as an explicit DFN.

The approach is illustrated in Figure 5-1. The rock and its constituent fractures (Figure 5-1a) are analysed in terms of statistical homogeneity. Rock volumes within which the variability for a chosen set of fracture properties is smaller than in adjacent rock volumes are defined as fracture domains. These fracture domains host DFN models that aim to honour the fracture characteristics sampled during site investigations. The modelled boundaries of fracture domains can be geological structures, e.g. deformation zones (Figure 5-1b) or rock contacts, the bedrock or ground surface (the upper boundary of FD3 in Figure 5-1b,c) or an interpreted boundary such as the lower boundary of FD3 in Figure 5-1b,c. Artificial boundaries are necessitated by sometimes diffuse transitions of a property, for example the fracture intensity. Similarly, the boundaries of deformation zones can be difficult to outline, especially if the zone is surrounded by a prominent damage zone (Kim et al. 2004, Choi et al. 2016). Nevertheless, deformation zones can themselves be defined as fracture domains (Figure 5-1c) with their own specific set of fracture properties, as a basis to generate individual fractures within them, or modelled as sub-planar surfaces with effective properties that somehow reflect the cluster of fractures they represent. The choice depends on the level of detail required and processes of interest. Modelling swarms of fractures may be appropriate for tunnel scale stability, flow or transport simulations, but perhaps unnecessarily elaborate for regional- or local-scale bulk flow calculations. In that case, deformation zones can be represented by triangulated surfaces with properties such as transmissivity defined on the scale of the triangles, spatially varying to represent gaps in continuity or changes in stress with depth, for example.

This chapter gives a general introduction on the approach to identifying and describing boundaries for each type of domain. Chapter 5 provides general theories and methods for describing fracturing.
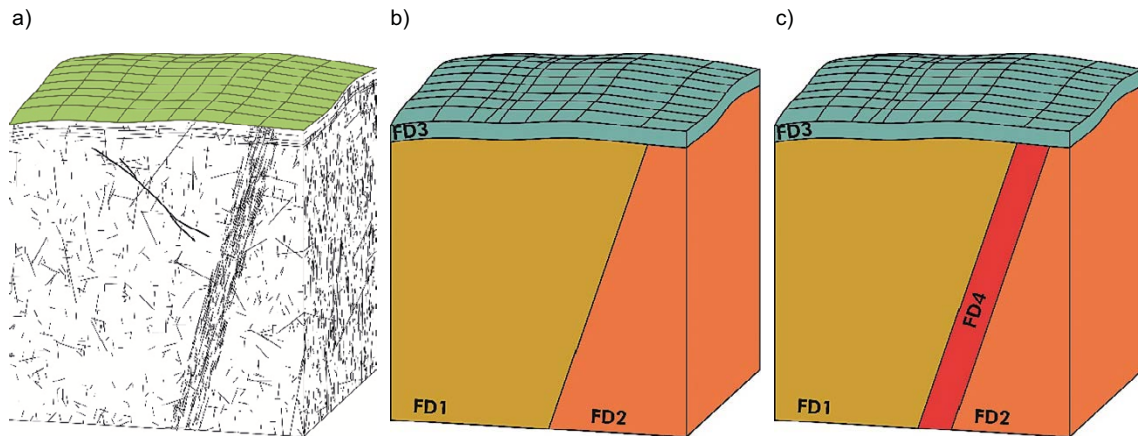

Figure 5-1. *Illustration of the fracture domain concept. See text for further explanation.*

5.1   Homogeneity, spatial variations and anisotropy

The use of "homogeneity" can be ambiguous in the context of geological- and stochastic DFN modelling, whether applied to qualification of a model, a geological process or geological datasets and observations. Strictly homogeneity is uniformity – i.e., a property is constant within a volume (e.g. domain), but this definition is too restrictive within the context of DFN modelling. We aim to clarify this below.

A simple DFN model, over a given domain, can be defined by a single, therefore constant and homogeneous, intensity value (e.g. over the domain volume, the fracture surface per unit volume is equal to X). The density value is coupled to a continuously uniform spatial probability density function (Figure 5-2) as a starting point of the stochastic generation process.

When going a step further, a DFN generated from such a model will display local spatial variations of any volume-average property measurement (e.g. number of fracture, or fracture surface, per unit volume), simply due to the DFN discrete nature and to the stochastic generation process. The magnitude of these variations decreases with increasing averaging volume size, in a manner that can be modelled. In such a case, while the observed property (on the generated DFN) is never truly constant, the fluctuations can be too small to be detected, or below a given "acceptable" variation threshold defined by modelling purposes, or be modelled as an outcome from the stochastic generation process if the model is known (e.g. Lavoine et al. 2020). Then the DFN model is denoted homogeneous, and by extension the property under consideration may be considered homogeneous above a certain sampling size. The expression "statistically homogeneous" is also used to refer to this combination between uniform underlying density distributions and stochastic generation processes.

In realistic conditions, and for scales relevant to site modelling requirements, geological- and DFN properties are always more variable than can be predicted by an underlying uniform probability density distribution model. Moreover, realistic density distribution models are commonly described as non-uniform (e.g. a Correlated Random Field with finite correlation length, Figure 5-3), non-stationary (e.g. fractal) or anisotropic (e.g. different model parameters in different directions, Figure 5-4). Therefore, even if a single or a few constant parameters define a density distribution model, the resulting spatial distribution of the density model may be spatially variable, and the DFN realizations even more variable, due to additional variability linked to the stochastic generation processes. Still in such conditions, the term homogeneous may be used if the spatial variations are below a certain threshold.

This is illustrated further with the following examples:

- When spatial variations decrease with increasing sampling volume size, fracture density might be considered homogenous on the scale of a larger rock volume but at the scale of the fracture, the density is highly heterogenous; the fracture either exist or it does not, with no intermediate state.

- Figure 5-3 shows three spatial distributions of a rock property (e.g. quartz mineralization in the rock) over a given volume. Each distribution in Figure 5-3 is defined from a Correlated Random Field (CRF) model defined by a mean, a standard deviation and a correlation length (λ). In the three examples, only the value of λ changes. When the volume over which the property is averaged is increased, the resulting value tends towards the theoretical mean of the distribution with less and less fluctuations. The local fluctuations are linked to the parameters of the model(s) (standard deviation and correlation length). The distributions are not themselves spatially uniform, but their resulting property tend to become homogeneous above a certain sampling size scale.

- Stationary density distribution models will tend to the above defined homogeneity of a property, when the averaging volume scale is much larger than the correlation length of the density distribution.

Finally, spatial fluctuations and homogeneity (as defined above) may be different depending on the direction of investigation. For example: Most fracture systems display preferential orientations; fractures and deformation zones are themselves highly anisotropic structures; the bulk rock strength (and other bulk properties) may be anisotropic, steered by e.g. foliation; the fracture aperture is different parallel to- than perpendicular to shear. This is illustrated in Figure 5-4 where the anisotropic nature of a rock property is increased due to an increased correlation length in one direction compared to the others.
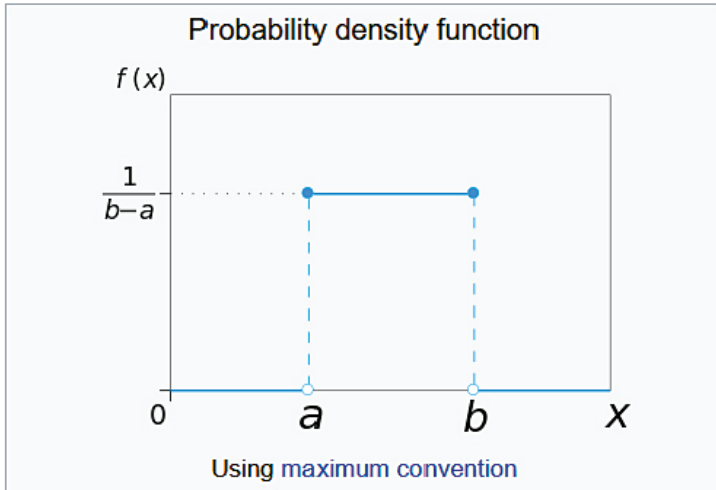
Figure 5-2. *Recall of the simple mathematical expression of a continuous uniform probability density distribution over one direction and for a spatial range [a;b].*
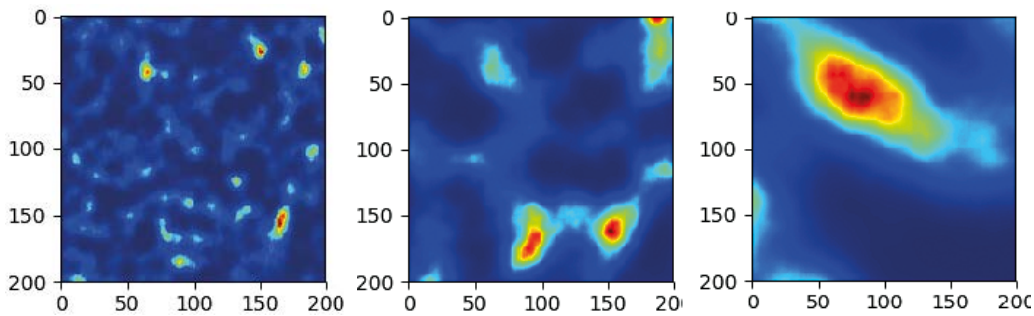
Figure 5-3. *Spatial distribution based on correlated random field with correlation length λ. From left to right λ = 20, 60 and 140.*
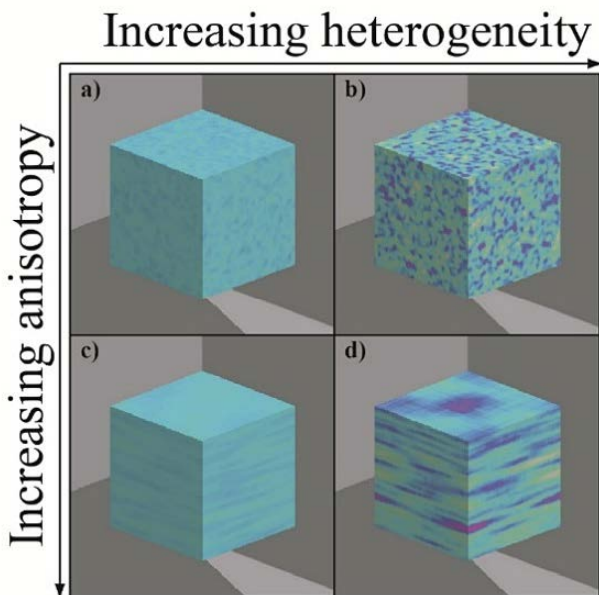
Figure 5-4. *Model realization of volumetric distribution of a hypothetical rock property. From left to right the intensity of the variations increases. From top to bottom the anisotropy increases with an increased correlation length in one direction.*

5.2   Variability within deformation zones

Brittle deformation zones are essentially two-dimensional structures (sub-planar structures with a small thickness relative to their lateral extent) along which there is a concentration of brittle, ductile or combined ductile and brittle deformation. In crystalline rocks, fault cores with associated damage zones can form preferential groundwater pathways with both the fault zone structure and the deformation history of the fault having a considerable impact on its hydraulic properties. Caine et al. (1996) in their description of fault zone architecture and permeability structure define the fault core as the "*lithologic, and morphologic portion of a fault zone where most of the displacement is accommodated*" and may include: "*single slip surfaces; unconsolidated clay-rich gouge zones; brecciated and geochemically altered zones; or highly indurated, cataclastic zones*". Typically, the propensity of the fault core to support groundwater flow is a function of the grain-scale of rocks with smaller grain sizes and/or mineral precipitations resulting in lower permeabilities whereas fault cores with larger grain sizes or intense fracturing tend to be more permeable. The damage zone, according to the definition of Caine et al. (1996) comprises a "*network of subsidiary structures that bound the fault core and may enhance fault zone permeability relative to the core and the undeformed protolith*" (wall rock). The damage zone will spread non-uniformly into the hanging and footwall of the fault and will be variable over the spatial extents of the deformation zone. Some examples of deformation zones are shown in Figure 1-17 and Figure 1-18. A schematic of the variable geometry of deformation zones at Forsmark is shown in Figure 5-5.

The hydraulic conductivity of the damage zone is controlled by the extent, intensity and hydraulic properties of its composite structures. Considering the evidence for reactivation of zones at Forsmark, it is likely that open or partly open fractures bearing groundwater will be most frequent in the damage zone, and likely located adjacent to the undeformed wall rock (Stephens et al. 2007). As such, deformation zones can be significant for flow and transport, affecting both the degree of connectivity and the available fracture surface area for diffusion and water-rock interaction processes. In addition, the spatial and orientation models within deformation zones have significance for dynamic mechanical effects and seismic hazards.
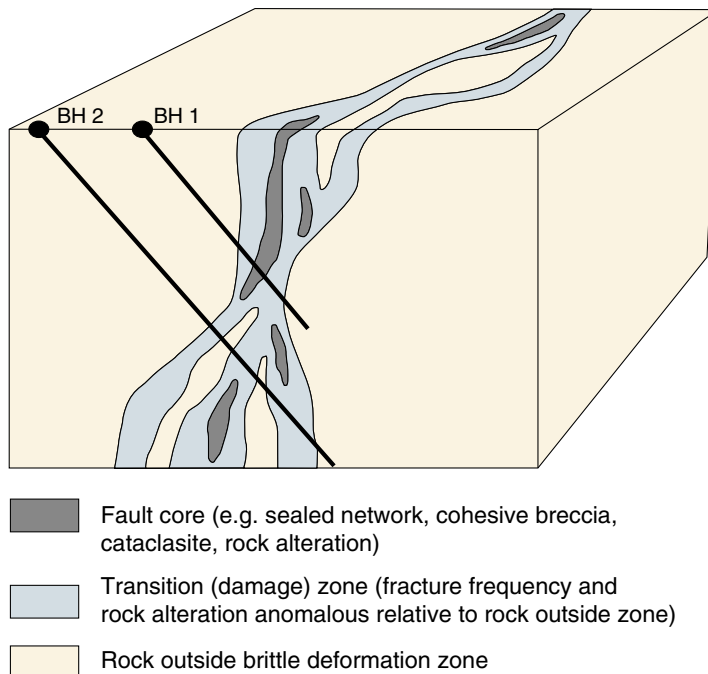
Figure 5-5. *Three-dimensional cartoon illustrating a conceptual geometric model for a brittle deformation zone at Forsmark along which shear displacement has occurred (redrawn after Caine et al. 1996). Note the variable character of the zone along the two borehole intersections. This figure is reproduced from Stephens et al. (2007).*

Each deterministically modelled deformation zone is essentially modelled as its own domain in which fracture data from boreholes and rock surfaces are isolated and analysed using the general methods described in Chapter 5 to derive a fracture conceptual model. Zones may be grouped according to orientation, size and/or deformation type (e.g. brittle, semi-brittle structures or sense of movement from kinematic indicators) to pool data for statistical analyses.

In Subsection 5.2.1 we discuss methods appropriate for describing zones modelled as sub-planar surfaces. The modelling of individual fracturing within deformation zones, modelled as tabular volumes, is discussed in Subsection 5.2.2.

5.2.1 Variability in deformation zone geometry

The description of the deformation zone structures involves analyses of their:

- Orientation, relative age, interaction (intersection/terminations) and kinematics (see Subsection 1.3.2),

- size of structures and their scaling,

- geometry and properties of zone core(s),

- geometry and properties of damage zone,

- thickness, correlation of maximum thickness and size and the variability in thickness,

- mechanical significance, effective properties,

- hydraulic significance, continuity and effective (mean) transmissivity, and

- alteration of the rock within and around the structure.

Of these, thickness, hydraulic properties and amounts of rock alteration can vary significantly between structures, but also across and along an individual structure.

Considering Figure 5-5 the thickness of the core and damage zone can be interpreted from borehole intercepts, with the damage zone thickness split between footwall and hanging wall thicknesses. Two separate damage zones develop on either side of a core with, usually, asymmetric thickness (Aydin and Johnson 1978). Asymmetry in fracture patterns can arise from differences in rock properties or from different stress conditions acting on the footwall and hanging wall respectively (Mandl 1988, 1999, Knott et al. 1996).

The core is characterised by anomalously high frequency of fractures, but also by cohesive breccia and cataclasite, while the damage zone may display moderately elevated fracture intensity and rock alteration. The variability in thickness between zones can be assessed by comparing the mean and maximum thickness for each zone and an assessment of whether this correlates with size and/or orientation. For example, a ratio of 100:1 damage zone thickness to length is proposed in Scholz (2002). For brittle fault zones at Olkiluoto, this was found to provide an upper estimate for width, with an alternative fit of width $\sim 11(Log_{10}(Length)-2)$ being used (Hartley et al. 2018b), such that zones essentially become single fractures below 100 m length and large faults have widths of a few tens of metres. The derived correlation can then be used to calculate an expected thickness for zones lacking measurements or by sampling the measured distribution if using a Monte Carlo approach.

Spatial variability of thickness within a zone can be analysed using variography (Matheron 1962) and interpolated using geostatistical methods (e.g. Matheron 1963, Isaaks and Srivastava 1989, Journel and Huijbregts 1991). Since this requires several boreholes or tunnels to intersect a deformation zone, this is likely only possible for a small number of large well-characterised deformation zones in the access area once the shafts and ramps have been constructed and in the deposition areas once several deposition tunnels and their pilot holes have been completed. The derived variograms can be used both to create conditioned realisations for the thickness of well-characterised zones or used as a proxy for generating realisations of spatial variability in other zones with few or no measurements. An example of this type of geostatistical method applied to Olkiluoto is given in Baxter et al. (2019).

Likewise, transmissivities of zones (see Chapter 8) can be described by geostatistical methods. The transmissivity of a structure as seen in a borehole intersecting is calculated from the sum of discrete flows measured within the damage zone or from a hydraulic packer test that straddles the zone. Hydraulic variability between zones can be assessed in terms of variations relative to size and set. However, because there is often a significant depth trend (Follin et al. 2007a, Follin 2008, Follin and Stigsson 2013), variations need to be calculated relative to this trend. As with thickness, geostatistics can be used to interpolate transmissivity over well-characterised zones or generate realisations of spatially varying transmissivity on those with few or no measurements. Variograms measure how much two samples will vary depending on the distance between those samples. An example of a variogram is given in Figure 5-6. The parameters defining the variogram are:

- Sill: The size of the maximum variance between two correlated points, as measured by the experimental variogram (height of plateau in Figure 5-6);

- Nugget: The size of the essentially random noise or measurement error that causes the appearance of a non-zero variance at zero or very small distance (intercept with the y-axis in Figure 5-6); and

- Range: The distance over which the variogram first reaches the sill in each of its major, medium and minor directions.

If correlations are more pronounced in one direction than another, i.e., anisotropic, the variograms can be derived for different directions, e.g. along the strike and down dip in a deformation zone.
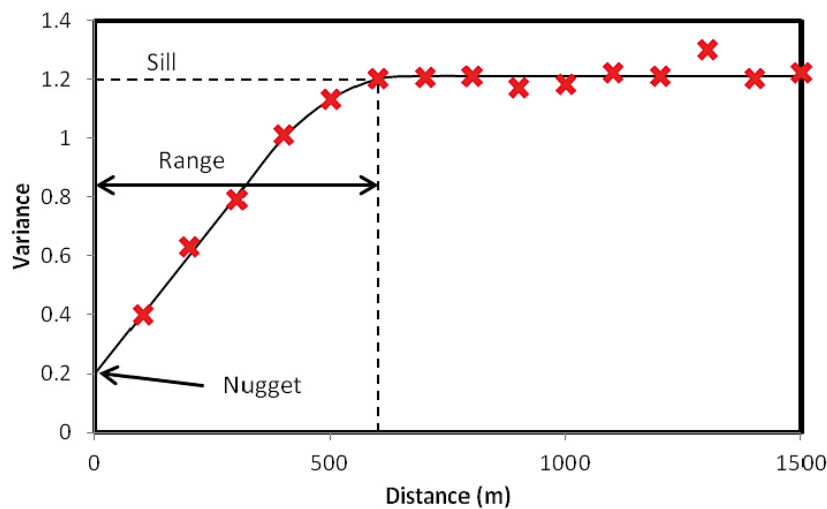
Figure 5-6. *Example variogram to transmissivity data in a single deformation zone. Here, a Gaussian variogram is used with sill 1.2, nugget of 0.2, and a range of 600 m (reproduced from Baxter et al. 2019).*

5.2.2　Variability of fracturing within deformation zones

The previous subsection covers methods appropriate for describing zones treated as sub-planar with effective properties. To model the individual fracturing within deformation zones modelled as tabular volumes, the following analyses need to be made:

- Outlining of deformation zone boundary. This may include division of the zone volume into subvolumes defining core(s) and damage zone(s).

- Orientations of fractures within the fracture zone domains, how these vary relative to the orientation of the general orientation of the structure.

- Intensity of fracturing within the fracture zone domains, how this varies with distance to the core plane (e.g. Du Bernard et al. 2002), between footwall and hanging wall and with elevation.

- Size distribution of fractures, from trace mapping in tunnels, within zones.

- Aperture, transmissivity and storativity of fractures.

- Morphology (roughness and undulation), mineralogy and alteration of fractures.

Fracture orientations within deformation zones typically differ from the rock mass because of localised displacement and stress conditions that have occurred. The orientations of fractures within the volume associated to the deformation therefore need to be analysed separately for each zone. Since deformation zones represent the most intensely fractured parts of the system in otherwise sparsely fractured rock, the local fracture patterns determine network connectivity and flow anisotropy. Often fracturing is locally sub-parallel to the general orientation of the structure (core), but there can also be obtuse angle fracturing.

To gain insight into the pattern of fracturing within a deformation zone domain it is appropriate to characterise the proportions of fractures that have dihedral angles less than 30º on either side of the main fault plane, and at dihedral angles 30º–60º, and > 60º. Decisions can then be made on an appropriate orientation model within each zone.

Fracture intensity as a function of distance to the fault core is another important measure controlling the connectivity of the fracture system within a zone (e.g. Du Bernard et al. 2002). Intensity commonly shows an exponential decrease with distance from fault core (Vermilye and Scholz 1998, Mitchell and Faulkner 2009) in brittle rocks corresponding to the decay of stress away from a fault tip as predicted from fracture mechanics models. This implies variations in properties across a damage zone shown illustratively in Figure 5-8. Fracture intensity relative to distance from core can be calculated from data including all fracture domains, inside and outside zones, and in fact can be used as input to determining damage zone extent where intensity decays to background levels. This relationship of intensity to distance to core can be calculated from borehole data for individual deformation zones or pooled amongst fractures of similar orientation or size. Fitting an exponential decay function, for example, to such data can then be used to generate fractures seeded around a fault core. It is a key parameter affecting connectivity of fracture swarms around deformation zones and an important parameter when calibrating models on large-scale hydraulic interferences (Hartley et al. 2018b).
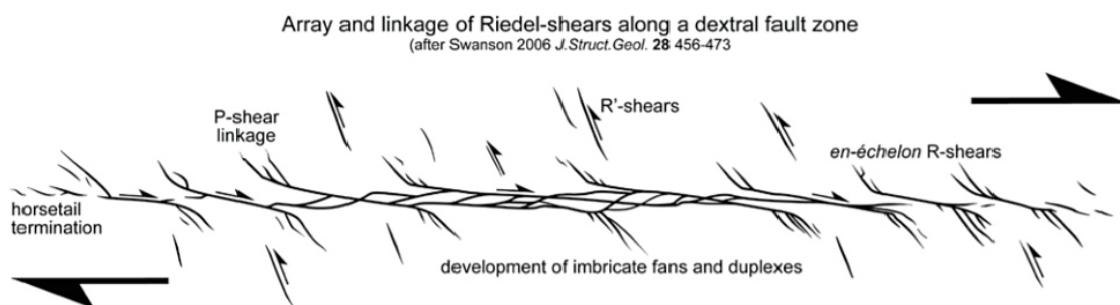
Figure 5-7. *Schematic of different types of shear fractures and the patterns they form in a strike-slip fault (after Swanson 2006).*
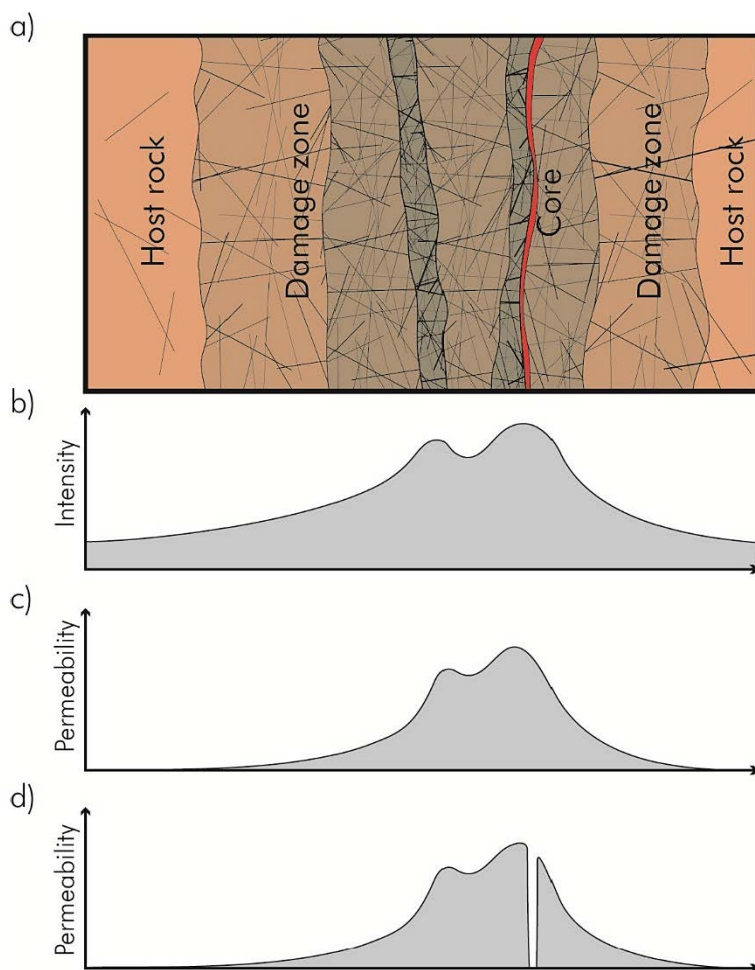
Figure 5-8. a) Idealization of deformation zone properties related to fracturing (cf Figure 1.18). b) Fracture intensity, c) Transverse permeability assuming transmissive core, d) Transverse permeability assuming either impermeable core or abundant fracture terminations against the core. Note that impermeable cores, e.g. due to fault gouge, are rare at Forsmark.

Fracture size distribution within deformation zones requires analysis of traces from those parts of rock surfaces, such as tunnels, within the domain associated to zones. Having sufficient data to perform such analysis involves data from several deformation zone intercepts, and so quantifying variability is unlikely.

Aperture and transmissivity of individual fractures vary significantly within deformation zones, and so their distributions need to be characterised along with any correlations. During tunnel construction it may be possible to link geological apertures and transmissivities measured in pilot holes with fracture traces seen on the subsequent tunnel walls and thereby correlate these properties to an indication of size. Transmissivities of individual fractures within deformation zones may follow similar distributions to those in the rock mass (e.g. Hartley et al. 2018b), with increased intensity and hence connectivity being the main difference. However, some deformation zones may show anomalously high transmissivities, requiring zone-specific properties to be calibrated.

Morphology is likely to vary with depth, with more rough fractures near the surface than at depth, and possibly with size (e.g. Hartley et al. 2018b). Mineralogy and alteration within deformation zones also vary with depth (e.g. Callahan et al. 2019), and it is important for transport modelling to identify deformation zones in which alteration is most prevalent, see Subsection 9.1.5 (on transport classes).

5.3 Variability within and between Fracture Domains

Having separated the deterministically modelled deformation zones as the primary brittle structures, the remaining bedrock is divided into fracture domains as the next most important level in describing spatial variability in fracturing. A fracture domain refers to a rock volume in which the bedrock shows similar statistical characteristics of fracturing and is distinct from adjacent domains (see Subsection 5.3.2).

From the initial division of the bedrock by the Deformation Zones, the consecutive division into Fracture Domains can be mostly geologically driven (Subsection 5.3.1) or result from a balance between geological arguments and a fully quantitative approach for defining DFN model statistical properties (DFN statistical models and hence the Statistically Driven Fracture Domains in Subsection 5.3.3).

The geologically-driven fracture domains, as implemented in e.g. Olofsson et al. (2007), typically extend over the facility-scale volume, c 1 km or more, and hence describe variability on the scales of a whole repository or deposition areas within the layout. Strictly, the concept of a fracture domain treats the volume within a domain as statistically homogeneous, and although variability can be generated stochastically, any particular structure or property value is equally likely anywhere in the domain.

5.3.1 Geologically-driven fracture domains

The boundaries of fracture domains are usually defined on geological factors such as contacts between bulk rock types, major deformation zones, ductile shear zones and tectonic units (see Figure 5-9 for application to Forsmark). The most important fracture characteristics for defining domains are fracture intensity and orientations. Other factors like magnitudes and directions of principal stresses, occurrence and magnitudes of flow and groundwater chemistry may also provide inputs to subdividing the rock mass. For example, contacts between rock units and several large deformations zones, both sub-vertical and gently dipping were used to define the fracture domains at Forsmark stage 2.2 (Olofsson et al. 2007), see below. In the DFN modelling of Olkiluoto they are based on tectonic units in which the orientation and types of foliation are considered "statistically homogeneous" (Aaltonen et al. 2016).

The definition of fracture domains is an iterative, multi-disciplinary task to identify sub-volumes that display a degree of statistical homogeneity relative to the variations in statistics between different domains. The aim is to define a spatial framework for explaining observed variability in bedrock fracturing and its relation to mechanical, flow and transport properties for the purpose of DFN modelling. The number of domains that can be managed from a practical point of view is usually of the order of 5–20. For a local-scale model, this implies fracture domains on the scale of a few kilometres, while for a facility-scale model this may reduce to a few hundred metres. If possible, natural domain boundaries such as the bedrock surface, rock contacts and deformation zones should be used in the first iteration (e.g. Olofsson et al. 2007) as it is reasonable to assume that the first order variability can be coupled to lithology.
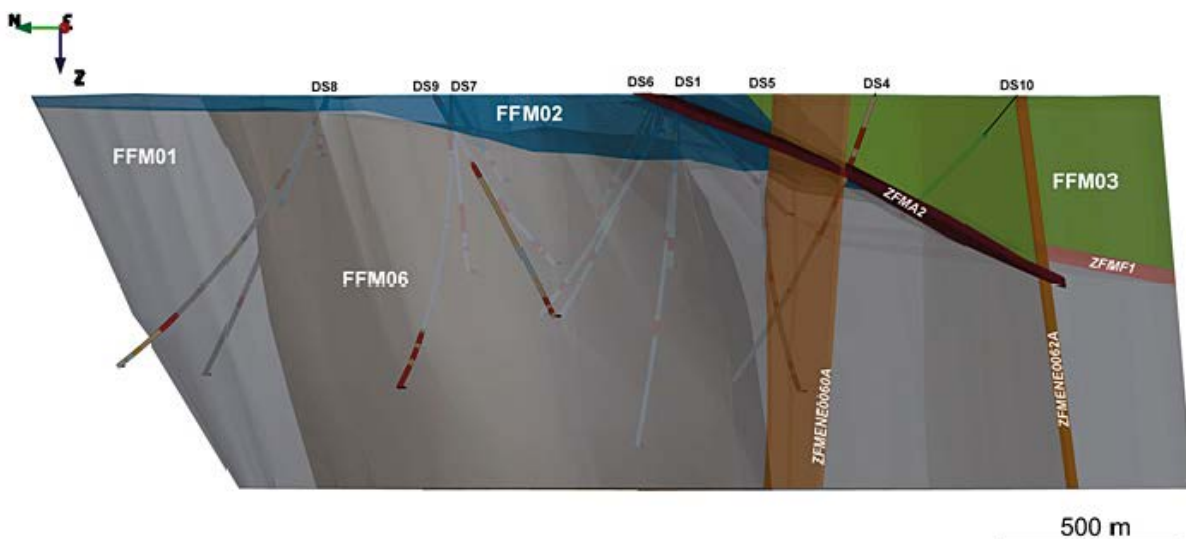
Figure 5-9. *Fracture domains (FFM) and deformation zones (ZFM) at the Forsmark site (from Joyce et al. 2015).*

The characteristics that may be considered include:

1. Fracture orientations and relative importance of fracture orientation sets (see Subsection 6.6.1). Note that intensity (next point) and orientation can also be analysed simultaneously as explained in Darcel et al. (2009).

2. Fracture intensity (see Section 6.3).

3. Degree of openness (e.g. fraction of open versus sealed fractures as observed in core) and fracture mineralogy (see Section 6.7).

4. Orientation, intensity and type of foliation (see Subsection 6.6.2).

5. Intensity and magnitude of discrete flows (see Chapter 7).

6. Hydrogeochemistry of water samples from fractures (see Chapter 8).

The approach used at Forsmark modelling stage 2.2 (Olofsson et al. 2007) primarily used quantitative measures of items 2, 3, and 4 to identify fracture domains as shown in Subsection 4.3.3. Items 1, 5, and 6 were secondarily used to provide confirmation of the approach to domain definition. The information was presented graphically on composite log plots for each borehole and manually interpreted for consistent changes in the indicators across geological boundaries such as:

1. Ductile deformation zones.

2. Brittle deformation zones.

3. Lithological units/rock domains.

4. Depth.

The Forsmark stage 2.2 model defined domains using of all of these boundary types, see Section 4.3:

- FFM01 is associated with rock domain RFM029.

- FFM03 lies in the hanging wall of the gently dipping modelled deformation zones ZFMA2 and ZFMF1.

- Deformation zone ZFMWNW0123 forms the south–west boundary of FFM01/FFM03.

- FFM04 is associated with a belt of strong bedrock anisotropy including high ductile strain and ductile structures that dip steeply to the south–west, associated with rock domains RFM012 and RFM018, forming the western boundary of FFM01.

- FFM05 is associated with strong bedrock anisotropy including high ductile strain and folded ductile structures, as well as the occurrence of fine-grained, felsic meta-igneous rocks of RFM044 and RFM032, forming the north–west boundary of FFM01/FFM06.

- FFM06 is associated with rock domain RFM45.

- The fracture domains are limited in vertical extent to an elevation of –1 100 m.

The result as seen in Figure 4-8 and Figure 5-9 is that the Forsmark tectonic lens is currently subdivided into domains FFM01, FFM02, FFM06 and FFM03, whose flanks are bounded by ductile structures associated with FFM04 and FFM05 to the south and north, respectively. Immediately outside of these ductile based bounds, major WNW–NW brittle structures also provide potential boundaries: ZFMWN0123, ZFMNW1200 to the south, and ZFMWNW0809A to the north. FFM02 is a near-surface domain.

Another common form of spatial variability in fracture properties is a trend with depth and is a feature of the sites that have been characterised for repositories in the Fennoscandian Shield (Fox et al. 2007b, La Pointe et al. 2008, Darcel et al. 2013, Hartley et al. 2018b). An illustration of this for Forsmark from Darcel et al. (2013) is given in Subsection 5.3.3. A higher fracture intensity, particularly sub-horizontal fracturing, occurs in the top c 200 m of bedrock outside of deterministic deformation zones, which also displays significantly higher flow and greater influence of relatively recent surface water infiltration. Outside of deformation zones in bedrock below c 300–400 m depth, fracture intensity is typically lower, flow is limited to a small minority of fractures, and groundwater composition is that of ancient brines and other relic waters. These trends can be expected from the increasing stress on fracture planes

with depth in the region. Mattila and Follin (2019) show that flow is more likely to occur in fractures at low normal stress at both Forsmark and Olkiluoto. Further, since the maximum horizontal stress in the near-surface at both sites is about 10 MPa (Glamheden et al. 2007, Posiva 2012) compared to near zero vertical stress, sub-horizontal fractures are more likely to conduct flows and at higher magnitudes than sub-vertical structures, assuming otherwise identical properties. In addition, the more significant changes in stress that occur in the near-surface during glacial loading/unloading can create extensional sheet joints (also called sheeting fractures) and buckling in the near-surface (Jahns 1943, Hencher et al. 2011, Leith et al. 2014, Martel 2016, Moon et al. 2017). At depths greater than c 300–400 m, normal stress on all fracture planes, irrespective of their orientation, exceeds shear stress, implying slip on fracture planes is unlikely to occur.

There are, therefore, mechanistic reasons for, in addition to subdivision into domains as described above, expressing the intensity variation with depth. It makes sense to explicitly create a sub-horizontal domain for the near-surface, due to its unique characteristics in terms of sheet joints, high hydraulic conductivity and low mechanical strength. However, whether the remaining domains should be further subdivided into discrete horizons or if the decay of intensity with depth should be expressed parametrically, will be a modelling decision, dependent on model scale and purpose. Regardless of approach, objective measures for choosing these horizons include:

- changes in mean intensity of all or sub-horizontal fractures,

- changes in water conducting fracture intensity (see Chapter 8),

- changes in fractions of carbonate-, sulphate-, or clay-rich fracture minerals, and

- changes in mean concentrations of groundwater signatures (e.g. Cl, SO_4, HCO_3, Br) may additionally provide indirect indications of division into horizons.

These changes can be calculated over fixed or moving intervals in elevation on the order of 30–50 m length (for models with local scale resolution) to identify where the most pronounced changes take place. These changes can be pooled over all data to identify horizons of uniform elevation. For example, hydrogeological DFN modelling (Follin et al. 2007b), split domains FFM01/FFM06 into elevation sub-domains above –200 m, –200 m to –400 m and below –400 m. Alternatively, the changes can be identified in individual boreholes to create markers through which a boundary surface can be interpolated. For example, at Forsmark stage 2.2, a highly fractured near-surface domain, FFM02, was identified as overlying FFM01/FFM06, characterised by a complex network of gently dipping and sub-horizontal, open and partly open fractures implying a base of FFM02 that tilted south–east from c –30 m elevation at the tip of the tectonic lens to c –100 m where it merges with the base of ZFMA2 in the south–east. In Version 2 of the Olkiluoto DFN (Hartley et al. 2013a), four layers of sub-domains were created by marking each of 54 boreholes according to changes in water conducting fracture intensity and groundwater chemistry, and then interpolating horizons between these markers.

Whereas the above-described steps require some subjective judgement from the expertise represented by the site geologists, a complementary step is introduced in the Fracture Domains evaluation (Subsection 5.3.4. It consists of more elaborate systematic and quantitative statistical analyses (e.g. Darcel et al. 2009, 2013). The aim is to identify the need to further subdivide the domains, by adding additional, statistically based, boundaries within or across the originally defined volumes, or to merge domains with similar properties. This step requires a definition of statistical distances (Subsection 5.3.3) and variability terms (intrinsic and extrinsic variability terms as introduced in Subsection 5.3.2). The statistical analyses provide an objective and reproduceable rationale for the domain definitions and delineations that eventually form input to the DFN modelling.

5.3.2 Variability terminology

Variability is a key concept to defining Fracture Domain models, such that the observed variability of the critical DFN properties is larger between the defined domains than within the domains. The limit between both results *i*) from the variability intrinsic to the fracturing process which cannot be explained by significant geological/tectonic observations and *ii*) from a strong dependence on the amount of available data. If data are scarce, then potential existing domains cannot be distinguished from each other and defined domains display a high intra-domain variability.

This is illustrated schematically in Figure 5-10 with fracture intensity variations, as observed from core logging data. In the plot, a few sharp intensity maxima are combined with less intensive local variations that result in a two-level description:

- First by domains over which the average intensity is well-defined (the plateaus in Figure 5-10). The change in average intensity from one domain to the other is called extrinsic variability.

- Second, by less intensive variations to be included in the DFN model of each domain. These variations are called intrinsic variability and their definition is statistical.

With **intrinsic** variability is meant a variability inherent in the property or object at hand, for instance fracture intensity. It can be regarded as an inherent variability given by Nature. However, the intrinsic variability is also closely connected to, but often mistakenly seen as synonymous to, the aleatoric uncertainty of the property or phenomena under study. Within a domain, the intra-domain variability is an intrinsic property of the domain expressing the natural variability of the fracture system and its undefined uncertainties. The **extrinsic** variability is dependent or related to other objects or external boundary conditions. Thus, the inter-domain variability can be said to be predominantly extrinsic in nature.

In summary, the terms inter- and intra-variability refer to the spatial aspect of variability ("where"), whereas the terms intrinsic and extrinsic refer to the nature of this variability ("how", "why").

The inter-domain variability may be systematic and correlated with geological indicators, such as changes in lithology or proximity to a deformation zone. If this is indeed the case, the geological indicators can be used, at a first order, to subdivide the bedrock into domains, and correlate fracture parameters (particularly orientation and intensity) to the geological properties. However, the fracturing process in-itself produces a multiscale variability which may not be unambiguously linked to the geological context. To conclude, the following definitions are therefore used:

- Intra-domain variability is spatial variation of the fracture intensity and orientations (deviations from the mean background values), that cannot be correlated to geological structures and can thus not be delimited deterministically. A model of intra-variability is required for each domain in any DFN model.

- Inter-domain variability refers to the average intensity variations which can be either explained by geology, or whose variations are significant and cannot be obtained by the intra-variability model. The inter-variability model is therefore the division of the bedrock according to deterministic boundaries delimiting fracture domains. These boundaries can be readily determined for the data but may be extrapolated either deterministically or simulated statistically away from data controls.
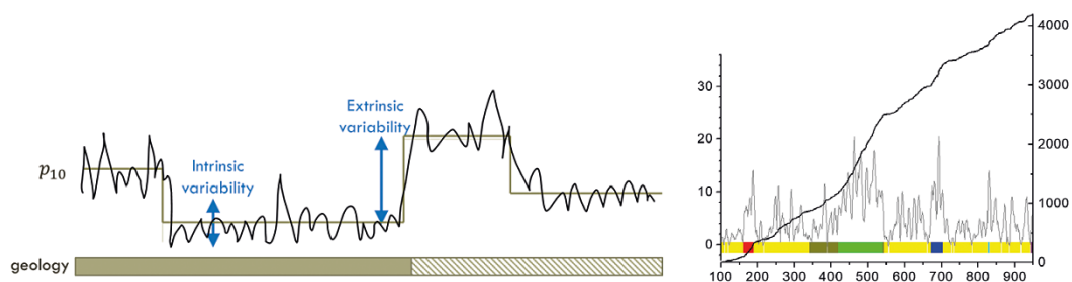
Figure 5-10. *a) Schematic view of the variations of P_{10} on a core section. Variations of P_{10} (black line) are viewed as a combination between a "constant average density" (brown line) and an internal variability component (intrinsic variability). The extrinsic variability corresponds to the jumps of average density. b) data (Darcel et al. 2013).*

5.3.3 Statistical distance

The formalism of fracture domains can be expressed as follows: Fracture Domains are expressed in Euclidean space, whereas Statistical Fracture Domains (Darcel et al. 2012) are defined in statistical space. Just like the Euclidian space familiar to humans, in which proximity is expressed in terms of metric distance, the proximity in statistical space is expressed in terms of statistical distance (Savazzi and Reyment 1999, Dodge 2006) and is a measure of statistical similarity of two entities (e.g. rock volumes). Though this may be perceived as a play on words, this formalism is necessary to differentiate between modelling of domain geometries, which takes place in the Euclidian space, from modelling of statistical domains, which takes place in statistical space.

The statistical distance is not only a measure of difference between, say, average values or variance of entities, it also expresses the strength of correlation between these entities. We model in the realm of a multidimensional (statistical) space and the entities may be either random variables or a collage of such, along each axis in this multidimensional statistical space. This may be perceived as somewhat abstract, but it simply boils down to properties, familiar to us, which define the genome of each DFN model, namely: Intensity, size, orientation, transmissivity, connectivity, location (Euclidian coordinates) and time to name but a few of the most obvious.

Any multidimensional (statistical or Euclidean) space can be sliced so the result is somewhat comprehensible to humans, by slicing it such that the slice itself lies in one of either *1D*, *2D* or *3D* space, which enables visualisation of complex parameter spaces. In analogy to Euclidian space, locations in the statistical space can be expressed in terms of coordinates. The example shown on Figure 5-11 displays the correlation and magnitude of two hypothetical entities a and b respectively. These should be understood as either being single properties (e.g. intensity and size) or as a combination of many properties (e.g. size/intensity and orientation/age) expressed as an appropriate metric stemming from investigation data (with or without Euclidian coordinates), assumptions or inferences. In the example shown here, the points $(\alpha 1, \beta 1)$ and $(\alpha 2, \beta 2)$ are considered statistically close whereas the point $(\alpha 3, \beta 3)$ is considered statistically distant in the α-β plane. Naturally, the distance can also be computed in the α-β-Magnitude volume and the statistical coordinates are instead expressed as triplets (e.g $(\alpha, \beta, Magnitude)$). This notion can be expanded to a statistical space of any dimension but cannot with ease be visualised in any comprehensible manner.

The next step consists of evaluating the statistical distance for a number of key properties. The purpose is to evaluate if the variability of the key properties is larger between the previously defined geometric (geologically driven) domains than within the domains. If the variability between two adjacent domains, evaluated by means of e.g. statistical distance, is smaller than a predefined metric the domains can be merged into a single domain. On the other hand, if the variability within a predefined geometric domain exceeds a certain predefined threshold (the statistical distance exceeds a pre-defined value), the domain needs to be split into two or several smaller domains.
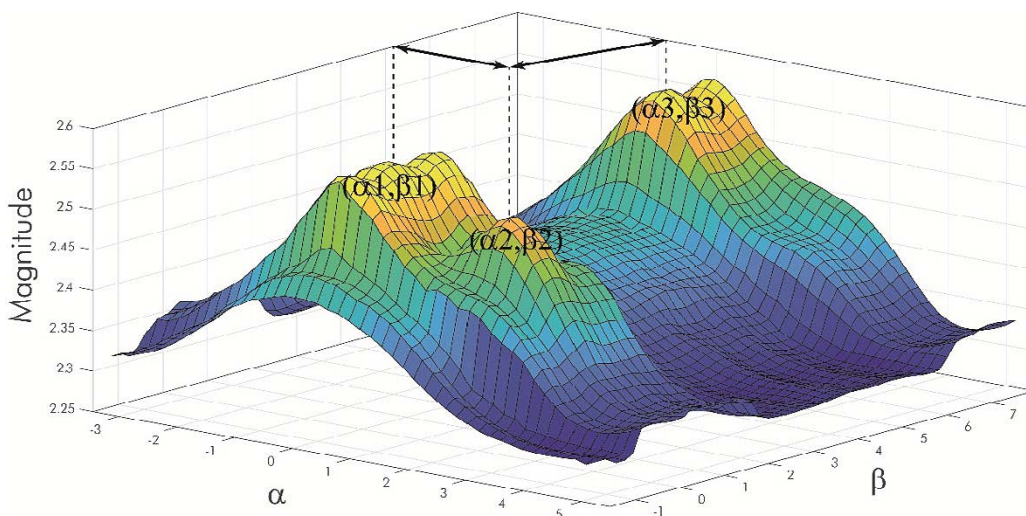
***Figure 5-11.** Illustration of the notion statistical distance, using a hypothetical example for illustrative purposes only.*

5.3.4   Statistically driven fracture domains

Fracture domains can also be identified by sub-dividing datasets, such as boreholes, and sorted into domains using an objective classification system according to statistics of fracture orientations and/or intensity, which therefore can be described as **statistically driven domains** (Darcel et al. 2013). In the example where intensity is used as the primary basis for classifying domains, borehole data are subdivided into sections, and the mean and variance estimates are calculated within each section. Initially, each section is allocated to it its own class. In an iterative process, the two classes that are closest together, based on some predefined metric of statistical proximity (see Darcel et al. 2013 for details), are merged thereby reducing the number of classes by one, and the maximum amount of statistical variation between any pair of the sections in a class is calculated. This process is repeated until the maximum statistical distance between any two sections in a class reaches some pre-defined limit. The result is the number of statistically compatible classes and the sets of borehole sections pooled into those classes. These classes are the statistically driven fracture domains. Note that in this method, the domains are not spatially contiguous (in a Euclidean sense) but statistically compatible. Figure 5-12 shows an example where the Forsmark SDM-site borehole data are sub-divided into 148 sections and sorted into six classes ordered by total intensity (open or sealed, any orientation). Sections within deformation zones mainly fall in high intensity classes (Darcel et al. 2013).

In a second example, the same data are split according to the dip angle of fractures: sub-horizontal, moderately dipping, and sub-vertical, and a similar process repeated for each group of orientations. This time seven classes remained when target maximum statistical distance between pairs was achieved. In this case the results revealed an interesting spatial pattern with depth, see Figure 5-13, with the sub-horizontal fracturing showing a distinct depth trend and sub-vertical fracturing not. For the sub-horizontal, the highest intensity occurs above 100 m and in deformation zones, there is then a steady decrease until c 400 m depth and then relatively uniform below that. There is also more variability below 100 m depth.

This method provides an objective classification into regions of statistically compatible intervals, that helps identify spatial trends and provides an indicator of spatial clustering along the boreholes. However, as it does not provide any spatial framework for extrapolating variability beyond the boreholes, i.e., it provides measures of variability along the boreholes but not transverse to their axes, it is best suited as an objective guide to help characterise and subdivide geologically driven fracture domains into subdomains.

Though data mainly based on boreholes is sparse, previous applications showed that statistical distance can be successfully used with non-trivial results (Darcel et al. 2013).
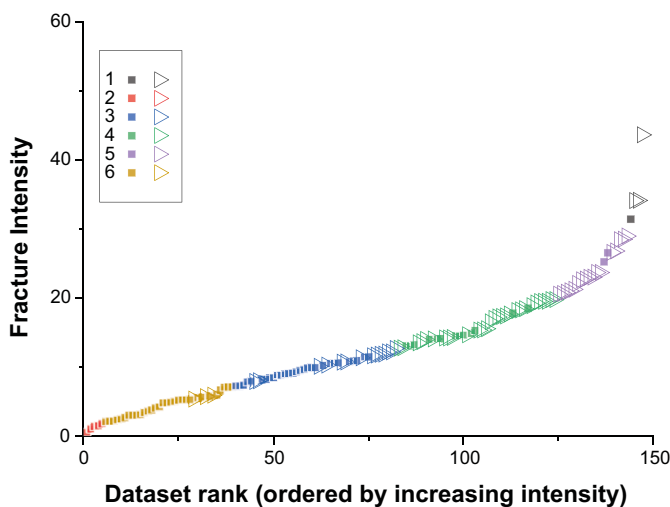
Figure 5-12. *Fracture intensities by borehole section, ordered by increasing intensity and coloured by reference to the statistically driven class index. The filled squares and the empty triangles correspond to Fracture Domains and Deformation Zones borehole sections, respectively.*
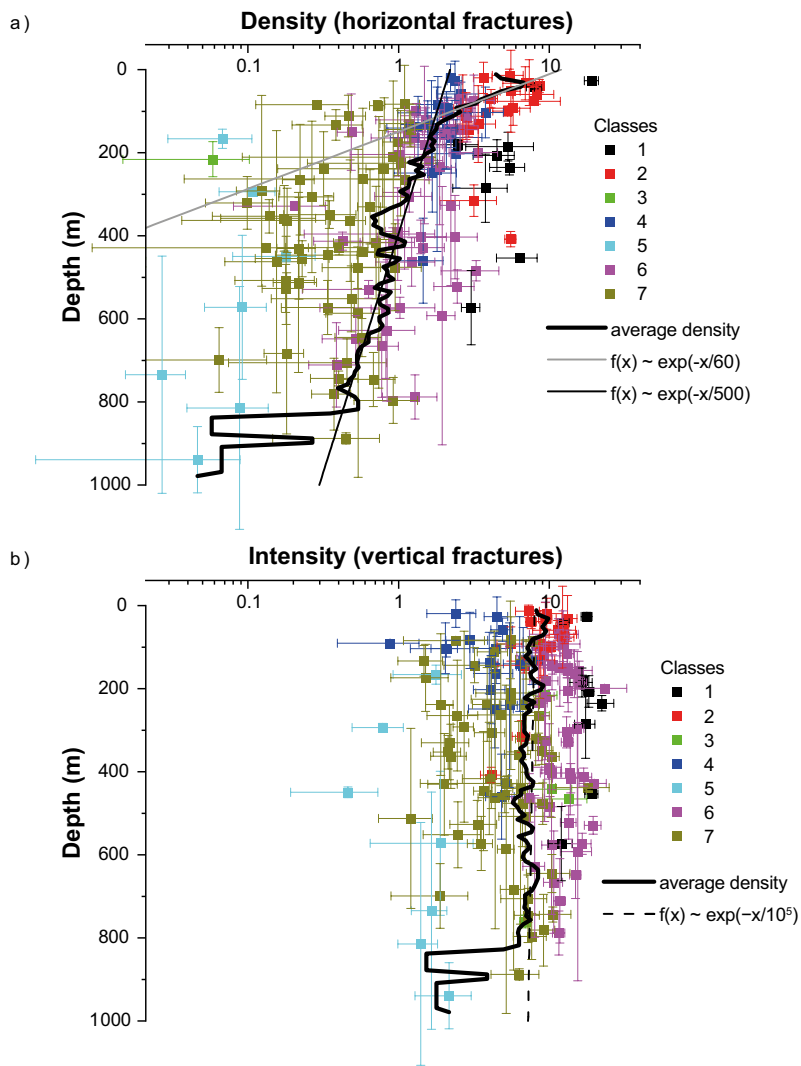
Figure 5-13. *Evolution of fracture intensity with depth when split into three groups by dip angle. The 7 final classes are represented by the different colours (see inlet), intensity vs. depth and here showing a) sub-horizontal fractures and b) sub-vertical fractures. The "depth error bars" represent the borehole section min and max depth.*

5.3.5 Synergy between Geologically and Statistically based rules for defining the Fracture Domains

The process of defining domains is quite simple though it obviously contains complex components. The first step consists of identifying natural domain boundaries (Figure 5-14 and Subsection 5.3.1). The next step is to investigate whether there exists any significant variability that necessitate either a merge of the defined domains or a split of domains. New information in terms of additional data, e.g. from boreholes or tunnel mapping, new model results (e.g. palaeohydrological) or the need to reassess assumptions triggers a reiteration of the process (Figure 5-14).
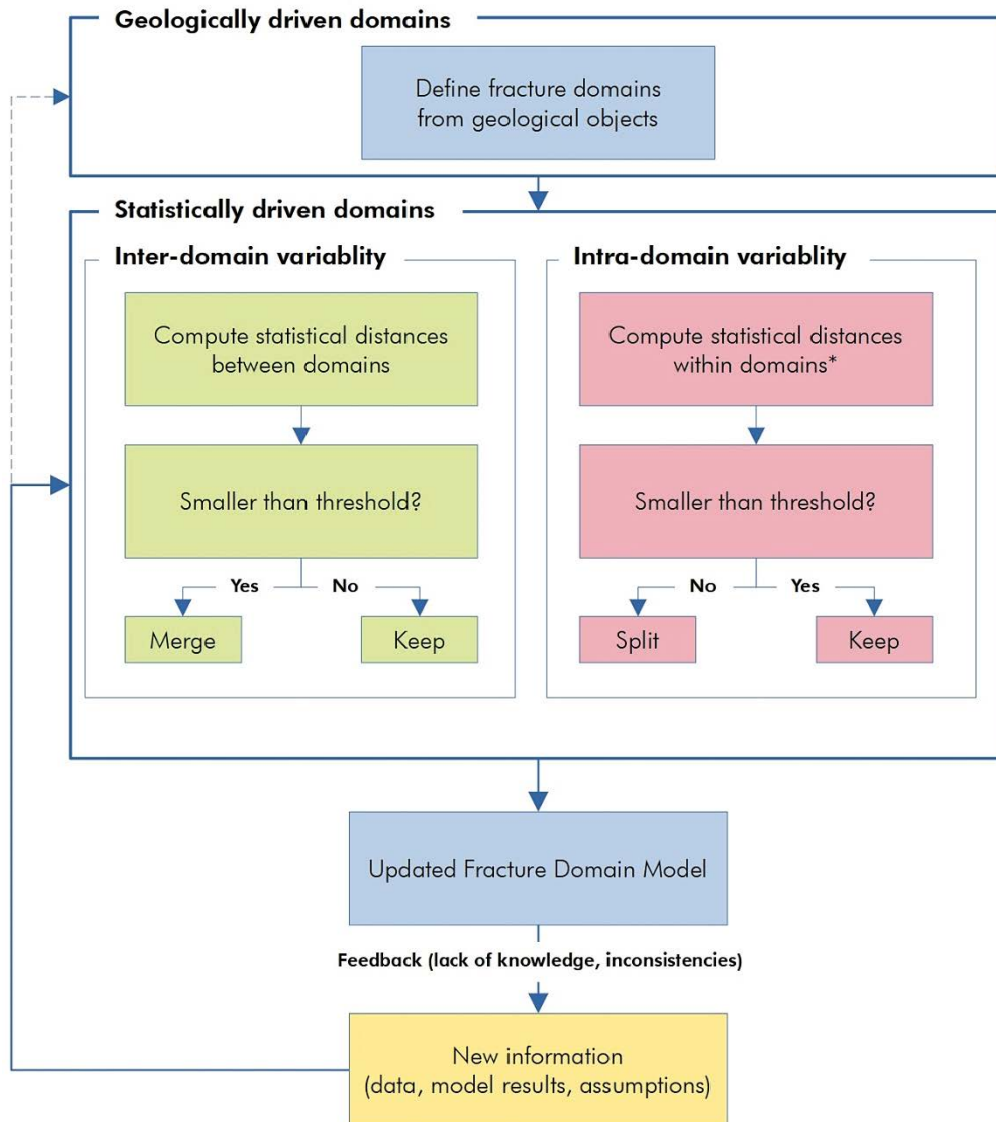
Figure 5-14. The modelling of fracture domains is an iterative process which includes creation of volumes based on a geological model, computation of statistical distance between key properties or combinations thereof, from the statistical distance create statistical domains (volumes in statistical space) and updating the fracture domain model to reflects inference from the statistical domains.(*) Within a domain, statistical distances are computed between the datasets which are the elementary bricks of the analyses (Darcel et al. 2012).

5.4 Underdetermined deformation zones

There are essentially three challenges for the modeller in representing relatively large-scale structures, in the size range 100s of metres to perhaps kilometres. These are:

- Yet undetected **deformation zones** of lengths greater than c 2 km outside the area of focused investigations.

- **Possible deformation zones** of lengths greater than c 100 m in the repository area, intersected by one or more tunnels or preceding pilot boreholes.

- **Sheet joints** and surface-parallel structures of lengths greater than c 100 m intersected by one or more boreholes and accesses (shafts and access ramp). Sheet joints need special attention because they are very important in terms of flow and constructability of the upper part of ramp and shafts. From a modelling point of view, they create challenges similar to the possible deformation zones.

It is expected that such structures will be partially determined by subsurface intersections and that they can be modelled semi-stochastically.

Figure 5-15 illustrates the challenge in simulating undetected deformation zones. It is expected that most zones of lengths greater than c 500 m will be detected and modelled deterministically in and around the facility-scale area of focused investigations. Outside of this area only the largest zones, and only the sub-vertical ones, are detected and modelled deterministically based on lineaments. This gives a variable resolution with the repository target area having the appearance of being the most faulted part of the bedrock. A more plausible structural model would require the generation of additional stochastic deformation zones in the far-field such that the distribution of intensity and orientations of deformation zones are more consistent across the modelled volume, whether local-scale or regional-scale. To achieve this, the target intensity and orientation models for the facility scale (or facility part scale) are extrapolated to the surrounding volumes, or deduced from detailed structural mapping in parts of the surrounding volumes. Hence, a stochastic prescription for the geometries of deformation zones is required, along with any rules for terminating the generated zones against the deterministically modelled ones.

As part of the deterministic geological modelling updates during construction and operation, if no geometric constraints can be obtained by investigations, deformation zones will be represented as extrapolations of tunnel/borehole intersects 1/3 the distance between the closest tunnel intercepts along strike and 40 m vertically above and below, (as detailed in **DGMM)**, see Figure 5-16 for example application. The challenge for DFN modelling will be to extrapolate these rectangles to represent semi-stochastically sampled planes using a defined statistical model of fracture size and applying rules for terminations between fractures.
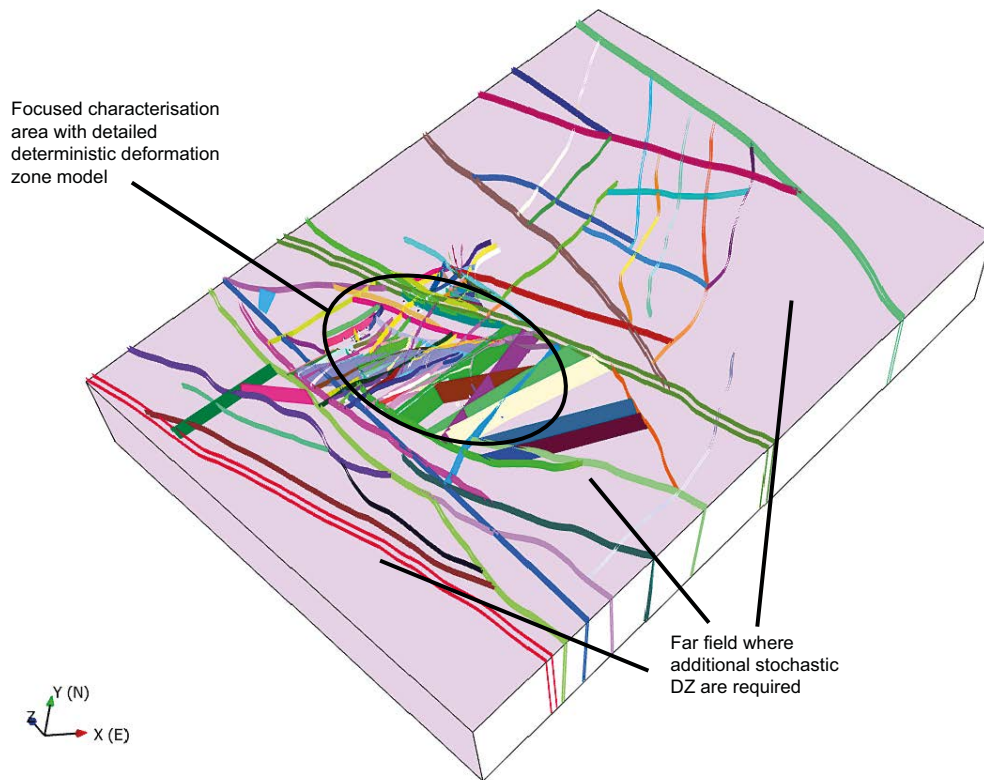
*Figure 5-15. The current deterministic deformation zones (shown as two bounding planes) projected on to the local-scale modelling domain to illustrate the non-uniformity of structural representation due to the repository area and planned underground openings. The model is described in **DGMM**.*
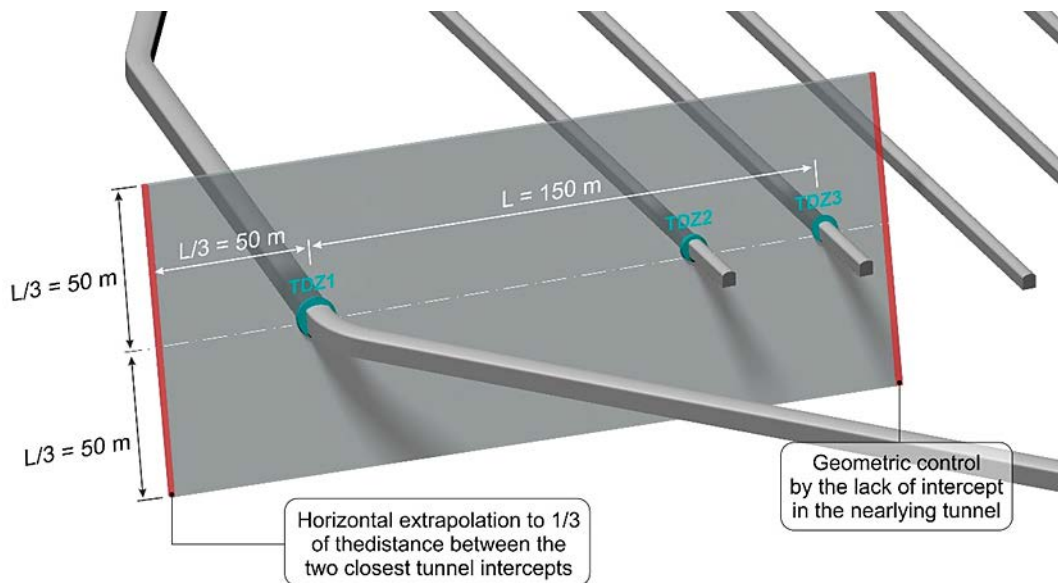
*Figure 5-16. A tentative deformation zone in the repository area modelled on the basis of observation points along three tunnels. A limited extrapolation is made by the geologist along the strike and to vertically 40 m above and below the tunnels (from **DGMM**).*

Sub-horizontal sheet joints, more or less filled with soft sediments, are conspicuous at Forsmark with geological aperture greater than 10 mm, with transmissivities greater than 10^{-6} m²/s, see Figure 5-17 and Figure 5-18. Above elevation –30 m they are pervasive enough that hydraulic connections may be inferred laterally between holes, while they are generally too sporadic to make hydraulic connections at greater depths. Again, the challenge is to sample semi-stochastic planes conditioned on these intersections and being made consistent with the inferred connections (both geometric and hydraulic) between boreholes.

Modelling of the deformation zones discussed above therefore requires the development of a DFN description of geometric parameters for structures on the scale of c 100 m to several kilometres, methods for describing terminations of fractures against one another and methods for conditioning fracture networks.
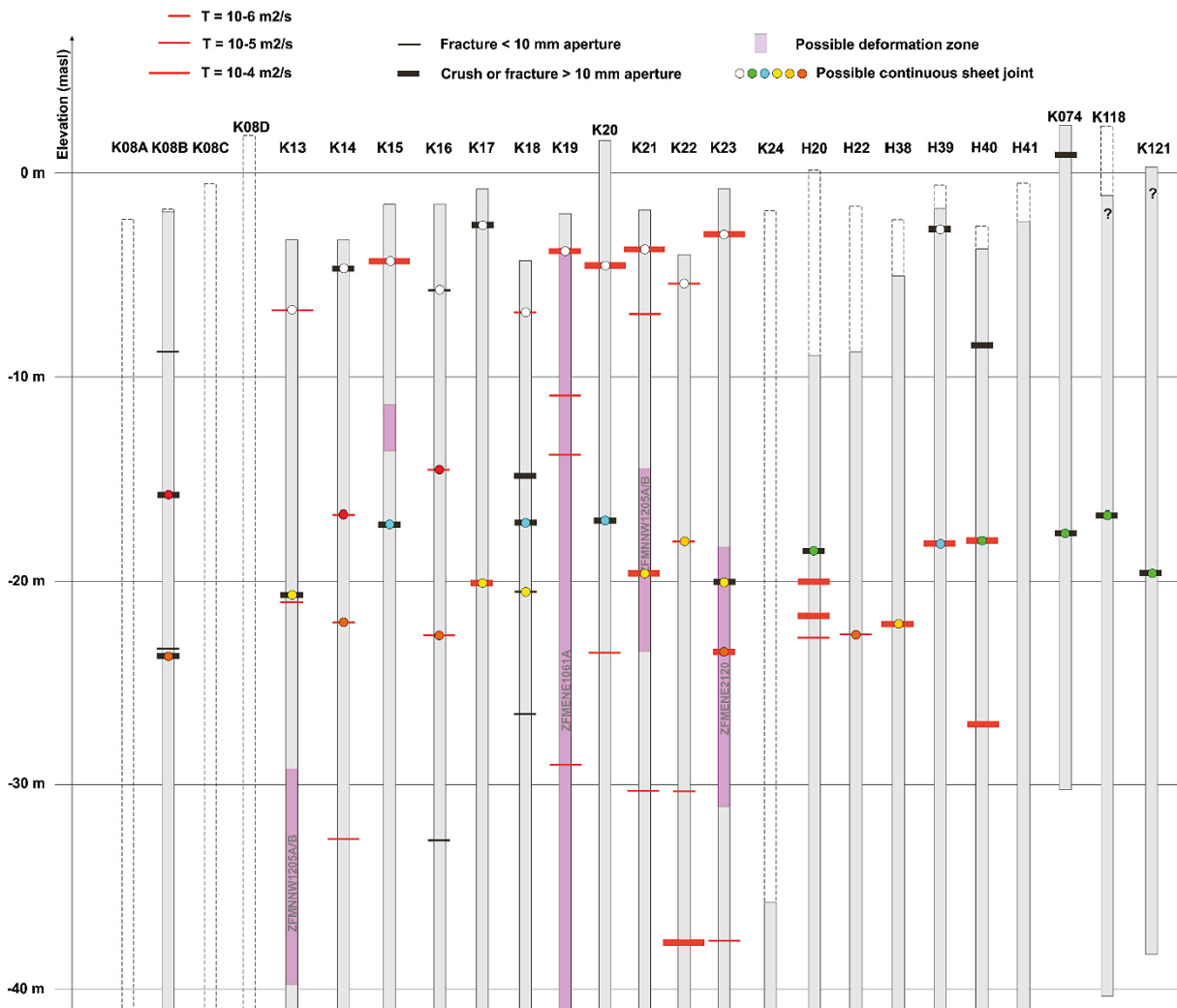
Figure 5-17. *An illustration of borehole intersects with significant near-surface sub-horizontal structures in the array of relatively closely spaced shallow holes in the access area of the Forsmark tectonic lens. The subset of structures shown are either crush zones (highly fractured, non-cohesive rock) or fractures of high transmissivity. Here, boreholes are projected on to a thick section, but spaced regularly.*

Figure 5-18. Map showing locations of boreholes shown in Figure 5-17.

6 Geometrical properties of fractures

6.1 Introduction to a DFN framework for rock masses

All energy based theories on fracturing (e.g. Griffith 1920) rely on the observation that the process of fracturing in rock, in response to imposed loads, basically consists of the creation of pairs of roughly parallel surfaces with an empty or fluid-filled void. The main macroscopic measure of a fracture system is thus the total fracture surface area[1] created per unit volume, commonly called P_{32} (Dershowitz and Herda 1992). A full description of a fracture system should identify, deterministically or statistically, all fracture surfaces in a rock. In practice, an exhaustive identification is impossible on all but small rock samples e.g. with computed tomography techniques. Hence the fracturing state of the rock must be estimated from limited exposures such as those provided by boreholes, outcrops or inferred from geophysical data.

The DFN methodology addresses the major issues raised by the characterisation and modelling of fractured systems:

- The fracture system is a complex, inaccessible, set of geological objects with intricate geometrical properties. An approach is required to identify a limited, but sufficient, number of parameters, which are quantitatively measurable, either deterministically or statistically, and which also enable the modelling of connectivity, transport, deformability and strength (see Chapter 2). Since the fracture system can be viewed as an ensemble of roughly planar structures, with lateral extension (size), shape, orientation, and void size, it is appropriate to describe it as a population of planar objects, which is the essence of the DFN method.

- Fractures exist at all scales, likely down to nanometre-scale crystal dislocations, resulting in an essentially infinite, necessitating that P_{32} must be qualified with respect to minimum scale for it to have meaning. A hierarchical approach, which sorts fractures according to a scale factor, is therefore required to assess the relative contribution of the different fracture scales to specific physical processes, e.g. hydraulic and or mechanical processes.

- Acknowledging the occurrence of fractures at all scales (Bonnet et al. 2001), the existence of a representative elementary volume (REV) above which the medium can be described by continuum theories is questioned for fractured geological systems (Freeze 1975, Long et al. 1982).

The DFN methodology and modelling framework considers the fractured rock as a *3D* volume populated with discrete fracture-like objects embedded in a homogeneous rock matrix (Long et al. 1982, Jing 2003, Jing and Stephansson 2007). It relies on the prevailing contribution of fractures to the mechanical and hydraulic properties of crystalline- and, to a lesser extent, sedimentary rocks (Barton et al. 1974). It aims to integrate field data into simulations of flow and/or deformation (Andersson et al. 1984, Cacas et al. 1990). This framework differs from classical continuum approaches for two main reasons:

- The medium model (Chapter 1, Figure 1-20) mimics the real system, i.e., the fractured geological rock mass, in such a way that any available geological information about fractures is easily integrated into the DFN.

- Unlike continuum methods, no homogenisation scale is required *a priori*.

In the light of the stochastic nature of a DFN model, it should be understood that a DFN model should primarily be viewed as a statistical ensemble of which the target site constitutes one of the many equiprobable possibilities.

In the following Sections 6.2 to 6.6, the properties of the DFN model(s) are described at the network scale (i.e., the fracture population). The steps related to the definition of individual fracture properties, based on the fracture in-plane variations, are reviewed in Section 6.7.

---

[1] Note that P_{32} is calculated on the assumption that fractures have zero thickness and thus only include one (of two) fracture surfaces.

6.2 Idealisation of fractures

The fractures of a DFN are, *fracture-like*, idealised objects, defined by their geometrical and physical properties. This idealisation refers to several assumptions:

- The lateral extent of a fracture is much larger than the aperture (and its in-plane variations), so that it can be represented by a *2D* surface. However, in the purely geometrical description, large fractures may require an explicit definition of their aperture, with a tabular and/or undulating representation.

- A fracture is roughly planar (and again the deviation from idealised planarity is small compared to the lateral extent), so that it can be represented by a *2D* surface.

- A fracture can be represented by a disc, an ellipse or a rectangular convex polygon, assuming that in any case the aspect ratio of fractures is sufficiently low (and therefore can be neglected).

- A mean fracture aperture may be defined. However, the resolution scale for the heterogeneity representation of a fracture plane (e.g. self-affine distribution of fracture aperture) is an open and debated issue (see also 6.7).

- Deviations from an idealised *2D* disc shape, including in-plane variations of fracture surface properties (roughness, matedness, aperture change, self-affinity of the surface), are potentially directly accounted for in the definition of the physical properties of the fractures (e.g. transmissivity, stiffness, strength etc), without any explicit geometrical representation. These physical properties are defined from physical or heuristic laws, at the fracture scale, between realistic geometries and effective physical properties.

Thus, the DFN supporting geometrical structure is a population of *2D* surfaces onto which attributes are associated to define physical values by fracture (effective values) or distributions of micro properties (on the discretised fracture plane). Accordingly, fractures have in most DFN models previously produced been conceptualised as planar, circular discs possessing zero thickness while the fractures in the rock are almost certainly neither strictly circular nor planar or infinitely thin. Ongoing DFN modelling applications take a step forward and combine a still simplified geometrical representation with in-plane heterogeneity of physical properties indirectly correlated to the real fracture shape.

Due to sampling difficulties, there is truly little empirical data on true fracture shapes, as this would require a complete dismantling of the rock mass under study and thus not sufficient data exist to mathematically characterise deviations from the abovementioned idealisations. Yet, a few studies of *faults*, (e.g. Rippon 1985, Walsh and Watterson 1988) indicate elliptical shapes with a major axis parallel to the direction of slip, and an axial length ratio of 2:1 to 3:1. On the other hand, studies of *joints* (e.g. Aydin and Johnson 1978) indicate that a circular shape is a reasonable assumption. Site investigations (e.g. at Forsmark or Laxemar) have not produced sufficiently firm kinematic evidence to address the ellipticity of fractures. To our knowledge, there are no known mechanical reasons to support that the actual fracture shapes may not tend towards being equant in crystalline rocks and as long as there is no observed mechanical layering. This differs from sedimentary rocks, where mechanical layering promotes non-equant fracture shapes. Notwithstanding, analyses of variations relative to the aspect ratio of the perimeter shape of an idealised planar fracture could be justified because fractures with a consistent and high aspect ratio may be more likely to intersect other fractures, and hence will increase network connectivity (de Dreuzy et al. 2000, Mourzenko et al. 2005, Yi and Tawerghi 2009, Barker 2018). The effect of ellipticity can be explored by e.g. treating the axial ratio as a stochastic variable. This would, however, only have a minor impact if the model contains fracture to fracture terminations which results in most fractures being n-sided polygons.

A fracture commonly undulates in 3-dimensions so that its strike and dip varies in different locations on its surface (Newman and Mitra 1993). It is also known that the undulation of fracture surfaces varies in amplitude with direction. Such variation in its local orientation occurs on many scales and can be considerable. For instance, the amplitude of undulation parallel to the shear vector is at least 10 times less than in a perpendicular direction (Power et al. 1987, Power and Tullis 1991). Using a self-affine fractal approach, a number of studies (e.g. Okubo and Aki 1987, Hirata 1989, Chilès and Delfiner 1999) report dimensions that would correspond to an amplitude of 2–15 % of the fracture diameter.

In most DFN applications, fractures are simplified to planar discs as the use of more realistic shapes (e.g. self-affine surfaces) is simply not computationally feasible, nor perhaps necessary for certain modelling scales (e.g. facility-scale DFN models). Yet, most modelling efforts require some degree of idealisations, both to tailor the description in terms of complexity to the problem at hand and to ease computational burden without oversimplification. Naturally, therefore, a great deal of the fundamental work on discrete fracture modelling (e.g. Baecher et al. 1977, Barton 1978, Dershowitz et al. 1979, Long et al. 1985) and stereology (e.g. Warburton 1980, Berkowitz and Adler 1998, Darcel et al. 2003) relies on the assumption of disc shaped fractures.

As for the abovementioned examples, the DFN modelling generally assumes that these idealisations do not induce systematic biases in the applications and that the related uncertainties are minor when compared to the uncertainties arising from the stochastic generation of fractures as used in this DFN modelling framework. It is, however, recognised that the consequences of these assumptions should where possible be addressed by sensitivity analyses e.g. analyses of the sensitivity of intersection statistics and flow to variations in fracture eccentricity.

Finally, for the simplest geometrical representation of a fracture, the disc-shape, only three parameters are required; two for angles (for the orientation of the fracture pole) and one for size, the diameter of the disc. The fracture surface area and fracture diameter are univocally related to each other. If the fracture geometrical shape is more complex but still planar, more parameters are needed to describe the shape and the fracture surface is not univocally related to a size. If the shape aspect ratio is low, the fracture typical size can be defined as the diameter (or radius) of an equivalent disc of the same surface of the fracture surface.

6.3   General Framework (theory)

6.3.1   Definitions

The **fracture density distribution, n_{3D} (P),** is a statistical characterisation of a fracture system. It is a **function** which, when integrated over the whole range of values of each fracture parameter, defines the total number of fractures per unit volume. In its most general expression P is a vector/set representation of all the fracture parameters. Typically, these are the fracture size, l, and orientation terms – **trend** θ and **plunge** ϕ. They may also be extended to any additional relevant fracture property (e.g. aperture, roughness, transmissivity, stiffness, friction coefficient, etc), noted u. P is thus the ensemble of fracture parameters: $P = [l, \theta, \phi, u]$.

By definition, a fracture density distribution n_{3D} (P) defines a number of elements per unit volume, whose parameter vector P' is in a given range $P' \in [P, P + dP]$, in the limit where $dP \to 0$. Vector notation simply expresses that each element of the parameter vector is valid within a given range: $l' \in [l, l + dl]$, $\theta' \in [\theta, \theta + d\theta]$, $\phi' \in [\phi, \phi + d\phi]$ and $u' \in [u, u + du]$.

Let us consider a fracture density distribution defined for a volume V. For fractures only partially included in V the contribution to the density distribution is calculated by attributing to each fracture a probability to belonging to V: $\pi_f (V)$. Several expressions can be used for $\pi_f (V)$. The simplest states that $\pi_f = 1$ if a specific point of the fracture (e.g. its barycenter) is within V, and 0 otherwise. $\pi_f (V)$ can be defined as the ratio between the surface of the fracture f included in the volume V and the total fracture surface. Then the number of fractures in V with parameters in $[P + dP]$ writes as:

$$N_V(P) = \sum_{f(P';P' \in [P,P+dP])} \pi_f (V)$$

Equation (6-1)

And the fracture density distribution is:

$$n_{3D}(P) = \frac{1}{V} \lim_{dP \to 0} \frac{N_V(P)}{dP}$$

Equation (6-2)

The fracture density distribution n_{3D} (P) is particularly suitable for dealing with multiscale fractured systems for representing the scale evolution of the fracture density and for combining analyses for data coming from different (in scale and in dimension) sampling supports (see Section 6.4).

The fracture density distribution $n_{3D}(P)$, once integrated over all the parameters in P and parameter ranges, ultimately expresses a number of fractures per unit volume of rock, a quantity (not a function), often noted $\boldsymbol{P_{30}}$. In this notation, the subscript 3 refers to the dimension of a volume (cubic meters) and the subscript 0 refers to the dimension of the object (in this case a point). Although this quantity is basically a density quantity, it is commonly denoted **fracture intensity**, following the terminology from Dershowitz and Herda (1992) (see further details in Subsection 6.3.3). P_{30} is the direct expression of the integration of the fracture density distribution functions over all the fractures in a given volume.

It is worth noting too that the **density distributions** used to define the DFN models must not be mistaken for **probability density functions**: the integral, over the whole range of values of a parameter, of the density distribution gives a number of fractures (per unit of rock volume) while the integral of the **probability density function** is equal to one by definition of what is a probability.

The density distribution $n_{3D}(P)$ as above expressed is the most general expression for DFN models. In most application cases, the number of fracture parameters is reduced to a few and the fracture density distribution accordingly simplified. It can be simply expressed for any subset of parameters P_1 irrespective of the others P_2 ($P = [P_1, P_2]$) with:

$$n_{3D}(P_1) = \int_{P_2} n_{3D}(P_1, P_2)\, dP_2 \qquad\qquad \text{Equation (6-3)}$$

In practice, one may define the density distribution of each individual fracture parameter (e.g. size or orientation) independently (Darcel et al. 2004, 2006, 2009) or split the density distribution into several separate contributions based on specific observations (e.g. division into fracture orientation sets as in Fox et al. 2007b, Hartley et al. 2018b).

Density distributions are also defined to describe the DFN models as they appear from the intersection between any surface of exposure – *2D* and *1D* sampling supports- and the *3D* DFN. The list of parameters P is adapted to the observations.

In *2D*, the sampling support is a surface S and the intersection between the sampling support and the DFN is a set of traces. Then the parameter vector P contains at least fracture trace lengths and, if possible, orientations, apertures, …, measured on traces. The fracture density distribution in *2D* thus

$$n_{2D}(P) = \frac{1}{S} \lim_{dP \to 0} \frac{N_S(P)}{dP} \qquad\qquad \text{Equation (6-4)}$$

where $N_S(P)$ is number of fracture traces on the surface of area S and with parameters P' in $[P + dP]$.

In *1D*, the sampling support is a line of size L. If sampling is strictly *1D*, fracture sizes can certainly not be measured and the parameter list contains only intercept positions; if it is not strictly *1D*, e.g. a borehole with a defined diameter, it contains all the measurable characteristics (potentially orientations and aperture, mineralogy, openness) of the fracture. The fracture density distribution in *1D* thus becomes:

$$n_{1D}(P) = \frac{1}{L} \lim_{dP \to 0} \frac{N_L(P)}{dP} \qquad\qquad \text{Equation (6-5)}$$

The possibility to infer the *3D* fracture density distribution from density distributions of lower dimensions and the characterization of *1D* and *2D* density distributions from commonly available data is further discussed in Section 6.4.

6.3.2 Scaling issues

As stated above, the DFN framework is foremost a hierarchical approach to assess the relative contribution of different fracture scales to specific applications (Davy et al. 2018b). The capacity to derive good predictions for a given process is intimately related to the capacity to have the right prediction at the scales relevant to this process. A DFN scaling relationship is a modelling tool to assess the adequacy between data and predictions and to understand to which scales the integrated measurements, such as P_{32}, correspond. A proxy of fracture scale is fracture size: In addition to the obvious fracture property, its size, it is a measure of the potential connectivity and the scale of the individual flow segments. It also controls the deformation and stress fluctuation induced by the fracture.

A critical indicator of the DFN scaling relationship is the size exponent (k), defined by:

$$k(l) = -\frac{d \log n_{3D}(l)}{d \log l} - 1$$

Equation (6-6)

The contribution of fractures according to their size is controlled by k. This is used to assess the range of scales that control a parameter or a physical process. For instance, the network connectivity depends on the third moment of the size distribution $n_{3D}(l)$ (Bour and Davy 1998, de Dreuzy et al. 2000). If $k > 3$, the contribution of the smallest fractures is dominant, and, conversely, large fractures control connectivity for $k < 3$. A similar discussion is developed in Davy et al. (2018b) for effective elastic mechanical properties.

The counterpart of scaling laws are characteristic scales, which give limits to fracture contributions and changes in the density scaling. Identifying them is an important part of the DFN methodology since most of the physical processes are controlled by a small range of characteristic sizes, either defined by the physical process itself or by the DFN characteristic scales (see the example in Davy et al. (2018a)).

Several statistical models adapted to multiscale distributions of fracture sizes are listed in Subsection 6.6.4.

6.3.3 Intensity terms and moments of the density distribution function

In general terms, the moments of a statistical density distribution are useful to characterise and analyse typical characteristics of the distribution. The moment of order 0 defines the number of elements, the moment of order 1 defines the average, the distribution standard deviation derives from a combination between the moment of order 1 and 2, and moments of order n, with n larger than 2, define higher level statistical indicators.

Some moments of the fracture density distribution specifically express a physical meaning essential to DFN modelling. They allow for establishing comparisons between different models, between observations and models and between theoretical models and their numerical realisations. The statistical moments of fracture density distributions are integrated values. They are defined in the general framework below (Equation (6-7) to Equation (6-10)).

Classically some of these moments are referred to as **fracture intensity** terms and summarised with the notation P_{XY} introduced by Dershowitz and Herda (1992) to describe fracturing properties. In this notation (see Figure 6-1), X is the dimension of the sampling domain (3 for a volume, 2 for a surface and 1 for a line) and Y is the dimension of the object. Hence, for a specific range of parameters (e.g. sizes within $[l_{min} - l_{max}]$), P_{32} is the fracture surface per unit of volume, P_{30} is the number of fractures per unit of volume, P_{21} is the fracture trace length per unit surface, P_{10} is the number of fractures per unit length and P_{33} is the fracture volume (void) per unit volume. These quantities are commonly used as measures of the fracturing intensity as observed on outcrops (P_{21}) or along boreholes (P_{10}) or as the main macroscopic measure of a fractured system as the total fracture surface area (P_{32}).

In the general framework, M_0 is the moment of order 0, already introduced in the previous section as the total number of fractures per unit of volume:

$$M_0 = \int n_{3D}(P) dP$$

Equation (6-7)

where P refers to all the properties (l, θ, ϕ, u) of the fracture density distribution.

M_0, or P_{30}, is the total number of fractures per unit volume, when integrated over all their properties.

The moments of order 1 of the fracture density distribution, for any parameter p, are defined as:

$$M_1^p = \int n_{3D}(p) \, p \, dp$$

Equation (6-8)

The ratio M_1^p/M_0 defines the average of the parameter p (the fracture size l, for instance).

Higher level moments, especially when defined for the fracture size density distribution – $n_{3D}(l)$ – are also of importance. For fracture sizes, the moment of order 2 reflects the total surface of fracture per unit volume. The expression below is adapted to disc-shaped fractures, where the fracture size is the fracture diameter and the fracture surface is $\pi l^2/4$ (any other expression can be used to account for different shapes):

$$M_2^l = \int n_{3D}(l)\frac{\pi}{4}l^2 \, dl \qquad\qquad \text{Equation (6-9)}$$

Thus defined, M_2^l is fracture intensity term P_{32}.

The last, but not least, significant moment of the fracture size density distribution (modified with a given normalization $\pi^2/8$, as explained below), is the moment of order 3, M_3^l:

$$M_3^l = \int n_{3D}(l)\frac{\pi^2}{8}l^3 \, dl \qquad\qquad \text{Equation (6-10)}$$

This dimensionless moment of the distribution is a cornerstone of the percolation theory and thus often called percolation parameter (Bour and Davy 1998, de Dreuzy et al. 2000, Barker 2018). It is primary a statistical indicator of the degree of connectivity within a DFN, and therefore it is an essential indicator for all flow applications (see Section 8.6).

To keep the formalism simple, integration boundaries were not specified in the preceding Equation (6-7) to Equation (6-10). But in every case, the final number of fractures, the parameter averages, the intensity P_{32} or the percolation parameter, all density distribution moments or intensity terms are dependent on the range of values over which the density distribution parameters are integrated.

		Number of fractures	Trace length	Fracture area	Fracture volume
		0	1	2	3
1D	1	P_{10}	P_{11}		
2D	2	P_{20}	P_{21}	P_{22}	
3D	3	P_{30}	P_{31}	P_{32}	P_{33}

Figure 6-1. *Conceptual representation of intensity terms P_{xy} in different spatial dimensions x (lines in the table) and for geometrical objects of dimensions y (columns in the table). Modified from Dershowitz and Herda (1992).*

6.3.4 Representativeness of the density distribution

The representativeness of fracture density distribution measurements is a key issue of the DFN modelling workflow. Identifying fracture domains from a geological point of view, as it is discussed in Chapters 3 and 5, is a necessary first step. Going further requires the capacity to model the natural spatial variations, and domain scale dependency, of the fracture density distribution. This has been solved for two reference models: randomly uniform (Poisson) and fractal distributions (see Subsection 6.6.5).

The former is addressed by Lavoine et al. (2019), who demonstrates that the average of n_{3D} (P) does not depend on the measurement volume V, but the variability depends on V in a way which relates to the size distribution of fractures.

For the latter, if the fractal dimension is less than the Euclidean dimension, the fractal model yields large, and irrespective of scale, fluctuations of the average density (see Figure 6-2 right column) and a decrease with scale of the average density proportional to $V^{D/3-1}$ (with D the fractal dimension and V the volume of interest). We note that to observe this scale dependency (Bonnet et al. 2001), the density measures must be done on the fracture structure (i.e., avoiding empty volumes of fractures). Otherwise, if the measures are randomly located from one scale to the other, the fluctuations still vary as $V^{D/3-1}$ but the apparent average density evolution with scale (volume V) becomes scale independent.

It is a key step, though challenging, of the DFN modelling process, to consistently estimate and model the spatial variations of real fracture systems and so to evaluate the representativeness of the measures (see also 5.3).

6.3.5 Beyond the fracture density distribution

Density fluctuations, scaling and spatial organisation

The fracture density distribution n_{3D} (P) as defined above mainly defines the density as a whole, thus determining the amount of fractures per unit volume, but not how these fractures are spatially organized. The most widespread model for describing the spatial distribution of density is using a Poisson point process (see below). In such a model the density is scale independent, i.e., the density of fracture is linearly proportional to the Euclidean dimension of the sampled volume, which means that area normalisation, the procedure of extrapolating e.g. outcrop samples of fracture intensity to a larger area or volume, is also linear.

However, numerous studies emphasise significant spatial correlations in fracture systems that can be expressed as a fractal organization of the DFN density scaling or as correlations between fracture position, orientation, size and terminations (both discussed below). The latter are also key components of the genetic models for DFN growth.

Poisson point process

Models based on Poisson point processes are historically the most widely used form of DFN model (Baecher et al. 1977, Dershowitz and Einstein 1988), where the spatial distribution of fractures is assumed to be statistically homogeneous. In a Poisson process, fractures with uniformly random positions are independently added until a target intensity is reached in a given generation region (Figure 6-2, left column bottom). On average, the intensity is scale invariant, which means that it is constant with change of size of the sampling support. Intensity variability results naturally from the Poisson generation process, which is scale dependent, and can be quantified and compared to measured variability (Lavoine et al. 2020).

Fractal organization

Many studies (Bonnet et al. 2001, Bour et al. 2002, Marrett et al. 2018, Moein et al. 2019) and references therein have reported a potential fractal organization of fracture systems, with consequences on the scaling of the DFN density distribution.

The classical definition for a **fractal object** is given by the number of segments, circles or spheres of dimension D equal to 1, 2 or 3, and of characteristic length scale r, necessary to cover a fractal object included in a volume R^D. This number should vary as:

$$N(r, R) \approx \left(\frac{R}{r}\right)^D,$$

<div align="right">Equation (6-11)</div>

where D denotes the fractal dimension.

When applied to DFN models, the consequences of the fractal organization are twofold. First the scaling properties of the density distribution are dependent on the fractal dimension:

$$n_{3D}(l, L) = L^D n_{3D}(l)$$

<div align="right">Equation (6-12)</div>

With $n_{3D}(l)$ defined in Equation (6-2), D the fractal dimension and L the domain size extent. If the 3D DFN density model is homogeneous, then $D = 3$ and the number of fractures in a volume is simply proportional to the volume, it is scale independent and thus equivalent to a Poisson point process. If $D < 3$, the density model is fractal.

The second consequence of the fractal organization is illustrated in Figure 6-2. Visually the fractal dimension reflects the spatial distribution through the degree of clustering and holes.
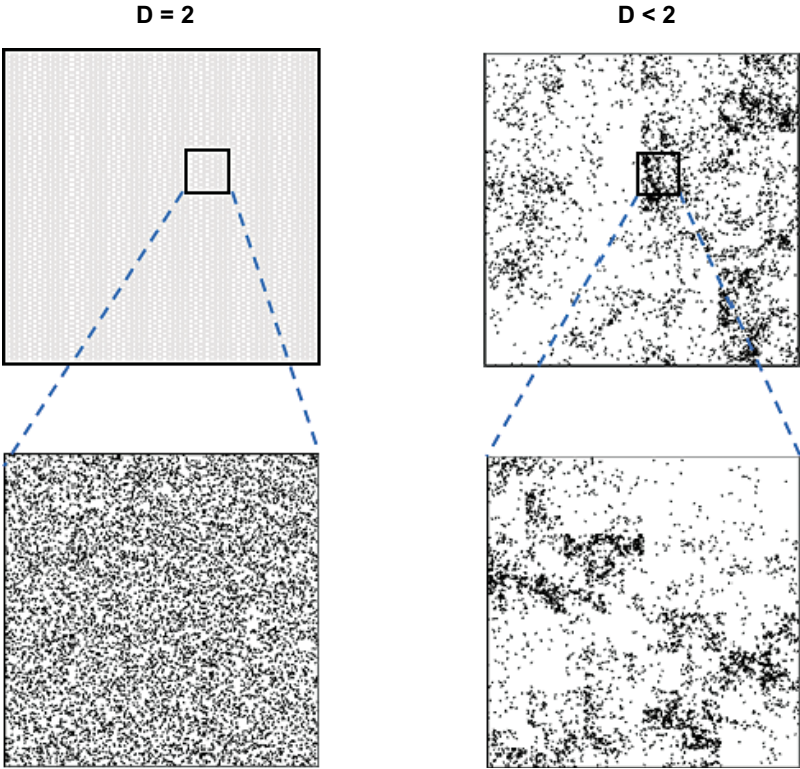
Figure 6-2. *Fracture positions of a 2D DFN are determined by a Poisson process on the left (D = 2) and by a fractal process with D < 2 on the right. From top to bottom is illustrated the hierarchical nature of the clustering. From Darcel et al. (2004).*

Limits of the density scaling distribution model

The density distribution $n_{3D}(P)$ defines only scaling and statistical relationships of the DFN. Spatial density variations (clustering, anti-clustering, fracture domains, etc) can be easily added to the framework in a deterministic mode, with change of parameters in different fracture domains, or in a stochastic mode with the fractal or Poisson's organization (see above).

However, these add-ons do not define existing, local, correlations between the positions of neighbouring fractures, which are reflected by specific fracture terminations (e.g. T-terminations) and intersections or by local clustering or anti-clustering of fractures around smaller or larger structures. Neglecting these aspects of the fractured system may thus lead to the negligence of critical properties of the DFN structure, starting by a misunderstanding of the DFN structures emerging properties, such as the density scaling itself, the connectivity or the flow structure.

The processes at the origin of abovementioned correlations are the same as those that control the other scaling and statistical aspects of the density distribution (Davy et al. 2010, 2013). To overcome the limits of the basic density distribution, it is recommended to improve the knowledge on the dominating processes which drive the DFN growth and to identify further measurable indicators of spatial correlations. We introduce below two classes of the DFN modelling framework which not only rely on the final statistics of the fractured system but aim to reproduce, with a more or less significant degree of realism, the physical rules behind the DFN growth.

Geomechanical models

Geomechanical approaches aim at applying various laws of physics to simulate ductile and brittle failure of rock, with all the inherent complexity. For example, Renshaw and Pollard (1994) simulated fracture growth in *2D* with feedback through the stress field with fractures growing where the stress at their tips exceed a critical threshold. This produces many realistic features like fractures curving toward each other, bridging gaps between fractures. More recently, Paluszny and Zimmerman (2011, 2013) presented methods for fracture generation in a full *3D* stress state, generating a *3D* DFN model by applying basic geomechanical laws, adaptive finite elements meshes, and impulse based methods for collision. Their method generates realistic looking fracture patterns, allowing for quantification of fracture interactions based on mechanical principles and creates aperture distributions that depend on local interaction effects. Methods based on geomechanical principles do not use information about observed fractures directly and are based purely on stress states and constitutive laws of the material. The drawbacks of such methods are that they are computationally very expensive and, as of yet, the match of modelled to observed fractures, i.e., conditioning, is yet unresolved.

Genetic models

Genetic models are mainly based on the life cycle of fractures (Renshaw and Pollard 1994, Renshaw 1996, Olson 2004, Davy et al. 2010, 2013). They describe, in a simplified way, the fracturing processes relative to initial fracture **nucleation**, then **growth** and finally "pseudo-mechanical" interactions with potential potentially **coalescence** and **arrest**. These models are a compromise on the complexity scale of DFN modelling, between the highest level represented by geomechanical models and the level where only statistical density distributions are simulated. Accordingly, the final scaling nature of the fracture size density distribution, or the topology of the fracture terminations should be emerging properties of the genetic approach rather than purely calibration parameters. A genetic model should be defined by a clear set of rules for growing the fracture network, where the rules are a sound simplification underlying physical and geomechanical true processes.

Nucleation is a time-wise fracture birth process controlled by a certain rate of nucleation. Once created, fractures **grow** at a rate dependent on the stress intensity factors at their tip and on the physical or chemical nature of fracturing (Paris and Erdogan 1963). For a constant nucleation rate, the emerging size density distribution of growing fractures is governed by the growth law. If the growth law is a power-law (Charles 1958), then the emerging fracture size density distribution will tend to be a power-law too (Davy et al. 2010, 2013).

During the growth process, mechanical interactions potentially become predominant when the fractures become larger and larger, and closer to each other, affecting their growth. Then, either their growth speeds up due to fracture **coalescence**, or it slows down and even **stop** due to mechanical inhibitions (Davy et al. 2010, 2013). The coalescence mechanism was shown on *2D* numerical simulations with subparallel fractures (Spyropoulos et al. 1999, 2002, Hardacre and Cowie 2003a, b), while the arrest or stop mechanism was suggested by Davy et al. (2010, 2013) to account for the observation of a large proportion of T-shape intersections (also shown on analogue experiments by Davy et al. (1990) and Sornette et al. (1990, 1993). In both cases, the resulting fracture size density distribution of the interacting regime and of larger fractures is significantly affected. One expects an exponential fracture size distribution for coalescence and a power-law for inhibition. A main difference between both processes is that coalescence leads to larger fracture densities for large fractures than for small ones, while inhibition leads to the opposite.

The inhibition model, as developed by Davy et al. (2010, 2013), hereafter called **UFM** by reference to Davy et al. (2010), is based on the assumption that, when two fractures intersect, the smallest is likely to stop while the largest continues to grow. This simple hierarchical rule leads to a quasi-unique self-similar scaling trend for the fracture size distribution (a power-law of scaling exponent equal to −4) whereas the total fracture density is a function of the complexity of the orientation distribution.

To sum-up, the size distribution readily emerging from the UFM model, as defined in Davy et al. (2010, 2013), is a doubly power-law model whose scaling exponent at small scales is deduced from the fracture growth rate law and whose scaling exponent at larger scales is unique and correspond to self-similar properties. The UFM model also determines the proportion of T and X terminations in the DFN. The transition scale between the two regimes is a major feature of the DFN geometrical and connectivity structure. It defines the largest typical size of "intact blocks", i.e., the blocks that are not crossed by fractures. It also controls the connectivity level. This model relies on strong physical bases for defining the genetic rules and has adequately reproduced the multiscale fracture size density distribution from the Forsmark fractured system (Davy et al. 2010, 2013).

The reliability of genetic models for the DFN methodology relies on 3 points:

- relevance of the underlying physical rules,

- ability to understand the geological processes that led to the observed fracturing patterns,

- capacity to generate realistic density distributions and fracture pattern.

Adaptation of genetic models to site conditions

As a trade-off between genetic models and models based on statistical analyses of observed fractures, several attempts are currently being made to increase the realism of DFN models by combining calibration steps, especially by introducing the steps of the deformation history into the growth processes, final statistical distributions and genetic-like rules.

For instance, with the Grown DFN (G-DFN) method (Libby et al. 2019) fractures are nucleated and grown by some sets according to the deformation history and are parameterised by an expected size model and termination probability matrix (see Subsection 6.6.5). There are also rules for the effects of shadowing around existing fractures preventing new fractures nucleating next to ones of the same generation, and for changing the shape of fractures if they propagate into more ductile rock (i.e., the growth of fracture tips decelerates as they encounter such rock). The inputs for these methods are a combination of probability density distributions and can include geocellular based parameters and the growth rules. However, these inputs can represent *a priori* assumptions that affect properties that emerge as results from the growth process, such as fracture size distribution and proportions of terminations. Hence, some iteration can be involved to reproduce observed characteristics of the network.

Adaptation of the UFM framework to account for major stress conditions representative of the deformation history, and therefore steps of the deformation history is also ongoing. This is firstly done by refining the nucleation and growth laws according to stress conditions.

Regardless of which DFN model is chosen for a particular task, it is of critical importance to explicitly and clearly state the rules of the DFN growth process and the modelling assumptions, that is, whether or not the spatial correlations are emerging properties from the generation process or purely a result

of calibration, as the emerging spatial correlations may be very different for the different driving conditions. It is also worth mentioning that stages of the deformation history are themselves models with significant uncertainties.

We review in the Subsection 6.6.6 the data interpretations which can be used to compare the results of genetic-based DFN and observations.

6.4 From data to models

6.4.1 Strategy for estimating the density model for different set of parameters

The calculation of n_{3D} (P) for a set of parameters P requires the binning of all the parameter ranges and to count the fractures that fulfil the binning conditions, e.g. size between l and $l + dl$, strike between θ and $\theta + d\theta$, dip between ϕ and $\phi + d\phi$, etc. The reliability of the density measure depends on the number of fractures in each multi-parameter bins $P + dP$. The bin widths can be adapted for this as already suggested in Section 6.3, but this may not be sufficient if the amount of data is not large enough for the number of screened parameters.

In practice, it may be convenient to calculate partial densities for a subset of parameters as indicated in Section 6.3, e.g. first calculating the size distribution n_{3D} (l) and then the orientation distribution n_{3D} (θ, ϕ). If both subsets of parameters are uncorrelated, the full distribution is:

$$n_{3D}(l, \theta, \phi) = \frac{n_{3D}(l) * n_{3D}(\theta, \phi)}{\int_l \int_{\theta,\phi} n_{3D}(l, \theta, \phi) \, dl \, d\theta d\phi}$$

Equation (6-13)

The double integral to the denominator is simply the number of mapped fractures.

In general, the conditions under which partial density distributions can be recombined to get a complete 3D distribution are:

- If the subset of parameters is uncorrelated (as abovementioned);

- If one parameter derives from the others, e.g. if u depends on size and orientations, u (l, θ, ϕ), then n_{3D} (l, θ, ϕ, u) reduces to n_{3D} (l, θ, ϕ);

- If the total population can be split into groups of fractures (like the fracture sets, see Subsection 6.6.1) where one of the above assumptions can be applied.

Whatever the conditions, if n_{3D} (l, θ, ϕ, u) derives from partial density distribution measurements, all the assumptions used to derive it should be clearly stated in the modelling exercise.

6.4.2 Completeness of the fracture density distribution

The fracture density distribution n_{3D} (P) defines the intrinsic density of DFN properties, so, when inferred from data, it should be independent from mapping biases and of sampling volume limits (see also the discussion further in this section). In practice, the density distribution in Equation (6-2) is reliable only if the fracture counting is exhaustive in the domain V and in the range $[P, P + dP]$ or if unexhaustive counting can be quantitatively modelled and compensated for.

The completeness of data is not possible for all the parameters and parameter ranges. Sampling issues occur due to resolution effects (limit below which small events are not detected), censoring effects (events that are partially known because the probability to observe them is small) or shadow effects (events that are not well placed with respect to the sampling support).

Let us illustrate the consequences with the issue of fracture sizes, for which sampling effects affect both ends of the size distribution: No fracture can be observed below l_{min} (resolution effect); the largest fracture that can be mapped in the sampling domain is l_{max} (censoring effect). The integrals of the density distribution C_{3D} $(l_1, l_2) = \int_{l_1}^{l_2} n_{3D}$ $(l)dl$ are independent of sampling biases only if the lower bound of the integral is larger than l_{min} and the upper bound smaller than l_{max}. It means that both the cumulative and the complementary cumulative density distributions, $C(0, l)$ and $C(l, \infty)$ respectively, are affected by sampling biases.

The total number of fractures per unit volume is theoretically $C(0, \infty)$ but the actual value is limited due to the resolution and censoring scales: $C(l_{min}, l_{max})$. As a consequence, the probability density distribution function of fracture sizes, $pdf(l) = \frac{n_{3D}(l)}{C(0,\infty)}$ cannot be estimated. The "pseudo" pdf calculated from the dataset – i.e., $\frac{n_{3D}(l)}{\int_{l_{min}}^{l_{max}} n_{3D}(l)dl}$ – is always larger than the real pdf since it is affected by resolution and censoring effects.

This example can be generalized to any fracture parameter affected by sampling biases. It illustrates why it is necessary to pay attention to the use of cumulative distributions and probability density functions.

6.4.3   From *1D* and *2D* data to *3D* models

One objective of fracture field mapping is to collect as much information as necessary to characterise statistically the fracture population ($n_{3D}(P)$, the fracture density distribution). There are inherent limitations with this process, as individual fractures cannot be entirely sampled, and as only a small portion of the entire population can be sampled.

This is in practice one fundamental problem of DFN modelling: DFN models require a *3D* parametrization that can never be measured directly but rather must be inferred from *1D* (boreholes) and *2D* (surfaces) data. Hence, the vast majority of fracture data are incomplete fracture geometries, predominantly fractures traces which are defined as intersections with the surface of the physical sampling support (outcrop, tunnel, drill core).

The scientific field called *Stereology* studies the intersections between objects of various dimensions and build rules to link the *3D* properties to the *1D* and *2D* properties. Applied to a DFN context, stereology explores relationships between the models and parameters of the volumetric DFN, i.e., relative to the density distribution n_{3D} and the distributions of lower dimensions, resulting from the intersection between the 3D DFN with any physical sampling support. Sampling supports can be sorted into 4 main types, as:

*   Scanline (1*D*).
*   Roughly planar surface (2*D*).
*   Curved surface (2*D*), e.g. tunnel wall (side walls, ceiling and floor).
*   Volume (3*D*), e.g. CT scan of whole core.

Stereological analyses in the DFN context not only involve intersection and dimensional aspects, but also mapping resolution (traces smaller than the resolution are not mapped), censoring (traces larger than the sampling map) and statistical representativity conditions. These are particularly critical to build up the *3D* fracture size density distribution (n_{3D}) from the lower dimension distributions (n_{2D} or n_{1D}).

Conceptually, both core logs/borehole image logs and tunnels can be viewed as approximately cylindrical shapes whose main difference is their diameter scale. At one extreme, and depending on the resolution conditions, if the sampling diameter vanishes (i.e. if the sampling diameter is much smaller that the smallest fracture radius), the sampling support becomes a line (1*D*). Then the sampled data should be interpreted from a 1*D*-3*D* stereological framework, where fracture traces are reduced to intersection points between fracture and sampling support. On the other extreme, if the traces are much smaller than the cylinder diameter, the resulting data can be interpreted from a 2*D*-3*D* stereological framework. In-between, if the sampled fractures are larger than the cylinder diameter (with full perimeter intersection fractures), then the 1*D*-3*D* framework is applicable with the addition of the orientation information. The latter is the common framework for interpreting core-log data. Finally, specific stereological rules can be used when the sampling conditions cannot be simplified into the 1*D*-2*D*-3*D* framework.

Stereological rules, thus, aim to determine the relationships between a lower dimension distribution and the 3*D* fracture density distribution. The definition of n_{2D} and n_{1D} is given in Section 6.3. In case of drill core mapping and in the absence of fracture size information, it is convenient to map fractures that overlaps the core centreline. It has been demonstrated that this is a way to select fractures whose size is larger than the core diameter (Davy et al. 2006). The number of fractures per unit core length L is:

$$n_{1D}\left(P_{p\neq l}\right) = \frac{1}{L}\int_{d_o}^{\infty} n_{1D}\left(l, P_{p\neq l}\right)dl \qquad\qquad \text{Equation (6-14)}$$

l the size of the fracture f, d_0 the core diameter, $P \neq l$ is the set of all fracture parameters except l, and L the length of the sampled core section. When integrated over all the parameters $P_{P\neq l}$, n_{1D} is simply the number of fracture intercepts per unit of sample length, otherwise commonly denoted P_{10}.

As already mentioned before in Subsection 6.3.2, any use of cumulative density distributions must inform on the range of fracture sizes which are effectively sampled, at least the resolution limit. If it is unknown, the density estimate cannot be used to reconstruct the 3D density distribution. Once the 3D, 2D and 1D fracture density distributions are analytically defined, the correspondence between their respective parameters is established by stereological rules (Warburton 1980, Piggott 1997, Berkowitz and Adler 1998, Zhang et al. 2002, Darcel et al. 2003, Wang 2005, Davy et al. 2006). It is noteworthy that in theory most of the parameters can be related to each other, there are practical limitations due to sampling conditions. One can predict the apparent density distribution resulting from the sampling of a 3D distribution with a physical sampling support, but the reverse is not straightforward.

The key concept of the stereological framework relies on the definition of the probability of intersection between fractures and sampling support.

For the 2D-3D relation, the density distribution of traces derives from the probability for a fracture of size l and orientation (θ, ϕ), located at a distance z from the 2D outcrop surface, to give a trace t on the outcrop, $\pi_i(l, \theta, \phi, z \to t)$:

$$n_{2D}(t, \theta, \phi) = \int_z dz \int_{l > 2z/\sin\beta_s} \pi_i(l, \theta, \phi, z \to t)\, n_{3D}(l, \theta, \phi)dl \qquad\qquad \text{Equation (6-15)}$$

The second integral is the contribution of fractures larger than $2z/\sin\beta_S$, where β_S is the dihedral angle between the normals (poles) of fractures and 2D plane, while the probability of intersection is null for smaller fractures in the domain specified by z. $\pi_i(l, \theta, \phi, z \to t)$ has an analytical expression for fracture discs and the integral can be calculated analytically in the case of a Poisson distribution of fracture centres and for a wide range of fracture size distributions (Warburton 1980, Piggott 1997, Berkowitz and Adler 1998, Zhang et al. 2002).

A similar combination between 3D and 1D fracture density distributions can be derived. In this case, a strict 1D sampling comes to directly measure the fracture frequency P_{10} along the sampling line. The probability of intersection between the sampling line and a fracture of the 3D density distribution, $\pi_i(l, \theta, \phi, \beta_L)$ is:

$$\pi_i(l, \theta, \phi, \beta_L) = \frac{\pi l^2}{4}\cos\beta_L, \qquad\qquad \text{Equation (6-16)}$$

where β_L is the dihedral angle between the fracture pole and the direction of the sampling line ($\beta_L = 0$ if the fracture pole is parallel to the line), l the fracture size and (θ, ϕ), angles. The 1D-3D stereological then expression is:

$$P_{10} = \frac{1}{L}\int_{\theta,\phi}\int_l \pi_i(l, \theta, \phi, \beta_L)n_{3D}(l)dl\, d\theta d\phi, \qquad\qquad \text{Equation (6-17)}$$

By combining Equation (6-16) with Equation (6-9), it follows that:

$$P_{32}(l \geq l_o) = P_{10}(l \geq l_o) \cdot f(\beta_L) \qquad\qquad \text{Equation (6-18)}$$

where l_0 is the lower boundary of the fracture size density distribution and $f(\beta_L)$ is simply a term integrated over the angle distribution of the DFN relative to the line direction. This shows that for such simplified conditions, the ratio of the 3D cumulative density distribution to the 1D fracture frequency is a factor only dependent of the fracture orientation distribution. In practice, if all fractures of the DFN are perpendicular to the sampling line direction, one gets $P_{32}(l \geq l_o) = P_{10}(l \geq l_o)$. Apart from the P_{32} to P_{10} ratio, the total frequency or cumulated density is dependent on the details of the fracture size density distribution, especially on its lower boundary.

This 1D-3D stereological framework can be adapted to core logging by considering a virtual sampling line at the centre of the core log and by selecting the sub-set of fractures which intersect the core or central line and whose trace is observed on the core log. By doing this one can replace the lower boundary of the fracture size distribution l_0 in Equation (6-18) by d_o the core log diameter.

More elaborated expressions of the intersection probability π_i and of stereological relationships can be found in the literature for different sampling supports and 3D density distributions n_{3D}. These are generally well established for 2D planar outcrops (Piggott 1997, Berkowitz and Adler 1998), scanlines and boreholes (Peacock et al. 2003, Davy et al. 2006, Peacock 2006), but cannot be univocally defined for conditions where the mapping surface cannot be approximated by a 1D or a 2D sampling support, like for tunnel mapping conditions (Mauldon and Mauldon 1997, Mauldon et al. 2001, Gupta and Adler 2006, Patriarche et al. 2007).

Depending on the type of available datasets, one can only partially reconstruct the complete density distribution n_{3D}. The usual way to estimate n_{3D} is to model it by a parametric analytical expression, and to derive its parameters from an inverse procedure.

6.4.4   Building the DFN models for a site

Building numerical models is the core of the DFN methodology. This is based on: (i) integration of data from different sources, (ii) extrapolation beyond data measurements, and (iii) building application models by generating "medium" models , i.e., models that represent the fractured system with its properties (Davy et al. 2018a).

A DFN model relies on deterministic data, specific statistical laws derived from datasets and density measurements, and assumptions based on prior knowledge that compensates for data scarcity and/or incompleteness (for instance, mathematical extrapolations). The determination of the fracture density distributions, in terms of orientations and fracture sizes, are major steps of the DFN model. As an example, the DFN models from the Forsmark SDM 2.2 stage (Fox et al. 2007b) are composed of a mix of Fisher distributions for the orientations and power-law distributions for the fracture sizes, all combined within the global density distribution framework.

We distinguish two main techniques of DFN modelling. The first are "data-driven" DFNs in that fracture properties are modelled stochastically (Monte Carlo) from distributions derived from sampled data. The sampling may use deterministic values, the raw data distributions, or interpreted data distributions (e.g. a density distribution n_{3D}, sets of Fisher models for orientations or power-law model for sizes). Thus, the DFN fracture density distribution model interpreted from measurements is used directly in the simulation process. When sampled values are fixed at measurements at the observation points, the model can be said to be "conditioned".

The second class of models are process-based models (e.g. the geomechanical and genetic models from Subsection 6.3.5). These models mimic the growth of a DFN, and potentially the tectonic deformation history or parts thereof. They constitute another way to generate systems with increased geological realism (see above Subsection 6.3.5).

The two techniques lie on a spectrum between fully statistical (Poisson point process models) and detailed mechanistic models of fracture growth, with the two methods often being combined to account for fracture interactions such as fracture clustering or T-intersections (e.g. Bonneau et al. 2013, 2016).

In the following sections, we review the type of available interpretation methods and models successively for the partial density distributions defined in Section 6.3 as part of the complete DFN density distribution. This part of the DFN methodology shall next be combined with the site scale variability analysis of Chapter 5.

All modelling allows, and requires, interpretations to various degrees. Even if the interpretation process is standardized, successive assumptions are made to complement the relative weakness or scarcity of data. Therefore, no order is specified in the next sections, but the DFN modeller should clearly state and document, in e.g. a modelling logbook, the successive modelling choices and assumptions made during each step of the process.

6.4.5 Modelling the anatomy of deformation zones

As sketched in Figure 5-1, deformation zones can be treated as specific fracture domains with distinct descriptions of the fracturing within them. A photograph of such a zone is shown in Figure 1-18. The variable connectivity, extent and properties of these "fault-related" fractures likely give rise to significant heterogeneity in the mechanical, hydraulic and transport properties of the composite zone, see Subsection 5.2.1. This heterogeneity would imply that deformation, flow and transport may be much more localised than would be predicted by a model where the zone is represented by a continuous plane with properties either uniform or having some simple trend. To gain an understanding of this heterogeneity it is necessary to describe the internal structural anatomy of the zone, considering them as essentially tabular fracture domains with different properties, e.g., intensity, orientation, mineralogy compared to the background rock. Once this has been achieved, it is possible to simplify the explicitly modelled zones by upscaling them to represent their spatial variability as effective properties on a sub-planar structure (Baxter et al. 2019).

In principle, the parameterisation of each deformation zone can be different, or they can be grouped by orientation set, size or some other characteristics. The analysis of each fracture property therefore has to be made by first separating the fracture borehole data using the Geological single hole interpretation (GSHI) and tunnel data by Single tunnel interpretation (STI). The deformation parameterisation should then include:

- **Intensity, sizes and orientation** of fractures within deformation zones and whether there are correlations in these to the zone's properties such as extent and orientation of the zone. For example, what is the enhancement and relative orientation of fracturing within the core and damage zone of the deformation zone? Orientation and intensity can be measured in boreholes, but size requires outcrop data, or ideally tunnel mapping of deformation zone intercepts.

- The hanging and footwall **thicknesses** of the damage zone of the deformation zone. The thickness of the damage zone is most important, rather than the fault core, since water conducting fractures often cluster outside the fault core and may even be concentrated to the flanking contacts to the wall rock. Typical conceptual questions may be: Is there any typical ratio of the hanging to footwall thickness and, if so, what is it? What is the spatial variability in hanging and footwall thicknesses? How do hanging and footwall thicknesses correlate with size and orientation of the deformation zone? How to adequately determine the boundaries of the damage zone for the purpose of DFN modelling?

- The **apertures, degree of openness and mineralogy** of fractures within deformation zones and prevalence of **rock mass alteration** within the damage zone. Other related properties for use in mechanical, hydraulic or transport properties should also be characterised separately for zones.

The deformation zone model is used to make appropriate subdivision of the fracture database between fault-related fractures and flows from individual fractures in the intervening wall rock, i.e., to make separate analyses of volumes suitable for disposal from those potentially less favourable for long-term safety. As such, the definition of the zone thickness should be the *total zone thickness,* including both core and damage zone, and will be defined by the primary indicators: fracture intensity, fault rocks, shear striae, and displacement; and secondary indicators: mineralogy, alteration, fracture apertures, caliper anomalies, flows, and decreased resistivity/magnetic susceptibility (**DGMM**).

Having made deformation zone-specific analyses, models can be extrapolated across both deterministic and stochastic deformation zones, constraining values to observations at borehole intersections. Several modelling approaches are available to explicitly represent the anatomy of deformation zones, the main ones being:

- **Parent-daughter methods** where fractures are generated around triangulated semi-planar midplanes of the deformation zones, assuming a spatial correlation of "daughter" fractures to larger "parent" fractures, e.g. to represent the damage zone around a fault (Billaux et al. 1989). More generally the parent can be a tabular non-planar structure and the parent can be removed after the generation of the daughters if there is no apparent discontinuity at the fault core. The centres of the daughter fractures are spatially distributed with a decay of fracture intensity, away from the core plane, that is steered by a probability distribution, e.g. exponential as proposed by Faulkner et al. (2011). The decay constant scales with the damage zone thicknesses and is tuned to ensure the total fracture count of deformation related fractures in simulations of the boreholes is on average consistent with mapping.

- **Gridded faults** the properties of a deformation zone can be described on a grid that provide input to generating fractures and their properties in each fault-related grid cell. This grid used can be a so called geocellular model (see Subsection 4.3.4) of the whole domain, but then the grid needs to be fine enough to describe the thickness of the deformation zones and any internal variability within them. Alternatively, a local grid can be constructed with the boundaries of the damage zone of each fault and used to describe the input to fracture generation specific to that fault.

With either method the fault-related fractures are generated separately from the surrounding fractures domains and combined by superposition.

Once a detailed representation of the internal structure of deformation zones has been created its hydraulic properties need to be calibrated against hydrogeological data (see Section 8.8) and possibly against mechanical data. Hydraulic calibration is most useful when done on multiple scales, e.g. flow logging in single boreholes or discrete tunnel inflow measurements, to quantify the distribution and intensity of individual fault-related flows, and multi-hole, e.g. interference tests or hydraulic monitoring during drilling and construction, to quantify the inter-connectivity of open fractures within zones (e.g. Chapter 9 of Hartley et al. 2018b). After calibration, the complexity of representing each zone in this way can be simplified to a more conventional model of equivalent mechanical, hydraulic and transport properties defined on the semi-planar fault zone mid-plane. Such an approach has been demonstrated by Baxter et al. (2019). Simplifying the fracture swarm description in this way provides (i) a mechanism to analyse the variability in the effective transmissivity, porosity, and flow wetted surface of the fault for communication purposes; (ii) provides input to downstream modellers requiring a simplified representation for deformation zones; and (iii) allows generation of realisations of transmissivity and porosity (through geostatistical models) as an expedient way to assess stochastic uncertainty (i.e., without having to run several large DFN realisations).

6.5 Sources and types of fracture geometry data

A summary of the types of existing geological information relevant to fracture modelling is listed in Subsection 4.1.1. In this section, we introduce the information currently available and data types which are expected to emanate from the planned access tunnels and shafts.

6.5.1 Data from surface-based investigations

Fracture data stemming from surface investigation are commonly available in 3 basic forms: remote geophysical data, ground geophysical data and data from outcrop mapping. Remote geophysical methods may include airborne magnetic measurements, airborne gravity measurements, airborne electric measurements, lidar measurements and, recently, drone imagery.

The remote sensing data is used to construct large-scale maps of lineaments (Figure 6-3), preliminarily assumed to represent the intersections of larger fractures and deformation zones with the surface. Remote methods can be complemented with ground magnetic surveys (Isaksson et al. 2006a, b) to locally increase the resolution. Detailed investigations of a relevant subset of these lineaments may reveal whether or not these are deformation zones, for example by trenching across the lineament and mapping the fractures using either scanline or area mapping (see below). Lineaments that are considered to represent deformation zones constitute the foundation of a *2D* deformation zone model. Such a model, together with borehole information and outcrop mapping are the building blocks for the *3D* geological model and DFN models of a site.

Outcrop mapping is commonly performed in any of the following forms: Area mapping (Figure 6-4), scanline mapping or non-systematic mapping. The area mapping method (e.g., Mauldon et al. 2001, Peacock et al. 2003) has the advantage of being systematic, objective and allows for robust handling of sampling bias but is, on the other hand, time consuming. The scanline method (Priest and Hudson 1981, Mauldon et al. 2001, Peacock et al. 2003) is also objective and systematic, much faster but is more challenging with regards to correction for sampling bias (Kulatilake and Wu 1984, La Pointe and Hudson 1985, Wathugala et al. 1990, Priest 1993, Mauldon 1994, Mauldon and Mauldon 1997, Mauldon et al. 2001) compared to area mapping. Non-systematic mapping has the advantage of covering large areas fairly rapidly but suffers from subjectivity and can only be used for qualitative purposes, e.g. inference on relative ages, kinematics, etc.
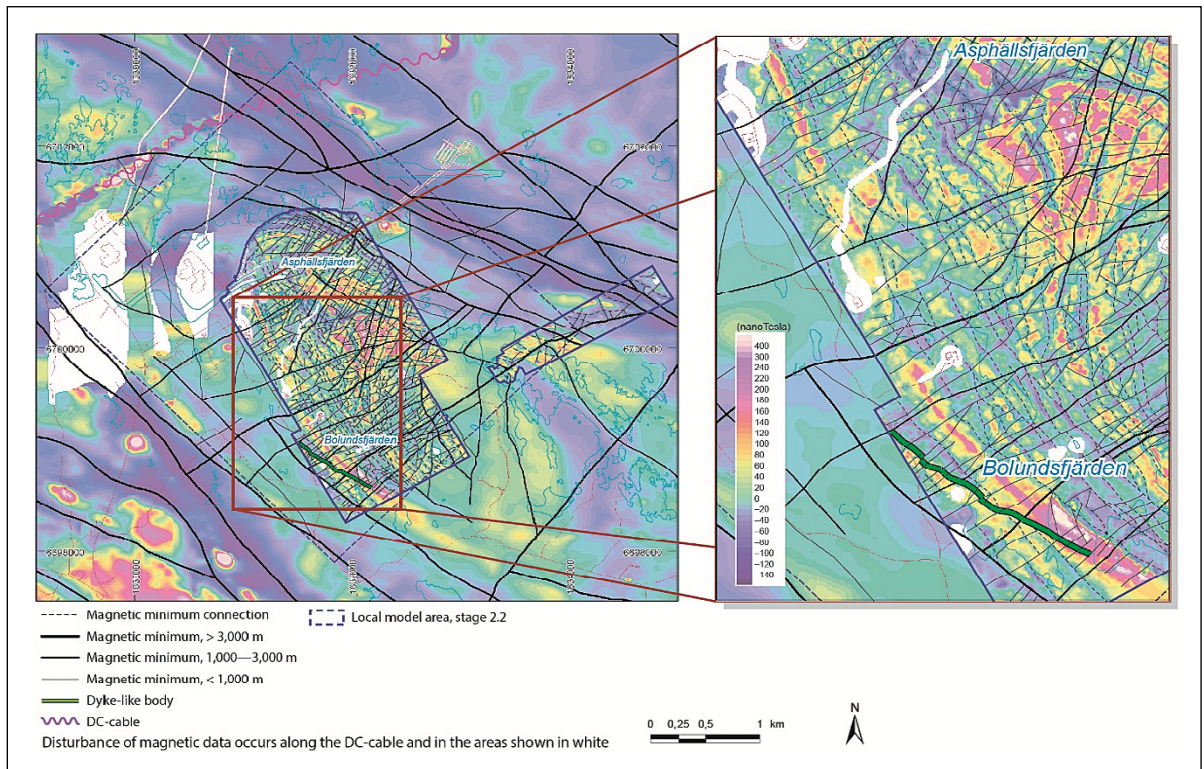
Figure 6-3. *Low magnetic lineaments identified inside and immediately around the Forsmark local model area (after Stephens et al. 2007, Figure 3-39) using a combination of airborne and ground based geophysics.*

At Forsmark, both area- and scanline mapping were used. The latter to locally sample fracture trace lengths below the truncation limit (0.5 m) set by sampling policy for area sampling. Locally, the truncation limit was set to 0.1–0.25 m.

Surface data, i.e., lineaments and outcrops, are primarily used to assess the trace length distribution and intensity distribution, and its scaling, from which the *3D* fracture density distribution of the fracture network can be inferred.
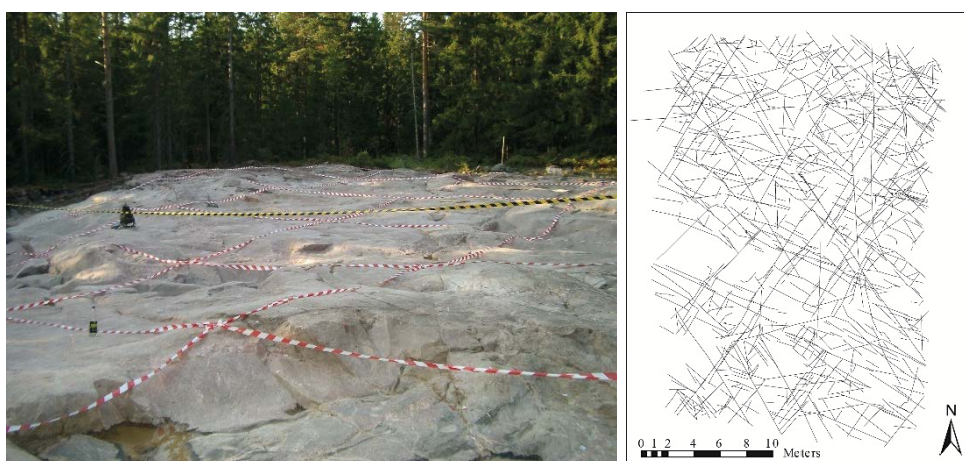
Figure 6-4. *a) Exhumed outcrop at drill site BP2 at Forsmark showing the grid used for area mapping. b) Fracture trace map from mapping of outcrop BP2.*

Surface data also provide a more reliable source for fracture orientations as data is sampled from the traces and not, as in boreholes, from small intercepts which only reflect the local orientation of the sampled fracture. However, a known weakness is the bias towards sampling fractures with high angles to the sampling surface, i.e., sub-horizontal fractures are systematically under sampled in outcrop mapping and lineament studies. Their density must be inferred by modelling.

Finally, outcrop data is essential for the inference of fracture T,Y and X (see e.g. Peacock et al. 2016 for terminology) terminations and, implicitly, relative ages, which for some modelling forms assist in simulating an evolution of a fracture network (see Subsection 6.6.6).

6.5.2   Data from surface-drilled boreholes

The structural mapping of boreholes is stored as a composite of core description and image log data in the SKB database SICADA. It is expected that new cored investigation and pilot boreholes drilled underground, with associated drill cores, will be characterised in a similar way as the cored surface drilled holes. The current surface drilled borehole database (September 2019) includes:

- 42 cored holes up to 1 000 m long in Forsmark, KFM01X–KFM09X (where X corresponds with up to 4 holes A–D drilled independently from the same pad), KFM10A–KFM23 (single holes), and the shallow KFM90B–F holes.

- There are also 46 percussion drilled holes up to 300 m long in Forsmark, HFM01–HFM46.

- There are an additional 19 core drilled holes, KFR, in conjunction with the adjacent SFR facility, and 4 percussion holes, HFR.

The structural description is stored in separate files for i) fracture, ii) for crush zones where the core is very fragmented and for iii) "sealed networks". As of April 2021, there are 141 395 fractures interpreted in cored boreholes (93 248 in KFM, 48 147 in KFR) and 408 crush zones of which 360 are mapped in cored holes (206 in KFM, 154 in KFR) and 48 mapped in percussion holes at Forsmark.

Of the fractures interpreted in Forsmark cored holes, 74 169 (80 %) and 31 815 (66 %), in KFM and KFR boreholes respectively, are visible in the borehole imagery system (BIPS) used SKB. The proportions of fractures without any orientation measurement are 14 % and 26 % for KFM and KFR boreholes respectively, whereas the proportions of fractures without any alpha value (minimum angle between borehole trajectory and fracture plane) are 2 % and 23 % for KFM and KFR boreholes respectively. The alpha angle is used to calculate an intensity weighting to compensate for orientation bias when calculating fracture intensity (see Subsection 6.6.3). The depths of fractures are given with a precision of centimetres. The detailed borehole mapping of fractures includes the following properties:

- Open, partly open or sealed. With open fractures being record with confidence: certain, probable or possible. Of the KFM hole fractures, 25 % are recorded as open and 2 % as partly open (the corresponding proportions are 27 % and 2 % in KFR holes). In the HFM and HFR percussion holes, 49 % of the fractures are mapped open and 4 % partly open. Most percussion drill holes are short and do not reach below the highly fractured near-surface bedrock, which explains parts of the difference in the relative frequency of open fractures as compared to cored bore holes. For comparison, the top 200 m of the cored boreholes (KFM and KFR) contain 37 % open or partly open fractures. The difference between cored holes and percussion holes in the top 200 m can be due to a sampling bias towards larger and more open structures in percussion holes, as well as effects due to the differences in drilling techniques.

- Strike and dip from image log, with support of core recordings.

- Alpha and Beta angles to core axis and uncertainties in these.

- Geologic aperture in mm (estimated representative value).

- Mineralogy is given as the 1st, 2nd, 3rd and 4th dominating mineral types. Note however the uncertainty in sampling as shown in Figure 1-16.

- Fracture alteration as Fresh, Slightly altered, Moderately altered, Highly altered and Gouge. Also, Joint alteration, *Ja*, as used by the Q-system.

- Roughness as (Planar, Irregular, Stepped and Undulating) and surface (smooth, slickensided and rough) that together can be converted to Q-system Joint roughness, *Jr*.

- Rock type the fracture is in, from querying the rock type log at the fracture depth.

Other structures are identified (banded, foliated, ductile shear zone, brittle-ductile shear zone, lineated, massive, cataclastic, brecciated) and assigned strike and dip or trend and plunge for planar and linear structures respectively, which provide the input to check for possible correlations between intensity and orientation of fractures with the surrounding rock fabric.

Other types of relevant borehole data are geophysical data and hydraulic data, the latter is dealt with in Section 8.7. Borehole geophysics essential for adequate fracture characterisation includes (see e.g. Petersson et al. 2018 for application):

- Gamma-gamma to measure density and can be used as input for interpretation of sonic logs.

- Various resistivity logs including high resolution "focused" and single point resistivity that can be used to identify open fractures or conductive fracture fills on the borehole wall to confirm core descriptions of openness.

- Full wave sonic to measure P-wave and S-wave velocities that can be used to calculate dynamic elastic properties, which can in turn be used to indicate intervals of increased extensive fractures and tied with rock mass descriptions.

- Fluid resistivity is used in normalising resistivity logs and in determining the salinity of inflowing and outflowing water in fractures intersecting the borehole.

- Temperature is used in combination with fluid resistivity to calculate salinities. Anomalous spikes in temperature logs can also show locations of water conducting fractures.

The richness of the information contained in the well log and the correspondence with the geological interpretation are illustrated in Figure 6-5 and in Figure 6-6. The motivation for plotting stereographic projections of borehole mapped fractures as shown in the examples of Figure 6-5 is explained in Subsection 6.6.2. In Figure 6-5 several types of stereonet are used for the same data showing:

- Depth – to help identify whether orientation clusters are associated with a particular depth or zone,

- contours – to help identify sets,

- alteration or mineralogy – to indicate age or using alteration as a proxy for size, and

- ductile structures – to reveal possible correlations with foliation.

In Figure 6-6 different types of geophysical logs and mapping are combined to aid integrated interpretations: "tadpole" plots of individual fracture orientations are shown alongside Terzaghi corrected intensity within a moving window to help analyse clustering of fractures.
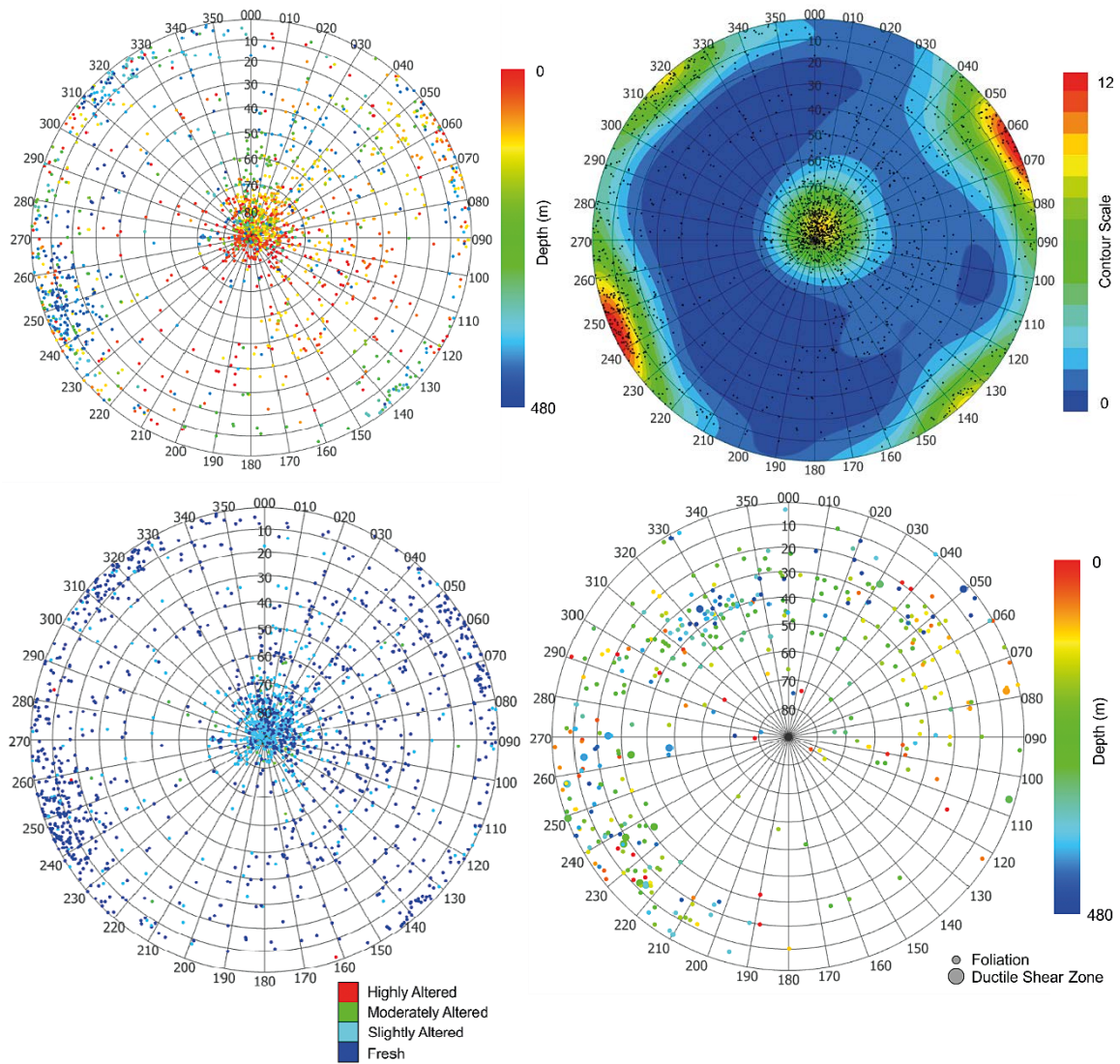
Figure 6-5. *Examples of stereonets for KFM01B. Top left: All fractures poles coloured by depth. Top right: Terzaghi-corrected contour plot. Bottom left: All fractures poles coloured by alteration. Bottom right: foliation and ductile shear zone poles coloured by depth.*
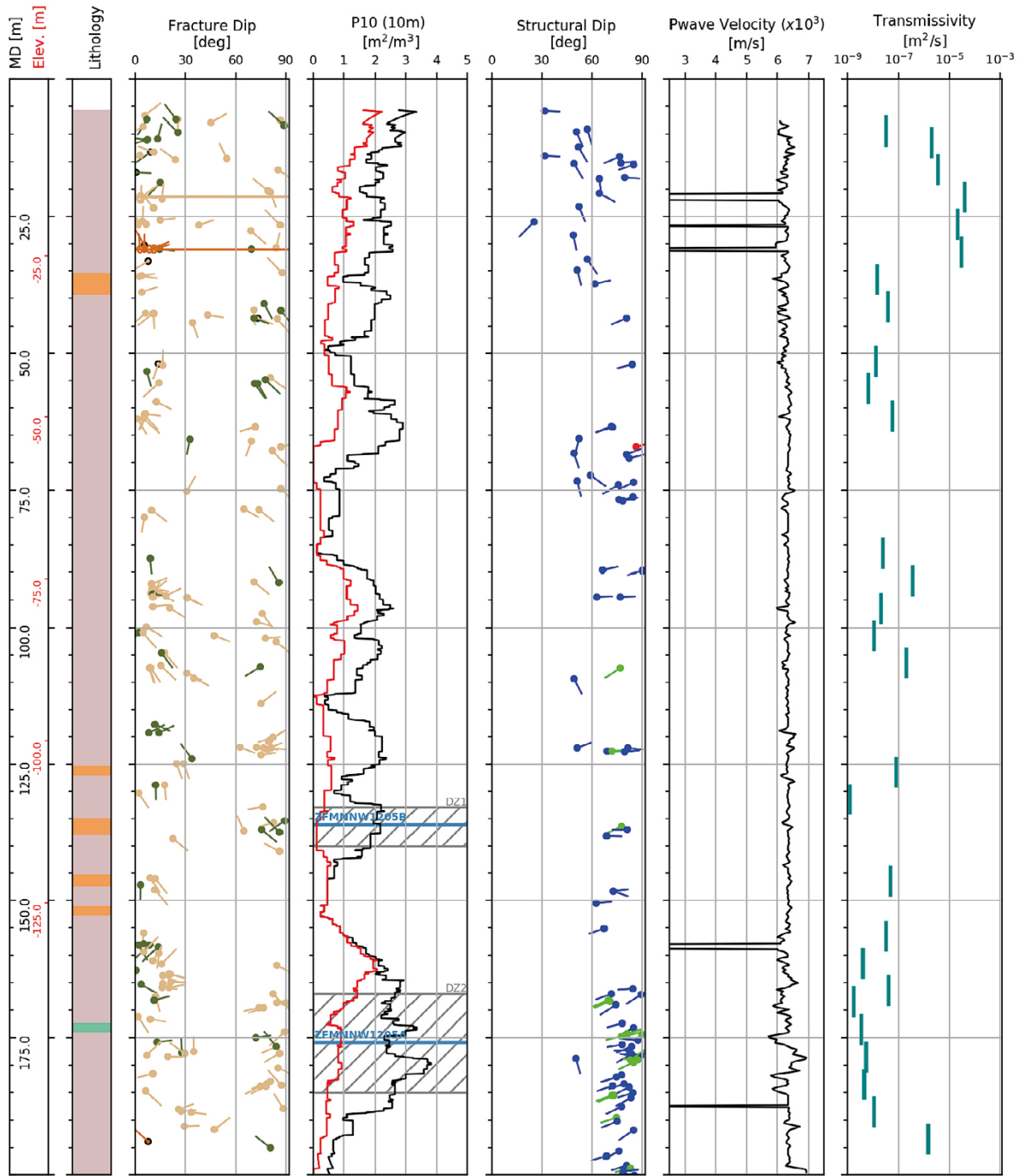
Figure 6-6. *Example composite log plot for open and partly open fractures in the top 200 m of KFM08B. The columns show (left to right) measured depth and elevation, lithology, fractures (shown as tadpoles with tail pointing down dip, N is up, coloured by alteration – green = fresh, tan = slightly altered, orange = moderately altered), horizontal lines indicate crush zones; rolling average Terzaghi corrected intensity of fractures (black) and gently dipping fractures (red) and single-hole interpretations of deformation zones (hashed); ductile structures (shown as tadpoles, blue = foliation, green = ductile shear zone, red = brittle-ductile shear zone); p-wave velocity from sonic logs; and specific capacity from PFL sequential logging.*

6.5.3   Data from tunnels and boreholes drilled from tunnels

New geological data will be acquired once construction starts on the access shafts and tunnels. The excavation cycles for tunnelling and shaft sinking, include the following steps, assuming employment of careful drill and blast excavation (Figure 6-7):

1. Core drilling of a pilot borehole, including measurements while drilling (MWD), and borehole investigations during and after drilling for assessment of the rock properties along a tunnel length of 100–300 m (e.g. the entire length of deposition tunnels will be pilot hole drilled).

2. Percussion drilling of probe boreholes, including MWD and hydrogeological borehole investigations during and after drilling for assessment of the rock properties for the next 4–5 blasting rounds (i.e., approximately 20–25 m) which might also include probe holes used for grouting measures if deemed required.

3. Overview geological tunnel mapping, employing a photogrammetric record. Detailed geological mapping of an individual blast round, done remotely using photogrammetric record.

4. Points 3 and 4 are repeated until the end of the probe holes is reached.

5. Points 2, 3 and 4 are repeated until the end of the pilot hole is reached. Then the sequence 1–6 is repeated.

The same types of geological, structural and geophysical logging as performed in the surface-drilled (76 mm) cored holes will be acquired for the pilot holes, and from dedicated "investigation boreholes" when needed. The latter holes are not consumed by subsequent development of a corresponding underground opening. There is currently no suite of geophysical logs for probe holes (64 mm). However, SKB intends to furnish a packer system to facilitate flow logging and hydraulic tests in the probe holes (so-called "FLS").
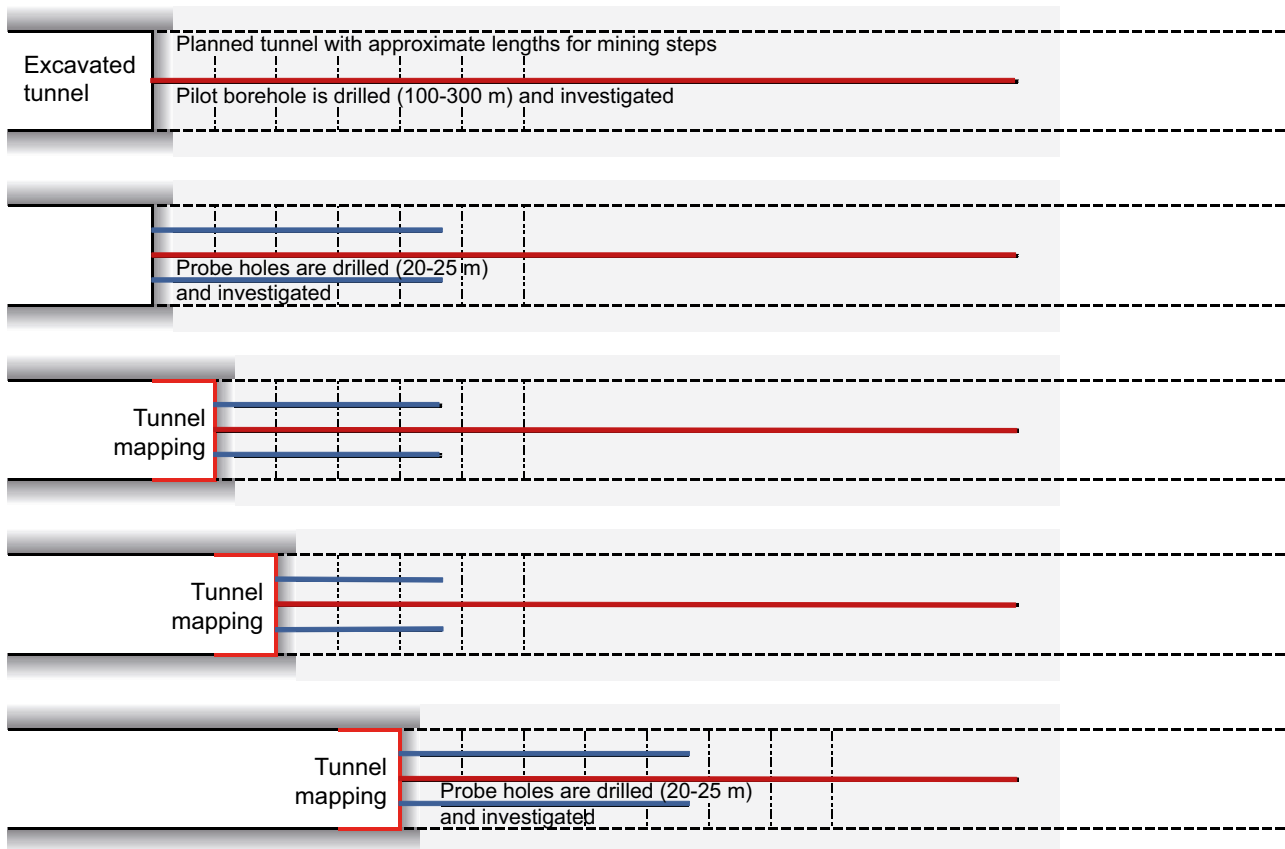
Figure 6-7. *Schematic illustration of the routine tunnelling and investigation sequence with pilot and probe hole drilling, borehole investigations, excavation and overview tunnel mapping (SKB 2011b).*

Structural logging in gently dipping pilot holes will provide better understanding of fracture intensities and orientations of sub-vertical fractures, and more data from the near-surface. In addition, the pilot holes for the spiral ramp and tunnels will potentially form a relatively dense array of rock samples compared to the surface-drilled holes, allowing spatial variability in lithology and structures to be analysed in different orientations and on different scales. Cross-hole geophysics may be used to support identification and modelling of critical structures (Munier and Mattila 2015) which affect decisions on deposition hole acceptance.

6.5.4 Tunnel mapping data

More significant for structural characterisation, mapping of underground constructions provides direct observation of fractures underground on the surfaces of the excavations, revealing fracture properties over a length scale larger than evident from drill cores. In particular fracture sizes/trace length will be mapped at relevant depths in the bedrock, measured on surfaces complementary to the existing data from horizontal surface outcrops.

These will be a significant addition to the eight existing surface outcrops (six exposed areas and two trenched outcrops) used for structural mapping in SDM-Site (Stephens et al. 2007).

Geologic mapping is planned to be carried out in all underground excavations and to take place after each blasting round in the time window between the scaling/cleaning of the tunnel and the installation of the temporary support (bolts and shotcrete, see below). All mapping, whether in situ and remote, of exposed rock surfaces along underground openings and exposed surface outcrops is made using RoCS (Rock Characterization System), developed by SKB (SKB 2014). RoCS is a system based on a digital mapping record created by photogrammetric means. Data obtained by this method will be the primary basis for analysing the bedrock geology and fractures during the successive development of the excavation of the underground facility, i.e., in situ and remote mapping is done on the *3D*-photogrammetric image (Hultgren and Munier 2012). In the deposition areas, it is herein assumed that geologic mapping and pilot holes logging will be available for each tunnel, whereas in the access and Central area, pilot holes will have limited coverage.

Overview mapping of each blasting round including the tunnel face is mainly done to monitor structures of importance for excavation progress and to provide a framework and platform for the subsequent detailed mapping. When passing through deformation zones, shotcrete rock support will limit this mapping to a remote mode. This step is followed by detailed geological tunnel mapping performed at distance behind the excavation front. The detailed tunnel mapping is, close to the tunnel front, done remotely to ensure workers safety and minimise impact on tunnel excavation. However, as the front has advanced sufficiently far, and for the detailed mapping, in situ mapping will be carried out. If remote mode cannot be implemented from the onset of this programme, i.e., in the upper part of the skip shaft and ramp tunnel, *in situ* detailed mapping is mandatory before this can be turned into a completely remote procedure.

In situ overview mapping of each blast round (ca. 5 m length) will record the following:

- Dominant rock type;
- Subordinate rock types;
- Rock type alterations;
- Prominent structures (zones and individual fractures, cut-off trace length ≥ 3 m);
- Rock mass quality (Q and RMR_{BAS});
- Inflows along individual fractures (presence of water).

Once the excavation has advanced a sufficient distance from a safety perspective, detailed remote tunnel mapping is performed of the tunnel/shaft section, during which detailing of the in situ mapping (e.g. smaller structures are added) is carried out. In addition to the in situ mapping, the following will be documented:

- Structures (fractures) with a cut-off fracture trace length ≥ 1 m; and
- Detailing and adjustment of potential deformation zones, using Full Perimeter Intersection structures (FPIs) as proxies for potentially critical structures.

DFN model may call for focused fracture mapping campaigns with even shorter cut-off fracture trace length, say 0.25 m (Nordbäck and Engström 2016, Hartley et al. 2018b). Opportunities for this type of detailed fracture mapping are likely to be in niches connecting the ramp and shafts. Important for DFN modelling, it allows inference of correlations between fracture properties and the size of structures, based on either the trace length or the linking of structures between different boreholes/tunnels which is anticipated to be feasible in, mainly, the deposition areas. The focused detailed mapping in niches, for example, can provide higher resolution analysis of the ends or fractures to derive cross-cutting and termination relationships.

Geophysical tunnel investigations include:

- Tunnel seismics enabling tomography to image large structures into the walls around and between tunnels.

- Ground-penetrating radar (GPR) to image the extent of fractures beneath the floors of tunnels.

- Resistivity tomography to image the connectivity of fractures between tunnels or boreholes.

6.6 Data analyses and parameterisation

6.6.1 Conceptual framework for sets and domains

From a geological standpoint, the fracture network has resulted from a long geological development history with several phases of deformation at different depth, changes in both pressure and temperature, chemical alterations and evolving stress conditions. Considering the complexity of the fracture network geometry and the sparseness of data, it is convenient to utilise some aspects of the geological history of fracturing to guide the statistical analysis of fracture networks.

The classical method for identifying fracture sets is to group them according to their orientations (Subsection 1.3.3), assuming that orientations are the key marker of the deformation history (geologic age) and paleo stresses seen as the main driving force for DFN growth.

In this way, a "fracture set" (an "age set") should ideally be defined according to mapped fractures with similar orientations (roughly sub-parallel) that are of the same type and age (NRC 1996, Chapter 2). The reason for linking these properties is because fracture orientations are indicative of both the type of tectonic event and the local orientation of stresses present when brittle failure first occurred. Successive paleo stress conditions therefore produce new sets of fractures whose orientations are directly related to the principal stress directions and whose interactions with former sets can be related to fracture terminations, potentially leading to an unambiguous combination between fracture orientation, age, termination and even with internal properties (mineral filling etc).

This idealised division of the fracture population into geological sets must, however, be weighed against the full complexity of the rock mass and it neglects critical and somehow elementary aspects of the fracture system dynamics and structure:

- Several orientation sets can be coeval for a given state of stress and grow concurrently (for example 2 sets form in mode II, 1 set forms in mode I),

- the density scaling is likely resulting from the linkage and reactivation or fractures potentially at different tectonic stages,

- the fracturing process intrinsically induces spatial heterogeneity of structures and stress at different scales, and

- in situ rock properties also control the spatial variability of fractures.

This prevents definition of a unilateral link between age, orientation and statistical fracture properties. In short, definition of fracture sets should not be restricted to a subdivision by clustering of orientation poles.

Joints, faults and deformation zones are likely to result from different fracturing processes. They form a size continuum as a consequence of the DFN scaling laws, but they may differ statistically in terms of orientations or terminations.

When performing the data analyses for building the DFN model(s), any property of the DFN model can be analysed independently from the others or in relation with the others. Trace size distributions may be analysed by fracture orientation-set or age-sets and orientations may be analysed by range of fracture sizes, etc. Moreover, datasets are also aggregated according to their location within the site, with the Fracture Domain and spatial variability as described in Chapter 5.

The geology needs to constitute the key guideline for the DFN modelling, but the importance of the orientations with respect to other properties of the DFN model, especially the density scaling and spatial heterogeneity, should not be overestimated. Thus, the modeller should, to a reasonable extent, test and evaluate as much as possible the degree of correlation between the different parameters of the DFN by calculating DFN density distribution parameters for subsets of properties, but to refine the DFN model into sub-DFN only if their respective properties are distinct.

Overall, the tested sub-sets may be relative to a geometrical characteristic (e.g. orientation, range of sizes), to a location (specific zone or volume, e.g. the Fracture Domains, or depth), to the geologic age (of the fracture creation or reactivation) if it can be determined as part of the deformation history, to typical infilling properties, or to a combination of the above.

To avoid a terminology and modelling confusion, the term "set" in the present report refers by default to the grouping of fractures according to orientations, so is basically an "orientation set". The term "age set" refers to the deformation history and age of the fractures.

6.6.2 Orientations

Conceptual framework and models (Overview)

The conceptual framework of the fracture orientation density distribution relies on the partial density distribution n_{3D} (θ, ϕ), as defined from Section 6.3.

In this section, the interpretations focus primarily on the identification of typical sets of fractures whose orientation are similar, and whose probability distribution models are defined. The orientation density distribution n_{3D} (θ, ϕ) is then equal to the sum of the contribution of each set, as its probability distribution model weighted by its density term.

The orientation analysis generally consists of three main steps:

1. The identification and classification of fracture sets (groups of fractures with a similar orientation and age). Set identification is generally done qualitatively by visual inspection of fracture orientations plotted on contoured stereonets. Statistical methods can also be used to quantitatively divide fractures into sets. Munier (2004) offers an introduction into the advantages and disadvantages of several of these approaches. Identifying typical orientations involves looking for clusters of fracture poles (vectors orthogonal to the fracture plane) or distinct spatial trends in orientations (Figure 6-8).

2. The evaluation of the correlation between orientation-sets and age-sets. The qualitative interpretation of the stereonets can be completed by analyses of termination relationships between different fractures (Bridges 1990) on mapped surfaces or by any age marker, e.g. mineral infill or alteration. If consistent results are obtained, the modeler may decide to replace the orientation-sets by age-sets.

3. The mathematical quantification of the orientation distribution model, by orientation- or age-set. For any defined group of fractures, the statistical variability can be described by estimating probability distributions for fracture orientations around a mean vector (pole). At this step, the orientation distribution models may be limited to probability density functions or directly integrated with density information, using the orientation-density distribution functions as described in Darcel et al. (2013).

These steps are repeated over successive datasets and aggregations of datasets. Automated or manual methods may be used for defining how many sets are meaningful (in a geometrical and or geological sense) and identifying bounds on their range of orientations (which may be distinct or overlapping). Automated methods of fracture set identification, such as stepwise bootstrap methods (Hsu et al. 1986) cluster analysis (Hammah and Curran 1998, Marcotte and Henry 2002) and probabilistic methods (Dershowitz et al. 1996, Peel et al. 2001) are acknowledged. Quantitative methods can be used further

to evaluate the statistical distance between the resulting fracture sets (Darcel et al. 2009, 2012, 2013) and thus evaluate the balance between refinement into many sets and statistical convergence of moments for individual sets.

The manual method can be applied easily over a few datasets but becomes more and more subjective as more and more datasets are added. The geologically based interpretation may be selected to define a first order division of the DFN model(s) into age sets, provided that its adequacy with other parameters of the DFN model (intensity, scaling, spatial distribution and correlations) is demonstrated.

Interpretation methods

Stereographic projection

The basic tool for a qualitative set analysis is the stereonet, which is a *2D* projection of the intersection of poles with a unit sphere or hemisphere. Fracture sets are generally identified by looking for clusters of features with similar orientations on the stereonet (see Figure 6-5). The standard orientation convention chosen here is that the orientations of fractures, faults, foliation, and structural contacts are represented by the **trend [0–360°]** and **plunge [0–90°]** of the **pole to the plane**, mapped in a **lower hemispherical projection**. While other conventions of orientation (dip magnitude and direction; strike and dip) are often used when recording planar data in the field, they are converted to pole trend and plunge for data analysis which enables a coherent handling of both linear and planar geological structures.

A lower-hemisphere projection should be used since all structural elements are defined to be inclined below the horizontal, using the right-hand rule for azimuth (i.e., 0–360 degree notation). Also, the convention of equal-area (Schmidt) stereonets should be used because they present no statistical bias when large numbers of data are plotted. On the equal-area stereonet, area is preserved so, for example, each 10° polygon on the net has the same area. For consistency of style it is also suggested individual structures where required as poles rather than great circles, polar or equatorial plots can be shown by choice. Contour plots of orientations from borehole data should be weighted to correct for bias. Depending on the sampling conditions, adapted corrections should be used (Terzaghi 1965, Mauldon 1994, Davy et al. 2006) and their choice motivated. The stereonet contour plot emphasises the concentration distribution of the pole orientations, so that preferential directions are easily visualized.

Stereonets can be applied to borehole data, outcrop/tunnel mapping data, lineaments and deformation zones. It is important to make an overall assessment of appropriate sets for these different scales of data before finalising the framework for sets.

Combination with Deformation history

For age-set determination, the interpretation is generally done qualitatively by a trained structural geologist who considers the geologic and tectonic history of the site, mainly based on cross-cutting relationships of mineralised fractures and supported by absolute dating measurements. Based on the understanding of deformation history in Forsmark, as shown in Figure 4-3 and Figure 4-4, at least four sub-vertical typical orientations can be expected (NW/WNW, NS/NNE, NE, ENE) and a gently dipping set striking NE–ENE and dipping SE. This provides a local-scale context for the identification of sets.

Identification of sets goes hand-in-hand with the conceptualisation of deformation history (Section 4.2) and determining suitable domains for describing variability (Chapter 5) as shown in the workflow indicated in Figure 6-8.
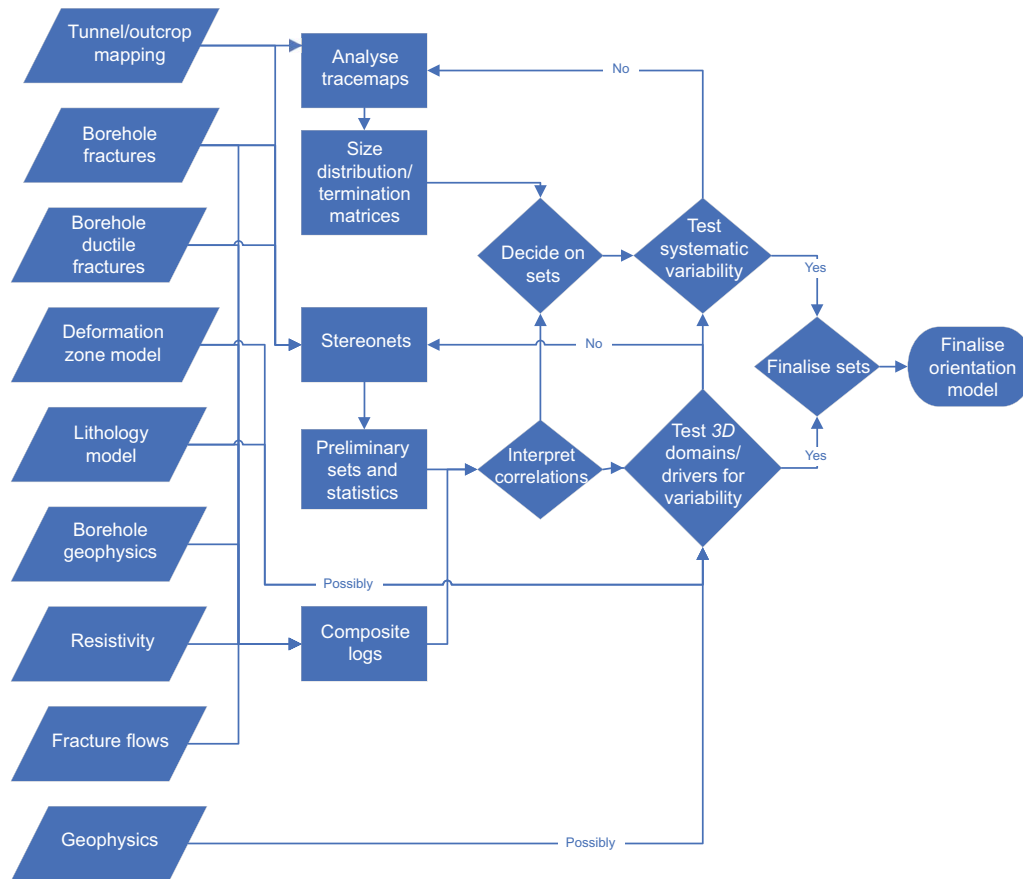
Figure 6-8. *Workflow for identification of fracture age sets and deriving an orientation model for each defined set. Rhombi represent data, rectangles are processes and diamonds are decision.*

The steps are as follows:

1. Produce contour and pole plot stereonets from all the available datasets, with poles coloured by various geological markers (Figure 6-5), and the composite plots as in Figure 6-6.

2. Compare the resulting trends with the *3D* geological model and with fracture terminations and in-filling material, if available. Using surface outcrop trace maps, tunnel wall mapping or *3D* structural models, termination relationships can also be used to divide fracture data into sets. The age relationship of truncating and truncated fractures is unambiguous; truncated fractures are younger than the fractures they truncate against (Pollard and Aydin 1988). Additional geological parameters such as fracture mineralisation, shape (roughness, planarity), alteration, lithology or termination type can be used to aid in set identification in cases where overlapping or diffuse sets exist (Dershowitz et al. 1996).

3. Assign each fracture to an orientation/age set.

4. Interpret the orientation density model for each set.

Illustrative example

Here, we describe an example from a single borehole to illustrate the process of age set interpretation. Example stereonets and typical distribution of orientations are shown in Figure 6-5 for KFM01B. The hole is just north of the Eckarfjärden deformation zone (ZFMNW0003). The contour plot indicates clear NW (to NNW) and NE sub-vertical sets and a sub-horizontal set that is mainly horizontal, but has moderately dipping fractures dipping from SW to NW. The sub-vertical sets extend almost all the way around the circumference. The depth-coloured pole plot shows that horizontal fractures are mostly in the top 100 m, the NW moderately dipping fractures are also mainly in the top 100 m, while the NS and ENE fractures seem to be sporadic in narrow depth ranges. Each of these localized trends may be related to the proximity with identified deformation zones or lithologies.

The NE fractures seem to rotate from moderately dipping to steeply dipping with depth. Such observations typically obscure the age vs. orientation set modelling, since then one typical orientation is no longer representative of an age. Moreover, each age of the deformation history is also associated with stress variability (change with location, e.g. depth or proximity to larger DZ), which makes the correlation between orientation and age even more uncertain. The best age marker is something that can be dated, e.g. minerals. So the correlation between age and orientation could be considered by first determining relative ages, then group fractures into these ages and analyse orientations.

The alteration-coloured pole plot reveals that alteration occurs mainly in sub-horizontal and NW fractures that dip moderately SW. The depth-coloured ductile structure pole plot shows that the NW fracture set is parallel to the main sub-vertical foliation orientation and with most ductile shear zones, with other NE foliations dipping moderately SE and also NW dipping moderately SW. Foliations striking between NNW and NS are often moderately dipping, as with fractures in these orientations, and so perhaps a distinct NS set could be considered.

An example of a composite log plot for the top 200 m of KFM08B is shown in Figure 6-6 to illustrate possible data that can be plotted to aid DFN modelling. Fracture orientations are shown as tadpoles with the tail pointing to the dip azimuth (with N up the page), the dip shown on the abscissa and depth on the ordinate axes and coloured here by alteration. The plot is useful for showing clustering of orientations at certain depths and where there are deformation zones, changes in lithology or spikes in the sonic logs as well as flow. Such plots can also be used to help guide an integrated interpretation of the damage zones flanking deformation zones and any local changes in orientation within them.

Understanding the relationships between fractures and geology puts the fracture geometrical description into context, and once implemented in the DFN model, provides improved predictive power.

Probabilistic description of fracture orientations

The final step (bullet 4 above) is to describe the statistical orientation distributions in the selected sets. This is done through the use of spherical or hemispherical probability distributions (Mardia and Jupp 2000). The probability distribution describes the dispersion of fracture orientations in terms of a mean pole and the variation (or concentration parameters) around that mean pole (see Figure 6-9 for examples). The distribution parameters for each set are estimated from fracture information as divided according to the sets. The hemispherical probability distributions typically used include:

- Univariate Fisher (Fisher 1953): Is the most commonly used for directional data. It is radially-symmetric and a *3D* equivalent to the normal distribution about a mean pole. Fisher-distributed data forms circular clusters around a mean pole on a stereonet with variation measured by a concentration parameter. Fisher distributions are widely used in geology due to their relatively straightforward and easy-to-parameterise nature.

- Bivariate Bingham (Bingham 1974): A bivariate distribution on the sphere, used to describe either elliptical or girdle distributions of fracture orientations created e.g. by folding. The bivariate Bingham distribution requires the specification of a mean direction, two concentration parameters and the orientation of the minor axis of the ellipse on the sphere. It can be used to fit a wide variety of pole cluster shapes.

- Bivariate Fisher (Fisher et al. 1993): Is the generalised version of the Univariate Fisher. The Bivariate Fisher distribution specifies the concentration around the mean orientation as a ratio in concentrations in two axial directions such as strike and dip. The primary use is for steeply- to moderately-dipping fractures that have a much larger variation in strike orientation than dip magnitude, often evident in field data, mostly likely an artefact of sampling strike and dip with different precisions and errors.

- The Elliptical Fisher distribution (Dershowitz et al. 1979). It is the generalization of the univariate Fisher distribution and parametrised by two direction vectors /trend and plunge) and two dispersion factors. When the dispersion factors are equal, the bivariate Fisher distribution reduces to the univariate Fisher distribution.

- Bootstrap: The bootstrap (e.g., Chernick 2007) is a method of doing inference in a way that does not require assuming a parametric form for the population distribution. It does not treat the original sample of orientations as if it is the population even though it involves sampling with replacement

from the original sample. It assumes that sampling with replacement from the original sample of size, *n*, mimics taking a sample of size *n* from a larger population. It has many variants such as the *m* out of *n* bootstrap which re-samples *m* times from a sample of size *n* where *m* < *n*. The bootstrap does, however, not contain more information about the population than what is given in the original sample. For that reason, it sometimes does not work well for e.g. small samples.

In Forsmark DFN2.2 (Fox et al. 2007b) each outcrop and borehole was split into between four and six sets. All four of the above distributions were tested for each set and each outcrop, while only univariate Fisher was tested for the boreholes data. In the outcrop tests, the quality of fit seemed to be more a function of the dataset itself than the distribution used. Overall, combinations of Fisher for circular and Bivariate Bingham for elliptical distributions may suffice.

Goodness of fit measures

The goodness of a fit of an inferred distribution either to the originating data or a new dataset can be quantified by the non-parametric Kolmogorov-Smirnov (K-S) test (Massey 1951) comparing the cumulative distribution function (CDF) and a dataset. Two measures can be calculated. The first number is the K-S statistic, a measure of the largest difference between CDF's for the model and fracture data (low is good). The second number a measure of the goodness-of-fit (the level at which the null hypothesis is rejected) of the fracture data against the orientation model (high is good).

Relation between orientation sets and DFN density distribution

The identification of orientation- or age- sets provides an intermediate layer of the DFN modelling which ultimately relates to a global density distribution of individual fractures. The probabilistic description of fracture sets lacks the density term and the size scaling terms.
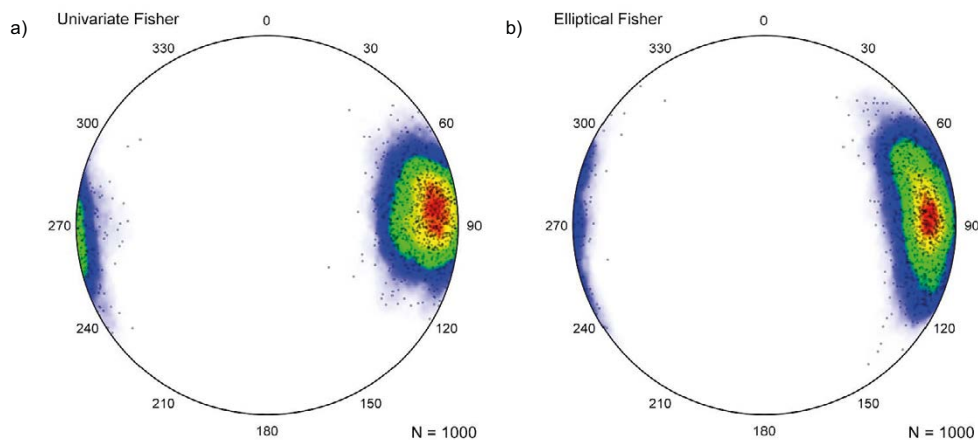
Figure 6-9. *Example of two different orientation distributions, both with mean pole orientation 085/15. In a) a Univariate Fisher (Fisher 1953) with k (concentration parameter) = 20 and in b) an Elliptical Fisher (Dershowitz et al. 1979) with k = 20 and an aspect ratio of 2 between the longest and shortest axes of the ellipse. Stereonets were made using a spherical Kamb algorithm (Vollmer 1995, 2015, 2021).*

6.6.3 Shape

The fracture shape is not very well constrained in *3D* since exposures of fractures tend to be limited to fracture traces on the sampling support. There is little information that can be derived concerning fracture shape from borehole data. Underground tunnel maps provide some data concerning shape, especially where fractures intersect corners of tunnels or niches, where some fractures can be inspected along more than one axis. However, many fractures are larger than the underground opening, and hence the traces of the fracture along the wall, floor and roof are likely to be censored approximations of the fracture size and shapes. More often than not, fracture shape is assumed based on analogues or other soft or lightly constrained data, and subsequently refined during validation modelling as a free parameter if required.

Some characteristics relating to fracture shape and to consequential physical properties of the fractures are described in Section 6.7. This includes the description of the fracture surface roughness (see Subsection 6.7.1), and whether it is made up of a single or multiple planar stepped segments (see Subsection 6.6.4 below).

6.6.4 Sizes

Scaling models

Fracture size implicitly refers to the fracture area. However, it is practical to express the area in terms of radius or diameter, for assumed circular fractures, or **equivalent radius** (r) or **equivalent diameter** (l) for irregularly shaped fracture tips (e.g. polygons).

The literature on fracture size distribution models is very broad (Bonnet et al. 2001), supported by many observations, experiments, numerical simulations and theoretical arguments. The review below is not exhaustive but focused on the type of scaling models adapted to a broad range of fracture sizes, as it is very common for crystalline rocks that fractures are observed on all scales (see the multiscale maps in Figure 6-10 from the Hornelen basin from Odling (1997)), as is the case in Forsmark.
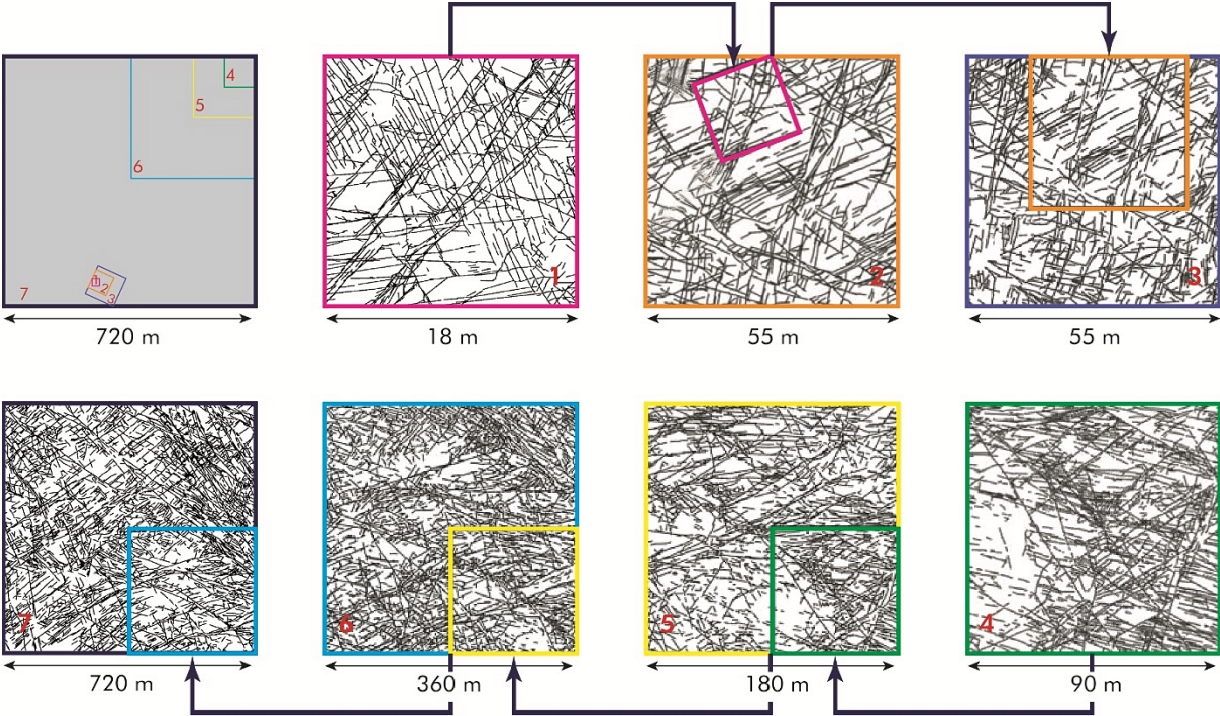
Figure 6-10. *Maps of the seven fracture patterns from the Hornelen basin (Odling 1997) and reworked from Bour et al. (2002).*

The analysis of fracture traces across wide ranges of scales from core through outcrop to aerial photographs and satellite image scales has been an active area of research and has shown that the fractures exist on a wide and continuous range of scales, from microns to zones of hundreds of kilometres. There are many examples in the literature of the derivation of scaling laws for fault size related statistics, such as of earthquake frequency versus magnitude (Gutenberg and Richter 1954, Utsu 1999), fault density versus size (King 1983, Hirata 1989, Barton and Zoback 1992, Davy 1993), slip displacement versus fault length (Walsh and Watterson 1988, Cowie and Scholz 1992a, c), and displacement (Marrett et al. 1999), for joint network (Bour et al. 2002) and for fracture networks (Davy et al. 2010). We recall below the definitions of the main models which have been used to model these scaling relationships, as the log-normal, the negative exponential and the power-law distributions. The latter has proven its efficiency to describe the fracture size density distribution evolution from the core scale and up to the lineament scale in Forsmark (Fox et al. 2007a, Darcel et al. 2009, Davy et al. 2010).

In all cases, the fracture size scaling model is critical to predict how fracture intensity is distributed over different sizes of structures. The fracture size density distribution function $n_{3D}(l)$, as defined in Equation (6-3) with ($P_1 = l$), basically gives the number of fractures per unit volume, whose size is in the range l; $l + dl$. The number of fractures per unit volume $N(l \in [l_1; l_2])$, corresponding to a given size range is readily given by the integration of $n_{3D}(l)$ over the given size range:

$$N(l \in [l_1; l_2]) = \int_{l_1}^{l_2} n_{3D}(l)dl \qquad\qquad \text{Equation (6-19)}$$

The use of the general framework and fracture density distribution for a DFN model has the advantage to readily define how many fractures there are per unit area or volume.

It is also recalled that the datasets used to derive the size density distribution firstly relies on 2D-type datasets and that a stereological analysis is necessary to infer the 3D model from the analyses of the 2D dataset.
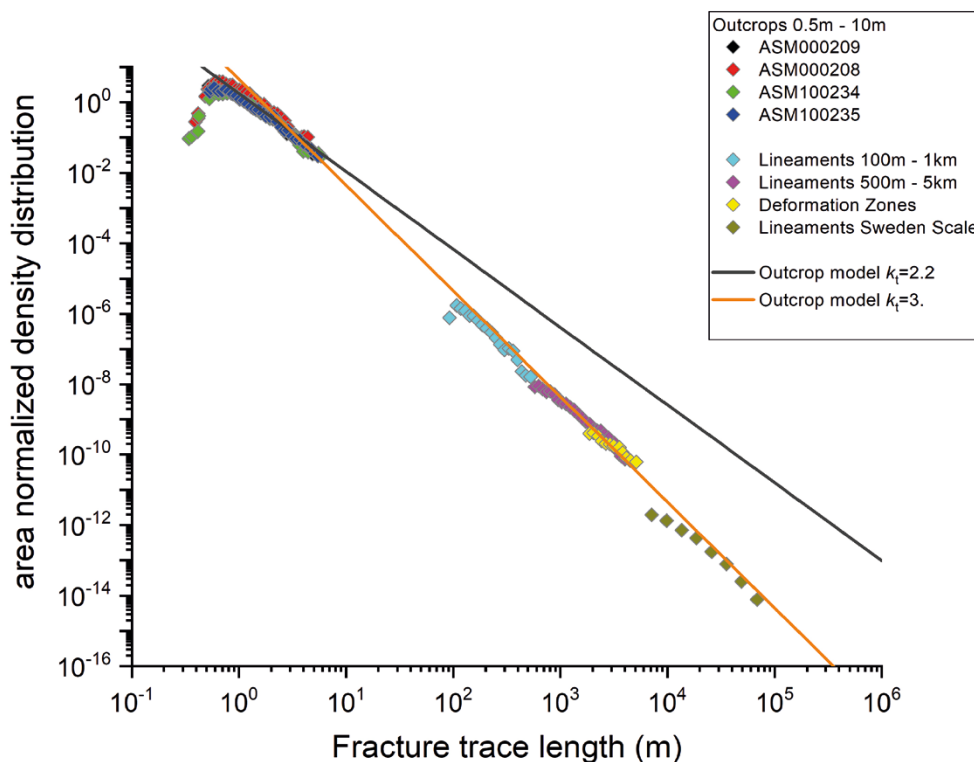
Figure 6-11. *Areal fracture trace length density distribution for different outcrop or lineament maps from the Forsmark area (Sweden), from Davy et al. (2010). Several surface outcrop (blue square symbols) and lineament (green, red and yellow dots) map dataset are combined in the plot. Two power-law models (blue and black straight line in the plot) are also plotted in in blue and black.*

Statistical laws for size distribution

The statistical laws presented hereafter have in common that they are all negatively skewed. For this reason, their parameters can be quite easily tuned to match fracture datasets over limited/narrow fracture trace size ranges. However, the reason for choosing one over another is also based on the physics/mathematics behind fracturing processes and the capacity to identify the size model beyond the data acquisition limitations (censoring and truncation effects).

Several statistical laws commonly used to model fracture size distributions are recalled hereafter. They are expressed as probability density functions. Their integration in the DFN modelling framework, which requires to switch from a probability density function to the fracture density distribution is introduced in the Section 6.3.

The most commonly used statistical laws to model the multiscale distribution of fracture sizes are the lognormal, the negative exponential and the power-law distributions.

Their mathematical expressions in term of probability distribution functions requires the definition of r_0 the radius of the smallest fracture of the distribution, and the functions are defined for $r \geq r_0$.

The lognormal law is, with $r > r_0$, equal to:

$$p_{3D}(r) = \frac{1}{(\sigma(r-r_0)\sqrt{2\pi})\exp\left(\frac{(\ln(r-r_0)-\mu)^2}{2\sigma^2}\right)},$$
Equation (6-20)

where the two parameters μ and σ are the logarithmic mean and variance, respectively, of the fracture radius. The lognormal law displays a characteristic scale around the logarithmic mean μ.

The negative exponential law is, with $\lambda > 0$, $r > r_0$, equal to:

$$p_{3D}(r) = \frac{exp\left(\frac{r_0-r}{\lambda}\right)}{\lambda},$$
Equation (6-21)

Like the log-normal law, the exponential law has a characteristic scale, equal to λ. Note that σ = μ = 1/λ.

The power law, with $k_r > 0$, $r > r_0$, is defined by Evans et al. (1993):

$$p_{3D}(r) = k_r\, r_0{}^{k_r} \times r^{-(k_r+1)}$$
Equation (6-22)

Where k_r describes the scaling characteristics of fractures as a function of size. The power-law is the only function with no characteristic scale except its limits.

Finally, the transition from the probability density function to the fracture density distribution model is defined as:

$$p_{3D}(r) = \frac{n_{3D}(r)}{\int_{r_0}^{\infty} n_{3D}(r)}$$
Equation (6-23)

The integral of the probability function p_{3D} over the whole range of fracture sizes is equal to 1 whereas the integral of the density distribution $n_{3D}(r)$ is equal to the total number of fractures per unit volume over the whole range (as in Equation (6-7)) or to the number of fractures (per unit volume) over any specific range (as in Equation (6-19)).

As introduced in Subsection 6.4.2, determination of a fracture density distribution model from data interpretations is less sensitive to data sampling truncation and censoring effects (see also Figure 6-15).

Arguments and counterarguments for lognormal distributions and fragmentation model

The lognormal model is potentially an appealing distribution for describing rock block size distributions arising from sequences of successive fragmentation iterations (Kolmogoroff 1941, Epstein 1947). Considering a rock fragmentation process, if fracturing locations are random, then the successive block segments have diameters d_i given by $d_{i+1} = f_i \cdot d_i$, where f_i is drawn from a random distribution on (0,1). Equivalently one can write that $\ln(d_{i+1}) = \ln(f_i) + \ln(d_i)$. The increments of $\ln(d_i)$ are random, and thus

the central limit theorem implies that for large number of fragmentation cascades n, $\ln(d_n)$ is normally distributed, i.e., the block size d_n is lognormally distributed. However, the model has been found to adequately describe the distribution of fragment sizes only in specific cases (Ishii and Matsushita 1992). Lognormal distributions are still possible models for block size distributions (Korvin 1989) and, for some specific geometries where fractures and blocks have similar sizes, models of fracture size distribution are also lognormal (Priest and Hudson 1981, Rouleau and Gale 1985, Turcotte 1986, Zhang and Einstein 2000).

In many real fragmentation processes, the breakage probability depends on the fragment size and thus the resulting distribution tends to exponential or power laws (Baker et al. 1992, Krapivsky and Ben-Naim 1994, Grady 2010, Davydova et al. 2014). Moreover, fractures can be much larger than blocks.

Finally, we notice that even if the lognormal distribution often provides a good fit to fracture size distribution over a single scale, such as over an outcrop, it fails to describe scaling behaviour over larger ranges of scales. One explanation is that the apparent lognormal distribution is an artefact of censoring and truncation at the limits of the measurement scale (Einstein and Baecher 1983, Segall and Pollard 1983, La Pointe 2002).

Arguments for Negative exponential distributions

The exponential scaling distribution has been used to describe fracture sizes in the continental crust (Cruden 1977, Hudson and Priest 1979, Priest and Hudson 1981, Nur 1982). In these cases, fracture growth results from a uniform stress distribution (Dershowitz and Einstein 1988), and fracture propagation can be compared to a Poisson process (Cruden 1977) resulting in an exponential distribution. Numerical experiments by Olson et al. (2001) have also shown the exponential size distribution results when Mode I fractures propagate through randomly distributed parallel flaws such that of fractures arrest under subcritical fracture growth (stress intensity less than fracture toughness).

Arguments for Power-law distributions

With the definition in Equation (6-19), the size distribution is a power-law when k_r, the dimensionless exponent of Equation (6-6), is independent of l over a certain range of scales. Such distributions seem to be ubiquitous in natural systems (Bonnet et al. 2001). The widespread use of power law models across a range of tectonic processes is natural given the physical correlations between rupture length, earthquake magnitudes, and seismic energy (e.g. Ben-Zion 2008). This introduces a rationale for the observations that fractures exists at all scales (Tchalenko 1970). Power-law distributions are emerging properties of several physical processes of fractures and fracture network growth. It is the case for:

- The stationary size distribution of growing fractures, when the growth rate is a power function of their size: $v(l) = dl/dt = Cl^b$ (Sornette and Davy 1991, Davy et al. 2010, 2013). In this case, the growth exponent b sets the power-law size exponent: $k_r = (b-1)$.

- The size distribution of fractures that grow and abut on the nearest larger fracture (Davy et al. 2010, 2013). In this case, $k_r = 3$, which corresponds to a self-similar geometry (i.e., the number of fractures that cross through systems from one end to another is independent of the system size).

Numerous studies (King 1983, Barton et al. 1985, Hirata 1989, Sornette and Davy 1991, Barton and Zoback 1992, Davy 1993, Davy et al. 2010) including fracture size interpretations in Forsmark and Laxemar-Simpevarp in Sweden (Andersson J et al. 2002a, Darcel 2003, Darcel et al. 2003, 2006, Hermanson et al. 2005, Fox et al. 2007b) have concluded that a power-law behaviour of fracture size provides a best-fit to observed data where all scales of fractures are considered simultaneously.

Interpretation methods for a statistical characterisation

Scope

The interpretation of fracture size density distribution models has critical implications for the DFN model building. There are two main stages: first the interpretation of individual fracture trace datasets (potentially decametre-scale outcrops, metre-scale tunnel walls or (deca)kilometre-scale aerial photographs), and second a combination between the datasets to define the multiscale density distribution. We review these two steps below.

Building the fracture density distribution model from outcrop trace maps

Typical outcrop trace maps are shown in Figure 6-12. The process of building the fracture density distribution model from outcrop trace maps consists of the following steps:

- Fracture trace linkage.

- Area correction.

- Computation of n_{2D} the size density distribution (including identification of censoring and resolution effects, parameter interpretations and stereological analysis).

Fracture trace linkage

On outcrops, it is quite common to observe sets of very close and closely aligned fracture traces, see Figure 6-12. Whether these configurations should be treated as linked traces or as independent shorter traces has potentially strong consequences on the resulting proportion of smaller and larger fractures in the fracture density distribution model.

These typical configurations may be a true consequence of the fracturing process, as are *en echelon* "Riedel" structures, or be an artefact due to the exposure quality of outcrops (ponds, grass, outcrop weathering …). In the latter case, the interpretation procedure should correct this sampling bias and link the fracture traces. In the former case, despite locally the trace may look disconnected on the outcrop, they may be connected at depth. Moreover, the set of aligned traces defines a highly correlated and aligned structure which is unlikely to be sampled by chance in the generation process of a DFN model. It is asserted that it is more consistent to consider these aligned structures as single idealised fractures and thus start the interpretation process by linking these stepped segments into simplified single traces.

The process is described in Darcel et al. (2009) and in Fox et al. (2007b). Linkable traces are first identified based on several criteria: two traces shall be linked if their respective pole orientations are sufficiently similar and if the distance between their tips is not too large (Figure 6-13a). An additional condition defines the portion of acceptable overlap between both pairs (Figure 6-13b and c). If the criteria are fulfilled, the traces are linked (Figure 6-13d and e). No linkage is done in the schematic case of Figure 6-13c.
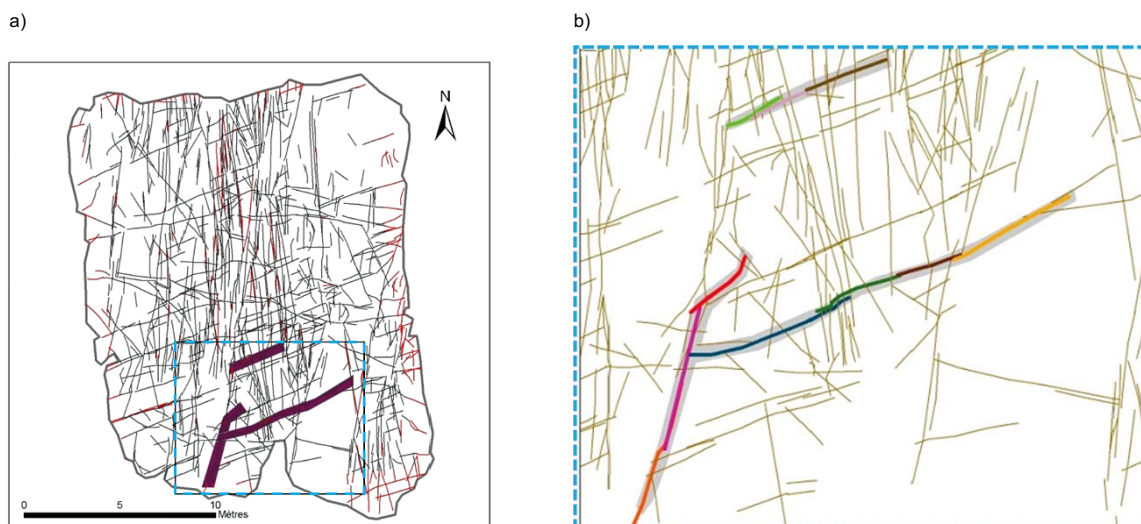
Figure 6-12. *a) Outcrop trace map from outcrop ASM100235 near the powerplant at Oskarshamn, Sweden. Several successions of traces highlighted in bold lines. b) zoom view (dashed blue line in a) to highlight the succession of aligned sub-segments (several colors). Modified from Darcel et al. (2009).*
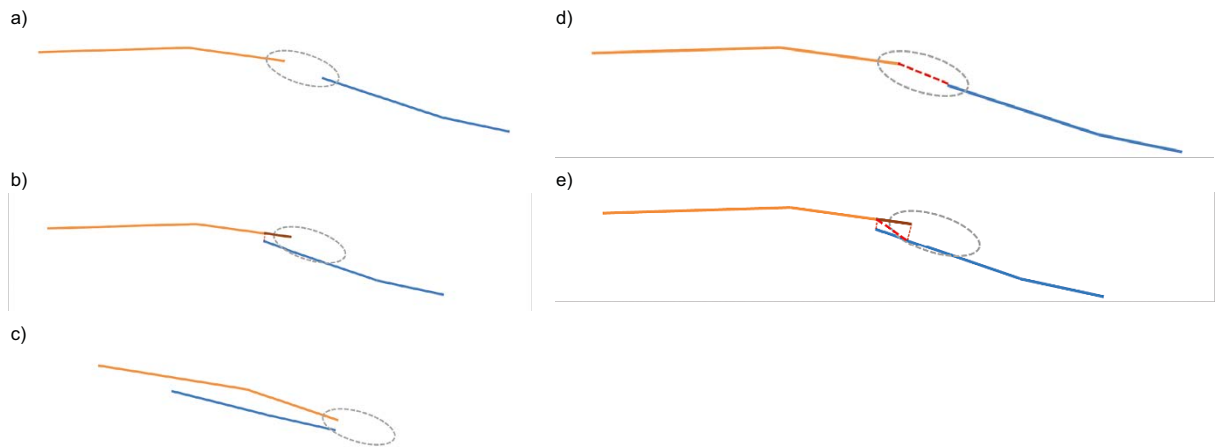
Figure 6-13. *a), b) and c) Example of non-Poisson structures in natural fractures. d) and e) Schematic linkage process. Modified from Darcel et al. (2009).*

There are no *ad hoc* limits between the amount of linkage and the criteria threshold. When applying the procedure, it is first recommended to visually check if the linkage process does not create unrealistic shapes. In addition, it is suggested to compare the proportion of identified segmented sets, for a certain level of identification criteria, to the number of segmented sets which would be identified in a basic and Poisson DFN model defined by the same set of segment-traces. The selected criteria must be sufficiently low such that no fake configurations are identified.

Area correction

In area sampling (and actually also scanline sampling) all fractures that intersect the sampling domain must be characterised, down to a reasonable censoring limit, in terms of their trace length. Although fractures crossing the sampling boundary will suffer from truncation, this can be overcome by restricting the analysis to the surface where all fractures with a well-defined trace can be counted. This amounts to removing a thick rim inside the mapping borders, whose width is equal to the trace size considered. The area that can be used in the fracture trace length density calculation thus decreases when trace size increases.
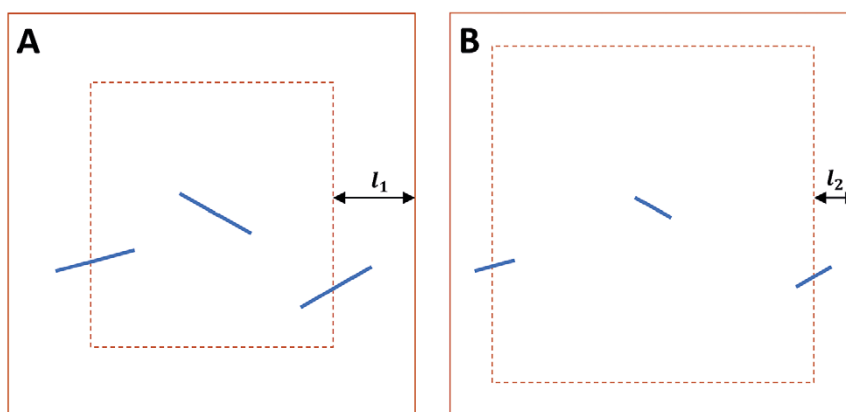
Figure 6-14. *Representation of area normalisation accounting for the finite-size effect. The normalisation surface is indicated by the dashed line for two different trace sizes (A and B).*

Building the fracture size density distribution

The key issues to compute the density distribution from a discrete dataset are related to the multi-scale character of the underlying fracture size density distribution model. In simplistic terms, the cumulative intensity term P_{21} is commonly dominated by the smaller range of trace sizes while the occurrence of larger traces is significantly lower. Resolution effects thus tunes P_{21} towards small sizes, whereas censoring effects limit the possibility to observe large traces, further increasing the difficulty to obtain a statistically relevant sampling procedure for these sizes.

Computing the density distribution, over a fracture trace range l, $l + dl$, comes to count how many traces fall in that range and to normalize it by the bin size dl and by the sampling surface S. The preferred method is to fix the binning dl so that the number of fractures N within each bin is statistically sufficient, and that the bin is small enough to consider that the distribution is locally well approximated (Davy 1993). A simple logarithmic binning is also well adapted to the abovementioned density scaling trend (a lot of small traces and few larger ones). Let l_{lo} and l_{up} be the lower and upper boundaries within which the logarithmic binning is defined. The logarithmic binning is defined by a logarithmic progression of the bin positions l_i, with:

$$l_i = l_{lo} \cdot (L_b)^i \qquad \text{Equation (6-24)}$$

$$L_b = \left(\frac{l_{up}}{l_{lo}} \right)^{1/N_{bin}} \qquad \text{Equation (6-25)}$$

with N_{bin} the number of bins, i defined between 0 and N_{bin}, and the size dl_i of a bin equal to $(l_{i+1} - l_i)$. With N_i the number of traces whose length is between $[l_i; l_{i+1}]$, the local density distribution is approximated by:

$$n_{2D}(l) \rightarrow \frac{1}{S} \cdot \frac{N_i}{l_{i+1} - l_i} \qquad \text{Equation (6-26)}$$

where S is the surface area over which the traces are defined.

A second possibility exists to compute, not the density distribution itself, but the complementary cumulative density distribution, $C_{2D}(l)$ defined as:

$$C_{2D}(l) = \int_l^{l_M} n_{2D}(l') \, dl' \qquad \text{Equation (6-27)}$$

where l_M is the upper limit of the underlying fracture size distribution.

Since this value is a cumulative density, computing it from a discrete dataset does not require definition of a specific binning, the number of traces larger than a given value is just cumulated from the largest to the smallest trace size.

However, as illustrated in Figure 6-15, this way to compute the density distribution is much more sensitive to finite size effects and makes the interpretation less accurate. The example shown is from an outcrop trace map from Simpevarp (ASM000206) with both the density distribution and the cumulative density distribution plotted.

At the low range of trace sizes, the distribution is affected by resolution effects. In addition, the long traces, in combination with area correction, will also affect the distribution. This by the censoring effects due to a smaller probability to get long traces in a finite system.

Cumulative distributions can be used to derive the density distribution, but the effect of the largest trace recorded (the upper bound l_M of the cumulative integral, Equation (6-27)) is important as illustrated in the Figure 6-15. Not considering the upper bound in the fit of the cumulative distribution leads to an overestimation of the exponent k.

The most relevant interpretation model in Forsmark is the power-law model. The fit can be done manually or automatically. The confidence in the model is reinforced by the comparisons between data from different locations, sampling supports and scales.
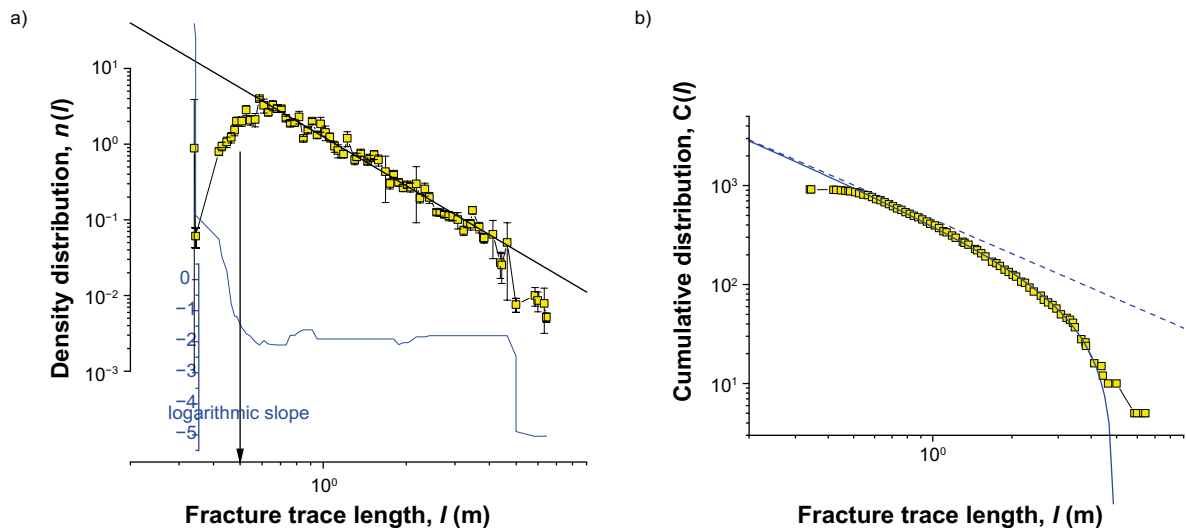
Figure 6-15. 2D size density distribution model. Outcrop ASM000206. Figure adapted from Darcel et al. (2009). Left) density distribution and right) cumulative distribution function. The dashed line is the power-law fit for both distributions. The solid line in the cumulative graph is the power-law integral with l_M = 5 m.

6.6.5 Density scaling and density fluctuations

Stochastic and deterministic representation

Modelling spatial variations of density has two main components: one is deterministic (see Chapter 5) spatially confined by the Fracture Domain boundaries (inter-variability), and the other is stochastic (intra-variability). The intra-variability reflects variations coming from the nature of the fracturing process which cannot be explained by geological/tectonic indicators, whether due to a lack of observations or to intrinsic variations within the fractured system.

The intrinsic variations result from the mechanical and physical interactions during fracture growth, which are reflected in the spatial distribution of volumetric intensity and in the local arrangement between fractures (T-terminations, space around each fracture) which in turn also affect the size and orientation model. The current subsection focuses on:

* Spatial distribution of density, how it varies in space and with scale; and

* Spatial interactions between fractures (i.e., the positions of the fractures relative to each other).

Interpretation methods

Fractal dimension D

Different methods (box counting, mass dimension, correlation dimension, (see Figure 6-16)) of determining the fractal dimension are used, depending on the DFN quantity measured (Bonnet et al. 2001). A widely used method relies on the mass of the fractal object rather than on the volume (Equation (6-11)). It defines the evolution with the characteristic length scale r of the mass of the fracture pattern, $L(r)$, as:

$$L(r) = r^{D_M},$$

Equation (6-28)

where D_M is called the mass dimension. Since it refers to different geometrical properties, D_M is not necessarily equal to the fractal dimension D in Equation (6-11). When applied to outcrop fracture trace maps (Figure 6-16a), the mass of the fracture pattern is defined as the total fracture length $L(r)$ included in discs of radius r and centred on the traces. In practice, $L(r)$ is averaging hundreds of discs to define the fractal behaviour as defined in Equation (6-11). The method was also applied in the DFN modelling during the Forsmark SDM stage 2.2 (Fox et al. 2007b). In the box counting method, the number of boxes of size r, $N(r)$, required to cover a fractal object (Figure 6-16b) of dimension D, is defined in Equation (6-11). For both methods, the plot of Equation (6-11) and Equation (6-28) in a bi-logarithmic diagram defines a straight line whose slope is equal to the fractal dimension.

The box-counting method also allows a generalization to the concept of *multifractality* (Grassberger and Procaccia 1983, Hentschel and Proccacia 1983). The basic version of the box-counting, which only defines the scaling properties of the spatial occupancy of an object, is completed by considering the scaling properties of the DFN density through the moments of order q. In practice, the measured quantity in each box i (Figure 6-16c) is the total fracture length in the box $L_i(r)$:

$$P_i(r) = L_i(r)/\sum_{i=1}^{n} L_i(r) \qquad \text{Equation (6-29)}$$

The moments of order q are then constructed:

$$M_q(r) = \sum_{i=1}^{n}[p_i(r)]^q \qquad \text{Equation (6-30)}$$

And should scale as:

$$M_q(r) \approx r^{(q-1)D_q} \qquad \text{Equation (6-31)}$$

where $\{D_q \text{ for } q = -\infty \text{ to } +\infty\}$ forms the multifractal spectrum of generalized fracture dimensions (Hentschel and Proccacia 1983). By definition, $D_{q=0} = D$. In general, multifractal measures give the distribution of physical or other quantities on a geometric support (Feder 1988). The multifractal spectrum can be determined for any measure defined for the object (i.e., not only the mass).

The mass method and the box-counting based methods can be equally applied to fracture systems seen as a whole or as a DFN. More specifically for DFN, an additional characterization method is proposed, the two-point correlation function $C_2(r)$. This function gives the probability that two points belong to the same structure. It is defined as:

$$C_2(r) = \frac{1}{N^2}N_d(r), \qquad \text{Equation (6-32)}$$

where N is the total number of points and N_d the number of pairs of points whose distance is less than r (Hentschel and Proccacia 1983). For a fractal population of points $C_2(r)$ should vary as r^{D_c}, where D_c is the correlation dimension, or dimension of order 2 of the multifractal spectrum. This method is used in Darcel et al. (2004, 2006) to measure the fractal dimension of outcrop trace maps and core sections from boreholes at the Laxemar and Forsmark sites or in Bour et al. (2002) for an application to the joint networks of the Hornelen basin.

The apparent fractal dimension deduced from a 2D The interpretation of the 1D-like fractal dimension deduced from core logging data is however not independent from the rest of the fracture density distribution model; the fractal nature of the 3D density distribution may be hidden by the variability resulting from the size distribution. Nonetheless, measures of fractal dimensions from 2D or 1D-like datasets (i.e., dimensions lower than the sampling support Euclidean dimension) are an unambiguous indication of the underlying fractal structure and multiscale organization, of the DFN model.
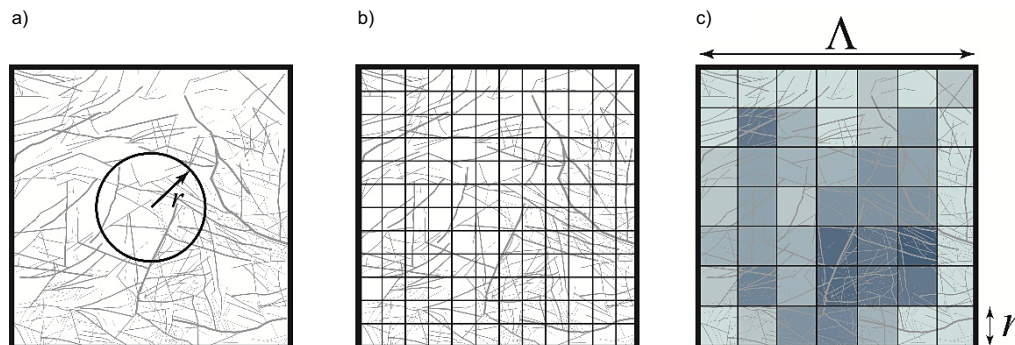
Figure 6-16. *Classical methods used to calculate the fractal dimension. These are (a) the mass dimension, where the total length of fracture traces lying in a disc of radius r is calculated, and (b) the box-counting method, for which the system of size L is covered by a regular mesh of size r. In (c) the multifractal analysis derived from the box-counting method for which each box of size r is weighted by the total length included in it. The darker the box, the greater the fracture length found inside it (figure and caption modified from Bonnet et al. 2001).*

Intensity variability

All the DFN models that mimic natural fractured systems are based at least partly on stochastic processes (Poisson, fractal, process-based, or a hybrid of these) which give rise to spatial variability in the properties of the DFN model, whether it be intensity, spacing or connectivity. This variability introduces uncertainties when inferring true (3D) parameters of the fracture system from finite datasets. It is also good practice to quantify the variability to make statistical comparisons between different datasets (and Fracture Domains). Their scaling nature is likely a significant characteristic of the underlying model since intensity is important for connectivity and intact block size distribution (Darcel et al. 2014, Lu et al. 2017).

The intensity variability $\sigma_\mu(s)$, of a fracture density term μ is defined at the observation scale s, as the standard deviation of μ estimates at the scale s. A complete theoretical description of the variability terms relative to the intensity estimates P_{Dd} (with D is the dimension of the sampling region and d the dimension of the sampled feature) for Poissonian DFN models is found in Lavoine et al. (2019). Following Plotnick et al. (1996), Lavoine et al. (2019) systematically derive the dimensionless ratio between the variance $\sigma^2(\mu)$ and the square of the mean $\bar{\mu}$:

$$\lambda_\mu(s) = \left[\frac{\sigma_\mu}{\bar{\mu}}\right]^2 \qquad \text{Equation (6-33)}$$

In the fractal theory, $\lambda(.)$ is called *lacunarity* (Plotnick et al. 1996). This is a scale dependent measure, whose analysis gives an idea of the scaling of fracture network textural heterogeneity and potentially on different regimes (Plotnick et al. 1996, Roy et al. 2014). The theoretical analysis of the intensity variability resulting from a Poisson process based DFN model shows that (Darcel et al. 2014, Lu et al. 2017, Lavoine et al. 2020) the variability term of the fracture intensity term measured on a 1D line (so $\mu \equiv P_{10}$) evolves as:

$$\sigma_{P_{10}}(s) \propto \sqrt{\frac{P_{10}}{s}} \qquad \text{Equation (6-34)}$$

This expected evolution of the variability term for Poisson process-based models is used further as a comparison reference to evaluate the meaning of variability terms measured from the real data. It can also be used as a proxy to evaluate the dimensions a dataset should have (relatively to the sample size and density) to achieve a certain estimation accuracy.

In practice, the variability term, associated with a dataset of length L (like the P_{10} log in Figure 6-17b), is calculated in a two-steps process. First the variation of $\sigma_{P_{10}}(s)$ are evaluated from a sliding box algorithm to compute the local means and the standard deviations (Figure 6-17a). A departure from the theoretical behaviour of the above-defined equation is observed as soon as the condition $s \ll L$ is not fulfilled. The dramatic decrease of the variability term is related to the finite size L of the data set and as such can be modelled as a finite effect. The second step of the process is the determination of the scaling exponent β of the evolution of $\sigma_{P_{10}}(s)$ as $s^{-\beta}$, over the range $s \ll L$ (straight lines in Figure 6-17a), and the extrapolation of the latter up to the dataset size (symbolized as a vertical dashed line in the figure).

The effective intensity variability extrapolated at the sample size L is a key output when identifying statistically-driven fracture domains (Subsection 5.3.3).

The scaling exponent β reflects the variability structure of the DFN and emphasises the potential departure from a basic Poisson equivalent model (Darcel et al. 2009). If β is lower that 0.5, the variability of the intensity of a fracture dataset is higher than the density variability one would expect from a Poissonian model.

Finally, the ratio of the density variability to the density estimate is a direct indication of the density estimate accuracy which will eventually be used as an input parameter of the DFN model(s).
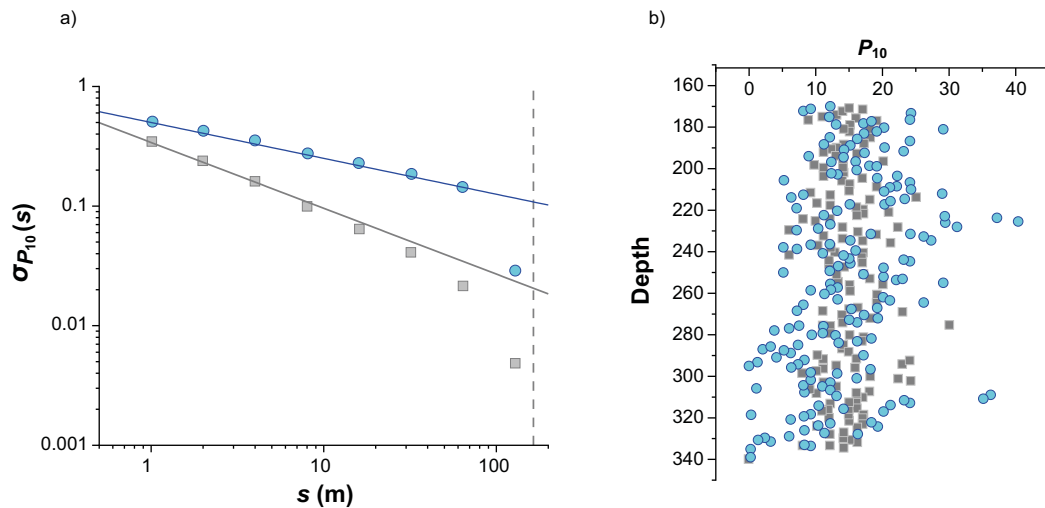
Figure 6-17. *Variability scaling, comparison between a dataset (blue symbols and blue line) and an equivalent Poisson's model (grey symbols and grey line). The dataset sampling support is a 1D-like core log of length equal to 164 m (vertical dashed lined, Figure a). a) Evolution of the variability term $\sigma_{P_{10}}(s)$ as function of s the sampling box. b) log of the local P_{10} values. From Figure 4-8 in Darcel et al. (2009).*

6.6.6 Local topology and terminations

The 3-dimensional fracture system consists of a number of finite surfaces or planes that either terminate at fracture tips, intersect with other planes at intersection (or branch) lines, or "float" isolated in free space. On a 2D slice through such a system, as seen on e.g. a relatively flat outcrop, the tips of fracture traces or segments terminate as so called Y- or T-intersections against other fractures, cross other fractures as X- intersections, join other tips as V or, is isolated in one or both ends, as I. The topology of the network as apparent on such 2D sample can be characterised by assigning the nodes of each fracture trace to one of these five types of vertices, see Figure 6-18. This topological description proposed by Sanderson and Nixon (2015) provides a description of the observed local connectivity between fractures and can be used to calibrate genetic-based DFN models to 2D observations.

As underlined by Sævik and Nixon (2017), counting the relative proportions of fracture ends and intersects in this way provides a way to classify fracture patterns and compare simulated patterns with those observed.
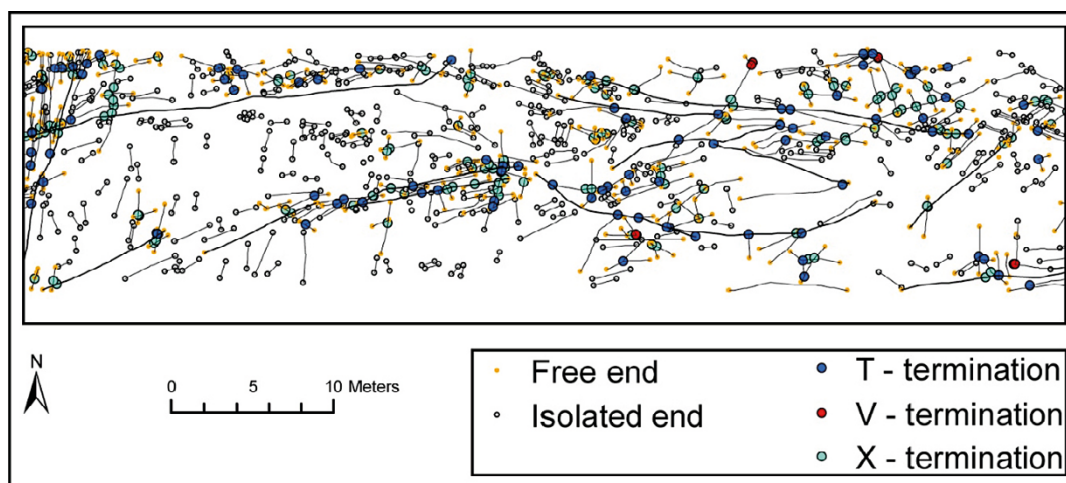
Figure 6-18. *Example of identification of node types from fracture traces on part of the tunnel floor of Parking Hall 1 in the ONKALO at Olkiluoto.*

The relative proportions of Y+V, X and I nodes can be plotted on a ternary diagram to classify different types of networks (Sanderson and Nixon 2015). This is illustrated in Figure 6-19 with a ternary diagram that provides a visual classification system of fracture patterns. Quantitative measures are given by the calculation of n_Y, n_X, n_V and n_I as the number densities of Y, X, V and I nodes per unit area, respectively. These can readily be calculated from an accurately digitised outcrop/tunnel surface (Figure 6-18). Several fracture patterns from Poisson or genetic-based DFN models are shown in Figure 6-19. In this representation, networks with similar local connectivity properties will appear in the same neighbourhood. In cases where many fracture traces are long compared to the dimensions of the mapped surface, the end node intensities can provide unambiguous measures of the fracture patterns.

Such representation of fracture traces is, however, dependent on the orientation (and shape) of the sampling plane, sampling resolution and is not related to the scaling properties of the DFN. The ternary representation and classification is a valuable tool for evaluating the local interactions between fractures which helps constraining the rules of genetic models.

Sævik and Nixon (2017) have made some investigations of possible functional relationships between hydraulic conductivity (in 2D) and these measures of connectivity.
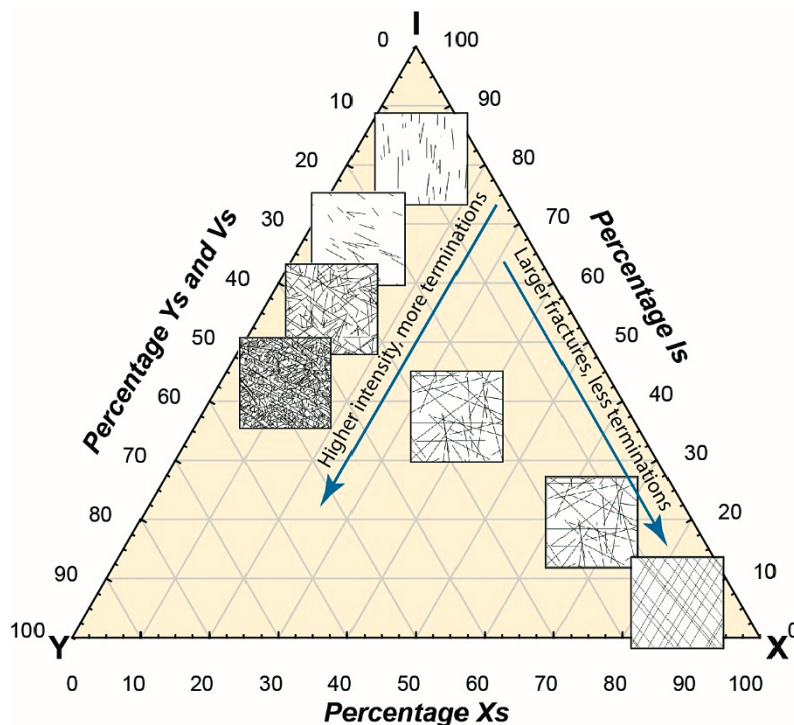
Figure 6-19. *Ternary diagram of proportions of different types of node for different example networks (edited from Libby et al. 2019).*

The present analysis of the topology of local connectivity can be used to assess the termination probabilities from one fracture set to another and, further, be used to combine the genetically-based DFN sequence of a site deformation history. The probability that a fracture trace terminates against another when they meet can be calculated from the number of ends as:

$$P(termination) = (n_Y + n_V)/(n_Y + n_V + n_X)$$

Equation (6-35)

where n_Y, n_X and n_V are the numbers of Y, X and V nodes per unit area, respectively. The termination probability can also be calculated between individual fracture sets (see Subsection 6.6.2 and fracture sets identified on an outcrop in Figure 6-20). Equation (6-35) can also be used to calculate a termination probability matrix for each set against every other, including itself. The result of such an interpretation is displayed in Table 6-1. The rows and columns of the matrix are ordered according to the relative ages of the sets as inferred from the deformation history, the termination probabilities of younger fractures on older ones should then be more apparent. The results for the example shown in Figure 6-18 are tabulated in Table 6-1, 40 % of the NW set terminates on itself, 26 % of NS sets terminate on the NW set and 7 % of the NW set terminates on the NS set. It is expected that probabilities are higher above the diagonal (i.e., "younger" terminating on "older") than below the diagonal (i.e., "younger" terminating on "older") as here. However, the relationship between orientation sets and age is rarely clear-cut, with fractures of different orientations being concurrent, or fractures of a certain orientation reactivating during a later tectonic era, giving the possibility of terminations against fractures of a different orientation that formed in the intervening time. Also, the intensity of the stress field or its alignment with weak planes may mean that the probabilities of termination of a relatively young set are low. Nonetheless, termination matrices provide another characteristic of network interaction and provide necessary input to genetic methods of fracture generation.

Table 6-1. Example of termination matrix from the mapping of traces on a tunnel floor of ca 120 m length by 15 m of ONKALO at Olkiluoto according to the six global sets in order (left to right) of the inferred age. A fracture belonging to the set listed in the columns has a probability that it will terminate on a fracture belonging to sets in the rows is given in the corresponding matrix.

PERCENTAGE OF (Y+V) nodes	Probability that fracture in column set terminates when intersecting fracture in row set					
	NW	NS	NE	EW_h	EW	FP
NW	40 %	26 %	43 %	25 %	27 %	50 %
NS	7 %	42 %	35 %	38 %	26 %	8 %
NE	33 %	0 %	100 %	50 %	29 %	33 %
EW_h	33 %	0 %	0 %	-	25 %	100 %
EW	15 %	17 %	9 %	14 %	61 %	28 %
FP	33 %	0 %	14 %	-	13 %	-

——— NW ——— NS ——— NE ——— EW_h ——— EW ——— FP
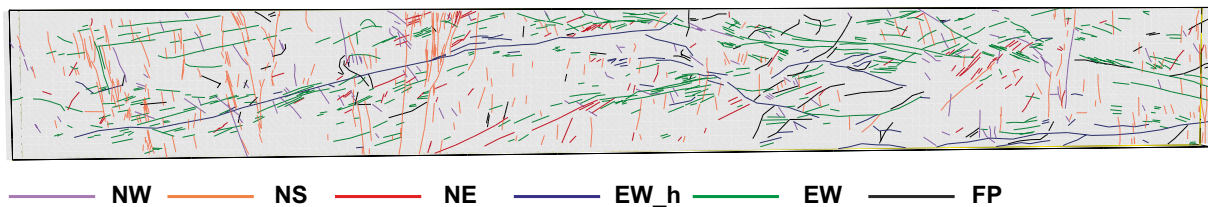
Figure 6-20. Example assignment of fracture to sets from the floor of Parking Hall 1 in the ONKALO, Olkiluoto (ca 120 m by 15 m). The traces are coloured by set, ordered left to right by an inferred relative age. Source: Posiva, reworked from Figure 14-5 in Hartley et al. (2018b).

6.7 Fracture in-plane characteristics

6.7.1 Conceptual framework and models

The concepts of **aperture** (geological, mechanical, hydraulic, transport, etc), **openness**, **roughness**, **waviness**, **matedness**, in-filling, **mineralogy** and **alteration** all relate to the geometrical description of space variations between fracture walls (Figure 6-25). All these properties potentially display local but significant spatial variations below the fracture size scale, whose nature can be captured by the former list of concepts. They basically all contribute to defining and characterizing fracture process properties relative to mechanical, hydraulic, transport and coupled processes (transmissivity and hydraulic aperture in Chapter 6, fracture mechanical properties in Chapter 7 and transport properties in Chapter 8).

The fracture in-plane characteristics can be partially observed from core or surface mapping and thus recorded in the systematic data sampling campaigns, as empirical rates or direct physical measures. Then, potentially combined with additional field or lab experiments (e.g. flow testing for hydraulic aperture, lab testing for relation to mechanical aperture to stress), they are used to support the assignment of fracture process properties.

Fracture surface roughness

A fracture is defined by two walls with each surface quantified as a height distribution. The so-called fracture roughness, or fracture morphology, refers to this height distribution.

A qualitative description derived from geotechnical charts (Chapter 6), is based on a two-scale description of this **roughness**, in terms of the irregularities of the surface on a scale smaller than the aperture; and **waviness** on a scale much larger than the aperture, but smaller than the length. These two scales of surface irregularity are shown in Figure 6-21. Fracture core interpretations in Forsmark record a roughness (waviness) and surface profile of fractures mapped in core; where the roughness may be *Irregular*, *Planar*, *Stepped*, or *Undulating*; and the surface profile may be *Smooth*, *Rough*, or *Slickensided*.

Roughness is also typically quantified by the joint roughness coefficient, JRC, which can be determined subjectively by comparing roughness profiles (at a 10 cm scale) to a set of standard profiles Barton and Choubey (1977). It can be measured precisely using tilt tests Barton (1973) but only by testing samples in the laboratory, not in situ. Many methods have since been proposed that overcome the weakness of the originally proposed JRC, some of which are reviewed in Grasselli (2006) who also introduced a quantitative surface parameter to replace JRC. However, the method of Grasselli (2006) presumes the fracture surface to be fully exposed which, unfortunately, is rarely the case in engineering applications. Thus, there is still a need to infer fracture roughness from field data, preferentially from fracture traces. This need has been addressed by Stigsson and Mas Ivars (2018) who advocate the use of fractal geometry (Mandelbrot and Van Ness 1968, Mandelbrot 1982) for the assessment of fracture roughness.
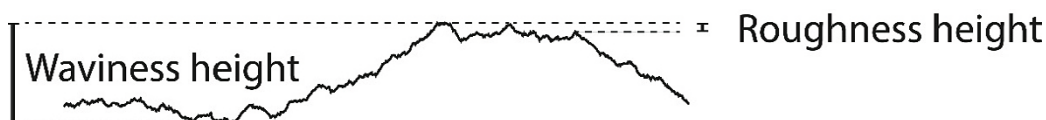
Figure 6-21. Schematic diagram showing the difference in scales of surface irregularities.

A more complete description of fracture surfaces relies on a self-affine or self-similar representation (Méheust and Schmittbuhl 2001). Describing fracture surface geometries as self-similar fractals means they are scale invariant, i.e., they 'look the same' whatever the scale of observation. The self-affine, in contrast to the self-similar, character implies that the 'elevation' axis, perpendicular to the average fracture plane and which defines the 'roughness' of the fracture surface, is statistically related to the fracture plane coordinates but has distinct magnitude. The self-affinity of fracture surfaces was early proposed by Mandelbrot (1985) and was later confirmed in numerous publications (e.g. Den Outer et al. 1995, Russ 2013). Moreover, Renard et al. (2006), Candela et al. (2009, 2012) and Brodsky et al. (2011, 2016) have shown in different studies that fractures are mono-fractal, self-affine surfaces over at least six orders of magnitude. From a DFN modelling perspective, these findings are intriguing as the implementation will push our computational efforts to the limit if fully implemented. At the same time, these findings offer some comfort to the modeller as it enables extrapolation and inferences from one scale to another.

Whereas a self-similar fractal is constrained solely by its fractal dimension, D, a self-affine fractal needs, in addition to its dimension, a scaling measure to be fully constrained. While the dimension of a self-affine fractal steers the persistence or correlation between points at various distances, the scaling measure steers the magnitude of the differences between the same points.

The dimension of a self-affine fractal can span between the topological and the Euclidian dimension of the object. This means that the dimension of a self-affine trace is a real number between 1 and 2, as a fracture trace is topologically a line, i.e., a *1D* object defined in a Euclidean *2D* space. In the same way the dimension of a self-affine fractal surface must be a real number between 2 and 3.

A slice through a N-dimensional fractal will yield a fractal with dimension N-1, i.e., a slice through a *2D* fractal surface with dimension D will yield a fractal curve with dimension D-1. This fundamental aspect of fractals thus enables the geologist to sample a fracture trace and from its dimension, deduce the fractal dimension of the fracture itself, assuming the surface is isotropic. Should this not be the case, two fracture traces sampled at a large angle (ideally perpendicular) would be necessary for the assessment.

It is not uncommon in the geological literature to express the dimension in terms of the Hurst exponent, after an early study by Hurst (1957) on the fluctuations of the Nile river. The fractal dimension, D, relates to the Hurst, H, exponent as:

$$H = 2 - D_{Line}$$ Equation (6-36)

$$H = 3 - D_{Surface}$$ Equation (6-37)

Thus, H is equal for the trace and the surface from which the trace is extracted, which makes the use of H rather than D quite practical in the context discussed here. It also implies that, to have a physical meaning, H is restricted to the interval [0–1] though, theoretically, H can be larger than 1. This would results in a line with voids (a so called Cantor dust (Cantor 1883)). H can also, theoretically, be less than 0, which results in a curve that wiggles so much that it fills more than the *2D* space. However, as far as we currently know, such obscure fractal curves are of limited value for the DFN applications discussed herein and will not be discussed further.

In time series analysis, it is common to quantify the so-called "persistence" of a series. As time and space are interchangeable in this context, the notion of persistence is also applicable to fracture traces (changing time for space in the abscissa). For $H > 0.5$, the trace is persistent with long range correlation in the sense that the probability is high that, for any studied point along the trace, the trace will in neighbouring points continue along the same direction. The opposite applies for $H < 0.5$ which has anti-persistent behaviour: The probability for a curve (or surface) at any given point to continue in the same direction as the neighbouring points is low. The very special case of H = 0.5 is called Brownian motion (sometimes also Wiener process) in which there is, ideally, no correlation at all. In the fractal terminology, self-affine curves are often called fractional Brownian motion of which the Brownian motion, proper, is a special case. However, as nicely summarised in Korvin (1992), most natural phenomena including fracture surfaces tend to have H roughly within the range 0.75–0.85.
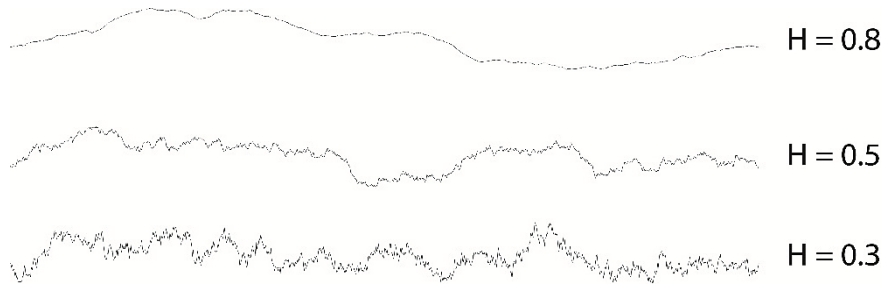
Figure 6-22. Examples of fractional Brownian motions with various Hurst exponents created with the random midpoint displacement algorithm (Fournier et al. 1982) and scaled vertically to yield the same amplitude.

Any complex motion can be broken down to a superimposed series of sinusoidal waves (Fourier 1822) which also applies to self-affine fractal curves. Fast Fourier Transform, FFT, makes use of Fourier's theorem, but uses a fast algorithm attributed to Cooley and Tukey (1965). Analysing a self-affine curve with FFT will render an array with complex numbers. From this array the power, i.e., the square of the amplitude, can be calculated for each frequency. A plot of the power as a function of each frequency will, in logarithmic space, render a straight line from which H can be deduced by (Russ 2013):

$$H = \frac{\beta - 1}{2},$$

Equation (6-38)

where β is the slope of the power spectrum in logarithmic space and is between 1 and 3 for a fractal curve to have a geologically meaning.

Whereas the Hurst exponent gives a measure of the correlation of relative heights of a fractal curve, the scaling parameter expresses the range of absolute heights. The standard deviation of height differences at different length intervals, Δl, denoted $\sigma \delta h(\Delta l)$, has proven to be an efficient metric for the scaling (Renard et al. 2006, Candela et al. 2009, Stiggson 2015). The scaling factor of two adjacent points (or vertices on a finite resolution curve) can be estimated from a power spectrum as (Stigsson and Mas Ivars 2018, Equation 4-9 in Supplementary material 1):

$$\sigma \delta h(1p) \approx \frac{2\sqrt{2}}{N} \cdot \sqrt{c_I} \cdot \sqrt{\sum_{f=1}^{\left(\frac{N}{2}\right)-1} \left(f^{-\left(H+\frac{1}{2}\right)} \cdot sin\left(\pi \cdot \frac{f}{N} \right) \right)^2},$$

Equation (6-39)

where c_I is the intercept of the power spectrum, f the frequency, i.e., number of waves per trace length, N the number of vertices of the fractal line and H the Hurst exponent.

To rescale for a different length interval, x, the following expression can be used:

$$\sigma \delta h(x) = \sigma \delta h(1) \cdot x^H,$$

Equation (6-40)

where $\sigma \delta h(1)$ is the standard deviation of vertices 1 unit apart, x the distance and H the Hurst parameter.

Typically $\sigma \delta h(1 \text{ mm}) = 0.05$–$0.4$ mm for $H = 0.8$ (Stiggson 2015, Stigsson and Mas Ivars 2018). Thus, a fracture trace with $H = 0.8$ should be sampled every mm over, say, a 1 metre long section of the trace, the undulation over a 100 m long section (of a theoretically infinitely long) trace can be computed to be (using 0.15 for $\sigma \delta h(1 \text{ mm})$):

$$\sigma \delta h(100m) = 0.15 \cdot 100000^{0.8} = 1500mm$$

This means that, with a probability of 68 %, a randomly chosen, 100 m long section, along a much longer trace will have an undulation smaller than 1.5 m. This insight not only enables the modeller to create realistic fracture geometries (Figure 6-23) over many scales, it also enables modelling of geometric uncertainty of modelled geological structures. Though both aspects stem from the same fundamental ideas, the target audience and practical implication is different.
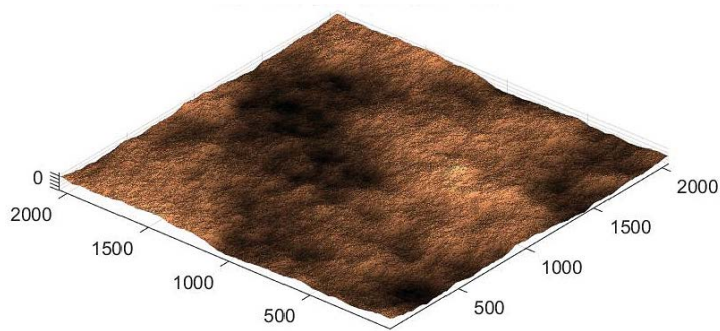
Figure 6-23. Example of a self-affine, isotropic, fractal surface produced using the method of Candela et al. (2009). The Hurst exponent, H, is in both x- and y- direction equal to 0.8. The surface was rescaled according to Stigsson and Mas Ivars (2018).

A related property of importance is the degree of **matedness** of the two fracture walls (see Figure 6-24) that affects fracture normal and shear stiffness as well as shear strength and dilation and how they all scale (Johansson and Stille 2014, Johansson 2016), see Chapter 6. Matedness can be decreased when asperities become damaged during shear under high normal stress.
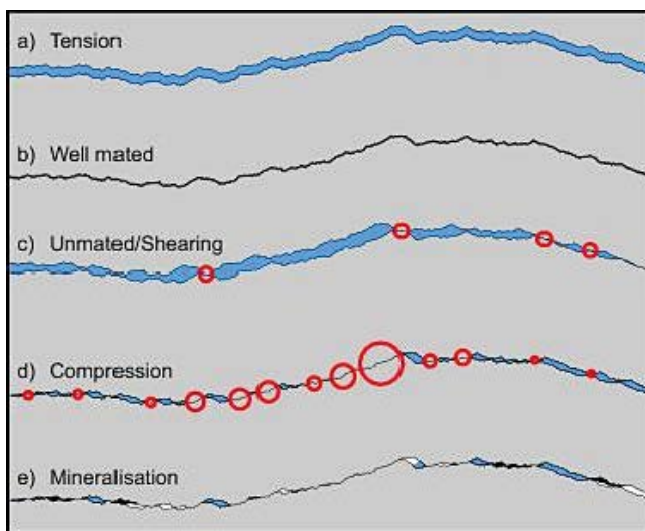
Figure 6-24. Schematic diagram showing the concept of matedness under different stress and mineralogical conditions.

Aperture(s), infilling and openness

Figure 6-25 shows a schematic conceptualisation of a fracture studied in the Äspö HRL, including an indication of the various apertures for this case.

The spacing between the fracture walls is referred to as the **geometric aperture** (sometimes known as geological aperture), defined as the distance between the surfaces of intact rock. Thus, the geological aperture is conceived as a measure of the "thickness" of a fracture orthogonal to the general fracture orientation.

The geometric aperture may be filled with minerals, gouge, rock fragments, and/or fluid filled openings in any combination. The **mechanical aperture** coincides with the geometric aperture. Both the geometric- and mechanical apertures can, however, be approximated in certain conceptual applications by, for example, the arithmetic average distance between the surfaces. The mechanical aperture of a fracture changes according to the applied stress acting normal (perpendicular) to the fracture plane. In the laboratory the mechanical aperture is often taken to be the average closure relative to a maximum closure, under a load applied normal to the fracture surface. Maximum closure is defined as the closure beyond which there is no deformation in excess of that in the intact rock.

A fracture's capacity for fluid flow is often characterised by measurement of the flow-rate through the fracture under a known hydraulic gradient. Assuming smooth and parallel plates, an equivalent **hydraulic aperture** is calculated in which flow-rate follows a cubic law (Snow 1965, Witherspoon et al. 1980), see Equation (8-3). Further characterisation of fracture hydraulic aperture and transmissivity, together with in-plane and DFN connectivity, is developed in Chapter 7. The compressibility of the mechanical aperture determines the storativity/hydraulic diffusivity of a fracture, which governs the rate at which pressure transients propagate, see Section 8.4.

In Figure 6-25, the geometric aperture varies along the fracture and includes fluid filled voids, fault gauge and rock fragments, but not altered zones. The average mechanical aperture is larger than the idealised smooth wall hydraulic aperture due to roughness of the fracture surfaces and the materials between them. An effective so called **transport aperture** (and closely related to storage) is also defined for transport modelling purposes (see Chapter 8 for further details). Geometric, mechanical and transport apertures are essentially the same, conceptually, but are measured in discipline-specific and scale dependent ways.

Much research has been focussed on deriving empirical relationships between equivalent hydraulic and mechanical fracture apertures, taking into consideration hydro-mechanical coupling, the role of applied stress and the relationship to geological aperture variations (see Chapter 7 for details).
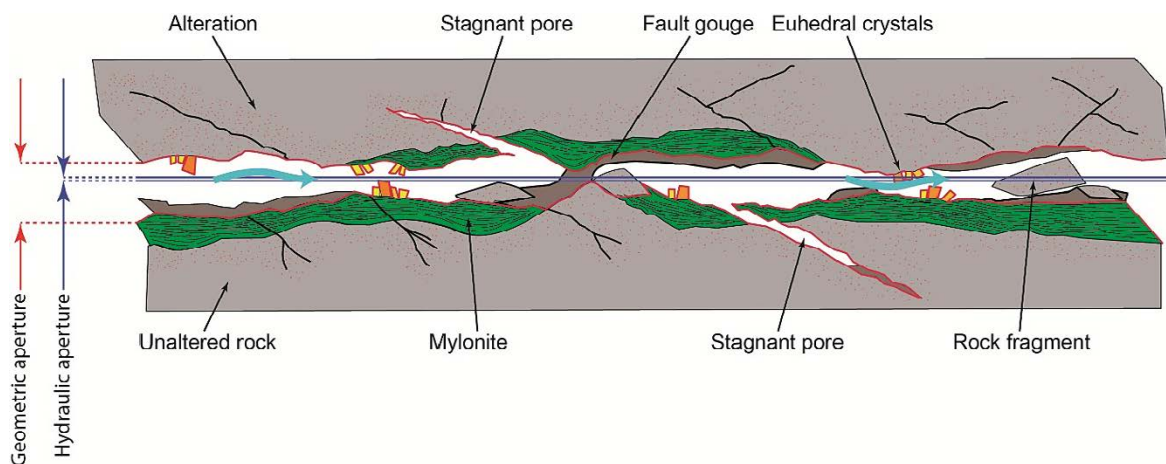
Figure 6-25. *Schematic illustration of fracture surfaces, mineralogy, and different types of aperture on a cross section through a fracture. Redrawn from Winberg et al. (2000). Geometric aperture is indicated as it may, locally, be directly measured, while other apertures will be interpreted as averages over a measurement scale drawn here as sub-volumes within the geologic aperture. Note that the geologic aperture is to approximate scale. The thickness of the remainder of the constituents is not to scale, e.g. the altered zones may extend several centimetres.*

The variations of average aperture (mechanical) with fracture size has been extensively studied e.g. (Cowie and Scholz 1992a, c, Clark and Cox 1996, Scholz 2002, Olson 2003, Schultz et al. 2008a, b, Klimczak et al. 2010). Commonly, the relation between geometric aperture (e) and fracture size (l) is described as follows:

$$e_m \sim Cl^b,$$ Equation (6-41)

with C a scaling constant and b commonly between 0.5 and 1.

However, Nordbäck (2014) showed at ONKALO underground research facility that there is a significant variation in geologic aperture for any given length, though in terms of general trends, both median and mean apertures correlate well with length. Analysis of aperture-size scaling of ONKALO for DFN modelling (Hartley et al. 2018b) interpreted a scaling between c 0.3–0.7 with 0.5 being used in simulations.

Figure 6-25 shows a schematic illustration of an open fracture. In addition to the notion of aperture, as described above, there is a need to introduce an additional term that expresses the portion of the fracture that is open or sealed, respectively (see details in Chapter 7). We note that fracture mapping in Forsmark recorded fractures as either being *Sealed*, *Open* or *Partially Open* based on core and BIPS observations.

Mineralogy and alteration

Identifications of mineralogical fracture infillings have been recorded in Forsmark through a sampling process of the drill core which includes the regular use of hand lens, binocular microscope, polarizing microscope, scanning electron microscope with an energy dispersive spectrometer (SEMEDS), and X-ray diffraction (XRD). The abundance of different fracture minerals in all fractures (open and sealed) in Forsmark shows a large variation (Sandström et al. 2008b), as summarised in Figure 6-26.

Other minerals have only been found as minor occurrences although they can be more common in particular rock volumes (e.g. asphaltite). It is noteworthy that borehole mapping in Forsmark does not differentiate between different clay minerals (e.g. Corrensite, Illite, Kaolinite). An open fracture, coated with a coating of euhedral quartz together with calcite and clay minerals (samples from KFM06B, 90.6 m – 90.85 m) is shown in Figure 1-13.
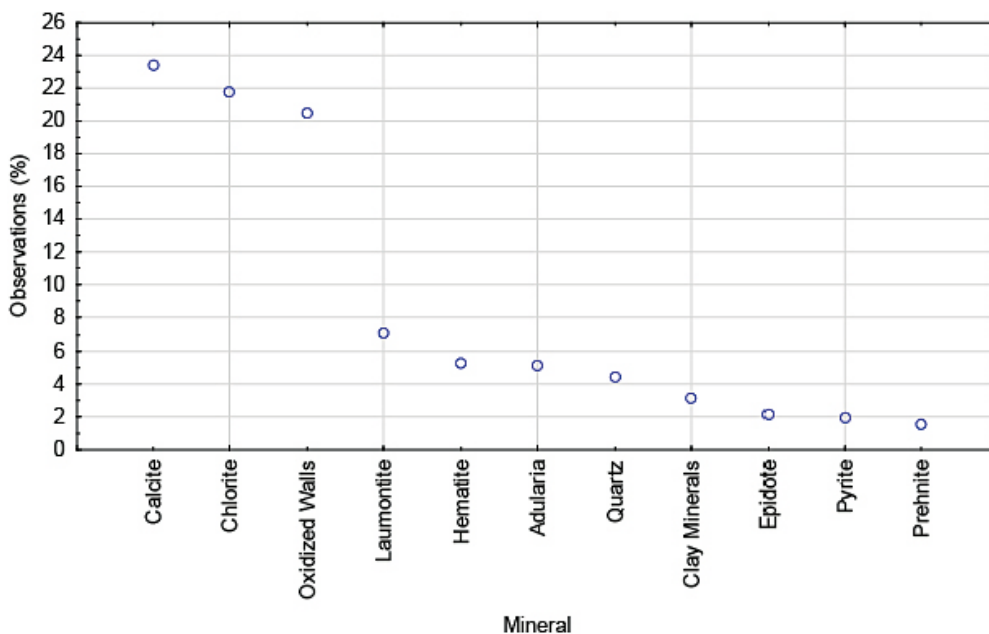
Figure 6-26. *Relative abundance of the most common fracture minerals in all fractures (both open and sealed) in Forsmark.*

The fracture alteration rate, J_a, is a simplified recording of the rate of alteration and mineralogy, for the rock quality classification system Q. The lowest values are for tightly-healed and unaltered fractures, where the rock walls are in contact, and the highest for thick mineral-filled fractures. Tight and healed fractures are classified with J_a of 0.75. Fractures with thin fillings and hard minerals, such as calcite, pyrite and quartz, are classified with J_a of 1. Fractures with thin coatings of, for example, kaolinite and/or chlorite are classified with J_a of 2, and with additional Illite and/or other clay minerals being classified with J_a of 3. Thicker (> 1 mm) fillings with graphite, chlorite and/or clay minerals can increase the J_a to 4 and fractures that are clearly clay-filled or grain-filled or are otherwise significantly altered with thicknesses of several millimetres have J_a of 6 or 8. The J_a value is mapped as standard for all fractures identified in core. Fractures with $J_a = 0.75$ are closed, while the likelihood of fractures being open and connected (at some point in history) increases with J_a.

The prediction of the spatial distribution of alteration of the rock walls and mineralogy, as distributed in the fracture system, is an important factor for describing retention properties (see Chapter 8).

Typical types of rock alteration in Forsmark are shown in Figure 6-27 and Figure 6-28, with red-staining of the wall rock due to hematite dissemination associated with hydrothermal alteration, and in Figure 6-29 with development of episyenite which is associated with the dissolution of quartz with subsequent precipitation of calcite in the voids.

Figure 6-27. Steeply dipping fractures with an orientation 350°/80° showing a reddish wall-rock hydrothermal alteration related to the growth of small grains of hematite.
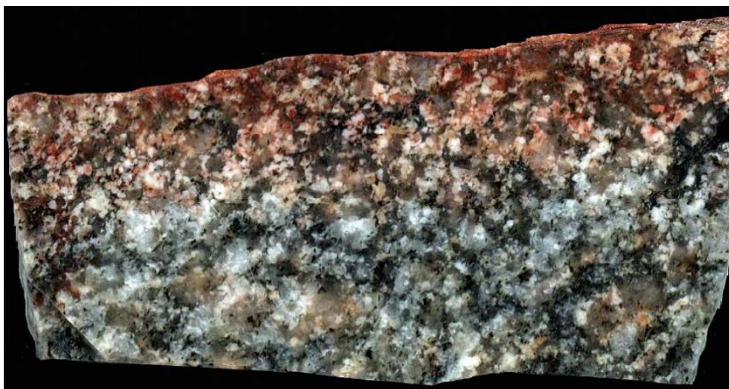
Figure 6-28. Red-stained hydrothermally altered rock adjacent to a laumontite sealed fracture (generation 2). The red-staining can be seen to gradually disappear ~ 1.5 cm out from the fracture. KFM09A 145.84 m. The base of the picture is ~ 4.5 cm. This photo is reproduced from Sandström et al. (2008b).

Figure 6-29. *Episyenite where the quartz has been dissolved. The voids have later been filled with calcite (white in figure). The diameter of the drill core is c 5 cm. KFM08A 410.60–411.04 m.*

6.7.2 Interpretation methods

The contribution of the abovementioned descriptive properties in term of fracture process properties (hydraulic aperture, transmissivity, hydraulic diffusivity, storativity, normal and shear stiffness, strength, retention properties etc., but also geological set and age), are further developed in Chapters 6, 7 and 8.

Some of the descriptive properties, i.e., defined from direct observations, like the openness (*Sealed, Open,* or *Partially Open*) can be complemented by high resolution resistivity such as "focused resistivity" or the single point resistivity (SPR) logs performed during PFL logging. It provides an independent check of whether the recorded open fractures contain either fluid or minerals (e.g. clays). Detection of local minima in the resistivity logs can be implemented based on the local derivative and variability of each log, to check if recorded open fractures consistently lie close to minima. It is proposed to use this to constrain the likely fraction of open fracture area (Hartley et al. 2018b).

In general, the distribution of openness Figure 1-15, of mineralogy classes (Figure 1-16 and Subsection 4.2.1) or of any other fracture in-plane characteristic, should be evaluated as a function of domain, depth, orientation set, age set and as function of distance to deformation zones. Preliminary analysis suggests these will give significant fractions of fractures in each generation, and so could be a viable partitioning of fractures according to mineralogy, that could then be used as part of the transport description.

Once tunnel mapping data becomes available from the access ramp and shafts, mapping of fracture properties and traces will allow correlation of alteration and mineralogy with fracture size. For example, one may expect large fractures to have a propensity to complex mineral assemblages and high alteration. Measurements of fracture apertures in tunnel mapping will also support analysis of potential aperture-size correlations.

There is inter-dependence between the properties of fracture apertures, surfaces and fillings and what they imply for mechanical, hydraulic and transport properties of fractures as portrayed in Table 6-2. It is therefore important to investigate these relationships, create suitable fracture classification systems that capture what is important for these properties, and implement them in numerical DFN models. The sorts of analyses this implies include:

- Determining correlations between fracture morphology measures with fractions of fractures that are water conducting and their transmissivity.
- Determining correlations between fracture alteration and mineralogy with fractions of fractures which are water conducting and their transmissivity.
- Determining relationships between fracture normal- and shear stiffness with fracture morphology measures and alteration.
- Determining correlation between orientation and mineralogy/alteration.
- Determining scaling relationships between aperture and fracture size.
- Determining any scaling relationship between mineralogy and alteration with fracture size.
- Determining any correlation between rock wall alteration with fracture size.

The first four bullets relate to statistical analyses of parameters measured on core samples, which are only of diameter 76 m in the slim holes at Forsmark. The last three bullets require mapping of fractures and their properties on exposed surfaces in tunnels. Aperture variability is another important property to characterise from a combination of direct observation of core, fractures on walls, fractured block samples, CT-scans, and from indirect indicators of the effects of aperture variability from e.g., transient hydraulic tests, tracer tests or injection of grout or resins.

Table 6-2. Relationships of mapped fracture properties to mechanical, hydraulic and transport behaviour of fractures.

		Mechanical	Hydraulic	Transport
Fracture properties	Mineralogy and alteration	Normal and shear stiffness, shear strength, shear dilation	Hydraulic aperture	sorption/diffusion
	Roughness	Normal and shear stiffness, shear strength, shear dilation	Hydraulic aperture	sorption
	Aperture and open fraction	Normal and shear stiffness, shear strength, shear dilation	Hydraulic aperture	Sorption, diffusion, retention

6.8 Sources of uncertainty

The sources of uncertainty are of three types: measurement resolution, absence of data and modelling interpretations. The spatial variability of the DFN properties (in term or density, scaling, orientation and correlations) accentuates their consequences. These are reviewed below, in light of the experience gained during the site investigations.

6.8.1 Overall technical/measurement uncertainties

- Fracture size related issues
  - Censoring effects – detecting small fractures, large fractures (few on scale of surface).
  - Small windows of observation on core, outcrops and tunnel surfaces, rarely on a full range of scales – the small and the large with a gap on the scale of tens of metres until several parallel deposition tunnels are excavated.
  - Under-sampling of large fractures, e.g., those unfavourably oriented relative to seismic reflection.
  - Extent of deterministic zones under-estimated due to lack of peripheral data.
- Precision of digitisation of traces and the types of ends and in associating orientations to traces.
- Shape is difficult to observe except in a few tunnel junctions, so has to be something we model.
- Stereological analysis.
- Variability terms.

6.8.2 Orientation uncertainties

Measurements of fracture orientations are afflicted with uncertainties that include instrument imprecision, external disturbances and human factors. A systematic assessment of these uncertainties in SKB's site investigations (Munier and Stigsson 2007, Stigsson and Munier 2013) estimated overall uncertainty to be about 20°, although this reduced below 10° for fractures interpreted in both core and borehole imagery. This cross-checking and avoiding drilling steeper than 80° are the main mitigations to constrain measurement uncertainties. Orientations supported by borehole imagery data are typically more reliable than those from the oriented core alone.

Of the interpreted fractures in the SKB database, 18 % lack strike and dip, which may bias interpretations should these records happen to be systematic in regards to particular sets.

The experiences for deriving the **DFN model** in Forsmark (Fox et al. 2007b) emphasised the difficulty to reconcile the complexity of the site DFN model into just 3–4 broad but ubiquitous age sets and the difficulty for the DFN model to account for spatial variations of properties, among which orientations, in a deterministic (increasing the number of sets and thus decreasing their internal variability) or stochastic representation (having less sets but with more internal variability).

Close to deformation zones, fracture statistics, including those of orientations, are often affected by the presence of the zone itself (Stephens and Simeonov 2015). Part of the affected region may lie inside the damage zone of the DZ but may also arise in a wider region after the formation of the zone. Hence, an approach to separating likely DZ-related fractures from those in intervening volumes should to be applied so that orientation and other properties can be analysed for the different volumes.

6.8.3 Fracture roughness

The main uncertainty is associated with the assignment of roughness to fractures mapped in boreholes, as the sample is mostly very small in relation to the size of the fracture and may therefore not provide any representative value. This uncertainty is inherent in the data and will be addressed once fracture mapping information becomes available from underground openings such as the ramp and Central area. Data stemming from the mapping of traces are inherently less uncertain though we note that the sampling and interpretation of traces is also associated with bias, inaccuracy and, to some extent, repeatability.

Methodologies are being developed for representation of the multiscale variability of fracture roughness in DFN models, see Subsection 6.7.1, but sampling plans and strategies need to be developed for the characterisation (including sampling strategy) of fracture roughness and for assessing, through modelling, the consequences of roughness on mechanical, flow and transport properties. The implications of necessary simplifications in the representation of in-plane variability can then be quantified.

6.8.4 Openness

Forsmark drillcore measurements include an analysis of whether individual fractures are **Sealed**, **Open** or **Partially Open**. With this, the geologists assigns a confidence in the interpretation of openness, expressed as **Certain**, **Probable**, or **Possible** which can be compared with discrete flow metering and used to understand bounds and uncertainty in the percentage of fractures, or the percentage of fracture area, open to flow.

6.8.5 Aperture

It is a working assumption that aperture follows a power-law scaling relationship with fracture size (Equation (6-41)), which in turn implies that transmissivity too is a function of fracture size (see Chapter 7). However, at present, with only surface-based borehole investigations available, there is limited data to support and characterise such correlations in Forsmark. Therefore, fracture aperture-size correlations are instead inferred from hydraulic modelling, by e.g. using the aperture model to match the shape of distribution of the specific transmissivities, and scaling relationships of flow over different borehole intervals or using cross-hole interference tests. However, matching such data is non-unique as model calibrations could be made using other fracture properties, for example the size scaling model.

Once underground construction begins, it is anticipated that mapping data from the ramp and Central area will provide the required data to further constrain these models, even more so when data can be analysed from the deposition areas.

6.8.6 Mineralogy and alteration

Extensive data collection and analysis has been performed for the mineralogical filling of fractures interpreted from drill core as synthesised by Sandström et al. (2008b), although it is acknowledged that this analysis should be updated for drilling campaigns made in Forsmark since the application for license in 2011. However, comparison of the mineral composition of fractures and PFL anomalies identify a number of water-conducting fractures without any visible fracture coatings (Claesson-Liljedahl et al. 2011). Although this lack of mineralogy could signify recent fracturing of the rock, it could also be a consequence of, for example, the drilling campaign causing mineral flushing of existing fractures or induced fracturing related to the sharpening of the drill crown.

As with many other fracture properties, it is challenging to extrapolate mineralogy beyond the borehole observations. A methodology is outlined above to perform analyses of various spatial correlations as the basis for making hypotheses in describing systematic spatial variability. As construction of the access areas proceeds, the interpretations can be further tested and refined using pilot hole and tunnel mapping data for the ramp and Central Area, and ultimately for the deposition areas.

7 DFN Descriptions for rock mechanics

DFN and rock mechanics models intertwine in several aspects of the Site Descriptive Modelling process. In this chapter, we describe this coupling between DFN and rock mechanics modelling, recognizing that, while the sequential integration of the modelling steps is well identified (Figure 7-1), their implementation is still challenging. We provide below an overview, including both standard approaches and developments in progress. We also provide multiple references to other chapters in this report (DFN Methodology Part 1), to the methodology for rock mechanics modelling of the Forsmark site (**RMMM**) and to Part 2 of this Methodology report, to facilitate the understanding of the coupling between rock mechanics, DFN geometries and hydraulics.

The current strategy for rock mechanics site descriptive modelling (**RMMM**) is still in line with the former strategy for rock mechanics site descriptive model, presented in Staub et al. (2002) and Andersson J et al. (2002b). It is defined to serve as a basis for design and safety assessment, and for the analyses performed during these steps. The key elements the site descriptive model should describe are recalled here:

- The distribution of rock mechanics properties such as deformation and strength properties for the intact rock, for fractures and for deformation zones in the rock volume, these three being taken separately, and of the rock mass viewed as a unit consisting of intact rock and fractures.
- The initial in situ stress conditions.
- The rock quality regarding its constructability.

It was already understood, in the strategy elaborated in 2002, that further developments were needed to implement the required key components in the site descriptive model. The updated strategy is strengthened by the improved understanding and the developments during the last 20 years. Additional key components are also identified:

- The effect of stress on fracture aperture and hence on transmissivity and hydraulic properties.
- Scaling issues to derive effective mechanical properties. While conceptually "intact rock" refers to pieces of rock free of fractures, and "rock mass" refers to rock volumes taken as a whole (rock and fractures), in practice rock pieces may contain some fractures, in a proportion correlated to the size scale (rock block dimensions). The concept of matrix rock can be used to refer to an "effective rock" into which the contribution of fractures below a certain size scale are merged with the intact rock to form an effective rock.

The concepts and methods to address these issues are described in the present document and in **RMMM**. This combines current knowledge and practices with ongoing developments. Significant steps forward were achieved in the past 15 years, so that numerical and analytical approaches to predict the rock mass properties, which take DFN models as input, are becoming new standards and valuable alternatives to the classical empirical approaches (see below).

The relations between the DFN modelling workflow and rock mechanics are schemed in Figure 7-1 with: *i*) Rules deriving from rock mechanics are an input to process-based DFN models (see Section 7.1), *ii*) DFN models are an input to the assessment of rock mass properties (see Section 7.2) which is an input for building stress models, and *iii*) rock mechanics are an input for assigning transmissivities to fractures (see Section 7.3), based on hydromechanical coupling processes in fractures.
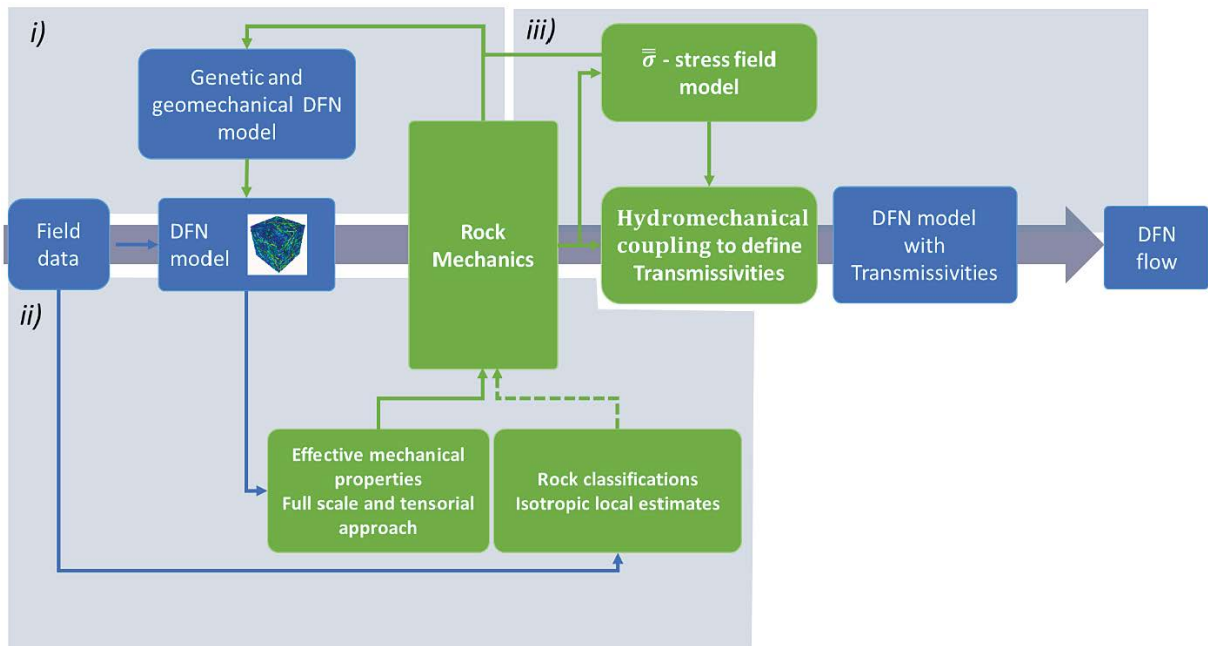
Figure 7-1. *Overview of the links between DFN and rock mechanics modelling. (i) Defines the use of rock mechanics as an input to DFN modelling, reflects the relation from rock mechanics to DFN (Section 7.1), box (ii) emphasises the relation from DFN model(s) to effective mechanical properties and box (iii) reflects the hydromechanical coupling relation with transmissivities and DFN flow (Section 7.3).*

7.1 From rock mechanics to DFN

DFN geometrical models can be significantly improved if they are process-based (geomechanical and genetic models below, Figure 7-1*i*), i.e., built from physical and mechanical arguments of fracture and fracture network growth, rather than only defined from statistical observations. We summarize below the current thinking and ongoing development efforts made with this approach. Most of the mentioned developments will be exemplified in Part 2. Giving a physical basis to fracturing from the laws of rock mechanics should bring more geological realism to DFN modelling. It potentially compensates the lack of knowledge (due to lack of information) to constrain some aspects of the models. This affects, for instance, individual fracture properties (e.g. fracture shapes, whose limited conceptual description is in Subsection 6.6.3), fracture local spatial configurations (intersections) and scaling organization (as introduced in Subsection 6.3.5 and 6.6.6) or fracture hydromechanical properties (e.g. aperture versus size and stress, see below in Section 7.3). However, although considerable progress has been made in understanding and modelling fracture mechanics since the pioneering work of Griffith (1920), the applications to geological contexts and to DFN modelling are still rudimentary in their ability to model the geometrical complexity of the fracture networks.

The degree of "geomechanics" integration in the DFN model(s) is basically null for purely statistically based DFN models (Section 6.3) and it increases more and more from the genetic DFN model(s) to fully geomechanical models (Subsection 6.1.9). One condition for rock mechanics based DFN model(s) to be sound alternatives to purely statistical DFN is that they still statistically reproduce the available observations. Also, using a rock mechanics based approach may give a physical rationale to local observations and therefore help the modeller to decide whether they can be generalized to the whole DFN modelling process.

Geomechanical models simulate a realistic propagation of fractures by solving the elastic, friction and rupture equations on *3D* models (Renshaw and Pollard 1994, Renshaw and Park 1997, Paluszny and Matthäi 2009, 2010 Ord and Hobbs 2010). The different numerical methods (adaptive finite elements, finite differences, discrete elements, etc) generate realistic looking fracture patterns, enabling quantification of fracture interactions based on mechanical principles and create aperture distributions that depend on local interaction effects. The main limitations of geomechanical models are the lack of knowledge of some of the constitutive rheological equations in natural conditions – e.g. friction,

crack growth – and the difficulty to model very complex or large systems (e.g. with millions of fractures) due to computational burden. Also, it is commonly not evident how to parameterise the models to match observed fractures.

Genetic models represent a promising way to approach the multiscale complexity of fracture networks, see Subsection 6.3.5. The main purpose of "genetic DFN models" is to mimic, as far as possible, the fracture pattern that would have evolved if a truly geomechanical model had been employed. They can be defined as the study of the growth trajectory of individual fractures (Kirkpatrick and Heckman 1989). The "genes" constitute the rules that define any fractures' growth and its adaptation to external stresses. For fracturing, the genetic models implement simplified mechanical rules for fracture nucleation, propagation and termination/arrest that are supported by experiments and/or theoretical considerations (see the discussion in Davy et al. 2013). The fracture network results from a time-wise collision process involving a very large number of interacting fractures. The genetic model developed by Davy et al. (2013) is able to reproduce the power-law distributions of fracture sizes and to provide a rationale for their parameters.

The development of genetic DFN models adapted to site conditions such as in Forsmark is still in its first stages. There is still a true R&D component in their developments. This includes for instance the consideration of varying stress conditions applying during tectonic phases of the development of fracture networks. The genetic and geomechanical models can be used to address yet unsolved critical modelling issues, e.g. whether one or several fracture orientation sets can develop concomitantly during a tectonic phase which is a critical assumption that controls the eventual network pattern and density.

Mixing geomechanical models, for their realism in considering the laws of physics, and genetic models, for their ability to reproduce complex fracture networks, is a key aspect for building confidence and reducing the uncertainties of DFN modelling. In practice, the developed models should be evaluated as developments occur, as part of the overall confidence building process (Chapter 10).

7.2 From DFN and fracture properties to rock mechanics

Rock mass deformability and strength arise from the ensemble behaviour of its constituents, which are the intact rock and the fractures. Since the DFN models are, currently, the best possible *3D* quantitative conceptualisation of the fractures in the rock, they are as such a key constituent of the rock mechanics modelling strategy. The consideration of the fracture system in the estimation of the rock mass effective properties has evolved considerably over the past 60 years and is now at a crossroads where several modelling approaches coexist. Building a quantitative approach to derive effective rock mass properties from DFN models, or directly from DFN model(s) parameters, is a ground-breaking research recently developed by different groups (see below). This evolution is only briefly recalled below. The reader is referred to **RMMM** and references therein for further discussion of the methods and their parameters, and to the planned Part 2 of this methodology for implementation and application examples.

The way the fractures are considered in the estimation of the rock mass properties has indeed evolved significantly since the first empirical classifications with the Rock Mass Quality Designation (RQD) introduced by Deere (1963) which preceded the *Q* system (Barton et al. 1974), the *RMR* (Bieniawski 1973) and the *GSI* with the associated Hoek-Brown constitutive model for rock mass strength envelope (Hoek and Brown 1997, 2018, Hoek et al. 2013). These empirical methods for rock mass classification were developed for use in civil and mining engineering in response to the need for ways to "rank" the mechanical quality of a specific rock mass, based largely upon the fractures and their weakening and softening effects on the rock material. They are defined by a combination of simplified fracture system geometry (e.g. fracture frequency noted P_{10} in Subsection 6.4.2) and fracture surface quality "conditions" (e.g. roughness, quality from fresh to weathered and/or altered, see Section 6.7). The fracture system is seen as an assembly of blocks rather than as a network of discrete fractures. In addition, empirical methods rely on readily available observations – core log or outcrop cell mapping data – to derive rock mass equivalent modulus and strength envelope. Hence the true nature of the fracture system (as a *3D* system) is reduced to the local available observations, assuming that an apparent fracture frequency and number of fracture sets (main orientations) are sufficient to constrain the impact of the fractures on the rock mass modulus and strength.

Even though empirically-based relations are in widespread use in engineering design, where they appear as fast and well suited for standard construction and design purposes (Staub et al. 2002), their scope of use is becoming narrower (Hoek et al. 2013). Their limited accuracy is increasingly questioned (Pells et al. 2017) and their inability to consider strength anisotropy (resulting from a preferred fracture orientation), scale effect (resulting mainly from the combined effect of fracture intensity and fracture size), and strain softening/weakening is a strong drawback (Mas Ivars et al. 2011). This is even more so for the conditions prevailing in the Fracture Domains in Forsmark, where the fracture system is rather sparse compared to the standard conditions for which the empirical methods for rock mass characterisation were originally developed (Hoek et al. 2013).

New comprehensive and quantitative approaches are now emerging, with numerical modelling of Synthetic Rock Masses (SRM), as initiated by Mas Ivars et al. (2007, 2011) and Pierce et al. (2007) and with the development of analytical relationships between the DFN model parameters and the rock mass properties (Darcel et al. 2018, Davy et al. 2018a). One of the core components of these approaches is the DFN model(s) definition (Chapter 6).

A SRM numerical model simulates the mechanical response of an idealised rock mass, viewed as a population of discrete fractures embedded in a matrix rock, with constitutive micromechanical models for both the rock and the fractures. This approach is being increasingly used, as shown by recent publications such as Min and Jing (2003), Pierce et al. (2007), Esmaieli et al. (2010), Mas Ivars et al. (2011), Harthong et al. (2012), Hoek et al. (2013) and Poulsen et al. (2015)). SRM modelling is based on Distinct Element Methods (DEM): The discontinuous medium model is represented as an assembly of discrete polyhedral blocks or spherical particles. All the particles (or blocks) are interacting at pair-wise contacts where the locally applied contact models reflect matrix rock or fractures' mechanical properties. These numerical models are adapted to simulate the deformability, strength, and spatial distribution of stresses which arise from the ensemble behaviour of the SRM constituents. SRM modelling provides means to analyse and assess the role played by DFN on the rock mass behaviour. Their ability to simulate very large domains and/or sufficiently large ranges of fracture sizes (multiscale fracture size density distribution, see Subsection 6.3.2 and 6.6.4) is however, limited by current computing capability.

An alternative approach to bridge the gap between an increasing understanding of the complexity of naturally fractured systems on the one hand (the DFN model(s)), and of the rock mass deformability and strength on the other, is developed since a few years. It consists in building the quantitative relationship between the DFN relevant geometrical and mechanical properties and the rock mass effective elastic and strength properties. Following the fundamental work in Kachanov and Laures (1989), Kachanov (1993) and Guéguen and Kachanov (2012) for populations of frictionless cracks, Davy et al. (2018a) are currently further developing the approach for multiscale DFN models considering the Coulomb slip model to describe the mechanical behaviour of each fracture. In short, the method, at present, takes as input an entire DFN embedded in a matrix rock (defined by elastic properties), including for each fracture the mechanical normal and shear stiffness and friction angle (and optionally also cohesion, tensile strength and dilation angle). The rock mass equivalent elastic properties (stiffness tensor) are thus analytically calculated at a chosen scale. Davy et al. (2018a) show how the latter tend to vary with scale (size of the rock mass), until a threshold is reached, beyond which the scale effect vanishes. The transition scale, between the scale dependent and independent regimes, results from a combination between fracture sizes, stiffnesses and the rock matrix modulus. This analytical DFN based method has several advantages:

- It provides a direct prediction of rock mass properties, based on individual fracture mechanical properties and on DFN structure.

- It is adapted to quantify scale, anisotropy and spatial variability effects.

- It is a tool for upscaling of properties in the context of multiscale DFN systems.

Its development is still ongoing (Darcel et al. 2018). Combination between the alternative analytical-based (Davy et al. 2018a) approach and the SRM numerical modelling is a key component for future modelling of stress distribution at different scales.

This alternative approach for rock mechanics is very close to the logic behind DFN flow modelling applied to hydrogeological modelling. It is quantitative, based on the complete DFN description, and adapted to upscale properties, including their scaling and anisotropy effects.

During the future phases of the development of the Rock Mechanics SDM, it is envisioned that both the empirical and the analytical/numerical approaches shall be evaluated to solve potential discrepancies and to redefine the scope of use of each of them (**RMMM**).

7.3 Hydromechanical coupling in fractures – basic mechanisms

The capability of a DFN to carry flow comes from the DFN connectivity structure and from the ability of each individual fracture to carry a certain amount of flow. Flow modellers commonly use the fracture transmissivity (see definition in Section 8.2) as the metric to quantify it. Since about twenty years, there is a growing attention to observe and quantify how hydromechanical coupling effects may significantly affect fracture transmissivities and DFN hydraulic properties.

In situ observations from the Forsmark or Olkiluoto sites (Martin and Follin 2011, Mattila and Tammisto 2012) emphasise correlations between fracture transmissivity and fracture orientation, likely in relation to mechanically induced change of fracture aperture resulting from the stress acting on it.

Numerous studies, based on lab- and field-testing, empirical, analytical and numerical modelling (Barton et al. 1985, Cook 1992, Esaki et al. 1999, Hopkins 2000, Pyrak-Nolte and Morris 2000, Olsson and Barton 2001, Min et al. 2004, Zimmerman and Main 2004, Auradou et al. 2005, 2006, Baghbanan and Jing 2008, Zangerl et al. 2008, Watanabe et al. 2009, Liu et al. 2013, Thörn 2015, Fang et al. 2018) emphasise a strong correlation between effective stress conditions and fracture mechanical and hydraulic apertures. The natural fracture is described as a pair of rough-walled surfaces with an in-plane distribution of contact areas and void spaces, whose heterogeneity prevents from defining an univocal relationship (like the parallel plate model and cubic law, see Chapter 8 and Equation (8-3)) between transmissivity, hydraulic aperture and mechanical aperture. The change of transmissivity is firstly related to a mechanically driven change of aperture, with opening/closure effects due to variations of fracture normal stress, changes in the relative position of the fracture walls in relation with shear stress, but also with potential damage and erosion of the asperities and additional clogging processes. Anisotropy of the transmissivity field may also result from these complex mechanical processes. The dominating effects are anyway locally controlled by the fracture shear and normal stresses, themselves defined by the fracture orientation and local in situ stress conditions. The latter results from a combination of regional stress conditions, stress redistribution close to underground openings (surrounding excavations, etc), rock matrix heterogeneity and also the surrounding fracture system itself.

There are several emblematic transmissivity-aperture-stress candidate models, widely referenced in the literature. They define a relationship between the normal and shear stress acting on a fracture and the hydraulic aperture (and transmissivity), whose parameters can be tuned according to the fracture in-plane shape and mechanical properties. The most well-known are the hyperbolic model from Goodman (1974), Barton (1982), Bandis et al. (1983), Willis-Richards et al. (1996), the exponential model from Liu et al. (2004) or the power-law model from Raven and Gale (1985).

Former DFN flow modelling for the Forsmark site (Follin et al. 2007b, 2014) did not consider a quantitative, stress based, hydromechanical coupling to define transmissivities, but rather a qualitative and empirical relation, based on hydraulic tests in boreholes and core logging, involving the fracture sets and the flow logs. More recent work, carried out by SKB, investigate hydromechanical coupling to define the fracture transmissivities. This encompasses the following:

- Determination of a sound transmissivity stress law, i.e., conceptualization of the relationship (Zou et al. 2018, Stigsson 2019, Stigsson et al. 2019, Zou and Cvetkovic 2020). This ongoing research is further discussed in **RMMM**.

- Sensitivity analyses, with preselected transmissivity models based on the exponential model of Liu et al. (2004) and Follin and Stigsson (2013) (see Equation (9-4)), to evaluate the increased variability and equivalent conductivity anisotropy evolution with scale, for rock mass block dimensions from a few to about a hundred of meters (Darcel et al. 2021).

- Parameter calibration of a selected transmissivity law (Willis-Richards et al. 1996) for DFN flow and transport prediction (Hartley et al. 2016, 2018b). The steps of the calibration process are briefly summarized in Table 8-2 of this report.

The stress field, the fractures and intact rock and rock mass mechanical properties, and the model parameters, necessary to define the hydromechanical properties are discussed in **RMMM**. The main components include:

- The regional stress field tensorial description.

- The calculation process, for each fracture, to derive the normal and shear stress components and the fracture normal and shear displacements.

- The fracture mechanical model(s) and parameters, including at least the fracture shear and normal stiffnesses, the cohesion, the friction angle and the dilation angle.

- The intact rock and rock mass mechanical properties, e.g. the Young's modulus and Poisson ratio and strength envelope.

The DFN and individual fracture geometrical properties, in-plane properties (e.g. roughness, matedness, etc) and the fracture scale properties (orientation, size), are defined in Chapter 6, Section 6.7 and 6.6 respectively.

7.4 DFN and transmissivity changes due to stress perturbations

While present day DFN models and natural conditions tend to demonstrate a low incidence of shear stress and critically stressed fractures on current fracture transmissivities, these conditions may change in the long term due to glaciation/deglaciation episodes and earthquakes. Furthermore, also on shorter time scales, the construction of the site infrastructure and the thermal loading phase will induce stress changes. These loading scenarios may induce stress and fluid pressure variations with significant consequences on the DFN and on the transmissivities. Though basic concepts of hydromechanical coupling in fractures were addressed in the previous section, we here provide a short summary of the current knowledge and discuss potential permanent changes of the fracture network and transmissivities due to stress perturbations.

Fracture reactivation is the most likely process, with high impact on hydraulic properties, that may occur during a change of the stress conditions. Even if generation of new fractures and propagation of existing ones cannot be discarded at the moment, fracture reactivation is more likely to occur than creation of new fresh fractures in the intact rock. The estimated values of cohesion of sealed fractures based on laboratory shear tests range between 2.2 and 7.5 MPa and the friction coefficient values range between 1.1 and 1.6 (Glamheden et al. 2007, Hakami et al. 2008), whereas the estimated tensile strength of the intact rock at Forsmark ranges between 7.9 and 20.9 MPa and the cohesion ranges from 17 to 42 MPa (Glamheden et al. 2007). The fracture reactivation mechanism would lead to reopening some sealed fractures and possibly to increasing the aperture of critically-stressed fractures by dilatancy. Considering that fracture networks are currently close to the percolation threshold[2] (Follin and Stigsson 2014), a small increase of the open portion of the fracture network has potentiality large consequences on flow as it is observed after earthquakes at short but also long distances to the source (Brodsky et al. 2003, Manga et al. 2012, Wang and Manga 2014, Wang et al. 2016).

Fractures are reactivated when their state of stress is modified enough to reach the failure condition either by shearing when they are critically stressed, or by tensile opening if the normal effective stress is low enough (Ferrill and Morris 2003, Ramsey and Chester 2004, Rozhko et al. 2007). Erosion, earthquakes, glaciations, thermal loading or tunnel drilling are natural or anthropogenic processes that can achieve these conditions. Regardless of whether the fracture is reactivated by tensile opening or shearing, the reactivation process involves both the stress applied on the fracture plane, which can be estimated, and the fluid pressure P_f at the time the fracture is reactivated, which is generally unknown. In well-connected networks, we may expect P_f to be close to the hydrostatic pressure, but in weakly connected networks or below impervious caprock, P_f can raise to the lithostatic pressure causing the effective stress to vanish (Sibson 2003). An increase of the fluid pressure is also expected when an ice sheet is close, but not exactly above, the site. The diffusion at depth of water over-pressurized by the

---

[2] An argument for considering fracture networks close to the percolation threshold is the number of flowing fractures (PFL in the report) compared to the total number of fractures recorded along boreholes.

ice sheet potentially leads to a build-up of the fluid pressure, which may cause hydraulic fracturing (Chan and Stanchell 2005, Lemieux et al. 2008, Vidstrand et al. 2008, Lönnqvist and Hökmark 2013, Hökmark and Lönnqvist 2014, Rühaak et al. 2014, Talbot 2014).

Whatever the reason for the fluid pressure increase, it tends to decrease the effective normal stresses without changing shear stresses, and thus to shift the Mohr circle to the left, closer to the failure envelope. Recent analysis of the open fraction of the fracture network (f_{op}) in Forsmark suggests that part of the distribution of f_{op} is controlled by fracture reactivation induced by fluid pressure build-up (Doolaeghe 2021), which sheds light on the fluid pressure as a driving force for reactivation, and on the consequences of past and maybe future glaciation/deglaciation events in the open structure of a DFN. These processes will certainly affect the shallow bedrock. However, they cannot be discarded at depth, even if the prevailing higher confinement may inhibit, to a certain extent, their effect.

There are not yet recipes to define how much a fracture network can grow or open due to stress change episodes, but there are ways to understand and quantify future loading scenarios as well as their consequences in terms of flow regimes.

8 DFN models for flow

8.1 Introduction

Crystalline rocks typically have low rock matrix permeability such that the effective hydraulic conductivity of the rock mass is controlled by fractures. For example, the measured hydraulic conductivity of intact rock samples from borehole KFM01D range between 4×10^{-14} to 5×10^{-12} m/s (Vilks 2007a) for different rock samples and confining pressure, with values typically reducing by an order of magnitude between confining pressures that may be encountered at the surface of the bedrock and those at repository depth. In contrast, the equivalent bulk hydraulic conductivity of the rock mass at Forsmark is much higher, when including both fractures and deformation zones, the average hydraulic conductivity of the top 200 m of bedrock is c 1×10^{-6} m/s, c 2×10^{-8} m/s between –200 and –400 m elevation, and c 3×10^{-9} m/s below –400 m elevation (Follin et al. 2007b). The hydraulic characteristics of any volume of rock mass are controlled both by the hydraulic characteristics of the largest and most conductive fractures within that volume and the degree of interconnections between the fractures. Hydraulic characteristics of individual fractures are controlled by surface morphology properties such as fracture aperture and its spatial correlation and variability, contact/infilled area, roughness, matedness (see Section 6.7), together with mechanical properties of normal and shear stiffness and in situ stress (see Chapter 6). The connectivity of the network depends on structural properties such as the spatial distribution of fractures, their intensity, size distribution and orientation of fractures (see Section 6.6). Hence, a systematic description of fracture hydraulics involves the integration of the concepts and fracture properties discussed in the previous chapters together with concepts specific to the measurement and prediction of fluid flow through fractures both inside and outside brittle deformation zones, see Subsection 6.4.5.

8.2 Modelling flow in DFNs – parameters (T and S) and dimensions

Under laminar flow conditions where viscous forces dominate inertial forces, which is generally the case for natural groundwater flow in low-permeable fractured rocks (i.e., low Reynold's number flows), the following equation of mass conservation is used to describe transient flow through a fracture network in the case of constant density flow:

$$\frac{S}{\rho_0 g} \frac{\partial P}{\partial t} = \nabla \cdot (Q) \qquad \text{Equation (8-1)}$$

P is the pressure (Pa), ρ_0 is a reference fluid density of freshwater (kg·m³), g is gravitational acceleration (m·s⁻²), S is the storativity of the fracture (-) representing both fracture and fluid compressibility, Q is flow-rate per unit width of fracture (m²·s⁻¹). Here, a pressure rather than a head formulation is used to allow for variable density flow which is relevant to the saline groundwaters in the deep bedrock at Forsmark.

Transmissivity (m²·s⁻¹) is the property that directly defines the flow-rate per unit width of fracture (m²·s⁻¹), Q, assuming flow inside the fracture follows Darcy's Law:

$$Q = -\frac{T}{\rho_0 g} \nabla(P - \rho g z) \qquad \text{Equation (8-2)}$$

where ρ is fluid density (kg·m⁻³), z is elevation (m). With these assumptions, the transmissivity T is the only hydraulic property required to perform steady flow simulations. A second parameter, the storativity S is required for transient conditions (see below).

In practical field testing terms, one actually measures specific capacity (flow-rate divided by drawdown Q/s, from which T can be inferred from e.g. DFN modelling), and the time at which hydraulic disturbances at monitoring points are observed (from which hydraulic diffusivity, η, (m²·s⁻¹) can be inferred, and then $S = T/\eta$).

With the above-mentioned equations, the DFN flow model is a *3D* system of inter-connected *2D* fracture planes to which transmissivities are assigned and whose local apertures are not explicitly required for the flow simulation but are possibly integrated into the transmissivity definition (see below). This locally defined *2D* description of the DFN flow model is the key modelling assumption since it directly combines the initial geometrical/structural description of a DFN with each fracture's capacity to bear flow, i.e., with its transmissivity.

Depending on the modelling application purpose, flow within a rock volume can be conceived as either fully continuous (i.e., *3D*) when using an upscaled ECPM model to simulate bulk flows, constrained to discrete fractures (i.e., locally *2D*), or constrained to channels within a fracture (i.e., locally *1D*). The Darcy law and mass conservation equations can be expressed either for *3D*, *2D* and *1D* elements, with the correspondence between element dimension and flow property illustrated in Figure 8-1. The transition from a DFN model to an ECPM model is commonly required when model dimensions are too large to afford DFN simulations (with current modelling capacities). The flow property of relevance is then the equivalent hydraulic conductivity tensor, K. When flow within fractures is highly heterogeneous such that flow within fracture planes occurs in sparse channels, then the flow within planes can be reduced to *1D* pipes to which a conductance C (m^3·s^{-1}) is assigned. Both alternatives, *3D* and *1D*, offer a reduction of the underlying fracture system in terms of numerical size.

At individual fracture scale, the fracture transmissivity results from the local distribution of connected voids between the fracture walls, see Section 6.7. For an idealised fracture, such as the well-known parallel plate model, defined by a constant hydraulic aperture e_h (m), the flow can be described by the Boussinesq equation (a simplification of the Navier-Stokes equations where fluid density is only important in the buoyancy term (Boussinesq 1868)) based on the integral of the parabolic flow profile between the walls. The resulting flow-rate is proportional to the aperture to the cube. This result, known as the cubic law, gives the following relation between the aperture and the transmissivity (Equation (8-2)):

$$T = \frac{\rho g}{12\mu} e_h^3$$

<div align="right">Equation (8-3)</div>

where μ is the fluid viscosity (Pa·s). In practice, transmissivity is calculated from measuring flow-rates under a known pressure gradient, Equation (8-2), and hydraulic aperture is evaluated based on the cube root implied by Equation (8-3).

The cubic law remains a good proxy of the transmissivity aperture relationship under the approximation that fractures are planar on the scale of the fracture length, i.e., with low tortuosity and surface roughness. Zimmerman et al. (1991) concluded that the cubic law (Equation (8-3)) also provides a reasonable representation of flow through rough fractures provided the wavelength of the dominant variations in aperture is greater than the amplitude of the variations. Witherspoon et al. (1980) demonstrated the validity of the cubic law in rock samples of granite, basalt and marble, as well as considering perturbations from this model due to roughness, normal load and higher Reynold's number (up to about 100).
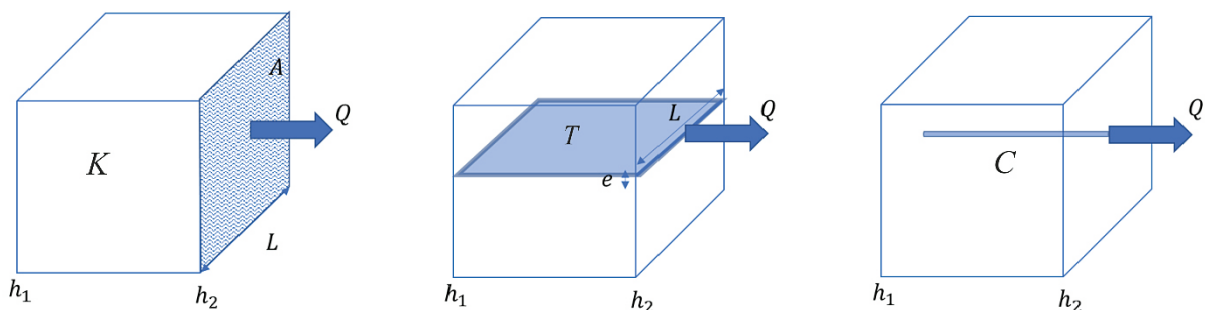

Figure 8-1. *Schematic illustration of Darcy law principle with* $\frac{Q\left[\frac{m^3}{s}\right]}{\nabla h} = KA = TL = C$ *for a) 3D medium and b) fracture of a DFN c) pipe/channel, respectively.*

It is noteworthy that in the general case fracture roughness cannot be neglected and the hydraulic aperture differs from the mechanical aperture. However, Equation (8-3) is still used to deduce a reference equivalent hydraulic aperture, e_h, from a prior flow-rate estimate (or measure) directly expressed as a transmissivity T. In such cases, the equivalent hydraulic aperture tends to be much smaller than the mechanical one (see Section 6.7). For natural and rough fractures subjected to varying loading conditions, many researchers (e.g. Barton et al. 1985, Tsang 1990, Zhao and Brown 1992, Pyrak-Nolte and Morris 2000, Watanabe et al. 2009, Xiao et al. 2013, Nishiyama et al. 2014) attempted to derive the relationship between fracture equivalent hydraulic aperture (or transmissivity), fracture in-plane characteristics and stress conditions (Section 8.4). These provide a general background for the models used in Table 8-2.

The second fracture flow property, the storativity parameter denoted S in Equation (8-1). This is derived from the hydraulic diffusivity, η, that governs the rate at which transient pressure disturbances transmit through the fracture system, which is dependent both on fluid and rock compressibilities. It can be interpreted in terms of the underlying rock and fluid properties, and can be calibrated to transient hydraulic tests, as developed in Section 8.4. In field tests, η is most reliably determined from cross-hole hydraulic tests based on the time for pressure disturbances to be detected in monitoring holes (Streltsova 1987), noting that Equation (8-1) represent a diffusion equation in pressure with a hydraulic diffusivity parameter $\eta = T/S$. Hence, storativity is calculated from interpretations of η and T, $S = T/\eta$.

The hydraulic characteristics of any volume of rock mass are thus controlled both by the geometrical structure, principally the intensity and connectivity, of fractures and by the spatial distribution of the transmissivities. Midway between connectivity and transmissivity is the binary description of open and sealed portions of the fracture surfaces, and the spatial distribution of openings. This is an intermediate step between the geometrical description of the DFN (Chapters 5 and 6) and the flow simulations. Flow cannot take place in the sealed part of fractures, but flow in the open parts depends on the spatial distribution of openings and local hydraulic boundary conditions. The open part of fractures being split between flowing parts where advection dominates and stagnant areas where voids are isolated, dead ends or subject to very low gradients, see Figure 8-7. Stagnant areas can contribute to flow when gradients are induced by pumping or excavation.

In high strength crystalline rocks of interest to host a repository, flow is typically concentrated in a small fraction of the total fracture area due to limited connectivity, heterogeneity of the fracture walls and infilling, the low incident hydraulic gradient, and compressive stresses. This channelling of flow then is created directly by closure of fractures over parts of their surface (see Section 8.3) and indirectly through roughness of the remaining open parts of the surface (see Sections 8.4 and 8.5). A necessary first step in the hydraulic DFN modelling is therefore to conceptualise and parameterise the spatial distribution of openings, Section 8.3. Followed by describing the spatial distribution of aperture voids and transmissivities in Section 8.4. We note that the primary control on hydraulic connectivity comes from the geometrical structure of the DFN combined with the spatial distribution of openings (Section 8.6), whereas flow channelling (Section 8.5) potentially results from the superposition of all these properties with the spatial distribution of transmissivity/apertures properties and boundary conditions.

8.3 Spatial distribution of openings

The fraction of fracture surface area completely sealed by mineral infilling and/or physical contact between fracture walls can be quantified from core characterisation. At Forsmark, this information is systematically recorded (as one of the fracture mapping attributes recorded in the database Sicada in the p_frac_core table), where each fracture intercept is qualified as sealed, open or partly open. This information may be supplemented by high-resolution resistivity logs that can also reveal the fraction of electrically conductive fractures that may correlate with water filled or clay filled fractures, as a downhole indicator of the fraction of potentially transmissive fractures.

Prior analyses of the available cored boreholes show that, overall, only about 25 % of the total fracture intercepts are open or partly open. This provides an estimate of the fraction of open fracture surface area, f_{op}, as assessed over all fractures logged in boreholes within some domain. These estimates can be refined and redefined by any relevant set/assembly of fracture as part of the site-descriptive modelling, to identify if this open fracture may significantly vary between different fracture domains or deformation zones, orientation or age set, depth etc. This the fraction of surface area open, but not necessarily connected to a source of water and conductive to sustained flows. Once the proportion of open fractures (or proportion of open fracture area) has been estimated from analysis, the spatial distribution of these openings between and within fractures, needs to be considered. For hydraulic modelling it is only necessary to consider that part of the fracture system that is open and connected, recognising that this is a subsystem of the Open fracture system and that in turn is a subsystem of the All (or Geometrical) fracture system.

Although the fraction of open fracture area is likely a critical property determining the connectivity of that part of the network able to conduct flow, its spatial distribution of openings is also likely to be an important factor. However, there is no direct observation or evidence to define this spatial distribution within the fractures and possible correlations with fracture size. Once geological tunnel mapping is available, one can make some limited use of indicators, such as hydrothermal alteration, clay minerals and slickensides, as to where flow or movement of fracture surfaces has occurred at some time in the geological record. These can be used as proxies for the existence of openings and whether such indicators correlate to fracture trace length. Direct observations of the openness distribution may be done at a decimetre scale, e.g. from resin injection experiments followed by over-coring, e.g. (Winberg 2010). At scales from metres to tens of metres some tests (hydraulic or electrical cross-hole) may be performed, as in Hurmerinta et al. (2012), Ludvigson and Hjerne (2014) and Krietsch et al. (2018), to identify interconnectivity of fracture opening between parallel boreholes. However, the resulting interconnectivity arises from both network and fracture in-plane properties, so that no direct/unique distribution of openness can generally be deduced.

How the openings are distributed between and within fractures is therefore an uncertainty that should be managed through considering alternative plausible hypotheses and testing these through sensitivity analyses, calibration and rejection. The range of hypotheses considered should postulate distributions that result in significantly different outcomes for safety critical properties such as the flow distribution, flow-related transport resistance and channelling. One extreme is that variability in openness is all inter-fracture variability, i.e., whole fractures are either open or closed, and another that intra-fracture variability in openness is dominant. The scale and shape of intra-fracture variability are other factors to be analysed. At the same time, they should all be conditioned on the measured fraction of opening and its correlations to other geometrical parameters. Sensitivity analyses can then be used to give quantitative understanding of how the alternative hypotheses affect safety critical properties and how they may be differentiated through indirect measurements (e.g. hydraulic tests, grouting operations or inflows).

The formulation of hypotheses should be guided by general and site-specific empirical considerations. For instance, shear and reactivation are more likely to occur on large fractures, and so they are more likely to be open, hence f_{op} is likely to increase with size. Of particular importance is the conceptualisation of openings within critical structures (SKB 2018) of Class 3 which form significant flow paths for groundwater, or structures where secondary shear movements may be triggered in conjunction with earthquakes and where the movements could be so large that they may damage a canister.

Note that the intensity-size scaling graph for open fractures will be beneath the distribution of all fractures, and have a different shape. Further, large fractures are more likely to connect than small ones compounding this difference. A simple schematic of possible density functions for all fractures and open fractures is shown in Figure 8-2. In the two simple examples shown, f_{op} is either a constant or a function of size $f_{op}(r)$ and applied as the probability whether any given fracture is completely open or completely sealed. This notion of different subsets of fractures with different size density models is a useful mental image for the density model relevant to hydraulics.
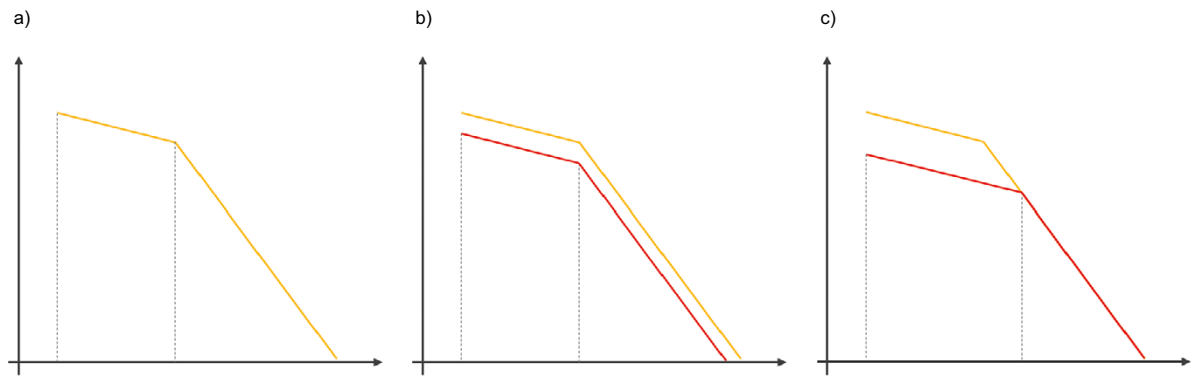
Figure 8-2. *Schematic of different fracture size density models on a log-log plot of density (ordinate) and abscissa (size): a) All fractures (orange color), b) a hypothesis for the open fractures assuming a fixed f_{op} across all scales (red color) c) a hypothesis for the open fractures assuming a lower f_{op} for small fractures increasing to 100 % for large fractures (red color). Minimum size and a transition size between different regimes are indicated with vertical grey dashed lines.*
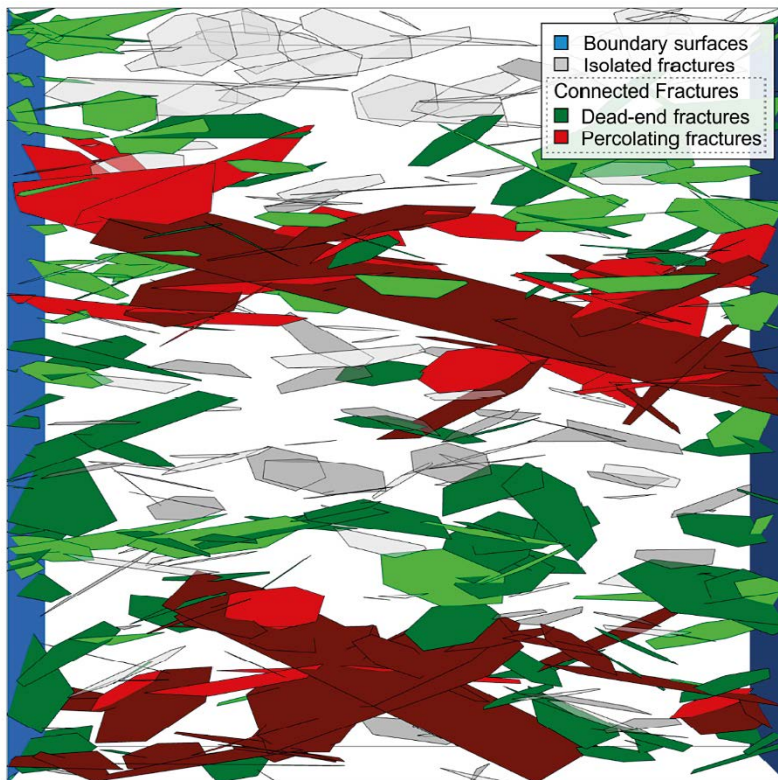
Figure 8-3. *Illustration of isolated, dead-end and percolating fracture in a 3D network.*

Potential hypotheses for openings can be grouped in two classes: ones that distribute openings between fractures (Figure 8-4a); and ones that distribute them within fractures (Figure 8-4b,c and d), including continuity of openings across them. The models used for SDM-Site (Follin et al. 2007b) simply assumed f_{op} was constant within a fracture domain, see Figure 8-4a. An alternative would be including size dependence such that $f_{op}(r)$ decreases below some critical size (Le Goc et al. 2018). An example of a model that distributes openings within fractures is the chequerboard type model for Olkiluoto (Hartley et al. 2013a) where a fracture is divided into tessellates and each assigned to open or sealed by a uniform random distribute using f_{op} as a probability, see Figure 8-4b. This was later elaborated to make $f_{op}(r, z)$ a function of size and elevation using the correlation of fracture mineral alteration with trace size seen in mapping of the access tunnel and the increased open fraction inside deformation zones as proxies for openness versus size (Hartley et al. 2018b). Building further realism, one can distribute openings as random binary fields Figure 8-4c, e.g. based on the fractal properties of fracture walls as described in Méheust and Schmittbuhl (2001).

With these models, the sealed part of the DFN is hydraulically inactive and can without any loss of detail be removed from the continuation of the flow analysis. In so doing, the inter-connectivity of the fracture system is likely reduced and potential pathways for flow are restricted with some portion of openings becoming isolated and others become essentially dead-ends (in *3D*, defined as fractures with only one intersection to that part of the network that connects to a boundary, see Figure 8-3). A hydraulic gradient cannot develop across dead-ends for steady flow, so that they only contribute to storage for transient flow and diffusion for transport. Prior to assignment of transmissivities and flow simulation, one can perform a connectivity analysis (Section 8.6) on the system of fracture openings comparing to the frequency of observed inflows in boreholes, providing high-resolution low-detection limit flow measurements are available. Sensitivity analyses on the size distribution of fractures, distribution of openings and parameters governing the persistence of openings can be used as the basis for early rejection of models or conditioning of parameter ranges potentially consistent with flow data. For example, the modelled system should give at least as frequent connections as the frequency of discrete flows, and should commensurate with the frequency of flowing intervals in boreholes (accounting for the detection limit of hydraulic measurements).

Screening hypotheses for the spatial distribution of openings and other uncertain parameters such as size using connectivity analyses, essentially a geometrical analysis, is an efficient first process for model reduction prior to the more computationally expensive process of flow simulation.
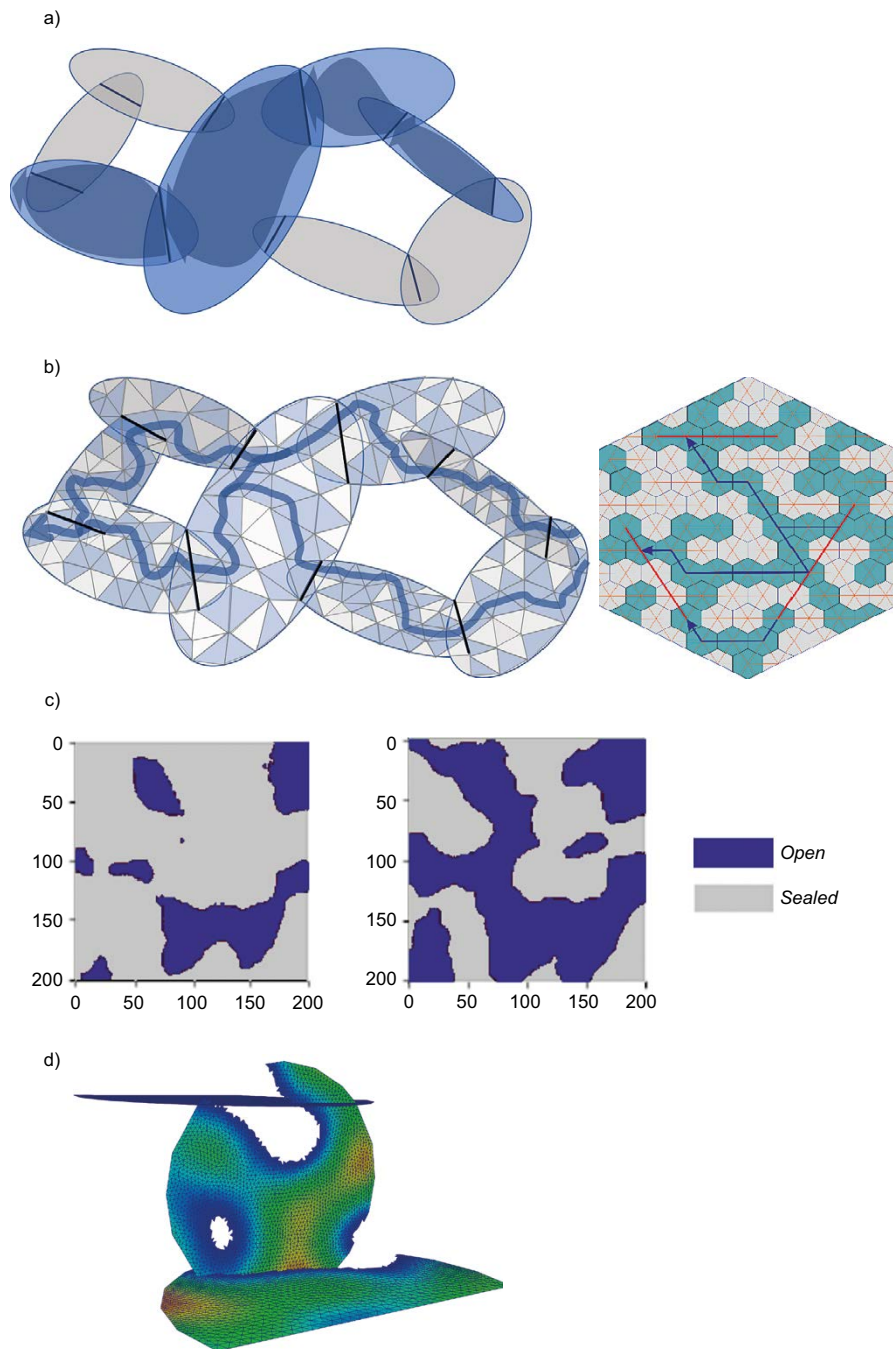
Figure 8-4. *Openings distributed: a) as two sub-sets of fractures (sealed = grey, open = blue) causing diffuse flow in the open fractures; b) as a chequerboard of openings distributed randomly over tessellated fractures (implemented on triangles on the left, or on a hexagonal Voronoi mesh on the right), creating channelised flow as indicated by the arrows. Transverse diffusion into the adjacent areas of poorly connected blue triangles; c) as a binary field of openings distributed over each fracture plane, also leading to channelised flow and stagnant areas; d) Example of the mesh resulting from tessellation of the fracture plane according to open patch (open fraction) and aperture distribution. The holes in the mesh are the sealed part. In the example the characteristic scale of the openness and of the aperture variations are correlated and the mesh size is significantly smaller than the aperture field characteristic size.*

8.4   Spatial distribution of transmissivity and storativity

The frequency of flowing fractures will be controlled by the connectivity of the open fracture system, so that it is usually calibrated first using a sensitivity analysis. Having defined models for distributing openings, the model for how transmissivity is distributed on the openings is next defined for use in hydraulic simulations. For transient simulations, storativity is also required, usually formulated as being correlated with transmissivity.

Before flow simulation, one can guess values for transmissivity and its correlation with size and simply simulate the distribution of specific capacity of fractures intersecting a borehole or set of boreholes based on geometry/connectivity only. The resulting distribution can then be compared to the measured distribution of specific capacities from flow tests as a first rough calibration. The distribution of specific capacities will be beneath this distribution of transmissivities, as flow can be choked by constrictions and low transmissivity bottlenecks in sparse networks, see Figure 8-5.

In crystalline rocks the distribution of transmissivity in a deep borehole can vary over 5–6 orders of magnitude or more, and hence it is important to examine the geological framework for the transmissivity variations in order to identify a site-specific framework for describing them. A consistent pattern between boreholes and sites is that the geometric mean transmissivity decreases with depth (Follin et al. 2007b, Rhén and Hartley 2009, Hartley et al. 2018b). For SDM-Site, depth dependency was described by defining three elevation intervals as $z > -200$ m, -200 m $> z > -400$ m and $z < -400$ m. A simple approach is then to fit a transmissivity distribution to statistics of the data within each elevation region, see Table 8-1. Another common characteristic of the data is that $log(T)$ distribution displays a power-law type distribution (i.e., a triangle tapering at lower values), although there may be a flattening at low transmissivities due to the effects of detection limits measuring small flows. This is coincident with typical distributions of fracture size inferred in the geometrical DFN (see Subsection 6.6.4) as intersected in a borehole, and so correlating transmissivity with size is one way to reproduce the observed flow distribution, and this is consistent with the expected correlation of fracture apertures. Alternatives are to include some statistical variability or just to have a lognormal distribution with large variability, see the examples inferred for the deep bedrock after flow simulation at Forsmark in Table 8-1. As mentioned above, the simulated specific capacity is less than the transmissivity specified for the fracture due to hydraulic choking by the typically sparse network (i.e., the supply of water from the surrounding network is restricted by poor connectivity or lower transmissivity bottlenecks). An example from Forsmark DFN flow simulations is shown in Figure 8-5, see Section 8.9. The simulated specific capacity of individual intersecting fractures, flow-rate (Q) to the hole over drawdown, is generally less than the transmissivity of each fracture and can be significantly less in the most transmissive fractures in sparsely fractured rock at depth because of a poor supply of water from the surrounding network.

Table 8-1. Example empirical models for transmissivity (m$^2 \cdot$s^{-1}) as a function of size as used for fracture domain FFM01/06 below –400 m. From Table 11-20 of Follin et al. (2007b).

Designation	Model	Parameters
Correlated (C)	$log(T) = log(a_T r^b)$	$a_T = 1.8 \times 10^{-10}$
		$b = 1.0$
Semi correlation (SC)	$log(T) = log(a_T r^b) + \sigma_{log(T)} N[0,1]$	$a_T = 5.3 \times 10^{-11}$
		$b = 0.5$
		$\sigma_{log(T)} = 1.0$
Uncorrelated (UC)	$log(T) = \mu_{log(T)} + \sigma_{log(T)} N[0,1]$	$\mu_{log(T)} = -8.8$
		$\sigma_{log(T)} = 1.0$
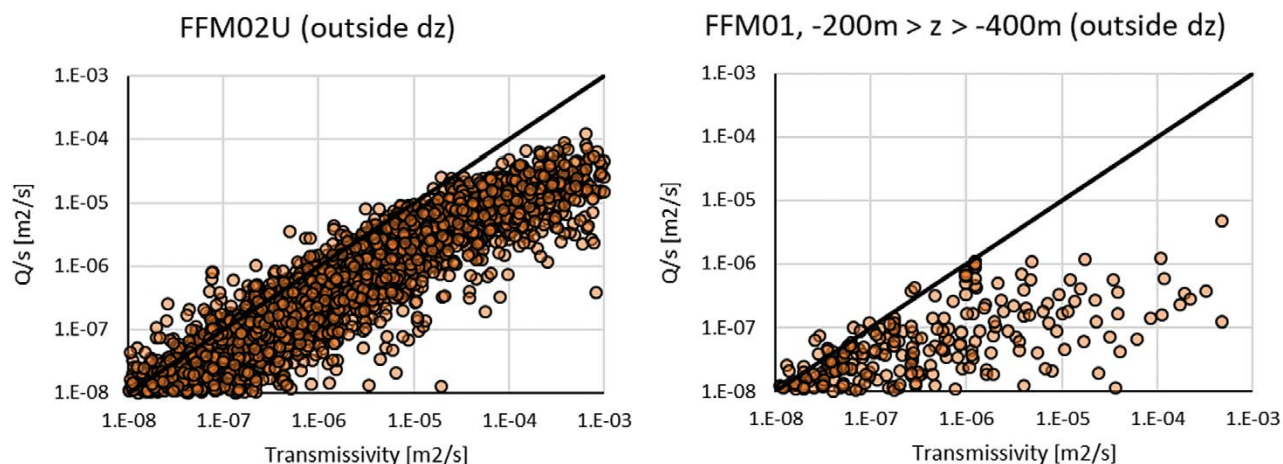
Figure 8-5. *Examples of the effects of hydraulic choking of flow magnitudes by variable connectivity and transmissivity based on DFN flow simulations. The input transmissivity of individual fractures connecting to the borehole is shown on the x-axis, while the simulated specific capacity, flow-rate (Q) from each fracture to the hole divided by drawdown (s), is shown on the y-axis. Left: moderate hydraulic choking in the intensely fracture near-surface bedrock; Right: significant hydraulic choking in the sparsely fractured deep bedrock.*

The limitations of fitting empirical models for transmissivity are that they require large statistical databases to support inference of any trends with respect to depth, orientation, fracture or domain given the large variability, and they don't provide a basis for extrapolating what transmissivities are appropriate to different structural domains or different loading conditions, e.g. due to excavations, dewatering or hydraulic tests, or ice loading.

Mechanistic models relating transmissivity to in situ stress conditions provide a means to predict likely trends with depth, fracture orientation and structural position in case a calibrated *3D* stress model is available. They also provide a means to predict the changes in transmissivity due to local or general changes in mechanical load. Hydromechanical modelling in this way involves an integration of fracture mechanical models from the laboratory scale, characterisation of fracture geometry and morphology distributions from core and tunnel mapping, with confirmatory testing against hydraulic predictions on the field scale. An example of a stepwise process followed by Hartley et al. (2018b) for deriving a hydromechanical model and suitable mathematical models is given in Table 8-2. The basis for the first step is given in Section 6.7 and can be confirmed against tunnel mapping of fracture aperture and sizes. The second step is based on laboratory tests of fracture normal stiffness. The final step involves confirmation of an integrated model against statistics of measured specific capacity, a site model for stress distribution and characterisation of fracture roughness either from detailed scanning of surfaces or statistics or fracture roughness from core and tunnel mapping. In Step 3 it should be noted that the predicted *T* is the geometric mean, and statistical variability can be super-imposed as in Table 8-1. Going from step 2 to 3 assumes that hydromechanical behaviour and properties can be reasonably extrapolated between the laboratory and field scales. Having discrete flow measurements from fractures with different orientations, depths and morphology allow the applicability of this assumption to be confirmed.

A few examples of applications where hydromechanics has been found to be a useful foundation for describing field scale fracture flows include (Mas Ivars 2006, Fransson et al. 2007, Follin and Stigsson 2013, Hartley et al. 2018a, Mattila and Follin 2019) from repository applications (Willis-Richards et al. 1996, Barton et al. 2013, Fang et al. 2015, Ishibashi et al. 2016) from geothermal energy (Tsang et al. 2007) from CO_2 storage (Cappa et al. 2006, Schweisinger et al. 2009) from hydraulic testing, and (Myer 1991, Moos and Barton 2008, Barton and Quadros 2014) from petroleum engineering. These provide some of the inspiration for the example formulations given in Table 8-2.

There are several alternative formulations of hydromechanical relationships that can be used such as that suggested by Liu et al. (2004) which was used in SR-Can thermal-hydromechanical modelling by Hökmark et al. (2006):

$$e_h = e_{hr} + e_{hmax} \exp(-\alpha \sigma_n')$$

<div align="right">Equation (8-4)</div>

Here, e_{hr} is a residual hydraulic aperture e_{hmax} is the hydraulic aperture when the effective normal stress, σ_n', is relaxed and α relates to the fracture normal stiffness. These parameters can be derived either by fitting to laboratory measurements or inferred from trends in fracture transmissivity statistics.

Table 8-2. Summary of hydromechanically based equations used to formulate hydraulic parameters of single fractures in Hartley et al. (2018b).

Parameter equation	Basis for parameter estimate
Step 1: Relating aperture to size (r)	
$e_{m0} = ar^b$	a can be estimated from intact rock elastic properties
	$b \sim 0.5$ expected, and can be estimated from focused mapping underground
Step 2: Relating aperture to normal load	
$e_m = e_r + \left(\dfrac{A}{1 + \dfrac{9\sigma'_n}{B}} \right)$	$e_r \sim 10^{-5}$ m, assumed
	For laboratory tests, A and B are constant deduced from fracture normal loading tests
	For field scale application, A accounts for scale (fracture size) so that $A \equiv e_{m0}$
Step 3: Relating transmissivity to size, load and roughness	
$e_h = e_{hr} + \dfrac{1}{f} \left(\dfrac{ar^b}{1 + \dfrac{9\sigma'_n}{B}} \right)$	$e_{hr} \sim 10^{-6}$ m, assumed low value
	$f \sim 3 - 20$ expected, obtained from characterisation of fracture surfaces in core or tunnel mapping
	$\frac{1}{f}$ is calibrated on measured flow distribution
$T = \dfrac{\rho g}{12\mu} e_h^3$	Choice of b can be confirmed against the shape of distribution of specific capacities from hydraulic tests
	Choice of B can be confirmed against the variation of specific capacity of fractures at different depths and orientations against their modelled normal stress
Step 4: Relating to transport aperture	
$e_t \sim e_m = e_h \cdot f$	f can also be confirmed from in situ tracer or grout injection tests if available

Storativity S can be interpreted in terms of the underlying physical parameters, being the fracture normal stiffness, k_n, compressibility of water, β, and mechanical aperture, e_m, (Doe et al. 1982, Geier et al. 1992):

$$S = \rho g \left(\frac{1}{k_n} + e_m \beta \right)$$

<div align="right">Equation (8-5)</div>

The compressibility of water is about 5×10^{-11} Pa^{-1} (Fine and Millero 1973), mechanical apertures of individual fractures are of order 10^{-3} m, while fracture normal stiffness are of order 10^2–10^3 GPa/m (SKB 2008). Hence, the compressibility of the fracture tends to dominate and implying a storativity around 10^{-8} to 10^{-7} for individual fractures. However, fracture normal stiffness is not a constant; it tends to decrease with increasing fracture aperture and size. One can derive an expected scaling between storativity and transmissivity from the assumed hydromechanical model. For example, using a hyperbolic function for mechanical aperture in step 2 shown in Table 8-2, the fracture normal stiffness becomes:

$$\frac{1}{k_n} = -\frac{\partial e_m}{\partial \sigma_n'} = \frac{9}{AB} \left(\frac{A}{1 + \frac{9\sigma_n'}{B}} \right)^2 \sim \frac{9}{AB} e_m^2$$

<div align="right">Equation (8-6)</div>

implying that storativity scales as the square of mechanical aperture. From the assumed linear scaling of hydraulic aperture with mechanical aperture then it follows that:

$$S \sim (\rho g)^{\frac{1}{3}} \frac{9}{AB} (12\mu)^{\frac{2}{3}} f^2 T^{\frac{2}{3}}$$

<div align="right">Equation (8-7)</div>

The key result being that storativity may be expected to scale as transmissivity to a power 2/3.

Previously, attempts have been made to derive a generic storativity model by pooling transient hydraulic interference test results conducted in several boreholes and sites, and fitting a function of the form:

$$S = a_s T^{b_s}$$

<div align="right">Equation (8-8)</div>

For example, at Simpevarp Rhén et al. (2009) proposed a_s = 0.01, b_s = 0.71. Hjerne et al. (2010) interpreted a_s = 0.0012 and b_s = 0.56 by collating hydraulic tests for several brittle deformation zones at several sites (Äspö, Finnsjön, Studsvik, Stripa, Forsmark and Laxemar) in Sweden, and by combining with tracer test data inferred a near quadratic dependence (exponent 1.8) of storativity on transport aperture (see definition below). Niemi et al. (2000) found a similar square root relation, a_s = 0.001 and b_s = 0.5 worked best for hydraulic tests at the Romuvaara site.

8.5   Flow channelling

Flow channelling expresses the fact that flow within the fractures is likely not homogeneously distributed over the total fracture surface but localised into restricted portions still connected to active hydraulic boundaries. In a fracture system hydraulic boundary conditions are not only defined by rock surfaces (topography, tunnel and borehole walls) but also by the intersections between fractures. The geometry of intersections can influence the distribution of flow channels and stagnant areas within a fracture to a similar degree as the spatial variability of aperture. The experiences from Äspö TRUE block provide excellent practical examples of flow channelling (Poteri et al. 2002, Winberg et al. 2003, 2013).

The total surface of a fracture may therefore be divided into so-called flowing areas (where the flow is significant), stagnant areas (small flows) and sealed/closed portions (with no flow).

8.5.1   Observations

Evidence of flow channelling has been observed in several laboratory and field experiments. A review of experimental observations was already produced by Tsang and Neretnieks (1998). The authors analysed 15 laboratory and field experiments, representative of spatial scales spanning five orders of magnitude, from a few centimetres to one kilometre. All these experiments were characterised by anomalous behaviour (e.g. multi-modal tracer breakthrough curves, water outflow observed in sparse locations, etc) that were directly or indirectly related to underlying channelling mechanisms.

Brown et al. (1998), Watanabe et al. (2009) or Zou et al. (2017) all show the in-plane flow heterogeneity with lab experiments at the cm to ten cm scale. Brown et al. (1998) obtained, at a 12 cm scale, a precise replica of a natural fracture using transparent epoxy resin and injected dye into the water-saturated fracture with steady state fluid flow. The visual analysis of dye concentration shows that dye enters and flows preferentially along the large channel but then diffuses into constricted regions (Figure 8-6), which points out the importance of diffusion into stagnant water regions as a mechanism for radionuclide retention. In a more recent work, Watanabe et al. (2009) performed integrated experimental-numerical analyses on flow through shear (Mode II) fractures and quantified the channels and proportions of contact and noncontact areas (Figure 8-7 left).

An example of how surface roughness affects flow – and transport – across a fracture surface of lateral dimensions 2.5 cm by 2.5 cm is provided by Zou et al. (2017), using a high resolution laser scan of the surface (Figure 8-8 left). The Navier-Stokes equation was solved explicitly and the resulting velocity field (Figure 8-8 right) showed significant heterogeneous patterns, with areas of low velocity localised around asperities and channels of higher velocity zones. Zou et al. (2017) also emphasise a correlation between local roughness (and shear) and dispersion of transport breakthrough curves.
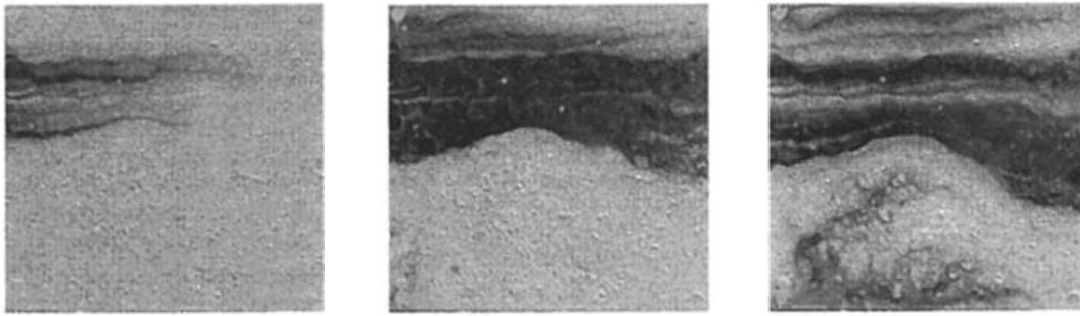
Figure 8-6. *Dye and water entering the replica fracture. Increasing dye concentration is indicated by darker shades of grey relative to clear water (left: after 17 sec; centre: after: 35 sec; right: 71 sec). The fracture has a length of 12 cm and a width, perpendicular to flow, of 7.8 cm. Figure modified from Brown et al. (1998).*
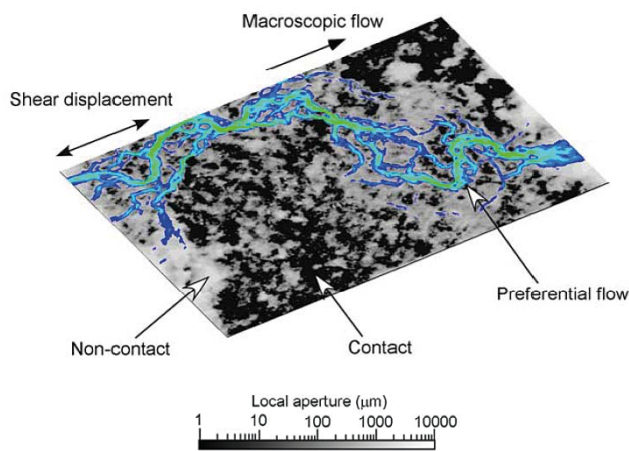
Figure 8-7. *Composite image showing fracture aperture and the development of preferential flow paths from Watanabe et al. (2009) in a core sample of dimensions 95 mm by 150 mm.*
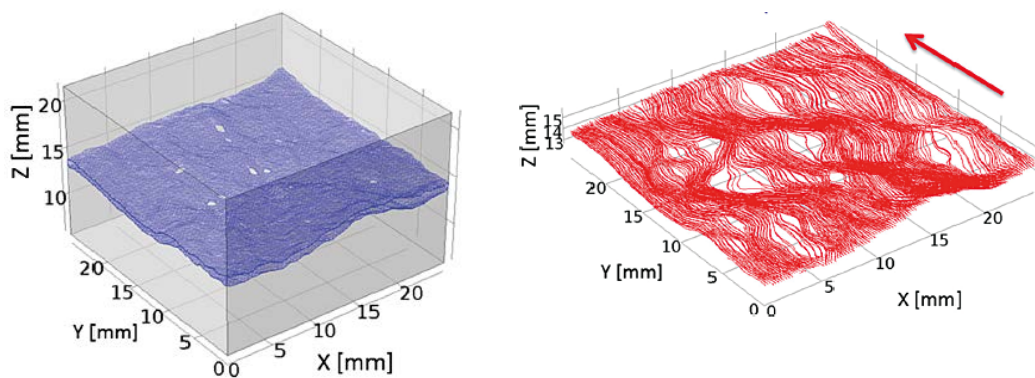
Figure 8-8. *(left) Rough-walled fracture-matrix system and (right) streamlines. White points in the figure on the left indicate asperities where the fracture is completely closed. Figure modified from Zou et al. (2017).*

Hence, if on the scale of a single fracture the effect of in-plane channelling is evident (see also the Stripa 2-D experiment in Abelin et al. (1985)); on the larger scale it is not obvious how to separate effects of intra-fracture (within) from the effect of structural or inter-fracture (between) heterogeneity, illustrated by the cartoon of Figure 8-4 and Figure 8-9.

Hence, flow channelling results from the superposition of fracture in-plane heterogeneity (Figure 8-9a), spatial organisation of the fractured system, as intersections between fractures (Figure 8-9b) and scaling structure, and connection to boundary conditions. The flow channelling indicator as defined in Subsection 8.8.4 is a first step to quantify the flow channelling.

In addition to describing in-plane variability between intersections, one could also consider the possibility of enhanced apertures around intersections forming *1D* conduits flow along the intersections between two fractures (Dershowitz and Klise 2002, Winberg et al. 2003, Einstein and Locsin 2012, Pusch et al. 2014) called "fracture intersection zones" with enhanced aperture. These can arise from greater deformation of the rock around fault and fracture intersections (Peacock et al. 2016). Under extension, intersections may form enlarged openings as pull-aparts along an extensional bend or an extensional step between two faults. The aperture around fracture intersections may be more likely to stay open due to higher strain concentrating around such weaknesses, the surfaces may not mate under compression, or the enhanced connectivity around intersections may result in a higher chance of dissolution of minerals.

Intuitively a "flow channel" refers to the restricted portion of the fracture plane where flow is significant and forms narrow paths (narrow relatively to their length) between an entry and an exit intersection on the fracture plane and linking up with flow channels on other planes either by the persistence of the opening or via fracture intersection zones. This opens the possibility to restricting the hydraulic system description to a network of flow channels, see below. However, when considering transport, this approach would neglect the mixing that takes place with water in stagnant areas due to transverse diffusion into the adjacent areas with non-zero aperture.
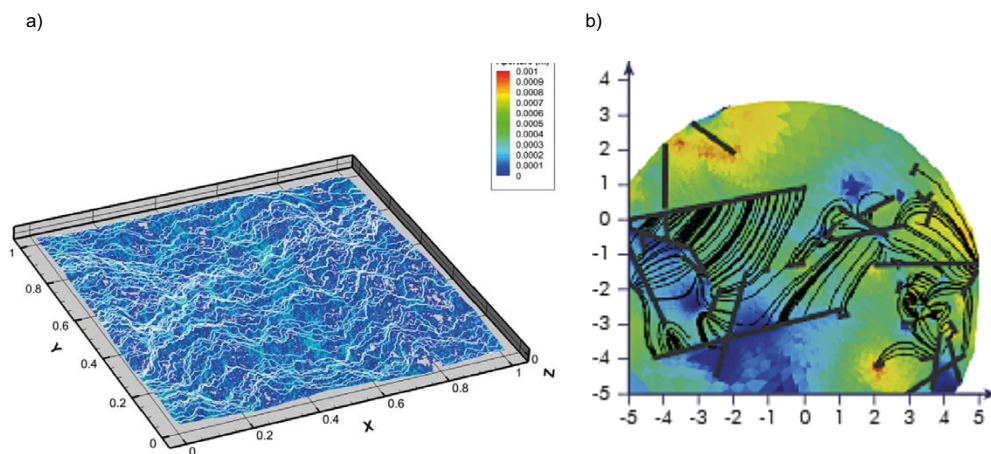
Figure 8-9. *Schematic illustration of flow heterogeneity for a) (Stigsson et al. 2019) single fracture plane with a local distribution of aperture and resulting flow lines (white lines) b) Plan view of the flow field (colours according to flow magnitude) and flow lines on a fracture extracted from a DFN (intersections to the other fractures of the DFN in dark grey) where the transmissivity is constant in the fracture.*

8.5.2 Describing and modelling in-plane variability

At the scale of a single fracture (Figure 8-9), local variations of transmissivity result from local variations of morphology and stress (Table 8-2). It is beyond the scope of the present chapter to resolve how hydromechanical coupled processes lead to observed in-plane variability of mechanical and hydraulic aperture. These questions are addressed in **RMMM**. We review below how models of local hydraulic aperture (or transmissivity) distributions can be used to model in-plane heterogeneity.

A common way to model fracture in-plane variability is to initially describe aperture (as the distance between the rough walls of a fracture) as a continuous field (Figure 8-8 and Figure 8-9) represented on a high resolution mesh (e.g. Makedonska et al. 2016, Frampton et al. 2017, Bym et al. 2018), see also Section 6.7. With this type of model, it can be argued that resulting flow channel widths should be of the scale of the correlation length of the underlying continuous random field. If the latter can be related to true properties of the fracture, e.g. scale of roughness or displacement of the opposite wall, one can argue that the width of the flow channels are likely comparable to this scale. In practice this can be in the range from centimetres to several metres.

Returning to the schematic illustrations of flow distributions shown in Figure 8-4, in sketch a) the channels are assumed to be of the scale of the fractures themselves. Sketch b) is appropriate when the primary cause of channel is perceived to be due to the prevalence of null or closed apertures, so that the above-mentioned continuous correlated random fields can be represented on a coarser resolution scale, so that their complexity is reduced to simplified Boolean description on tessellates within each fracture. In the simplest model a uniform distribution can be used to generate a so-called "chequerboard" model, see illustration in Figure 8-4b. Use of this type of approach has been explored for Olkiluoto (Hartley et al. 2018b). Channel widths are then of the scale of the tessellates, metres to tens of metres. In this case, flow is focused in the open tessellates with the greatest connectivity to other open tessellates, but in-plane diffusive exchange takes place with less connected open areas, but not in sealed or isolated openings.

Two other concepts for flow distribution arising from in-plane variability come to mind as sketched in Figure 8-10. The first, Figure 8-10a, is where transmissivity is represented on a fine-scale and flow channelling is calculated explicitly. The second, Figure 8-10b, is where the flow channels are replaced with a set of pipes (*1D* objects) whose number, widths and conductance are postulated, perhaps based on detailed simulation or some empirical evidence. Channel widths are assumed from centimetres to tens of metres. For illustration purposes the pipe geometry itself can be postulated as a sparse subset of connections between a regular lattice of nodes (e.g. Black et al. 2007). For more structural consistency, the channels can be postulated within the geometric DFN model (e.g. Cacas et al. 1990, Figueiredo et al. 2016, Dessirier et al. 2018).
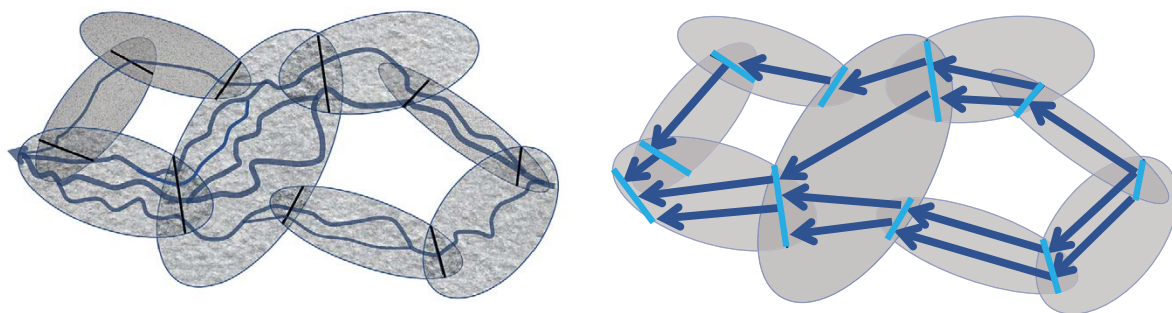
Figure 8-10. *a) Schematic of a small connected fracture network where the variability in transmissivity of all fractures is generated as a spatial process on a fine grid on each fracture. The fracture intersections shown as black lines. The arrows indicate channels where advective flows are most concentrated. b) model simplification based on a), where narrow channels (blue) are postulated between fracture intersections with additional channels along fracture intersection to connect these.*

It is however a significant simplification to reduce the DFN flow structure to narrow channels. One is essentially choosing some threshold on flow-rate to isolate the dominant flow paths and derive channel widths under a particular hydraulic gradient, which may not describe the connectivity of the flow conditions under different hydraulic boundary conditions. A particular challenge is how to capture the channels around a pumped borehole when attempting to calibrate a model to hydraulic test data in a way that is conceptually consistent with a sparse channel network, because by definition, a borehole is unlikely to intersect a channel. It also excludes important transport processes, namely the potentially significant lateral diffusion of solutes into areas of lower aperture, which makes the effective channel width far larger if advective flow rates are low (Neretnieks 2006).

The selection of the fracture in-plane heterogeneity model, ranging from a *2D* high-resolution tessellation to a simplified *1D* channel network, with each channel having an equivalent conductance, can offer distinct alternatives to describing hydraulic and transport properties appropriate to representing in-plane heterogeneity and the consequent channelling of flow and transport processes. However, if one starts with a mechanistic and detailed description of how fracture surface and aperture properties vary in single fractures, then these methods are in fact progressively more simplified numerical implementations of the same concept, and differences in results are as much artefacts of these simplifications than stemming from fundamental conceptual uncertainty. Nonetheless, the degree and nature of aperture variability on relevant scales is hard to measure, and so alternative models and sensitivity analyses provide a means to better understand what hydraulic data is telling us about the system and what consequences the uncertainties have for predictive modelling.

8.6 DFN connectivity

A necessary condition for having flow when the matrix is impervious is to have at least one connected fracture path between boundaries. Predicting, evaluating and characterising the connectivity structure of a DFN model provides the first, but essential, step towards a DFN flow model. The connectivity of a DFN model can be compared to in situ hydraulic data and combined to the metrics defined in Subsection 8.8.4 for calibration purposes. A sound understanding of DFN model connectivity structure is also essential for addressing the model parameter reduction (see Chapter 10) stage of the DFN modelling workflow.

Characterising the connectivity properties of a DFN relies on identifying intersections between fractures and then clusters of connected fractures and percolating cluster(s). If there is a path connected to the system boundaries, the DFN is percolating. The probability for a system to percolate, e.g. the percolation probability, was found to be determined by a dimensionless number, the percolation parameter, p, which is defined from the fracture size, shape and orientation density functions (Bour and Davy 1998, de Dreuzy et al. 2000). When the percolation parameter of a network is above the percolation threshold, which is a given dimensionless number, the network statistically percolates; below it, it is disconnected.

Thus, the percolation parameter is a robust statistical indicator of connectivity that can be calculated from the statistical properties of networks. Moreover, according to percolation theory (Stauffer and Aharony 1992), the percolation parameter informs on the connectivity structure: the size of the largest cluster in the unconnected network, or the size of the largest unconnected volume for connected networks. Percolation theory was originally developed for objects of constant size (Berkowitz and Balberg 1993), see Figure 8-11a, and it has been extended to fracture networks with a wide range of sizes (Bour and Davy 1998, de Dreuzy et al. 2000) and to fractures of mixed shapes (Barker 2018). In the specific case of a power-law fracture size density distribution (Equation (6-2)), the percolation parameter is scale dependent for exponents $k_r \leq 3$, (see Equation (6-22)) meaning that the connectivity increases with the size of the target system (Figure 8-11b). For this case, the percolation threshold is a scale, which corresponds to the largest unconnected block in the system (Bour and Davy 1997).
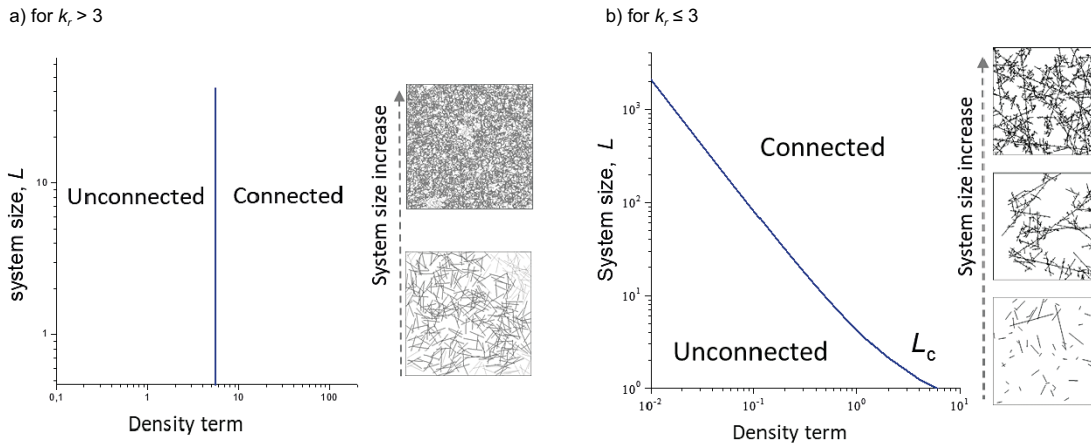
Figure 8-11. *Illustration of DFN connectivity state dependency with system size, modified from Bour and Davy (1997). Connected and unconnected domain limits are delineated by the solid blue lines. a) The DFN connectivity state is scale independent, as for DFN power-law models with $k_r > 3$, and b) the connectivity is scale dependent, as for DFN power-law models with $k_r \leq 3$. Is this case the percolation parameter increases when increasing the system size. The solid blue line symbolizes the critical size scale L_C at which the percolation threshold is reached. The illustrative DFN slice views on the right of each plot illustrate the unchanged connectivity state for case a) and the increasing connectivity with system size for case b). The dashed grey lines on the right of each plot symbolizes the increase of the system size.*
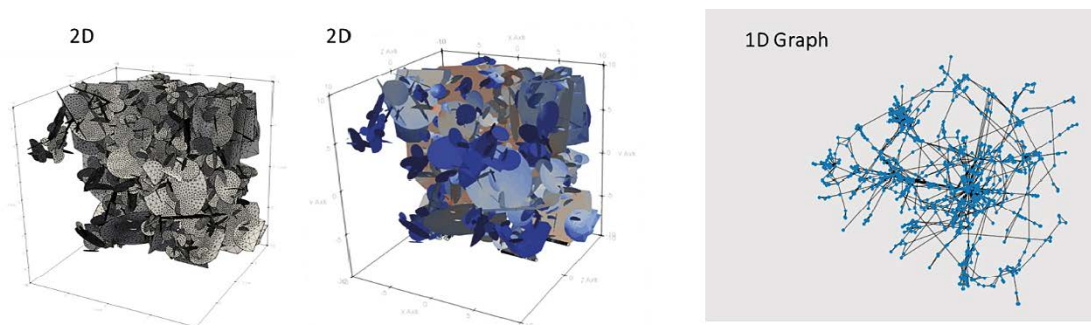
Figure 8-12. *DFN flow modelling approaches. DFN in a 3D volume, built 2D fractures in a) and b); with meshed fractures in a) and head field in b). c) Schematic graph structure computed from the same DFN, where fractures are represented as nodes and intersections between fractures as link (or pipes).*

In systems with a sparse flow distribution, such as Forsmark, the sparsity of flow apparent on different scales provides characteristics against which models can be rejected or uncertain parameters can be conditioned based on hydraulic data. Those characteristics include the:

- intensity of flows seen in discrete flow measurements in borehole sections,

- frequencies of packed-off intervals providing measurable transient flow,

- fractions of monitoring intervals that respond in hydraulic cross-hole tests, and

- presence of finite boundaries, i.e., flow compartments and non-percolating clusters.

In the first case the relevant percolation length scale is distance between the borehole and a known source of water, e.g. the surface or a deformation zone; in the second, it is the interval scale; and in third it is the distance between the pumped and monitoring holes. Together such data can provide connectivity characteristics on different scales. Understanding the scaling of connectivity for different models and its sensitivity to uncertain parameters is therefore a useful tool to narrow the range of possible models consistent with flow measurements. For example, the intensity-size scaling model can first be tested, followed by the model for the spatial distribution of openings.

A more elaborate version of connectivity analysis is to perform a complete topological analysis of the connectivity structure. A graph analysis of the network with nodes (either fracture or intersection) and links allows for analysing details of the connectivity and is one method to construct an equivalent network of *1D* pipes, see Subsection 8.5.2, as a numerically efficient way to estimate flow. The network topology, basically the distributions of fracture interconnections in the system, provides additional metrics of connectivity, e.g. robustness (Viswanathan et al. 2018)) or assortativity. Assortativity is a graph metric, for the nodes of a network, of their degree of connectivity to nodes of similar connectivity level (Andresen et al. 2013). Hope et al. (2015) shows that genetic and Poissonian DFN have distinct assortativity ratios (nodes to links ratio).

8.7 Sources of supporting site hydraulic data

The projected primary data on hydraulic properties of the bedrock at Forsmark comes from the fracture transmissivity measurements from difference flow logging in most surface-drilled boreholes and pilot holes to be drilled ahead of construction of the access ramp, central area, and deposition areas. These are augmented by double-packer injection tests within intervals chosen to isolate and characterise the main hydraulic structures encountered in each hole. In the surfaced-based investigations injection tests were made sequentially on 100 m, 20 m and 5 m intervals, homing in on the most conductive intervals. For the underground operational programmes, injection tests will focus on sections identified by the preceding difference flow logging, i.e., employing section lengths optimised to the width of the structures to be tested. Comparative measurements of flow logging versus injection tests exist from the surface-based site investigations (Follin et al. 2007b).

Impeller logging is also used to identify major flowing zones in the shallow holes, including HFM holes and KFM13–23. As well as these single-hole tests, interference tests have been performed in HFM14, HFM33 and KFM24. Such tests have sometimes been used as a precursor to flow difference logging.

By optimising these tests, the statistical and spatial distributions of flow (specific capacity) of individual fractures can be characterised. Characterisation of network properties around deposition holes and tunnels would also benefit from hydraulic interference tests or the monitoring of disturbances from drilling and construction. These can provide a form of hydraulic tomography (Ludvigson and Hjerne 2014) to reveal in part the spatial architecture of the hydraulic fracture system. These would also provide additional metrics for model selection/calibration on the connectivity of the network on an intra-tunnel (tens of metres) scale, the anisotropy of this connectivity, and the storativity of the network.

There are additional interference tests available from SFR. Once construction of the accesses begins, hydraulic disturbances detected in monitoring holes and intervals, alongside measurements of inflows to the underground openings (including pilot boreholes), are expected to provide insight into facility-scale hydraulic connectivity and characteristics. Finally, there are groundwater head, electrical conductivity and groundwater hydrogeochemical sample data from the deep boreholes. The data sources for these observations and studies are presented briefly in the following subsections, see **HGMM** for more details.

8.7.1 Single-hole flow log measurements

The main database for fracture-specific hydraulic properties contains the specific capacities of individual fractures (commonly referred to as PFL transmissivities and named PFL-f) measured with the difference flow logging tool (Öhberg and Rouhiainen 2000). Modelled transmissivities (and other fracture parameters such as size) are calibrated through flow simulation against the measured distribution of specific capacities to account for network and heterogeneity effects, rather than being directly parameterised on the measurements.

Techniques for performing flow logging of discrete fractures near horizontal probe and pilot holes drilled from the tunnel face have also been developed (Pekkanen 2009, Pekkanen and Hurmerinta 2013). Recently, greater control of the pressure changes in the hole during the test has been achieved with the use of a sealing mechanism (Pekkanen 2019), reducing uncertainties in the specific capacity of each fracture logged.

Specific capacities are measured with the PFL tool by guiding the water through an isolated borehole section past a flow sensor, while moving the section continuously along the borehole isolating the top and bottom of the borehole section by means of rubber disks. Transmissivity is determined by the Thiem equation, Equation (8-9). The whole borehole is pumped over several days with limited disturbance by the tool by means of a by-pass tube through the isolated section, see Figure 8-13. The tool also includes fine-scale measurements of single point resistivity (PFL-SPR) that are used to identify the depths of electrically-conductive features likely associated with the flow measurements to increase the precision in the location of flows to about ± 0.1 m. The linking of measured specific capacities to the geological fractures based on the integration of detailed geological borehole mapping is described in Forsman et al. (2004), Forssman et al. (2006, 2008) and Teurneau et al. (2008). The detection limit of the PFL-f method varies depending on the *in situ* conditions and on the way the PFL measurement device is operated (Öhberg and Rouhiainen 2000, Ludvigson et al. 2002, Öhberg 2006, Aalto et al. 2019). As a rule of thumb, the lower detection limit of the flow meter device used is approximately 30 mL/h (8.3×10^{-9} m³/s). The upper detection limit is 300 L/h (8.3×10^{-5} m³/s). Typically, a drawdown of 5–10 m is used in surface-drilled holes, implying a range of measured transmissivities from about 10^{-9} to 10^{-5} m²/s, although the observed lower detection limit can be as high as 10^{-8} m²/s in some borehole sections. The drawdown can be significantly larger in underground pilot holes, providing increased sensitivity to lower transmissivity fractures, typically a minimum of about $3–10 \times 10^{-11}$ m²/s (see e.g. Komulainen and Pöllänen 2016, Tammisto et al. 2019). In total, 889 discrete flow measurements by the difference flow method are available covering 16 surface boreholes KFM01A–KFM11A and KFM24, as well as 663 discrete measurements in 8 KFR holes at SFR.

The linking of PFL-f measurements to individual fractures provides the basis for analysing the relationship between flow and other fracture properties, such as orientation (and hence anisotropy with differential stress), morphology, alteration and mineralogy. Such analyses in turn provide the means to conceptualise Mechanical-Hydraulic-Retention relationships, see Subsection 6.7.2.

The PFL tool can also be used to provide 5 m sequential transmissivity measurements using the PFL-s method. That provides 1 469 measurements in the same KFM holes, giving 7 345 m of measured intervals in total for Forsmark; there is 1 530 m of measurements for SFR holes. This continuous data can be used to analyse scaling relationship for hydrogeological properties, e.g. statistics for how many 5 m intervals have transmissivity above a certain value, and by amalgamating adjacent intervals, forming transmissivity distributions on 5 m, 20 m and 100 m, for example.
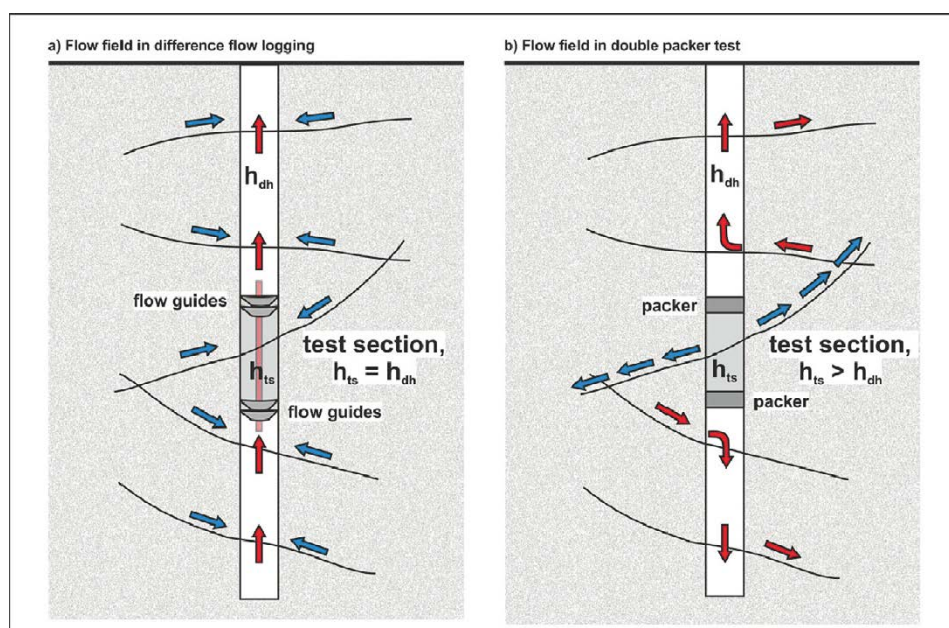

Figure 8-13. *Flow field around the borehole and the test section in a) flow logging and b) PSS tool using a double-packer to isolate the test section. Source: Posiva, Aalto et al. (2019).*

8.7.2 Single-hole injection tests

The description of hydraulic testing and how they are used given here is largely a retrospective account of how they have been integrated in DFN modelling during the surface-based investigations. Some remarks as to how the approach is expected to be adapted for underground investigation are included though.

The pipe-string system (PSS) works by injecting water at constant overpressure from a double-packer drillhole interval into the bedrock (e.g. Ludvigson et al. 2004). The injection stage of a PSS test normally lasts 20 mins and the fall-off stage 10 mins. The estimation of PSS transmissivity is based on the Moye-interpretation (Moye 1967) using the shut-in rate, i.e., the rate at the end of injection time. Moye is essentially the same as Thiem with different assumptions about constant-head boundary and flow geometry to which the results have limited sensitivity. For the PSS method, the accuracy of the flow rate measurements depends on the actual flow rate. As a rule of thumb, the lower detection limit of the PSS flow meter device used is approximately 60 mL/h (1.7×10^{-8} m^3/s), defining the measurement limit for flow. The upper limit for pumping is about 40 L/min. First the tests employing 100 m test sections were performed. For 100 m test-sections showing flow rates above the measurement limit for the flow, tests with 20 m test sections were performed. Subsequently, the tests with a test section length of 5 m were performed for those 20 m test sections showing flow rates above the measurement limit for flow. For a typical injection pressure corresponding to 20 m head, the detection limit means transmissivities of borehole sections above approximately $7 \times 10^{-10}/9 \times 10^{-10}/1 \times 10^{-9}$ m^2/s are observed for test scales 5/20/100 m, respectively. Due to the short duration of this type of test, a transmissivity may also be interpreted for isolated fractures, or isolated clusters of fractures, connected to the test section that would not be expected to yield a value for the longer duration PFL tests. Hence, it is important to note that the PSS method may yield an apparent higher number of borehole sections with flow.

The PSS method has been used to identify the main water conducting intervals in HFM11–HFM13 (5 measurements in total), and in 18 cored holes KFM01A–KFM12A, giving 6 000 m of tests in total at Forsmark, with an additional 4 KFR holes at SFR. As for PFL-s data, PSS can be used to analyse scaling relationship for hydrogeological properties.

Aggregated PFL-f transmissivities over the same intervals as isolated by PSS typically give consistent values above transmissivity of 10^{-8} m^2/s, but PSS suggests more flowing intervals of low transmissivity than PFL. Quantifying the cumulative distributions of the number of 5 m interval transmissivity above different magnitudes provides insight into this issue (see Table 4-4 and Figure 4-19 of Follin et al. (2007b)). The distributions were very similar for values $> 10^{-8}$ m^2/s. PFL-f tests indicated 8.1 % of 5 m intervals had transmissivities $> 10^{-8}$ m^2/s against 9.6 % for PSS; 11 % versus 17 % $> 10^{-9}$ m^2/s; and, 14 % versus 20 % above the respective detection limits. It is not clear which method best reflects actual flow conditions around and below 10^{-9} m^2/s; however, the two methods provide consistent indication that only a small minority, 11–17 % of 5 m borehole intervals conduct flow above 10^{-9} m^2/s.

It should be noted that the hydraulic tests performed in the surface-based investigations are performed in steeply dipping boreholes with propensity for intersecting sub-horizontal fracturing, making it necessary to estimate intensity of sub-vertical water conducting fractures by bias correction techniques. Such techniques can only partially compensate for the drilling bias. Performing hydraulic tests for substantial lengths of pilot holes drilled for the access ramp is therefore essential for a balanced characterisation to properly appraise the flow distribution between sub-vertical and sub-horizontal fractures, the anisotropy of the hydraulic system and directional circulation of flow.

Furthermore, while hydraulic testing in underground sub-horizontal pilot holes will give an improved characterisation of fracture hydraulics at repository depth, it will be biased towards sub-vertical fractures. However, flows surrounding deposition holes will be most affected by flows in sub-horizontal fractures. Hence, there is also a need to perform hydraulic test in vertical holes, so as to assess both parts of the flow system at depth. In practice this means performing detailed injection tests of flow logging in probe holes drilled ahead of the shafts or in the pilot holes for deposition holes.

8.7.3 Impeller logging and near-surface testing

The hydraulic data in percussion boreholes are referred to as HTHB data, which is a combination of borehole-scale pumping tests and impeller flow-logging, which typically registers the largest 2–3 bore-hole inflows. The latter is reported to have a detection limit on the order 10^{-7} to 10^{-6} m²/s. It measures cumulative flow, and therefore it may be expected that the practical detection limit depends on the inflow at depth. Owing to its high detection limit, HTHB data do not provide detailed information on the flowing fracture network. However, it provides auxiliary information on identified large transmissivities. 26 HFM holes with 3 770 m of hole length have been measured in this way, and 12 KFM holes with 887 m of measurement. The individual high flow intervals range from c 1–10 m, of which there are 169 in total.

Impeller logging is limited to shallow depth c 200 m. It can be used to identify the most transmissive zones in the shallow bedrock. Usually there are several open fractures within the logged interval and so it is ambiguous which individual or combination of fracture is responsible for the flow. Sonic log indications of low p-velocity may provide some narrowing of candidates. The orientations of fractures most likely giving rise to the flow can be interpreted and used to identify the elevation and orientation of highly transmissive sheet joint in the upper bedrock, for example.

In 2018, focused hydraulic characterisation of the near-surface bedrock was made in the access area with PFL testing in the core drilled holes KFM14, KFM15, KFM16, KFM20, KFM21, KFM22 and KFM23 (Komulainen et al. 2019). This allowed the distribution of discrete transmissivities and its structural context to be inferred, and in particular, the role that sheet joints play in the near surface hydrogeology. Interference tests were also performed in this area (Föhlinger et al. 2020). The interpretations made from these new holes and tests formed the basis for an exploratory update of the DFN description of the upper 200 m of bedrock (Hartley et al. 2020). It remains to fully integrate the learnings from that exercise with the wider and deeper site model.

8.7.4 Interference tests and hydraulic disturbance data

The single-hole tests described above characterise individual parts of the hydrogeological system according to their structural domain: deformation zones, the intervening fracture domains and the near-surface fracture system, typically measuring flows on the scale of individual fractures or small networks over some tens of metres. Hydraulic interferences observed in pilot holes for deposition areas (main, transport and deposition tunnels) will characterise small networks over scales of some tens or hundreds of metres. Monitoring of responses to hydraulic disturbances created by drilling or construction will characterise the overall system on scales of hundreds of metres or more.

To date, long-term interference tests have been performed in HFM14 (Gokall-Norman and Ludvigson 2008a), HFM33 (Gokall-Norman and Ludvigson 2008b) and KFM24 (Harrström et al. 2018). Several smaller interference tests have been performed, e.g. (Gokall-Norman et al. 2004, 2005a, b, 2006 Gokall-Norman and Ludvigson 2005, Föhlinger et al. 2020). These are usually run as a constant rate test with pressure monitoring in several holes, and so the rate and duration of pumping is needed. The spatial distribution of pressure drawdowns and the time at which the pressure drawdowns occur and stabilise can be used to infer transmissivity, storativity and the hydraulic connectivity of the system. Spatial heterogeneity in the levels and times of responses are of interest as indications of anisotropy or sparsity of connections, including intervals that do not respond. Precipitation (rain) events can attenuate drawdowns, and so meteorological data are an important input to simulating interference tests.

As indicated in Figure 3-2, interference tests (Datasets DS2) are used in a second stage (Step BS5) of hydraulic calibration. They are the only means of determining hydraulic diffusivity and infer relations between storativity and transmissivity. Often, they are dominated by the connectivity and of fracturing within and around deformation zones, as well as connectivity to surface recharge via sub-vertical defor-mation zones and near-surface fracturing. Nonetheless, the hydraulic connectivity of the background fracture network can also be constrained to some extent on this sort of test, as it can contribute to the attenuation of hydraulic drawdowns over long distances. For significant drawdowns to be transmitted laterally over several hundred metres, the system must on the one hand have high diffusivity, and on the other, poor connections to a source of water, e.g. at the surface.

Drainage water into underground facilities can also be used as a type of large-scale interference test, dataset DS4 in Figure 3-2 both to confirm/calibrate the integrated DFN (Step BS5) and in confirming ECPM models (Step BS8). As well as measuring drawdowns, it is essential that operational records be kept of drainage water inflows into water-rings and weirs, construction progress, meteorology and pressure monitoring in borehole intervals. This is so that causes (inflows) and effects (drawdowns) can be visualised and correlated, particularly whether the deformation zone model, deterministic or semi-stochastic, provides the observed hydraulic connections or lack thereof. Of particular interest are transient responses seen following the breakthrough of construction through deformation zones to understand their connectivity. Such measurements were found to be very useful in understanding structural connections at Olkiluoto (Hartley et al. 2018b). Follin (2008) reports the abstraction of drainage water at SFR causes significant drawdowns in HFM34 and HFM35 located 500 m away, and also the nearby KFM11A, including at depth. For planning purposes, it is expected that drilling and excavation records, measured inflows to discrete chainages and pressure monitoring in surface-drilled holes would be used on completion of the repository accesses to check the performance of the structural model in describing hydraulic connections and to validate and iterate the DFN model.

Tunnel-scale single-hole transient and interference tests are also expected to be performed between closely spaced pilot holes, first in the central access area at repository depth, and later between deposition tunnel pilot holes. These will provide data to validate the hydraulic connectivity of individual large fractures (10s-100 m) and small networks, their heterogeneity and anisotropy in the background rock outside of deformation zones at repository depth.

8.7.5 Hydrogeochemical data

Groundwater samples of shallow and deep groundwaters have been collected at Forsmark (Laaksoharju et al. 2008). This baseline groundwater data provides the basis for integrated interpretations of the circulation of different water types that have resulted from changes in the climate, changes in surface water chemistry and water-rock interactions. The main groundwater transitions indicating dynamic changes are from Littorina Sea Water to Deep Saline Water at depth that can be differentiated by Br/Cl ratios, and from Present-day Meteoric Water to Littorina Sea Water shown by HCO_3 at moderate depths. The depths of such transitions in different deformation zones can be used as markers for the relative rate of mixing and the hydraulic significance of the zones. Thereby, providing indicators of depth related fracture domains, the vertical connectivity of fracture systems and the importance of increasing stress with depth. As shown in Figure 3-2, simulations of palaeohydrogeology (Dataset DS5), including the evolution of surface and groundwater chemistry, can be used as a confirmatory test of the integrated bedrock description either using a DFN model (Step BS5) or an ECPM model (Step BS8). To date upscaled ECPM models have been used for this step because it involves simulations over long timescales and large volumes with complex boundary conditions and rock matrix diffusion. The use of hydrogeochemical data is further covered in the Hydrogeological and Transport Modelling Methodologies.

8.8 Data interpretations

8.8.1 Transmissivity distribution from high resolution flow logging

For interpretation of field measurements, such as the PFL tests, a transmissivity of each flowing interval is usually reported. The interpretations are made under assumed steady-state radial constant density flow around a borehole intersecting with a fracture, then transmissivity can be estimated by Thiem's Equation (Thiem 1906) as:

$$T = \frac{Q_w}{2\pi\Delta h} \ln\left(\frac{R}{r_w}\right),$$

Equation (8-9)

where Q_w is the flow-rate injected/abstracted, r_w is the radius of the borehole, Δh is the head difference between the heads at the borehole radius and a radius of influence, R. This assumes that a constant transmissivity plane extends over a distance R. Under steady-state conditions, i.e., long duration pumping, the interpreted values of transmissivity should not be viewed as necessarily the transmissivity of individual fractures, or the transmissivity of the fracture local to the borehole intersect. They are more indicative of the effective transmissivity of the adjacent network over a larger scale.

An appropriate choice for the radius of influence should be the distance to a position beyond which the pump test has limited effect, which in practice should correspond to the distance to fractures having significantly higher transmissivities. A constant-head boundary is assumed to occur, otherwise a steady flow will never be reached. Fractures that are much more transmissive than the one intersecting the borehole may serve as a constant-head boundary, but if such a fracture is not intersected, then the "choking" effects of the network will prevent steady conditions. At Forsmark the spacing of higher transmissivity fractures is on the order of several tens to hundreds of metres (Follin et al. 2007b). This formula has been used to interpret the PFL tests, which being performed after several days of pumping are assumed to result in steady-state conditions. Values used in the formula are: r_w is 0.038m and R/r_w is assumed to be 500, or $R \sim 19$ m (e.g. Väisäsvaara et al. 2006), and in so doing the interpreted transmissivity is close to the specific capacity of the fracture $T \approx \frac{Q_w}{\Delta h}$. Because of the logarithmic form, the results are only slightly sensitive to the choice of radius of influence – if R increased to 100 m, T only increases by 25 %. There is therefore a distinction between the measured specific capacity $Q_w/\Delta h$ (often reported as transmissivity) and the model transmissivity of individual fractures.

8.8.2 Transient flow tests

Transient single-hole tests and interference tests can provide additional information beyond the hydraulic characterisation derived from flow logging. This includes quantification of flow dimension, heterogeneity, channelling and storativity.

In surface based investigations, tests between packers, PSS tests, have been performed with constant-head injection tests typically run with three different test section lengths, 100 m, 20 m and 5 m. The length of the injection period of the 5 m tests is 20 minutes, which means that the state of flow during constant-head injection is likely to be more transient than that during difference flow logging. Ludvigson and Hansson (2007) present the standard interpretation procedure used for interpretation of test interval transmissivity, based on Theis' classic theory for transient radial flow to well in an infinite two-dimensional, homogeneous porous medium (Theis 1935). Separate transient evaluations are made of the injection and recovery periods of each test. Interpretation of the transient tests can estimate the transmissivity averaged over the fracture affected by the test, essentially measuring how the effective transmissivity changes over distance as the test proceeds. In contrast, steady-state and PFL measure the transmissivity local to the borehole. Hence, interpretation of transient tests can yield higher transmissivities than steady-state where fractures are heterogeneous. Transient tests can also detect finite compartments, i.e., more intensity of flowing intervals than seen by PFL. The measurement of flow over different interval lengths provides a scaling relationship for bulk flows which emerges from the underlying spatial arrangement of flow in the fracture network.

Additional transient single-hole tests (Subsection 8.7.1 and 8.7.2) and interference tests (Subsection 8.7.4) will be essential during the underground investigations in order to characterise flow dimension, heterogeneity, channelling (Section 8.5) and storativity (Section 8.4) at the target depth. They are all properties resulting from the spatial arrangement of flow within the fracture system and have significant bearing on the prediction of post-closure flow and transport. Alternative models and structural interpretations can also be tested against such data to build confidence in or reject models.

Diagnostic analysis during the injection period is mainly performed from log-log plots of the inverse of the flow rate for a constant drawdown (*dh/Q*) together with the corresponding semi-log derivative plot. For the recovery period, an equivalent analysis is made on pressure and its derivative, see Figure 8-14. Analysis of flow regimes during the test is performed, e.g. wellbore storage (WBS), pseudo-linear flow (PLF), pseudo-radial flow (PRF) and pseudo-spherical flow regime (PSF), respectively. During some tests, transitions between different flow regimes occur. In addition, indications of outer boundary conditions, i.e., apparent no-flow boundaries (NFB) or constant-head boundaries (CHB), during the tests are identified. In constant-head tests, effects of wellbore storage are assumed to be negligible during the injection period since pressure is constant. Flow regimes may be described in terms of a generalised radius of influence from the borehole:

- Inner zone (iz). Representing very early response which reflects the hydraulic interaction between the borehole and rock close to the borehole. It may be deteriorated by turbulent head losses or other head losses (drilling debris) or improved by fractures intersecting the borehole. The hydraulic properties of the inner zone are generally expressed in terms of skin factor and WBS (for the recovery period). Skin can arise due to local heterogeneity around the hole. No fracture has uniform transmissivity, and one is likely to drill a borehole into a portion of the fracture that has lower transmissivity than the effective average (geometric mean).

- Middle zone (mz). Representing the first response from which it is considered possible to evaluate representative hydraulic properties of the fracture near the borehole, in the time span from t_1 to t_2.

- Outer zone (oz). Representing the response of fracture network/boundary conditions connected to the actual fracture interpreted from the middle zone, at times later than t_2. Sometimes it is possible to deduce the possible character of the network or boundary and sometimes possible to evaluate the hydraulic properties or boundary conditions.

In particular, time intervals with pseudo-radial flow, reflected by a constant (horizontal) derivative in log-log diagrams, are identified. Pseudo-linear flow, indicating flow in a single confined hydraulic channel, is reflected by a straight line of slope 0.5 (1:2) or less at the beginning of the test, both for the inversed flow rate and its derivative. In many cases, pseudo-linear flow is transitioning to pseudo-radial during the test, see Figure 8-14, implying a growing connect area or array of channels within a fracture plane. A true spherical flow regime (*3D*), indicating an array of inter-connected channels within a network of fractures, is reflected by a straight line with a slope of –0.5 for the derivative. Steeper slopes of the derivative may indicate transitions to pseudo-spherical (leaky) or ultimately, pseudo-stationary flow caused by apparent constant-head boundaries, reflected by almost steady-state conditions with a rapidly decreasing derivative. Pseudo-spherical flow, as defined here, may be conceptually interpreted in several ways, for example an increasing cross- sectional flow area with distance away from the borehole (e.g. flow in a thick, well-connected fracture zone), or an increasing transmissivity with distance away from the borehole (e.g. due to interconnecting fractures with higher transmissivity at some distance).

An increasing gradient can be indicative of a hydraulic choke or a no-flow boundary, i.e., a finite fracture cluster not connected to a source of water. Such features are not detected by PFL testing because the borehole is pumped for a much longer time, and so these would go dry. This is one key difference between the flow system as characterised by the two test methods.
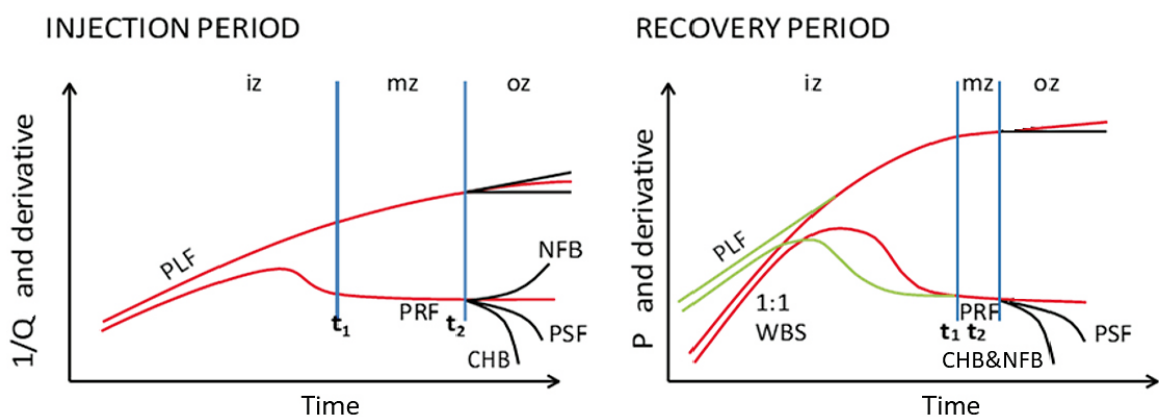

Figure 8-14. Schematic log-log plots of transient test responses and associated derivatives during the injection period and the recovery period of a constant-head injection test. The notation and symbols are explained in the text.

Transient tests can therefore reveal additional characteristics of the fracture network flow system, providing some additional insights, albeit non-unique, in the spatial distribution of transmissivity of the fracture connecting to the borehole, the adjacent network and its relative connectivity, see Figure 8-5. In summary:

- Transmissivity is obtained from transient tests (steady flow measures specific capacity) and that error has to do with biases to the near-hole transmissivity

- Transient tests identify boundaries and major features of the connected fracture geometry. Geometric interpretations from derivatives are non-unique but that does not mean they are not constrained. A half slope implies linear (pipe) flow and a zero slope implies radial flow. There are different ways to arrange fractures to get those responses (i.e., non-unique) but that does not mean it can be anything. With knowledge of the geology and some geophysics, you can significantly constrain the interpretation.

- Matching transient data are an important criterion for testing DFN models.

8.8.3   Review of discrete flows and selection of hydromechanics model

A key step in the structural-hydraulic integration is the linking of discrete flow measurements to individual fractures recorded in the core/image log interpretations, see Subsection 8.7.1. This integration provides the database for inferring the spatial distribution of flow against e.g. orientation, size, mineralogy, alteration, roughness etc. Given a *3D* stress field, the location and properties of a flowing fracture, the effective normal and shear stress on the fracture can be calculated to investigate the relationship between the occurrence and magnitude of flow and in situ stress, as follows.

The effects of stress on flow can be revealed by plotting Mohr diagrams of the calculated shear and normal stresses on each fracture and indicating the stresses on those that are water conducting, highlighting those that are of relatively high transmissivity. Because stress increases with depth, such plots have to be made for different depth intervals and the stress normalised with respect to one of the principal stresses, usually the maximum. The importance of low normal stress and/or high shear/normal stress ratios for flow can then be analysed and used to fine-tune the hydromechanics model used in the DFN modelling. One possible hypothesis is that high flows are more likely in critically stress fractures (Zoback 2010), i.e., close to shear failure leading to small shear displacements such that the two surfaces of a fracture become un-mated. This issue is considered in Figure 8-15 from Forsmark (Hartley et al. 2020), here showing a majority of flow occurring in fractures with $\sigma' < \sigma'_h$ (minimum horizontal stress) and most high flows have $\sigma' < (\sigma'_h + \sigma'_v)/2$ (the mean of the vertical and minimum horizontal stress), so low normal stress seems to be more of an indicator for flow likelihood than critical stress. Hence, this needs to be reflected in the aperture model used. It should be noted that a simplified *1D* stress field (varying only with depth) was used in this particular analysis. This is consistent with findings from the Olkiluoto dataset (Hartley et al. 2018b, Mattila and Follin 2019).

However, it is clear from these plots that the incident stress on a fracture is not a sufficient indicator of transmissivity alone, the fracture also needs to be open and connected. Hence, the many black points in Figure 8-15 at low stress but without flow. It can also be seen that there are several flowing fractures outside of the low normal stress region, albeit far less concentrated than in the low stress region. Possible causes for these outliers are numerous and so deserve focused analysis. This includes further analyses of variations of the *3D* stress model and data interpretation process for linking flow measures to mapped fractures. Nevertheless, high flow outliers may also be due to critical paths in the DFN connectivity structure and/or local conditions which maintain openness despite high stresses (e.g. fault gouge or minerals).

Hence, it is an important part of structural-hydraulic integration to make Mohr plots like this using the latest *3D* stress field model as an aid to review the reliability of the flow-fracture linking process, prior to its use in detailed model calibration, to reduce uncertainty in the anisotropy of flow.

The effects of fracture roughness and alteration can also be assessed by looking at differences in transmissivity distribution according to these properties under different normal stress magnitudes. For example, alteration may function as a proxy (or indicator) of size as more alteration occurs in large, connected fractures. If transmissivity then correlates with alteration it provided support for a correlation

between transmissivity and size. Hence, the DFN model can be further elaborated to include the dependence of both fracture mechanical and hydraulic properties on the statistical and spatial distribution of roughness through factors such as *f* in Table 8-2.
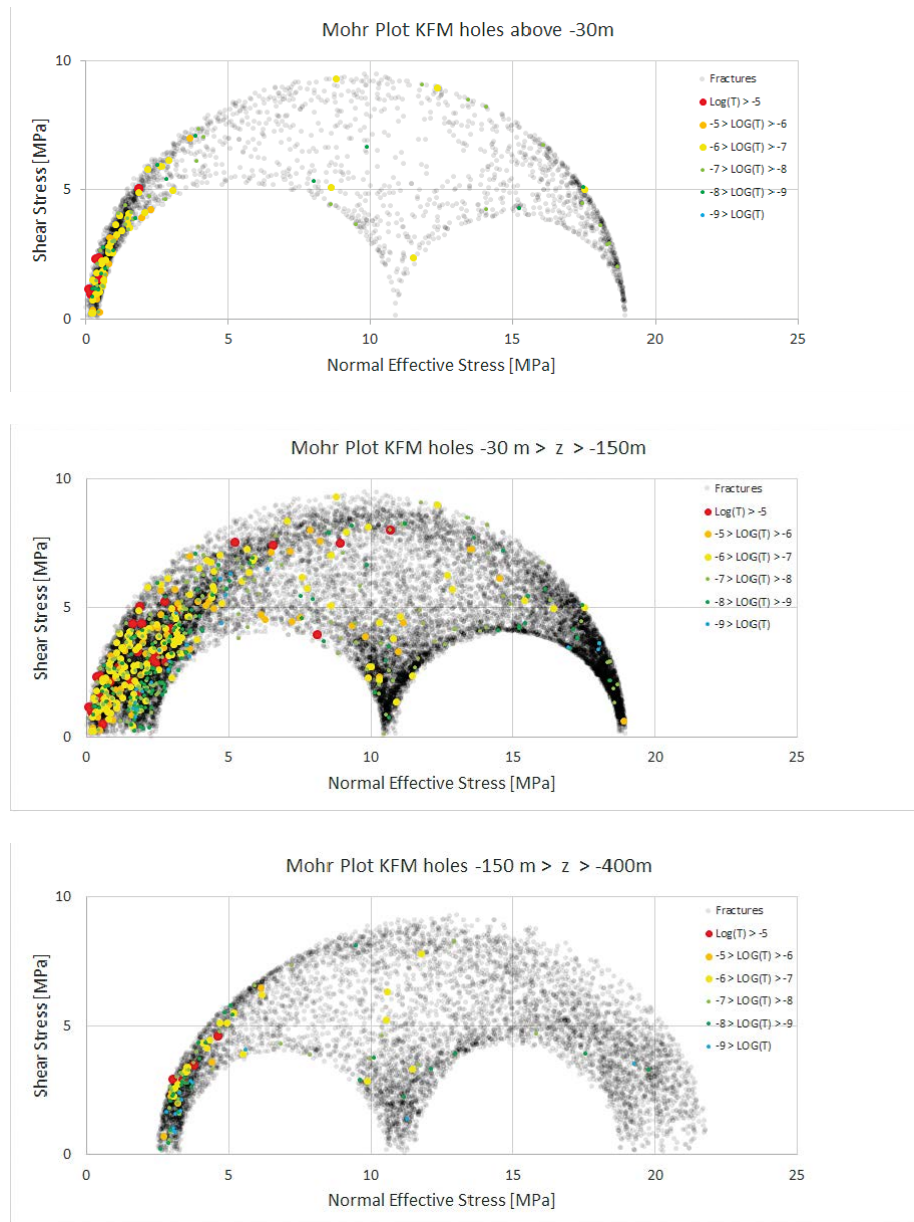

Figure 8-15. *Mohr plots for each observed fracture in FFM02 above elevation −30 m(top), in FFM01/06 with elevations −30 m to −150 m (middle) and FFM01/FFM06 in FFM01/06 with elevations −1 500 m to −400 m (bottom), and each outside deformation zones with transmissive fractures overlain coloured by their magnitude of interpreted transmissivity.*

8.8.4 Channelling indicator and equivalent hydraulic conductivity scaling

Additional metrics of the measured flow-rate and the flux distributions can be characterised for various purposes. Here, we discuss how equivalent block hydraulic conductivities can be calculated to support ECPM models, and how the channelling indicator can be introduced as a metric to evaluate the heterogeneity of the flow distribution (and consequence on transport characteristic). Both equivalent conductivity and channelling indicator values and potential scale dependency can be evaluated from the single-hole flow log measurements.

Discrete flow logging at Forsmark clearly shows that a very small portion of the fracture system carry the most significant part of the flow. The question is then how to describe this sparsity of flow and what portion of the fracture system carries the most significant part of the flow? The channelling indicator defined in Maillot et al. (2016) was introduced as a metric to quantify this channelling effect. It has since been used at Olkiluoto (Hartley et al. 2018b) to effectively differentiate the flow-related transport properties of different models in sensitivity analyses.

Ideally, the flow structure could be characterised in *3D*, but this is possible only for models. Ideally, indicators should also be possible to relate to available observations. Therefore, we develop indicators from models and simulations, but we link them to the discrete flow data.

The flow channelling indicator was chosen so that it can be applied to *3D* models, but also adapted for application to the in situ discrete flow data to allow comparison between models and data. The *3D* flow channelling indicator d_{qnet} (m^{-1}) for application to DFN flow simulations, is defined from local flow-rates in each modelled fracture plane (they are computed in mesh elements for the flow simulation):

$$d_{q_{net}} = \frac{1}{V} \cdot \frac{[\sum_m S_m \cdot q_m]^2}{\sum_{m \in V_s} S_m \cdot q_m^2}$$

Equation (8-10)

where the sub-index m refers to a mesh element, S_m is its area (m^2), q_m is the volumetric flow-rate (m$^3 \cdot$s^{-1}) going through it and V is the model volume over which it is computed. d_{qnet} provides an indication of the flow channelling within a DFN model, which cannot be directly estimated in situ. The ratio d_{qnet}/P_{32} (-) is a very useful measure, as it reflects the ratio of flowing fracture surface to the total fracture surface. However, the indicator can also be estimated from single-hole discrete flow measurements, as a *1D* flow channelling indicator with:

$$P_{10_q}(l) = \frac{1}{l} \frac{(\sum q_m)^2}{\sum q_m^2}$$

Equation (8-11)

where q_m is the flow-rate of the discrete inflow m over an interval of length l. $\frac{1}{P_{10_q}}$ can be considered as the statistical distance between two major flow paths.

One can also calculate equivalent block hydraulic conductivities to support ECPM models, recognising that they tend to be scale dependent because fractures tend to occur on a variety of scales and their properties often correlate with scale. Equivalent block hydraulic conductivities can be computed in *3D* from DFN flow models, but the latter cannot directly be compared to in situ data. The scale evolution of the equivalent hydraulic conductivity, K_{eq}, as defined from (*1D*) single-hole flow logs, is defined as follows over a borehole section of size l:

$$K_{eq}(l) = \frac{1}{l} \sum_{f \in l} T_{PFL,f} = \frac{T_{PFL}(l)}{l}$$

Equation (8-12)

where $T_{PFL,f}$ is the equivalent transmissivity of each observed inflow f, in the section l. A sliding box method is applied to sample a flow log dataset and to finally compute the geometrical average of the equivalent hydraulic conductivity $K_g(l)$, over a section length l, as:

$$K_g(l) = \exp\left(\frac{1}{N(K_{eq}(l_i)>0)} \sum_{\{l_i \in L | K_{eq}(l_i)>0\}} \log K_{eq}(l_i)\right)$$

Equation (8-13)

with $N((l_i)_{>0}) (K_{eq}(l_i) > 0)$ the number of sampling segments (over the entire core size) of size l with at least one measured inflow. An example of this metric applied to Forsmark data is shown in Section 10.2.

8.9   Flow simulation, model conditioning and calibration

The processes described in Sections 8.1 through 8.6 primarily involve characterisation of the hydraulic data prior to numerical simulation. They are used to condition the selection of models consistent with observations and for narrowing down parameter space accordingly, see Chapter 10. Generally, the model conditioning on hydraulic data starts with the geometrical parameters, then alternative models for the spatial distribution of openings or dimensionality of the flow system, and finally the spatial distribution of transmissivity, as pre-cursors to model calibration using flow simulations in a DFN model, Figure 8-16.

This model conditioning is performed for each part of the fracture system: deformation zone, fracture domains and near-surface system where clear statistical differences are apparent, although typically different alternative models will be applied consistently across the system but adapting the parameter space to each part.

Having conditioned each part of the DFN, flow simulations are used to reduce parameter space. This is usually done in three steps: sensitivity analyses/rejection, calibration and prediction/confirmation, see Chapter 10. In brief, sensitivity analyses are used to understand the relative importance of parameters and how they affect flow characteristics that can be calculated from measurements, using this knowledge the range of parameters giving models statistically consistent with data is obtained, and then the resulting models are used to predict other types of data or new measurements to confirm, re-calibrate or reject the model.
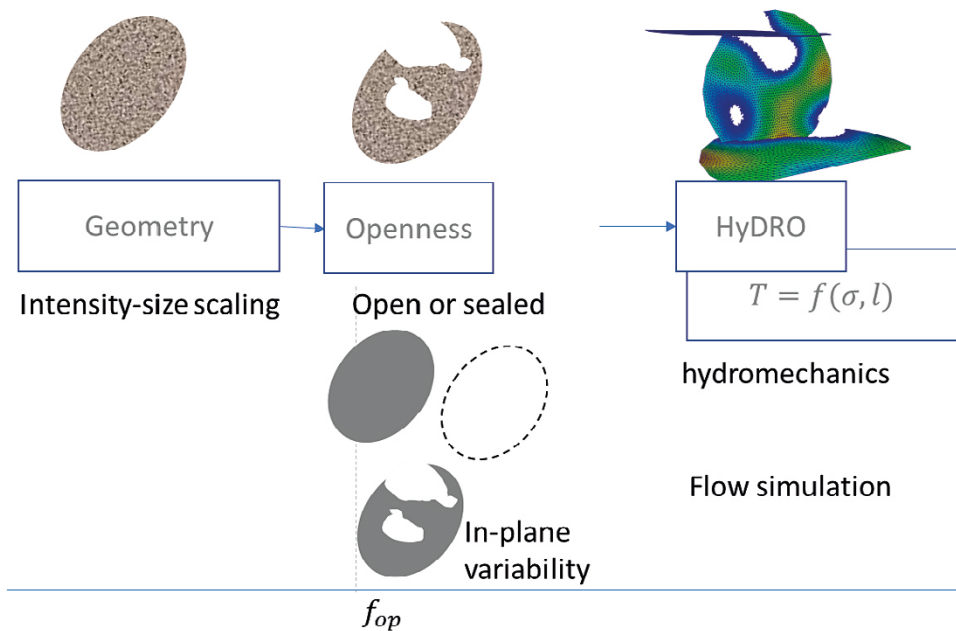

Figure 8-16. *The main steps in conditioning model space for fracture hydraulic description.*

8.9.1 Sensitivity tests

Initial sensitivity tests are used to provide insights into the behaviour of alternative models (see terminology in Chapter 10) and the importance of model parameters using a set of metrics and characteristics. These metrics may be related to properties critical to safety or engineering evaluations as part of model selection to ensure that alternative models chosen will have significance for the ultimate purpose of the models. Metrics can also be chosen that reflect flow and transport characteristics of the fracture system, such as percolation scaling, conductivity scaling and channelling indicators introduced in Subsection 8.8.4. By comparing flow simulation results with measured characteristics, sensitivity tests allow the screening out of models that cannot describe flow observations, and the identification of the set of equally viable hydrogeological models. Sensitivity tests are primarily used to illustrate what range of alternative conceptual models that can honour the observed data, i.e., result in equally good calibration results relative to the defined set of hydraulic metrics and quantify the significance of these alternatives for performance measures related to post-closure safety or metrics that can be used to discriminate between models. The most valuable sensitivity tests are those that aim to bound sensitivities to uncertainties that are difficult to constrain by data, such as size distribution, shape and spatial distribution of openings. Ideally, these are explored through defining bounding assumptions. Other sensitivities are parametric and numerical uncertainties, such as boundary conditions, spatial and temporal discretisation.

8.9.2 Formulation and calibration of hydraulic properties

Having formulated a model for transmissivity as a function of incident stress on the fracture and size, which in turn are functions of location and orientation, the absolute magnitude of transmissivity is calibrated through simulating hydraulic tests with a DFN model for flow simulations (as built using the process illustrated in Figure 8-16). In the calibration process, some parameters are selected, and their values fine-tuned within a defined range to improve the calibration. If mapping of lineaments and rock exposures on several scales has provided reasonable confidence for the geometrical model, primarily intensity-size, then the hydraulic calibration focuses on tuning parameters controlling the distributions of openings and transmissivity to obtain the observed flow statistics and connectivity. If, however, the simulated flow system is either under-connected or over-connected when varying the hydraulic parameters within their uncertainty ranges, then one needs to reassess uncertainties in geometric parameters, such as intensity-size scaling and connections within the deterministic structural model.

The integration of data for flow calibration can be made in three main steps:

1. Simulate steady-state flow tests of specific capacities and single hole scale, as in Figure 10-3 (Step BS3 and BS4 Figure 3-2) – adjusting the magnitude of transmissivity and its relationship to size that affects the shape of flow distribution, and the hydromechanics model that affects trends with orientation and location.

2. Compare with the scaling behaviour of flow statistics, for equivalent conductivity and channelling indicator see Subsection 8.8.4 Figure 10-4 and pursue the process of screening out or accepting models.

3. Simulate transient interference tests or hydraulic disturbances (Step BS6 in BS4 Figure 3-2) over inter-hole scale, with focus on the deformation zones, including storativity of the zones.

The first step is approached by constructing many realisations of the DFN around each borehole or drill pad, simulating both background and DZ-related fractures (since they affect the connectivity of each other), and then simulating steady-state flows to the borehole to derive the distribution of flow at each intersecting fracture. For logistical reasons, all fractures down to a few decimetres need to be simulated around the borehole, but only the fractures larger than a few metres need be simulated away from the hole, as the small fractures only contribute to porosity and storage. The simulated distributions of flows over several tens of realisations are then compared with measured distributions.

The database of flowing fractures from flow-logging is used to quantify the intensity of fracture-specific flows, as well as the overall distribution of specific capacity, and can be subdivided according to being inside/outside DZ and fracture set to provide additional detailed characteristics of flow patterns to match models against. The set of calibration targets formulated from the flowing fractures database include:

1. the ensemble distribution of specific capacities,

2. the overall numbers of flowing fractures with specific capacity $> 10^{-10}$ m^2/s,

3. the distribution of specific capacities outside a DZ,

4. the distribution of specific capacities inside a DZ,

5. the distribution of specific capacities by set,

6. the total specific capacity by elevation region inside/outside DZ, and

7. the total specific capacity summed for each borehole by elevation region inside/outside DZ.

The 1st target ensures that the overall range of transmissivities is correct, i.e., the variability in flow magnitudes. The 2nd target ensures that the connectivity of the flow system is reproduced. The 3rd and 4th targets ensure that the spatial distribution of flow between inside DZ damage zones and in the rock mass are correctly simulated. The 5th target ensures that the correct flow distribution is simulated according to fracture orientation and the sensitivity to normal stress. The 6th target ensures that overall flows are correct. The 7th target tests that the spatial variability of flow within and outside DZ between the drillholes is captured by simulations. It is believed that together these targets provide stringent tests of the ability of the model to reproduce the important characteristics of fracture specific flows and their structural, spatial and mechanical contexts. The parameters typically adjusted to achieve a calibration are listed in the first step above.

In the second main step, the simulated flows are amalgamated over different scales to calculate equivalent conductivity and channelling indicator. Because of the significant differences in flow statistics with depth and in DZ compared to the rock mass these metrics need to be compared with statistically equivalent domains.

In the third main step, transient simulations are performed as multiple realisations. Predicted drawdowns in monitoring holes often vary a lot between realisations due to the use of stochastic DFN models, and hence it is appropriate to compare the range of simulated drawdowns over the realisations with the aim of simulating a majority of the correct intervals responding in each realisation. Usually this is achieved by adjusting the connectivity of the deformation zone model and fractures connecting to the pumping hole, as well as considering the top surface boundary, such as available recharge to bedrock. The transmissivity of fractures around the pumping hole needs to be calibrated to have any chance of predicting drawdowns in the surrounding holes. The storativity of the fractures also needs to be calibrated to get the correct time of drawdowns, which means adjusting the fracture normal stiffness in Equation (8-5). An example from the simulation of disturbances following construction of ONKALO at Olkiluoto is in Figure 8-17. Data are ordered by straight-line distance to the ONKALO. The first (upper) inset shows ten realisations of simulated and measured heads (groundwater levels) prior to the construction of ONKALO. The black horizontal line in each of the blue bars estimate the effects of variable groundwater density in the hole. The second (middle) inset shows the range of drawdowns over 10 realisations. In the third (lower) inset, this range is replaced by dots representing the individual realisations to reveal how some realisations such as Realisation 4 works well for some intervals (presumably having by chance a correct combination of connections in one area) and Realisation 7 works well for another set.
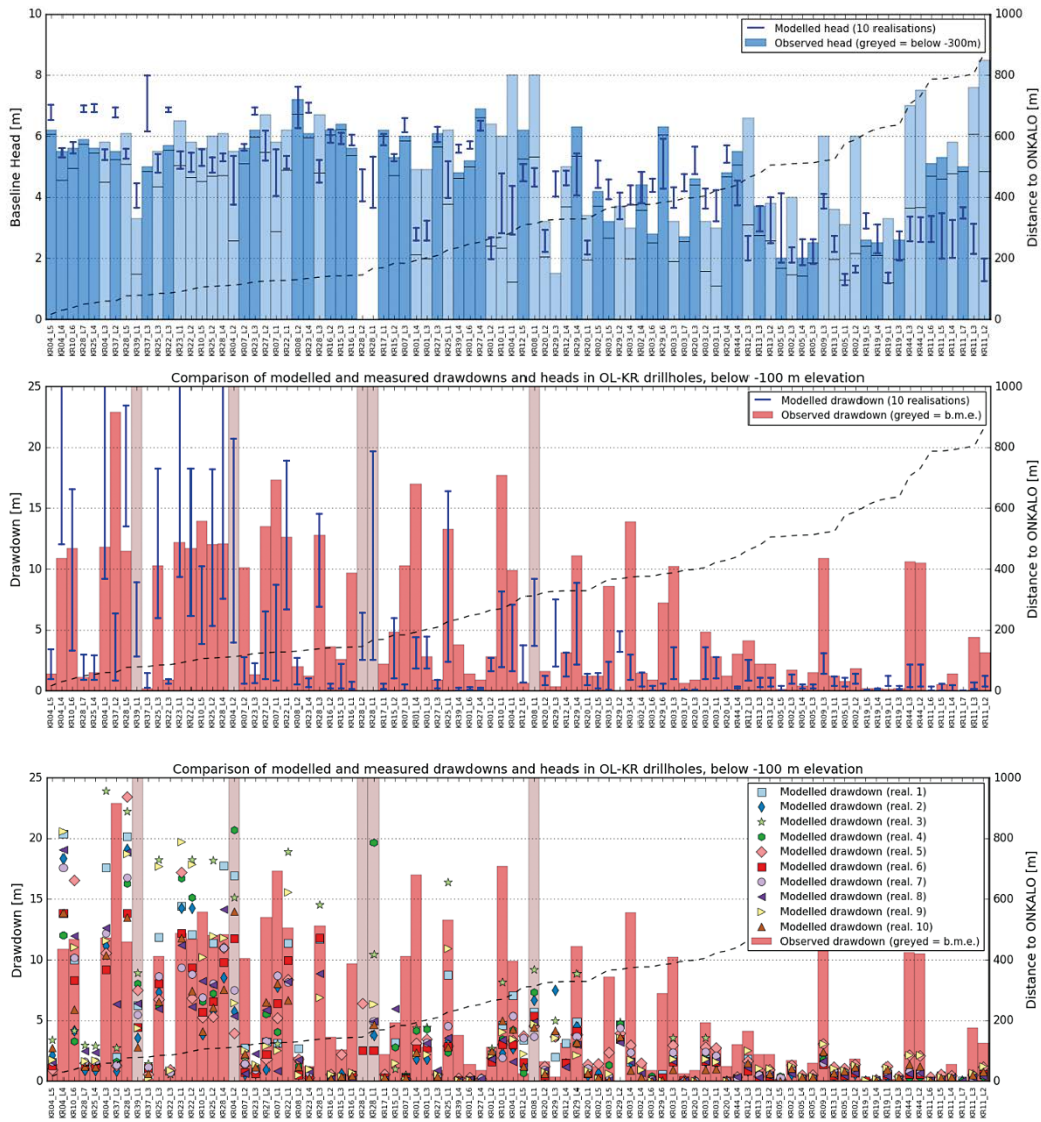
Figure 8-17. *Comparison over ten realisations of simulated and measured heads (blue bars) and drawdowns (red bars) in cored boreholes below −100 m elevation at Olkiluoto. Data are ordered by straight-line distance to the ONKALO. Dark blue lines show range spanned by 10 realisations of simulated heads and drawdowns. Individual realisations of simulated drawdowns are shown as coloured symbols, as per the figure legend, in the lowermost inset. Observed drawdowns marked as 'b.m.e.' (greyed) indicate pressure response is sufficiently strong such that the drawdown is below the measurement elevation, so are displayed as off the vertical scale. The black horizontal lines in the head plot estimate the effects of variable groundwater density. Source: Posiva, Figure 9-23 and Figure 9-24 in Hartley et al. (2018b).*

8.10 Expected sources of uncertainty and how they can be treated

8.10.1 Measurement limitations and detection limits

As mentioned in Section 8.7, magnitudes of flows in fractured rock can vary over several orders of magnitude, but flows can only be detected in certain ranges depending on the tool used and the conditions of the borehole and how the test was performed. A few high flows may be under-estimated, while low flows cannot be detected, making it uncertain if there is no flow or if it is just below the detection limit. PFL and PSS measurements generally capture flows over magnitudes that are of concern for assessments of post-closure safety, but small flows are still of interest when assessing issues such as availability of water for resaturation of the buffer. The detection of smaller magnitude flows measured by transient short interval PSS tests provide a possible bound on these low flows, although the short duration used may measure flows which would not be sustained over longer periods where local closed networks are injected into. Flow logging in underground conditions in pilot holes where a higher drawdown is used is another way to lower the detection limit.

Combining flow logging with transient hydraulic tests underground will provide improved understanding of the effects of a sparse, often non-percolating, network at depth and heterogeneity. Hypotheses for the spatial distribution of flow still need to defined and tested as whether they are consistent with the data and if so what consequence alternative hypotheses have for long-term safety.

Detailed hydraulic testing of the upper 100 m of the bedrock has been limited due to most KFM holes in this interval being equipped with metal casing. PSS testing has only been performed in KFM03B, KFM06B, KFM08B, KFM09B (without fracture logging), with PFL-f only in KFM24. These provide quite limited indications of flow statistics in the top 100 m and the degree of hydraulic coupling between the shallow and deep systems. Monitoring of hydraulic disturbances in shallow intervals during the construction of the access ramp and facilities, alongside measurements of inflows to the tunnels, would provide data to support understanding of this vertical coupling between the shallow and deep hydrogeological systems.

Impeller logging in this interval provides some indication of the magnitudes of the largest transmissivities in the top 100 m, and isolates the main flowing structures typically to a scale of a few metres, but leaves a lot of uncertainty in linking that flow to individual fractures, their orientations and properties. Recent characterisation of the KFM13–23 shallow holes around the access area has provided a significant new dataset to conceptualise fracture hydraulics in the top 100 m (Hartley et al. 2020). Sheet joints or reactivated fractures in the top 30 m of bedrock give rise to a particularly conductive system of sub-horizontal fractures in this depth interval. Fracture intensity is elevated in the SubH and ENE sets in this upper layer, and the ratio of open/closed fractures is also significantly higher for all orientations. This would suggest a horizontally conductive system in the top 30 m that will flatten lateral hydraulic gradients and divert surface groundwater from circulating to depth unless disturbed by unsealed constructions. An exploratory update of a DFN model for the near-surface quantifies fracture parameters for this top-most domain (Hartley et al. 2020), although it did not fully implement the methodology described here, such as the representation of intra-fracture variability.

8.10.2 Linking of flows to structures

The above workflow assumes flows have been linked to specific fractures. For the PFL-f logging, the flow can be isolated to a few decimetres, but it can still then be more than one fracture in this interval and there is room for uncertainty in the measurements of depth between the borehole image, core and flow measurements. The uncertainty in depth corrections and the most likely conductive fracture can be assisted by correlating flow with high resolution resistivity logs, e.g. as measured on the upper disc of the PFL device or on corresponding tool (FFLS) to be developed by SKB. In the fracture linking process (Forsman et al. 2004, Forssman et al. 2006, 2008, Teurneau et al. 2008) the best choice is indicated together with 1–3 alternatives fractures where there is possible ambiguity. It is difficult to assess these different possibilities. However, what can be tested is to make analyses and interpretation of correlations between occurrence of flow and transmissivity versus stress, morphology, alteration and mineralogy for the best choice fracture for each flow, (see Subsection 8.8.3) and then repeat selected analyses for the second choice to quantify how sensitive the interpretations are to this uncertainty. The number of alternatives varies with intensity of fracturing, and so broadly this uncertainty diminishes with depth.

The greater challenge comes in linking the impeller logging in the shallow bedrock to individual structures because the intervals are typically narrowed to c 1–10 m, which can span several or tens of fractures. Sometimes minima in the p-wave velocity can be used to narrow the likely water conducting fractures further, and this data exists for both percussion (HFM) and cored (KFM) holes. Another possibility is whether such flows are regularly coincident with fractures with clay minerals, for example. What can often be determined is whether the flow is mostly associated with sub-horizontal or sub-vertical fractures. Different hypotheses such as the high flow being predominantly associated with different orientation of structures and their extent can then be used to construct alternative models. These can then be tested/screened against interference tests data to reduce the plausible hypotheses.

8.10.3 Spatial distribution of flow and channelling

One of the most important and yet difficult uncertainties to characterise is how openings and apertures are distributed spatially. As described in Section 8.5 this has to be approached by considering alternative conceptual models, and testing how sensitive are the simulations of various types of measured flow behaviours: fracture-specific flow distributions, scaling behaviour for different intervals and hydraulic connectivity as measured by interference tests and inferences based on hydraulic disturbances. The significance of these uncertainties for performance measures, such as statistical distributions of flow rates around deposition holes, advective travel times and flow-related transport resistance can then be calculated. The channelling indicator, see Subsection 8.8.4, can also be used to quantify how concentrated bulk flows are into channels.

8.10.4 Non-uniqueness of model

It can be possible to produce an equally good match to individual hydraulic datasets by changing different model settings and parameters. For example, drawdowns in interference tests may be increased by reducing transmissivity or reducing the amount of recharge from the top surface. The best way to reduce the number of viable models is to test models against different sorts of hydraulic data and use a range of metrics that measure different characteristics of the hydraulic system and over different scales. For example, fracture-specific flow data from flow logging is ideal for calibrating the distributions of the hydraulic apertures over individual fractures, while interference tests measure large scale connectivity and anisotropy of the fracture system, and hydraulic conductivities on different scales measure the patterns of clustering of flows. Still, often the hydraulic data measure the integrated effects of several different parameters in combination rather than each directly, and so it may not be possible to distinguish between some models. The key is whether these alternatives have different consequences for post-closure safety and to constrain the possibilities.

8.10.5 Prediction-outcome

Once underground, suitable prediction metrics are the distributions of fracture-specific flows, especially the intensity of high flows of magnitudes above 10^{-8} m^2/s, and above 10^{-9} m^2/s at repository depth. These will be available from pilot holes drilled for the ramp. Because flows can be expected to be rare, then prediction-outcome exercises need to be made in a statistical approach amalgamating statistics from several pilot holes.

Focused prediction-outcome exercises on the hydraulic connectivity of scales of deposition holes and tunnels can be performed in investigation niches using closely spaced short boreholes. These may provide some useful input to testing concepts for the spatial distribution of openings. Larger-scale network connectivity can be tested by predicting responses in monitoring boreholes during construction periodically, especially as the "rectangular spiral" ramp intersects major deformation zones, with potential repeated intersects of the same deformation zone.

Quantifying inflows to tunnels underground is difficult because of the evaporation, practicalities of collecting the water, and for modelling it is difficult to describe the conditions in the tunnel. A non-linear seepage type boundary condition is best suited, allowing inflow to the tunnel at atmospheric pressure, but preventing water fluxes into the rock. If grouting and/or shotcreting is present, then fracture transmissivities in the sealed volume needs to be reduced or inflows will be over-predicted.

Stochastic modelling predicts a set of equally likely realities, and hence comparisons have to be made statistically. Appropriate acceptance criteria are then whether an observation sits within the predicted distribution, and sufficient realisation are required to achieve stable statistics for the quantities measuring the span of realisations, such as the variance or 95 % confidence interval. This might require several tens to hundreds of realisations.

9 DFN models for solute transport and retention properties

There are a number of issues that are of concern for post-closure safety of a deep geological repository for spent nuclear fuel and that need to be addressed by means of transport simulations. A non-comprehensive list includes the fate and migration of potentially harmful radionuclides, the ingress of oxygenated glacial meltwater (Sidborn et al. 2010, Trinchero et al. 2017), which is detrimental for the engineering barriers (Glynn et al. 1999, McMurry 2000, Puigdomenech et al. 2001), the dissolution of the cementitious grout used during tunnel construction, which may generate a hyper-alkaline plume (Sidborn et al. 2014, Molinero et al. 2016), and the progressive infiltration of altered meteoric water, which may alter the pH and redox conditions of the system (Salas et al. 2010).

Transport in fractured media is characterised by a dual behaviour (Bibby 1981), with advection being the main transport driver along water conducting fractures and with diffusion being the dominant process in the adjacent rock matrix. The description of the fractured medium as a dual-porosity system, with diffusion occurring only perpendicularly to the fracture surface, is obviously a highly simplified idealisation. For instance, in some non-granitic fractured media the rock matrix contributes significantly to the global flow and the medium effectively behaves as a dual-permeability system (Matthäi and Belayneh 2004). However, field and laboratory evidence have shown that in fractured crystalline rock, the matrix is essentially stagnant and thus the dual-porosity approximation is deemed to be reasonable (Vilks 2007a, b, Finsterle 2019).

Moreover, advection and matrix diffusion are tightly coupled (Neretnieks 1980, Tang et al. 1981, Cvetkovic et al. 1999). For this reason, the present transport chapter of this report includes not only a discussion of those processes and features that characterise in-plane solute transport but also an overview of retention processes in the adjoining matrix. Some of the topics presented in the following sections are related to matrix heterogeneity. The rock matrix of fractured crystalline media has, in fact, long been treated as being intact; i.e., characterised by homogeneous single values of porosity, diffusivity and sorption partition. However, recent micro-scale characterisation studies (Iraola et al. 2017, Svensson et al. 2018) have pointed out that the rock matrix is constituted by a complex distribution of diffusion-available pore space and by a sparse and heterogeneous distribution of reactive mineral grains, which has an impact on the underlying retention processes. Thus, available upscaling and averaging methodologies for use in large-scale (facility and local scale in SKB notation) transport simulations will be discussed.

Transport models are all based on the principle of mass conservation and the underlying mathematical equations require a number of parameter values. Some of these parameters may be obtained from laboratory measurement, whereas other parameters are usually inferred from either lab-scale or *in situ* scale experiments. Flow related transport parameters in the fracture system are typically obtained by numerical modelling.

An important aspect of transport modelling is the definition of a transport aperture. In fact, transport aperture is used to convert computed fluxes per unit of fracture aperture into Darcy fluxes (and thus, groundwater velocities) and it is also a key parameter affecting matrix diffusion (see Subsection 9.1.2). Real fractures are heterogeneous and thus their geometric aperture is given by a distribution. Single effective values are used in large-scale simulations and they are typically based on empirical relations with e.g. fracture transmissivity. Transport apertures are described more in detail in **TRPMM**.

In the framework of safety assessment (SA) studies of deep geological repositories, transport modelling entails the need to evaluate very long time scales; typically, thousands to hundreds of thousands of years, in large domains, of hundreds to thousands of meters. It turns out that parameters inferred from lab or field scales need to be upscaled (i.e., the small-scale information need to be transferred into a larger support volume; e.g. Fernàndez-Garcia et al. 2009) and evidence obtained from e.g. *in situ* tracer tests need to be extrapolated to the larger temporal scale of interest.

The following sections provide a general overview of specific transport processes and related parameters and features, discuss sources of supporting data, present different modelling approaches, some of them related to specific transport calculations (e.g. background geochemistry vs. radionuclide

transport), and, finally, wraps up with a discussion of uncertainties and guidelines on how they can be treated. The processes discussed in this chapter occur in fractured systems similar to that illustrated in Figure 2-2, although idealisations and model simplifications are made to render those processes numerically manageable.

9.1 Transport in fractured media: processes, parameters and features

9.1.1 Advection-dispersion in fractures

Advection is the phenomenon by which dissolved solutes are transported by fluid displacement.

If we consider a solute that is only displaced by advection in the fracture and is not affected by any other process, then mass fluxes, J, in the fracture can be expressed as

$$\boldsymbol{J} = C\boldsymbol{u}$$ Equation (9-1)

where C [M·L^{-3}] is the volumetric concentration and $\boldsymbol{u}$ [L·T^{-1}] is the water velocity. Mass balance in an elementary volume of fracture gives the advection equation, which relates mass fluxes to variations of mass per unit time:

$$\frac{\partial C}{\partial t} = -\nabla(C\boldsymbol{u})$$ Equation (9-2)

Equation (9-2) is known as the divergence form of the advection equation. With simple mathematical rearrangements, the advection equation can be reformulated; it is the so-called convective form, by analogy to heat transport (Diersch 1998).

$$\frac{\partial C}{\partial t} = -\boldsymbol{u}\nabla C$$ Equation (9-3)

The convective form is widely used as it is the base for most of the Eulerian-Lagrangian numerical formulations used for solving solute transport (Saaltink et al. 2004). So, we will use this canonical form from now on.

Flow and transport in open fractures is often channelised (Tsang and Neretnieks 1998), so it can sometimes be convenient to use a streamline representation and reduce the dimension of the problem by orientating the axis along the principal direction of flow. In this case, the advection equation for a single packet of contaminant mass reduces to:

$$\frac{\partial C}{\partial t} = -u_x\frac{\partial C}{\partial x}$$ Equation (9-4)

The variability of fracture velocity field within and between fractures leads to a spreading of the dissolved mass, which is observed both in space and in time. This phenomenon, denoted hydrodynamic dispersion, has an important effect on e.g. radionuclide breakthrough curves that are characterised by earlier initial arrival times and lower peak values.

When hydrodynamic dispersion is included, mass fluxes in the longitudinal direction need to be described by an additional term:

$$J_x = Cu_x - D_L\frac{\partial C}{\partial x}$$ Equation (9-5)

where D_L [L^2·T^{-1}] is the hydrodynamic dispersion coefficient in the longitudinal direction. The transport partial differential equation takes the form of the standard advection-dispersion equation (ADE):

$$\frac{\partial C}{\partial t} = -u_x\frac{\partial c}{\partial x} + D_L\frac{\partial^2 C}{\partial x^2}$$ Equation (9-6)

On the scale of a single fracture, hydrodynamic dispersion is the result of two different mechanisms: Taylor-Aris dispersion, i.e., variations in velocity across the aperture, and variations in the velocity field due to roughness and fracture aperture variations along the plane (Bodin et al. 2003).

Taylor-Aris dispersion is related to the parabolic velocity profile that is observed, under the assumption of laminar flow, between two parallel plates. Due to molecular diffusion, dissolved molecules of solute can sample different velocities. (Wooding 1960) quantified the asymptotic value of Taylor-Aris dispersion as:

$$D_{Tay} = \frac{2}{105} \frac{u_x^2 b^2}{D_m}$$

Equation (9-7)

where u_x has to be intended as the velocity in the middle of the aperture, b [L] is half of the distance between the two parallel plates and D_m [L$^2\cdot$T^{-1}] is the molecular diffusion in unconstrained solution. The time when asymptotic dispersion is reached (t_{ast} [T]) can be evaluated using the characteristic time for diffusion:

$$t_{ast} = \frac{b^2}{D_m}$$

Equation (9-8)

Roughness and local changes in fracture aperture (Section 6.7) are common in natural fractured rocks and they are typically induced by mechanical mechanisms, such as shear and compression. Gelhar (1993) used stochastic theory to provide an approximated solution for the equivalent homogeneous dispersion in a fracture with variable fracture aperture. However, the model was based on a somewhat simplified conceptualisation of fracture aperture variability. In a more recent work, Zou et al. (2017) used a realistic fracture-matrix model (denoted as the rough-wall fracture matrix model), based on laser-scanned surface tomography of a real rock sample, to assess the effect of roughness and variability in fracture aperture on radionuclide transport, see Subsection 9.1.4. The two dispersive mechanisms described above are in principle additive, although for reactive solutes there may be some interaction that makes the full hydrodynamic process more complex (Berkowitz and Zhou 1996).

Hydrodynamic dispersion is often approximated as:

$$D_L = D_m + \alpha_L.u_x$$

Equation (9-9)

where $\alpha_L\cdot$[L] is an empirical parameter denoted as longitudinal dispersivity.

In a recent paper, Molz (2015) stated that "*in any fluid flow, including groundwater flow, there is only advection and diffusion. So, if we could reproduce the true velocity field in a porous medium, all we would need in order to model solute transport would be molecular diffusion*". Although theoretically true, this statement has limited practical implications because it is impossible to obtain the true velocity field, particularly in complex systems such as natural fractures. Thus, a macroscopic representation of dispersion processes is still needed. It is worthwhile noting also that Equation (9-6) is only valid under the assumption of asymptotic or Fickian conditions. In the same paper, Molz revisited data from different *in situ* tracer tests pointing out that, even at relatively large scales, asymptotic behaviour is rarely reached. Evidence of scale dependency of hydrodynamic dispersion dates back to the pioneering work of Gelhar et al. (1979) and has been assessed in numerous scientific publications. A detailed review of these works is, however, out of the scope of this report. At the network scale, the strong variation in fluid velocities, which is often controlled by the structure of the fracture network, leads to additional dispersion mechanisms. This is discussed more in detail in Subsection 9.1.4.

Macro dispersion is typically inferred either (*i*) from spatial moments of the solute plume at given times or (*ii*) from the breakthrough curve of a tracer observed at a given location. In practical applications, the first approach is unfeasible as it requires a very large number of observation points. Thus, tracer test experiments, typically performed between two boreholes (one for the tracer injection and the second for observation of the breakthrough curve), are the most commonly used way to estimate values of macro dispersion. A large number of works have focused either on providing specific guidelines for the correct execution of the field tests (e.g.Novakowski 1992, D'Alessandro et al. 1997, Dorn et al. 2012) as well as for the interpretation of the experimental data (e.g. Harvey and Gorelick 1995, Novakowski et al. 1998).

9.1.2 Matrix diffusion

Solutes moving along water conducting fractures may diffuse into the adjacent rock matrix. A packet of radionuclide mass that has diffused into the matrix may decay or eventually re-emerge from the matrix and move along the remaining pathway (the meaning of the term "pathway" will be discussed in detail in Subsection 9.3.2).

In Lagrangian terms, the time spent by a packet of solute mass in the infinite matrix surrounding a water conducting fracture is described by the following cumulative distribution function (Painter et al. 2008):

$$F_T = erfc \left[\frac{\kappa \beta}{2\sqrt{t_{ret}}} \right]$$

Equation (9-10)

where $\kappa = \sqrt{D_e R_{im} \phi}$ [(L^2·T^{-1})$^{0.5}$] is a material parameter group, D_e [L^2·T^{-1}] is the effective diffusion coefficient, ϕ [-] is the matrix porosity, R_{im} [-] is the immobile (matrix) retardation factor, $t_{ret} = t - t_{gw}$ [T] is the retention time and t_{gw} [T] is the groundwater residence time, $erfc$ is the complementary error function, β [TL^{-1}] is a hydrodynamic control parameter denoted as transport resistance (Cvetkovic et al. 1999) and defined as:

$$\beta = \int_0^{t_{gw}} \frac{d\varepsilon}{b(\varepsilon)}$$

Equation (9-11)

where ε is the integration dummy variable and b [L] is the fracture half aperture. From Equation (9-10) it can be noticed that the distribution of t_{ret} is equally influenced by β and κ.

For fractures with constant aperture, transport resistance is equivalent to the Eulerian quantity denoted as F-factor (Moreno et al. 1997):

$$fquo = \frac{2WL}{Q}$$

Equation (9-12)

where W [L] and L [L] are the width and length of the fracture and Q [L^3·T^{-1}] is the fracture volumetric flow rate. The numerator of Equation (9-12) is the so-called flow-wetted surface area. It is worthwhile mentioning that in previous SKB reports the notation "transport resistance" and "F-factor" was used interchangeably. Since in fractures exhibiting internal heterogeneity, transport resistance and F-factor are different, here we propose to use transport resistance to refer to Lagrangian-based quantities (Equation (9-11)) and F-factor to refer to Eulerian-based effective values (Equation (9-12)).

There is a direct analogy between the retention time distribution (Equation (9-10)) and the Eulerian solution for a continuous injection. The latter in fact reads (Carslaw and Jaeger 1959):

$$C = C_o erfc \left[\frac{\kappa \beta}{2\sqrt{t - t_{gw}}} \right]$$

Equation (9-13)

Note that the hydrodynamic control parameter β is called the F-factor in an alternative notation (Larsson et al. 2012). This flow-related parameter, which establishes the coupling between advective processes in the fracture and diffusion mechanisms in the matrix, is of key importance for the simulation of contaminant transport in fractured media and thus it is discussed in detail in the next dedicated subsection.

The other controlling parameter, κ, depends on specific characteristics of the rock matrix; namely immobile retardation factor, connected matrix porosity and effective diffusion coefficient. The first parameter depends in turn on the available pool of sorption sites in the matrix and will be discussed in more detail in Subsection 9.1.4. Matrix porosity is typically inferred from laboratory measurements using e.g. water saturation techniques. Alternative approaches involve the use of C-14-PMMA autoradiography measurements (Hellmuth and Siitari-Kauppi 1990). Although there is no unified notation, the effective diffusion coefficient is usually defined as:

$$D_e = F_f D_m = \phi \frac{\delta}{\tau^2} D_m$$

Equation (9-14)

where F_f [-] is the formation factor, δ [-] is the constrictivity and τ [-] the tortuosity. The effective diffusion coefficient is often determined from laboratory or in situ experiments. Specific in situ tests, such as the Water Phase diffusion Experiment at ONKALO, Finland (Poteri et al. 2018) can be used to estimate the lumped retention capacity of the rock matrix (i.e., the κ value).

Equation (9-13) and all the discussion above assume that properties of the rock matrix are homogeneous. However, both laboratory micro-characterisation studies (Drake et al. 2006, Voutilainen et al. 2019) and results from *in situ* tracer tests have pointed out that the matrix is highly heterogeneous, both in terms of physical and mineralogical properties (Iraola et al. 2017). Notice that we refer here to "physical heterogeneity" to the heterogeneous distribution of the diffusion available pore space, and with "mineralogical heterogeneity" to the sparse distribution of sorbing minerals.

Recently, Svensson et al. (2018) have proposed an alternative approach to represent the heterogeneous rock matrix. The approach is based on a micro-Discrete Fracture Network (micro-DFN) which is in turn built using different fracture sets to mimic both intra- and inter-granular pore space. The proposed model, which was successfully calibrated against available measurements from rock samples taken at the Forsmark site, is deemed to be a useful tool for the evaluation of reactive transport processes occurring at the grain-scale as well as for designing upscaling procedures required to extend the signature of matrix heterogeneity to the scale of interest of a safety assessment.

On a larger scale (roughly speaking, on the scale of a single fracture), fractures and the adjacent rock matrix are heterogeneous as they may have been subject to different hydrothermal and tectonic alteration events. This fracture-scale heterogeneity is accounted for by means of transport classes, which are described in detail in Subsection 9.1.5.

Another important assumption related to Equation (9-10) and its Lagrangian counterpart (Equation (9-11)) is that both assume that the matrix has an infinite storage capacity. In real applications however, the amount of diffusion available pore space is limited. Typically, this is accounted for by means of a gross simplification; i.e., by assuming that transport occurs in a system of parallel fractures and that transport patterns are perfectly symmetric. For these conditions, the following analytical solution applies (Sudicky and Frind 1984):

$$\bar{C} = \frac{C_o}{s} exp(-t_{gw}s) exp\left[-\kappa\beta\sqrt{s} \tanh\left(\Delta \cdot \sqrt{\frac{R_{im}}{D_p}s} \right) \right] \qquad \text{Equation (9-15)}$$

where $\bar{C}$ is the Laplace transform of C, $D_p = D_e/\phi$ [L$^2\cdot$T^{-1}] is the pore diffusivity and Δ [L] is the available extent of the rock matrix. Notice that the solution of Equation (9-15) can be reinterpreted in a Lagrangian sense as the convolution between the water residence time distribution (first exponentiation) and the retention time distribution (second exponentiation).

The effect of a limited matrix is illustrated in Figure 9-1, which shows the breakthrough curves of a non-sorbing radionuclide for the case of infinite and finite matrix (the parameters of the model are based on the experiment WPDE-1 (Poteri et al. 2018)). For an infinite matrix, the tailing of the breakthrough curves shows the typical power-law behaviour with $C \sim t^{-3/2}$. When a limited matrix is considered, first a bump is observed until a cut-off is reached, when concentration decreases dramatically. The time when the bump and the cut-off are observed depends on $t_c \approx \Delta^2/D_p$.

Equation (9-15) (and its Lagrangian counterparts) along with the related underlying assumptions are used by most computer codes to simulate radionuclide transport in fractured media with a matrix of limited extent. Cvetkovic (2017a) has recently investigated the effect of an alternative model based on the assumption of zero concentration in the adjacent fracture. The effect of this alternative assumption on the breakthrough curve computed along a single pathway is shown to be very modest. Nevertheless, this alternative model has an important conceptual implication, as part of the solute advecting along a fracture may diffuse and start to advect along adjacent fractures.
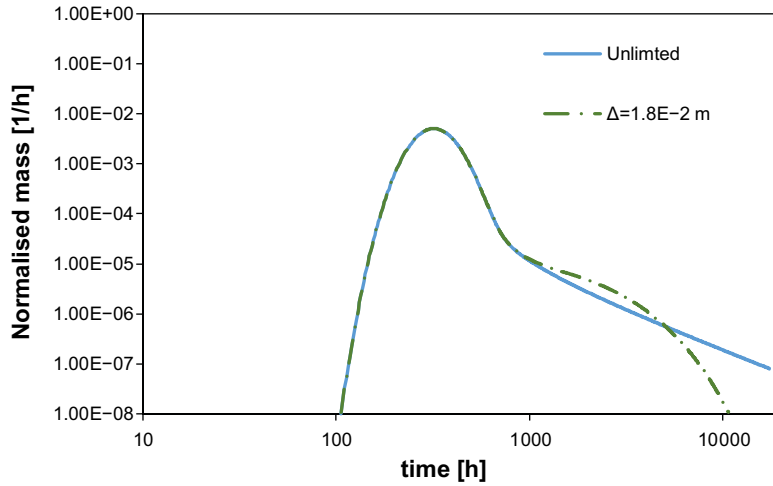
Figure 9-1. *Breakthrough curve of a non-sorbing radionuclide computed using unlimited and finite matrix ($\Delta = 1.8 \times 10^{-2}$ m). Parameters of the model are based on experiment WPDE-1. Source: Posiva, Poteri et al. (2018).*

9.1.3 Flow related properties and fracture-matrix coupling

We have already noted in the previous subsection that the radionuclide breakthrough curve at the fracture outlet (Equation (9-13)) depends on properties related to the hydrodynamic conditions in the water conducting fracture; namely the flow-wetted surface area and the fracture volumetric flow rate, which are lumped in a parameter denoted as F-factor. We have also discussed that the F-factor is equivalent to the Lagrangian expression denoted as transport resistance or β value.

Transport pathway delineation carried out using DFN models samples single fracture segments and thus transport resistance is defined on a segment-basis using the computed groundwater travel time and the assigned fracture half aperture (b), as shown in Equation (9-11). When using ECPM formulations, the F-factor is computed based on contributions from multiple intersecting fractures. This can be done using the following integral that is expressed in terms of local flow wetted surface:

$$ fquo = \int_{t_0}^{t} \frac{fws}{frevol} dt \qquad \text{Equation (9-16)} $$

where *fws* [L^2] is the local flow wetted surface and *frevol* [L^3] is the local free volume (i.e., fracture-filling water volume) along the particle trajectory. Equation (9-16) can be re-written as:

$$ fquo = \int_{t_0}^{t} \frac{SSA_b}{\epsilon} dt = \int_{t_0}^{t} SSA_f dt \qquad \text{Equation (9-17)} $$

here SSA_b [L^{-1}] is the bulk specific surface area, defined as the total flow wetted surface area per unit bulk volume of rock, SSA_f [L^{-1}] is the fracture specific surface area, defined as the total flow wetted surface area per unit fracture volume and ϵ [$-$] is the fracture volume fraction, defined as the ratio between the fracture volume and the bulk volume of rock. In Equation (9-17), the three parameters are defined in a local sense, i.e., relative to the size of the grid cells of the continuum model. It is worthwhile noting here that $SSA_b = 2P_{32}$. The factor of 2 is required since transport simulations and all the related quantities acknowledge the existence of two surfaces per each fracture, separated each other by the fracture volume whereas P_{32} treats fractures as planar objects. It is worthwhile noting that the aforementioned relation between SSA_b and P_{32} assumes a parallel plate model. In real fractures a correction factor is needed (Gylling et al. 1999). These few paragraphs highlight the importance of carefully characterising the connected P_{32} and the fracture volume fraction to properly capture mass exchange mechanisms between the fracture and the matrix.

Based on statistical and geometrical considerations Gylling et al. (1998a) showed that the specific flow-wetted surface area (*FWS* [L^{-1}]) can be directly estimated from the intersection frequency between boreholes and water conducting fractures, see Section 6.1 and Chapter **7**.

9.1.4 Processes specific for radionuclide transport

We have discussed in Subsections 9.1.1 and 9.1.2 transport mechanisms that control the migration of radionuclides in fractured media; namely: advection, in-plane dispersion and matrix diffusion. Other processes that may affect the fate of a radionuclide are:

- Sorption onto the fracture surface and/or in the rock matrix.
- Radioactive decay and ingrowth.
- Anion exclusion.
- Diffusion into stagnant water in the fracture.

The first three processes are general transport processes that can take place in both the fracture and pore water and hence are described in **TRPMM**. The fourth process is taking place only within fracture openings and so dealt with here.

Diffusion into stagnant water

Anionic species have a lower tendency to diffuse into the rock matrix due to electrostatic mechanisms that result in the so-called anionic exclusion effect. It turns out that negatively charged radionuclides pose the most serious challenges in terms of final radiological risk. For instance, in SR-Site, I-129 was one of the highest dose contributors (SKB 2010d). Nevertheless, SR-Site transport calculations of anionic species may have been over-conservative as a potential additional retention mechanism was not considered: the diffusion from the water conducting part of the fracture into the adjacent stagnant water in the same fracture (denoted diffusion into SW, from now on). Diffusion into stagnant water is strongly related to the channelling effects discussed in Section 8.5.

Analytical solutions for transport in fractured rock with diffusion into SW have been provided by Neretnieks (2006) (unlimited extent of matrix and stagnant water), Mahmoudzadeh et al. (2013) (limited extent of matrix and stagnant water with layered matrix) and Shahkarami et al. (2015) (decay chain for a channel with finite matrix and stagnant water).

Figure 9-2 shows the concentration of a non-sorbing tracer computed at the outlet of a 10-m flowpath, considering two different channel half widths (W [L]) (results taken from Neretnieks (2006)). The results show that the retention capacity of the stagnant water is strongly related to a new hydrodynamic control parameter analogous to the β value presented in Equation (9-11), which is defined as

$$\beta_{SW} = \frac{t_{gw}}{W} \qquad\qquad\qquad \text{Equation (9-18)}$$

notice that $P_{32,w} = 1/W$ [L^{-1}] is the specific surface area of the stagnant region. For relatively large channels the retention of diffusion into stagnant water is modest, whereas for narrower channels the effect of stagnant water is significant. The retention capacity of the stagnant water is also strongly dependent on the available extent of stagnant water in the fracture, which is typically conceptualised as the half distance between flowing channels (W_W [L]) (see Figure 9-3).

All the models discussed in this subsection assume that flowing channels are perfectly regular geometrical entities surrounded by completely motionless water in the stagnant region. However, reality is much more complex as water flows along irregular channels (Figure 8-7) and velocity is heterogeneously distributed in the fracture, which makes it difficult to draw an exact geometrical boundary between flowing and stagnant region. Thus, many efforts are being made to derive credible effective parameters that describe the mutual interplay between diffusion into the matrix and in the SW. Recently, Cvetkovic (2017b) presented a preliminary framework for the dynamic characterisation of the specific surface area of fracture networks. The key of the framework is the use of different sources of data ((i) flow rate data as obtained by a flow logging procedure; (ii) transmissivity data as obtained by pumping tests and (iii) fracture network data as obtained from outcrop and geophysical observations) along particle tracking calculations to infer statistical distributions of P_{32} and $P_{32,w}$ for use in radionuclide transport simulations. Other on-going efforts by Zou and Cvetkovic are focused on quantifying the influence that non-perfectly motionless water in the stagnant region has on radionuclide retention.
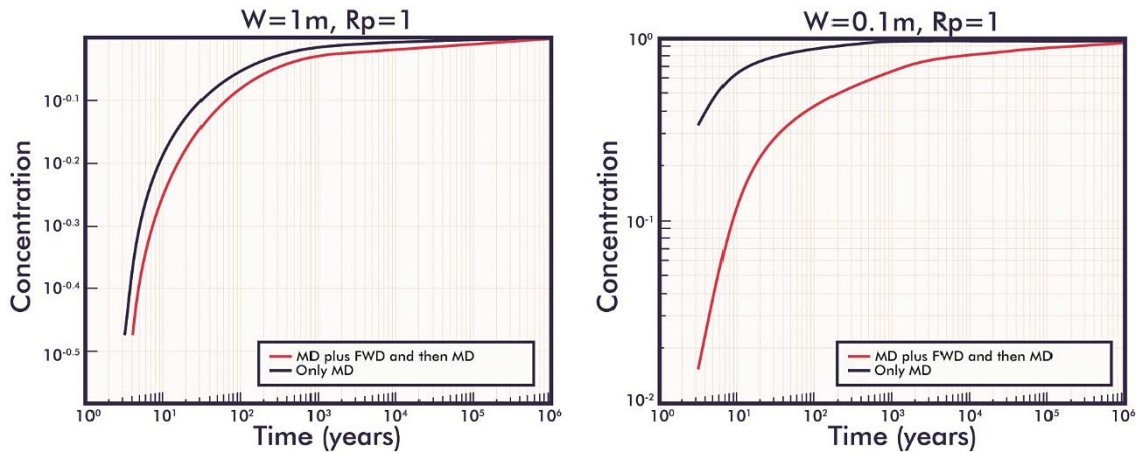
Figure 9-2. *Concentration computed at the outlet of a 10-m flow path for (left) a channel half width (W) of 1 m and (right) a channel half width of 0.1 m. MD = matrix diffusion, FWD = fracture water diffusion (reworked from Figure 7 in Neretnieks (2006)).*
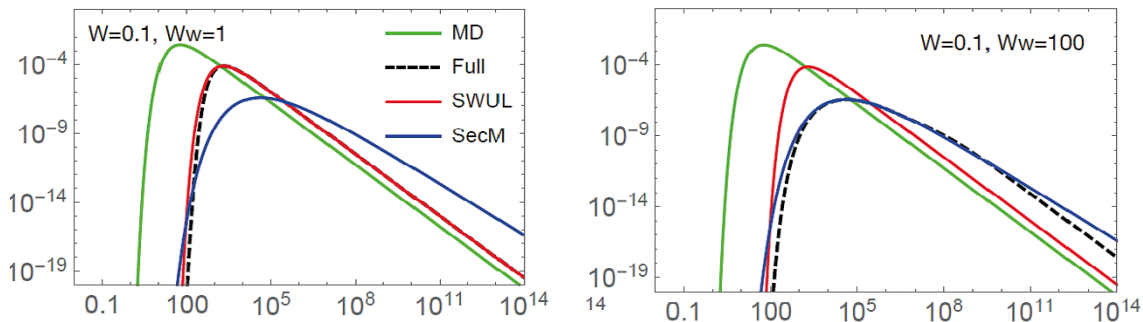
Figure 9-3. *Concentration computed at the outlet of a flow path with half width W = 0.1 m and with extent of the stagnant water equal to (left) $W_W = 1$ m and (right) $W_W = 100$ m right. The groundwater residence time is set to $\tau = 40$ y and the half fracture aperture is $b = 1.3 \times 10^{-4}$ m. Results are computed (MD – green continuous line) considering only diffusion into unlimited matrix; (Full- black-dashed line) considering the full solution with diffusion into unlimited matrix, diffusion into SW and secondary diffusion from stagnant water into the matrix; (SWUL – red continuous line) neglecting secondary diffusion and (SecM – blue continuous line) considering secondary diffusion but neglecting diffusion into stagnant water. From Cvetkovic (personal communication).*

9.1.5 Structural framework for transport properties and transport classes

Transport classes

Single open fractures typically have a discontinuous thin layer of secondary minerals, such as chlorite, calcite and mixed clay minerals. Precipitation of these secondary minerals has occurred during different time epochs due to, e.g. hydrothermal or low temperature alteration processes. In drill cores from the Forsmark site, it is common to observe "old" fractures completely sealed by filling material of hydro-thermal origin intersecting more recent fractures with filling material formed at low temperature. The variety of different alteration and reactivation processes explains why coating minerals are heterogene-ously and sparsely distributed in a patchwork like arrangement. Beyond the coating layer, if present, there may be an alteration rim that sometimes is visible by red staining due to the precipitation of oxide and hydroxide minerals. At Forsmark, the absence of minerals is recognised in about 2 % of fractures, and a small fraction of fractures lack a recorded mineral type in the earliest investigation holes.

Based on mineral mapping on open fractures, Byegård et al. (2008) identified eight different fracture groups, with related properties of fracture thickness and wall rock alteration (see Figure 9-4). In Crawford (2008), these fracture groups were related to retardation properties. For some of these groups, sorption coefficients were defined in terms of probability distribution functions for specific

radionuclides and specific hydrochemical conditions. The distribution and statistical frequency of each fracture group was analysed by Byegård et al. (2008) for the ensemble of open fractures (Figure 9-5 left), for the water conducting fractures only (Figure 9-5 right) and for transmissive fractures inside deformation zones (transmissive fractures were identified by means of PFL measurements) as a function of depth. A similar analysis, but with all open fractures grouped together, was carried out for different fracture domains (Figure 9-6).

A slightly different approach was used by Löfgren and Sidborn (2016) to assess the distribution of fracture minerals at Forsmark and Laxemar. In this work, mapped coating minerals were analysed individually by means of both parametric and non-parametric statistical methods and suggested cumulative distribution functions were provided (Figure 9-7).

In the recent DFN modelling report in support of Olkiluoto Site Description 2019 (ODFN3, from now on), transport classes were identified in a similar way to what was done in SR-Site; i.e., relating transport classes with hydrothermal filling systems. These filling systems were in turn restricted to three specific alteration events.

	Fracture coating	Thickness*	Wall rock alteration	Example	Mainly found in fracture generations, Subsection 4.2.1
A	**Chlorite + Calcite**	≤ 0.5 mm	Fresh		2, 3
B	**Chlorite + Clay** ± *Epidote* ± *Prehnite* ± *Calcite*	~1 mm	Altered ~1 cm		2, 3, 4
C	**Chlorite + Hematite** ± *other*	< 0.5 mm (0.1 mm)	Altered 0.5 cm		1, 2
D	**Chlorite** ± *other*	< 0.5 mm (0.1 mm)	Fresh		1, 2, 3, 4
E	**Laumontite** ± *Calcite* ± *Chlorite* ± *Clay*	0.1–2 mm	Altered 1–5 cm		2
F	**Calcite** ± *Quartz* ± *Pyrite* ± *other*	0.,1–2 mm	Fresh		3
G	**Clay** ± *other*	1–5 mm	Altered ≥ 5 cm		3.4
H	**No mineral**		Fresh		Not known

Figure 9-4. Fracture transport classes identified for the retardation model of SDM-Site (Byegård et al. 2008).

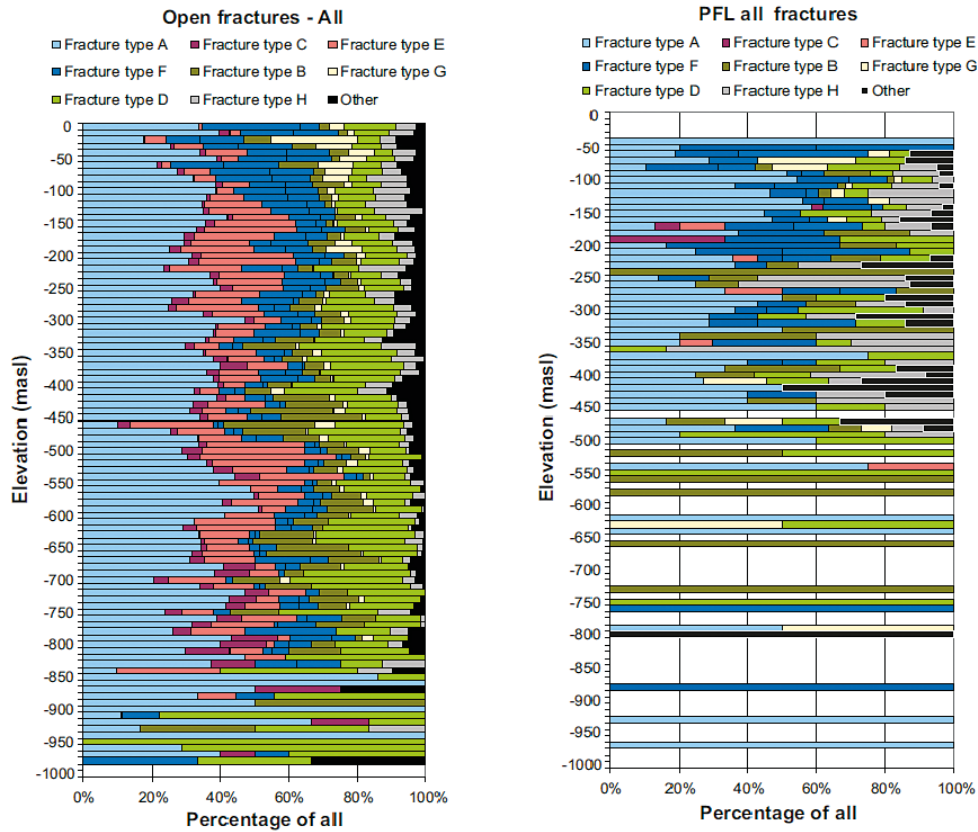**Figure 9-5.** *Relative frequency of different fracture types in (left) all open fractures at various elevations at the Forsmark site and (right) for all transmissive fractures as identified by PFL measurements. Figure modified from Byegård et al. (2008).*
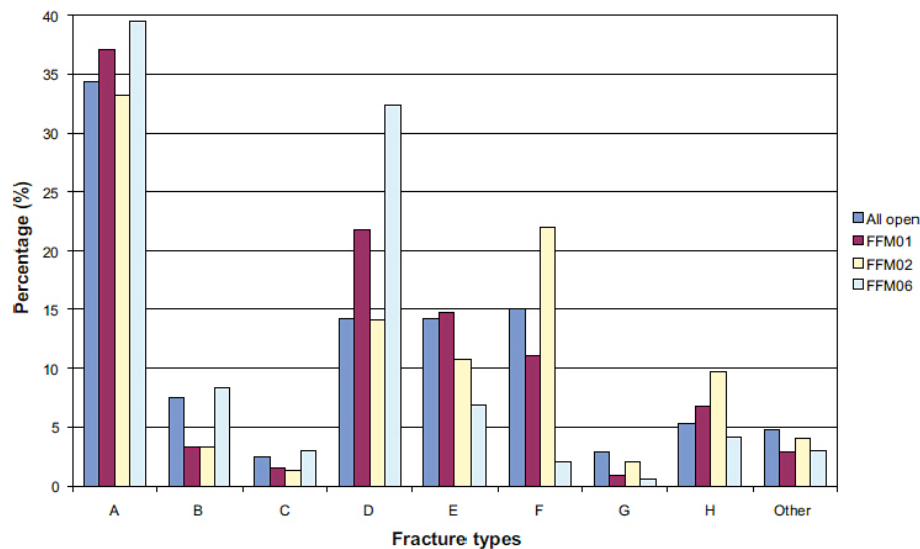

Figure 9-6. *Distribution of the different fracture types within different fracture domains at the Forsmark site. Figure taken from Byegård et al. (2008).*
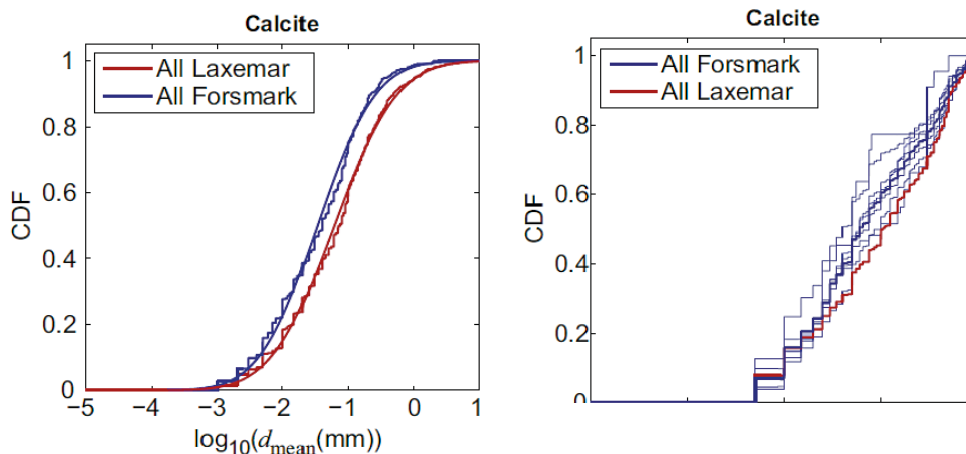
Figure 9-7. *Cumulative distribution function for (left) calcite coating thickness and (right) calcite coverage. Modified from Figures 5 and 6 in Löfgren and Sidborn (2016).*

Structural framework for property description

Despite the considerable effort placed in characterising fracture classes for the Forsmark site, the radionuclide calculations carried out for SR-Site (SKB 2010d) were based on aggregated values of τ and β, meaning that structural heterogeneity along a flow pathway was basically neglected. Uncertainty was assessed by means of Monte Carlo simulations in which aggregated retardation properties were drawn from probability distribution functions defined at the scale of a single fracture. This simplified approach was motivated by operational limitations of the numerical tools available at the time when the safety analysis was performed. Since then, the computer codes for radionuclide transport modelling, and in particular the particle-based code MARFA, have evolved and are now prepared to easily accommodate flow pathways built upon several different transport classes. More specifically, the DFN flow model provides an ensemble of particle pathways that are defined by successive fracture segments, each marked by a specific identifier. In MARFA, these identifiers can in turn be linked to specific transport classes (rock types in MARFA's notation) (Figure 9-8).

It is highly suggested that radionuclide transport simulations carried out in future safety assessment studies take profit of the significant operational improvement of computer codes discussed above and incorporate explicitly the comprehensive information of fracture types (and related transport classes) currently available (e.g. Byegård et al. 2008). However, transport classes are not explicitly resolved by the DFN flow model, whose level of granularity is limited to generic geological structures (e.g. fracture domains, deformation zones, etc). Thus, a probabilistic framework, establishing a link between transport classes and generic geological structures or lithologies, need to be formulated. To this end, it is useful to examine the implementation of transport classes as done in ODFN3, where the database of water conductive fractures was split in four different geologic structures (altered BFZ, other BFZ, PGR/MFGN, other), two different depths (above and below –200 m) and four different orientation of maximum principal stress. This split dataset was then used to define probability lookup tables (see example in Figure 9-9), which were used to sample the transport class conditioned on the geologic structure to which the considered fracture segment belongs to. A similar micro-structural framework was used in a semi-synthetic model of block scale conductive structures at the Äspö HRL (Dershowitz et al. 2003b). An approach based on statistical sampling of transport classes could be used in future transport calculations for the Forsmark site.
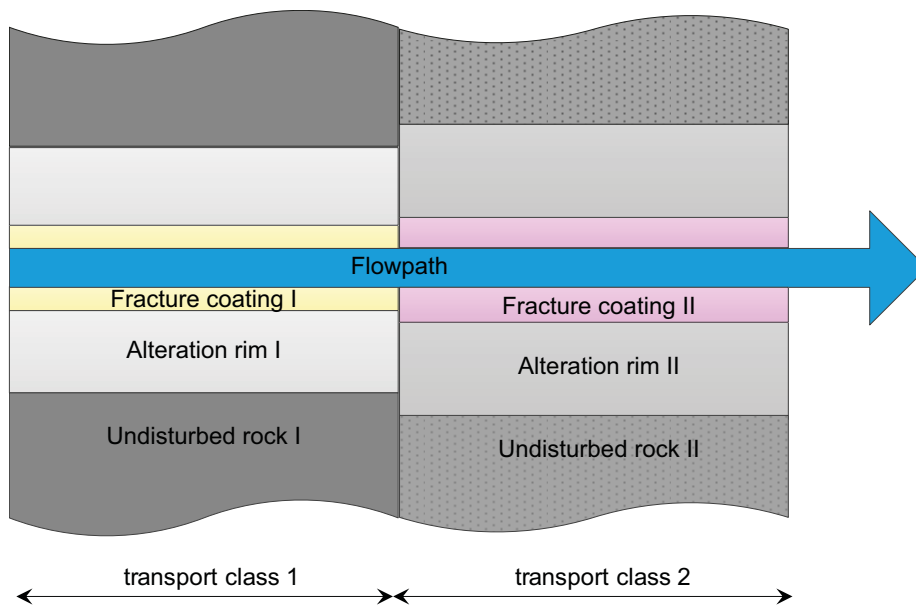
Figure 9-8. *Sketch of a flow pathway traversing two different transport classes (figure modified from Crawford and Löfgren (2019)).*

Minerals	Altered BFZ	Other BFZ	PGR/MFGN	Other
Above −200 m				
EW/NW – HT1	36 %	31 %	18 %	18 %
EW/NW – HT2/3	57 %	56 %	58 %	74 %
EW/NW – NHT	7 %	13 %	24 %	8 %

Figure 9-9. *Part of the lookup table used in ODFN3 to assign transport classes (Hartley et al. 2018b).*

Transport in deformation zones

Byegård et al. (2008) have identified four different types of altered bedrock as recurrent units within (or close to) deformation zones (Figure 9-10). Some of these units are thought to be commonly abundant in deformation zones, while other are less common but still have a significant importance for the overall retention capacity of the deformation zone.

On a larger scale, since ODFN3, deformation zones are explicitly represented by Posiva as swarms of individual fractures stochastically generated according to an exponential distribution of fracture centres around the core of each fault (Hartley et al. 2018b). Due to high computational costs, it is probably not feasible to use this explicit swarm representation of deformation zones to carry out all the particle tracking transport calculations required in a typical radionuclide transport simulation for a safety assessment study. Thus, an on-going project is focused on assessing possible strategies in which the deformation zone is simplified as a single collapsed plane (or an ECPM) and the transport heterogeneity of the fracture swarm is preserved by means of a downscaling algorithm (Painter and Cvetkovic 2005).

Regardless of the way deformation zones are represented in DFN flow models, their parameterisation in transport models is complex because deformation zones are very heterogeneous and most of them have been reactivated during different geological events and are characterised by a broad range of alteration types. Besides the alteration units shown in Figure 9-10 (which are related to corresponding transport classes in Subsection 4.5.3 of Crawford and Löfgren (2019)), the eight different fracture types discussed in the paragraph above may coexist within the same deformation zone. Byegård et al. (2008) showed an illustrative yet comprehensive example of how a description of a borehole intercept with a deformation zone (namely, ZFMA2) can be transferred for use in a retardation model. A similar approach can be used to construct look-up tables, conditioned on specific deformation zones

and e.g. different elevations, for use in radionuclide transport calculations. This look-up table can be probabilistically sampled to describe the transport class of a segment lying within a deformation zone in the same operational way as described in the paragraph above.

1) Strongly altered (tectonized and partly incohesive) wall rock, "fault rock".

   Altered rock fragments with varied mineralogy dependent on host rock. Chlorote, saussurite and clay are generally present.

   Potential impact on retardation: Partly very fine-grained material which may have significantly increased surface areas available for adsorbtion.

   Estimated occurrence[A]: Sparsely.

2) Sealed fracture networks, mainly with breccia and cataclasite. Different fracture fillings such as laumontite + calcite, epidote, chlorite.

   Potential impact on retardation: Increased porosity in the sealed fractures may constitute fast diffusion pathways.

   Estimated occurrence[A]: Relatively common.

3) Rock exposed to quartz dissolution, Vuggy rock.

   Potential impact on retardation: Extreme with respect to porosity due to the large voids in the material, may constitute fast diffusion pathways.

   Estimated occurrence[A]: Sparsely.

4) Oxidized wall rock, mainly medium or strong degree of alteration.

   Potential impact on retardation: Extreme with oxidized surfaces which may have an impact on adsorbtion of radionuclides influenced by surface complexation.

   Estimated occurrence[A]: Relatively common.

Figure 9-10. *Identified units inside deformation zones (figure taken from Byegård et al. (2008)).*
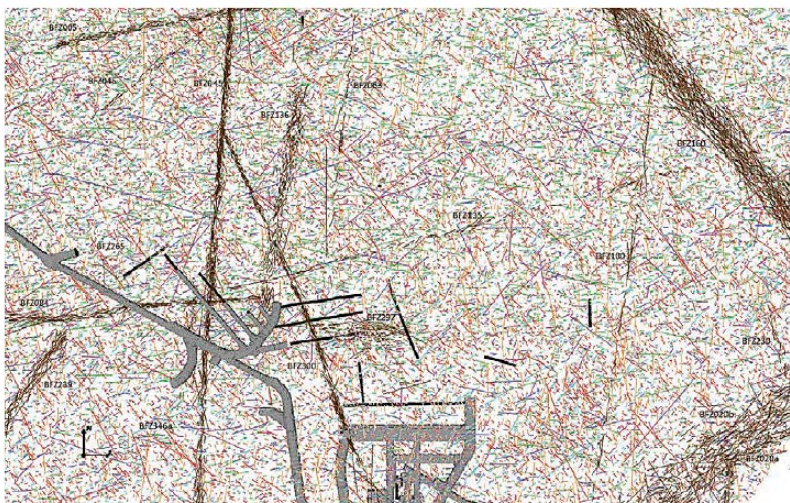
Figure 9-11. *View of different deformation zones in a slice at z = −420 m through Posiva's ODFN3 of the Olkiluoto site, Finland. Source: Posiva, Hartley et al. (2018b).*
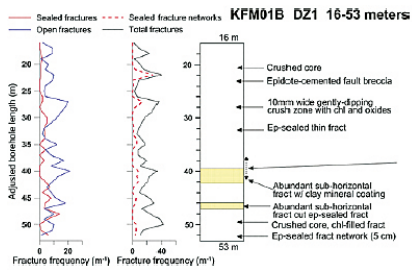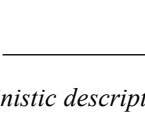
Fracture type/ Deformation zone unit	Percentage of open fracture (n = 259) for some of the fracture types in the zone intercept	Percentage of the borehole length in the zone intercept (37 m)
Fracture type A, **Chlorite + Calcite**	10 %	
Fracture type B, **Chlorite + Clay** ± epidote ± prehnite ± calcite	12 %	
Fracture type D, **Chlorite ± other**	15 %	
Fracture type F, **Calcite** ± quartz ± pyrite ± other	17 %	
Fracture type G, **clay** ± others	23 %	
Fracture type H and **group "others"**	12 % and 10 % respectively	
Oxidized wall rock, medium to strong degree of alteration (transition zone)		16 %
Fault rock (core)		Not estimated* (crush rock 5.5 %)
Sealed networks with **breccia and cataclasite** (core and transition zone)		3 %

Figure 9-12. *Example of how a deterministic description of a borehole intercept with a deformation zone can be used to define look-up table for the transport model (figure taken from Byegård et al. (2008)).*

Additional data

Fracture filling minerals, such as chlorite or clay minerals, have the potential to retard radionuclides due to sorption mechanisms, which are surface-mediated processes and thus depend on the available mineral surface area. Radionuclide sorption is typically stronger in the rock matrix, due to the larger available pool of sorption sites (larger mineral surface area). However, surface sorption may be not negligible and thus need to be properly accounted for in transport calculations. Appropriate K_a [L] values for a fracture entirely covered by a pure mineral phase ($C_{vis}^i = 1$) can be obtained by means of mechanistic reactive transport modelling and the related surface sorption coefficient for a given fracture segment can be probabilistically defined as:

$$K_a^{i,k} = \sum_{i=1}^{M} c_{vis}^j K_a^k \qquad \text{Equation (9-19)}$$

where K_a [L] is the surface sorption coefficient (as defined in Subsection 9.1.4), C_{vis}^j [-] is the coverage of mineral j, which is drawn from a corresponding probability distribution function (e.g. see Figure 9-7, right), M is the total number of pure mineral phases considered and indexes i and k indicate, respectively, the fracture segment and the geochemical condition representative of the computed value of surface sorption (e.g. Littorina water, brackish water, etc). K_a values can be updated in time as geochemical conditions evolve using the smart-K_d approach described in Subsection 9.3.2.

Fracture filling minerals, and in particular reduced iron-bearing minerals, are also important buffers against the infiltration of oxygenated water. Recently, Trinchero et al. (2017) presented an ECPM-based DFN-consistent numerical framework for the evaluation of these buffering mechanisms. The results of their reactive transport calculations (Figure 9-13) showed that chlorite, present in the fracture filling, is a very strong buffer against the infiltration of oxygenated glacial melt-water. Despite being based on a somewhat simplified model set-up, this modelling work shows how statistical information on fracture filling minerals (namely, probability distribution functions describing abundance of chlorite in fracture filling , as provided in Löfgren and Sidborn (2016)) can be included in reactive transport models to evaluate the buffering capacity of the medium.

a)

b)
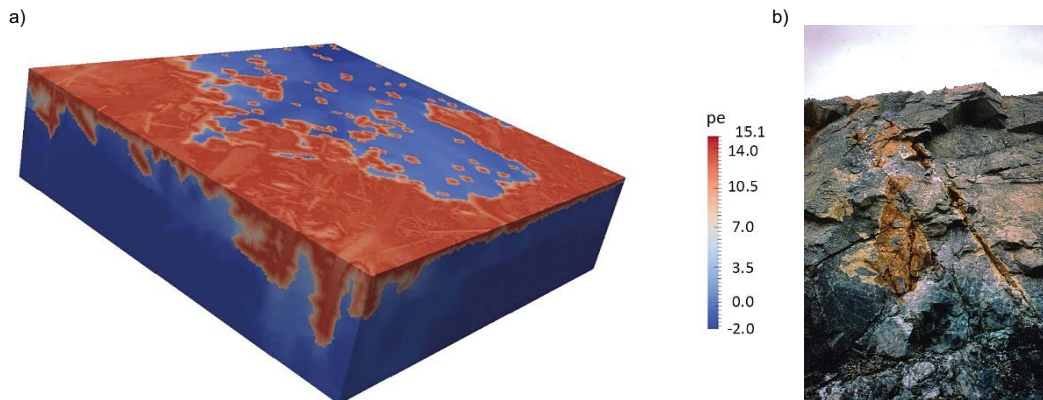
Figure 9-13. (a) Redox potential computed at time 340 (modified from Trinchero et al. (2017)). (b) Oxidised front (light brown) in the Osamu Utsumi uranium mine at Poços de Caldas (Brasil). The scale of the photography is 10 m, approximately. Source: Photography courtesy of the Swedish Nuclear Fuel and Waste Management Co (SKB).

General workflow

The general workflow for the definition of a structural framework for transport properties and transport classes is shown in Figure 9-14, noting that the development/definition of transport classes is described in more detail in **TRPMM**. The workflow is based on a stepwise approach, initially identifying several transport classes based on a framework of the mineral age of fracture infill. Spatial analysis of these classes provides statistics of transport classes by domain, by depth or whether inside or outside deformation zones and supports a preliminary spatial model for the transport class. The typical mineral assemblages in each of these transport classes can also be defined. Alongside this analysis, core samples can be analysed to describe the transport properties of the rock adjoining conductive fractures, including porosity profiles, diffusivities and intact rock mineralogy and alteration. Finally, the above are combined to provide a conceptualisation of transport classes and properties, including how these overlay the spatial framework already identified.

Once underground (e.g. during construction) the above framework for conceptualising transport classes and transport properties can be reviewed in light of the additional data available. For example, it is anticipated that the sub-horizontal excavations during construction will enhance the dataset of sub-vertically orientated structures, which have previously been under sampled due to the inherent orientation bias of surface based drillhole observations.
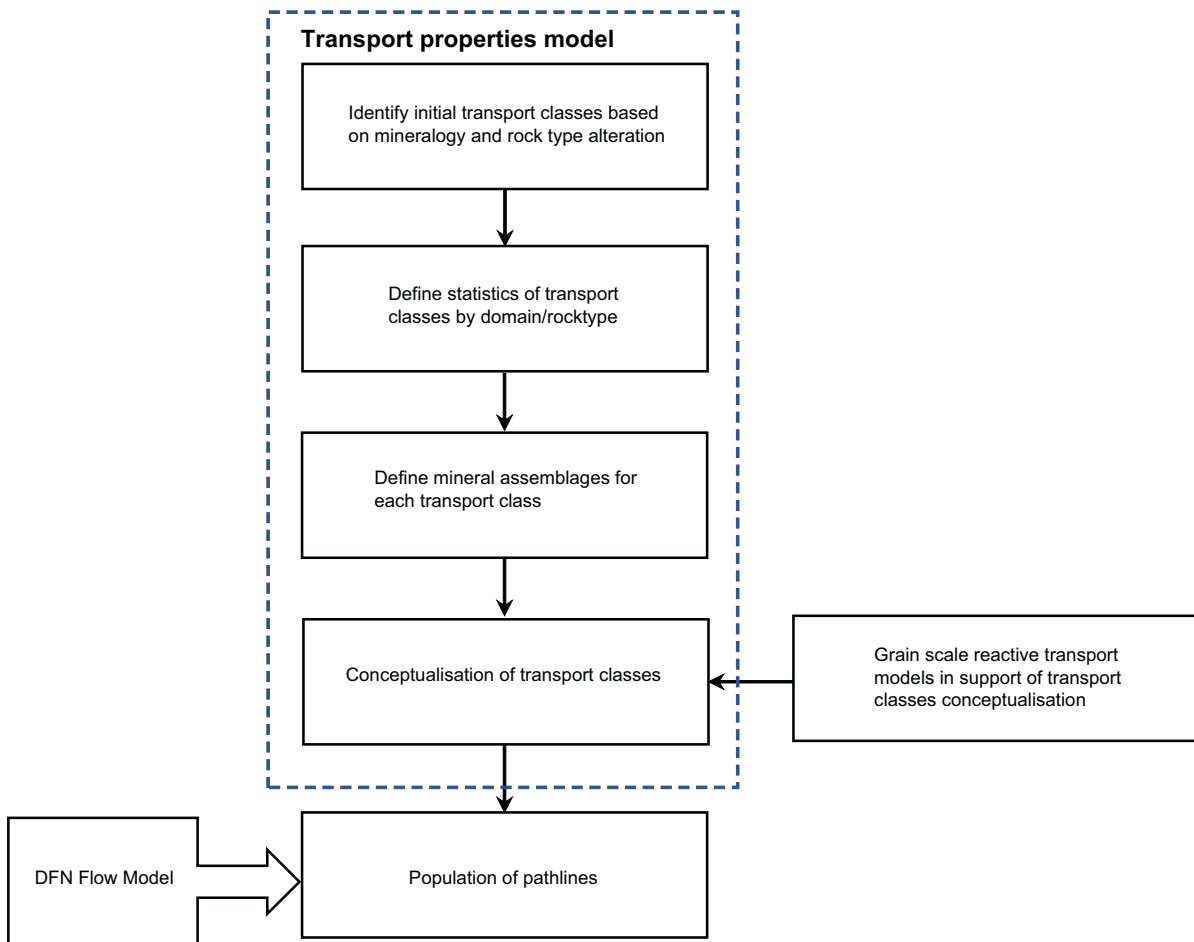
Figure 9-14. *General workflow for the formulation of the structural framework for transport properties and transport classes.*

9.2 Sources of supporting site data

9.2.1 Core interpretation and lab-scale characterization methods

Although they do not have a direct implication for transport parameters, fracture filling minerals may be related to hydrothermal alteration events, which may in turn be linked to specific transport classes (see Subsection 9.1.5). Moreover, the amount and spatial distribution of e.g. reduced iron-bearing minerals provides important information about the buffering capacity of the system. The determination of fracture filling minerals is usually done based on visual inspection (Figure 9-15), although the resulting information can be complemented by means of data based on digital image analyses of photographed drill core samples. Besides, qualitative information, Löfgren and Sidborn (2016) have mapped 2 071 open fractures in drillcores at Forsmark and provided quantitative information about: (i) visible coverage of layer, (ii) total coverage of layer and (iii) thickness of the mineral layer. The interpretation was analysed statistically, and recommended probability distribution functions (PDFs) were provided for use in reactive transport modelling. Recently, Trinchero et al. (2017) have used these PDFs to study the buffering capacity of the system against the infiltration of oxygenated glacial melt-water.

Lab-scale characterisation methods are used to characterise the properties of the rock matrix; namely porosity and effective diffusivity. The first parameter can be estimated by direct measurements (e.g. water saturation method or ^{14}C-PMMA method) while the second need to be indirectly inferred from lab experiments or measurements (e.g. through diffusion experiments or electrical resistivity measurements).

The total porosity of the rock matrix is typically divided into a connected and an unconnected part (Selnert 2008). The connected part is usually related to the void space around mineral grains while the unconnected part is usually associated to the intra-granular porosity. Svensson et al. (2018) showed that this division is somewhat artificial. Based on measurements and observations they interpreted the total porosity as being divided into three types: (i) relatively large micro-fractures that may transect mineral grains, (ii) inter-granular grain boundary pores and (iii) intra-granular pore space. The authors showed that all these three types may partly contribute to the bulk diffusive properties of the rock matrix. Thus, here we will use the term "diffusion-available porosity" to refer to the values of porosity obtained from lab-scale characterisation method (although the generic term "porosity" is used in the rest of the document; see e.g. Equation (9-13)). Notice also that the diffusion-available porosity may be radionuclide specific.

Figure 9-15. *Open fractures of borehole KFM09B at Forsmark, at borehole lengths 226 m, with coating of laumontite, calcite, pyrite, and quartz (figure modified from Löfgren and Sidborn (2016)).*

The most common method to measure the porosity of a rock sample is the water saturation method, which consists in first drying the sample and then saturating it by water in vacuum. Differences in weight are used to estimate the bulk porosity. Alternatively, diffusion-available porosity can be estimated using the ^{14}C-PMMA (PolyMethylMethAcrylate) method (Hellmuth and Siitari-Kauppi 1990), which consists in obtaining an autoradiograph of the ^{14}C-PMMA impregnated sample, which in turn provides a map of the diffusion-available pore space.

Effective diffusivity is most often determined by means of through-diffusion experiments, in which a thin slice of a drill core is placed between two chambers (see Figure 9-16). A synthetic groundwater tagged with a radionuclide (usually tritiated water, HTO) is placed in one chamber, while the raise in radionuclide concentration is observed in the second chamber (observation chamber, from now on), which initially contains radionuclide-free water. Using an analytical solution originally derived by Carslaw and Jaeger (1959), Skagius and Neretnieks (1986) provided the following mathematical expression that describes the increase in concentration in the observation chamber:

$$C_r = \frac{D_e t}{l^2} - \frac{\alpha}{6} - \frac{2\alpha}{\pi^2} \sum_{n=1}^{\infty} \frac{(-1)^n}{n^2} exp\left\{ -\frac{D_e n^2 \pi^2 t}{l^2 \alpha} \right\} \qquad \text{Equation (9-20)}$$

where l [L] is the length of the rock sample. At late times the expression reduces to:

$$C_r = \frac{D_e t}{l^2} - \frac{\alpha}{6} \qquad \text{Equation (9-21)}$$

In Equation (9-20) and Equation (9-21), the capacity factor is defined as:

$$\alpha = \phi + K_d \rho_d \qquad \text{Equation (9-22)}$$

where K_d [L^3·M^{-1}] and ρ_d [M·L^{-3}] are the distribution coefficient and bulk rock density. It is evident that for a non-sorbing radionuclide (like HTO) the rock capacity factor is equal to the diffusion-available porosity. By fitting Equation (9-20) or Equation (9-21) to the experimental data one can obtain an estimation of both the rock capacity factor and the effective diffusion coefficient.

We have already shown in Equation (9-14) that the effective diffusion coefficient is related to the molecular diffusion coefficient in unconstrained solution through the formation factor, F_f [-], which depends only on properties of the rock matrix. The formation factor can be estimated as (Selnert 2008):

$$F_f = \frac{\rho_w^e}{\rho_s^e} \qquad \text{Equation (9-23)}$$

where ρ_w^e and ρ_s^e are, respectively, the electrical resistivity of the soaking water and the saturated rock sample measured at 0.1 Hz. Electrical resistivity is the reciprocal of electrical conductivity and its SI units are ohm-metre (Ω·m). The formation factor inferred from electrical resistivity measurements can then be used to obtain estimations of effective diffusivity using Equation (9-14).
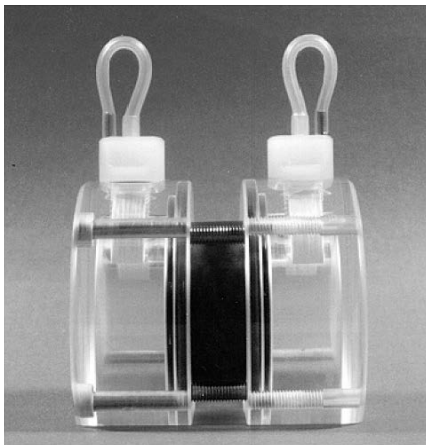
Figure 9-16. *Photograph of a rock sample assembled in a diffusion cell (figure taken from Selnert et al. (2008)).*

9.2.2   In situ tests

In situ tracer tests can be performed either in hydraulically conductive fractures or in the rock matrix adjacent to an investigated borehole. As pointed out in the very comprehensive review by Löfgren et al. (2007), field-scale tracer tests are mostly intended to support and corroborate the current conceptual understanding of solute transport in fractured media, although results of such field experiments can provide also important quantitative information about aggregated quantities that involve both matrix diffusion properties (9.1.2) and flow-related parameters (9.1.3). We have already discussed that the analytical solution for advective transport along a single fracture with infinite matrix (Equation (9-13) and Equation (9-10)) is a function of the product of the material parameter group (κ) and the transport resistance (β). In field experiments, radionuclides are typically injected as a short pulse (see Löfgren et al. (2007) for a comprehensive discussion about the injection mode), thus it is convenient to look at the unit response function, that at late times can be approximated as:

$$\gamma \sim \frac{\kappa\beta}{2\sqrt{\pi}} t^{-3/2}$$

Equation (9-24)

Equation (9-24) tells us two things:

1. In a log-log plot, the breakthrough curve shows a linear tailing with slope equal to $-3/2$ (see also Haggerty et al. (2000)).

2. The level of the tailing is directly dependent on $\kappa\beta$.

Point 1 above is particularly important for process understanding, as evidence of the $-3/2$ late-time slope is used to demonstrate the effectiveness of matrix diffusion as a retention process. Point 2 above is also important as provides a direct and simple way to estimate the lumped product of the material parameter group and the transport resistance. Decoupling κ from β requires some complementary information or assumption. Cvetkovic and Cheng (2002) interpreted data of the TRUE Block Scale experiment (Poteri et al. 2002) at the Äspö HRL by establishing a linear functional relationship between the transport resistance and the groundwater residence time. The empirical constant of this relationship was inferred using breakthrough curves of non-sorbing radionuclides and the resulting transport resistance was used to obtain estimates of κ for non-sorbing and sorbing radionuclides. Recently, Cvetkovic (2017a) has presented a statistical formulation of generalised tracer retention in fractured rock. The formulation has been used to infer key parameters of tracer retention (namely, the mean groundwater residence time and the diffusion-sorption forward rate) using both a lab-scale and an in situ tracer test (Cvetkovic et al. 2020). This new interpretation approach was motivated manly because it provided an improved understanding of the coupled hydrodynamic and retention processes, and the resulting parameters can in principle be used in site-scale radionuclide transport simulations.

In situ resistivity measurements can be used to infer fracture aperture and effective diffusivity of the rock matrix (see Appendix A of SKB 2010a). A sketch of the tool used to carry out these measurements is shown in Figure 9-17. The red square in the figure indicates the electrode that sends out the electrical current. Other electrodes are needed to force the current to be normal to the borehole axis. The orange curve in the same figure shows the resistivity log, with the minimum value indicating the presence of a water bearing fracture. Fracture aperture can be estimated as:

$$2b^e = \rho_w^e L_m \left(\frac{1}{\rho^e} - \frac{1}{\rho_r^e} \right)$$

Equation (9-25)

where L_m [L] is the thickness of the investigated section and ρ_w^e, ρ_r^e and ρ^e are, respectively, the resistivity of the groundwater in the fracture, in the non-fractured rock-matrix and the measured resistivity (superscript e indicates that the fracture aperture has been estimated by means of resistivity measurements). Equation (9-25) should be corrected when the fracture plane is not normal to the borehole axis.
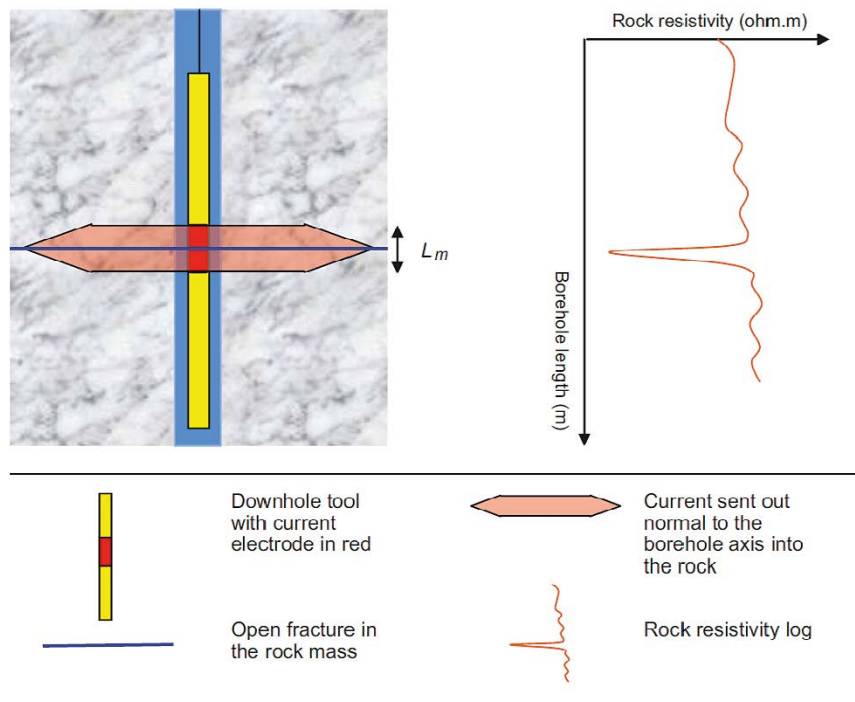
Figure 9-17. *Sketch of the tool used to perform* in situ *resistivity measurements (figure taken from SKB 2010a).*

9.3   Modelling methods for application

9.3.1   Overview of modelling approaches

Analytical models for solute transport in fracture networks are based on solutions derived for single fractures. The solution for the basic model of transport in a single fracture and diffusion in an infinite matrix (unlimited diffusion) was first presented by Neretnieks (1980), based on existing solutions for heat diffusion across parallel plates (Carslaw and Jaeger 1959). Tang et al. (1981) generalised this solution by including dispersion in fracture (in-plane dispersion) while Sudicky and Frind (1984) added the effect of limited matrix extent by means of a conceptualisation based on a symmetric system of parallel fractures. Both Tang's and Sudicky's solutions are provided in both Laplace space as well as in ordinary geometric space and they include also the effect of decay (but not a decay chain). Maloszewski and Zuber (1990) extended the solution of Neretnieks (1980) by including kinetic sorption. Cvetkovic (2010) derived an analytical solution for a single fracture and a limited matrix constituted by different layers with different properties. This solution was based on a previous recursive formulation presented by Ash et al. (1965). Neretnieks (2006) derived a semi-analytical solution (i.e., a solution in Laplace space) for transport in a single fracture and diffusion into both infinite matrix and infinite stagnant water. This solution, which included the so-called "secondary diffusion" (i.e., diffusion from stagnant water into the matrix), was further extended by Mahmoudzadeh et al. (2013), who accounted for the limited extent of bath matrix and stagnant region, and further generalised by Shahkarami et al. (2015), who introduced an arbitrary length decay chain.

Most of the analytical solutions provided in geometric ordinary space are based on multiple integrals and/or infinite series that need to be evaluated by means of accurate and, sometimes, computationally expensive numerical algorithms. Thus, it is often more practical to treat the analytical solutions in Laplace space and then computing the inverse Laplace transform numerically. A similar semi-analytical approach is used by the computer code FARF31 (see Subsection 9.3.2 for further details). The main advantage of analytical/semi-analytical models is that they provide accurate descriptions of radionuclide breakthrough curves, even for decay chains of arbitrary length, although, despite what is commonly thought, they are not exact solutions as their evaluation requires numerical approximations. Their main drawback is that their application is restricted to relatively simple transport configurations (e.g. homogeneous matrix, time constant sorption properties, etc).

Time-domain (TD) particle tracking methods are alternative approaches that combine the robustness of analytical solutions with the flexibility of particle-based simulations (Painter et al. 2008). TD methods differ from "standard" particle tracking random walk methods in that they use a fixed spatial displacement while randomising the time for the displacement, and this offers a significant computational gain as particles can be routed along a trajectory segment using a single step. Compared to analytical and semi-analytical methods, TD-based algorithms are less restrictive in terms of required model simplifications. For instance, TD particle tracking calculations have been previously used to simulate radionuclide transport along thousands of particle pathlines built upon several different rock types (a rock type denotes a part of the rock that can be described by the same homogeneous parameters) with time variable radionuclide sorption coefficients (see Subsection 9.3.2 for further details on how changes in radionuclide retention are described using the so-called smart-K_d approach) (Trinchero et al. 2016). A drawback of TD methods is that instantaneous breakthrough curves need to be reconstructed from the cumulative discharge. This reconstruction, which is typically done using kernel estimation techniques (Painter et al. 1997, Painter and Mancillas 2013), may result in some statistical noise, particularly when long decay-chains are involved.

Particle-based methods are free of numerical dispersion and, thus they are particularly suited to model radionuclide transport. However, they can only accommodate linear reactions and thus have a limited applicability for reactive transport modelling. Reactive transport models are instead commonly based on Eulerian formulations of the ADE. Existing numerical schemes include finite difference, finite element, finite volume, etc. Transport and reactions are either tightly coupled, by means of the so-called Global Implicit Approach (GIA), or loosely integrated if based on a split-operator technique. GIA methods offer better performance, particularly in the presence of complex chemical reactions (Saaltink et al. 2001), although they are more difficult to implement. Eulerian numerical schemes are in general not recommendable for simulating radionuclide transport because they are affected by numerical dispersion, which may lead to non-conservative artificial dilution.

9.3.2 Approaches specific for simulation of radionuclide transport

Pathway delineation and upscaling of flow-related properties

Radionuclide transport calculations are typically based on a set of fixed pathways that represent the movement of hypothetical, advectively transported groundwater tracers and are typically calculated by pathline tracing in a DFN or DFN/CPM flow code. The main parameters needed for the transport calculations are the groundwater residence time and transport resistance along trajectory segments (or fracture legs in another notation) that constitute the full pathway (i.e., from the source location to the release point). We will here briefly discuss how particle tracing and flow-related parameters are computed in ConnectFlow and DarcyTools.

The preferred method in ConnectFlow since ODFN3 (Hartley et al. 2018b) is the "mass-conserving method", which is based on the formulation presented by Cordes and Kinzelbach (1992). The mass-conserving method performs well if the flow solution is accurate. The same mass-conserving method applies to ECPM-based calculations.

DarcyTools particle tracking option is implemented in a subroutine called PARTRACK, which can be used in two different modes of operation; the first is the traditional way of moving the particle along the local velocity vector (similarly to what is done in the "standard method" of ConnectFlow), while the second method uses the so called "cell-jump" approach. In the second approach, a particle stays in a cell for a time equal to the free volume of the cell divided by the flow rate through the cell and then jumps to a neighbour cell that has an outgoing flow direction. The choice of the neighbour cell is made with a likelihood that is proportional to the flow rates, which means that complete mixing in a cell is assumed. DarcyTools uses an ECPM representation of the fractured system, which implies that transport resistance needs to be properly represented from the underlying DFN. As explained in Appendix E of Svensson et al. (2010), in DarcyTools transport resistance, is computed as:

$$F = a_r L / q \hspace{3cm} \text{Equation (9-26)}$$

where L [L] is the cell dimension, a_r [L^{-1}] is the FWS per unit of rock and q [L·T^{-1}] is the Darcy flux. In the same report, the authors discussed three different approaches for the estimation of a_r In the first, a_r is directly computed as the total fracture surface area that intersects the considered grid cell divided by the volume of the grid cell. The second method is based on the global value of P_{32}, which

is obtained from the underlying statistics of the DFN and is distributed to each cell proportionally to its value of kinematic porosity. The third method is based on an empirical relationship between transmissivity and hydraulic aperture. The three methods were thoroughly tested using a modified version of the Äspö HRL model (Svensson 2001b). The general conclusion of this assessment was that the three methods give global estimates of a_r that are in fair agreement with the expected value for the Äspö HRL (Andersson et al. 1998). Yet, method one is considered to be the best choice as it directly calculates a_r from the fracture network, without any additional assumption.

Another interesting particle tracking tool is dfnTrans, which is included in the software suite dfnWorks and makes use of a robust algorithm for velocity reconstruction (Painter 2011).

Treatment of transport/mineralogical classes

Previous safety assessment studies (e.g. Posiva 2013) have considered the rock matrix to be constituted by layers with different properties. Typically, three layers are considered: the fracture coating, the alteration rim and the undisturbed rock. However, the implementation of layered matrix in radionuclide transport calculations is not straightforward.

Poteri (2009) presented a mathematical model where adjacent layers were rearranged into successive fracture segments. The approach is particularly attractive as it can be implemented in existing computer codes as a simple pre-processing step. Nevertheless, it can only be applied when porosity is monotonically decreasing (i.e., smaller porosity in layers located far away from the fracture).

A more generic recursive solution was provided by Cvetkovic (2010). This solution, which is derived in Laplace space, can be used to compute look-up tables of the retention time distribution. These look-up tables can in turn be directly used in MARFA using the so-called tabular retention model.

9.4 Expected sources of uncertainty and how they can be treated

To put things simple, radionuclide discharge depends on the groundwater residence time, from the source to the release point, and the product of the material parameter group and the cumulative transport resistance ($\kappa\beta$). Two of these parameters, namely the groundwater residence time and the transport resistance, are flow-related quantities, which highlights the fact that uncertainty in radionuclide transport is strongly related with the underlying uncertainty in groundwater flow.

We have discussed earlier that the computed groundwater fluxes and velocities are related through the transport aperture, which is also related to transport resistance through Equation (9-11). Transport aperture is affected by a high level of empiricism (it is typically based on some empirical laws, which are in turn derived from field observations). It turns out that a significantly high uncertainty stems from the definition of transport aperture in the DFN model and this uncertainty affects the computed distribution of groundwater travel time (t_{gw}). It is worthwhile noting that, for a fracture segment, t_{gw} can be defined as follows:

$$t_{gw} = \int_\Gamma \frac{ds}{\|\boldsymbol{v}\|} = 2b \int_\Gamma \frac{ds}{\|\boldsymbol{q}^*\|} \qquad\qquad \text{Equation (9-27)}$$

where Γ is the trajectory (from fracture inlet to outlet), $\boldsymbol{v}$ [L/T] is the groundwater velocity and $\boldsymbol{q}^*$ [L^2/T] is the groundwater flux per unit fracture aperture. The latter is the natural output of DFN groundwater flow models used for transport pathway tracing. Given the linear relationship between the computed t_{gw} and the chosen value of b and given the expression of transport resistance (Equation (9-11)) we can see here that the definition of transport aperture has no impact on the computed distribution of transport resistance.

Again, roughly speaking, groundwater residence time depends on the actual structure and connectivity of the DFN, on its hydraulic and transport properties (transmissivity and kinematic porosity or mass balance aperture) and on the applied flow boundary conditions. Groundwater flow boundary conditions are typically treated as deterministic and depend mostly on companion landscape evolution models. Fracture hydraulic properties are usually determined from empirical relationship between fracture size

and transmissivity, and they might be conditioned to field measurements, thus they have a reasonably high level of confidence. The structure of DFN models is usually assessed by means of a limited number of realisations and the transport pathways used to run the transport calculations are usually obtained by "pasting" together pathways obtained from different realisations, which offers a plausible way to address source-to-discharge connectivity and thus to account for uncertainty in groundwater residence time. Notice that groundwater residence time is expected to have a significant effect only for the early part of the breakthrough curve of non-sorbing or weakly sorbing radionuclides. The late-time of the breakthrough curve of non-sorbing or weakly sorbing radionuclides and the whole breakthrough curve of strongly-sorbing radionuclides is instead mostly controlled by $\kappa\beta$. Notice also the strong correlation between the groundwater residence time and β (Cvetkovic et al. 1999), which "translate" the uncertainty in groundwater residence time into uncertainty in the cumulative transport resistance.

The material parameter group depends on specific properties of the rock matrix, namely effective diffusivity, porosity and retardation factor in matrix, and is spatially variable as the fractures and surrounding rock matrix may have experienced different hydrothermal alteration events. The structural framework for transport properties and transport classes discussed in Subsection 9.1.5 provides a statistical approach to sample heterogeneity of transport classes conditioned on e.g. field observations of fracture filling minerals and thus offers a quantitative way to handle uncertainty in the spatial distribution of κ. The parameters of each transport class can reasonably well be characterised from lab experiments (see Subsection 9.2.1); however, the retardation factor in the matrix deserves a separate discussion. This parameter is radionuclide-specific and linearly dependent on the radionuclide distribution coefficient (see Subsection 9.2.1). Since sorption is a surface mediated process (Crawford 2010), distribution coefficients obtained from batch experiments on crushed material provides K_d values that intrinsically account for the concentration of the sorbing mineral(s) in the rock matrix. In a recent work, Trinchero et al. (2020) showed that these values are appropriate for large to very large scale simulations. However, when the mineral is present in very small concentrations (think for instance on biotite), the radionuclide breakthrough curve is characterised by an anomalous signature (i.e., early first arrival compared to what predicted by a model based on the assumption of homogeneous matrix retardation) which has a surprisingly large spatial persistence. It turns out that the heterogeneous distribution of sorbing minerals leads to uncertainty that need to be quantified (in the same paper by Trinchero et al. (2020), an alternative three-parallel pathway model is proposed to include and evaluate the effect of heterogeneous retention).

While groundwater residence time and the material parameter group can be described with a relatively high level of confidence, by leveraging lab and field observations along with appropriate statistically or genetically based Discrete Fracture Network Models, a large uncertainty still resides in β. This parameter depends in fact on the fracture specific surface area, which is very difficult to characterise as it may change significantly due to e.g. changes in mechanical stress. If diffusion into stagnant water is also accounted for, things become even more difficult as a second hydrodynamic parameter comes into play. Ongoing efforts to characterise the interplay between flow, channelling and mechanical stress using state-of-the-art numerical tools (Zou et al. 2017) along with generalised statistical formulations of tracer retention (e.g. Cvetkovic 2017a) may lay the ground for alternative, and less uncertain, representations of radionuclide retention in heterogeneous fractures.

Reactive transport modelling of processes potentially affecting the post-closure safety of the repository (e.g. the infiltration of oxygenated glacial melt-water or the microbially mediated sulphide production) implies the need for defining of appropriate reaction rates. These are in turn dependent on e.g. the exposed mineral surface area. We have already discussed in subsection "additional data" that exposed mineral surface areas can be defined as a function of the underlying DFN statistics and used in DFN-based ECPM models. However, there is evidence that continuum-based models significantly over-estimate mixing, and thus the underlying reaction rates. Natural subsurface systems are in fact typically poorly mixed environments, in which mixing between potential reactants is hindered by mass transfer limitations (Dentz et al. 2011). However, in continuum-based reactive transport models the reaction rates are typically expressed based on transition state theory (e.g. Lasaga 2014) as a function of volume averaged species concentrations. This implies that perfectly mixed conditions are assumed on the given support scale and thus mass transfer limitation is neglected (e.g. Steefel et al. 2005, Lichtner and Kang 2007). Rolle and Le Borgne (2019) identified three potential mechanisms for mixing in porous media: shear flow, flow focusing and defocusing and twisting flow. In fractured media an additional, and probably dominant, mechanism is mixing at fracture intersections (Kang et al. 2015). This mechanism can be adequately described by reactive transport models based on explicit DFN representations.

10 Building model confidence

10.1 Building model confidence by model reduction

Development of a DFN methodology is a response to a need for various types of predictions of geosphere behaviour. It relies on building models that minimize deviation from the data or assumptions the model is conditioned to, while simultaneously complying with conditions required by the purpose of the modelling activity.

It is convenient to introduce a few terms relevant to the issues discussed in this chapter. The **model space** is the envelope of possible models, when describing bounds on the system of interest, from which relevant parameterisations, idealisations and modelling principles are chosen, in a process which eventually reduces the model space. The reduction of the model space results is carried out by different operations (Figure 10-1):

- Selection of the processes relevant to the prediction outcome (see Subsection 10.2.1). Essentially:
  1. Identification of the physical and/or chemical processes that are of relevance for the prediction.
  2. Identification of suitable qualitative or quantitative models that describe those processes and their interactions (that may involve simplifying assumptions).
  3. Listing of all parameters that define the model space.
  4. Identification of a prior probability distribution, and its moments, for each defined parameter.

- Conditioning the model space on prior data information (see Subsection 10.2.2) – i.e., data that are amenable for processing as model parameters (value, range or distribution).

- Calibration of the model on data (see Subsection 10.2.3) – i.e., assessing the probability of a chosen model parameter set to be consistent with data.

- Validation is a demonstration that the model is an adequate representation of the real system being modelled to make the predictions required (see Section 10.4).

The process can be iterated in different ways (see below) and the eventual output is the ensemble of Models Conditioned by the Data (MCD), where each model characterised by a set of parameters has a probability of occurrence. The model space is expected to be reduced as compared to the initial assessment through rejection of some selected models and/or constraining parameter space.
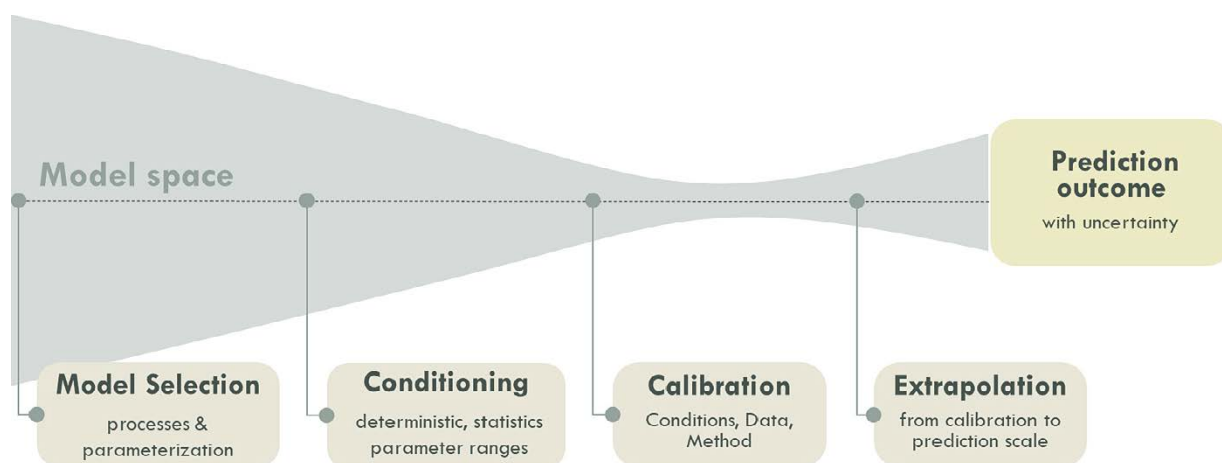
Figure 10-1. Sketch of the processes that make the model space evolve from hypothesis to prediction.

The prediction is an application of the MCD within the prediction space that defines all the conditions such as time, space, boundary conditions, etc. For operations that extrapolate the calibration conditions to much larger space and time scales, this entails not only an increase of the prediction uncertainty compared to the fitting under calibration conditions, but also likely an increase of the model space if new or modified physical/chemical processes that do not exist under the calibration conditions are expected to occur. Examples of such processes are changes in the boundary conditions (glaciations, elevation of temperature, mechanical load, sea level, etc), new chemical processes, etc. The extrapolation from calibration to prediction scale is the last step in Figure 10-1, although this whole process may be part of a repeated cycle during the main stages of the underground development and associated detailed site investigations and site-descriptive modelling.

The model space workflow is consistent with the Bayesian theory (Gelman et al. 2013), where the "prior" – what we think about the modelled system based solely on expert judgement and no data (model selection) – is combined with data (conditioning) to give the "posterior" distribution – e.g., the model space conditioned by the data – after estimating the likelihood of model parameter values given the observed data (calibration). The 'posterior' distribution is then represented by the reduced (i.e. constrained) model space after conditioning and calibration, which is then applied to the prediction space (extrapolation).

Note that conditioning and calibrating are similar ways of reducing the model space by using data. We find it convenient to differentiate a data comparison process that sets a priori the parameter value or range (conditioning) with a data comparison that calibrates parameters by letting the model run under calibration conditions (calibrating). There is a wealth of published theories on calibration, also called the inverse problem, of well-posed problems (processes and parameters are well known, a unique solution exists), with a lot of data, for which the calibration space is close to the prediction space (calibration experiments performed with conditions similar to the prediction) (Tarantola 2004, Stuart 2010). In that case, the calibration is essential to reduce the model space for prediction and it is different in nature and in techniques from the prior conditioning. In complex systems with sparse data compared to system heterogeneities, prior conditioning may be even more important than the calibration on experiments that are far from representing the natural conditions of the eventual prediction. In this case, prior conditioning and calibration are both important steps of model space reduction.

10.2   The stages of model reduction

In this section we elaborate on each of the processes of model reduction shown in Figure 10-1 to demonstrate that it comprises a cycle of iterative steps as shown in Figure 10-2.

Each of these processes is described below, including the main steps: Model selection, **s**ensitivity **a**nalysis, prior **c**onditioning, calibration, **re**jection (called SACRe process thereafter), and extrapolation.
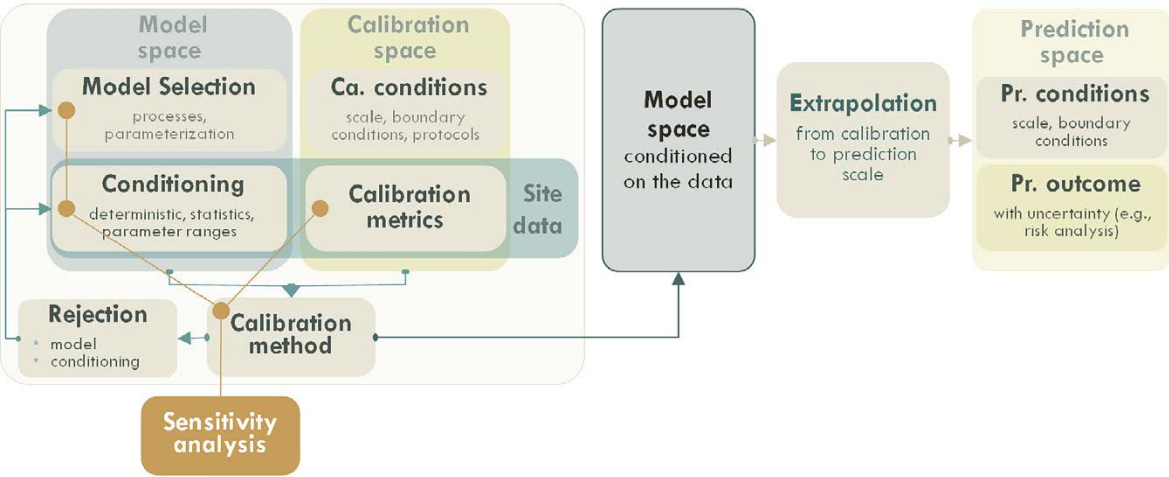
Figure 10-2. *A detail sketch of the model space reduction that gives the different stages, the way they combine and the semantics.*

10.2.1 Model selection

The model space (MS) is the ensemble of physical (in the broad sense) rules, mathematical equations and parameters that give a theoretical, observational and/or empirical description of the *processes* and *boundary conditions* that allow simulations of a system and its evolution. This definition implies a logical and objective formalism, which makes a model of MS amenable for testing and evaluation with data or experiments. In that sense, it is a step further in the formalism compared to a conceptual model that would rely only on ideas, words and schematics. For the purpose of traceability and repeatability (see Section 10.4), the rules, mathematical equations and parameters that define MS must be clearly set.

A model is obviously not the reality but a representation that contains hypotheses and simplifications of the real system. A key issue is its amount of complexity, which is a trade-off between the complexity of the real system so far as it can be observed, and the need to remain commensurate with the requirements for the model and what the available data can support. As for statistical models or machine learning, overfitting (over-determination) is an issue that needs to be avoided; although it allows for a better fit of the data, it makes model prediction/extrapolation less reliable (Hawkins 2004). The sensitivity analysis is a useful test for assessing the right level of model complexity, in the sense that additional complexity can only be justified if it demonstrably contributes to a reduction in model predictive uncertainty (see next section).

MS evolves as new information is gathered or different requirements are placed on the model. A prior estimate of the model parameter ranges can be required to avoid starting with a too large model space, or simply to avoid adopting unphysical parameter values.

MS is not a unique ensemble of relationships since it relies on an understanding of the nature of processes taking place in the system and that may not be complete. MS is underpinned by the relevant laws of physics, but it may also contain soft data, i.e., established geoscientific principles or commonly used models that practitioners have found to describe observations at other sites from personal experience, accepted practice or inspired by the scientific literature. Some of these empirical relationships and principles, which make up for the lack of data or knowledge, are hard to verify. To bracket the geological truth, it is recommended to test several hypotheses with different levels of scientific plausibility (e.g., if it is supported by physical principles, even simplified, or derived from data fitting, each one defining a sub-model space. It is convenient to define a *baseline MS*, which corresponds to either the most likely model from a scientific point of view or to the one most used in engineering practices of the day. The postulate is that predictions made with the *baseline MS* and *alternative MS* adequately span outcomes in the real system (see Section 10.4), which is not obvious a priori and must be questioned throughout the modelling phase.

10.2.2 Prior conditioning to site data

Prior conditioning is the process of constraining models with information about the model parameter ranges, the statistical targets, or the observations which must be respected by the models in a strict or statistical sense. Part of this conditioning belongs to the normal model selection process (previous section) when it consists in collecting generic – i.e., not specific to a site – information about the physical processes. Part relies on local observations made on the site – e.g., a structural model with the main geological domains and their boundaries defined by site geologists.

For the sake of clarity, we recommend identifying the prior conditioning related to site data as a step in model space reduction different from the model selection. The point is that this conditioning is complementary to the calibration, which also uses site data, but in a more indirect sense. It clarifies the DFN methodology to know at which level of the model reduction process the data are used.

Prior conditioning to site data is often used to implement the know-how of geologists and hydrogeologists in a series of constraints with potential to significantly reduce the model space and simplify the modelling process and the models stemming thereof. A sensitivity analysis is recommended both to evaluate the need and consequences of the prior conditioning in the prediction.

In the case of a multi-step process, where the calibration is applied several times, step by step (e.g., a structural model space conditioned on the data is an input of the hydrogeological model space), the prior conditioning of the last stage is the result of model calibration and conditioning of the previous stage. However, the conditioning may also be applied simultaneously such that the MS is constrained by e.g., combined geometrical and hydraulic conditions.

10.2.3 Calibration

Calibration space

Calibration is the process of reducing the model space by comparing model outputs to observed data (Tarantola 2004). This is not only the estimate of the best-fitting set of model parameters but the determination of an occurrence probability as in the Bayesian formalism (Bayes 1763, Stuart 2010, Gelman et al. 2013). This problem is known as "the inverse problem" (data/output → model parameter), which is the inverse of forward modelling (model parameter → output). But, as expressed by Tarantola (2004), *'while the forward problem has (in deterministic physics) a unique solution, the inverse problem does not'*. There are many reasons for this. Given uncertainties, poor or inadequate data quality and the complexity of the model itself, a number of different parameter combinations can render quite different, but equally "good" fits to the information to which the model is calibrated. A critical point, therefore, is that the conditions of calibration (e.g., the calibration space) are not necessarily adequate to explore all the model parameters which, in practice, imply that some parameters will remain undetermined after the calibration process. In this sense, calibration may be viewed as a probability density function filtering process, in which the uncertainty in the model's parameter values is *reduced*, rather than eliminated. The extent to which the uncertainty associated with a given parameter is reduced by calibration is a function of both the information content of the observed data (as it pertains to that parameter), as well as the extent to which that information is shared with other parameters in such a way that it cannot be uniquely resolved; itself a function of the model parameterisation, amongst other factors . Therefore, defining the conditions of calibration – e.g., the observed dataset with uncertainties and the physical conditions of calibration (volume and time scale explored, boundary conditions if necessary, etc) – is important information for any end-user of the calibrated model.

Metrics for calibration

Calibration metrics define practical measures for comparing model predictions with field observations of the fracture system and/or models with each other. When used to compare model and data, the metric must be applied to modelled conditions similar to those in which measurements are made.

Since DFN models are only representations of real fracture systems, i.e. aimed to show statistical equivalence, adequate metrics are not necessarily a 'local' measure, but it may be a global measure averaged over a certain volume (e.g., intensity), a statistical distribution (of e.g., sizes) or a scaling relationship (e.g., aperture scaling with fracture size). Examples of calibration metrics are:

- 'Local' metrics are defined by a quantity – e.g., transmissivity or inflow – and by the way it is measured including the position, sampling scale and uncertainty. It is only a relevant metric to calibrate DFN models, which have been heavily preconditioned on the data in the vicinity of the measurement.

- 'Density' metrics are the average of a quantity over a certain volume – e.g., trace density measured in tunnels or boreholes.

- Statistical distribution – e.g., trace size distribution, flow distribution or breakthrough curves – are relevant metrics to calibrate the spatial variability of parameters (measured/modelled on tunnel walls, and along and in between boreholes).

- Scaling relationships characterise the structure (correlations and spatial arrangement) across scales of the target quantity. An example is the equivalent hydraulic conductivity scaling (see Subsection 8.8.4) that can be computed from borehole intervals with PFL data to characterise the connectivity and spatial hydraulic structure.

Metrics should be chosen as a function of the prediction/outcome objective (i.e. related to properties affecting long-term safety or repository engineering) in order to increase the reliability of the calibrated model in its ultimate use. For this reason, the choice of suitable calibration metrics also reflects suitable prediction metrics (see Section 10.4). An example of prediction metrics used for validation of DFN models in the ONKALO is given in Table 10-1 classified according to their type and the components of MS they are used to validate. The issue of prediction metrics will be returned to in vol II of this DFN Modelling Methodology.

Table 10-1. Examples of prediction metrics (revised from Hartley et al. 2018b).

Property	Metric	Type
Fracture size and spatial distribution	Number of full perimeter intersections fractures in tunnel section	Density
	Number of gently dipping traces > > mapping resolution[3]	Density
Flow distribution	Number $T > 1 \times 10^{-8}$ m^2/s	Density
	Number $T > 1 \times 10^{-9}$ m^2/s	Density
	Total summed flow to boreholes	Density
Inflow distribution	Difference between geometric mean of simulated values and the measured value	Local
	Median of number of inflows lying correctly above/below detection limit	Density
Fracture size and spatial distributions	P_{10}[4] in pilot holes	Density
	P_{21} for traces lengths > > mapping resolution	Density
	Trace size distribution	Statistical
Orientation	Goodness of fit on stereoplots[5]	Statistical
Terminations	Percentages of one-end and two-end terminations	Statistical
Spatial model	Trends in relative intensity by lithology	Scaling
Aperture	Correlations of geological aperture with trace size	Scaling

Many quantities – e.g., transmissivity – cannot be measured directly but are instead derived from the interpretation of an experiment or a proxy measurement (e.g., ratio between inflow and hydraulic head as a proxy for transmissivity). It must be verified that the quantities simulated in the model and in the field represent the same physical or chemical parameters and conditions.

A sensitivity analysis (see Figure 10-2) is essential to demonstrate the ability of the metrics to make the model more reliable for a given prediction objective.

A statistical metric for calibrating flow distributions is shown in Figure 10-3 based on simulating single-hole PFL hydraulic tests in 17 deep core drilled KFM holes at Forsmark compared to measurements partitioned according to fracture domain and depth. This involves calibration of connectivity and transmissivity.

---

[3] The mapping resolution is the truncation limit dictated by the fracture sampling policy. This limit may vary within different parts of the repository, and with the purpose of the mapping, but is typically 0.25–0.5 m in nisches and 0.5–3 m in the main tunnels.

[4] The borehole intensity, P_{10}, can be based either on fractures intersecting the axis of the core, i.e. a scanline proper, or as fractures making a full perimeter intersection (FPI) with the core. The choice of mapping principle will affect, among other things, the choice of bias correction.

[5] There are many different techniques to compare fracture orientations but most favoured by practitioners are based on Stereoplots.
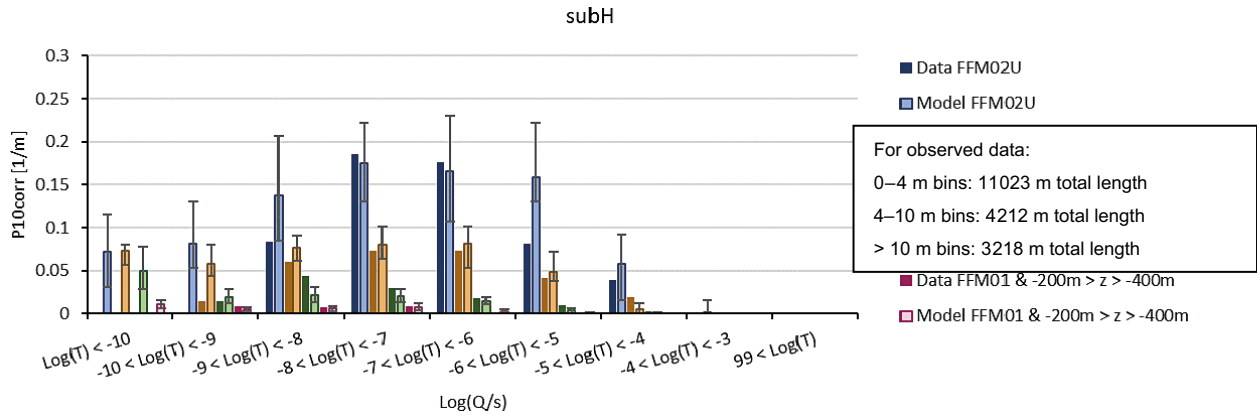
Figure 10-3. *Example statistical metric for the intensity of flowing fractures in different ranges of specific capacity by rock units FFM02(U/L) and FFM01 (above and below z = –200 m) for the sub-horizontal orientation set. Model results are the average over 10 realisations of a DFN model (simulated KFM holes only). Error bars indicate the maximum and minimum results across the realisations (Hartley et al. 2020).*

An example of a metric for the scaling relationship for flow is shown in Figure 10-4. The equivalent hydraulic conductivity, $K_g(l)$, computed from the available single-hole flow tests, performed over several cored boreholes at the Forsmark site is shown by grey lines with annotation of the mean scaling behaviour and how to interpret it. It has a V-shape evolution with first a decrease and next an increase phase. At sizes L_s smaller than the minimum distance between two inflows, $K_G(L_S)$ decreases as L_S^{-1} down to a minimum value (point 1 in the figure), then increases again once averaging begins of two or more inflow values within a section.
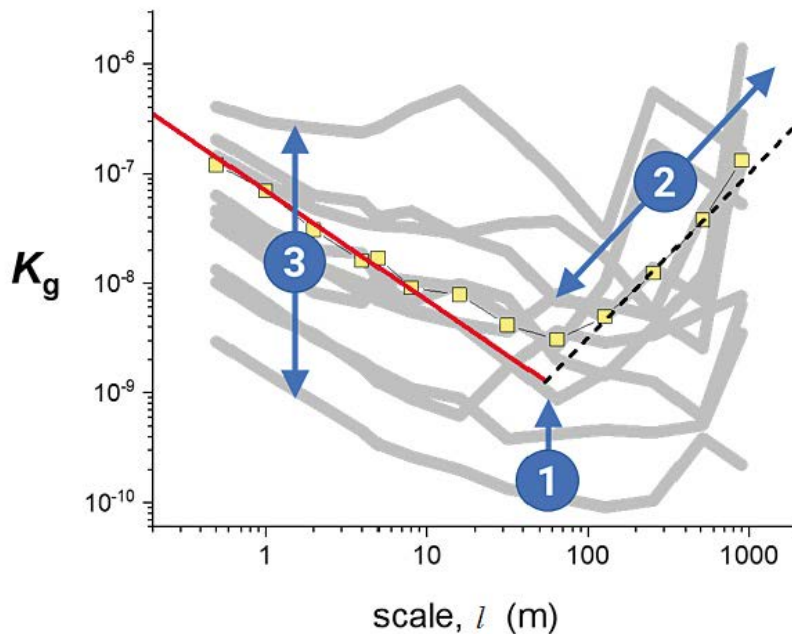
Figure 10-4. *Scaling relationships of the geometrical permeability average K_g calculated from core-log PFL transmissivity data by sampling different boreholes at different scales irrespective of vertical depth. The metrics that are used to calibrate models are 1) the scale at which K_g is minimum (interpreted as the network percolation scale), 2) the scaling of K_g above the percolation scale, and 3) the variability of K_g for different boreholes). The red and dotted lines illustrate this metric for one of the boreholes identified by the yellow squares. After Davy et al. (2019).*

The calibration process and the objective/likelihood function

The calibration process is related either to a minimisation of an objective function, which calculates the difference between model outputs and observed data (Gupta et al. 1998), or to the calculation of a likelihood of the observed data given a set of model parameters (the Bayesian approach (Bayes 1763, Gelman et al. 2013)). The former yields the best-fitting model with the range of plausible parameters; the latter gives a likelihood of the model space conditioned to the data.

The Bayesian approach allows the issue of over-parameterisation (e.g., the discussion in Brunetti et al. (2017): *'a parameter-rich, but geologically-unrealistic model may fit the data equally well or perhaps even better than a more parsimonious model'*) to be addressed quantitatively. Using the Bayesian approach to choose between different alternative model spaces is a possibility worth exploring. However, in the context of complex geological systems with sparse data sampling, the issue of finding the right trade-off between model complexity and goodness of fit is an open issue (see the discussion in the Section 10.4).

Calibration, reliability tests and model rejection

Reliability tests and model rejection are basic versions of the calibration process, which require defining an (un)acceptable deviation between the models and the data.

Early model rejections are important steps of the model space reduction since it allows for narrowing the options to the relevant alternative models. An example is a connectivity analysis for the open fracture system against the intensity of discrete flow measurements, see Section 8.6, where some alternative intensity-size scaling and spatial models for fracture openings may be rejected prior to flow simulation.

10.2.4 Sensitivity Analysis

Sensitivity analysis (SA) is defined "as the study of how the variability in the model output can be apportioned to the different sources of input" (Saltelli et al. 2006). It is a preliminary analysis of the models that underpins several important tasks of the global process:

- Model selection; Test which complexity is necessary, and which knowledge about processes and parameters is required.
- Conditioning; (i) Test which data accuracy is required (e.g., whether data can be considered deterministic or partly uncertain); (ii) test if new data bring more constraints.
- Calibration metrics; Test the ability of metrics to make the model more reliable for a given prediction objective, and
- Calibration process; The sensitivity analysis basic to parameter estimates.

How SA can be carried out is an open question given the non-linearity of the models. SA can be local, one parameter at a time or global in the allowable ranges of the input space (Leamer 1985, Baroni and Tarantola 2014), the latter being preferred for complex, non-linear, models. In the context of environmental models used for decision support purposes, a range of methods have been developed for evaluating model predictive uncertainty in non-linear models. These include Markov chain Monte Carlo (MCMC) simulation, calibration-constrained Monte Carlo analysis and Bayesian ensemble-based data assimilation methods.

We recommend starting from the simplest models that are close to reality (e.g., a 'site-like' modelling that reproduces site conditions as much as possible) and to test the importance of introducing a process, a parameterisation, or a data on the eventual prediction. That is to say, additional model complexity should only be justified if it can be demonstrated (via model predictive uncertainty analysis) that it improves the model's predictive power as it pertains to the key predictions of interest. This can occur in one of two ways, namely that the additional complexity either: (1) enhances the model's ability to express expert knowledge (i.e. in the form of the prior distributions); or (2) improves the model's ability to replicate relevant system behaviour (i.e. as expressed by the likelihood function). Since the model's predictive power varies strongly with the type of prediction it is asked to make, this raises the spectre that the model selection, conditioning and calibration processes should be tailored to specific predictions of interest.

10.2.5 Stochasticity

Most of the models in the DFN methodology are stochastic or partly stochastic, i.e., relying on random variables constrained by stochastic processes or statistical distributions. A realization is characterized by the set of stochastic/statistical parameters used to generate it, and the set of numbers which identify the realization in the random space. For DFN, the random space contains the parameters that position fractures and describe their properties under statistical/stochastic constraints. Given the number of fractures and of fracture properties, the random space is always orders of magnitude larger than the statistical/stochastic space (i.e., the number of independent statistical parameters used to generate realizations).

For a given set of stochastic/statistical parameters, the ensemble of realizations gives the mean and variability of stochastic model outputs.

The calibration of stochastic models applies on both set of parameters, stochastic/statistical and random, with the goal to find the set of realizations that match the data. Although there is no prescribed rule, calibration can be done as a two-step process:

- First, a "statistical calibration" investigates the ensemble of statistical/stochastic parameters with adapted metric (for instance, relying on the mean and standard deviation of outputs).

- Lastly, a "full calibration" aims at identifying the subset of realizations that match data.

The former calibration is reasonably achievable since the stochastic/statistical parameters are generally well constrained by data and they exert a strong control on the model outputs. The latter is more difficult to achieve because of the size of the random space, which leaves a wide range of possible realizations. This is very often the main source of uncertainty in stochastic model predictions.

This raises the issue of assessing the mean and variability of model outputs due to the random space – i.e., the space of stochastic realizations. The model outputs are the metrics chosen to quantify the impact of each realization, and their probability distribution (pdf) determines the ensemble of possible values of the metrics. The metrics average and variability are highly dependent on the shape of the pdf. If low-probability high-impact realizations contribute significantly to the mean or standard deviation of the impact metrics, good estimates of these terms require a significant number of the high-impact realizations and therefore an even greater number of realizations. For pure random Monte-Carlo methods, the ratio between these two numbers is inversely proportional to the survival probability of the low probability events, which gives an estimate of the number of realizations to be carried out. In practice, convergence tests can be used to estimate the quality of the mean and variability of the selected metrics.

Note that the realization number depends on the purpose of modelling, i.e., on the chosen metrics; it will be different for flow, residence time or channelling characteristics, for instance. Also note that, beyond the mean and standard deviation, it could be important to evaluate the probability of some highly impacting events if, for instance, a threshold not to be exceeded has been defined.

10.2.6 Extrapolation: Applying the model space conditioned on the data to the prediction space

The prediction space is defined in terms of:

- Time scales,

- spatial scales,

- spatial domains,

- boundary conditions, and

- an even process that may operate during the prediction time (e.g., glaciations for long term predictions).

For a repository project, prediction space has two main purposes: one in support of validation (see Section 10.4) and one in support of end users; environmental impact assessment (EIA), post closure safety assessment and repository engineering. Some predictions made for validation purposes will be

made for conditions close to those used in calibration, e.g., underground mapping and hydraulic tests, while others may be on a larger scale, such as hydraulic disturbances in monitoring holes distributed across the local-scale domain. Examples that require a longer time scales are palaeo-climate simulations. Predictions for engineering will likely include extrapolation to new construction areas, as yet unsampled, while forward modelling for long-term post-closure safety will include time scales and boundary conditions not considered during calibration.

Since the prediction space may be very different from the calibration space, the projection of the models conditioned by the data is not straightforward and may lead to additional, or revised, assumptions in terms of boundary conditions, processes, etc. This results in an increase in the range of models/ parameters and assumptions. The prediction-outcome must take this into account in order to deliver the likelihood prediction and its uncertainty.

Predictions used for validation are compared with outcomes derived from measurements, as part of prediction-outcome exercises using new or reserved information during ongoing investigations and site monitoring. In this context "outcome" is not just comparing model predictions and observations, but also describing what is learned about model space from making such a comparison.

10.3 A multistep multipurpose process

The process described above can be decomposed into several successive steps as shown in Figure 10-5 and adapted to different prediction spaces. We recommend each step to be described with the required elements (model space, prior conditioning, calibration space) in order to ensure the reliability of the whole process.

For example, the top line of the figure may represent the flow of Geometric DFN model space to Flow DFN model space to Transport DFN model space to safety assessment prediction space of flow and transport around the deposition areas, see Figure 3-1. The example here thus illustrates that conditioning can include data from multiple disciplines such as geology (e.g., geometries), hydrogeology (e.g., flow) and transport (e.g., breakthrough curves, i.e., travel times).

Several prediction spaces can be defined (e.g., repository area (facility scale) and individual deposition areas (facility part scale)).
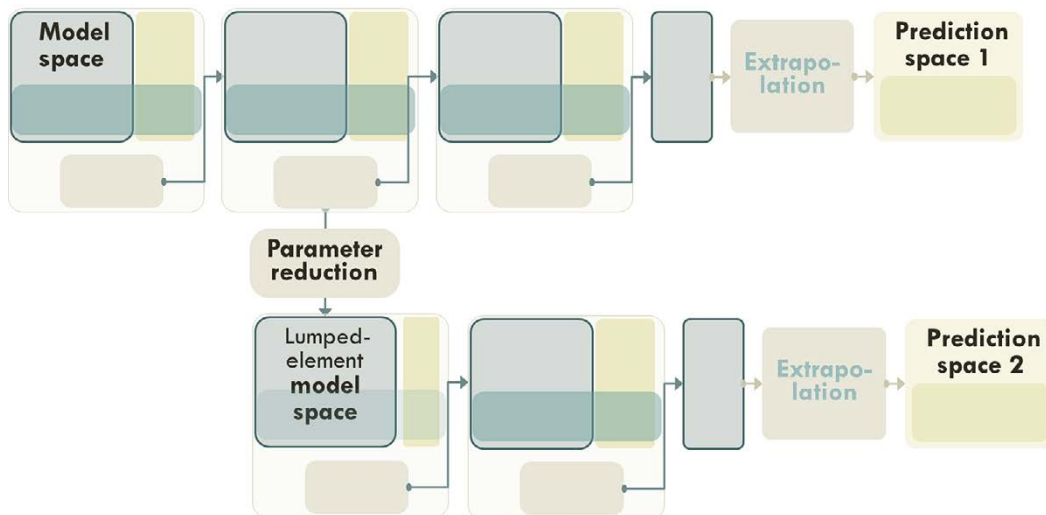

Figure 10-5. *Sketch of a multistep, multipurpose process.*

It may be necessary to use models with different degrees of complexity depending on the prediction space (especially for long-term, large-scale predictions). The new model space is then considerably reduced by integrating/averaging the local heterogeneity into a few "lumped" (effective) parameters (Incropera et al. 2007). The consistency between both models must be checked to ensure that the lumped-element model is still able to reproduce the main processes with a resolution consistent with what the prediction requires, and to evaluate the uncertainty due to the parameter reduction. For example, the DFN models for flow can be up-scaled to an ECPM for performing simulation of long-term evolution of groundwater flow and chemistry (as planned in steps BS8–9 in Figure 3-2.

The whole process is iterative if/when new data are acquired, or new processes identified.

10.4   A trade-off between model complexity and parsimony

An issue for validation is the trade-off between model complexity and parsimony, which deserves an explicit and motivated choice. Model complexity is usually defined as the richness of the model space, e.g., the number of free parameters (Ye 1998, Spiegelhalter et al. 2002), but also in machine learning, as a measure of how hard it is to learn from limited data.

The arguments for complex models are:

- Model confidence partly relies on their ability to reproduce geological systems in all their complexity and variability.

- Model complexity is also necessary to some extent to allow the models to be conditioned to data of different types (geological, hydrogeological, geochemical, etc) – e.g., prediction exercises on very specific areas.

- Important processes for prediction are partly controlled by the spatial variability of fluxes, e.g., flow channelling controls transport of radionuclides. Time and space variability is hardly obtained by the simplest models; it is rather an emergent property of the model complexity, which may be required for the prediction.

However, complex models with limited (and/or noisy) data may not perform well on new data and thus on prediction. They are commonly overparameterized, which reduces their prediction capability after calibration. This is the principle of Occam's razor, which implies that any given complex function is *a priori* less probable than any given simple function. Furthermore, the computational resources required to conduct sensitivity and uncertainty analyses on complex models can be significant.

On the contrary, simplified models are supposed to be easy to implement and fast to calculate. They are useful for several reasons, including (but not restricted to):

- To explore the model space by guiding the modeler in developing alternative conceptions.

- To make the calibration process easier by systematically identifying the main parameters and performing a complete sensitivity analysis.

- To provide a better understanding of the key processes and characteristics of system, which helps to increase confidence in the modelling through a fine understanding of the results.

Graph representations, effective field theories, sparse channels, or simplified parameter relationships are examples of simplified models.

If different kind of models from simplified to complex are necessary to increase the scientific relevance of the modelling approach, the "best" models for prediction are a trade-off between complexity and parsimony, which consists in reducing the complexity as much as possible[6] to increase the prediction capability, but not too much so as not to lose the model relevance to describe the main geological processes. Effective theories validated by complex modelling, or simplifications by removing structures and processes of minor importance are ways to reduce model complexity. The optimum for prediction models requires frequent iterations between models of different complexity level.

---

[6] The debate between model complexity and parsimony is well summed up by the sentence attributed to Albert Einstein "*Everything should be made as simple as possible, but no simpler*".

10.5 Validation

A vital component of the model building process is the validation of the whole process in the sense defined by the IAEA Safety Glossary (IAEA 2018): *The process of determining whether a model is an adequate representation of the real system being modelled.* IAEA (2018) also specifies that, in the case of geological disposal facilities that involves temporal scales and spatial scales for which no comparisons with system level tests are possible, models cannot be 'validated' for that which cannot be observed, so model validation implies showing that there is a basis for confidence in the model(s) by means of detailed external reviews and comparisons with appropriate field and laboratory tests, and comparisons with observations of tests and of analogous materials, conditions and geologies at the process level (IAEA 2018).

Part of the confidence is related to a clear description of the modelling workflow:

- Are the different stages (definition of the model space, calibration, …) clearly identified?
- Does the model selection and data rely on current scientific methods?
- Have the consequences for the prediction of the model selection, including the necessary simplification assumptions, of the prior conditioning, and of the calibration process, been sufficiently tested through a relevant sensitivity analysis?

The confidence also requires to understand as precisely as possible where the uncertainty in the prediction comes, and to quantify it after calibration. Most authors who have addressed this issue acknowledge that "verification and validation of numerical models of natural systems is impossible", because all such systems are open, with distributed input parameters that are incompletely known or conceptually inconsistent with their model counterparts (Oreskes et al. 1994). But models are proved to be useful to help engineers make the best decisions (de Marsily et al. 1992) if they are verified on data or if the sources of uncertainty due to assumptions and lack of data are well understood and quantified.

All the steps described above, including calibration, sensitivity analysis, fundamental understanding, and estimate of the stochastic uncertainties, are steps that contribute to giving confidence in the modelling predictions.

11 Summary

The current report provides a methodology for conceptualising and modelling fractured rock, and is to be applied for the Forsmark site in the municipality of Östhammar in Uppland, Sweden. This site is characterised by certain geological features, specifically deformation zones with elevated fracture intensity as compared to the rock mass in between the deformation zones. Additionally, extensive horizontal sheet joints in the near-surface rock combined with very sparsely fractured rock at depth, as outlined in Chapter 4, provide site-specific hydraulic characteristics. Discrete fracture network (DFN) modelling is advocated as providing a natural approach for achieving a quantitative and probabilistic description of the site. Nonetheless, the methodology is formulated such that it is applicable to any site located in crystalline, fractured rock.

Prior to the planning of detailed site investigations at Forsmark and Laxemar (2003–2010), SKB presented methodologies and strategies for the analysis and construction of Site Descriptive Models (SDMs). These strategies were manifested in the form of a series of methodology reports which offered the theoretical underpinning for the methods and best practices that were to be applied to the various aspects of site modelling. The objectives then were to develop a sufficient understanding in order to demonstrate a safety case could be made for a KBS-3 repository, and to select between sites. It was also recognised that some issues could not be resolved until underground investigations could be made. Thus, though adequate for the SDM and subsequent safety assessment SR-Site, SKB identified a need to update the methodology for DFN modelling to meet challenges anticipated during the construction of the repository and to reflect the state-of-the-art in this complex field of science. The new methodology presented now is tailored to utilise data from underground investigations, and should thereby provide the means necessary for further modelling and development of details related to post-closure safety, design and operations of a repository.

Due to lessons learnt from SDM-Site, the governing principle of this work has been to ensure the creation of a common, general and multidisciplinary DFN framework that can be used in any application required for modelling in support of site-description, safety assessment or repository engineering for any chosen crystalline fractured rock site. Specific new features of the methodology include hydromechanical coupling, introduction of in-plane heterogeneity of individual fractures, genetic fracture generation, description of deformation zones through a DFN approach and a framework for uncertainty management. Some of these key aspects are elaborated below, and an overall assessment of how the various aspects presented are to be used in conjunction is attempted.

A key notion of discrete fracture network modelling is spatial variability, implying aleatoric uncertainty, since several fracture attributes manifest great variation in space. A probabilistic framework is thus needed since we will never have exhaustive information to avoid remaining uncertainties. Identifying regions within the domain of interest with internally similar fracture properties; i.e., regions exhibiting statistical quasi-homogeneity, is an important first step in the assessment. Specifically, individual fracture domains of the rock mass and deformation zones, with their unique fracture characteristics, need to be identified. It is noted that deformation zone geometries largely are provided by the deterministic litho-structural modelling; however, some zones, e.g. those intercepting repository components, may be unknown in their extents. The methods for extrapolating such structures are also provided by the DFN modelling methodology. Furthermore, the methodology needs to provide means, in a structurally consistent way, to fill the model volume with deformation zones where these have not been characterised, and to fill in zones below the scale of detection.

Once the sub-domains of interest have been identified, the geometrical properties of the fractures within each domain are to be described; this pertains to both fracture domains and deformation zones. These properties include location, orientation, shape, size and density of fractures. Possible correlations between these properties need also to be described, among which fracture termination characteristics are one aspect.

If fractures terminating against each other is a prominent feature, this must be considered in DFN models as it is for example in so-called genetic (or grown) models since termination is a critical control of the network connectivity. More importantly, the genetic models also provide a means for reducing the uncertainty in fracture size scaling since fracture size distribution becomes an emergent property rather than an input. Traditionally, so-called stattistical models using pre-defined probability density functions of the different attributes have been used. An example of a statistical model is the Poissonian model

where fracture centres are distributed in space with uniform probability. The current methodology aims to provide the theoretical concepts behind both statistical and genetic approaches to fracture generation. Also, a spectrum of alternative methods to include fracture in-plane heterogeneity (aperture, surface roughness) are discussed, ranging from Boolean representations of open/sealed fractures to random fields mapped onto the modelled fracture planes.

With the geometrical framework in place, the fractures are parameterised for different applications. A key notion adopted in the methodology is that aperture depends on the stress field. Thus, a fracture's location and orientation relative to other fractures and to the stress field will affect its aperture. Additionally, other characteristics such as fracture size may be included as drivers for assigning aperture. A transmissivity for each fracture or portion of open fracture space is then assigned through the stress field-dependent aperture. The assignment of the distribution of open and sealed fractures, i.e., the distribution of fracture openings, is the key notion going from all fractures in the discrete fracture network to those that may be hydraulically active. Ensuring that the open fractures are a true statistical subset of all fractures, the consistency between geological and hydrogeological DFN disciplines is maintained. The proposed methodology presents several means of arriving at the size distribution for open fractures based on the corresponding relationship for all fractures. Furthermore, the spatial arrangement of the open and closed parts of a fracture are discussed, and a range of models to quantify such distributions are proposed.

The distribution of open and sealed fracture space or spatial variability in aperture, together with the network connectivity structure, will govern the flow distribution and the resulting channelling of flow. The methodology discusses channelling characterization, metrics and modelling strategies. Specifically, a flow channelling indicator is presented, which can be applied both at single fracture scale (when individual fractures have varying aperture) and network scale. Also, various field tests that can be used when parameterising models are presented, and sensitivity analysis, calibration and conditioning methods in this context are discussed.

Resulting flow channelling will strongly affect transport of dissolved solutes in the network system. The methodology highlights the relevant transport processes, and the links between the flow field and retention of mass, primarily through matrix diffusion, as quantified by the hydrodynamic transport resistance. Besides transport resistance, which is a Lagrangian quantity integrated along flow paths, its Eulerian counterpart, denoted as F-factor or F-quotient, is also presented. The latter is to be intended as an average value representative of the bulk retention capacity of the fracture while the former is a distribution, which is often long-tailed because of fracture internal variability. Furthermore, the concept of transport classes is introduced, which is a means to relate retention models to fracture types, as provided through a site-descriptive model, to individual fractures or fracture segments of the DFN model. Thus, the notion of Transport classes merges the site-descriptive understanding of retention properties with the quantitative geometrical-hydraulic DFN fracture description.

The final chapter of the report brings up various issues related to model confidence. Even if the chapter comes last, many of the aspects brought up here are relevant for the full process of building a DFN model. Specifically, the methodology introduces the notion of model space, which can be reduced through model selection/rejection, conditioning, and calibration. When the model is used for extrapolation, i.e., prediction, the model space will again increase.

Sensitivity analysis is a prominent feature of the proposed methodology. Specifically related to model confidence, the steps in the model reduction process are model **s**election, **s**ensitivity **a**nalysis, prior **c**onditioning, **c**alibration, and **re**jection (denoted as the SACRe process). Sensitivity analysis is an important component in model selection, conditioning, calibration, rejection and prediction by assessing how the variability in the model output depends on the model inputs. Sensitivity analysis thus provides an increased understanding of the modelled system. Finally, the challenging subject of model validation is briefly touched upon.

The presented methodology for DFN modelling in each main chapter provides recommended methods and best practices. The methodology is structured in a modular way so that specific pieces of the framework can be replaced if better practices, tools and methods become available. Due attention is paid to other methodologies developed by SKB, in particular the methodologies for geological modelling, for rock mechanical modelling, for hydrogeological modelling and for transport modelling. The presented methodology is aimed towards a broad audience, thereby enabling both practitioners and theoreticians alike to appreciate the information provided.

References

SKB's (Svensk Kärnbränslehantering AB) publications can be found at www.skb.com/publications. SKBdoc documents will be submitted upon request to document@skb.se.

Aalto P, Ahokas H, Hurmerinta E, Komulainen J, Pentti E, Tammisto E, Vaittinen T, 2019. Quality assessment of transmissivity data acquired over time in surface drillholes at the Olkiluoto site. Posiva Working Report 2018-29, Posiva Oy, Finland.

Aaltonen I (ed), Engström J, Front K, Gehör S, Kosunen P, Kärki A, Mattila J, Paananen M, Paulamäki S, 2016. Geology of Olkiluoto. Posiva 2016-16, Posiva Oy, Finland.

Abelin H, Neretnieks I, Tunbrant S, Moreno L, 1985. Final report of the migration in a single fracture Experimental results and evaluation. Stripa Project Technical Report 85-03, Svensk Kärnbränslehantering AB.

Allaby M (ed), 2013. A dictionary of geology and earth sciences. 4th ed. Oxford: Oxford University Press.

Andersson C, 2002. Djupförvarsteknik. Äspö Pillar Stability Experiment. Feasibility study. SKB TD-02-07, Svensk Kärnbränslehantering AB.

Andersson J, Shapiro A M, Bear J, 1984. A stochastic model of a fractured rock conditioned by measured information. Water Resources Research 20, 79–88.

Andersson J, Hermansson J, Elert M, Gylling B, Moreno L, Selroos J-O, 1998. Derivation and treatment of the flow wetted surface and other geosphere parameters in the transport models FARF31 and COMP23 for use in safety assessment. SKB R-98-60, Svensk Kärnbränslehantering AB.

Andersson J, Berglund J, Follin S, Hakami E, Halvarson J, Hermanson J, Laaksoharju M, Rhén I, Wahlgren C-H, 2002a. Testing the methodology for site descriptive modelling. Application for the Laxemar area. SKB TR-02-19, Svensk Kärnbränslehantering AB.

Andersson J, Christiansson R, Hudson J, 2002b. Site investigations strategy for rock mechanics. Site Descriptive Model. SKB TR-02-01, Svensk Kärnbränslehantering AB.

Andersson J, Skagius K, Winberg A, Lindborg T, Ström A, 2013. Site-descriptive modelling for a final repository for spent nuclear fuel in Sweden. Environmental Earth Sciences 69, 1045–1060.

Andersson P, Byegård J, Dershowitz B, Doe T, Hermanson J, Meier P, Tullborg E-L, Winberg A (ed), 2002. Final report of the TRUE Block Scale project. 1. Characterisation and model development. SKB TR-02-13, Svensk Kärnbränslehantering AB.

Andresen C A, Hansen A, Le Goc R, Davy P, Hope S M, 2013. Topology of fracture networks. Frontiers in Physics 1. doi:10.3389/fphy.2013.00007

Ash R, Barrer R, Palmer D, 1965. Diffusion in multiple laminates. British Journal of Applied Physics 16, 873.

Auradou H, Drazer G, Hulin J-P, Koplik J, 2005. Permeability anisotropy induced by the shear displacement of rough fracture walls. Water Resources Research 41. doi:10.1029/2005WR003938

Auradou H, Drazer G, Boschan A, Hulin J-P, Koplik J, 2006. Flow channeling in a single fracture induced by shear displacement. Geothermics 35, 576–588.

Aydin A, Johnson A M, 1978. Development of faults as zones of deformation bands and as slip surfaces in sandstone. Pure and Applied Geophysics 116, 931–942.

Baecher G B, Einstein H H, Lanney N A, 1977. Statistical description of rock properties and sampling. In Proceedings of The 18th US Symposium on Rock Mechanics (USRMS), Golden, Colorado, June 1977. Paper ARMA-77-0400.

Baghbanan A, Jing L, 2008. Stress effects on permeability in a fractured rock mass with correlated fracture length and aperture. International Journal of Rock Mechanics and Mining Sciences 45, 1320–1334.

Baker L, Giancola A, Allahdadi F, 1992. Fracture and spall ejecta mass distribution: Lognormal and multifractal distributions. Journal of Applied Physics 72, 2724–2731.

Bandis S C, Lumsden A C, Barton N R, 1983. Fundamentals of rock joint deformation. International Journal of Rock Mechanics and Mining Sciences & Geomechanics Abstracts 20, 249–268.

Barker J A, 2018. Intersection statistics and percolation criteria for fractures of mixed shapes and sizes. Computers & Geosciences 112, 47–53.

Baroni G, Tarantola S, 2014. A General Probabilistic Framework for uncertainty and global sensitivity analysis of deterministic models: A hydrological case study. Environmental Modelling & Software 51, 26–34.

Barton C A, Zoback M D, 1992. Self-similar distribution and properties of macroscopic fractures at depth in crystalline rock in the Cajon Pass Scientific Drill Hole. Journal of Geophysical Research: Solid Earth 97, 5181–5200.

Barton C, Moos D, Hartley L, Baxter S, Foulquier L, Holl H, Hogarth R, 2013. Geomechanically coupled simulation of flow in fractured reservoirs. In Proceedings of Thirty-Eighth Workshop on Geothermal Reservoir Engineering, SGP-TR-198. Stanford University, Stanford, California, 11–13 February, 2013. SGP-TR-198.

Barton N, 1973. Review of a new shear-strength criterion for rock joints. Engineering Geology 7, 287–332.

Barton N, 1978. Suggested methods for the quantitative description of discontinuities in rock masses. International Journal of Rock Mechanics and Mining Sciences & Geomechanics Abstracts 15, 319–368.

Barton N, 1982. Modelling rock joint behavior from in situ block tests: implications for nuclear waste repository design. ONWI--308, Office of Nuclear Waste Isolation, Battelle Project Management Division.

Barton N, Choubey V, 1977. The shear strength of rock joints in theory and practice. Rock Mechanics 10, 1–54.

Barton N, Quadros E, 2014. Gas-shale fracturing and fracture mobilization in shear: Quo vadis? Proceedings of ISRM Conference on Rock Mechanics for Natural Resources and Infrastructure – SBMR 2014, Goiania, Brazil, September 2014. International Society for Rock Mechanics and Rock Engineering, paper ISRM-SBMR-2014-016.

Barton N, Lien R, Lunde J, 1974. Engineering classification of rock masses for the design of tunnel support. Rock Mechanics 6, 189–236.

Barton N, Bandis S, Bakhtar K, 1985. Strength, deformation and conductivity coupling of rock joints. International Journal of Rock Mechanics and Mining Sciences & Geomechanics Abstracts 22, 121–140.

Bates R, Jackson J (eds), 1987. Glossary of geology. 3rd ed. Alexandria, VA: American Geological Institute.

Baxter S, Hartley L, Hoek J, Myers S, Tsitsopoulos V, Williams T, 2019. Upscaling of brittle deformation zone flow and transport properties. SKB R-19-01, Svensk Kärnbränslehantering AB.

Bayes T R, 1763. An essay towards solving a problem in the doctrine of chances. Republished in Biometrika 45, 296–315.

Ben-Zion Y, 2008. Collective behavior of earthquakes and faults: Continuum-discrete transitions, progressive evolutionary changes, and different dynamic regimes. Reviews of Geophysics 46. doi:10.1029/2008RG000260

Bergman T, Andersson J, Hermansson T, Zetterström Evins L, Albrecht L, Stephens M B, Petersson J, Nordman C, 2004. Forsmark site investigation. Bedrock mapping. Stage 2 (2003) – bedrock data from outcrops and the basal parts of trenches and shallow boreholes through the Quaternary cover. SKB P-04-91, Svensk Kärnbränslehantering AB.

Berkowitz B, Adler P M, 1998. Stereological analysis of fracture network structure in geological formations. Journal of Geophysical Research 103, 15339–15360.

Berkowitz B, Balberg I, 1993. Percolation theory and its application to groundwater hydrology. Water Resources Research 29, 775–794.

Berkowitz B, Zhou J, 1996. Reactive solute transport in a single fracture. Water Resources Research 32, 901–913.

Berkowitz B, Bour O, Davy P, Odling N, 2000. Scaling of fracture connectivity in geological formations. Geophysical Research Letters 27, 2061–2064.

Bibby R, 1981. Mass transport of solutes in dual-porosity media. Water Resources Research 17, 1075–1081.

Bieniawski Z, 1973. Engineering classification of jointed rock masses. Civil Engineer in South Africa 15. doi:10.1016/0148-9062(74)90924-3

Bieniawski Z T, 1989. Engineering rock mass classifications: a complete manual for engineers and geologists in mining, civil, and petroleum engineering. Wiley.

Billaux D, Chiles J, Hestir K, Long J, 1989. Three-dimensional statistical modelling of a fractured rock mass—an example from the Fanay-Augères mine. Proceedings of International Journal of Rock Mechanics and Mining Sciences & Geomechanics Abstracts, 1989. Elsevier.

Billaux D, Guérin F, Wendling J, 1994. Hydrodynamic modelling of the Äspö HRL. Discrete fracture model. HRL ICR Reports SKB ICR-94-14, Svensk Kärnbränslehantering AB.

Bingham C, 1974. An antipodally symmetric distribution on the sphere. J The Annals of Statistics. p. 1201–1225.

Black J H, 2012. Selective review of the hydrogeological aspects of SR-Site.

Black J H, Barker J A, Woodman N D, 2007. An investigation of 'sparse channel networks'. Characteristic behaviours and their causes. R-Reports SKB R-07-35, Svensk Kärnbränslehantering AB.

Bodin J, Delay F, De Marsily G, 2003. Solute transport in a single fracture with negligible matrix permeability: 1. fundamental mechanisms. Hydrogeology Journal. Volume 11, issue 4, p. 418–433

Bonneau F, Henrion V, Caumon G, Renard P, Sausse J, 2013. A methodology for pseudo-genetic stochastic modeling of discrete fracture networks. Computers & Geosciences 56, 12–22.

Bonneau F, Caumon G, Renard P, 2016. Impact of a stochastic sequential initiation of fractures on the spatial correlations and connectivity of discrete fracture networks. Journal of Geophysical Research: Solid Earth 121, 5641–5658.

Bonnet E, Bour O, N.E. O, Davy P, Main I, Cowie P, Berkowitz B, 2001. Scaling of fracture systems in geological media. Reviews of Geophysics 39, 347–384.

Bour O, Davy P, 1997. Connectivity of random fault networks following a power law fault length distribution. Water Resources Research 33, 1567–1584.

Bour O, Davy P, 1998. On the connectivity of three-dimensional fault networks. Water Resources Research 34, 2611–2622.

Bour O, Davy P, Darcel C, Odling N, 2002. A statistical scaling model for fracture network geometry, with validation on a multiscale mapping of a joint network (Hornelen Basin, Norway). Journal of Geophysical Research: Solid Earth 107, ETG 4-1–ETG 4-12.

Boussinesq J, 1868. Mémoire sur l'influence des frottements dans les mouvements réguliers des fluids. Journal de mathématiques pures et appliquées 13, 377–424. (In French.)

Bridges M, 1990. Identification and characterisation of sets of fractures and faults in rock. In Barton N, Stephansson O (eds). Rock joints: proceedings of the International Symposium on Rock Joints, Loen, Norway, 4–6 June 1990. Rotterdam: Balkema, 19–26.

Brodsky E E, Roeloffs E, Woodcock D, Gall I, Manga M, 2003. A mechanism for sustained groundwater pressure changes induced by distant earthquakes. Journal of Geophysical Research: Solid Earth 108. doi:10.1029/2002jb002321

Brodsky E E, Gilchrist J J, Sagy A, Collettini C, 2011. Faults smooth gradually as a function of slip. Earth and Planetary Science Letters 302, 185–193.

Brodsky E E, Kirkpatrick J D, Candela T, 2016. Constraints from fault roughness on the scale-dependent strength of rocks. Geology 44, 19–22.

Brown S R, 1987. Fluid flow through rock joints; the effect of surface roughness. Journal of Geophysical Research: Solid Earth 92, 1337–1347.

Brown S R, Scholz C H, 1985. Broad bandwidth study of the topography of natural rock surfaces. Journal of Geophysical Research: Solid Earth 90, 12575–12582.

Brown S, Caprihan A, Hardy R, 1998. Experimental observation of fluid flow channels in a single fracture. Journal of Geophysical Research: Solid Earth 103, 5125–5132.

Brunetti C, Linde N, Vrugt J A, 2017. Bayesian model selection in hydrogeophysics: Application to conceptual subsurface models of the South Oyster Bacterial Transport Site, Virginia, USA. Advances in Water Resources 102, 127–141.

Byegård J, Selnert E, Tullborg E-L, 2008. Bedrock transport properties. Data evaluation and retardation model. Site descriptive modelling SDM-Site Forsmark. SKB R-08-98, Svensk Kärnbränslehantering AB.

Bym T, Follin S, Hermanson J, 2018. A numerical study of channeling in heterogeneous vs. calibrated homogeneous discrete fracture network realizations. Proceedings of 2nd International Discrete Fracture Network Engineering Conference, Seattle, Washington, USA, June 2018. American Rock Mechanics Association. Paper ARMA-DFNE-18-1296.

Bäckblom G, 2008. Excavation damage and disturbance in crystalline rock – results from experiments and analyses. SKB TR-08-08, Svensk Kärnbränslehantering AB.

Börgesson L, Sandén T, Dueck A, Andersson L, Jensen V, Nilsson U, Olsson S, Åkesson M, Kristensson O, Svensson U, 2015. Consequences of water inflow and early water uptake in deposition holes. EVA Project. SKB TR-14-22, Svensk Kärnbränslehantering AB.

Cacas M-C, 1989. Développement d'un modèle tridimensionnel stochastique discret pour la simulation de l'écoulement et des transferts de masse et de chaleur en milieu fracturé. PhD thesis. Ecole Nationale Supérieure des Mines, Paris, France. (In French.)

Cacas M C, Ledoux E, Marsily G d, Tillie B, Barbeau A, Durand E, Feuga B, Peaudecerf P, 1990. Modeling fracture flow with a stochastic discrete fracture network: calibration and validation. 1. The flow model. Water Resources Research 26, 479–489.

Caine J S, Evans J P, Forster C B, 1996. Fault zone architecture and permeability structure. Geology 24, 1025–1028.

Callahan O A, Eichhubl P, Olson J E, Davatzes N C, 2019. Fracture mechanical properties of damaged and hydrothermally altered rocks, Dixie Valley-Stillwater Fault Zone, Nevada, USA. Journal of Geophysical Research: Solid Earth 124, 4069–4090.

Candela T, Renard F, Bouchon M, Brouste A, Marsan D, Schmittbuhl J, Voisin C, 2009. Characterization of fault roughness at various scales: Implications of three-dimensional high resolution topography measurements. Pure and Applied Geophysics 166, 1817–1851.

Candela T, Renard F, Klinger Y, Mair K, Schmittbuhl J, Brodsky E E, 2012. Roughness of fault surfaces over nine decades of length scales. Journal of Geophysical Research: Solid Earth 117. doi:10.1029/2011jb009041

Cantor G, 1883. On infinite, linear point-manifolds (sets). Mathematishe Annalen 21, 545–591.

Cappa F, Guglielmi Y, Rutqvist J, Tsang C-F, Thoraval A, 2006. Hydromechanical modelling of pulse tests that measure fluid pressure and fracture normal displacement at the Coaraze Laboratory site, France. International Journal of Rock Mechanics and Mining Sciences 43, 1062–1082.

Carlsson A, 1979. Characteristic features of a superficial rock mass in southern central Sweden: horizontal and subhorizontal fractures and filling material. PhD thesis. Uppsala University, Sweden.

Carslaw H S, Jaeger J C, 1959. Conduction of heat in solids. 2nd ed. Oxford: Clarendon.

Carter T, Jefferies M, Rombough V, Dershowitz W, 2015. Aperture controlled grouting – benefits of the discrete fracture network approach. Mining Technology 124, 188–202.

Chan T, Stanchell F W, 2005. Subsurface hydro-mechanical (HM) impacts of glaciation: Sensitivity to transient analysis, HM coupling, fracture zone connectivity and model dimensionality. International Journal of Rock Mechanics and Mining Sciences 42, 828–849.

Charles R J, 1958. Dynamic fatigue of glass. Journal of Applied Physics 29, 1657–1662.

Chernick M R, 2007. Bootstrap methods: a guide for practitioners and researchers. 2nd ed. John Hoboken, NJ: Wiley.

Chilès J-P, Delfiner P, 1999. Geostatistics: modeling spatial uncertainty. New York: Wiley.

Choi J-H, Jin K, Enkhbayar D, Davvasambuu B, Bayasgalan A, Kim Y-S, 2012. Rupture propagation inferred from damage patterns, slip distribution, and segmentation of the 1957 M_w8.1 Gobi-Altay earthquake rupture along the Bogd fault, Mongolia. Journal of Geophysical Research: Solid Earth 117. doi:10.1029/2011jb008676

Choi J-H, Edwards P, Ko K, Kim Y-S, 2016. Definition and classification of fault damage zones: A review and a new methodological approach. Earth-Science Reviews 152, 70–87.

Claesson-Liljedahl L, Munier R, Sandström B, Drake H, Tullborg E-L, 2011. Assessment of fractures classified as non-mineralised in the Sicada database. SKB R-11-02, Svensk Kärnbränslehantering AB.

Clark R M, Cox S J D, 1996. A modern regression approach to determining fault displacement-length scaling relationships. Journal of Structural Geology 18, 147–152.

Cook N G W, 1992. Natural joints in rock: mechanical, hydraulic and seismic behaviour and properties under normal stress. International Journal of Rock Mechanics and Mining Sciences & Geomechanics Abstracts 29, 198–223.

Cooley J W, Tukey J W, 1965. An algorithm for the machine calculation of complex Fourier series. Mathematics of Computation 19, 297–301.

Cordes C, Kinzelbach W, 1992. Continuous groundwater velocity fields and path lines in linear, bilinear, and trilinear finite elements. Water Resources Research 28, 2903–2911.

Cosgrove J, Stanfors R, Röshoff K, 2006. Geological characteristics of deformation zones and a strategy for their detection in a repository. SKB R-06-39, Svensk Kärnbränslehantering AB.

Cosma C, Enescu N, Balu L, 2005. Forsmark site investigation. Vertical seismic profiling from the boreholes KFM01A and KFM02A. SKB P-05-168, Svensk Kärnbränslehantering AB.

Cowie P A, 1992. The growth of faults. PhD thesis. Columbia University, New York.

Cowie P A, Scholz C H, 1992a. Physical explanation for the displacement-length relationship of faults using a post-yield fracture mechanics model. Journal of Structural Geology 14, 1133–1148.

Cowie P A, Scholz C H, 1992b. Growth of faults by accumulation of seismic slip. Journal of Geophysical Research 97, 11085–11095.

Cowie P A, Scholz C H, 1992c. Displacement-length scaling relationship for faults; data synthesis and discussion. Journal of Structural Geology 14, 1149–1156.

Crawford J, 2008. Bedrock transport properties Forsmark. Site descriptive modelling SDM-Site Forsmark. SKB R-08-48, Svensk Kärnbränslehantering AB.

Crawford J, 2010. Bedrock K_d data and uncertainty assessment for application in SR-Site geosphere transport calculations. SKB R-10-48, Svensk Kärnbränslehantering AB.

Crawford J, Löfgren M, 2019. Modelling of radionuclide retention by matrix diffusion in a layered rock model. SKB R-17-22, Svensk Kärnbränslehantering AB.

Cronquist T, Forssberg O, Maersk Hansen L, Jonsson A, Koyi S, Leiner P, Vestgård J, Petersson J, Skogsmo G, 2005. Detailed fracture mapping of two trenches at Forsmark. Forsmark site investigation. Site Investigation Reports; P-Reports SKB P-04-88, Svensk Kärnbränslehantering AB.

Cruden D, 1977. Describing the size of discontinuities. Proceedings of International Journal of Rock Mechanics and Mining Sciences & Geomechanics Abstracts, 1977. Elsevier.

Cvetkovic V, 2010. Significance of fracture rim zone heterogeneity for tracer transport in crystalline rock. Water Resources Research. Volume 46, issue 3.

Cvetkovic V, 2017a. Statistical formulation of generalized tracer retention in fractured rock. Water Resources Research 53, 8736–8759.

Cvetkovic V, 2017b. Dynamic characterisation of the specific surface area for fracture networks. Proceedings of AGU Fall Meeting 2017, abstract #NG52A-02.

Cvetkovic V, Cheng H, 2002. Äspö Hard Rock Laboratory. TRUE Block Scale project. Evaluation of block scale tracer retention understanding experiments at Äspö HRL. SKB IPR-02-33, Svensk Kärnbränslehantering AB.

Cvetkovic V, Selroos J-O, Cheng H, 1999. Transport of reactive tracers in rock fractures. Journal of Fluid Mechanics 378, 335–356.

Cvetkovic V, Poteri A, Selroos J O, Zou L, 2020. Inference of retention time from tracer tests in crystalline rock. Water Resources Research 56. doi:10.1029/2019WR025266

D'Alessandro M, Mousty F, Bidoglio G, Guimera J, Benet I, Sánchez-Vila X, Gutiérrez M G, De Llano A Y, 1997. Field tracer experiment in a low permeability fractured medium: results from El Berrocal site. Journal of Contaminant Hydrology. Volume 26, issue 1-4, p. 189–201.

Darcel C, 2003. Äspö Hard Rock Laboratory. True Block Scale continuation project. Assessment of the feasibility of tracer tests with injection in "background fractures" using a model based on a power law fracture length distribution. SKB IPR-03-41, Svensk Kärnbränslehantering AB.

Darcel C, Bour O, Davy P, 2003. Stereological analysis of fractal fracture networks. Journal of Geophysical Research: Solid Earth 108. doi:10.1029/2002jb002091

Darcel C, Davy P, Bour O, de Dreuzy J R, 2004. Alternative DFN model based on initial site investigations at Simpevarp. SKB R-04-76, Svensk Kärnbränslehantering AB.

Darcel C, Davy P, Bour O, de Dreuzy J-R, 2006. Discrete fracture network for the Forsmark site. SKB R-06-79, Svensk Kärnbränslehantering AB.

Darcel C, Davy P, Le Goc R, Bour O, de Dreuzy J R, 2009. Statistical methodology for Discrete Fracture Models – including fracture size, orientation uncertainty together with intensiy uncertainty and variability. SKB R-09-38, Svensk Kärnbränslehantering AB.

Darcel C, Davy P, Le Goc R, 2012. Statistical fracture domain methodology for DFN modeling applied to site characterization. Proceedings of EUROCK 2012, Stockholm, 28–30 May 2012. BeFo (Bergteknisk Forskning) and International Society for Rock Mechanics (ISRM).

Darcel C, Le Goc R, Davy P, 2013. Development of the statistical fracture domain methodology – application to the Forsmark site. SKB R-13-54, Svensk Kärnbränslehantering AB.

Darcel C, Le Goc R, Davy P, Olofsson I, 2014. Including variability into a quantitative DFN modeling approach– application to SKB sites. In Kennard D S, Eberhardt E, Elmo D (eds). Proceedings of 1st International Conference on Discrete Fracture Network Engineering DFNE 2014, Vancouver, BC, Canada, 19–22 October 2014. The Canadian Rock Mechanics Association (CARMA).

Darcel C, Davy P, Le Goc R, Mas Ivars D, 2018. Rock mass effective properties from a DFN approach. Proceedings of 2nd International Discrete Fracture Network Engineering Conference, Seattle, 20–22 June 2018. American Rock Mechanics Association.

Darcel C, Davy P, Le Goc R, 2021. Alternative Hydro DFN modeling at the Forsmark site – phase I. 016R-017. Under review, Svensk Kärnbränslehantering AB.

Davy P, 1993. On the frequency-length distribution of the San Andreas fault system. Journal of Geophysical Research: Solid Earth and Planets 98, 12141–12151.

Davy P, Sornette A, Sornette D, 1990. Some consequences of a proposed fractal nature of continental faulting. Nature 348, 56–58.

Davy P, Darcel C, Bour O, Munier R, de Dreuzy J R, 2006. A note on the angular correction applied to fracture intensity profiles along drill core. Journal of Geophysical Research: Solid Earth 111. doi:10.1029/2005jb004121

Davy P, Le Goc R, Darcel C, Bour O, de Dreuzy J-R, Munier R, 2010. A likely universal model of fracture scaling and its consequence for crustal hydromechanics. Journal of Geophysical Research: Solid Earth 115. doi:10.1029/2009jb007043

Davy P, Le Goc R, Darcel C, 2013. A model of fracture nucleation, growth and arrest, and consequences for fracture density and scaling. Journal of Geophysical Research: Solid Earth 118, 1393–1407.

Davy P, Darcel C, Le Goc R, Mas Ivars D, 2018a. Elastic properties of fractured rock masses with frictional properties and power law fracture size distributions. Journal of Geophysical Research: Solid Earth 123, 6521–6539.

Davy P, Darcel C, Le Goc R, Munier R, Selroos J-O, Mas Ivars D, 2018b. DFN, why, how and what for, concepts, theories and issues. In Proceedings of the 2nd International Discrete Fracture Network Engineering Conference, Seattle, Washington, 20–22 June 2018. American Rock Mechanics Association.

Davy P, Goc R L, Darcel C, Selroos J-O, Dooleaghe D, 2019. Validation of hydraulics models in fractured rocks. Application to the Forsmark site (Sweden). Abstract H41H-1760, AGU Fall Meeting, San Fransisco, California.

Davydova M, Uvarov S, Chudinov V, 2014. Scaling law of quasi brittle fragmentation. Procedia Materials Science 3, 580–585.

de Dreuzy J R, Davy P, Bour O, 2000. Percolation parameter and percolation-threshold estimates for three-dimensional random ellipses with widely scattered distributions of eccentricity and size. Physical Review E 62, 5948–5952.

de Marsily G, Combes P, Goblet P, 1992. Comment on 'Ground-water models cannot be validated', by L.F. Konikow & J.D. Bredehoeft. Advances in Water Resources 15, 367–369.

Deere D, 1963. Technical description of rock cores. Geologie und Bauwesen 28.

Deere D, Hendron A, Patton F, Cording E, 1966. Design of surface and near-surface construction in rock. In Proceedings of the 8th US symposium on rock mechanics (USRMS), Minneapolis, Minnesota, 15–17 September, 1966. American Rock Mechanics Association.

Den Outer A, Kaashoek J, Hack H, 1995. Difficulties with using continuous fractal theory for discontinuity surfaces. International Journal of Rock Mechanics and Mining Sciences & Geomechanics Abstracts 32, 3–9.

Dentz M, Le Borgne T, Englert A, Bijeljic B, 2011. Mixing, spreading and reaction in heterogeneous media: A brief review. Journal of Contaminant Hydrology 120, 1–17.

Dershowitz B, Eiben T, Follin S, Andersson J, 1999. SR 97 – Alternative models project. Discrete fracture network modelling for performance assessment of Aberg. SKB R-99-43, Svensk Kärnbränslehantering AB.

Dershowitz B, Shuttle D, Klise K, Uchida M, Metcalfe R, Cave M, 2000. Äspö Hard Rock Laboratory. Fracman modelling of geochemical end-member transport pathways Äspö HRL, Äspö Sweden. Task 5. SKB IPR-02-37, Svensk Kärnbränslehantering AB.

Dershowitz W, 1985. Rock joint system. PhD thesis. Massachusetts Institute of Technology, Cambridge, Massachusetts.

Dershowitz W S, Einstein H H, 1988. Characterizing rock joint geometry with joint system models. Rock Mechanics and rock Engineering 21, 21–51.

Dershowitz W, Herda H H, 1992. Interpretation of fracture spacing and intensity. In Proceedings of the The 33rd U.S. Symposium on Rock Mechanics (USRMS), Santa Fe, New Mexico, 3–5 June 1992.

Dershowitz W, Klise K, 2002. Äspö Hard Rock Laboratory. TRUE Block scale project. Evaluation of fracture network transport pathways and processes using the Channel Network approach. SKB IPR-02-34, Svensk Kärnbränslehantering AB.

Dershowitz W, Baecher G, Einstein H, 1979. Prediction of rock mass deformability. In Proceedings of the 4th ISRM Congress, Montreux, Switzerland, 2–8 September 1979. Vol. 1, 605–611.

Dershowitz W, Busse R, Geier J, Uchida M, 1996. A stochastic approach for fracture set definition. In Proceedings of the 2nd North American Rock Mechanics Symposium, Montreal, Canada, 19–21 June 1996. American Rock Mechanics Association.

Dershowitz B, Shuttle D, Klise K, Uchida M, Metcalfe R, Cave M, 2000. Äspö Hard Rock Laboratory. Fracman modelling of geochemical end-member transport pathways Äspö HRL, Äspö Sweden. Task 5. SKB IPR-02-37, Svensk Kärnbränslehantering AB.

Dershowitz W, Uchida M, Shuttle D, 2003a. Äspö Hard Rock Laboratory. Äspö Task Force. GoldSim and FrackMan/LTG Modeling Task 6A, 6B and 6B2. Performance assessment modeling using site characterisation data (PASC). SKB IPR-04-32, Svensk Kärnbränslehantering AB.

Dershowitz W, Winberg A, Hermanson J, Byegård J, Tullborg E-L, Andersson P, Mazurek M, 2003b. Äspö Hard Rock Laboratory. Äspö Task Force on modelling of groundwater flow and transport of solutes. Task 6c. A semi-synthetic model of block scale conductive structures at the Äspö HRL. SKB IPR-03-13, Svensk Kärnbränslehantering AB.

Dessirier B, Tsang C-F, Niemi A, 2018. A new scripting library for modeling flow and transport in fractured rock with channel networks. Computers & Geosciences 111, 181–189.

Diersch H-J G, 1998. About the difference between the convective and the divergence form of the transport equation. FEFLOW Software White Papers, Vol. 1, Chapter 6.

Dodge Y (ed), 2006. The Oxford dictionary of statistical terms. Oxford: Oxford University Press.

Doe T, 1999. Äspö Hard Rock Laboratory. TRUE Block Scale project. Reconciliation of the March´99 structural model and hydraulic data. SKB IPR-01-53, Svensk Kärnbränslehantering AB.

Doe T W, Long J C S, Endo H K, Wilson C R, 1982. Approaches to evaluating the permeability and porosity of fractured rock masses. In Proceedings of the 23rd U.S. Symposium on Rock Mechanics (USRMS), Berkeley, California, 25–27 August 1982. American Rock Mechanics Association.

Doolaeghe D, 2021. Colmatage des réseaux de fractures, modèles et conséquences hydrologiques. PhD thesis. University of Rennes. (In French.)

Dorn C, Linde N, Le Borgne T, Bour O, Klepikova M, 2012. Inferring transport characteristics in a fractured rock aquifer by combining single-hole ground-penetrating radar reflection monitoring and tracer test data. Water Resources Research 48. doi:10.1029/2011WR011739

Drake H, Sandström B, Tullborg E-L, 2006. Mineralogy and geochemistry of rocks and fracture fillings from Forsmark and Oskarshamn: Compilation of data for SR-Can. SKB R-06-109, Svensk Kärnbränslehantering AB.

Drake H, Heim C, Roberts N M, Zack T, Tillberg M, Broman C, Ivarsson M, Whitehouse M J, Åström M E, 2017. Isotopic evidence for microbial production and consumption of methane in the upper continental crust throughout the Phanerozoic eon. Earth and Planetary Science Letters 470, 108–118.

Duba A G, Durham W, Heard H C, Handin J, Wang H (eds), 1990. The brittle-ductile transition in rocks: the Heard volume. Washington, DC: American Geophysical Union.

Du Bernard X, Labaume P, Darcel C, Davy P, Bour O, 2002. Cataclastic slip band distribution in normal fault damage zones, Nubian sandstones, Suez rift. Journal of Geophysical Research: Solid Earth 107, ETG 6-1–ETG 6-12.

Durlofsky L J, 1991. Numerical calculation of equivalent grid block permeability tensors for heterogeneous porous media. Water Resources Research 27, 699–708.

Eftekhari M, Baghbanan A, Bagherpour R, 2014. The effect of fracture patterns on penetration rate of TBM in fractured rock mass using probabilistic numerical approach. Arabian Journal of Geosciences 7, 5321–5331.

Einstein H H, Baecher G B, 1983. Probabilistic and statistical methods in engineering geology. Rock Mechanics and Rock Engineering 16, 39–72.

Einstein H H, Locsin J-L Z, 2012. Modeling rock fracture intersections and application to the Boston area. Journal of Geotechnical and Geoenvironmental Engineering 138, 1415–1421.

Elmo D, Rogers S, Stead D, Eberhardt E, 2014. Discrete Fracture Network approach to characterise rock mass fragmentation and implications for geomechanical upscaling. Mining Technology 123, 149–161.

Epstein B, 1947. The mathematical description of certain breakage mechanisms leading to the logarithmico-normal distribution. Journal of the Franklin Institute 244, 471–477.

Ericsson L O, Thörn J, Christiansson R, Lehtimäki T, Ittner H, Hansson K, Butron C, Sigurdsson O, Kinnbom P, 2015. A demonstration project on controlling and verifying the excavation-damaged zone. Experience from the Äspö Hard Rock Laboratory. SKB R-14-30, Svensk Kärnbränslehantering AB.

Esaki T, Du S, Mitani Y, Ikusada K, Jing L, 1999. Development of a shear-flow test apparatus and determination of coupled properties for a single rock joint. International Journal of Rock Mechanics and Mining Sciences 36, 641–650.

Esmaieli K, Hadjigeorgiou J, Grenon M, 2010. Estimating geometrical and mechanical REV based on synthetic rock mass models at Brunswick Mine. International Journal of Rock Mechanics and Mining Sciences 47, 915–926.

Evans M, Hastings N, Peacock B, 1993. Statistical distributions. 2nd ed. New York: Wiley.

Fang Y, Elsworth D, Cladouhos T T, 2015. Estimating in situ permeability of stimulated EGS reservoirs using MEQ moment magnitude: an analysis of Newberry MEQ data. In Proceedings of the 40th Workshop on Geothermal Reservoir Engineering, Stanford University, 2015.

Fang Y, Elsworth D, Ishibashi T, Zhang F, 2018. Permeability Evolution and Frictional Stability of Fabricated Fractures With Specified Roughness. Journal of Geophysical Research: Solid Earth 123, 9355–9375.

Faulkner D R, Mitchell T M, Jensen E, Cembrano J, 2011. Scaling of fault damage zones with displacement and the implications for fault growth processes. Journal of Geophysical Research: Solid Earth 116. doi:10.1029/2010jb007788

Feder J, 1988. Fractals. New York: Plenum Press.

Fernàndez-Garcia D, Llerar-Meza G, Gómez-Hernández J J, 2009. Upscaling transport with mass transfer models: Mean behavior and propagation of uncertainty. Water Resources Research 45. doi:10.1029/2009WR007764

Ferrill D A, Morris A P, 2003. Dilational normal faults. Journal of Structural Geology 25, 183–196.

Figueiredo B, Tsang C-F, Niemi A, Lindgren G, 2016. Review: The state-of-art of sparse channel models and their applicability to performance assessment of radioactive waste repositories in fractured crystalline formations. Hydrogeology Journal 24, 1607–1622.

Fine R A, Millero F J, 1973. Compressibility of water as a function of temperature and pressure. The Journal of Chemical Physics 59, 5529–5536.

Finsterle S, 2019. Overall evaluation of Tasks 8A–D, F, and water-uptake test related to modelling of the interaction between engineered and natural barriers. Task 8 of SKB Task Forces EBS and GWFTS. SKB TR-17-08, Svensk Kärnbränslehantering AB.

Fisher N I, Lewis T, Embleton B J, 1993. Statistical analysis of spherical data. Cambridge: Cambridge University Press.

Fisher R, 1953. Dispersion on a sphere. Royal Society of London Proceedings 217, 295–305.

Follin S, 2008. Bedrock hydrogeology Forsmark. Site descriptive modelling, SDM-Site Forsmark. SKB R-08-95, Svensk Kärnbränslehantering AB.

Follin S, Hermanson J, 1996. A discrete fracture network model of the Äspö TBM tunnel rock mass. SKB Djupförvar Arbetsrapport AR D-97-001, Svensk Kärnbränslehantering AB.

Follin S, Stigsson M, 2013. A transmissivity model for deformation zones in fractured crystalline rock and its possible correlation to in situ stress at the proposed high-level nuclear waste repository site at Forsmark, Sweden. Hydrogeology Journal 22, 299–311.

Follin S, Stigsson M, 2014. A transmissivity model for deformation zones in fractured crystalline rock and its possible correlation to in situ stress at the proposed high-level nuclear waste repository site at Forsmark, Sweden. Hydrogeology Journal 22, 299–311.

Follin S, Johansson P-O, Hartley L, Jackson P, Roberts D, Marsic N, 2007a. Hydrogeological conceptual model development and numerical modelling using CONNECTFLOW. Forsmark modelling stage 2.2. SKB R-07-49, Svensk Kärnbränslehantering AB.

Follin S, Levén J, Hartley L, Jackson P, Joyce S, Roberts D, Swift B, 2007b. Hydrogeological characterisation and modelling of deformation zones and fracture domains, Forsmark modelling stage 2.2. SKB R-07-48, Svensk Kärnbränslehantering AB.

Follin S, Hartley L, Rhén I, Jackson P, Joyce S, Roberts D, Swift B, 2014. A methodology to constrain the parameters of a hydrogeological discrete fracture network model for sparsely fractured crystalline rock, exemplified by data from the proposed high-level nuclear waste repository site at Forsmark, Sweden. Hydrogeology Journal 22, 313–331.

Forsman I, Zetterlund M, Rhén I, 2004. Correlation of Posiva flow log anomalies to core mapped features in Forsmark (KFM01A to KFM05A). SKB R-04-77, Svensk Kärnbränslehantering AB.

Forssberg O, Mærsk Hansen L, Koyi S, Vestgård J, Öhman J, Petersson J, Albrecht J, Hedenström A, Gustavsson J, 2007. Forsmark site investigation. Detailed fracture and bedrock mapping, Quaternary investigations and GPR measurements at excavated outcrop AFM001264. SKB P-05-269, Svensk Kärnbränslehantering AB.

Forssman I, Zetterlund M, Forsmark T, Rhén I, 2006. Correlation of Posiva Flow Log anomalies to core mapped features in KFM06A and KFM07A. Forsmark site investigation. SKB P-06-56, Svensk Kärnbränslehantering AB.

Forssman I, Forsmark T, Rhén I, 2008. Forsmark site investigation. Correlation of Posiva Flow Log anomalies to core mapped features in KFM02B, KFM08D and KFM11A. SKB P-07-128, Svensk Kärnbränslehantering AB.

Fourier J, 1822. Theorie analytique de la chaleur. Paris: Firmin Didot, père et fils.

Fournier A, Fussell D, Carpenter L, 1982. Computer rendering of stochastic models. Communications of the ACM 25, 371–384.

Fox A, Dershowitz W, Ziegler M, Uchida M, Takeuchi S, 2005. Äspö Hard Rock Laboratory. TRUE Block Scale continuation project. BS2B experiment: Discrete fracture and channel network modeling of solute transport modeling in fault and non-fault structures. SKB IPR-05-38, Svensk Kärnbränslehantering AB.

Fox A, La Pointe P, Hermanson J, 2007a. Techniques for large-scale site characterization and fracture domain modeling at the Forsmark Site, Uppland, Sweden (Poster),. 50th Annual Meeting of the Association of Engineering and Environmental Geologists (AEG), Universal City, CA., September 2007.

Fox A, La Pointe P, Hermanson J, Öhman J, 2007b. Statistical geological discrete fracture network model. Forsmark modelling stage 2.2. SKB R-07-46, Svensk Kärnbränslehantering AB.

Frampton A, Hyman J, Zou L, 2017. Internal fracture heterogeneity in discrete fracture network modelling: Effect of correlation length and textures with connected and disconnected permeability field. Proceedings of AGU Fall Meeting Abstracts, 2017.

Fransson Å, Gustafson G, 2006. Efterinjektering: inläckageprognos och design – förslag till analys. SveBeFo Rapport 75, SveBeFo – Stiftelsen Svensk Bergteknisk Forskning (Swedish Rock Engineering Research). (In Swedish.)

Fransson Å, Tsang C-F, Rutqvist J, Gustafson G, 2007. A new parameter to assess hydromechanical effects in single-hole hydraulic testing and grouting. International Journal of Rock Mechanics and Mining Sciences 44, 1011–1021.

Freeze R A, 1975. A stochastic-conceptual analysis of one-dimensional groundwater flow in nonuniform homogeneous media. Water Resources Research 11, 725–741.

Funehag J, 2012. Guide to grouting with silica sol: for sealing in hard rock. BeFo Report 118, Stiftelsen Bergteknisk Forskning, Sweden.

Fälth B, 2018. Simulating earthquake rupture and near-fault fracture response. PhD thesis. Uppsala University, Sweden.

Fälth B, Hökmark H, Lund B, Mai P M, Roberts R, Munier R, 2014. Simulating earthquake rupture and off-fault fracture response: Application to the safety assessment of the Swedish nuclear waste repository. Bulletin of the Seismological Society of America 105, 134–151.

Fälth B, Hökmark H, Lund B, 2016. Simulation of co-seismic secondary fracture displacements for different earthquake rupture scenarios at the proposed nuclear waste repository site in Forsmark. International Journal of Rock Mechanics and Mining Sciences 84, 142–158.

Fälth B, Lönnqvist M, Hökmark H, 2019. Co-seismic secondary fracture displacements under different stress conditions. Posiva Working Report 2019-10, Posiva Oy, Finland.

Föhlinger S, Koehler B, Harrström J, 2020. Hydraulic interference tests in HFM33 and HFM43–46. SKB P-19-11, Svensk Kärnbränslehantering AB.

Gale J E, 1999. Äspö Hard Rock Laboratory. Impact of flow geometry, flow regime, two-phase flow and degassing on the transmissivity of rough fractures. SKB IPR-99-08, Svensk Kärnbränslehantering AB.

Geier J E, 1996. SITE-94. Discrete-feature modelling of the Äspö Site: 2. Development of the integrated site-scale model. SKI Report 96:6, Swedish Nuclear Power Inspectorate.

Geier J E, Thomas A L, 1996. SITE-94. Discrete-feature modelling of the Äspö Site: 1. Discrete-fracture network models for the repository scale. SKI Report 96:5, Swedish Nuclear Power Inspectorate.

Geier J E, Axelsson C L, Hässler L, Benabderrahmane A, 1992. Discrete fracture modelling of the Finnsjön rock mass: Phase 2. SKB TR 92-07, Svensk Kärnbränslehantering AB.

Gelhar L W, 1993. Stochastic subsurface hydrology. Prentice-Hall.

Gelhar L W, Gutjahr A L, Naff R L, 1979. Stochastic analysis of macrodispersion in a stratified aquifer. Water Resources Research 15, 1387–1397.

Gelman A, Carlin J B, Stern H S, Rubin D B, Vehtari A, Dunson D B, 2013. Bayesian data analysis. 3rd ed. Boca Raton, FL: Chapman and Hall/CRC.

Gilbert G K, 1904. Domes and dome structure of the High Sierra. Bulletin of the Geological Society of America 15, 29–36.

Glamheden R, Fredriksson A, Röshoff K, Karlsson J, Hakami H, Christiansson R, 2007. Rock Mechanics Forsmark. Site descriptive modelling Forsmark stage 2.2. SKB R-07-31, Svensk Kärnbränslehantering AB.

Glynn P D, Voss C I, Provost A M, 1999. Deep penetration of oxygenated meltwaters from warm based ice sheets into the Fennoscandian shield. In Use of hydrogeochemical information in testing groundwater flow models: technical summary and proceedings of a workshop organised by the NEA Co-ordinating Group on Site Evaluation and Design of Experiments for Radioactive Waste Disposal (SEDE) and hosted by the Swedish Nuclear Fuel and Waste Management Company (SKB), Borgholm, Sweden, 1–3 September 1997. Paris: NEA/OECD.

Gnirk P, 1993. OECD/NEA International Stripa Project 1980–1992. Overview volume II: Natural barriers. Svensk Kärnbränslehantering AB.

Gokall-Norman K, Ludvigson J-E, 2005. Forsmark site investigation. Hydraulic interference tests. Boreholes HFM16, HFM19 and KFM02A. SKB P-05-78, Svensk Kärnbränslehantering AB.

Gokall-Norman K, Ludvigson J-E, 2008a. Forsmark site investigation. Large-scale interference test with borehole HFM14 used as pumping borehole, 2007. SKB P-07-228, Svensk Kärnbränslehantering AB.

Gokall-Norman K, Ludvigson J-E, 2008b. Hydraulic interference test with borehole HFM33 used as pumping borehole, November of 2007. SKB P-07-229, Svensk Kärnbränslehantering AB.

Gokall-Norman K, Svensson T, Ludvigson J-E, Jönsson S, 2004. Forsmark site investigation. Hydraulic interference test. Boreholes HFM18 and KFM03A. SKB P-04-307, Svensk Kärnbränslehantering AB.

Gokall-Norman K, Ludvigson J-E, Jönsson S, 2005a. Forsmark site investigation. Hydraulic interference test. Boreholes KFM04A, HFM10, HFM13, HFM19 and HFK252. SKB P-05-186, Svensk Kärnbränslehantering AB.

Gokall-Norman K, Ludvigson J-E, Jönsson S, 2005b. Forsmark site investigation. Hydraulic interference test in borehole HFM01. SKB P-05-236, Svensk Kärnbränslehantering AB.

Gokall-Norman K, Ludvigson J-E, Jönsson S, 2006. Forsmark site investigation. Hydraulic interference test. Boreholes KFM02A and KFM03A. SKB P-06-09, Svensk Kärnbränslehantering AB.

Goodman R, 1974. The mechanical properties of joints. In Proceedings of the Third Congress on ISRM, Denver. Vol. 1A. Washington, DC: National Academy of Sciences, 127–140.

Grady D E, 2010. Length scales and size distributions in dynamic fragmentation. International Journal of Fracture 163, 85–99.

Grassberger P, Procaccia I, 1983. Measuring the strangeness of srange attractors. Physica D. Nonlinear Phenomena 9, 189–208.

Grasselli G, 2006. Manuel Rocha medal recipient shear strength of rock joints based on quantified surface description. Rock Mechanics and Rock Engineering 39, 295. doi:10.1007/s00603-006-0100-0

Griffith A A, 1920. The phenomena of rupture and flow in solids. Philosophical Transactions of the Royal Society of London. Series A 221, 163–198.

Grigull S, Luth S, 2018. Detailed structural geological mapping on Äspö. SKB P-16-33, Svensk Kärnbränslehantering AB.

Guéguen Y, Kachanov M, 2012. Effective elastic properties of cracked rock – an overview. In Lehner Y M, Lehner F K (eds). Mechanics of crustal rocks. Vienna: Springer, 73–125.

Gupta A K, Adler P M, 2006. Stereological analysis of fracture networks along cylindrical galleries. Mathematical Geology 38, 233–267.

Gupta H V, Sorooshian S, Yapo P O, 1998. Toward improved calibration of hydrologic models: Multiple and noncommensurable measures of information. Water Resources Research 34, 751–763.

Gustafson G, Hodgkinson D, Ström A, 1995. Modelling groundwater flow and transport in fractured crystalline rock. Experiences from the OECD/NEA Stripa Project and the Äspö Hard Rock Laboratory, Sweden. In Proceedings of the International Conference On Mathematics and Computations, Reactor Physics, and Environmental Analyses, Portland, Oregon, 30 April – 4 May, 1995.

Gutenberg B, Richter C, 1954. Seismicity of the earth and related phenomena. Princeton, NJ: Princeton University Press.

Gylling B, Birgersson L, Moreno L, Neretnieks I, 1998a. Analysis of a long-term pumping and tracer test using the channel network model. Journal of Contaminant Hydrology 32, 203–222.

Gylling B, Moreno L, Neretnieks I, 1998b. Channel network model for flow and radionuclide migration. In Modelling the effects of spatial variability on radionuclide migration, Proceedings of the 2nd GEOTRAP Workshop, Paris, France, 279–289.

Gylling B, Moreno L, Neretnieks I, 1999. The channel network model – A tool for transport simulations in fractured media. Groundwater 37, 367–375.

Haggerty R, McKenna S A, Meigs L C, 2000. On the late-time behavior of tracer test breakthrough curves. Water Resources Research 36, 3467–3479.

Hakami E, Fredriksson A, Lanaro F, Wrafter J, 2008. Rock mechanics Laxemar. Site descriptive modelling SDM-Site Laxemar. SKB R-08-57, Svensk Kärnbränslehantering AB.

Hammah R, Curran J, 1998. Fuzzy cluster algorithm for the automatic identification of joint sets. International Journal of Rock Mechanics and Mining Science 35, 889–905.

Hardacre K M, Cowie P A, 2003a. Variability in fault size scaling due to rock strength heterogeneity: a finite element investigation. Journal of Structural Geology 25, 1735–1750.

Hardacre K M, Cowie P A, 2003b. Controls on strain localization in a two-dimensional elastoplastic layer: Insights into size-frequency scaling of extensional fault populations. Journal of Geophysical Research: Solid Earth 108. doi:10.1029/2001jb001712

Harrström J, Sjöberg O, Öhman J, 2018. Evaluation of Hydraulic Interference Tests in Forsmark with KFM24 as pumping borehole. SKB P-17-17, Svensk Kärnbränslehantering AB.

Harthong B, Scholtès L, Donzé F-V, 2012. Strength characterization of rock masses, using a coupled DEM–DFN model. Geophysical Journal International 191, 467–480.

Hartley L, Appleyard P, Baxter S, Hoek J, Roberts D, Swan D, 2013a. Development of a hydrogeological discrete fracture network model for the Olkiluoto site descriptive model 2011. Posiva Working Report 2012-32, Posiva Oy, Finland.

Hartley L, Hoek J, Swan D, Appleyard P, Baxter S, Roberts D, Simpson T, 2013b. Hydrogeological modelling for assessment of radionuclide release scenarios for the repository system 2012. Posiva Working Report 2012-42, Posiva Oy, Finland.

Hartley L, Baxter S, Williams T, 2016. Geomechanical coupled flow in fractures during temperate and glacial conditions. Posiva Working Report 2016-08, Posiva Oy, Finland.

Hartley L, Baxter S, Fox A, Poteri A, Aaltonen I, Koskinen L, Suikkanen J, 2018a. Status and outline planning report for discrete fracture network concepts, data, methods and models for the Olkiluoto site 2015. Posiva 2016-21, Posiva Oy, Finland.

Hartley L, Appleyard P, Baxter S, Hoek J, Joyce S, Mosley K, Williams T, Fox A, Cottrell M, La Pointe P, Gehör S, Darcel C, Le Goc R, Aaltonen I, Vanhanarkaus O, Löfman J, Poteri A, 2018b. Discrete fracture network modelling (Version 3) in support of Olkiluoto Site Description 2018. Posiva Working Report 2017-32, Posiva Oy, Finland.

Hartley L, Baxter S, Carty J, Follin S, Libby S, 2020. Exploratory integration of discrete fracture networks with hydrogeology for the upper bedrock at the Forsmark site. Svensk Kärnbränslehantering AB.

Harvey C F, Gorelick S M, 1995. Temporal moment-generating equations: Modeling transport and mass transfer in heterogeneous aquifers. Water Resources Research 31, 1895–1911.

Hawkins D M, 2004. The problem of overfitting. Journal of Chemical Information and Computer Sciences 44, 1–12.

Hellmuth K H, Siitari-Kauppi M, 1990. Investigation of the porosity of rocks. Impregnation with ^{14}C-polymethylmethacrylate (PMMA), a new technique. STUK-B-VALO 63, Finnish Centre for Radiation and Nuclear Safety Helsinki Finland.

Hencher S R, Lee S G, Carter T G, Richards L R, 2011. Sheeting joints: characterisation, shear strength and engineering. Rock Mechanics and Rock Engineering 44, 1–22.

Hentschel H G E, Proccacia I, 1983. The infinite number of generalised dimensions of fractals and strange attractors. Physica D: Nonlinear Phenomena 8, 435–444.

Hermanson J, Hansen L, Olofsson J, Sävås J, Vestgård J, 2003a. Forsmark. Detailed fracture mapping at the KFM02 and KFM03 drill sites. SKB P-03-12, Svensk Kärnbränslehantering AB.

Hermanson J, Hansen L, Vestgård J, Leiner P, 2003b. Forsmark site investigation. Detailed fracture mapping of the outcrops Klubbudden, AFM001098 and drill site 4, AFM001097. SKB P-03-115, Svensk Kärnbränslehantering AB.

Hermanson J, Hansen L, Wikholm M, Cronquist T, Leiner P, Vestgård J, Sandahl K-A, 2004. Oskarshamn site investigation. Detailed fracture mapping of four outcrops at the Simpevarp peninsula and Ävrö. SKB P-04-35, Svensk Kärnbränslehantering AB.

Hermanson J, Forssberg O, Fox A, La Pointe P, 2005. Statistical model of fractures and deformation zones. Preliminary site description, Laxemar subarea, version 1.2. SKB R-05-45, Svensk Kärnbränslehantering AB.

Hermansson T, Stephens M B, Corfu F, Andersson J, Page L, 2007. Penetrative ductile deformation and amphibolite-facies metamorphism prior to 1 851 Ma in the western part of the Svecofennian orogen, Fennoscandian Shield. Precambrian Research 153, 29–45.

Hermansson T, Stephens M B, Corfu F, Page L M, Andersson J, 2008a. Migratory tectonic switching, western Svecofennian orogen, central Sweden: Constraints from U/Pb zircon and titanite geochronology. Precambrian Research 161, 250–278.

Hermansson T, Stephens M B, Page L M, 2008b. $^{40}Ar/^{39}Ar$ hornblende geochronology from the Forsmark area in central Sweden: Constraints on late Svecofennian cooling, ductile deformation and exhumation. Precambrian Research 167, 303–315.

Hirata T, 1989. Fractal dimension of fault systems in Japan; fractal structure in rock fracture geometry at various scales. Pure and Applied Geophysics 131, 157–170.

Hjerne C, Nordqvist R, Harrström J, 2010. Compilation and analyses of results from cross-hole tracer tests with conservative tracers. SKB R-09-28, Svensk Kärnbränslehantering AB.

Hoek E, Brown E T, 1997. Practical estimates of rock mass strength. International Journal of Rock Mechanics and Mining Sciences 34, 1165–1186.

Hoek E, Brown E T, 2019. The Hoek–Brown failure criterion and GSI – 2018 edition. Journal of Rock Mechanics and Geotechnical Engineering 11, 445–463.

Hoek E, Carter T, Diederichs M, 2013. Quantification of the geological strength index chart. In Proceedings of the 47th US Rock Mechanics/Geomechanics Symposium, San Francisco, CA, 23–26 June 2013. American Rock Mechanics Association.

Hollmén K, 2008. R20 Programme: The development of grouting technique – Stop criteria and field tests. Posiva Working Report 2007-101, Posiva Oy, Finland.

Hope S M, Davy P, Maillot J, Le Goc R, Hansen A, 2015. Topological impact of constrained fracture growth. Frontiers in Physics 3. doi:10.3389/fphy.2015.00075

Hopkins D, 2000. The implications of joint deformation in analyzing the properties and behavior of fractured rock masses, underground excavations, and faults. International Journal of Rock Mechanics and Mining Sciences 37, 175–202.

Hsu Y-S, Walker J J, Ogren D E, 1986. A stepwise method for determining the number of component distributions in a mixture. Mathematical Geology 18, 153–160.

Hudson J, Priest S, 1979. Discontinuities and rock mass geometry. International Journal of Rock Mechanics and Mining Sciences & Geomechanics Abstracts 16, 339–362.

Hultgren P, Munier R, 2012. RoCS; a time efficient and precise underground mapping system. In Proceedings of the 34th International Geological Congress, IGC 34, Brisbane, Australia, 5–10 August 2012.

Hurmerinta E, Pekkanen J, Komulainen J, Rouhiainen P, 2012. Pressure, flow and hydraulic interference measurements in ONKALO at Olkiluoto, drillholes ONK-PP262 and ONK-PP274. Posiva Working Report 2011-86, Posiva Oy, Finland.

Hurst H E, 1957. A suggested statistical model of some time series which occur in nature. Nature 180, 494.

Hökmark H, Lönnqvist M, 2014. Reply to comment by Christopher Talbot on "Approach to estimating the maximum depth for glacially induced hydraulic jacking in fractured crystalline rock at Forsmark, Sweden". Journal of Geophysical Research: Earth Surface 119, 955–959.

Hökmark H, Fälth B, Wallroth T, 2006. T-H-M couplings in rock. Overview of results of importance to the SR-Can safety assessment. SKB R-06-88, Svensk Kärnbränslehantering AB.

Hökmark H, Lönnqvist M, Fälth B, 2010. THM-issues in repository rock. Thermal, mechanical, thermo-mechanical and hydro-mechanical evolution of the rock at the Forsmark and Laxemar sites. SKB TR-10-23, Svensk Kärnbränslehantering AB.

IAEA, 2018. IAEA safety glossary: 2018 edition. Vienna: International Atomic Energy Agency.

Incropera F P, Lavine A S, Bergman T L, DeWitt D P, 2007. Fundamentals of heat and mass transfer. 6th ed. New York: Wiley.

Iraola A, Trinchero P, Voutilainen M, Gylling B, Selroos J-O, Molinero J, Svensson U, Bosbach D, Deissmann G, 2017. Microtomography-based Inter-Granular Network for the simulation of radionuclide diffusion and sorption in a granitic rock. Journal of Contaminant Hydrology 207, 8–16.

Isaaks E H, Srivastava R M, 1989. An introduction to applied geostatistics. Oxford: Oxford University Press.

Isaksson H, Pitkänen T, Thunehed H, 2006a. Forsmark site investigation. Ground magnetic survey and lineament interpretation in an area northwest of Bolundsfjärden. SKB P-06-85, Svensk Kärnbränslehantering AB.

Isaksson H, Thunehed H, Pitkänen T, Keisu M, 2006b. Forsmark site investigation. Detailed ground and marine magnetic survey and lineament interpretation in the Forsmark area – 2006. SKB P-06-261, Svensk Kärnbränslehantering AB.

Isaksson H, Thunehed H, Pitkänen T, Keisu M, 2007. Forsmark site investigation. Detailed ground magnetic survey and lineament interpretation in the Forsmark area, 2006–2007. SKB R-07-62, Svensk Kärnbränslehantering AB.

Ishibashi T, Watanabe N, Asanuma H, Tsuchiya N, 2016. Linking microearthquakes to fracture permeability change: The role of surface roughness. Geophysical Research Letters 43, 7486–7493.

Ishii T, Matsushita M, 1992. Fragmentation of long thin glass rods. Journal of the Physical Society of Japan 61, 3474–3477.

Jackson C P, Hoch A R, Todman S, 2000. Self-consistency of a heterogeneous continuum porous medium representation of a fractured medium. Water Resources Research 36, 189–202.

Jahns R H, 1943. Sheet structure in granites: its origin and use as a measure of glacial erosion in New England. Journal of Geology 51, 71–98.

Jing L, 2003. A Review of Techniques, Advances and Outstanding Issues in Numerical Modelling for Rock Mechanics and Rock Engineering. In: International Journal of Rock Mechanics and Mining Sciences 40, 283–353.

Jing L, Stephansson O, 2007. Fundamentals of discrete element methods for rock engineering: theory and applications. Amsterdam: Elsevier.

Johansson F, 2016. Influence of scale and matedness on the peak shear strength of fresh, unweathered rock joints. International Journal of Rock Mechanics and Mining Sciences 82, 36–47.

Johansson F, Stille H, 2014. A conceptual model for the peak shear strength of fresh and unweathered rock joints. International Journal of Rock Mechanics and Mining Sciences 69, 31–38.

Journel A G, Huijbregts C J, 1991. Mining geostatistics. London: Academic Press.

Joyce S, Simpson T, Hartley L, Applegate D, Hoek J, Jackson P, Swan D, Marsic N, Follin S, 2010. Groundwater flow modelling of periods with temperature climate conditions – Forsmark. SKB R-09-20, Svensk Kärnbränslehantering AB.

Joyce S, Applegate D, Appleyard P, Gordon A, Heath T, Hunter F, Hoek J, Jackson P, Swan D, Woollard H, 2015. Groundwater flow and reactive transport modelling in ConnectFlow. SKB R-14-19, Svensk Kärnbränslehantering AB.

Juhlin C, Bergman B, 2004. Reflection seismics in the Forsmark area. Updated interpretation of Stage 1 (previous report R-02-43). Updated estimate of bedrock topography (previous report P-04-99). SKB P-04-158, Svensk Kärnbränslehantering AB.

Juhlin C, Palm H, 2005. Forsmark site investigation. Reflection seismic studies in the Forsmark area, 2004: Stage 2. SKB R-05-42, Svensk Kärnbränslehantering AB.

Juhlin C, Zhang F, 2010. Site investigation SFR. Reprocessing of reflection seismic profiles 5b and 8, Forsmark. SKB P-10-50, Svensk Kärnbränslehantering AB.

Juhlin C, Bergman B, Palm H, 2002. Reflection seismic studies in the Forsmark area – stage 1. SKB R-02-43, Svensk Kärnbränslehantering AB.

Kachanov M, 1985. A simple technique of stress analysis in elastic solids with many cracks. International Journal of Fracture 28, R11–R19.

Kachanov M, 1993. Elastic solids with many cracks and related problems. In Hutchinson J W, Wu T T (eds). Advances in applied mechanics. Vol. 30. New York: Academic Press, 259–445.

Kachanov M, Laures J P, 1989. 3-dimensional problems of strongly interacting arbitrarily located penny-shaped cracks. International Journal of Fracture 41, 289–313.

Kang P K, Dentz M, Le Borgne T, Juanes R, 2015. Anomalous transport on regular fracture networks: Impact of conductivity heterogeneity and mixing at fracture intersections. Physical Review E 92, 022148. doi:10.1103/PhysRevE.92.022148

KBS, 1983a. KBS 3 – Final storage of spent nuclear fuel – KBS-3, IV Safety. Svensk Kärnbränsleförsörjning AB.

KBS, 1983b. KBS 3 – Final storage of spent nuclear fuel – KBS-3, III Barriers. Svensk Kärnbränsleförsörjning AB.

KBS, 1983c. KBS 3 – Final storage of spent nuclear fuel – KBS-3, I General. Svensk Kärnbränsleförsörjning AB.

KBS, 1983d. KBS 3 – Final storage of spent nuclear fuel – KBS-3, Summary. Svensk Kärnbränsleförsörjning AB.

Kim Y-S, Sanderson D J, 2005. The relationship between displacement and length of faults; a review. Earth-Science Reviews 68, 317–334.

Kim Y-S, Peacock D C P, Sanderson D J, 2004. Fault damage zones. Journal of Structural Geology 26, 503–517.

King G, 1983. The accommodation of large strains in the upper lithosphere of the earth and other solids by self-similar fault systems; the geometrical origin of b-value. Pure and Applied Geophysics 121, 761–815.

Kirkpatrick M, Heckman N, 1989. A quantitative genetic model for growth, shape, reaction norms, and other infinite-dimensional characters. Journal of Mathematical Biology 27, 429–450.

Klimczak C, Schultz R A, Parashar R, Reeves D M, 2010. Cubic law with aperture-length correlation: implications for network scale fluid flow. Hydrogeology Journal 18, 851–862.

Knott S D, Beach A, Brockbank P J, Brown J L, McCallum J E, Welbon A I, 1996. Spatial and mechanical controls on normal fault populations. In Cowie P A, Knipe R J, Main I G, Wojtal S F (eds). Scaling laws for fault and fracture populations: analyses and applications. Journal of Structural Geology 18, 359–372.

Koistinen T, Stephens M B, Bogatchev V, Nordgulen O, Wennerström M, Korhonen J, 2001. Geological map of the Fennoscandian Shield, Scale 1: 2 000 000. Geological Surveys of Finland, Norway and Sweden and the North–West Department of Natural Resources of Russia.

Koittola N, 2014. Geological 3D model of the investigation niche in ONKALO, Olkiluoto, southwestern Finland. Posiva Working Report 2014-35, Posiva Oy, Finland.

Kolmogoroff A, 1941. Über das logarithmisch normale Verteilungsgesetz der Dimensionen der Teilchen bei Zerstückelung. Comptes Rendus (Doklady) de l'Academie des Sciences de I'URSS, 31: 99.

Komulainen J, Pöllänen J, 2016. KBS-3H – DETUM. Difference flow logging in boreholes K03009F01 and K08028F01. SKB P-15-13, Svensk Kärnbränslehantering AB.

Komulainen J, Pekkanen J, Ripatti K, 2019. Forsmark site investigations. Difference flow logging in boreholes KFM14, KFM15, KFM16, KFM20, KFM21, KFM22 and KFM23. SKB P-19-19, Svensk Kärnbränslehantering AB.

Korvin G, 1989. Fractured but not fractal: Fragmentation of the gulf of suez basement. Pure and Applied Geophysics 131, 289–305.

Korvin G, 1992. Fractal models in the earth sciences. Cambridge: Cambridge University Press.

Krapivsky P, Ben-Naim E, 1994. Scaling and multiscaling in models of fragmentation. Physical Review E 50, 3502. doi:10.1103/physreve.50.3502

Krietsch H, Doetsch J, Dutler N, Jalali M, Gischig V, Loew S, Amann F, 2018. Comprehensive geological dataset describing a crystalline rock mass for hydraulic stimulation experiments. Scientific Data 5, 180269. doi:10.1038/sdata.2018.269

Kulatilake P, Wu T, 1984. Sampling bias on orientation of discontinuities. Rock Mechanics and Rock Engineering 17, 243–253.

Kvartsberg S, Fransson Å, 2013. Hydrogeological characterisation and stochastic modelling of a hydraulically conductive fracture system affected by grouting: A case study of horizontal circular drifts. Tunnelling and Underground Space Technology 38, 38–49.

Laaksoharju M, Smellie J, Tullborg E-L G M, Hallbeck L, Molinero J, Waber N, 2008. Bedrock hydrogeochemistry Forsmark. Site descriptive modelling. SDM-Site Forsmark. SKB R-08-47, Svensk Kärnbränslehantering AB.

La Pointe P, 2002. Derivation of parent fracture population statistics from trace length measurements for fractal fracture populations. International Journal of Rock Mechanics and Mining Sciences 39, 381–388.

La Pointe P R, Hudson J A, 1985. Characterization and interpretation of rock mass joint patterns. Boulder, CO: Geological Society of America. (Geological Society of America Special Paper 199.)

La Pointe P, Fox A, Hermanson J, Öhman J, 2008. Geological discrete fracture network model for the Laxemar site. Site Descriptive Modelling SDM-Site Laxemar. SKB R-08-55, Svensk Kärnbränslehantering AB.

Larsson M, Niemi A, Tsang C-F, 2012. A study of flow-wetted surface area in a single fracture as a function of its hydraulic conductivity distribution. Water Resources Research 48. doi:10.1029/2011WR010686

Lasaga A C, 2014. Kinetic theory in the earth sciences. Princeton University Press.

Lavoine E, Davy P, Darcel C, Le Goc R, 2019. On the density variability of Poissonian discrete fracture networks, with application to power-law fracture size distributions. Advances in Geosciences 49, 77–83.

Lavoine E, Davy P, Darcel C, Munier R, 2020. A discrete fracture network model with stress-driven nucleation: impact on clustering, connectivity, and topology. Frontiers in Physics. doi:10.3389/fphy.2020.00009

Leamer E E, 1985. Sensitivity analyses would help. The American Economic Review 75, 308–313.

Le Goc R, Darcel C, Selroos J-O, Maillot B, Davy P, 2018. Progress on Discrete Fracture Network (DFN) flow modeling. In Proceedings of CMWR2018: Computational Methods in Water Resources XXII, Saint-Malo, France, 3–7 June 2018.

Leijon B, 2005. Forsmark site investigation. Investigations of superficial fracturing and block displacements at drill site 5. SKB P-05-199, Svensk Kärnbränslehantering AB.

Leith K, Moore J R, Amann F, Loew S, 2014. Subglacial extensional fracture development and implications for Alpine Valley evolution. Journal of Geophysical Research: Earth Surface 119, 62–81.

Lemieux J-M, Sudicky E, Peltier W, Tarasov L, 2008. Simulating the impact of glaciations on continental groundwater flow systems: 2. Model application to the Wisconsinian glaciation over the Canadian landscape. Journal of Geophysical Research: Earth Surface 113. doi:10.1029/2007JF000929

Libby S, Hartley L, Turnbull R, Cottrell M, Bym T, Josephson N, Munier R, Selroos J-O, Ivars D M, 2019. Grown Discrete Fracture Networks: A new method for generating fractures according to their deformation history. In Proceedings of the 53rd US Rock Mechanics/Geomechanics Symposium, June 2019, New York City. American Rock Mechanics Association, ARMA 19–1559.

Libby S, Catley J, Hartley L, 2020. Shaft data heterogeneity analysis. Posiva Project Memorandum, Posiva Oy.

Lichtner P C, Kang Q, 2007. Upscaling pore-scale reactive transport equations using a multiscale continuum formulation. Water Resources Research 43. doi:10.1029/2006WR005664

Lidmar-Bergström K, 1994. Berggrundens ytformer (Morphology of the bedrock surface). In Fredén C (ed). Sveriges nationalatlas, Berg och jord. Stockholm: Sveriges nationalatlas, 44–54. (In Swedish.)

Liu H-H, Rutqvist J, Zhou Q, Bodvarsson G S, 2004. Upscaling of normal stress-permeability relationships for fracture networks obeying fractional Levy motion. In Stephansson O, Hudson J A, Jing L (eds). Coupled thermo-hydro-mechanical-chemical processes in geo-systems. Elsevier Science. (Elsevier Geo-Engineering Book Series 2), 263–268.

Liu H-H, Wei M-Y, Rutqvist J, 2013. Normal-stress dependence of fracture hydraulic properties including two-phase flow properties. Hydrogeology Journal 21, 371–382.

Long J C S, Remer J S, Wilson C R, Witherspoon P A, 1982. Porous Media Equivalents for Networks of Discontinuous Fractures. Water Resources Research 18, 645–658.

Long J, Gilmour P, Witherspoon P A, 1985. A model for steady fluid flow in random three-dimensional networks of disc-shaped fractures. Water Resources Research 21, 1105–1115.

Lu Y C, Tien Y M, Juang C H, 2017. Uncertainty of 1-D fracture intensity measurements. Journal of Geophysical Research: Solid Earth 122, 9344–9358.

Ludvigson J-E, Hansson K H C, 2007. Forsmark site investigation. Method evaluation of single-hole hydraulic injection tests at site investigations in Forsmark. SKB P-07-80, Svensk Kärnbränslehantering AB.

Ludvigson J-E, Hjerne C, 2014. Detailed analysis of selected hydraulic interference tests and review of new test analysis methods. SKB R-10-73, Svensk Kärnbränslehantering AB.

Ludvigson J-E, Hansson K, Rouhiainen P, 2002. Methodology study of Posiva difference flow meter in borehole KLX02 at Laxemar. SKB R-01-52, Svensk Kärnbränslehantering AB.

Ludvigson J-E, Jönsson S, Levén J, 2004. Forsmark site investigation. Hydraulic evaluation of pumping activities prior to hydro-geochemical sampling in borehole KFM03A – Comparison with results from difference flow logging. SKB P-04-96, Svensk Kärnbränslehantering AB.

Luna M, Arcos D, Duro L, 2006. Effects of grouting, shotcreting and concrete leachates on backfill geochemistry. SKB R-06-107, Svensk Kärnbränslehantering AB.

Lundberg E, Juhlin C, Zhang F, Behrendt R, 2018. Seismic reflection, refraction and tomography results from 3D seismic data, Forsmark. SKB P-17-25, Svensk Kärnbränslehantering AB.

Lundqvist J, 1994. The deglaciation. In Fredén C (ed). Sveriges nationalatlas, Berg och jord (Geology). Stockholm: Sveriges nationalatlas.

Löfgren M, Sidborn M, 2016. Quantitative mapping and statistical evaluation of fracture minerals in the granitic bedrock at Forsmark, Sweden. Mineralogy and Petrology 110, 663–680.

Löfgren M, Crawford J, Elert M, 2007. Tracer tests – possibilities and limitations. Experience from SKB fieldwork: 1977–2007. SKB R-07-39, Svensk Kärnbränslehantering AB.

Lönnqvist M, Hökmark H, 2010. Assessment of potential for glacially induced hydraulic jacking at different depths. SKB R-09-35, Svensk Kärnbränslehantering AB.

Lönnqvist M, Hökmark H, 2013. Approach to estimating the maximum depth for glacially induced hydraulic jacking in fractured crystalline rock at Forsmark, Sweden. Journal of Geophysical Research: Earth Surface 118, 1777–1791.

Mahmoudzadeh B, Liu L, Moreno L, Neretnieks I, 2013. Solute transport in fractured rocks with stagnant water zone and rock matrix composed of different geological layers – Model development and simulations. Water Resources Research 49, 1709–1727.

Maillot J, Davy P, Le Goc R, Darcel C, de Dreuzy J R, 2016. Connectivity, permeability, and channeling in randomly distributed and kinematically defined discrete fracture network models. Water Resources Research 52, 8526–8545.

Makedonska N, Hyman J D, Karra S, Painter S L, Gable C W, Viswanathan H S, 2016. Evaluating the effect of internal aperture variability on transport in kilometer scale discrete fracture networks. Advances in Water Resources 94, 486–497.

Maloszewski P, Zuber A, 1990. Mathematical modeling of tracer behavior in short-term experiments in fissured rocks. Water Resources Research 26, 1517–1528.

Mandelbrot B B, 1982. The fractal geometry of nature. San Fransisco: Freeman.

Mandelbrot B B, 1985. Self-affine fractals and fractal dimension. Physica Scripta 32, 257.

Mandelbrot B B, Van Ness J W, 1968. Fractional brownian motions, fractional noises and applications. SIAM Review 10, 422–437.

Mandl G, 1988. Mechanics of tectonic faulting: models and basic concepts. Amsterdam: Elsevier.

Mandl G, 1999. Faulting in brittle rocks: an introduction to the mechanics of tectonic faults. Berlin: Springer.

Manga M, Beresnev I, Brodsky E E, Elkhoury J E, Elsworth D, Ingebritsen S E, Mays D C, Wang C-Y, 2012. Changes in permeability caused by transient stresses: Field observations, experiments, and mechanisms. Reviews of Geophysics 50. doi:10.1029/2011rg000382

Marcotte D, Henry E, 2002. Automatic joint set clustering using a mixture of bivariate normal distributions. International Journal of Rock Mechanics, Mining Sciences 39, 323–334.

Mardia K V, Jupp P E, 2000. Directional statistics. 2nd ed. Chichester: Wiley.

Marrett R, Ortega O J, Kelsey C M J G, 1999. Extent of power-law scaling for natural fractures in rock. Geology 27, 799–802.

Marrett R, Gale J F W, Gómez L A, Laubach S E, 2018. Correlation analysis of fracture arrangement in space. Journal of Structural Geology 108, 16–33.

Martel S J, 2006. Effect of topographic curvature on near-surface stresses and application to sheeting joints. Geophysical Research Letters 33. doi:10.1029/2005gl024710

Martel S J, 2011. Mechanics of curved surfaces, with application to surface-parallel cracks. Geophysical Research Letters 3. doi:10.1029/2011gl049354

Martel S J, 2016. Effects of small-amplitude periodic topography on combined stresses due to gravity and tectonics. International Journal of Rock Mechanics and Mining Sciences 89, 1–13.

Martin D, Follin S, 2011. Review of possible correlations between in situ stress and PFL fracture transmissivity data at Forsmark. SKB R-08-69, Svensk Kärnbränslehantering AB.

Mas Ivars D, 2006. Water inflow into excavations in fractured rock—a three-dimensional hydro-mechanical numerical study. International Journal of Rock Mechanics and Mining Sciences 43, 705–725.

Mas Ivars D, Deisman N, Pierce M, Fairhurst C, 2007. The synthetic rock mass approach – A step forward in the characterization of jointed rock masses. In Proceedings of 11th Congress of the International Society for Rock Mechanics, Lisbon, Portugal, 9–13 July 2007.

Mas Ivars D, Pierce M E, Darcel C, Reyes-Montes J, Potyondy D O, Young R P, Cundall P A, 2011. The synthetic rock mass approach for jointed rock mass modelling. International Journal of Rock Mechanics and Mining Sciences 48, 219–244.

Massey F J Jr, 1951. The Kolmogorov–Smirnov test for goodness of fit. Journal of the American Statistical Association 46, 68–78.

Matheron G, 1962. Traité de géostatistique appliquée. Vol. 1. Editions Technip.

Matheron G, 1963. Principles of geostatistics. Economic Geology 58, 1246–1266.

Matthäi S K, Belayneh M, 2004. Fluid flow partitioning between fractures and a permeable rock matrix. Geophysical Research Letters 31. doi:10.1029/2003GL019027

Mattila J, Follin S, 2019. Does in situ state of stress affect fracture flow in crystalline settings? Journal of Geophysical Research: Solid Earth 124, 5241–5253.

Mattila J, Tammisto E, 2012. Stress-controlled fluid flow in fractures at the site of a potential nuclear waste repository, Finland. Geology 40, 299–302.

Mattila J, Viola G, 2014. New constraints on 1.7 Gyr of brittle tectonic evolution in southwestern Finland derived from a structural study at the site of a potential nuclear waste repository (Olkiluoto Island). Journal of Structural Geology 67, 50–74.

Mauldon M, 1994. Intersection probabilities of impersistent joints. International Journal of Rock Mechanics and Mining Sciences & Geomechanics Abstracts 31, 107–115.

Mauldon M, Mauldon J G, 1997. Fracture sampling on a cylinder: From scanlines to boreholes and tunnels. Rock Mechanics and Rock Engineering 30, 129–144.

Mauldon M, Dunne W M, Rohrbaugh M B, 2001. Circular scanlines and circular windows: new tools for characterizing the geometry of fracture traces. Journal of Structural Geology 23, 247–258.

McMurry J, 2000. Evaluating effects of deep recharge by a low-salinity, oxidizing groundwater: a geochemical modelling case study. Report 06819-REP, 1300-10007, Ontario Power Generation, Nuclear Waste Management, Canada.

Méheust Y, Schmittbuhl J, 2001. Geometrical heterogeneities and permeability anisotropy of rough fractures. Journal of Geophysical Research: Solid Earth 106, 2089–2102.

Milnes A G, 2006. Understanding brittle deformation at the Olkiluoto site. Literature compilation for site characterization and geological modelling. Posiva Working Report 2006-25, Posiva Oy, Finland.

Min K-B, Jing L, 2003. Numerical determination of the equivalent elastic compliance tensor for fractured rock masses using the distinct element method. International Journal of Rock Mechanics and Mining Sciences 40, 795–816.

Min K-B, Rutqvist J, Tsang C-F, Jing L, 2004. Stress-dependent permeability of fractured rock masses: a numerical study. International Journal of Rock Mechanics and Mining Sciences 41, 1191–1210.

Mitchell T, Faulkner D, 2009. The nature and origin of off-fault damage surrounding strike-slip fault zones with a wide range of displacements: A field study from the Atacama fault system, northern Chile. Journal of Structural Geology 31, 802–816.

Moein M J A, Valley B, Evans K F, 2019. Scaling of fracture patterns in three deep boreholes and implications for constraining fractal discrete fracture network models. Rock Mechanics and Rock Engineering 52, 1723–1743.

Molinero J, Trinchero P, de Vries L M, Ebrahimi H, Svensson U, 2016. The BRIDGE Project. Development, testing and application of a high performance computing framework for reactive transport modelling in crystalline rocks (iDP). SKB R-15-17, Svensk Kärnbränslehantering AB.

Molz F, 2015. Advection, dispersion, and confusion. Groundwater 53, 348–353.

Moon S, Perron J, Martel S, Holbrook W, St. Clair J, 2017. A model of three-dimensional topo-graphic stresses with implications for bedrock fractures, surface processes, and landscape evolution. Journal of Geophysical Research: Earth Surface 122, 823–846.

Moos D, Barton C, 2008. Modeling uncertainty in the permeability of stress-sensitive fractures. In Proceedings of the 42nd U.S. Rock Mechanics Symposium (USRMS), San Francisco, California, 29 June – 2 July 2008. American Rock Mechanics Association.

Moreno L, Neretnieks I, 1991. Fluid and solute transport in a network of channels. SKB TR 91-44, Svensk Kärnbränslehantering AB.

Moreno L, Gylling B, Neretnieks I, 1997. Solute transport in fractured media – the important mechanisms for performance assessment. Journal of Contaminant Hydrology 25, 283–298.

Mourzenko V V, Thovert J-F, Adler P M, 2005. Percolation of three-dimensional fracture networks with power-law size distribution. Physical Review E 72, 036103. doi:10.1103/PhysRevE.72.036103

Moye D G, 1967. Diamond drilling for foundation exploration. Civil Engineering Transactions April. 95–100.

Munier R, 1993. Four-dimensional analysis of fracture arrays at the Äspö Hard Rock Laboratory, SE Sweden. Engineering Geology 33, 159–175.

Munier R, 2004. Statistical analysis of fracture data, adapted for modelling Discrete Fracture Networks – Version 2. SKB R-04-66, Svensk Kärnbränslehantering AB.

Munier R, 2008. Methodology for iterative and integrative geomodelling in a multidisciplinary workspace. 33rd international geological congress, Oslo, Norway, Aug. 6–14, 2008, 2008. Congres Geologique International, Resumes, vol. 33, Abstract 1292656.

Munier R, 2010. Full perimeter intersection criteria. Definitions and implementations in SR-Site. SKB TR-10-21, Svensk Kärnbränslehantering AB.

Munier R, Hermanson J, 2001. Metodik för geometrisk modellering Presentation och administration av platsbeskrivande modeller. SKB R-01-15, Svensk Kärnbränslehantering AB. (In Swedish.)

Munier R, Mattila J, 2015. Memo on terminology. POS-021685, Posiva Oy. SKBdoc 1496284 ver 1.0, Svensk Kärnbränslehantering AB.

Munier R, Stigsson M, 2007. Implementation of uncertainties in borehole geometries and geological orientation data in Sicada. SKB R-07-19, Svensk Kärnbränslehantering AB.

Munier R, Stenberg L, Stanfors R, Milnes A G, Hermanson J, Triumf C-A, 2003. Geological Site Descriptive Model. A strategy for the model development during site investigations. SKB R-03-07, Svensk Kärnbränslehantering AB.

Myer L R, 1991. Hydromechanical and seismic properties of fractures. In Proceedings of the 7th ISRM Congress, Aachen, Germany, 16–20 September 1991. International Society for Rock Mechanics and Rock Engineering.

Neretnieks I, 1980. Diffusion in the rock matrix: An important factor in radionuclide retardation? Journal of Geophysical Research: Solid Earth 85, 4379–4397.

Neretnieks I, 2006. Channeling with diffusion into stagnant water and into a matrix in series. Water Resources Research 42. doi:10.1029/2005WR004448

Newman J, Mitra G, 1993. Lateral variations in mylonite zone thickness as influenced by fluid–rock interactions, Linville Falls Fault, North Carolina. Journal of Structural Geology 15, 849–863.

Niemi A, Kontio K, Kuusela-Lahtinen A, Poteri A, 2000. Hydraulic characterization and upscaling of fracture networks based on multiple-scale well test data. Water Resources Research 36, 3481–3497.

Nishiyama S, Ohnishi Y, Ito H, Yano T, 2014. Mechanical and hydraulic behavior of a rock fracture under shear deformation. Earth, Planets and Space 66, 108. doi:10.1186/1880-5981-66-108

Nordbäck N, 2014. Tunnel Crosscutting Fractures (TCF) in ONKALO (chainage 0-4986). Posiva Working Report 2014-58, Posiva Oy, Finland.

Nordbäck N, Engström J, 2016. Outcome of geological mapping and prediction/outcome studies of ONKALO. Posiva 2016-14, Posiva Oy, Finland.

Nordbäck N, Mattila J, 2018. Brittle fault systems of the ONKALO Underground Research Facility. Posiva Working Report 2018-20, Posiva Oy, Finland.

Nordgulen O, Saintot A, 2006. Forsmark site investigation. The character and kinematics of deformation zones (ductile shear zones, fault zones and fracture zones) at Forsmark – report from phase 1. SKB P-06-212, Svensk Kärnbränslehantering AB.

Nordgulen O, Saintot A, 2008. Forsmark site investigation. The character and kinematics of deformation zones (ductile shear zones, fracture zones and fault zones) at Forsmark – report from phase 3. SKB P-07-111, Svensk Kärnbränslehantering AB.

Nordstrom D K, 2012. Models, validation, and applied geochemistry: Issues in science, communication, and philosophy. Applied Geochemistry 27, 1899–1919.

Novakowski K S, 1992. The analysis of tracer experiments conducted in divergent radial flow fields. Water Resources Research 28, 3215–3225.

Novakowski K, Lapcevic P, Voralek J, Sudicky E, 1998. A note on a method for measuring the transport properties of a formation using a single well. Water Resources Research 34, 1351–1356.

NRC, 1996. Rock fractures and fluid flow: contemporary understanding and applications. National Research Council: National Academies Press.

Nur A, 1982. The origin of tensile fracture lineaments. Journal of Structural Geology 4, 31–40.

Oda M, 1985. Permeability tensor for discontinuous rock masses. Géotechnique 35, 483–495.

Odén M, Follin S, Öhman J, Vidstrand P, 2014. SR-PSU Bedrock hydrogeology. Groundwater flow modelling methodology, setup and results. SKB R-13-25, Svensk Kärnbränslehantering AB.

Odling N E, 1997. Scaling and connectivity of joint systems in sandstones from western Norway. Journal of Structural Geology 19, 1257–1271.

Okubo P G, Aki K, 1987. Fractal geometry in the San Andreas fault system. Journal of Geophysical Research: Solid Earth 92, 345–355.

Olofsson I, Simeonov A, Stephens M, Follin S, Nilsson A-C, Röshoff K, Lindberg U, Lanaro F, Fredriksson A, Persson L, 2007. Site descriptive modelling Forsmark, stage 2.2. A fracture domain concept as a basis for the statistical modelling of fractures and minor deformation zones, and interdisciplinary coordination. SKB R-07-15, Svensk Kärnbränslehantering AB.

Olson J E, 2003. Sublinear scaling of fracture aperture versus length: An exception or the rule? Journal of Geophysical Research: Solid Earth 108. doi:10.1029/2001jb000419

Olson J E, 2004. Predicting fracture swarms; the influence of subcritical crack growth and the crack-tip process zone on joint spacing in rock. Geological Society Special Publications 231, 73–88.

Olson J E, Yuan Q, Holder J, Rijken P, 2001. Constraining the spatial distribution of fracture networks in naturally fractured reservoirs using fracture mechanics and core measurements. Proceedings of SPE Annual Technical Conference and Exhibition, New Orleans, Louisiana, 30 September – 3 October 2001. Society of Petroleum Engineers.

Olsson R, Barton N, 2001. An improved model for hydromechanical coupling during shearing of rock joints. International Journal of Rock Mechanics and Mining Science 38, 317–329.

Ord A, Hobbs B E, 2010. Fracture pattern formation in frictional, cohesive, granular material. Philosophical Transactions of the Royal Society A: Mathematical, Physical and Engineering Sciences 368, 95–118.

Oreskes N, Shrader-Frechette K, Belitz K, 1994. Verification, validation, and confirmation of numerical models in the earth sciences. Science 263, 641–646.

Outters N, Shuttle D, 2000. Sensitivity analysis of a discrete fracture network model for performance assessment of Aberg. SKB R-00-48, Svensk Kärnbränslehantering AB.

Page L, Hermansson T, Söderlund P, Andersson J, Stephens M B, 2004. Forsmark site investigation. Bedrock mapping U-Pb, ^{40}Ar/^{39}Ar and (U-Th)/He geochronology. SKB P-04-126, Svensk Kärnbränslehantering AB.

Page L, Hermansson T, Söderlund P, Stephens M B, 2007. ^{40}Ar/^{39}Ar and (U-Th)/He geochronology: Phase 2. SKB P-06-211, Svensk Kärnbränslehantering AB.

Painter S, 2011. User's manual for Walkabout Version 1.0. Technical Report LA-UR-11-01952, Los Alamos National Laboratory, Los Alamos, NM.

Painter S, Cvetkovic V, 2005. Upscaling discrete fracture network simulations: An alternative to continuum transport models. Water Resources Research 41. doi:10.1029/2004WR003682

Painter S, Mancillas J, 2013. MARFA user's manual: Migration analysis of radionuclides in the far field. Posiva Working Report 2013-01, Posiva Oy, Finland.

Painter S, Paterson L, Boult P, 1997. Improved technique for stochastic interpolation of reservoir. SPE Journal 2, 48–57.

Painter S, Cvetkovic V, Mancillas J, Pensado O, 2008. Time domain particle tracking methods for simulating transport with retention and first-order transformation. Water Resources Research 44. doi:10.1029/2007WR005944

Palmström A, 2005. Measurements of and correlations between block size and rock quality designation (RQD). Tunnelling and Underground Space Technology 20, 362–377.

Paluszny A, Matthäi S K, 2009. Numerical modeling of discrete multi-crack growth applied to pattern formation in geological brittle media. International Journal of Solids and Structures 46, 3383–3397.

Paluszny A, Matthäi S K, 2010. Impact of fracture development on the effective permeability of porous rocks as determined by 2-D discrete fracture growth modeling. Journal of Geophysical Research 115, B02203. doi:10.1029/2008jb006236

Paluszny A, Zimmerman R W, 2011. Numerical simulation of multiple 3D fracture propagation using arbitrary meshes. Computer Methods in Applied Mechanics and Engineering Failure Analysis 200, 953–966.

Paluszny A, Zimmerman R W, 2013. Numerical fracture growth modeling using smooth surface geometric deformation. Engineering Fracture Mechanics 108, 19–36.

Paris P, Erdogan F, 1963. A critical analysis of crack propagation laws. Journal of Basic Engineering 85, 528–533.

Paris P C, Sih G C, 1965. Stress analysis of cracks. Fracture toughness testing and its applications. ASTM International.

Patriarche D, Pili E, Adler P M, Thovert J-F, 2007. Stereological analysis of fractures in the Roselend tunnel and permeability determination. Water Resources Research 43. doi:10.1029/2006wr005471

Peacock D C P, 2006. Predicting variability in joint frequencies from boreholes. Journal of Structural Geology 28, 353–361.

Peacock D C P, Harris S D, Mauldon M, 2003. Use of curved scanlines and boreholes to predict fracture frequencies. Journal of Structural Geology 25, 109–119.

Peacock D C P, Nixon C W, Rotevatn A, Sanderson D J, Zuluaga L F, 2016. Glossary of fault and other fracture networks. Journal of Structural Geology 92, 12–29.

Peel D, Whiten W J, McLachlan G J, 2001. Fitting mixtures of Kent distributions to aid in joint set identification. Journal of the American Statistical Association 96, 56–63.

Pekkanen J, 2009. Difference flow measurements and hydraulic interference test in ONKALO at Olkiluoto. Drillholes ONK-PP125, ONK-PP127 and ONK-PP129. Posiva Working Report 2009-40, Posiva Oy, Finland.

Pekkanen J, 2019. Flow measurements in ONKALO at Olkiluoto. Probe holes in ONK-TR-TT-4505, Investigation Holes ONK-KR17 and ONK-PP408 and Pilot Hole ONK-PH28. Posiva Working Report 2018-21, Posiva Oy, Finland.

Pekkanen J, Hurmerinta E, 2013. Äspö Hard Rock Laboratory. Difference flow logging in borehole KA2051A01. SKB P-13-25, Svensk Kärnbränslehantering AB.

Pells P, Bieniawski Z, Hencher S, Pells S, 2017. Rock quality designation (RQD): time to rest in peace. Canadian Geotechnical Journal 54, 825–834.

Petersson J, Andersson U B, Berglund J, 2007a. Scan line fracture mapping and magnetic susceptibility measurements across two low magnetic lineaments with NNE and NE trend, Forsmark. In Stephens M B, Skagius K (eds). Geology – Background complementary studies. Forsmark modelling stage 2. SKB R-07-56, Svensk Kärnbränslehantering AB, 6–15.

Petersson J, Skogsmo G, Vestgård J, Albrecht J, Hedenström A, Gustafsson J, 2007b. Forsmark site investigation. Bedrock mapping and magnetic susceptibility measurements, Quaternary investigations and GPR measurements in trench AFM001265. SKB P-06-136, Svensk Kärnbränslehantering AB.

Petersson J, Hultgren P, Stenberg L, Mattsson H, 2018. Äspö Site descriptive Model. Simplified geological single-hole interpretation of drill cores from KA1061A, KA1131B and KBH02. SKB P-17-28, Svensk Kärnbränslehantering AB.

Pierce M, Mas Ivars D, Cundall P, Potyondy D, 2007. A synthetic rock mass model for jointed rock. Rock mechanics: meeting society's challenges and demands. In Proceedings of the 1st Canada–U.S. Rock Mechanics Symposium, Vancouver, BC, 27–31 May 2007.

Piggott A, 1997. Fractal relations for the diameter and trace length of disc-shaped fractures. Journal of Geophysical Research 102, 18121–18125.

Plotnick R E, Gardner R H, Hargrove W W, Prestegaard K, Perlmutter M, 1996. Lacunarity analysis: a general technique for the analysis of spatial patterns. Physical review E 53, 5461. doi:10.1103/PhysRevE.53.5461

Pollard D D, Aydin A, 1988. Progress in understanding jointing over the past century. Geological Society of America Bulletin 100, 1181–1204.

Posiva, 2012. Olkiluoto site description 2011. Posiva 2011-02, Posiva Oy, Finland.

Posiva, 2013. Safety case for the disposal of spent nuclear fuel at Olkiluoto – Performance assessment 2012. Posiva 2012-04, Posiva Oy, Finland.

Posiva SKB, 2017. Safety functions, performance targets and technical design requirements for a KBS-3V repository. Conclusions and recommendations from a joint SKB and Posiva working group. Posiva SKB Report 01, Posiva Oy, Svensk Kärnbränslehantering AB.

Poteri A, 2009. Retention properties of flow paths in fractured rock. Hydrogeology Journal 17, 1081–1092.

Poteri A, Billaux D, Dershowitz W, Gómez-Hernández J J, Cvetkovic V, Hautojärvi A, Holton D, Medina A, Winberg A, 2002. Final report of the TRUE Block Scale projekt. 3. Modelling of flow and transport. SKB TR-02-15, Svensk Kärnbränslehantering AB.

Poteri A, Nordman H, Pulkkanen V-M, Smith P, 2014. Radionuclide transport in the repository near-field and far-field. Posiva 2014-02, Posiva Oy, Finland.

Poteri A, Nilsson K, Andersson O, Siitari-Kauppi M, Helariutta K, Voutilainen M, Kekkäälääinen P, Ikonen J, Sammaljärvi J, Lindberg A, Byegård J, Skålberg M, Kuva J, Timonen J, 2018. The first matrix diffusion experiment in the water phase of the REPRO Project: WPDE 1. Posiva Working Report 2017-23, Posiva Oy, Finland.

Poulsen B, Adhikary D, Elmouttie M, Wilkins A, 2015. Convergence of synthetic rock mass modelling and the Hoek–Brown strength criterion. International Journal of Rock Mechanics and Mining Sciences 80, 171–180.

Power W L, Tullis T E, 1991. Euclidean and fractal models for the description of rock surface roughness. Journal of Geophysical Research, B, Solid Earth 96, 415–424.

Power W L, Tullis T E, Brown S R, Boitnott G N, Scholz C H, 1987. Roughness of natural fault surfaces. Geophysical Research Letters 14, 29–32.

Priest S D, 1993. Discontinuity analysis for rock engineering. London: Chapman & Hall.

Priest S D, Hudson J A, 1981. Estimation of discontinuity spacings and trace length using scanline surveys. International Journal of Rock Mechanics and Mining Sciences & Geomechanics Abstracts 18, 183–197.

Puigdomenech I, Ambrosi J-P, Eisenlohr L, Lartigue J-E, Banwart S A, Bateman K, Milodowski A E, West J M, Griffault L, Gustafsson E, Hama K, Yoshida H, Kotelnikova S, Pedersen K, Michaud V, Trotignon L, Rivas Perez J, Tullborg E-L, 2001. O_2 depletion in granitic media. The REX project. SKB TR-01-05, Svensk Kärnbränslehantering AB.

Pusch R, Popov V, Adey R, Kasbohm J, Knutsson S, 2014. Rational and economic disposal of hazardous waste: Use of abandoned mines. Journal of Earth Sciences and Geotechnical Engineering 4, 33–54.

Pyrak-Nolte L, Morris J, 2000. Single fractures under normal stress: The relation between fracture specific stiffness and fluid flow. International Journal of Rock Mechanics and Mining Sciences 37, 245–262.

Ramsey J M, Chester F M, 2004. Hybrid fracture and the transition from extension fracture to shear fracture. Nature 428, 63–66.

Rauséus G, Petersson J, 2020. Geological single-hole interpretation of HFM42–HFM47 and KFM25–KFM27. SKB P-20-13, Svensk Kärnbränslehantering AB.

Raven K G, Gale J E, 1985. Water flow in a natural rock fracture as a function of stress and sample size. International Journal of Rock Mechanics and Mining Sciences & Geomechanics Abstracts 22, 251–261.

Renard F, Voisin C, Marsan D, Schmittbuhl J, 2006. High resolution 3D laser scanner measurements of a strike-slip fault quantify its morphological anisotropy at all scales. Geophysical Research Letters 33. doi:10.1029/2005GL025038

Renshaw C E, 1996. Influence of subcritical fracture growth on the connectivity of fracture networks. Water Resources Research 32, 1519–1530.

Renshaw C E, 1999. Connectivity of joints networks with power law length distributions. Water Resources Research 35, 2661–2670.

Renshaw C E, Park J C, 1997. Effect of mechanical interactions on the scaling of fracture length and aperture. Nature 386, 482–484.

Renshaw C E, Pollard D D, 1994. Numerical simulation of fracture set formation; a fracture mechanics model consistent with experimental observations. Journal of Geophysical Research: Solid Earth 99, 9359–9372.

Rhén I, Hartley L, 2009. Bedrock hydrogeology Laxemar. Site descriptive modelling SDM-Site Laxemar. SKB R-08-92, Svensk Kärnbränslehantering AB.

Rhén I, Smellie J, 2003. Task force on modelling of groundwater flow and transport of solutes. Task 5 Summary report. SKB TR-03-01, Svensk Kärnbränslehantering AB.

Rhén I, Forsmark T, Hartley L, Jackson P, Roberts D, Swan D, Gylling B, 2008. Hydrogeological conceptualisation and parameterisation. Site descriptive modelling SDM-Site Laxemar. SKB R-08-78, Svensk Kärnbränslehantering AB.

Rhén I, Forsmark T, Hartley L, Joyce S, Roberts D, Gylling B, Marsic N, 2009. Bedrock hydrogeology. Model testing and synthesis. Site descriptive modelling SDM-Site Laxemar. SKB R-08-91, Svensk Kärnbränslehantering AB.

Rippon J H, 1985. Contoured patterns of the throw and hade of normal faults in the Coal Measures (Westphalian) of north–east Derbyshire. Proceedings of the Yorkshire Geological Society 45, 147–161.

Robinson P C, 1984. Connectivity, flow and transport in network models of fractured media. PhD thesis. Oxford University.

Rolle M, Le Borgne T, 2019. Mixing and reactive fronts in the subsurface. Reviews in Mineralogy and Geochemistry 85, 111–142.

Rouhiainen P, Sokolnicki M, 2005. Forsmark site investigation. Difference flow logging in borehole KFM06A. SKB P-05-15, Svensk Kärnbränslehantering AB.

Rouleau A, Gale J E, 1985. Characterization of the fracture system at Stripa with emphasis on the ventilation drift. Technical information report no. 52. LBL-14875 SAC-52, A joint project of Swedish Nuclear Fuel Supply Co. Stockholm, Sweden and Lawrence Berkeley Laboratory, Earth Sciences Division, University of California, Berkeley, California, USA.

Roy A, Perfect E, Dunne W M, McKay L D, 2014. A technique for revealing scale-dependent patterns in fracture spacing data. Journal of Geophysical Research: Solid Earth 119, 5979–5986.

Rozhko A Y, Podladchikov Y Y, Renard F, 2007. Failure patterns caused by localized rise in pore-fluid overpressure and effective strength of rocks. Geophysical Research Letters 34, L22304. doi:10.1029/2007gl031696

Russ J C, 2013. Fractal surfaces. Springer Science & Business Media.

Rühaak W, Bense V F, Sass I, 2014. 3D hydro-mechanically coupled groundwater flow modelling of Pleistocene glaciation effects. Computers & Geosciences 67, 89–99.

Rønning H J S, Kihle O, Mogaard J O, Walker P, 2003. Helicopter borne geophysics at Simpevarp, Oskarshamn, Sweden. Simpevarp site investigation. SKB P-03-25, Svensk Kärnbränslehantering AB.

Saaltink M W, Carrera J, Ayora C, 2001. On the behavior of approaches to simulate reactive transport. Journal of Contaminant Hydrology 48, 213–235.

Saaltink M W, Carrera J, Olivella S, 2004. Mass balance errors when solving the convective form of the transport equation in transient flow problems. Water Resources Research 40. doi:10.1029/2003WR002866

Sævik P, Nixon C, 2017. Inclusion of topological measurements into analytic estimates of effective permeability in fractured media. Water Resources Research 53, 9424–9443.

Sainsbury B, Pierce M, Mas Ivars D, 2008. Simulation of rock mass strength anisotropy and scale effects using a Ubiquitous Joint Rock Mass (UJRM) model. Proceedings of the 1st International FLAC/DEM Symposium on Numerical Modelling, Minneapolis, Minnesota, 25–27 August 2008.

Saintot A, Nordgulen O, 2007. Forsmark site investigation. The character and kinematics of deformation zones (ductile shear zones, fracture zones and fault zones) at Forsmark – report from phase 2. SKB P-07-101, Svensk Kärnbränslehantering AB.

Saintot A, Stephens M B, Viola G, Nordgulen Ø, 2011. Brittle tectonic evolution and paleostress field reconstruction in the southwestern part of the Fennoscandian Shield, Forsmark, Sweden. Tectonics 30. doi:10.1029/2010tc002781

Salas J, Gimeno M J, Auquè L, Molinero J, Gómez J, Juárez I, 2010. SR-Site – hydrogeochemical evolution of the Forsmark site. SKB TR-10-58, Svensk Kärnbränslehantering AB.

Saltelli A, Ratto M, Tarantola S, Campolongo F, 2006. Sensitivity analysis practices: Strategies for model-based inference. Reliability Engineering & System Safety 91, 1109–1125.

Sanderson D J, Nixon C W, 2015. The use of topology in fracture network characterization. Journal of Structural Geology 72, 55–66.

Sandström B, Tullborg E-L, 2005. Forsmark site investigation. Fracture mineralogy. Results from fracture minerals and wall rock alteration in boreholes KFM01B, KFM04A, KFM05A and KFM06A. SKB P-05-197, Svensk Kärnbränslehantering AB.

Sandström B, Tullborg E-L, Page L, 2008a. Forsmark site investigation. Fracture mineralogy and $^{40}Ar/^{39}Ar$ ages of adularia in fracture filling and K-feldspar in breccia. Data from drill cores KFM01C, KFM01D, KFM02B, KFM04A, KFM06A, KFM06B, KFM07A, KFM08A, KFM08B, KFM08C, KFM08D, KFM09A, KFM09B, KFM10A and KFM11A. SKB P-08-14, Svensk Kärnbränslehantering AB.

Sandström B, Tullborg E-L, Smellie J, MacKenzie A B, Suksi J, 2008b. Fracture mineralogy of the Forsmark site. SDM-Site Forsmark. SKB R-08-102, Svensk Kärnbränslehantering AB.

Sandström B, Tullborg E-L, Larson S-Å, Page L, 2009. Brittle tectonothermal evolution in the Forsmark area, central Fennoscandian Shield, recorded by paragenesis, orientation and $^{40}Ar/^{39}Ar$ geochronology of fracture minerals. Tectonophysics 478, 158–174.

Savazzi E, Reyment R A, 1999. Aspects of multivariate statistical analysis in geology. Amsterdam: Elsevier.

Sawada A, Saegusa H, Takeuchi S, Sakamoto K, Dershowitz W S, 2015. Äspö Task Force on modelling of groundwater flow and transport of solutes. Task 7 – Groundwater flow and transport modelling of fracture system at regional, block, and single-fracture scale flow and transport, Olkiluoto. SKB P-13-46, Svensk Kärnbränslehantering AB.

Scholz C H, 2002. The mechanics of earthquakes and faulting. 2nd ed. Cambridge: Cambridge university press.

Scholz C H, Dawers N H, Yu J Z, Anders M H, Cowie P A, 1993. Fault growth and fault scaling laws; preliminary results. Journal of Geophysical Research: Solid Earth 98, 21951–21961.

Schultz R A, Fossen H, 2002. Displacement-length scaling in three dimensions: the importance of aspect ratio and application to deformation bands. Journal of Structural Geology 24, 1389–1411.

Schultz R A, Mège D, Diot H, 2008a. Emplacement conditions of igneous dikes in Ethiopian Traps. J Journal of Volcanology, Geothermal Research 178, 683–692.

Schultz R A, Soliva R, Fossen H, Okubo C H, Reeves D M, 2008b. Dependence of displacement–length scaling relations for fractures and deformation bands on the volumetric changes across them. J Journal of Structural Geology 30, 1405–1411.

Schweisinger T, Svenson E J, Murdoch L C, 2009. Introduction to hydromechanical well tests in fractured rock aquifers. Groundwater 47, 69–79.

Segall P, Pollard D D, 1983. Joint formation in granitic rock of the Sierra Nevada. Geological Society of America Bulletin 94, 563–575.

Selnert E, 2008. Laboratory investigations of porosity, diffusivity and sorption characteristics of crystalline rock. In Ahlbom K, Stephens M (eds). Investigations of potential repository sites for spent nuclear fuel at Forsmark and Laxemar-Simpevarp, Sweden. Abstracts, 33rd International Geological Congress, Oslo. SKB R-08-97, Svensk Kärnbränslehantering AB, 15.

Selnert E, Byegård J, Widestrand H, 2008. Forsmark site investigation. Laboratory measurements within the site investigation programme for the transport properties of the rock. Final report. SKB P-07-139, Svensk Kärnbränslehantering AB.

Selroos J-O, Follin S, 2010. SR-Site groundwater flow modelling methodology, setup and results. SKB R-09-22, Svensk Kärnbränslehantering AB.

Selroos J-O, Walker D D, Stöm A, Gylling B, Follin S, 2002. Comparison of alternative modelling approaches for groundwater flow in fractured rock. Journal of Hydrology 257, 174–188.

Shahkarami P, Liu L, Moreno L, Neretnieks I, 2015. Radionuclide migration through fractured rock for arbitrary-length decay chain: analytical solution and global sensitivity analysis. Journal of Hydrology 520, 448–460.

Sibson R H, 2003. Brittle-failure controls on maximum sustainable overpressure in different tectonic regimes. AAPG Bulletin 87, 901–908.

Sidborn M, Sandström B, Tullborg E-L, Salas J, Maia F, Delos A, Molinero J, Hallbeck L, Pedersen K, 2010. SR-Site: Oxygen ingress in the rock at Forsmark during a glacial cycle. SKB TR-10-57, Svensk Kärnbränslehantering AB.

Sidborn M, Marsic N, Crawford J, Joyce S, Hartley L, Idiart A, de Vries L M, Maia F, Molinero J, Svensson U, Vidstrand P, Alexander R, 2014. Potential alkaline conditions for deposition holes of a repository in Forsmark as a consequence of OPC grouting. Revised final report after review. SKB R-12-17, Svensk Kärnbränslehantering AB.

Skagius K, Neretnieks I, 1986. Porosities and diffusivities of some nonsorbing species in crystalline rocks. Water Resources Research 22, 389–398.

SKB, 1989a. FoU-PROGRAM 89. Kärnkraftavfallets behandling och slutförvaring. Program för forskning, utveckling och övriga åtgärder. [Del II Program 1990–1995]. Svensk Kärnbränslehantering AB. (In Swedish.)

SKB, 1989b. FoU-PROGRAM 89. Kärnkraftavfallets behandling och slutförvaring. Program för forskning, utveckling och övriga åtgärder [Del I Allmän]. Svensk Kärnbränslehantering AB. (In Swedish.)

SKB, 1992. SKB 91 – Final disposal of spent nuclear fuel. Importance of the bedrock for safety. SKB TR 92-20, Svensk Kärnbränslehantering AB.

SKB, 2008. Site description of Forsmark at completion of the site investigation phase. SDM-Site Forsmark. SKB TR-08-05, Svensk Kärnbränslehantering AB.

SKB, 2010a. Data report for the safety assessment SR-Site. SKB TR-10-52, Svensk Kärnbränslehantering AB.

SKB, 2010b. Geosphere process report for the safety assessment SR-Site. SKB TR-10-48, Svensk Kärnbränslehantering AB.

SKB, 2010c. Utvecklingen av KBS-3-metoden. Genomgång av forskningsprogram, säkerhetsanalyser, myndighetsgranskningar samt SKB:s internationella forskningssamarbete. SKB R-10-40, Svensk Kärnbränslehantering AB. (In Swedish.)

SKB, 2010d. Radionuclide transport report for the safety assessment SR-Site. SKB TR-10-50, Svensk Kärnbränslehantering AB.

SKB, 2011a. Long-term safety for the final repository for spent nuclear fuel at Forsmark. Main report of the SR-Site project. SKB TR-11-01, Svensk Kärnbränslehantering AB.

SKB, 2011b. Framework programme for detailed characterisation in connection with construction and operation of a final repository for spent nuclear fuel. SKB R-11-14, Svensk Kärnbränslehantering AB.

SKB, 2014. Äspö Hard Rock Laboratory. Annual report 2013. SKB TR-14-17, Svensk Kärnbränslehantering AB.

SKB, 2018. Detailed site investigation programme for the construction and operation of the Repository for spent nuclear fuel. SKB R-17-16, Svensk Kärnbränslehantering AB.

SKBf/KBS, 1983. KBS 3 – Final storage of spent nuclear fuel – KBS-3, II Geology. Svensk Kärnbränsleförsörjning AB.

Snow D T, 1965. A parallel plate model of fractured permeable media. PhD thesis. University of California.

Sornette D, Davy P, 1991. Fault growth model and the universal fault length distribution. Geophysical Research Letters 18, 1079–1081.

Sornette A, Davy P, Sornette D, 1990. Growth of fractal fault patterns. Physical Review Letters 65, 2266–2269.

Sornette A, Davy P, Sornette D, 1993. Fault growth in brittle-ductile experiments and the mechanics of continental collisions. Journal of Geophysical Research: Solid Earth 98, 12111–12139.

Spiegelhalter D J, Best N G, Carlin B P, Van Der Linde A, 2002. Bayesian measures of model complexity and fit. Journal of the Royal Statistical Society B 64, 583–639.

Spyropoulos C, Griffith W J, Scholz C H, Shaw B E, 1999. Experimental evidence for different strain regimes of crack populations in a clay model. Geophysical Research Letters 26. doi:10.1029/1999gl900175

Spyropoulos C, Scholz C H, Shaw B E, 2002. Transition regimes for growing crack populations. Physical Review E 65, 056105. doi:10.1103/PhysRevE.65.056105

SSM, 2018. Strålsäkerhet efter slutförvarets förslutning, Beredning inför regeringens prövning. Slutförvaring av använt kärnbränsle. Rapport 2018:07, Swedish Radiation Safety Authority. (In Swedish.)

Staub I, Fredriksson A, Outters N, 2002. Strategy for a Rock Mechanics Site Descriptive Model. Development and testing of the theoretical approach. SKB R-02-02, Svensk Kärnbränslehantering AB.

Stauffer D, Aharony A, 1992. Introduction to percolation theory. 2nd ed. London: Taylor & Francis.

Steefel C I, DePaolo D J, Lichtner P C, 2005. Reactive transport modeling: An essential tool and a new research approach for the Earth sciences. Earth and Planetary Science Letters 240, 539–558.

Stephens M B, 2009. Synthesis of the bedrock geology in the Bergslagen region, Fennoscandian Shield, south-central Sweden. Uppsala: Sveriges geologiska undersökning (SGU). (Serie Ba 58.)

Stephens M B, 2010. Forsmark site investigation. Bedrock geology – overview and excursion guide. SKB R-10-04, Svensk Kärnbränslehantering AB.

Stephens M B, Simeonov A, 2006. Site investigation, Forsmark: ductile and brittle structures and a conceptual model. Bulletin of the Geological Society of Finland Special Issue 1, 155.

Stephens M B, Simeonov A, 2015. Description of deformation zone model version 2.3, Forsmark. SKB R-14-28, Svensk Kärnbränslehantering AB.

Stephens M B, Skagius K, 2007. Geology – Background complementary studies. Forsmark modelling stage 2.2. SKB R-07-56, Svensk Kärnbränslehantering AB.

Stephens M B, Bergman T, Andersson J, Hermansson T, Wahlgren C-H, Albrecht L, Mikko H, 2003. Forsmark. Bedrock mapping. Stage 1 (2002) – Outcrop data including fracture data. SKB P-03-09, Svensk Kärnbränslehantering AB.

Stephens M B, Fox A, La Pointe P, Simeonov A, Isaksson H, Hermanson J, Öhman J, 2007. Geology Forsmark. Site descriptive modelling Forsmark stage 2.2. SKB R-07-45, Svensk Kärnbränslehantering AB.

Stephens M B, Simeonov A, Isaksson H, 2008. Bedrock geology Forsmark. Modelling stage 2.3. Implications for and verification of the deterministic geological models based on complementary data. SKB R-08-64, Svensk Kärnbränslehantering AB.

Stephens M B, Follin S, Petersson J, Isaksson H, Juhlin C, Simeonov A, 2015. Review of the deterministic modelling of deformation zones and fracture domains at the site proposed for a spent nuclear fuel repository, Sweden, and consequences of structural anisotropy. Tectonophysics 653, 68–94.

Stiggson M, 2015. Parameterization of fractures – methods and evaluation of fractal fracture surfaces. Posiva Working Report 2015-27, Posiva Oy, Finland.

Stigsson M, 2019. Structural uncertainties of rock fractures and their effect on flow and tracer transport. PhD thesis. KTH Royal Institute of Technology, Sweden.

Stigsson M, Mas Ivars D, 2018. A novel conceptual approach to objectively determine JRC using fractal dimension and asperity distribution of mapped fracture traces. Rock Mechanics and Rock Engineering 52, 1041–1054.

Stigsson M, Munier R, 2013. Orientation uncertainty goes bananas: An algorithm to visualise the uncertainty sample space on stereonets for oriented objects measured in boreholes. Computers & Geosciences 56, 56–61.

Stigsson M, Cvetkovic V, Mas Ivars D, Selroos J-O, 2019. A method to estimate flow and transport properties of sheared synthetic fractures in crystalline rock with different roughness under varying normal stress. In Stigsson M. Structural uncertainties of rock fractures and their effect on flow and tracer transport. KTH Royal Institute of Technology, Sweden.

Streltsova T D, 1987. Well testing in heterogeneous formations. New York: Wiley.

Ström A, Andersson J, Skagius K, Winberg A, 2008. Site descriptive modelling during characterization for a geological repository for nuclear waste in Sweden. Applied Geochemistry 23, 1747–1760.

Stuart A M, 2010. Inverse problems: A Bayesian perspective. Acta Numerica 19, 451–559.

Sudicky E A, Frind E O, 1984. Contaminant transport in fractured porous media: Analytical solution for a two-member dacay chain in a single fracture. Water Resources Research 20, 1021–1029.

Svensson U, 2001a. A continuum representation of fracture networks. Part I: Method and basic test cases. Journal of Hydrology 250, 170–186.

Svensson U, 2001b. A continuum representation of fracture networks. Part II: application to the Äspö Hard Rock laboratory. Journal of Hydrology 250, 187–205.

Svensson U, Follin S, 2010. Groundwater flow modelling of the excavation and operational phases – Forsmark. SKB R-09-19, Svensk Kärnbränslehantering AB.

Svensson U, Ferry M, Kuylenstierna H-O, 2010. DarcyTools version 3.4 – Concepts, methods and equations. SKB R-07-38, Svensk Kärnbränslehantering AB.

Svensson U, Löfgren M, Trinchero P, Selroos J-O, 2018. Modelling the diffusion-available pore space of an unaltered granitic rock matrix using a micro-DFN approach. Journal of Hydrology 559, 182–191.

Swanson M T, 2006. Late Paleozoic strike-slip faults and related vein arrays of Cape Elizabeth, Maine. Journal of Structural Geology 28, 456–473.

Söderbäck B, 2008. Geological evolution, palaeoclimate and historical development of the Forsmark and Laxemar-Simpevarp areas. Site descriptive modelling. SDM-Site. SKB R-08-19, Svensk Kärnbränslehantering AB.

Söderlund P, Juez-Larré J, Page L M, Stuart F M, Andriessen P A M, 2008. Systematic shift in apatite (U-Th)/He and fission track ages in Palaeoproterozoic domains, south–eastern Sweden. In Ahlbom K, Stephens M (eds). Investigations of potential repository sites for spent nuclear fuel at Forsmark and Laxemar-Simpevarp, Sweden. Abstracts, 33rd International Geological Congress, Oslo. SKB R-08-97, Svensk Kärnbränslehantering AB, 45.

Söderlund P, Hermansson T, Page L M, Stephens M B, 2009. Biotite and muscovite $^{40}Ar/^{39}Ar$ geochronological constraints on the post-Svecofennian tectonothermal evolution, Forsmark site, central Sweden. International Journal of Earth Sciences 98, 1835–1851.

Talbot C J, 2014. Comment on "Approach to estimating the maximum depth for glacially induced hydraulic jacking in fractured crystalline rock at Forsmark, Sweden" by M. Lönnqvist and H. Hökmark. Journal of Geophysical Research: Earth Surface 119, 951–954.

Tammisto E, Ahokas H, Komulainen J, Pekkanen J, 2019. Quality assessment of PFL transmissivity data identified in subsurface drillholes of ONKALO. Posiva 2017-04, Posiva Oy, Finland.

Tang D H, Frind E O, Sudicky E A, 1981. Contaminant transport in fractured porous media: Analytical solution for a single fracture. Water Resources Research 17, 555–564.

Tarantola A, 2004. Inverse problem theory and methods for model parameter estimation. Philadelphia, PA: Society for Industrial and Applied Mathematics.

Tchalenko J S, 1970. Similarities between shear zones of different magnitudes. Geological Society of America Bulletin 81, 1625–1640.

Terzaghi R, 1965. Sources of error in joint surveys. Géotechnique 15, 287–304.

Teurneau B, Forsmark T, Forssman I, Rhén I, Zinn E, 2008. Forsmark site investigation. Correlation of Posiva Flow Log anomalies to core mapped features in KFM01D, KFM07C, KFM08A, KFM08C and KFM10A. SKB P-07-127, Svensk Kärnbränslehantering AB.

Theis C V, 1935. The relation between the lowering of the piezometric surface and the rate and duration of discharge of a well using ground-water storage. Eos, Transactions American Geophysical Union 16, 519–524.

Thiem G, 1906. Hydrologische Methoden. Gebhardt.

Thörn J, 2015. The impact of fracture geometry on the hydromechanical behaviour of crystalline rock. PhD thesis. Chalmers University of Technology, Sweden.

Tillberg M, Drake H, Zack T, Kooijman E, Whitehouse M J, Åström M E, 2020. In situ Rb-Sr dating of slickenfibres in deep crystalline basement faults. Scientific Reports 10, 562. doi:10.1038/s41598-019-57262-5

Tirén S A, 2012. Initial Review Phase for SKB's safety assessment SR-Site: Geological structures and deformation zones, from site investigation to safety assessment. Technical Note 2012:54, Swedish Radiation Safety Authority.

Trinchero P, Painter S, Ebrahimi H, Koskinen L, Molinero J, Selroos J-O, 2016. Modelling radionuclide transport in fractured media with a dynamic update of K_d values. Computers & Geosciences 86, 55–63.

Trinchero P, Puigdomenech I, Molinero J, Ebrahimi H, Gylling B, Svensson U, Bosbach D, Deissmann G, 2017. Continuum-based DFN-consistent numerical framework for the simulation of oxygen infiltration into fractured crystalline rocks. Journal of Contaminant Hydrology 200, 60–69.

Trinchero P, Cvetkovic V, Selroos J-O, Bosbach D, Deissmann G, 2020. Upscaling of radionuclide transport and retention in crystalline rocks exhibiting micro-scale heterogeneity of the rock matrix. Advances in Water Resources 142. doi:10.1016/j.advwatres.2020.103644

Tsang C-F, 1990. Coupled behavior of rock joints. LBL-28600, Lawrence Berkeley Laboratory, University of California.

Tsang C F, Neretnieks I, 1998. Flow channeling in heterogeneous fractured rocks. Reviews of Geophysics 36, 275–298.

Tsang C-F, Rutqvist J, Min K-B, 2007. Fractured rock hydromechanics: from borehole testing to solute transport and CO_2 storage. Geological Society, London, Special Publications 284, 15–34.

Tullborg E-L, Larson S Å, Morad S, 2001. Dating methods and geochronology of fractures and movements in bedrock: a review. SKB R-01-25, Svensk Kärnbränslehantering AB.

Turcotte D L, 1986. Fractals and fragmentation. Journal of Geophysical Research: Solid Earth 91, 1921–1926.

Uchida M, Doe T, Dershowitz W, Thomas A, Wallmann P, Sawada A, 1994. Discrete-fracture modelling of the Äspö LPT-2, large-scale pumping and tracer test. SKB ICR-94-09, Svensk Kärnbränslehantering AB.

Utsu T, 1999. Representation and analysis of the earthquake size distribution: a historical review and some new approaches. In Wyss M, Shimazaki K, Ito A (eds). Seismicity patterns, their statistical significance and physical meaning. Springer, 509–535.

Vermilye J M, Scholz C H, 1998. The process zone: a microstructural view of fault growth. Journal of Geophysical Research: Solid Earth 103, 12223–12237.

Vidstrand P, Wallroth T, Ericsson L O, 2008. Coupled HM effects in a crystalline rock mass due to glaciation: indicative results from groundwater flow regimes and stresses from an FEM study. Bulletin of Engineering Geology and the Environment 67, 187–197.

Vidstrand P, Follin S, Zugec N, 2010. Groundwater flow modelling of periods with periglacial and glacial climate conditions – Forsmark. SKB R-09-21, Svensk Kärnbränslehantering AB.

Vilks P, 2007a. Forsmark site investigation. Rock matrix permeability measurements on core samples from borehole KFM01D. SKB P-07-162, Svensk Kärnbränslehantering AB.

Vilks P, 2007b. Oskarshamn site investigation. Rock matrix permeability measurements on core samples from borehole KLX03. SKB P-07-204, Svensk Kärnbränslehantering AB.

Viola G, Venvik Ganerød G, Wahlgren C H, 2009. Unraveling 1.5 Ga of brittle deformation history in the Laxemar-Simpevarp area, southeast Sweden: A contribution to the Swedish site investigation study for the disposal of highly radioactive nuclear waste. Tectonics 28. doi:10.1029/2009tc002461

Viola G, Mattila J, Zwingmann H, Todd A, Raven M, 2011. Structural and K/Ar illite geochronological constraints on the brittle deformation history of the Olkiluoto region, southwest Finland. Posiva Working Report 2011-37, Posiva Oy, Finland.

Viswanathan H S, Hyman J, Karra S, O'Malley D, Srinivasan S, Hagberg A, Srinivasan G, 2018. Advancing graph-based algorithms for predicting flow and transport in fractured rock. Water Resources Research 54, 6085–6099.

Vollmer F W, 1995. C Program for automatic contouring of spherical orientation data using a modified Kamb method. Computers & Geosciences 21, 31–49.

Vollmer F W, 2015. Orient 3: a new integrated software program for orientation data analysis, kinematic analysis, spherical projections, and Schmidt plots. Proceedings of Geological Society of America Abstracts with Programs, 2015.

Vollmer F W, 2021. Orient 3. Version: 3.13.0. Available at: http://www.frederickvollmer.com/orient

Voutilainen M, Miettinen A, Sardini P, Parkkonen J, Sammaljärvi J, Gylling B, Selroos J-O, Yli-Kaila M, Koskinen L, Siitari-Kauppi M, 2019. Characterization of spatial porosity and mineral distribution of crystalline rock using X-ray micro computed tomography, C-14-PMMA autoradiography and scanning electron microscopy. Applied Geochemistry 101, 50–61.

Väisäsvaara J, Leppänen H, Pekkanen J, Pöllänen J, 2006. Forsmark site investigation. Difference flow logging in borehole KFM08C. SKB P-06-189, Svensk Kärnbränslehantering AB.

Walsh J J, Watterson J, 1988. Analysis of the relationship between displacements and dimensions of faults. Journal of Structural Geology 10, 239–247.

Wang C-Y, Manga M, 2014. Earthquakes and water. In Meyers R A (ed) Encyclopedia of complexity and systems science. New York: Springer.

Wang C-Y, Liao X, Wang L-P, Wang C-H, Manga M, 2016. Large earthquakes create vertical permeability by breaching aquitards. Water Resources Research 52, 5923–5937.

Wang X, 2005. Stereological interpretation of rock fracture traces on borehole walls and other cylindrical surfaces. PhD thesis. Virginia Polytechnic Institute and State University.

Warburton P M, 1980. Stereological interpretation of joint trace data; influence of joint shape and implications for geological surveys. International Journal of Rock Mechanics and Mining Sciences & Geomechanics Abstracts 17, 305–316.

Watanabe N, Hirano N, Tsuchiya N, 2009. Diversity of channeling flow in heterogeneous aperture distribution inferred from integrated experimental-numerical analysis on flow through shear fracture in granite. Journal of Geophysical Research: Solid Earth 114. doi:10.1029/2008JB005959

Wathugala D N, Kulatilake P H, Wathugala G W, Stephansson O, 1990. A general procedure to correct sampling bias on joint orientation using a vector approach. Computers and Geotechnics 10, 1–31.

Wen X-H, Gómez-Hernández J J, 1996. Upscaling hydraulic conductivities in heterogeneous media: An overview. Journal of Hydrology 183, ix–xxxii.

Wickman F E, Åberg G, Levi B, 1983. Rb-Sr dating of alteration events in granitoids. Contributions to Mineralogy and Petrology 83, 358–362.

Willis-Richards J, Watanabe K, Takahashi H, 1996. Progress toward a stochastic rock mechanics model of engineered geothermal systems. Journal of Geophysical Research: Solid Earth 101, 17481–17496.

Winberg A (ed), 2010. Fault rock zones characterisation – Final report. TRUE-1 Continuation Project. SKB TR-10-36, Svensk Kärnbränslehantering AB.

Winberg A, 2017. Modelling scales applicable to detailed site investigations in the Forsmark area. SKBdoc 1409070 ver 1.0, Svensk Kärnbränslehantering AB.

Winberg A, Andersson P, Hermanson J, Byegård J, Cvetkovic V, Birgersson L, 2000. Äspö Hard Rock Laboratory. Final report of the first stage of the tracer retention understanding experiments. SKB TR-00-07, Svensk Kärnbränslehantering AB.

Winberg A, Andersson P, Byegård J, Poteri A, Cvetkovic V, Dershowitz W, Doe T, Hermanson J, Gómez-Hernández J J, Hautojärvi A, Billaux D, Tullborg E-L, Holton D, Meier P, Medina A, 2003. Final report of the TRUE Block Scale project. 4. Synthesis of flow, transport and retention in the block scale. SKB TR-02-16, Svensk Kärnbränslehantering AB.

Winberg A, Fox A, Pettersson A, Drake H, 2013. Detailed description of TRUE Block Scale Structure #20 based on intercepts in boreholes and intercepts in the TASS tunnel. SKB R-12-09, Svensk Kärnbränslehantering AB.

Witherspoon P A, Wang J S Y, Iwai K, Gale J E, 1980. Validity of cubic law for fluid flow in a deformable rock fracture. Water Resources Research 16, 1016–1024.

Wooding R A, 1960. Instability of a viscous liquid of variable density in a vertical Hele-Shaw cell. Journal of Fluid Mechanics 7, 501–515.

Xiao W, Xia C, Wei W, Bian Y, 2013. Combined effect of tortuosity and surface roughness on estimation of flow rate through a single rough joint. Journal of Geophysics and Engineering 10, 045015. doi:10.1088/1742-2132/10/4/045015

Ye J, 1998. On measuring and correcting the effects of data mining and model selection. Journal of the American Statistical Association 93, 120–131.

Yi Y, Tawerghi E, 2009. Geometric percolation thresholds of interpenetrating plates in three-dimensional space. Physical Review E 79, 041134. doi:10.1103/PhysRevE.79.041134

Zangerl C, Eberhardt E, Evans K, Löw S, 2008. Normal stiffness of fractures in granitic rock: a compilation of laboratory and in situ experiments. International journal of rock mechanics and Mining Sciences 45, 1500–1507.

Zhang L, Einstein H H, 2000. Estimating the intensity of rock discontinuities. International Journal of Rock Mechanics and Mining Sciences 37, 819–837.

Zhang L, Einstein H H, Dershowitz W S, 2002. Stereological relationship between trace length and size distribution of elliptical discontinuities. Géotechnique 52, 419–433.

Zhao J, Brown E T, 1992. Thermal cracking induced by water flow through joints in heated granite. International Journal of Rock Mechanics and Mining Sciences & Geomechanics Abstracts 29, 77–82.

Zimmerman R, Kumar S, Bodvarsson G, 1991. Lubrication theory analysis of the permeability of rough-walled fractures. International Journal of Rock Mechanics and Mining Sciences & Geomechanics Abstracts 28, 325–331.

Zimmerman R, Main I, 2004. Hydromechanical behavior of fractured rocks. In Guéguen Y, Boutéca M (eds). Mechanics of fluid-saturated rocks. Amsterdam: Elsevier. (International Geophysics Series 89), 363–422.

Zoback M D, 2010. Reservoir geomechanics. Cambridge: Cambridge University Press.

Zou L, Cvetkovic V, 2020. Impact of normal stress-induced closure on laboratory-scale solute transport in a natural rock fracture. Journal of Rock Mechanics and Geotechnical Engineering 12, 732–741.

Zou L, Jing L, Cvetkovic V, 2017. Modeling of solute transport in a 3D rough-walled fracture-matrix system. Transport in Porous Media 116, 1005–1029.

Zou L, Cvetkovic V, Jing L, Mas Ivars D, 2018. Impact of normal stress caused closure on fluid flow and solute retention in rock fractures. In Proceedings of the International Conference on Coupled Processes in Fractured Geological Media: Observation, Modeling, and Application (CouFrac), Wuhan, China, 12–14 November 2018.

Öhberg A, 2006. Investigation equipment and methods used by Posiva. Posiva Working Report 2006-81, Posiva Oy, Finland.

Öhberg A, Rouhiainen P, 2000. Posiva groundwater flow measuring techniques. Posiva 2000-12, Posiva Oy, Finland.

SKB is responsible for managing spent nuclear fuel and radioactive waste produced by the Swedish nuclear power plants such that man and the environment are protected in the near and distant future.

skb.se